Vol. 194, March 16, 1987
Complete in one issue

ISSN 0003-2670

ANALYTICA CHIMICA ACTA

International journal devoted to all branches of analytical chemistry

ELSEVIER

ANALYTICA CHIMICA ACTA

International journal devoted to all branches of analytical chemistry
Revue internationale consacrée à tous les domaines de la chimie analytique
Internationale Zeitschrift für alle Gebiete der analytischen Chemie

PUBLICATION SCHEDULE FOR 1987

	J	F	M	A	M	J	J	A	S	O	N	D
Analytica Chimica Acta	192	193	194	195	196	197	198	199	200	201	202	203

Scope. *Analytica Chimica Acta* publishes original papers, short communications, and reviews dealing with eve aspect of modern chemical analysis both fundamental and applied.

Submission of Papers. Manuscripts (three copies) should be submitted as designated below for rapid ar efficient handling:

Papers from the Americas to: Professor Harry L. Pardue, Department of Chemistry, Purdue University, We Lafayette, IN 47907, U.S.A.

Papers from all other countries to: Dr. A. M. G. Macdonald, Department of Chemistry, The University, P.O. Box 36 Birmingham B15 2TT, England. Papers dealing particularly with computer techniques to: Professor J. T. Cler Universität Bern, Pharmazeutisches Institut, Baltzerstrasse 5, CH-3012 Bern, Switzerland.

Submission of an article is understood to imply that the article is original and unpublished and is not beir considered for publication elsewhere. Upon acceptance of an article by the journal, authors will be asked to transf the copyright of the article to the publisher. This transfer will ensure the widest possible dissemination information.

Papers in English, French and German are published. There are no page charges. Manuscripts should conform layout and style to the papers published in this Volume. See inside back cover for "Information for Authors".

Reprints. Fifty reprints will be supplied free of charge. Additional reprints (minimum 100) can be ordered. A order form containing price quotations will be sent to the authors together with the proofs of their article.

Publication. *Analytica Chimica Acta* appears in 12 volumes in 1987. The subscription for 1987 (Vols. 192–203) Dfl. 2700.00 plus Dfl. 300.00 (p.p.h.) (total approx. US $1463.40). All earlier volumes (Vols. 1–191) except Vol 23 and 28 are available at Dfl. 231.00 (US $112.70), plus Dfl. 17.00 (US $8.30) p.p.h., per volume.

Our p.p.h. (postage, packing and handling) charge includes surface delivery of all issues, except to subscribers the U.S.A., Canada, Japan, Australia, New Zealand, P.R. China, India, Israel, South Africa, Malaysia, Thailan Singapore, South Korea, Taiwan, Pakistan, Hong Kong, Brazil, Argentina and Mexico, who receive all issues by a delivery (S.A.L. — Surface Air Lifted) at no extra cost. For the rest of the world, airmail and S.A.L. charges a available upon request.

Subscription. Subscription should be sent to: Elsevier Science Publishers B.V., Journals Department, P.O. Bo 211, 1000 AE Amsterdam, The Netherlands. Tel: 5803 911, Telex: 18582, to which requests for sample copies ca also be sent.

Claims for issues not received should be made within three months of publication of the issues. If not they cann be honoured free of charge.

Readers in the U.S.A. and Canada can contact the following address: Elsevier Science Publishing Co. Inc., Journ Information Center, 52 Vanderbilt Avenue, New York, NY 10017, U.S.A., Tel: (212) 916-1250, for furth information, or a free sample copy of this or any other Elsevier Science Publishers journal.

Advertisements. Advertisement rates are available from the publisher on request.

0003-2670/87/$03.

Printed in The Netherlands

CONTENTS

ANALYTICA CHIMICA ACTA
VOL. 194 (1987)

ANALYTICA CHIMICA ACTA

International journal devoted to all branches of analytical chemistry

ELSEVIER Amsterdam–Oxford–New York–Tokyo

0003-2670/86/$03.50

Printed in The Netherlands

Analytica Chimica Acta, 194 (1987) 1—9
Elsevier Science Publishers B.V., Amsterdam — Printed in The Netherlands

AUTOMATED ODOR-SENSING SYSTEM BASED ON PLURAL SEMICONDUCTOR GAS SENSORS AND COMPUTERIZED PATTERN RECOGNITION TECHNIQUES

HIDETSUGU ABE, TADAYOSI YOSHIMURA, SHIGEHIKO KANAYA, YOSHIMASA TAKAHASHI, YOSHIKATSU MIYASHITA and SHIN-ICHI SASAKI*

Department of Materials Science, Toyohashi University of Technology, Hibarigaoka, Tempaku, Toyohashi 440 (Japan)

(Received 18th November 1986)

SUMMARY

Although odor is an inherent characteristic of chemical substances, no methods to measure or identify odor objectively have been available. A computerized method for classification and identification of odor is reported. Odors are detected by using eight semiconductor gas-sensor elements which have different sensing properties for gases; the output from the odor-detecting apparatus for a gas sample is represented by an 8-dimensional vector. The vectors for 30 substances were examined by clustering analysis and four obvious clusters were observed. These clusters corresponded to ethereal, ethereal-minty, ethereal-pungent and pungent substances.

No reliable method except organoleptic tests by experienced human noses or taste-buds is known for identification of the odors of chemical substances, e.g., in perfume production.

The first aim of the present study is to classify the odors by computerized pattern-recognition technique and plural semiconductor gas-sensors. If the purpose can be achieved, a system of identifying the odors of specified substances should become possible. Fortunately, semiconductor gas-sensors possessing different sensitivities to various gases have become available, and an attempt to classify odors was made with the assorted sensors. A general idea of this system is presented in Fig. 1. Sensor units $s_1 - s_n$, give electric signals, $x_1 - x_n$, respectively, for a specified chemical substance. These electric signals can be regarded as n-dimensional pattern vectors. The pattern vectors are supposed to be different for different samples, i.e., each substance is to give its specific pattern vectors. Therefore, if there are m kinds of substances, they will give m sets of pattern vectors through this system. If the odors of m kinds of substances are classified into p categories ($m > p$), the pattern vectors belonging to each category are presumed to have some common features. The aim is to establish a system which can identify the odors objectively by discovering the above-mentioned common features by means of computerized pattern-recognition techniques.

0003-2670/87/$03.50

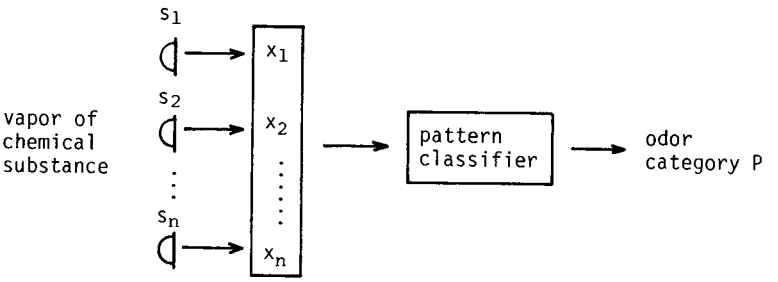

Fig. 1. General idea of the odor-sensing system.

EXPERIMENTAL

Apparatus

The sensor units used are all available on the market (Figaro Engineering Company, Minoo, Osaka, Japan); their types and the major gases detected are shown in Table 1. The principle of gas detection for this sensor unit is that its electric resistance changes when gas molecules are adsorbed on its surface. The change of resistance of the sensor unit is detected as a change of electric potential between the two ends of the load resistance (R_L) in the circuit shown in Fig. 2, where V_C is the circuit voltage and V_H is the heater voltage. The whole apparatus is shown in Fig. 3; the test box of about 5-l capacity is fitted, inside, with the eight sensor units listed in Table 1, a circulating fan, an air brush for cleaning the surfaces of the units, a sample input port, air inlet and air outlet. The signals were measured by a personal computer (NEC, PC-9801 VM2) via a multichannel A/D converter (12 bits, 8 channels), taking in the outputs from the eight sensor units at 1-s intervals.

Sample preparation and "odor" measurement

The substances used in these experiments are listed in Table 2. All the substances were of the highest grade available on the market and were used as received. The descriptions of their odors found in the literature [1] are also listed in Table 2. The substance (5 ml as liquid) was poured into a 500-ml glass bottle, which was sealed with a rubber stopper, and kept at 25°C for

TABLE 1

Sensor elements and the major gases sensed

No.	Element name	Gas sensed	No.	Element name	Gas sensed
1	TGS814D	Ammonia	6	TGS815D	General combustible gases
2	TGS711	Carbon monoxide	7	TGS816	General combustible gases
3	TGS812	Alcohols	8	TGS813	General combustible gases
4	TGS712D	Carbon monoxide			
5	TGS817	Alcohols Carbon monoxide Chlorofluorocarbons			

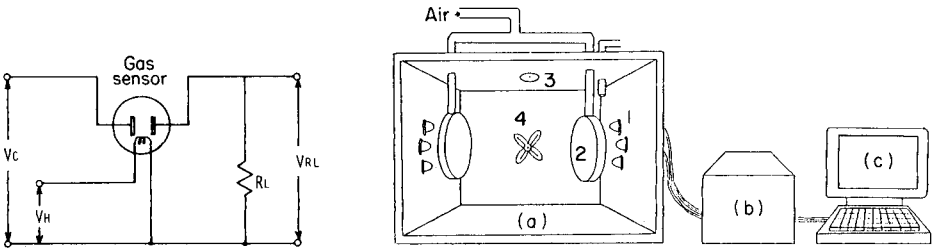

Fig. 2. Measuring circuit of semiconductor gas-sensors: V_C, circuit voltage; V_H, heater voltage; R_L, loading resistance; V_{RL}, output voltage.

Fig. 3. Arrangement of odor-sensing system. (a) Test box; (b) terminal box and power supply; (c) personal computer with A/D converter; (1) TGS sensors; (2) air brush; (3) sample injection point; (4) fan.

more than 10 min so that air saturation was achieved, in a constant-temperature chamber. Then, gas samples were taken from the bottle with a gas syringe with pressure compensation. Purified air was obtained from a compressed air cylinder.

Data processing

The measurement circuit for each sensor unit was shown in Fig. 2. The standard resistance of a sensor unit (R_{air}) can be calculated from the average value (V_{air}) of the electric potential (10 points) measured for ten seconds prior to sample input, between the ends of the load resistance (R_L = 3.9 kΩ) by using the following equation:

$$R_{air} = [(V_C/V_{air}) - 1]R_L \tag{1}$$

where V_C is the circuit voltage, 10.0 V.

From the maximum value (V_{gas}) of the electric potential (60 points) between the ends of R_L observed for 60 s after the sample injection, R_{gas} is calculated from the equation

$$R_{gas} = [(V_C/V_{gas}) - 1]R_L \tag{1'}$$

The ratio r is then calculated from R_{air}:

$$r = \log_{10}(R_{air}/R_{gas}) \tag{2}$$

As afore-mentioned, the data expressed by 8-dimensional vectors, (r_1, r_2, ... r_8), are obtained for each sample, because eight sensor units are used. Equation 2 is derived from the relation between gas concentration C and electric resistance of the sensor unit [2] expressed by the equation

$$R_{air}/R_{gas} = \exp(a \ln C + b) \tag{3}$$

where a and b are constants. Each of the eight sensor units used shows different behavior to the concentrations, i.e., they each have different a and b

TABLE 2

Substance used

No.	Name	Description of odor quality[a]
1	Methyl acetate	Sweet, and extremely diffusive, ethereal fruity odor of very poor tenacity
2	Diethyl ether	Very diffusive, sweet-ethereal odor
3	Acetone	Light ethereal-nauseating and powerful odor of very poor tenacity. Irritant at high concentration, rather pleasant in dilution
4	Ethyl acetate	Pleasant, ethereal-fruity, banana-like odor, somewhat nauseating in high concentration
5	Acetyl acetone	Ethereal-minty odor, somewhat metallic or "chemical"
6	Methyl formate	Very ethereal-diffusive odor of winey chloroform-type
7	Ethyl formate	Pleasant, ethereal, diffusive, warm-fruity rum-like odor
8	Acetaldehyde	Pungent ethereal-nauseating odor, in high dilution reminiscent of coffee or wine
9	Allyl acetate	Ethereal-winey odor, somewhat similar to that of ethyl acetate, but more pungent, rum-like fruity, arrack-like
10	Isobutyl methyl ketone	Powerful and diffusive ethereal-fruity odor of poor tenacity
11	Pentyl formate	Powerful ethereal-vinous, somewhat dry-earthy, yet fruity odor with earthy-green undertones
12	Isopropyl acetate	Very diffusive, fruity-ethereal odor of very poor tenacity
13	Tert-pentanol	Nauseating, camphor-like odor, also slightly cool minty, diffusive
14	2-Methylcyclohexanone	Somewhat harsh, minty-almondy, rather chemical odor. Poor tenacity
15	3-Methylcyclohexanone	Fresh, camphoraceous-minty, but rather weak odor of poor tenacity
16	4-Methylcyclohexanone	This isomer is the most pleasant-minty smelling in the three
17	Methyl butyrate	Very diffusive and penetrating sweet-ethereal fruity odor. In extreme dilution reminiscent of apple peel with a slight fatty peach-like undertone
18	Isobutylaldehyde	Extremely diffusive, penetrating odor, pungent and — undiluted — unpleasant, sour, repulsive. In extreme dilution it becomes almost pleasant fruity, banana-like, "overripe fruity like"
19	Menthone	Minty-refreshing and diffusive odor of moderate tenacity and slightly woody dry undertones
20	Acetic acid	Pungent, stinging sour odor, unpleasant when concentrated, less repulsive when diluted below 15% in water
21	Methyl valerate	Pungent-ethereal, green fruity apple-like odor of poor tenacity. The odor is heavier than that of methyl isovalerate
22	Furfural	Pungent, but sweet bread-like, caramel-like, cinnamon-almond-like odor of poor tenacity
23	Acrylic acid	Its odor resembles that of acetic acid, but more it is acrid, corrosive to human mucous membrane, irritating to the eyes

TABLE 2 (continued)

No.	Name	Description of odor quality[a]
24	Phenetole	Pleasant, warm-aromatic, but somewhat pungent odor, more attractive in dilution
25	Propionic acid	Pungent sour odor reminiscent of sour milk, cheese or sour butter
26	Dioxane	Very sweet, mild-ethereal odor
27	Chloroform	Diffusive, heavy, sweet-ethereal odor with considerable anaesthetic effect
28	Pyridine	Pungent, penetrating and diffusive odor, generally described as nauseating, but in extreme dilution warm, "burnt", smokey of very poor tenacity
29	2-Methyl-3-butanone	Diffusive, ethereal-camphoraceous odor, pleasant in dilution, somewhat pungent choking when concentrated
30	Pyrrole	Sweet and warm-ethereal, slightly burnt-nauseating odor, resembling the odor of propyl formate

[a]Taken from Arctander [1].

values. In order to compensate for this situation, the characteristic values, P_i ($i = 1, 2, \ldots 8$) were used as the data:

$$P_i = r_i / \sum_{i=1}^{8} r_i \tag{4}$$

Table 3 shows the P_i values for 30 substances obtained for 6-ml sample gas injections.

Dependence of the sensor response on sample concentration and reproducibility of the data

Equation 3 indicates that there is a linear relation between the logarithm of the gas sample concentration C and the value of r. Tests of the coefficients a and b for various concentrations were made by using the equation $r = a \log C + b$, which is derived from Eqn. 3. Table 4 shows the linear regression coefficients a and b, and the correlation coefficients R_c for the sensor units, which were obtained when the gas was diethyl ether and the injected volume was changed gradually from 0.1 ml to 9.0 ml. Average values, $\bar{P}_i$, for the characteristic values P_i for the sensors and the 95% confidence limits are included in Table 4. These results indicate that all the sensors have sufficient linearity for the concentration range in these experiments. To indicate reproducibility, the mean values of r_i and P_i for about 100 data points sampled periodically over five months with diethyl ether gas (6-ml injections) are shown in Table 5.

These results indicate that each sensor has enough stability and reproducibility to continue this investigation, because it was regarded as equal to the performance of the F-test (significance level $\alpha = 0.01$).

TABLE 3

P_i values of the eight sensors for all substances

Substance[a]	1	2	3	4	5	6	7	8
1	0.186	0.063	0.159	0.168	0.183	0.056	0.104	0.081
2	0.181	0.061	0.153	0.168	0.179	0.069	0.106	0.083
3	0.180	0.044	0.168	0.176	0.190	0.057	0.099	0.086
4	0.177	0.055	0.154	0.169	0.182	0.065	0.090	0.109
5	0.172	0.037	0.160	0.177	0.192	0.077	0.110	0.075
6	0.168	0.089	0.155	0.160	0.173	0.061	0.108	0.088
7	0.175	0.093	0.157	0.160	0.173	0.061	0.105	0.077
8	0.170	0.122	0.146	0.156	0.165	0.063	0.101	0.079
9	0.162	0.094	0.153	0.176	0.196	0.071	0.086	0.062
10	0.151	0.103	0.153	0.180	0.193	0.073	0.078	0.069
11	0.152	0.068	0.170	0.198	0.226	0.068	0.062	0.058
12	0.155	0.076	0.159	0.194	0.208	0.071	0.073	0.063
13	0.121	0.084	0.177	0.191	0.221	0.075	0.066	0.066
14	0.135	0.093	0.142	0.196	0.205	0.096	0.074	0.060
15	0.143	0.074	0.143	0.191	0.201	0.111	0.075	0.063
16	0.147	0.072	0.145	0.193	0.202	0.104	0.075	0.062
17	0.170	0.024	0.174	0.190	0.212	0.065	0.094	0.072
18	0.164	0.035	0.170	0.189	0.212	0.070	0.093	0.068
19	0.148	0.023	0.162	0.191	0.204	0.070	0.118	0.085
20	0.140	0.003	0.173	0.202	0.224	0.074	0.113	0.071
21	0.158	0.020	0.179	0.204	0.232	0.066	0.080	0.062
22	0.145	0.015	0.186	0.199	0.238	0.063	0.084	0.065
23	0.158	0.009	0.168	0.204	0.236	0.067	0.097	0.061
24	0.140	0.018	0.175	0.214	0.251	0.060	0.077	0.062
25	0.129	0.003	0.168	0.216	0.235	0.096	0.089	0.064
26	0.201	0.011	0.185	0.186	0.207	0.056	0.076	0.078
27	0.144	0.019	0.145	0.160	0.169	0.105	0.094	0.160
28	0.097	0.006	0.177	0.187	0.206	0.103	0.116	0.108
29	0.166	0.149	0.146	0.165	0.177	0.063	0.071	0.064
30	0.160	0.146	0.126	0.163	0.170	0.088	0.083	0.065

[a]For identification, see Table 2.

TABLE 4

Linear regression coefficients for the eight sensors obtained with diethyl ether

Sensor	1	2	3	4	5	6	7	8
a	0.730	0.334	0.603	0.648	0.652	0.306	0.437	0.391
b	1.356	0.511	1.146	1.192	1.299	0.505	0.779	0.619
R_c	0.993	0.978	0.999	0.998	0.997	0.998	0.998	0.981
P_i[a]	0.183	0.064	0.154	0.164	0.173	0.070	0.107	0.084
Confidence limits by t-test (α = 0.05)	0.008	0.014	0.002	0.004	0.004	0.002	0.001	0.002

[a]i = 1, 2, . . . 8 (Sensor No.)

TABLE 5

Reproducibility of each sensor for diethyl ether

Sensor	1	2	3	4	5	6	7	8
$\bar{r}_i$	1.91 ± 0.12	0.67 ± 0.16	1.65 ± 0.06	1.72 ± 0.11	1.83 ± 0.11	0.74 ± 0.03	1.12 ± 0.04	0.89 ± 0.02
$\overline{P_i}$	0.183 ± 0.010	0.064 ± 0.016	0.154 ± 0.002	0.164 ± 0.005	0.173 ± 0.005	0.070 ± 0.002	0.107 ± 0.001	0.084 ± 0.002

Pattern recognition of the sensor data

To investigate whether or not there is any correlation between the sensor data and the odors of the substances, an unsupervised pattern classification method, cluster analysis [3] was applied. The similarity measure for the evaluation was the 8-dimensional Euclidian distance. The resulting dendrogram is shown in Fig. 4. Four obvious clusters can be seen, corresponding to substances 1—8 (cluster I), 9—16 (cluster II), 17—26 (cluster III), and 29 and 30 (cluster IV). Only two data sets corresponding to substances 27 and 28 were not clustered.

Inspected from the standpoint of the odors of the substances in each cluster, all substances in cluster I have ethereal odor and almost all substances in clusters III and IV have pungent odors. Cluster II consists of ethereal and minty substances, and most minty substances are present in this cluster.

To visualize the 8-dimensional data structure, the K-L plotting method [4] was applied to the data. Figure 5A shows the plot for the first and the second principal components; the cumulative variance for the components was 78.2%. The plot for the first and the third principal components is shown in Fig. 5B, for which the cumulative variance was 70.5%. The cumulative variance for the first to third principal components was 92.2%. Clusters I—IV are delineated in the diagrams. As clearly displayed, the data points for minty substances in cluster II are condensed into a smaller sub-cluster and those for ethereal substances in this cluster are located close to the borderline of cluster I which consists of entirely ethereal substances. Moreover, the data points for pungent substances in cluster III also form a condensed sub-cluster.

These results show that there is indeed a correlation between the 8-dimensional sensor data and the odors of chemical substances.

DISCUSSION

Because odor is an inherent property of substances, identification of substances should correspond to identification of odors. It is true that many perfumery experts can identify thousands of substances by their odors, and primitive peoples are also very effective in identifying odors; but for ordinary people, odors can well be classified into a small number of categories, although the odors of the members of a category are not always identical.

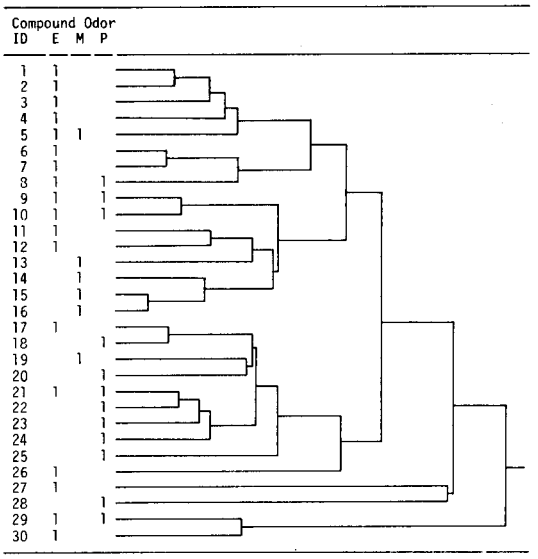

Fig. 4. The result of cluster analysis on the sensor data for 30 substances. E, Ethereal; M, minty; P, pungent.

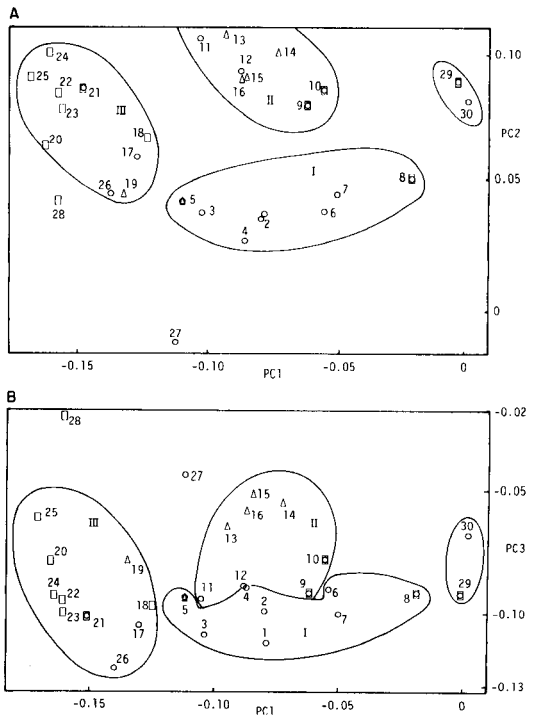

Fig. 5. K-L plots for the sensor data of 30 substances: (A) first and second principal components; (B) first and third principal components. Odor: (□) pungent; (○) ethereal; (△) minty.

Furthermore, it is known that there are groups of substances which have different chemical structures but similar odors. The man who has unskilled and not always sharp olfaction seems to be classifying odors of such substances into categories by using a pattern recognition method. The results presented above strongly suggest that the present plural semiconductor sensor system, though its sensing mechanism is quite different from that of biosystems, makes it possible to identify the odors of chemical substances. Better precision and higher sensitivity could be achieved by improvement of the sensor units so that the system would become more suitable for this purpose.

The authors thank Dr. Haruki Tsuruta of Takasago Corporation for helpful discussions about odor substances. Part of this work was financially supported by the Ministry of Education, Science and Culture through Grant-in-Aid for Scientific Research (No. 61127006).

REFERENCES

1 S. Arctander, Perfume and Flavor Chemicals I, II, P.O. Box 114, Elizabeth, NJ, 1969.
2 J. Watson, Sensors and Actuators, 5 (1984) 29.
3 Y. Takahashi, Y. Miyashita, H. Abe and S. Sasaki, Anal. Chim. Acta, 122 (1980) 241.
4 B. R. Kowalski and C. F. Bender, J. Am. Chem. Soc., 95 (1973) 686.

Analytica Chimica Acta, 194 (1987) 11—24
Elsevier Science Publishers B.V., Amsterdam — Printed in The Netherlands

DIFFERENTIAL CROSS-CORRELATION HIGH-PERFORMANCE LIQUID CHROMATOGRAPHY, A METHOD OF ESTABLISHING SMALL CONCENTRATION DIFFERENCES IN SAMPLES OF SIMILAR ORIGIN

J. M. LAEVEN, H. C. SMIT* and J. C. KRAAK

Laboratory for Analytical Chemistry, University of Amsterdam, Nieuwe Achtergracht 166, 1018 WV Amsterdam (The Netherlands)

(Received 22nd September 1986)

SUMMARY

A modified cross-correlation method is described, which eliminates the disadvantageous effects of the cross-correlation chromatographic (CC) method on baseline noise; such effects occur if the chromatographic system is not ideal. Deviations from the ideal behaviour of such a system can be caused by non-linear effects in the chromatographic system and by irreproducibility of the injections. If several main components are present in the sample besides the trace components to be evaluated, non-ideal behaviour of the CC system causes extra baseline noise. A theoretical discussion is given of the distortion of the correlogram caused by imperfect injection profiles and by non-linear phenomena in chromatography. This distortion appears to be partially proportional to the concentration differences between the compounds in sample and eluent. Thus a differential mode of CC, in which these differences can be decreased, is often advantageous. In the modified method the cross-correlation technique is used in the differential mode: the eluent is made equivalent to the sample by adding the main components present in the sample to the eluent, or another sample is used as eluent. Consequently, the method measures differences between samples and not absolute concentrations. The signal-to-noise ratio was evaluated experimentally in artificial samples and eluents with different phenol concentrations in order to verify the theoretical results. The advantages of the differential mode of cross-correlation chromatography are outlined.

The application of the cross-correlation technique in liquid and gas chromatography has been described in several papers [1—11]. Until now, the technique has mainly been applied in situations where the sample contains trace amounts of the compounds to be examined. It is to be expected, however, that the chromatogram (correlogram) resulting from the cross-correlation technique will be more affected by non-ideal behaviour of the chromatographic system if the difference in composition of sample and eluent increases. Two main aspects of the chromatographic system are responsible for this non-ideal behaviour. The first aspect originates from imperfections in the experimental design of the analyses and in the technical equipment itself, resulting in non-stationarities in the chromatographic system and in irreproducible injection profiles: the theoretically required injection pattern for correlation chromatography (CC), the pseudo-random binary sequence

0003-2670/87/$03.50

(PRBS), cannot be matched exactly in practice because of limitations of the injection valves. Also non-linear behaviour of the detector and instabilities in flow and pressure can play a significant role.

The second component originates from non-linearity of the distribution isotherm, which can be attributed to two effects: first, the mutual influence in the column of the components present in sample and eluent, and secondly, the mutual influence of molecules of the same type on their separation behaviour. In conventional chromatography, it is generally assumed that the physicochemical interaction of each compound in the sample with the column material is independent of time and position in the column. This assumption is often realistic; usually there is little competition for the active sites of the stationary phase between the different types of molecules in the solute, except near the column inlet. Competition is insignificant, as dilution of the sample increases rapidly during elution, and as separation of the compounds starts immediately. In cross-correlation chromatography, however, mutual influence of the sample components is likely, even for moderate concentrations, as at each moment on each position in the column statistically half of the compounds in the sample are present (Fig. 1). In this case, the physicochemical interaction of the compounds is time- and position-dependent, as all compounds always experience competition from changing amounts of the other compounds. This effect is stronger if some compounds equilibrate slowly between the mobile and stationary phases. Another consequence of the mutual influence can be a shift in retention times, because the adsorption characteristics of the stationary phase may be changed by the presence of main absorbing compounds.

In Fig. 2 it can be seen that in CC the axial concentration variation is higher than in conventional chromatography. As the axial diffusion is proportional to the concentration gradient, an extra axial dispersion is expected in CC. From another point of view, a second side-effect of CC can be expected: each point of the ultimate correlogram is the mean sum of concentrations over a wide range of the (non-linear) distribution isotherm; thus low as well as high concentrations of the compounds jointly determine each correlogram point, and hence the distribution isotherm is virtually linearized. Therefore the peaks in a correlogram are usually more symmetric than in a chromatogram. This effect is also known in process control and electronics as the dither effect. The net result of all the (partly competitive) effects occurring if non-linearity is observed in a CC system, is not clear yet and requires a thorough study in which the transport phenomena in such systems are investigated.

It is nevertheless possible to avoid serious contamination of the correlogram by the afore-mentioned effects by using differential cross-correlation chromatography (DCC). The basic idea behind DCC is to eliminate the disturbing influence of major components in the sample by adding these compounds in similar amounts to the eluent, while preserving the main advantage of normal cross-correlation chromatography, i.e., its high sensitivity to

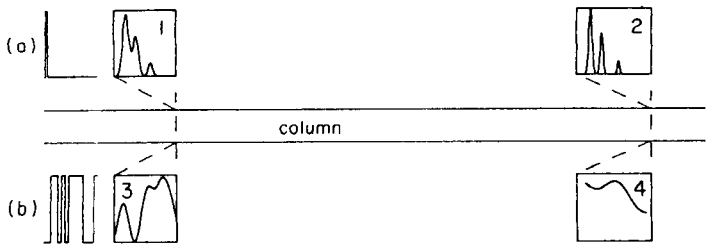

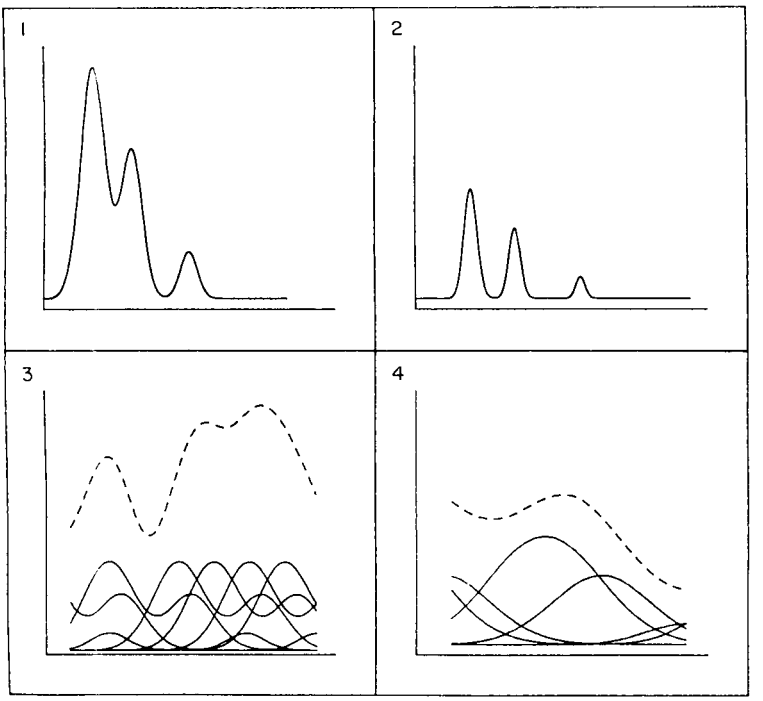

Fig. 1. Visualization of CC and single-injection chromatography. At the top, concentration profiles are shown passing through two cross-sections of a chromatographic column (flow from left to right), resulting from injection of a mixture of three compounds. (a) At the start of the column the situation resulting from a single injection is depicted. The concentration profile passing through the left cross-section is shown (enlarged in frame 1), followed by the profile passing the right cross-section (frame 2). (b) A similar situation is shown for CC: the same mixture is injected according to a PRBS of length 15, which results in the profiles depicted at the two cross-sections (enlarged in frames 3 and 4). Frames: (1) the compounds are incompletely separated at the first cross-section; (2) separation is complete near the outlet of the column; (3) in CC the concentration profile (— — —) is constituted by shifted single injection profiles; (4) a number of single injection concentration profiles shifted according to the PRBS constitute the resulting concentration profile at the cross-section near the outlet. Frames 3 and 4 show clearly that in CC a mixture will always elute at the outlet of the column, never a pure compound. The profiles shown are only part of the entire chromatograms; therefore the scaling is different for the left and right frames.

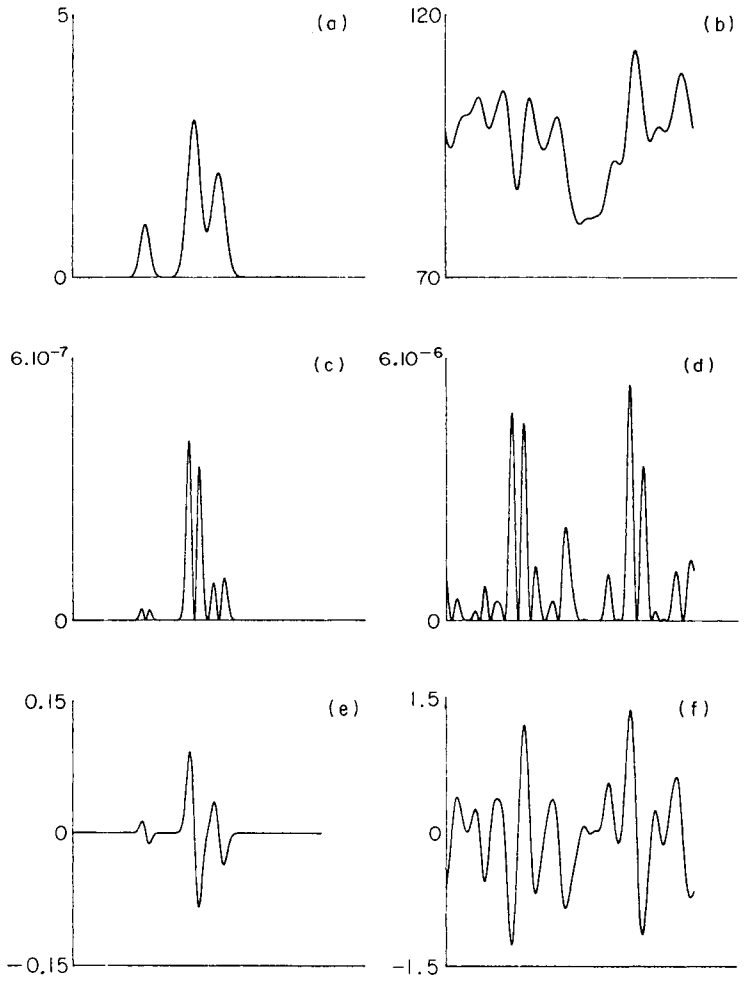

Fig. 2. Axial concentration gradient in CC and single injection chromatography: (a, c, e) single injection chromatography; (b, d, f) CC. Parts (a) and (b) represent the concentration measured at the detector; they show that in CC not only the mean concentration (baseline level) but also the concentration range (b) are much higher. In parts (c) and (d), the weighted square difference (Eqn. 20) is shown. Parts (e) and (f) show the weighted difference (Eqn. 19); in these, it can be seen that the gradient may be negative and positive, and for the calculation of the net mean gradient over the entire column the negative and positive contributions cancel. This cancellation does not occur in (c) and (d) because the differences are squared. Obviously, the mean local concentration variation is much larger in CC than in conventional chromatography, which might lead to a higher sensitivity to non-linearities.

trace components. It should, however, be noted that when these major compounds are added to the eluent, the column properties will change as the column is loaded with these compounds continuously, resulting in an altered separation behaviour of the column, which may even be favourable. Conse-

quently, the separation properties of the column have to be re-evaluated when the differential cross-correlation technique is applied. Another consequence is the possible presence of negative peaks in the chromatogram (correlogram) if the concentration of some compound is higher in the eluent than in the sample. This illustrates one of the basic features of the technique, its symmetry with respect to sample and eluent.

It is obviously impossible in practice to add the major disturbing compounds present in the sample to the eluent in exactly equal amounts. However, it is to be expected that addition of these compounds to the eluent, in order to create stable column conditions, will be adequate if the resulting concentration differences between sample and eluent are of the same order of magnitude as the concentrations of the trace compounds to be quantified. If one is just interested in evaluating concentration differences between two samples, e.g., between the inlet and outlet of a chemical process, DCC can be applied simply by adding the modifier to both samples in the same quantity, which is easily done by weighing, and then using one of the samples as eluent.

In order to investigate the viability and applicability of this differential cross-correlation technique, a theoretical and practical study was made of the signal-to-noise ratio and separation behaviour of correlograms resulting from high-performance liquid chromatographic (LC) separations for samples and eluents of different concentrations.

THEORY

The theoretical background of CC has been described in several papers [5, 9, 12]. The basic equations are summarized below. Symbols are defined in Table 1.

A chromatogram h_k, where k is (discrete) time, can be considered as the impulse response of the chromatographic system to an impulse input, i.e., the injection of sample. If instead of a single injection, multiple injections are made according to an input function x_k, where x_k is 0 (eluent) or 1 (sample), then the output at the column outlet is

$$y_k = \sum_{l=0}^{M-1} h_l \, x_{k-l} \tag{1}$$

Obviously y_k, the sum of shifted chromatograms, cannot be interpreted like a normal chromatogram (Fig. 1). If the input function is a PRBS (pseudo-random binary sequence) with levels 0 and 1, then it can be shown that the cross-correlation function of the functions y and x is

$$R_{xy}(n) = [(M + 1)/4M] \left(\sum_{l=0}^{M-1} h_l + h_n \right) \tag{2}$$

where M is the total number of injections of sample or eluent during the chromatogram.

TABLE 1

List of symbols and definitions

Symbol	Definition
k	Discrete time (in time units)
l	Relative discrete time (in time units)
M	Total number of injections
x_k	Injection function (0 or 1; eluent or sample, respectively)
x'_k	Injection function distorted by noise
y_k	Detector output
y'_k	Detector output, if x'_k is applied at the inlet instead of x_k
$R_{xx}(n)$	Autocorrelation function $R_{xx}(n) \equiv (1/M) \sum_{k=0}^{M-1} x_k x_{k-n}$
$R_{xy}(n)$	Cross-correlation function $R_{xy}(n) \equiv (1/M) \sum_{k=0}^{M-1} x_k y_{k-n}$
$R'_{xy}(n)$	Cross-correlation function obtained if x'_k is applied at the inlet
h_l	Chromatogram (impulse response)
h_l^s	Chromatogram contribution from the sample
h_l^e	Chromatogram contribution from the eluent
Δh_l	$h_l^s - h_l^e$
ϵ_k	Noise
σ_ϵ^2	Noise variance
σ_{cc}^2	Baseline variance in CC
σ_c^2	Baseline variance in conventional chromatography
$E[\ ]$	Expected value of the expression between the brackets
$R_{xx}(n)$	$[(M + 1)/4M]\ (1 + \delta_n)$, if x_k is a PRBS with levels 0 and 1. $\delta_n = 0$ if $n \neq 0$; $\delta_n = 1$ if $n = 0$
z	Disturbance

Equation 2 leads to

$$h_n = [4M/(M + 1)]\ R_{xy}(n) - \sum_{l=0}^{M-1} h_l \tag{3}$$

The second part of Eqn. 3 is independent of n, and can be considered as the baseline of the correlogram.

In DCC, the situation is slightly more complex than in CC because the ultimate correlogram is constituted from contributions of both sample and eluent. Here, h_l^s and h_l^e are defined as the response of the sample and of the eluent, respectively, and Δh_l as the differential chromatogram of sample and eluent. Because the input functions x_{k-l}^s and x_{k-l}^e of sample and eluent, respectively, are complementary (if no sample is injected, then eluent is injected and vice versa), the response at the detector can be written as

$$y_k = \sum_{l=0}^{M-1} [h_l^s x_{k-l} + h_l^e(1 - x_{k-l})] \tag{4}$$

whereafter the cross-correlation function $R_{xy}(n)$ is easily obtained:

$$R_{xy}(n) = [(M + 1)/4M] \left[\sum_{l=0}^{M-1} (h_l^s + h_l^e) + \Delta h_n \right] \tag{5}$$

The differential correlogram Δh_n is then

$$\Delta h_n = [4M/(M + 1)]\, R_{xy}(n) - \sum_{l=0}^{M-1} (h_l^s + h_l^e) \tag{6}$$

The second part is again independent of n and can be considered as the baseline of the differential correlogram.

Signal-to-noise ratio improvement by DCC

As mentioned before, several factors can influence the signal-to-noise ratio (S/N) in CC. Only the influence of detector noise and a corrupted input function are discussed here. The S/N improvement of CC has been discussed in several papers [5, 9, 13]. Only the result is given here:

$$\sigma_c^2/\sigma_{cc}^2 = (M + 1)/2 \tag{7}$$

This result is also applicable to DCC because changing the nature of sample or eluent does not affect the detector noise. The effect of distorted input signals on the S/N is more complicated, as follows from the description below. The cross-correlation function resulting from an undistorted input signal is

$$R_{xy}(n) = [(M + 1)/4M]\, (c + \Delta h_n) \tag{8}$$

where c represents the first part of Eqn. 5, which is independent of n.

If the input function is distorted according to

$$x_k' = x_k + z_k \tag{9}$$

then

$$y_k' = y_k + \sum_{l=0}^{M-1} \Delta h_l z_{k-l} \tag{10}$$

and

$$R_{xy}'(n) = R_{xy}(n) + \sum_{l=0}^{M-1} \Delta h_l R_{zx}(l-n) \tag{11}$$

Two different cases are distinguished here: (a) in which the disturbance z and the PRBS are not correlated; and (b) in which z and x are correlated.

Case (a): z and x are not correlated. If z and x are not correlated and z is white noise with variance σ_z^2, the variance of the baseline as a consequence of the distortion z is easily computed:

$$\sigma^2_{R'_{xy}(n)} \equiv E\,[R'_{xy}(n) - E(R'_{xy}(n)]^2$$

$$= \sum_{l=0}^{M-1} \sum_{j=0}^{M-1} \Delta h_l \Delta h_j E\,[R_{xz}(l-n)\,R_{xz}(j-n)]$$

$$= [(M+1)/2M]\;\sigma_z^2 \sum_{l=0}^{M-1} \Delta h_l^2 \tag{12}$$

In other words, the variance of the baseline noise resulting from stochastic ergodic input disturbances is independent of n, but appears proportional to the integrated squared chromatogram.

Case (b): z *and* x *are correlated.* It is assumed that distortion z of the input signal occurs only when it changes its value (switching from eluent to sample or vice versa) according to

$$z_{k-l} = -\epsilon\,(x_{x-l} - x_{x-l-1}) \tag{13}$$

where ϵ is a constant between 0 and 1 giving the magnitude of the deviation from ideal injection. For $\epsilon = 0$ no distortion is present, and for $\epsilon = 1$, corruption is complete. It is easily seen from Eqn. 13 that no distortion is assumed when successively two eluent (or sample) injections are made, as both values of the input function are then equal.
Cross-correlation of z and x yields

$$R_{xz}(l-n) = [(M+1)/4M]\;\epsilon\;[\delta\,(l+1-n) - \delta\,(l-n)] \tag{14}$$

and the distorted correlogram is

$$R'_{xy}(n) = [(M+1)/4M]\;[c + (1-\epsilon)\,\Delta h_n + \epsilon \Delta h_{n-1}] \tag{15}$$

In order to obtain the original correlogram from the distorted correlogram $R'_{xy}(n)$, it is necessary to transform the corrupted correlogram. The following terms are defined:

$$Q \equiv [(M+1)/4\,M]\;c, \quad t = \epsilon/(1-\epsilon) \text{ and } r = [(M+1)/4\,M)\,(1-\epsilon)$$

Transformation of Eqn. 15 according to

$$Z(n) = [R'_{xy}(n) - Q]/r \tag{16}$$

yields $\Delta h_n = Z(n) - t\Delta h_{n-1}$. From this result, the corrected chromatogram can be computed:

$$\Delta h_n = \sum_{k=0}^{M-1} \left\{ (-t)^k Z\,(n-k)/[1-(-t)^M] \right\} \tag{17}$$

Of course, the above calculation can be done only if the constant ϵ is known, which is usually not the case. Hence this constant has to be estimated from prior knowledge of the chromatogram. If part of the chromatogram is known (preferably the baseline near a peak), a good estimate of ϵ is obtained if the following condition is met:

$$[1-(-t)^M]\ [r\Delta h_j + Q/(1+t)] = \sum_{k=0}^{M-1} (-t)^k R'_{xy}(j-k) \qquad (18)$$

In other words, t (and hence r) are chosen such that the above equation is satisfied. From t, ϵ can be derived, and the transformation (Eqn. 16) can be made and the correlogram computed (Eqn. 17). If ϵ can be evaluated exactly, the imperfect injection profile does not contribute to the baseline noise.

Axial gradient in CC and conventional chromatography

As mentioned above, axial dispersion in CC is completely different from that in conventional chromatography. Use of CC implies that over the entire column, each component is present at all times in a varying concentration. This also implies that if there is mutual influence on the separation behaviour of the components, this influence and its consequences will be equally strong throughout the column, at all times, and will not decrease with increasing separation as in conventional chromatography. The exact consequences of non-linearity of the distribution isotherm on the ultimately observed "separation" properties of CC will be examined at a later date, but the concentration gradient as observed in CC is derived here because many transport phenomena are directly related to the concentration gradient.

As a measure of the gradient, the expression used is

$$(1/M) \sum_{k=0}^{M-1} \left[y_k (y_k - y_{k-1}) / \sum_{k=0}^{M-1} y_k \right]$$

where y_k is the detector output. This relatively complex measure is necessary in order to allow comparison of the variations in both CC and conventional chromatography. The measure weights the gradient: the higher the number of molecules that sense a certain gradient, the higher weight that gradient receives. For a single injection, the measure simply yields

$$(1/M) \sum_{k=0}^{M-1} \left[h_k (h_k - h_{k-1}) / \sum_{k=0}^{M-1} h_k \right]$$

and for CC,

$$(1/M) \sum_{k=0}^{M-1} \left[y_k (y_k - y_{k-1}) / \sum_{k=0}^{M-1} y_k \right]$$

$$= (1/2M) \sum_{k=0}^{M-1} \left[(h_k^2 - h_k h_{k-1}) / \sum_{k=0}^{M-1} h_k \right] \qquad (19)$$

Thus, in CC the mean weighted gradient is half that in conventional chromatography, which implies a lower sensitivity to non-linear effects.

The above chosen expression is a measure of the net mean gradient over the entire column. However, it should be noted that this net gradient is not an appropriate measure for the real local variation in the column because

gradients with opposite sign cancel each other. Therefore, the mean local variation itself should be a more suitable measure for investigating the effect of possible non-linearity in the column:

$$(1/M) \sum_{k=0}^{M-1} \left[y_k (y_k - y_{k-1})^2 / \sum_{k=0}^{M-1} y_k \right] \tag{20}$$

Simulation (Fig. 2) reveals the characteristics of both measures. In conventional chromatography, the weighted variation is significantly smaller than in CC. Possible consequences of non-linearity of the distribution isotherm are therefore conflicting: in CC the mean concentration gradient is lower, but the local concentration variation is larger, than in conventional chromatography.

Further theoretical evaluation of the complicated non-linear effects and their consequences on CC is not done in this study. A detailed study of the transport phenomena occurring in CC is necessary to establish how non-linear effects exactly influence the correlograms obtained ultimately in CC and DCC.

EXPERIMENTAL

In order to investigate the signal-to-noise ratio resulting from DCC, test samples of phenol were prepared and examined in a reversed-phase HPLC system. A special injection device designed for CC/HPLC [14] was used. The device consists of two thermostatted symmetrical cylindrical tubes, connected with the column by a T-piece with zero dead volume and a home-made correlator [15] capable of generating the appropriate injection pattern (PRBS) and of doing the data-acquisition and processing.

The equipment used included a Spectra-Physics (SP 740B) pump, a Hypersil SAS (Chrompak) column (4.6 mm i.d., 25 cm long) and a Perkin-Elmer LC-55 UV detector with a Princeton Applied Research model 113 instrument amplifier.

The operating conditions were as follows: detector wavelength, 254 nm; pressure drop, up to 95 bar; mobile-phase flow rate, 13 μl s^{-1}; thermostat, 26°C; chromatogram length, 1124.2 s; minimum injection length, 2.2 s; PRBS length, 511; number of sequences, 3; mobile phase, tetrahydrofuran/water (1:3 v/v); sample, 0.127—12.7 mg kg^{-1} phenol in mobile phase (see Table 2); and eluent, 0—10.9 mg kg^{-1} phenol in mobile phase (see Table 2).

In six of the eleven experiments, phenol was present only in the sample reservoir, whereas in five experiments different concentrations of phenol were also present in the eluent. The signal-to-noise ratio was evaluated as a function of the difference in phenol concentration between sample and eluent. Because these DCC experiments require relatively high volumes of sample and eluent (about 500 ml for each experiment), both sample and eluent were carefully prepared by adding a weighed amount of phenol to a weighed amount of mobile phase in order to avoid dilution errors.

TABLE 2

Concentrations of phenol in sample and eluent

Experiment	Phenol concentration[a] (μg kg^{-1})		
	Eluent	Sample	Difference
1	0	127 (1.3%)	127 (1.3%)
2	0	1270 (1.2%)	1270 (1.2%)
3	0	1270 (1.2%)	1270 (1.2%)
4	0	12 700 (1.1%)	12 700 (1.1%)
5	0	12 700 (1.1%)	12 700 (1.1%)
6	0	12 700 (1.1%)	12 700 (1.1%)
7	10 900 (±1.1%)	12 700 (1.1%)	1800 (170)
8	10 900 (±1.1%)	12 700 (1.1%)	1800 (170)
9	1090 (±1.2%)	1270 (1.2%)	180 (18)
10	1090 (±1.2%)	1270 (1.2%)	180 (18)
11	109 (±1.3%)	127 (1.3%)	18 (1.8)

[a]The numbers in parentheses represent the uncertainties of measurements.

RESULTS AND CONCLUSIONS

The results are shown in Fig. 3. The calibration curve obtained reflects the expected linear relation between the concentration differences and the resulting peak areas over about three concentration decades. This proves the practical suitability of DCC for determining concentration differences in samples of similar nature. The calibration curve calculated with the least-squares method adapted for the different baseline variances evaluated from the obtained correlograms (see Fig. 4) was $A = 3.11c - 74$. The correlation coefficient was 0.992.

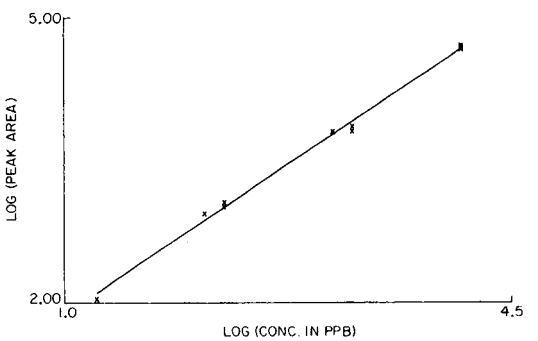

Fig. 3. Calibration plot for differential cross-correlation chromatography. Both axes are logarithmic. The x axis represents the concentration difference between sample and eluent in μg kg^{-1} (ppb) and the y axis the peak area in arbitrary units. The two measurements at 1.270 mg kg^{-1} coincide, and the three measurements at 12.700 mg kg^{-1} almost coincide.

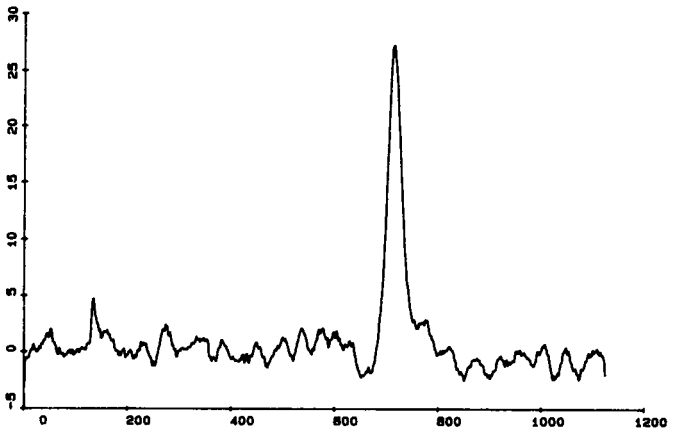

Fig. 4. Differential correlogram resulting from experiment 8. The sample contains 12.700 mg kg^{-1} phenol and the eluent 10.900 mg kg^{-1}.

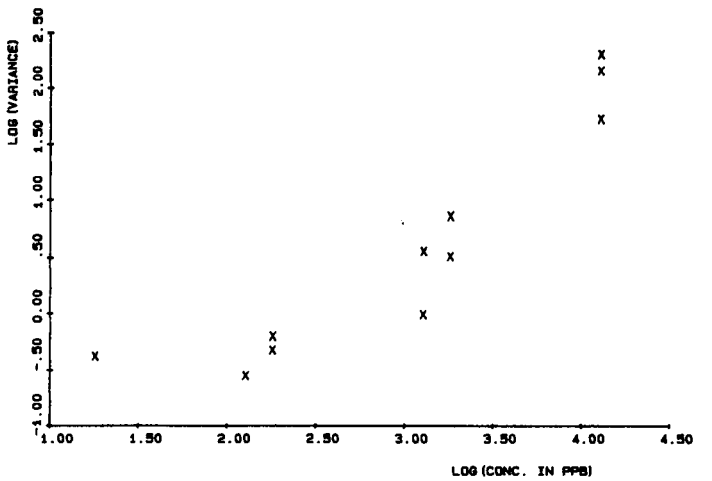

Fig. 5. Baseline variance in DCC as a function of the concentration difference between sample and eluent. Both axes are logarithmic.

The baseline variances calculated from the resulting correlograms are shown in Fig. 5. It is obvious that there is no clear linear relationship between these variances and the corresponding phenol concentrations. Such a relationship cannot be expected because the baseline variance results from four different noise sources: (a) detector noise which is (usually) independent of sample concentration; (b) random distortions of the injection pattern (PRBS), not correlated with the level of the injection pattern itself; (c) dis-

tortions of the injection pattern correlated with the level of the PRBS, caused by imperfect switching of sample and eluent; and (d) other contributions, e.g., unstable flow, changing column properties, fluctuations in the input concentrations at the inlet of the column, non-linearity of the distribution isotherm, and mutual influence of the compounds in sample and eluent. Contribution (b) to the baseline variance is proportional to the squared chromatogram. Distortions related to (c) have a deterministic effect on the correlogram (Eqn. 15), and are one of the causes of ghost peaks, as will be shown in a later paper. However, Fig. 5 clearly demonstrates that the correlation of the concentration differences between sample and eluent with the baseline variance is significant, as predicted in the theoretical section, which demonstrates the dominance of contribution (b) and possible other sources causing proportional noise. Non-linearities also contribute to the baseline noise, but do not seem to have a major influence on the correlograms obtained (at least in this case).

The main conclusion of this study should therefore be that CC shows the best performance if the concentration differences between sample and eluent are small, i.e., in trace analysis (if there is no main component other than that used as eluent), because CC easily suffers from proportional noise contributions. If the sample to be analyzed contains main components (sensed by the detector) in addition to the trace components of interest, it is recommended to use CC in the differential mode by adding these main components to the eluent in equal amounts. Although such an addition may not always be easy in practice, the resulting reduction of the signal-to-noise ratio, needed to quantify the trace components with sufficient accuracy, makes the effort involved worthwhile.

The DCC method also seems to be suitable if relative concentration changes between two sites, two points of time, inlet and outlet of some reactor etc. have to be determined. For such applications, it is not even necessary to add compounds to one of the two samples. The only requirement is to add the modifier in exactly the same amounts to both samples, one of which will be used as eluent. This can be done easily and accurately by using an analytical balance.

Applications of the differential mode of CC may be found in environmental analysis, where the problem of analyzing trace compounds in the presence of main compounds is ubiquitous. Also the monitoring of potential sources of pollution like the waste of a chemical plant in a river can be achieved by DCC by comparing samples taken before and behind the waste. Another property of DCC might lead to important applications in the analysis of samples with a complex matrix. In DCC, in contrast to conventional chromatography, the compounds in sample and eluent are not actually physically separated. At each position and at each moment in the column, all the compounds are present, albeit in different concentrations. This implies that all compounds remain in their matrix during the entire "separation" process. This property of DCC could be very useful for the analysis of pro-

teins or drugs in tissue fluids. Addition of the matrix to the eluent and use of the DCC method may then prevent the irreversible adsorption phenomena that frequently affect conventional separations. Further applications of DCC may be found in analyzing the influence of time on the degradation of complex mixtures, because the compounds not sensitive to time processes will not be visible in the differential correlogram obtained from two samples taken at different times. In such an application, all peaks (both positive and negative) in the differential correlogram reflect the influence of the time processes on the compounds concerned.

REFERENCES

1 K. Izawa, Ind. Chim. Belge, 32 (1967) 223.
2 H. C. Smit, Chromatographia, 3 (1970) 515.
3 R. Annino and L. E. Bullock, Proc. 9th Int. Symp. on Gas Chromatography, Montreux 1972, Applied Science, 1973, p. 171.
4 C. Largeau and F. Barras, Chromatographia, 12 (1973) 160.
5 M. Kaljurand and E. Kuellik, J. Chromatogr., 186 (1979) 145.
6 R. Annino and E. Grushka, J. Chromatogr. Sci., 14 (1976) 265.
7 J. B. Phillips and M. F. Burke, J. Chromatogr. Sci., 14 (1976) 495.
8 H. C. Smit, Tj. Th. Lub and W. J. Vloon, Anal. Chim. Acta, 122 (1980) 267.
9 T. T. Lub and H. C. Smit, Anal. Chim. Acta, 112 (1979) 341.
10 T. T. Lub, H. C. Smit and H. Poppe, J. Chromatogr., 149 (1978) 721.
11 R. Annino, M. Gonnord and G. Guiochon, Anal. Chem., 51 (1979) 379.
12 H. C. Smit, C. Mars and J. C. Kraak, Anal. Chim. Acta, 181 (1986) 37.
13 M. Koel, M. Kaljurand and E. Kuellik, eesti nsv teaduste akademia toimised 32 koide keemia 1983 nr. 2 (Academy of Sciences of the Estonian SSR).
14 J. M. Laeven, H. C. Smit and J. C. Kraak, Anal. Chim. Acta, 150 (1983) 253.
15 H. C. Smit, R. P. J. Duursma and H. Steigstra, Anal. Chim. Acta, 133 (1981) 283.

Analytica Chimica Acta, 194 (1987) 25—35
Elsevier Science Publishers B.V., Amsterdam — Printed in The Netherlands

IDENTIFICATION OF OIL SPILLS IN HARBOURS BY MEANS OF PATTERN RECOGNITION

M. M. A. RUYKEN and F. W. PIJPERS*

Institute for Theoretical Physics, Faculty of Science, University of Nijmegen, Toernooiveld, 6525 ED Nijmegen (The Netherlands)

(Received 1st September 1986)

SUMMARY

For environmental control purposes, floating oil spills in Europoort (Rotterdam) harbours must often be identified and their sources located. Pattern recognition, applied to gas chromatographic data for the spill and for various suspected sources such as oil from bunkers of passing ships and from harbour installations, can lead to definite conclusions, particularly after artificial weathering formulae have been used. The general approach for tackling these problems and the complicating factor of weathering of the oil spills is discussed.

The Europoort area, between Rotterdam and the North Sea, is highly industrialized. Apart from oil refineries, fertilizer plants and other manufacturing processes, sea and river traffic is heavy. In order to monitor and control the environmental effects of these activities, a governmental organization, the Dienst Centraal Milieubeheer Rijmond, DCMR (Central Environmental Control Agency) was founded. With an automatic network of air analyzers and a central laboratory, sources of air and water pollution, and noise, are monitored and the findings are reported to the provincial authorities (see, e.g. [1]).

The DCMR is occasionally confronted with floating oil spills in the Europoort area. The Rotterdam harbour police are instructed to sample such oil spills and take samples of oil bunkers of suspected ships or harbour installations. The DCMR laboratory produces gas chromatograms of the oil spill and of the suspected samples and compares them visually in order to find the organization or person responsible. This visual inspection has the important drawback that weathering of oil spill can make comparisons difficult.

Studies on weathering of oil have been reported [2, 3]. The most important alteration by weathering occurs during the first few days and is caused by selective evaporation of the lower alkanes up to octadecane [4]. Dissolution of aromatic hydrocarbons in water also occurs [5]. These processes are active during the first four days of an oil spill and depend on water and air temperature, wind speed, sunshine and thickness of the oil layer [6]. After this period, oxidation becomes the most important weathering process [7]. The light oil fractions seem more susceptible to weathering than heavy ones.

0003-2670/87/$03.50

Biodegradation rates decrease in the order n-alkanes > iso- and cyclo-alkanes (naphthenes) > aromatic hydrocarbons. These processes are operative during several years [8]. In spite of weathering, sufficient information often remains available to identify the culprit oil source within a considerable group of suspected sources [9].

Laboratory experiments with artificial weathering of oil often succeed in reproducing natural weathering [9, 10] as far as results from infrared spectroscopy (i.r.) and gas-chromatography (g.c.) are concerned. The applicability of these and other analytical procedures for the identification of oil fractions has been discussed by Bentz [7, 11]. Comparison of various chromatograms of oil fractions has been described [12]. Clark and Jurs [13] demonstrated how artificially-weathered oil samples can be compared by means of a Bayesian statistical method.

In this paper, it is shown that pattern recognition methods, applied to gas chromatograms of "fresh" oils and weathered oil spills, can serve to find the culprit source of oil spills more reliably than visual inspection can.

PREPROCESSING OF GAS CHROMATOGRAMS

The general appearance of gas chromatograms of oil fractions obviously depends on the detector and column used. Changing the immobile phase and/or replacing a packed column by a capillary one with a higher number of theoretical plates, or changing the recording speed or temperature program during elution will result in chromatograms with quite different appearances. Visual interpretation cannot cope easily with all the possible variations.

Apart from these factors, weathering causes changes in the appearance of chromatograms that may not be recognized visually. Figure 1 shows a representative chromatogram of an oil fraction; the sharp peaks result from

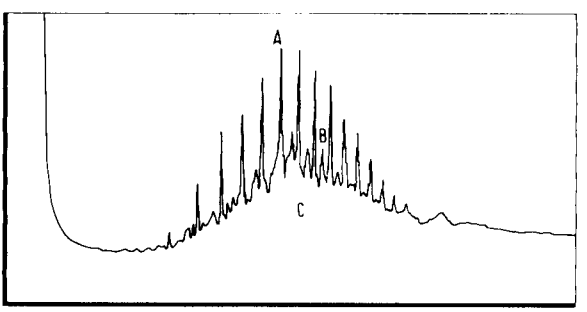

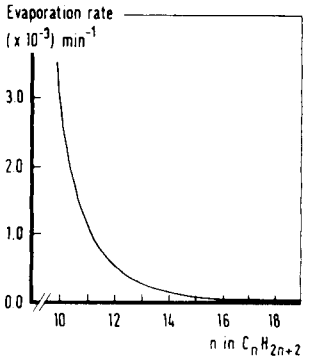

Fig. 1. Schematic representation of a chromatogram of an oil fraction: (A) n-alkanes; (B) iso-alkanes; (C) naphthenes and aromatic compounds.

Fig. 2. An empirical relationship between molecular weight (n in C_nH_{2n+2}) and evaporation rate for n-alkanes. Evaporation rate is given as percent/minute.

n-alkanes, while the small peaks and the elevated baseline result from iso-alkanes, aromatics and naphthenes. Such a chromatogram can be represented by a set of peak heights pertaining to the ensemble of n-alkanes, or by the individual integrations of these peaks. The shape of the elevated baseline or background signal can also be accounted for. A more abstract presentation can be produced from data on range, C-average, spread and highest n-alkane content; and if the background signal can be described by means of a Gaussian distribution function, skewness, kurtosis and higher moments of this distribution can be used. Before these data are extracted from the chromatograms, variations in amplification of the recorder and detector during the recording must be taken into account. Thus a normalization procedure is required to cope with variations of the sample size [10, 14, 15]. A generally accepted procedure is normalization of the sum of all peak heights of the n-alkanes encountered in the sample to 100%. Thereafter each peak is represented by a fraction of this normalized set.

Sometimes, an additional transformation on peak heights X is applied, viz., $X_i' = \ln (X_i + 1)$. This transformation aims to render insignificant any small differences between two small peaks where the measured peak heights are inaccurate; the differences between large peaks are virtually unaffected by this transformation.

Weathering of oil samples by selective evaporation of hydrocarbons of low molecular weight

Regnier and Scott [4] showed that, during weathering, hydrocarbons with low molecular weights evaporate more rapidly from an oil sample than hydrocarbons with high molecular weights. Comparisons between the original oil sample and the weathered one are thus hampered by changes in the chromatogram at the light end [16—18]. Neglect of the low-molecular-weight fractions in the comparison leads to a better correlation which, however, becomes less selective. Especially with light oils such as kerosenes, neglect of the light fractions tend to make conclusions ambiguous. A better approach would be to correct the light fractions in a manner that takes care of the differences in molecular weight and thus of the evaporation rates among the various fractions [4].

Figure 2 shows an empirical relationship between molecular weight and evaporation rate for n-alkanes. This curve can be described by the equation

$$F(n) = 64.1 \exp(-0.52n) - 0.154 \quad (n = 8, 9 \ldots 24) \qquad (1)$$

where n represents the number of carbon atoms per molecule. This equation can be used to correct data for an unweathered sample to obtain data for a weathered one from

$$P'(n) = P(n)\,[1 - k\,F(n)] \qquad (2)$$

where k is an integer $\geqslant 1$ which is found empirically by comparing an original sample with a weathered one. For each suspected original sample, com-

parison with the weathered sample is made and the one with the highest correlation is chosen.

PATTERN RECOGNITION TECHNIQUES

In order to distinguish between items such as mineral oil fractions that are characterized by many parameters, pattern recognition can be applied. In this technique, each item is represented by a collection of parameters, grouped as elements of a vector. This vector defines a point in a multidimensional vector space with as many dimensions as there are elements of the vector. Each item (pattern) is represented by one point in the vector space. The relative positions in the collection of patterns are studied.

For the description of oil samples, each sample is represented by a vector in which the vector elements comprise the n-alkane concentrations and proper measures to represent the background (e.g., a "mean" value, skewness, kurtosis and standard deviation). These vector elements (features) span the vector space. In order to construct a multidimensional space with equivalent axes in each direction, each axis is usually scaled by the same procedure. For example, in autoscaling the centre of the axis is placed at the mean value of the parameters ($\bar{x}$) that are plotted along the axis, and the standard deviation (s_x) is taken as the unit of length along the axis. This type of scaling makes all parameters equally important:

$$x' = (x - \bar{x})/s_x \tag{3}$$

In order to describe the location of the patterns in a multidimensional space, some information has to be sacrificed. In pattern recognition techniques, one chooses the inter-pattern distances to be kept unchanged whereas the mutual orientations of the patterns in space are neglected. Construction of the inter-pattern distance matrix is generally based on Euclidean distances, but other distance measures may also be used. With Euclidean distances, $D_{i,j}$, for n dimensions:

$$D_{i,j} = [\sum_{k=1}^{n} (x_{i,k} - x_{j,k})^2]^{0.5} \tag{4}$$

Visual representation of the distance matrix is provided by a hierarchical clustering procedure, where vicinal patterns are represented by a similarity number near unity, and patterns that are far apart have a similarity of about zero:

$$S_{i,j} = 1 - D_{i,j}/D_{\max} \tag{5}$$

Here, $S_{i,j}$ represents the similarity between i and j, $D_{i,j}$ their distance and $D_{\max}$ the maximal element in the distance matrix. The results of similarity calculations can be represented as in Fig. 3, where the ordinate lists the collection of all patterns investigated and the abscissa the similarity ($1 \rightarrow 0$). Vertical bars connect patterns and groups with high similarities.

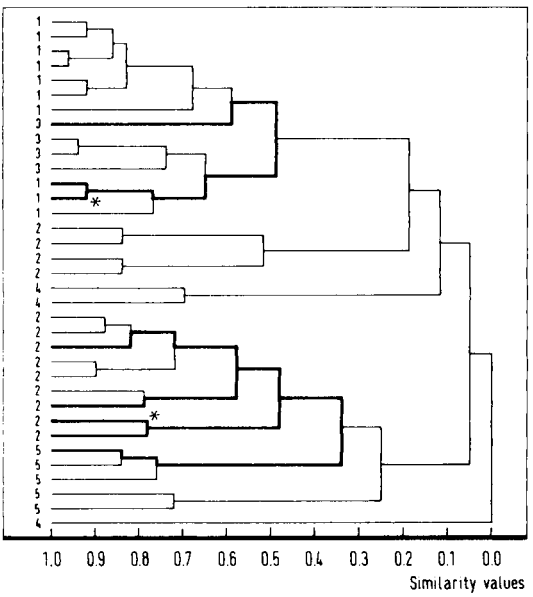

Fig. 3. Hierarchical clustering of oil samples according to their similarity. Two cases of identification of oil spills are asterisked.

The comparison between two oil samples becomes less complicated if the dimensionality of their representation can be reduced. The possibility of reducing dimensionality is seen from the inter-feature correlation matrix. When two features are highly correlated, one of them can be neglected without significant loss of information and thus dimensionality is reduced. Another way of reducing dimensionality is offered by construction of linear feature combinations as in the Karhuhnen-Loève procedure. Here the eigenvalue of the combination represents a portion of the variance as found in the variance/covariance matrix of all features. Grouping all eigenvectors in descending magnitude of the eigenvalues offers the possibility of describing the entire pattern space with two or three eigenvectors only, without appreciable loss of information.

RESULTS AND DISCUSSION

Table 1 shows an example based on the peak heights of 17 n-alkanes in the chromatograms of 35 oil samples. It can be seen that the first three eigenvectors of the 17-dimensional space account for about 69% of the total variance. This enables a projection of the patterns in this space on a plane spanned by, e.g., the first two eigenvectors that shows over 50% of the available information. The same procedure applied on the logarithmic peak heights (Table 1) provides more information (about 63% for the first two eigenvectors).

Figure 4 shows the projection of the 35 oil samples in the 17-dimensional

TABLE 1

Karhuhnen-Loève transformation, based on gas chromatograms, using normalized peak heights (x) of n-alkanes and logarithmic peak heights (ln (x + 1))

Feature (n-alkane)	Normalized peak heights[a]			Logarithmic peak heights[b]	
	Eigenvectors (squares of coefficients)			Eigenvectors (squares of coefficients)	
	First	Second	Third	First	Second
C-8	0.02	0.09	0.01	0.03	0.06
C-9	0.05	0.04	0.01	0.03	0.05
C-10	0.07	0.13	0.00	0.06	0.01
C-11	0.11	0.01	0.05	0.06	0.12
C-12	0.06	0.10	0.06	0.01	0.26
C-13	0.00	0.15	0.05	0.01	0.16
C-14	0.00	0.22	0.00	0.02	0.16
C-15	0.02	0.19	0.02	0.04	0.08
C-16	0.09	0.00	0.02	0.08	0.01
C-17	0.07	0.01	0.11	0.10	0.00
C-18	0.07	0.01	0.14	0.08	0.03
C-19	0.04	0.02	0.01	0.09	0.01
C-20	0.06	0.01	0.12	0.07	0.01
C-21	0.10	0.00	0.12	0.08	0.01
C-22	0.09	0.01	0.12	0.09	0.01
C-23	0.08	0.01	0.12	0.07	0.00
C-24	0.07	0.00	0.04	0.08	0.02
	1.00	1.00	1.00	1.00	1.00

[a]Eigenvalues (i.e., information) 35.3% + 19.1% + 14.5% = 68.9%. [b]Eigenvalue (i.e., information) 43.6% + 19.9% = 63.5%.

pattern space on the plane spanned by eigenvector 1 (x-axis) and 3 (y-axis) (see Table 1). It can be seen that various categories of oils encountered in the DCMR data set form clusters, as is denoted by different numbers. Based on these clusters and knowledge on the source of the samples, five oil categories can be distinguished. These categories are listed in Table 2, together with the ranges of n-alkanes in their chromatograms. The classification into five different categories offers a possibility for initial selection of one category to which a culprit sample might belong. The inter-category correlation matrix in Table 3 shows that the correlation within each category is generally higher than that between two categories: the diagonal elements are higher than the non-diagonal ones. This means that the choice of categories makes sense, although exceptions can occur in categories 1 and 2 when the distinction between heavy and light gas oils is based on n-alkanes in the range C-20–C-24. The "no name" oil of category 3 could be a heavy gas oil because of a correlation coefficient of 0.43 with category 1. The heavy fuel category is internally less homogeneous than the other categories. This follows not only from the value of the fourth diagonal element (0.39), which is relatively low, but also from the spread of its cluster in Fig. 4.

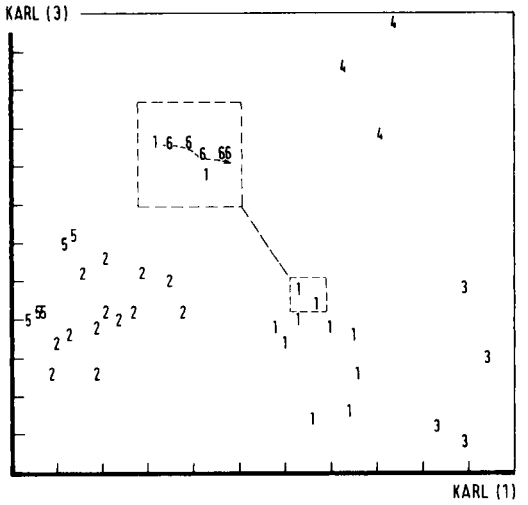

Fig. 4. Projection of the multidimensional pattern space of oil fractions on a plane spanned by the first (x-axis) and the third (y-axis) eigenvector. The eigenvectors are obtained from the variance/covariance matrix of all features by means of a Karhuhnen-Loève transformation. Numbers denote the oil fractions in Table 2. Insets represent the weathering process (see text).

TABLE 2

Oil categories encountered in the DCMR data set

Category	Name	n-Alkanes in chromatogram
1	Heavy gas oil	C-8—C-24
2	Light gas oil	C-8—C-20
3	"No name" oil	C-9—C-24
4	Heavy fuel	C-13—C-18
5	Kerosenes	C-8—C-13

TABLE 3

Inter-category correlation matrix based on gas chromatograms from 35 oil samples (Standard deviations are given in parentheses)

Category number	1	2	3	4	5
1	0.72(0.2)	0.47(0.2)	0.43(0.2)	0.23(0.2)	−0.06(0.3)
2	—	0.66(0.2)	−0.06(0.2)	−0.14(0.2)	0.27(0.3)
3	—	—	0.71(0.1)	0.38(0.2)	−0.31(0.2)
4	—	—	—	0.39(0.4)	−0.25(0.1)
5	—	—	—	—	0.57(0.3)

In seeking the answer to a problem of identification, the suspected oil sample and the sample taken from the spill location are positioned in the pattern space spanned by all relevant measured concentrations after correction for weathering. The oil spill is then attributed to the source that provided the sample nearest in composition to the spill. Figure 4 indicates the result of the correcting procedure for weathering according to Eqn. 2. In the central inset, point 1 at the left-hand side represents the composition of the culprit sample as it was taken from the oil bunker; point 1 at the right-hand side represents the weathered oil sample collected in the harbour. Points 6 represent the patterns artificially weathered according to Eqn. 2 with an increasing value of k. This demonstrates that the original sample shifts towards the oil spill, i.e., there is a decreasing distance in the multidimensional space and greater similarity.

Results after correction for evaporation

The procedure suggested was applied to a collection of 35 oil samples, analyzed by the DCMR laboratory. The culprit samples that caused the oil spills were known. In a first example, a comparison was requested between a weathered light gas-oil spill and a group of three gas oils among which the suspected sample was expected. For a start, the difference between two samples a and b was calculated from the sum of the quadratic logarithms of the peak heights i:

$$\mathrm{QSLR}(a, b) = \sum_{i=1}^{n} \Delta F^2 (a, b, i) \tag{6}$$

with

$$\Delta F(a, b, i) = \log P_{i,a}/P_{i,b} - (1/n) \sum_{i=1}^{n} (\log P_{i,a}/P_{i,b}) \tag{7}$$

where n represents the number of peak heights in the sample. This procedure was repeated for spill sample a and for all suspected samples b. Thereafter, the suspected samples were mathematically weathered with Eqn. 1 in an iterative fashion according to Eqn. 2. The value of k was adapted in integer steps from 1 up until the best possible match, i.e., the lowest QSLR(a, b), was obtained. The results of this procedure are listed in Table 4, together with the Euclidean distances between the spill and the suspected samples in the 17-dimensional pattern space. It can be seen in each case that sample 1, even without artificial weathering, shows the highest similarity with the spill. The distance between each two samples in the feature space can be diminished considerably by weathering although some of the other samples too become more like the spill on weathering, at least according to their QSLR values. In the pattern space, no increase in similarity was achieved by weathering the "innocent" samples 2 and 3 (or 4) in each case.

Figure 5 shows the effect of the weathering on the log-ratio calculations

TABLE 4

Euclidean distances between oil spills and suspected samples and QSLR values, without and with a correction for weathering[a]

Suspected samples	Before weathering		After weathering correction	
	Euclidean distance to spill sample	QSLR	Euclidean distance (k)	QSLR (k)
Case 1: a light gas-oil spill				
A-1 (*)	11.27	0.316	7.99(25)	0.197(7)
A-2	14.07	12.9	X	12.5(10)
A-3	15.71	12.8	X	12.8(6)
Case 2: a heavy gas-oil spill				
B-1 (*)	7.26	0.192	2.95(28)	0.048(8)
B-2	9.22	4.956	X	2.315(12)
B-3	9.22	0.769	X	0.716(6)
Case 3: a light gas-oil spill				
C-1 (*)	7.72	0.724	4.48(41)	0.53(8)
C-2	14.22	8.323	X	X
C-3	15.74	12.85	11.68(45)	X
C-4	22.95	14.32	X	X
Case 4: a heavy gas-oil spill				
D-1 (*)	10.6	1.18	4.83(29)	0.49(11)
D-2	4.6	3.65	X	1.54(11)
D-3	7.1	0.55	X	X

[a]Culprits are asterisked. X indicates that no improvement was possible with weathering corrections. The k values found for the best match obtained according to Eqn. 2 are given in parentheses.

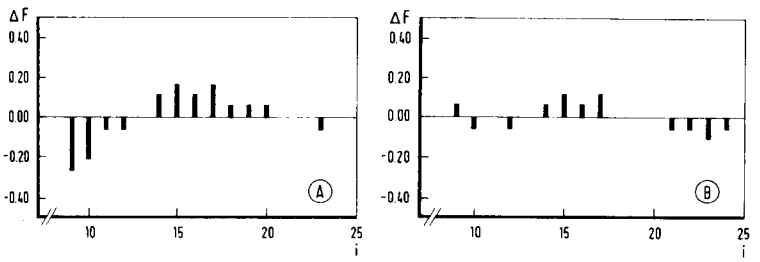

Fig. 5. The effect of the weathering procedure on the log-ratio calculation on a chromatogram: (A) before correction for evaporation; (B) after correction for evaporation by Eqn. 7.

on the chromatograms. The weathering results in a decrease of the log-ratio values for most of the n-alkane signals. Case 3 (Table 4) shows that sometimes the match between the spill and other samples may improve after a weathering correction, but only the real culprit shows a specific high match. Case 4 in this table shows an oil spill that was badly weathered. The match

TABLE 5

Contribution of iso-alkanes in the unresolved background of the chromatogram to the identification. Sample 2257-3 is correlated with the other samples listed

Sample	Correlation	
	Without iso-alkanes	With iso-alkanes
2257-1	0.89[a]	0.89[a]
2287-2	0.76	0.47
2287-1	0.73	0.48
2039-0	0.67	0.61
2263-1	0.66	0.58

[a]Culprit.

with the fresh sample of the culprit and of other samples is not high and sample D-2, which was not the culprit, shows the smallest distance towards the spill sample. However, on weathering, the culprit was found because of the considerable decreases in the Euclidean distance and in the QSLR value.

In these examples, identification was based only on the concentrations of n-alkanes in the sample. Table 5 indicates how the unresolved background of the gas chromatograms, which comes from iso-alkanes and other constituents, may help in the identification process. A set of 17 new features was created by adding the unresolved background under each n-alkane to the old features. Normalization was done in the same way as described above. When the information contained in the background was taken into account, the selectivity of the identification was enhanced considerably, because of the decreased correlation number of the non-culprit samples.

Conclusions

The identification procedure for oil spills as described was based on 35 oil samples only. In order to enhance the reliability of this method, the data set should be increased considerably. Recording of gas chromatograms with capillary columns provides more reliable identification of small iso-alkane and naphthene signals that would improve the selectivity of the identification. Extension of the procedure with measurement of i.r. absorption spectra would also improve selectivity without requiring a mathematical selection procedure different from the one described here.

Identification based on Euclidean distances in the pattern space independently from that based on QSLR values offers the advantage that when the two methods lead to conflicting results, the unreliability of the identification is obvious. Mathematical correction of oil samples for weathering, based on selective evaporation of the light-end fractions of the sample seems a powerful means of improving identification. Possible further improvement for the description of weathering must be based on better experimental evidence.

The authors thank Mr. Den Hartigh and Mr. Van Haagen of DCMR for providing the gas-chromatographic data and Prof. B. R. Kowalski for making the ARTHUR program available.

REFERENCES

1 F. W. Pijpers, in Joseph J. Breen and Philip E. Robinson (Eds.), A.C.S. symposium series, Vol. 292, Washington, 1985, p. 93.
2 P. J. Whittle and M. W. Horne, J. Inst. Eng. Sci., 34 (1980) 50.
3 J. S. Mattson, C. S. Mattson, M. J. Spencer and S. A. Starks, Anal. Chem., 49 (1977) 297.
4 Z. R. Regnier and B. F. Scott, Environ. Sci. Technol., 9 (1975) 469.
5 J. F. Zajc, B. Supplisson and B. Volesky, Environ. Sci. Technol., 8 (1974) 665.
6 W. C. Yang and H. Wang, Water Res., 11 (1977) 879.
7 A. P. Bentz, Anal. Chem., 48 (1976) 454A.
8 M. Blumer and J. Sass, Science, 176 (1972) 1120.
9 C. W. Brown and P. F. Lynch, Anal. Chem., 48 (1976) 191.
10 M. Ahmadjian, C. D. Baer, P. F. Lynch and C. W. Brown, Environ. Sci. Technol., 10 (1976) 777.
11 A. P. Bentz, Anal. Chem., 50 (1978) 655A.
12 D. V. Rasmussen, Anal. Chem., 48 (1976) 1562.
13 H. A. Clark and P. C. Jurs, Anal. Chem., 51 (1979) 616.
14 G. A. Flanigan, Proceedings of Workshop on Pattern Recognition Applied to Oil Identification, Coronado, CA, Nov. 1976, IEEE, 1977.
15 P. F. Lynch and C. W. Brown, Environ. Sci. Technol., 7 (1973) 1123.
16 O. C. Zafiriou, Anal. Chem., 45 (1973) 952.
17 E. R. Adlard, L. F. Creaser and P. H. D. Matthews, Anal. Chem., 44 (1972) 64.
18 M. E. Garza Jr. and J. Muth, Environ. Sci. Technol., 8 (1974) 249.

Analytica Chimica Acta, 194 (1987) 37—48
Elsevier Science Publishers B.V., Amsterdam — Printed in The Netherlands

REGISTRY AND SEARCH OF CHEMICAL COMPOUNDS ON GRAPHICS DISPLAY

SOHSUKE HANAI* and MASAMI MIYAKAWA

Ashigara Research Laboratories, Fuji Photo Film Co., Ltd., Minamiashigara, Kanagawa (Japan)

(Received 15th August 1986)

SUMMARY

The registry and substructure search component of in-house system SPHINCS (Structure/Property Handling Information Network for Chemical Substances) has been developed. For registry, a chemical structure is constructed on a graphics display by use of templates (e.g., 6N for pyridine, NH2 for amino group) and commands (e.g., BOND, EXCHANGE, DELETE). The generated connection table and atom coordinates are stored in a file. In a search, a query substructure is drawn on a graphics display. Special atom symbols (e.g., A for any atoms but hydrogen, HT for hetero atoms) can be used to represent the generic nature of a search. More than 1000 fragment codes (elements, rings, chains and augmented atoms), generated by computer analysis of connection tables, are used as primary search screens. An atom—bond—atom search program removes false drop structures. The structures retrieved are displayed in forms familiar to chemists with use of templates.

Chemistry deals with properties of substances and the atoms and molecules therein play important roles as basic elements in recognition, description, transfer and use of chemical information. Experimental or theoretical information about these basic elements, namely atoms or molecules, are of value for a long period. The situation is very different in other fields of science or technology, such as electronics or mechanical engineering, where the basic elements change rapidly; e.g., from vacuum tubes to transistors, to integrated circuits. To chemists, information described in Beilstein Handbooks several decades ago is still useful. Thus, storage and search systems for chemical information are necessary for chemists. With the advent of computer technology, especially in the fields of mass storage and international communication networks, the versatile substance search capabilities of such systems as CAS ONLINE [1], DARC [2] or CIS [3] are widely available. Published information on about seven million compounds in the CAS Registry can be searched and retrieved in a few minutes.

However, many companies have numerous confidential chemical compounds. Storage and search systems for these compounds are necessary for the effective use of in-house chemical information. Among the possibilities for producing such a system, use of a foreign private registry system (e.g., CAS [4]) must be regarded as impractical for various reasons. Another possibility

0003-2670/87/$03.50

would be to use one of the commercially available search software systems, like MACCS [5], DARC, SANSS, ORGANIC [6] or CROSSBOW [7]. But large chemical companies have many different kinds of functionally modified chemical compounds (e.g., co-polymers, surface-active compounds with repeating units, complex dye-forming branched molecules) and it is not easy to treat such a collection with generalized, commercially available structure-handling software. Moreover, the in-house system should have flexible functions to enable it to combine with property- or document-search systems or with programs for scientific calculations. In our particular case, the in-house document search system uses Kanji or Chinese characters, which are capabilities demanded by users in Japan today. Finally, the structure-handling system, which must be the core of the information system for a chemical company, must not be a black box in terms of effective use and future technical development. In order to satisfy these requirements, an in-house computer system for storage and search of chemical compounds has been developed. In this paper, the structure-handling component of SPHINCS (Structure/Property Handling Information Network for Chemical Substances) is described.

SYSTEM DESIGN

In the design of the structure-handling system, the following three goals were set: (1) registration or input of chemical structures can be handled by any clerical non-chemical staff; (2) structure search must be done comprehensively so that, in principle, any substructure which can be expressed in terms of chemical structure can be sought without noise; and (3) the retrieved structures must be displayed in two-dimensional forms which are familiar to chemists.

Several in-house structure search systems have been reported [8—10]. Starting from the fragmentation code systems in the 1960s, systems based on linear notation were widely utilized in the early 1970s. But now, with computer graphics technology and mass storage, it is possible to adopt the connection-table format for structure representations. By using connection tables, every detail of chemical structure information can be described, which is mandatory for flexible substructure search capabilities. Input of structural information by use of linear notation or nomenclature is not impossible, but giving correct notations or names for complex molecules requires much intellectual work and becomes very expensive.

The graphics display technique and connection-table format were selected. When a chemical structure is built up on a graphics display, chemical connectivity information and x and y coordinates for the two-dimensional structure drawing are completed. Atom codes, describing the specific characters of atoms in a molecule, are later added automatically and are utilized to make the substructure search more precise and effective.

Relations between the processes and information for substructure searching are shown in Fig. 1. Elements in bold-lined boxes are used in the SPHINCS

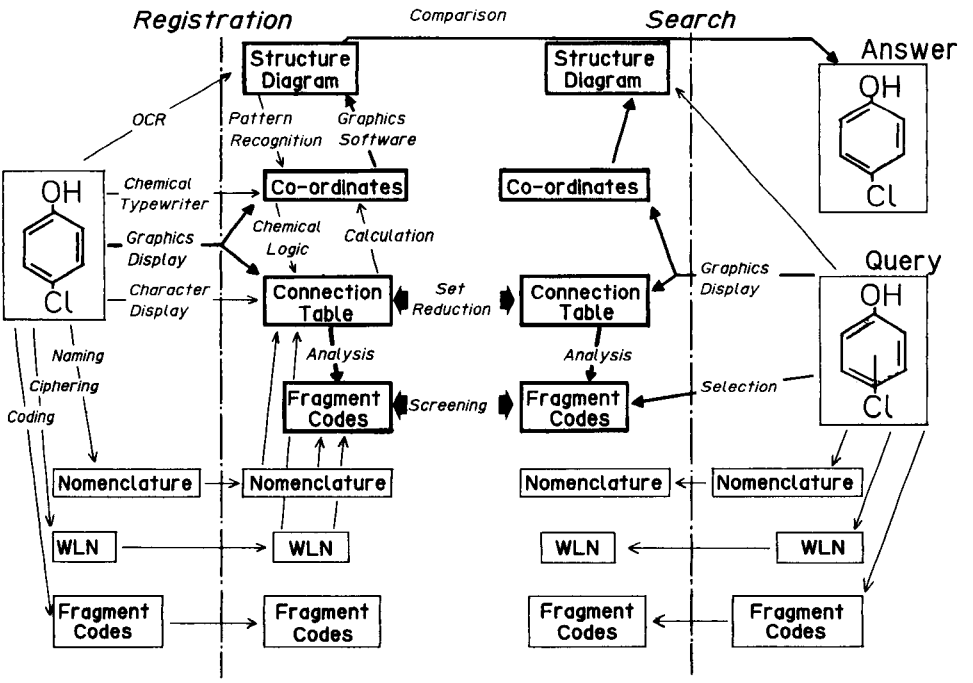

Fig. 1. Processes and information flow in substructure search. In SPHINCS, information flows along the bold lines.

system. Nomenclature, WLN or manually-coded fragment codes are not input into the system.

DETAILS OF SPHINCS

Registration.

Graphics display. Building blocks (fragments which comprise molecules) are called up on a graphics display and joined to make a full structure. The graphics display is divided into three areas (Fig. 2). Commands can be input in the C (Command) area, while building blocks are called onto the H (Hold) area and processed to make a larger structure in the W (Work) area. Directions for chemical bonds are normalized (Fig. 3), but any arbitrary direction can be specified with use of two points on the display.

Building blocks. More than 200 building blocks have been prepared (Fig. 4), and other elements can be added for use, if necessary. Each building block can be called up by use of chemically significant alphanumeric codes. Integer means an aromatic ring, e.g., 6 for benzene and 66 for naphthalene ring. An integer preceded by S (Saturation) indicates a saturated ring and alphabetic symbols describe atoms in a ring, e.g., S6N for piperidine. Functional groups are represented by alphabetic notations.

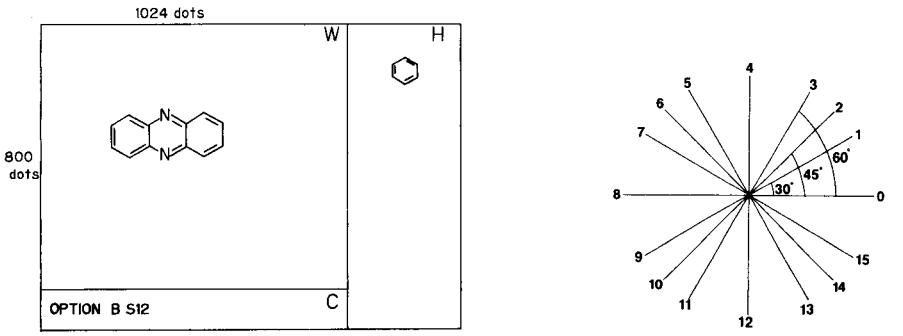

Fig. 2. Division of graphics display into three areas. C for commands, H for holding and W for working.

Fig. 3. Direction of bonds represented by numerical codes.

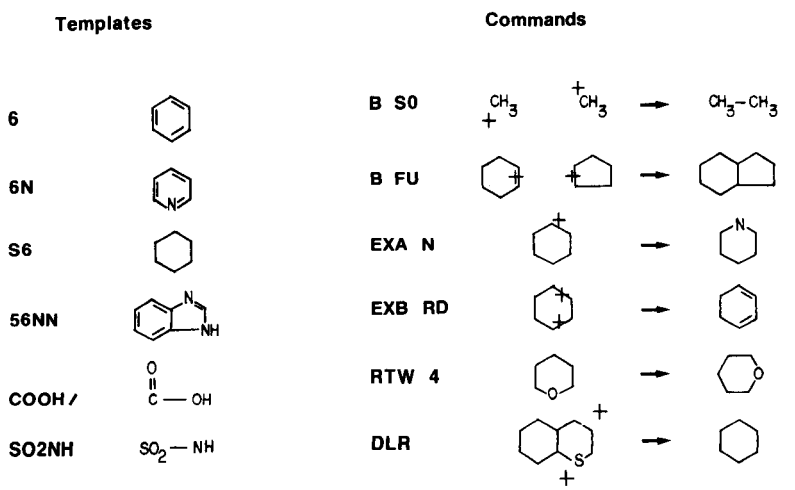

Fig. 4. Examples of building blocks and commands.

Commands. About 30 commands have been prepared (Fig. 4) to manipulate atoms and bonds to complete molecular structures, e.g., B for bonding, EXA for changing atoms and RTW for rotating a structure in the WORK area.

Examples. Figure 5 shows some examples of unit command operations. The atoms or bonds to be processed are indicated by use of the graphics hair cursor controlled with a joy-stick. The nearest elements are detected. The directions of bonds are indicated by use of 16 normalized numerical codes as described earlier. After the building is complete, every atom is checked for the standard valences of the element, and the calculated molecular formula is compared to the input formula. The discrepancies, if any, are indicated on the display so that any mistakes can be removed before input to the registry file.

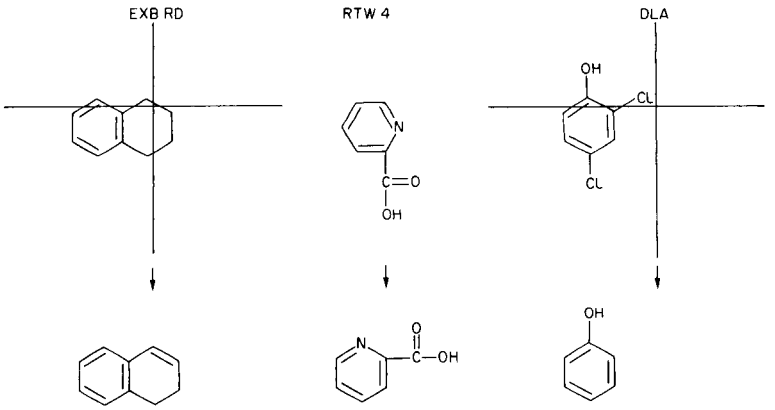

Fig. 5. Photocopies of examples for unit operations: EXB RD (EXchange Bond to Ring Double), DLA (Delete Atoms) and RTW 4 (RoTation in Working area for 90°).

Structure search

Substructure searching follows the usual two-step procedures (Fig. 6). Just after a molecule has been completed in the registration, the information of chemical connectivity in the connection table is analyzed by a program to generate detailed fragmentation codes, which are stored in the search files, as well as connection tables.

In a search, a query substructure, which is drawn on the graphics display by using the same procedures as in the registration, is analyzed to generate the above-mentioned fragmentation codes. Primary screening is done by comparing these fragmentation codes. The false drops, which cannot be eliminated with use of definite numbers of fragmentation codes, are excluded by use of a set-reduction algorithm. Application of Boolean AND, OR or NOT operations between the intermediate answer files narrows or broadens the search results to the desired extent.

SSSR (Smallest Set of Smallest Rings). The smallest set of smallest rings is detected to give the ring information as in the program by Schmidt and Fleischhauer [11]. Some improvements were introduced to the original program in order to handle the complex molecules often found in-house. Thus, the maximum connectivity of an atom is increased from 4 to 6; and in order to handle the mixtures or co-polymers, plural ring system units can be processed. Each isolated ring system gives the smallest set of smallest rings, respectively.

Fragmentation codes. After SSSR has been calculated, each ring system and the smallest rings are examined to give detailed ring information. Each smallest ring is labelled "isolated" or "imbedded". The latter means that the smallest ring is in a larger ring system, e.g., a benzene ring in a naphthalene system. Parts of a molecule other than ring systems are called "chain systems". Aliphatic skeletons, substituents on rings and links between the ring systems

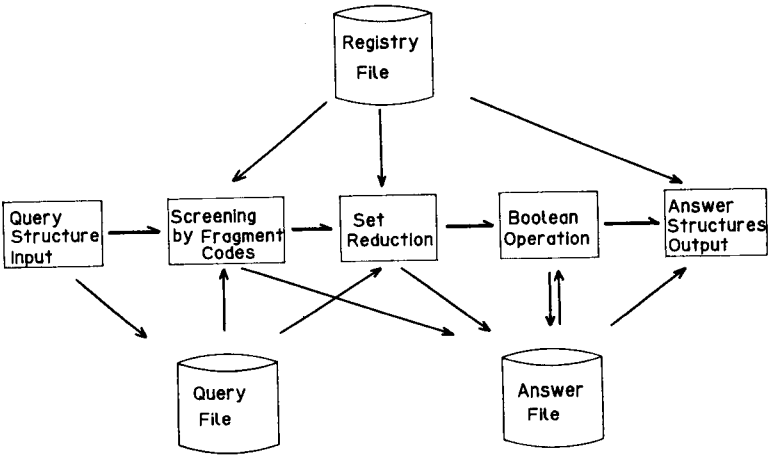

Fig. 6. Processes for substructure searching.

constitute the chain systems of a molecule. For each molecule, up to 30 ring systems, 30 smallest rings and 40 chain systems can be accommodated in the present version.

More than one thousand fragmentation codes are obtained through the computer analysis of the connectivity data. Some examples are as follows.

(1) Smallest rings: number of atoms in the ring, substituent patterns (*ortho*, *meta* or *para*) for 5- or 6-membered rings with the corresponding element pairs (e.g., *p*-(O, N)).

(2) Ring systems: number of atoms in the ring system, number of 5- or 6-membered rings in the ring system, number of aromatic bonds in the ring system.

(3) Chains: number of atoms in the chain, degree of branches in the chain, number of bonds (single, double or triple) in the chain.

(4) Common: number of elements, molecular weight, number of ring systems, rings and chains, isotopes, stereochemistry and charges.

(5) Augmented atoms: the detailed environmental information around every atom is examined; the connectivity (number of non-carbon atoms around the atom), charge and other information are given.

In primary screening, a comparison is made between the codes of a query structure and those of filed structures. Of all the codes generated for the query structure, several effective ones for rapid searching (i.e., those with the least frequencies in the registry file) are chosen.

Set reduction. Although the extensive primary screening is done by use of detailed fragmentation codes, the inevitable false drops remain as long as a fixed number of predefined codes is relied on. This noise can be eliminated by use of atom-by-atom analysis in the form of a set-reduction algorithm. The basic set-reduction algorithm of Sussenguth [12, 13] is used with some improvements for the description of each atom in the connection table by

use of the following atom codes: (1) stereochemistry (R, S, *cis*, *trans*, etc.); (2) chain or ring (if the atom is in a ring, then the number of atoms in the ring); (3) charge; (4) number of hydrogens attached to the atom; (5) mother and daughter relation for describing the generic nature of the molecule; (6) alkyl chain length; (7) isotopes; (8) ring system and ring (carbocyclic or heterocyclic, hetero atoms, saturated or unsaturated).

Boolean logic. Any concepts represented by chemical structures can be drawn on a graphics display and searched against the filed structures. The usual Boolean operations (AND, OR, NOT) can be used to reduce or extend the range of structure searching.

Devices for extensive and flexible substructure search

In order to endow the system with comprehensive search capabilities, the following devices are incorporated in addition to those described above.

Chemical hierarchy. Chemical elements have built-in hierarchy (Fig. 7). In a query structure, these special atoms can be used to represent some generic nature. The query structure in Fig. 8 searches all the compounds with any halogen (F, Cl, Br, I, At) substituted at the *para*-to-OH position on a benzene ring. These special atom representations are borrowed from CAS conventions [14].

Chemical bonds are likewise qualified by some chemical hierarchy, classified as follows: (1) multiplicity (single, double, triple); (2) environment (chain or ring, the latter classified as aromatic or aliphatic); (3) others: ionic, Markush, etc. The combination of these classes led to the adoption of the hierarchy for chemical bonds (Fig. 8).

SCR commands. In primary screening, by combining some of the >1000 fragmentation codes, the degree of membership in the set (e.g., in a chain, in a ring or in other circumstances) in which the substructure in question finds itself can be changed. Figure 9 indicates the performance of the SCR commands.

TSCR requires the exact match of every fragmentation code generated by analysis. With this command, the full structure search is conducted. SCR1

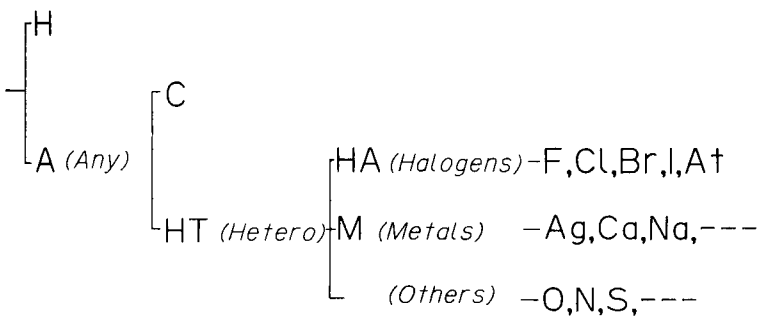

Fig. 7. Hierarchy of elements.

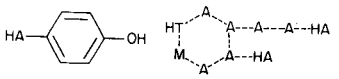

Fig. 8. Use of special atoms in query substructure representation.

		SCR Commands			
	Structures in File	TSCR	SCR1	SCR2	SCR4
A	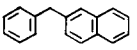	x	x	x	x
B	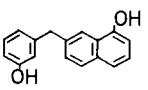	N	x	x	x
C	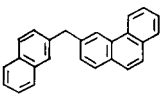	N	N	x	x
D	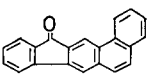	N	N	N	x

Query Structure

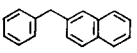

Fig. 9. SCR commands. X means matching; N means not matching.

differentiates between ring systems and chain systems. The codes for ring systems must exactly match. Thus, NH—CO—NH, with the SCR1 command retrieves every compound with a urea group in a chain (cf. SCR4). With SCR2, the ring systems of a query structure can be part of the larger ring systems. SCR 3 emphasizes aromaticity. Non-aromatic rings fused to any aromatic rings have the meaning of substituents on the ring. In the SCR4 command, only the topological connectivities between the atoms are compared. Chains or ring systems play no role in comparison. Thus, the urea group when sought under SCR4 command retrieves every compound with the urea moiety either in a chain or in a ring (Fig. 10).

Markush representation. Generic representation for query structures is useful for the efficient search for any compound class. SPHINCS has the following capabilities either for query structures or filed structures (Fig. 11): (1) position of substituents on a ring; (2) elements in a chain or in a ring; (3) links between rings; (4) substituents on a ring or a chain; (5) substituents on any part of the molecule.

The most frequent use of Markush representations for chemical structures is found in chemical patent specifications. The methods suggested here help in representation of patent claims to some extent, but as is often discussed [15], the claims in patents must be regarded as being expressed in natural

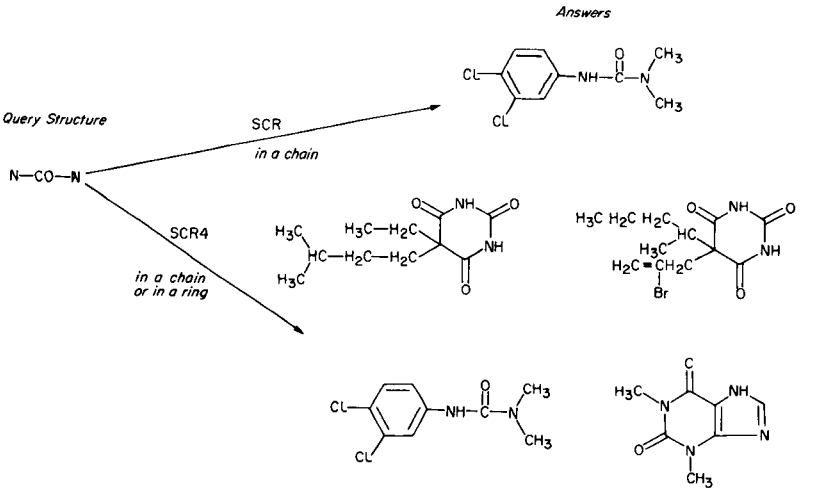

Fig. 10. Use of SCR and SCR4 commands.

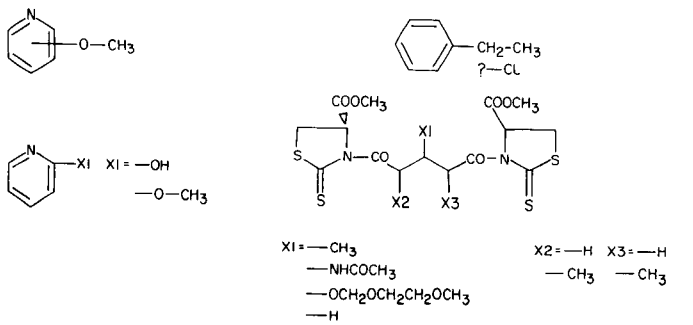

Fig. 11. Examples of generic representations in SPHINCS.

languages, so that the complete representations of chemical patent claims for comprehensive searches are far from being satisfactory.

Key commands. A general-purpose DBMS (ADABAS) is utilized for the primary screening. In addition to the computer-generated primary search fragmentation codes, specific codes for use with the KEY command can be selected manually. Indicating some key values searches the entire search file quickly (e.g., KEY LA/EQ/2 for two hetero atoms in a ring).

System installation

The SPHINCS system is implemented on the in-house mainframe computer (FACOM M-380S). Registration and searching can be conducted in the TSS mode on a graphics display (FACOM F9430) linked to the mainframe via an in-factory communication network (9600 bps line speed). The computer programs, as long as 60 000 lines including comments, are written mainly in

COBOL, with small portions coded in FORTRAN or assembly language. At the start of the system development, COBOL was the most favorable language in the general environment of program development because use of the mainframe computer and cooperation with the computer department were mandatory. Structure handling by computer consists mainly of processing characters or integers in tables. COBOL can be used for such applications and graphics subroutines, T-GSP (Fujitsu), are called from COBOL.

EXAMPLES

Figure 12 shows the flow of operations for building up a molecule with some repeating units. Figure 13 shows some examples of the flexible search capabilities of SPHINCS. The query structures on the left produce the answers on the right.

The searched and retrieved chemical structures are displayed on a graphics display in the following two modes: (a) one structure in one display frame; (b) four structures in one display frame.

Future developments

As was discussed above, a structure-handling information system is essential in a chemical industrial organization. Applications of computer technology in other fields of chemical structure information are being developed for future use. The following are of major concern.

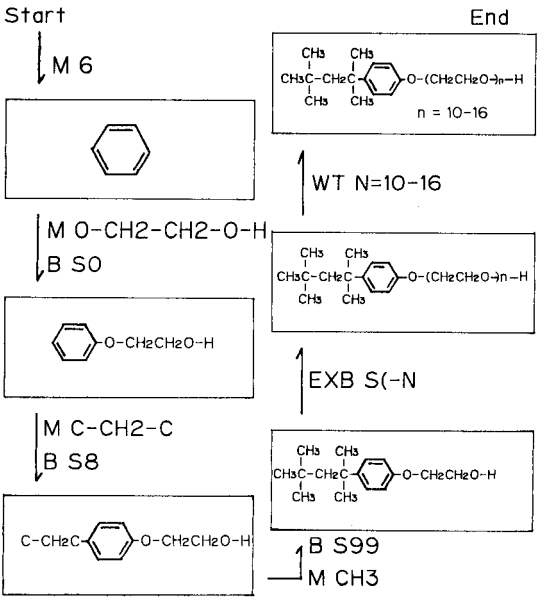

Fig. 12. An example of building a molecule with repeating units.

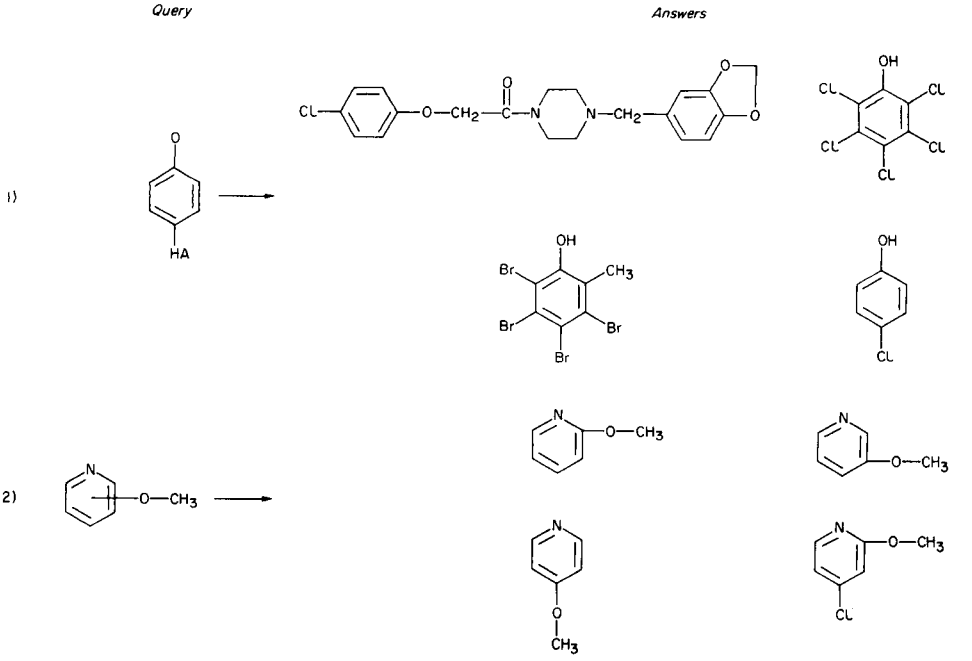

Fig. 13. Examples of substructure search: (1) any halogen attached to a benzene ring *para* to the oxygen atom; (2) methoxypyridines.

Links to other structure information processing are important. Calculations for molecular orbitals or molecular mechanics need initial three-dimensional coordinates. Input of two-dimensional coordinates by use of SPHINCS and conversion to coarse three-dimensional coordinates is easily used by chemists. The generation of structure descriptors for QSAR data analysis is vital; for multivariate data-analysis programs, substructural descriptors, generated automatically and extensively, are valuable [16]. The substructure search capabilities of SPHINCS can be applied. Combination with other substance-related search systems will be very useful. In-house information on substances can be combined through the structure-handling capabilities of SPHINCS. Handling of Chinese characters, or Kanji, and many kinds of numerical values describing chemical properties is important. The extensive and versatile structure-handling capabilities of the present system can also be applied to structure processing for the description, storage and search of chemical reactions, or for designing syntheses. Papers describing some of these applications will be reported in due course.

The authors express their thanks to Professor S. Sasaki of the Toyohashi University of Technology for helpful discussions and members of the computer department of this company for the development and installation of the system.

REFERENCES

1 R. E. Stobaugh, J. Chem. Inf. Comput. Sci., 25 (1985) 271; P. G. Dittmar, N. A. Farmer, W. Fisanick, R. C. Haines and J. Mockus, J. Chem. Inf. Comput. Sci., 23 (1983) 93.
2 R. Attias, J. Chem. Inf. Comput. Sci., 23 (1983) 102.
3 S. R. Heller, J. Chem. Inf. Comput. Sci., 25 (1985) 224; G. W. A. Milne and S. R. Heller, J. Chem. Inf. Comput. Sci., 20 (1980) 204.
4 R. Westland, in W. J. Howe, M. M. Milne and A. F. Pennell (Eds.), Retrieval of Medicinal Chemical Information. ACS Symposium Series, 84, 1978, p. 132.
5 W. T. Wipke, Proc. Soc. Polym. Sci. Jpn., (1983) 14.
6 M. Yoshida and Y. Mizobe, Proc. Soc. Polym. Sci. Jpn., (1983) 32.
7 D. R. Eakin and E. Hyde, in W. T. Wipke (Ed.), Computer Representation and Manipulation of Chemical Information, Wiley, New York, 1974, p. 1.
8 W. J. Howe and T. R. Hagadone, in Ref. 4, p. 107; J. Chem Inf. Comput. Sci., 22 (1982) 8, 182.
9 J. Kao, V. Day and L. Watt, J. Chem. Inf. Comput. Sci., 25 (1985) 129.
10 J. Kao, C. Eyermann, L. Watt, R. Maher and D. Leister, J. Chem. Inf. Comput. Sci., 25 (1985) 400.
11 B. Schmidt and J. Fleischhauer, J. Chem. Inf. Comput. Sci., 18 (1978) 204.
12 E. H. Sussenguth, J. Chem. Doc., 5 (1965) 36.
13 J. Figueras, J. Chem. Doc., 12 (1972) 237.
14 CAS ONLINE. The Registry File, Vol. II: Building Structures, Chemical Abstracts Service, April 1984, p. II-1-15.
15 M. F. Lynch, J. M. Barnard and S. M. Welford, J. Chem. Inf. Comput. Sci., 25 (1985) 264.
16 P. C. Jurs, T. R. Stouch, M. Czerwinski and J. N. Narvaez, J. Chem. Inf. Comput. Sci., 25 (1985) 296.

Analytica Chimica Acta, 194 (1987) 49—60
Elsevier Science Publishers B.V., Amsterdam — Printed in The Netherlands

A RANDOM-WALK SIMULATION OF FLOW-INJECTION SYSTEMS WITH MERGING ZONES

C. D. CROWE* and H. W. LEVIN[a]

Medical Products Department, E.I. du Pont de Nemours and Company, Inc., Wilmington, DE 19898 (U.S.A.)

D. BETTERIDGE and A. P. WADE[b]

Information Technology Research Unit, BP Research Centre, Chertsey Road, Sunbury-on-Thames, Middlesex, TW16 7LN (Great Britain)

(Received 25th February 1986)

SUMMARY

A flow-injection system with merging zones is simulated by using a random-walk stochastic (Markovian chain) model. Variables studied include reagent plug size and offset, reagent concentration and flow rate, injection delay time, reaction stoichiometry, rate constant, diffusion constants, viscosity, and temperature. The reaction of Ca(II) with *o*-cresolphthalein complexone was used to compare simulated and experimental results. In general, there was good agreement among computed and measured results.

The merging-zones flow-injection technique is a useful variant on the flow-injection approach to rapid semi-automated wet chemical quantitation [1—9]. In traditional flow-injection systems, a sample plug is injected into (or streamed together with) a continuous flow of reagent. In a merging-zones system (Fig. 1) plugs of sample and reagent are injected into separate streams. Reaction occurs when they meet at a tee-piece downstream. The merging zones method is advantageous in that smaller volumes of sample and/or reagent are consumed and complete mixing of these volumes can be rapidly achieved. In an investigation of the merging-zones technique, the analytical possibilities of offsetting the sample and reagent plugs were considered of interest. A reagent plug reaching the mixing point later than the sample plug would interact with in effect, a smaller sample size. In this way, the required reagent volume might be decreased further.

Betteridge et al. [10] developed a random-walk computer simulation to study the mixing processes at work in a simple flow-injection system. This model considers the sample as a discrete number of individual molecules. Each molecule is allowed to move under laminar flow for a discrete time

[a]Present address: Herman W. Levin Associates, 1919 Chestnut Street #2706, Philadelphia, PA 19103, U.S.A.
[b]Present address: The Chemistry Department, Michigan State University, E. Lansing, MI 48824, U.S.A.

0003-2670/87/$03.50

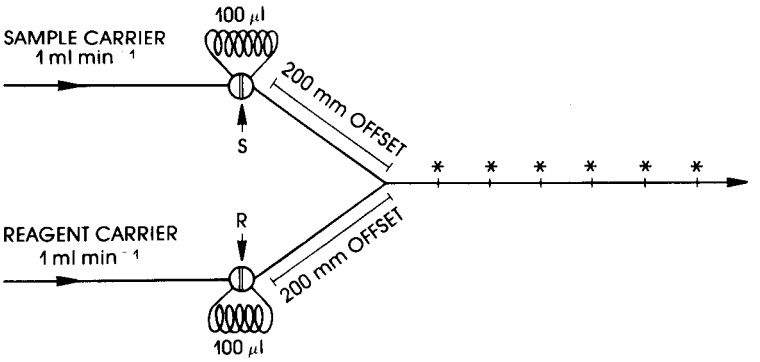

Fig. 1. Simulated flow-injection system with merging zones. Asterisks indicate detectors placed every 5 cm.

interval, and then takes a random step (cf. Brownian motion). The extent of reaction is then calculated. This process is repeated many times. In the work described here, their random-walk model [10] was modified to simulate an ideal merging-zones system. Further simulation studies are then reported which attempt to model an experimental system, namely the spectrophotometric quantitation of calcium with *o*-cresolphthalein complexone (CPC) [11—17]. This has led to an improved understanding of the effect that the basic parameters of a merging-zones apparatus have on the interacting processes of physical dispersion and chemical reaction.

EXPERIMENTAL

Instrumentation and reagents

The experimental apparatus consisted of a commercially available flow-injection analyzer (Tecator FIAstar), modified from a single- to a dual-injection valve, with an ultraviolet/visible spectrophotometer (Du Pont 837) as the detector. Glycine buffer (0.2 M, pH 9.7) was used as the reagent carrier, and water as the sample carrier stream. Sample (10^{-3} M calcium chloride) and reagent solutions (0.296, 0.148 and 0.076×10^{-3} M CPC) were prepared in both distilled water and glycine buffer.

Simulation studies of an ideal flow-injection system with merging zones

Typically, 1500 "molecules" of sample and reagent were simulated. Each molecule was represented by x,y (across tube) and z (axial, along tube) coordinates, and by its type (reagent, sample or product). The z-coordinate indicated the distance (in mm) of a molecule from the merging tee. The arms of the merging-zones system were denoted by negative z values and the merged stream by positive. Initial z values were calculated for each sample and reagent molecule so as to lie uniformly within the injection loops. The tubes were assumed to be of circular cross-section. Sample and reagent molecules were given randomly chosen x and y values constrained to lie within the boundaries of the tubes.

Sample and reagent plugs were "injected", (i.e., set in motion towards the tee-piece), whereupon the streams merged. After the tee-piece, the flow rate was the sum of those for the sample and reagent streams. The simulated tubes were divided into fixed-length segments. Each segment is divided into a number of concentric rings of equal volume ("reaction zones"). Under laminar flow conditions, all molecules equidistant from the center of the tube experience the same physical and chemical conditions. Where sample and reagent are present in the same zone, there exists a finite probability of reaction. The number of each to react in each zone is computed from the rate constant, reaction stoichiometry, initial concentrations and the time per step in the manner described below. (Symbols are defined in Table 1.) For the reaction, $S + R \overset{k_1}{=} P$ the rate of reaction zone i at time t is

$$Q = k_1 [S]_i^t [R]_i^t \tag{1}$$

By ratios, $[S]_i^t/[S]^0 = S_i^t/S^0$ and $[R]_i^t/[R]^0 = R_i^t/R^0$ and it follows that $Q = k_1 [S]^0 [R]^0 (S_i^t/S^0)(R_i^t/R^0)$. The number of simulated molecules which represents 1 mol l^{-1}, is

$$N_{AS} = S^0/[S]^0 = R^0/[R]^0 \tag{2}$$

The number of molecules that could possibly react in any zone in time interval, dt, is $N_{poss} = Q N_{AS} dt = k_{rel} S_i^t R_i^t$ where $k_{rel} = k_1 dt [R]^0/R^0$. The equation for N_{poss} is of the same form as Eqn. 1 for Q, is valid in each zone, uses the initial concentrations and is in terms of simulated molecules. There may be insufficient reagent or sample molecules present to fulfill this extent of reaction, and the reaction stoichiometry must be satisfied. Therefore, the number of sample and reagent molecules in any zone at time t that are actually allowed to react, NS_i^t and NR_i^t, is bounded by the following: NS_i^t, $NR_i^t \leqslant N_{poss}$; $NR_i^t = n NS_i^t$; $NS_i^t \leqslant S_i^t$; $NR_i^t \leqslant R_i^t$. For each dt, after the

TABLE 1

Symbols used

Symbol	Definition
t	Time after start of simulation (simsecs)
Q	Rate of reaction (l mol^{-1} s^{-1})
$[S]_i^t$	Sample concentration (M) in zone i at time t
$[R]_i^t$	Reagent concentration (M) in zone i at time t
$[S]^0$	Initial injected sample concentration (M)
$[R]^0$	Initial injected reagent concentration (M)
S_i^t	Number of simulated sample molecules in zone i after time t
R_i^t	Number of simulated reagent molecules in zone i after time t
S^0	Number of simulated sample molecules initially present in each zone of the injected sample plug
R^0	Number of simulated reagent molecules initially present in each zone of the injected reagent plug
n	Number of reagent molecules which react with each sample molecule
dt	Time interval for each cycle (stochastic step)

molecules have been allowed to move, the NS_i^t and NR_i^t values are calculated. The sample and reagent in each zone are then allowed to "react" (i.e., NS_i^t sample molecules are changed to "product" and NR_i^t reagent molecules are effectively removed from the simulation).

First, simulation studies of an ideal merging-zones system (Fig. 1) were done to evaluate the effects of ten variables. These were reagent plug size, offset, concentration, flow rate, injection delay, reaction rate constant, reaction stoichiometry, reagent diffusion constant, temperature, and system viscosity. The offsets (normally 200 mm) were measured from the middle of the sample and reagent loops so that, when equivalent, sample and reagent plugs of different sizes would travel the same mean distance to the tee. Sample and reagent plugs (100 μl, $C_s = C_r = 1 \times 10^{-3}$ M) were injected simultaneously into streams flowing at 1 ml min^{-1}. Diffusion constants for sample and reagents (D_s, D_r) were 1×10^{-3} mm^2 s^{-1} and viscosity was 1 cP. The rate constant (k_1) at 20°C was 10^5 l mol^{-1} s^{-1}. All tubes were 0.8-mm i.d. The time interval for each step was 1 simulated second (simsec).

In real flow-injection systems, the flow rates of the two streams and the angle at which they meet are well known to have a significant effect on the mixing process at the tee and immediately downstream thereof. For example, a layering effect is observed when a slowly flowing stream enters into the side of a faster stream. Visual inspection indicates that mixing takes place within a short distance (ca. 5—10 cm). It proved difficult to include this into the model without major changes in zone shape. In the experimental system, the streams are assumed to meet head on at a tee, rather than one entering the side of the other. Because of this, and the computational speed factor, complete mixing is assumed to occur at the tee.

Experimental studies

The test chemistry was the reaction of calcium with *o*-cresolphthalein complexone (CPC) [11—17]. The amount of purple product (1:1) formed is proportional to calcium concentration and is measured at 577 nm. Sample (100 μl of 10^{-3} M calcium chloride) and reagent (100 μl of 0.148×10^{-3} M CPC) were simultaneously introduced into 1.15 ml min^{-1} streams. The reagent carrier stream was 0.2 M glycine, which has a viscosity 1.05 cP at 20°C. The distance from the exit of the sampling valves to the tee-piece on the symmetric merging-zones system was 200 mm. Tubing of 0.8-mm i.d. was used throughout. The laboratory temperature was 22°C. Experiments and their equivalent simulations were then done in which the flow rate, concentration, plug offset and plug size for reagent were varied.

RESULTS AND DISCUSSION

Simulation of ten variables of the ideal flow-injection system with merging zones

Effect of reagent plug size. The results (Fig. 2A) show that where reagent and sample plugs are the same size and of equal concentrations, there is total

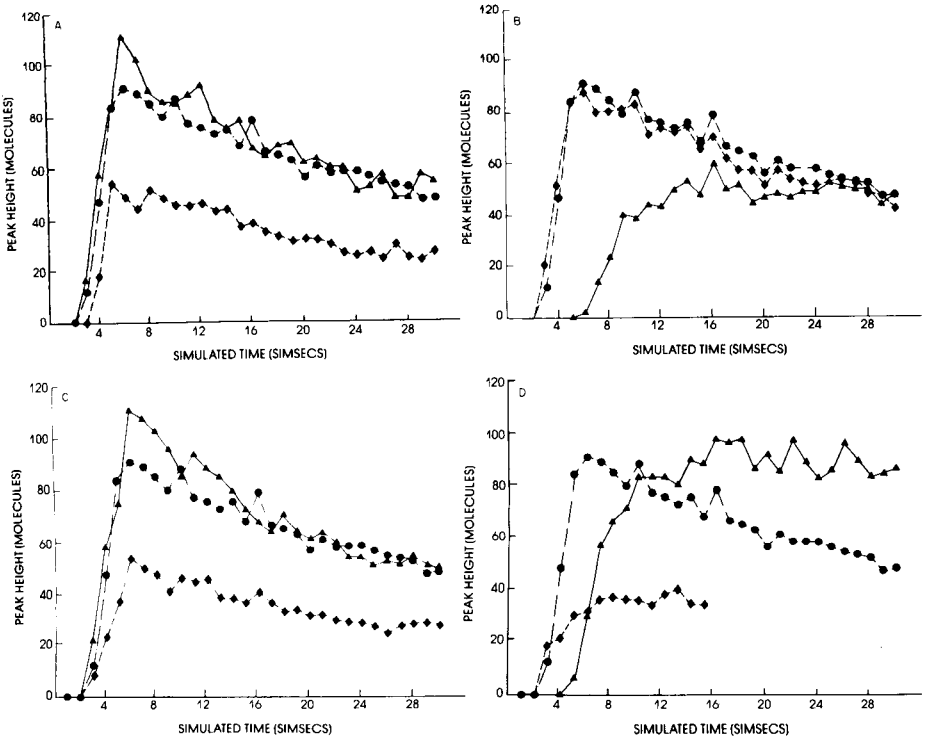

Fig. 2. (A) Effect of reagent plug size (μl) (100-μl sample plug): (♦) 50; (•) 100; (▲) 150. (B) Effect of reagent plug offset (mm) (200-mm sample plug offset): (♦) 150; (•) 200; (▲) 400. (C) Effect of reagent concentration (10^{-3} M) (1 × 10^{-3} M sample): (♦) 0.5; (•) 1.0; (▲) 2. (D) Effect of reagent stream flow rate (ml min^{-1}) (1 ml min^{-1} sample stream): (♦) 2.0; (•) 1.0; (▲) 0.5.

overlap, and kinetics are favorable, then complete reaction can occur and the initial rate of reaction is fast. When a smaller reagent plug is totally overlapped by a larger sample plug, the leading edge of the sample plug reaches the tee before the reagent plug; its tail reaches the tee after the reagent plug has completely passed through. The initial rate of reaction seen is slower as there is less reagent than sample present at the front of the reagent plug. This is accentuated by smaller values of the reaction rate constant than used here. The product maximum observed is not as high because of the overall lack of reagent. The peak area seen is only half that which would have been possible had it been possible for all sample to react. Where the reagent plug is larger than the sample plug, the rate of product formation is enhanced by an extended excess of reagent over sample. The same final peak area is seen as for the 1:1 case. From these results, a larger reagent plug than sample plug would appear generally more desirable.

Effect of reagent plug offset. This is shown in Fig. 2B and affects both the rate of reaction and amount of product formed [5]. When reagent offset is greater than sample offset, the reagent plug reaches the confluence later than the sample plug and (assuming equal diffusion constants) is more dispersed.

Product forms later than when sample and reagent offsets are matched and a lower maximum peak height is observed. An initially faster rate of reaction is seen when the reagent offset is a little less than the sample offset because here there exists an excess of reagent over sample at the leading edge of the sample plug.

Effect of reagent concentration. Figure 2C shows the simulation results for reagent/sample ratios of 2:1, 1:1 and 0.5:1. The rate of reaction increases with reagent/sample ratio. In the 2:1 and 1:1 cases, sufficient reagent is present for complete reaction and, although the early peak heights and initial rates increase with reagent concentration, both simulations finish on the same dispersion curve. In the case of 0.5:1 ratio, not only is reaction slower, but also at most only half the total product produced in the other cases can be formed. An excess of reagent is therefore expected to enhance the rate of product formation, and cause the maximum observed peak height to occur earlier and thus be higher. The findings agree with experimental experience [18].

Effect of reagent stream flow rate. The results are shown in Fig. 2D. The initial rate of reaction increases with reagent flow rate, because this determines the amount of reagent meeting the sample at the tee-piece. Concurrent with this is increased dilution of sample as it leaves the tee-piece and more rapid dispersion of the product formed. Moreover, decreased overlap of sample and reagent plugs means that reaction is not complete. In the longer term, while the slower reagent flow rate also does not give perfect overlap, where sufficient overlap exists it results in less dilution, less dispersion and better sensitivity.

For reasons of brevity, simulation results for the remaining six variables studied are not shown as figures, but are summarized below. Copies of these figures are available from the authors.

Effect of injection delay. In addition to the use of offsets, plug overlap can also be modified by means of a time delay between injection of sample and reagent. Here, assuming equal diffusion constants, the plugs reach the tee-piece in equally dispersed condition. This is not regular experimental practice because the valves should be independent; some tandem valves may be unsuitable. Time delays of −2, 0 and 2 s for reagent injection relative to sample injection were tried. The simulation predicted that (all other things being equal) simultaneous injection would give the best sensitivity and sample throughput.

Effect of reaction stoichiometry. For an A + 2B reaction with equal concentrations of A and B, early reagent depletion caused a slower reaction rate. Only half the usual (A + B case) peak height and area were seen. In this study, second-order kinetics were assumed. This can be changed readily in the model.

Effect of rate constant. In general, the observed behavior follows that for simple flow-injection systems [10] in that larger rate constants enhance the initial rate. The maximum peak height is also enhanced because it occurs

earlier on the dispersion curve. A decreased length of tubing between the tee and the detector is optimal.

Effect of reagent diffusion constant. The mean length of one step in the random walk is proportional to $D^{0.5}$ [19]. Values of 0.6, 0.8 and 1.0×10^{-3} mm^2 s^{-1} were used for D_R ; D_s was kept constant at 1.0×10^{-3} mm^2 s^{-1}. When D_s and D_R were equal, best overlap was obtained and hence maximum peak height and product formation were observed. Larger values for both D_R and D_s enhanced radial mixing and so improved sensitivity by decreasing axial dispersion.

Effect of system viscosity. Values of 0.5, 1.0 and 1.5 cP were tried. The effect of system viscosity was more marked than that of D_R . The mean length of one step in the random walk decreases with increasing system viscosity. A greater peak height is indicated for systems with higher viscosity. This is expected because the theoretical maximum peak height available (other than that caused by combination of flows) would be seen when there is zero dispersion.

Effect of temperature. Temperatures of 10, 20 and 40°C were used. Raising the temperature increased radial mixing and decreased axial dispersion caused by convection. The predicted enhancement of peak height was found experimentally [20].

Experimental and computer simulation studies of the calcium system

Further computer simulation studies were done which modeled the real experimental system as accurately as was possible. Four variables (reagent plug size, plug offset, flow rate and reagent concentration) were studied, both experimentally and by computer simulation. Instrumental limitations prevented experimental investigation of non-simultaneous injections and temperature. The effect of reaction rate was not studied, although this could be varied by pH control. The rate constant for the reaction (at pH 9.7) was not known exactly, but the kinetics were fast. Calcium (as $CaCl_2$) has a diffusion constant, D, of 1.2×10^{-3} mm^2 s^{-1} [21]. The D values for CPC and the Ca—OCPC complex were assumed to be about 0.6×10^{-3} mm^2 s^{-1}, based on those of similarly sized molecules; it was later suggested that a value of 0.3×10^{-3} mm^2 s^{-1} might have been more appropriate for CPC. In the experiments, the reagent was at 1/7th of the sample concentration, whereas the ideal simulation studies had used equal concentrations. This meant that only 1/8th of the 1500 molecules simulated could become product. With a 1:1 ratio, this would have been one in two. Because the accuracy of the model improves with the number of molecules simulated, Figs. 3, 4, 5 and 7 are subject to more statistical variations (cf. noise) than Fig. 2. The sample and reagent plug offsets used here were calculated as the length of tubing from the sampling valves (i.e., the front of the sample/reagent loops) as this was easier to implement experimentally.

The simulation results indicate the maximum product concentration observed by a number of detectors (at 5-cm intervals along the tube) with

time. The experimental apparatus used a single detector and therefore the data shown are in terms of time required for the product peak maximum to reach the detector. Six lengths of tubing between the tee and the detector (0, 30, 60, 90, 120, 150 cm) were used to vary the read time. The simulation predicts product absorbance from the moment product begins to form (i.e., 2—3 s after injection). Experimentally, the single detector did not respond until the product peak passed. Thus, each experiment gives one peak maximum value, and this only after at least 7.5 s have elapsed.

Effect of reagent plug size. The sample plug size was 100 μl. Reagent plug sizes of 50, 100 and 200 μl were tried. Sample and reagent flow rates were equal and injections were simultaneous. Figure 3 shows the experimental and simulation results, which used a 200-mm offset and flow rates of 1.15 ml min^{-1}. In each case, the leading edges of the sample and reagent plugs reached the confluence simultaneously. The concentrations chosen for the experiments caused reaction of sample to be incomplete. When the reagent plug was smaller than the sample plug, the tail of the sample interacted with little reagent and a smaller "effective sample size" resulted. Because sample was in excess over reagent and the sample plug completely overlapped the reagent plug, total reaction of reagent occurred. When the sample and reagent plug sizes were identical, a peak of approximately double the height of that for the 50-μl reagent plug was seen for both the experiment and the simulation. Larger reagent plugs (here 200 μl) completely enveloped the sample plug. In these cases, some reagent reached the tee after the sample had completely passed through, and so the resulting peak maximum obtained, while higher than the 100-μl example, was not twice as high, i.e., the effective reagent plug size with which the sample interacted was less than 200 μl. Good agreement between experimental and simulated behavior was observed.

Effect of reagent plug offset. The results are shown in Fig. 4. The sample offset (front of loop to tee) was 200 mm. Reagent offsets were 100, 200 and 400 mm. The simulation predicted that equal or decreased offsets would give the highest peak height and the maximum product formation. A further simulation with 150-mm offset predicted a slightly larger maximum peak height than for either the 100-mm or 200-mm cases. This most likely was a result of the difference between D_s and D_R. Kinetic factors may also be involved. In the 400-mm case, overlap was due solely to axial dispersion of the plugs; the reagent reached the tee later than the sample, product formation was delayed, and poor overlap resulted in low product concentration. The experimental results showed the 200-mm offset to be better than both the 100-mm and 400-mm results. The 400-mm offset, which had the poorest overlap and reached the tee in the most dispersed condition, gave a higher peak height than the 100-mm offset. This might occur if, for some reason, the rate of reaction was slower than expected because then parts of the (more concentrated) sample would have longer to react than in the 100-mm case. However, this result has not been fully accounted for by the known facts.

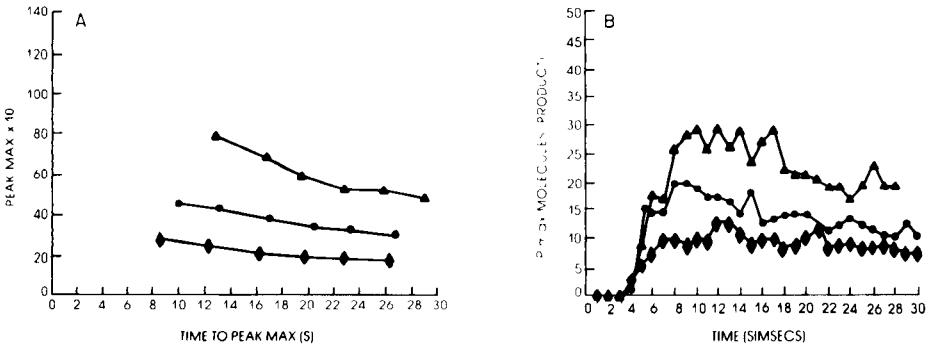

Fig. 3. Effect of reagent plug size: (A) results of experiment; (B) simulation. Plug size (μl): (♦) 50; (●) 100; (▲) 200. (100-μl sample plug.)

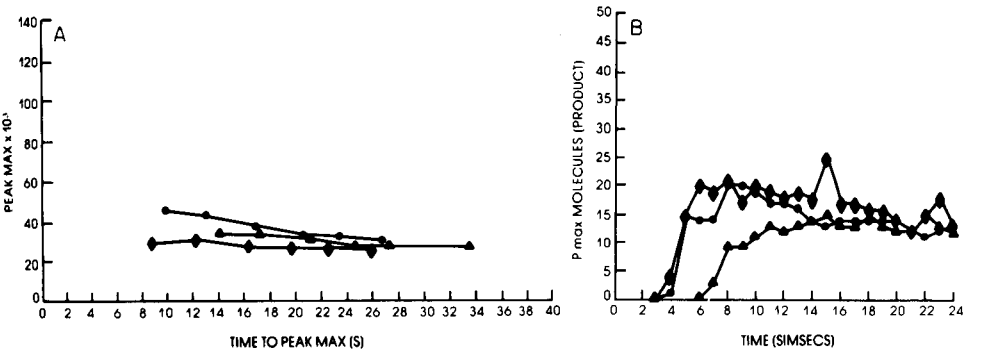

Fig. 4. Effect of reagent plug offset: (A) results of experiment; (B) simulation. Offset (mm): (♦) 100; (●) 200; (▲) 400. (200-mm sample plug offset.)

Effect of reagent concentration. Figure 5 shows the experimental and simulation results for reagent-to-sample ratios of 1:3.5, 1:7 and 1:14. As expected, the curves were of the same type as that in Fig. 2C where sample was in excess. The initial rate of reaction and the product concentration increase with reagent-to-sample ratio. Similarly, with complete reagent uptake, the areas of the peaks should be in the ratio 4:2.1. This is seen experimentally, with good, stable results for the 1:14 and 1:7 systems, but with peak area falling off with time for the 1:3.5 system. This would seem to be a feature of the chemistry. Once again, there is generally good agreement between model and experiment.

Effect of reagent stream flow rate. The experimental results (Figs. 6 and 7) were for reagent stream flow rates of 0.53, 1.15 and 2.00 ml min^{-1} and show the different times the peak maximum took to reach the detector. Increasing the reagent flow rate dilutes the sample after the tee and raises the amount of reagent available. The first experimental results (Fig. 6) showed the faster reagent flow rate to give maximum sensitivity. This conflicted with the model predictions and was considered worthy of further

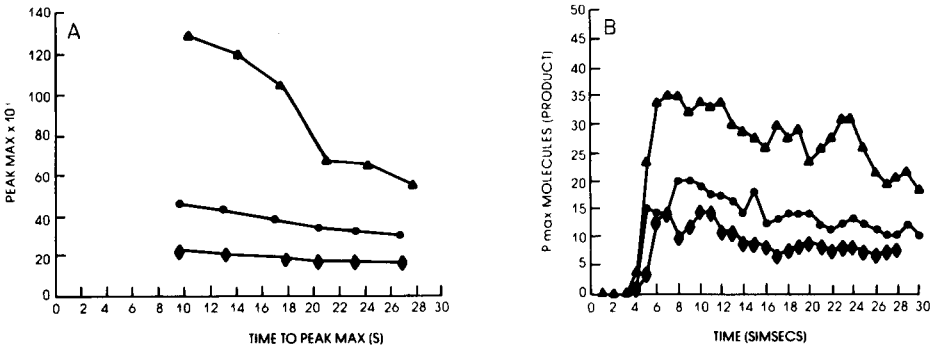

Fig. 5. Effect of reagent plug concentration: (A) results of experiment; (B) simulation. Reagent concentration (10^{-3} M): (♦) 0.076; (●) 0.148; (▲) 0.296. (1×10^{-3} M sample.)

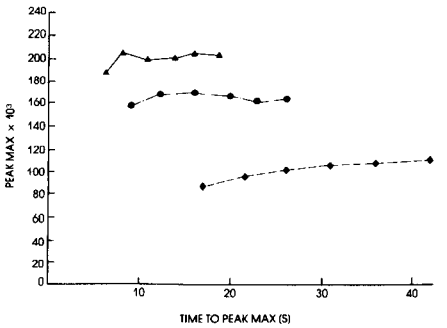

Fig. 6. Effect of reagent stream flow rate (results of initial experiments): (♦) 0.53; (●) 1.15; (▲) 2.0 ml min^{-1}. (Sample stream, 1.15 ml min^{-1}.)

investigation. The experiment had been done with sample and reagent solutions prepared in distilled water. The sample carrier solution was water, but the reagent carrier was glycine buffer. The reaction rate is highly pH-dependent, proceeding faster at pH 9.7 than at lower pH values. It was suggested that by the time the reagent plug (at ca. pH 4) reached the tee, it was sufficiently dispersed in the buffer (ca. pH 9.7) to cause a limited pH gradient. If this were so, then the faster reagent flow rate would enhance mixing of reagent and buffer, and hence give the highest reagent pH. To investigate this hypothesis, an experiment without any pH effect was done. In this, both carrier streams were glycine buffer, and both sample and reagent were prepared in glycine buffer. The results (Fig. 7) were substantially different, and correlated better with the predicted behavior. Without the simulation, the pH gradient might have gone unnoticed. The resulting system, in use in one of our laboratories, is now more stable.

Note on flow characteristics. The experimental results suggest that product formation is complete within 12—15 s from injection. In the simulation, peak area is still increasing after 12 s, because a few molecules of sample and

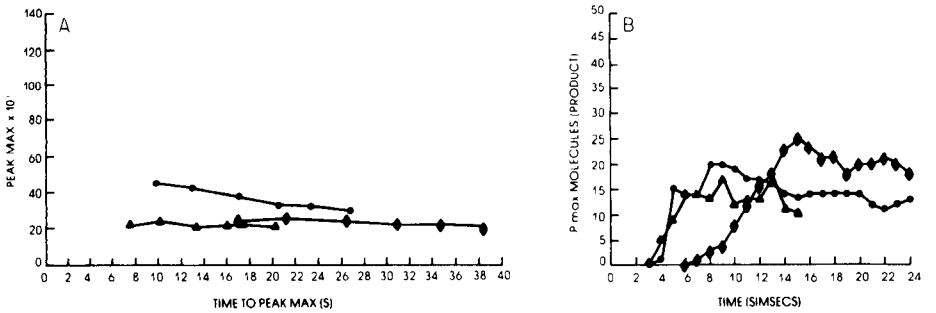

Fig. 7. Effect of reagent stream flow rate with pH gradient removed: (A) results of experiment; (B) simulation. Symbols and sample flow rate as for Fig. 6.

reagent are still coming through the arms of the tee and reacting. The model assumes a laminar flow pattern both before and after the tee-piece. It is very unlikely in practice that this is valid, as is evidenced by the limited tailing on peaks and subsequently higher sample throughput rates reported experimentally [22]. In real flow-injection systems, secondary flow [23, 24] also occurs. This enhances radial mixing and so decreases dispersion and tailing. Inclusion of secondary flow terms into the model would be possible. A further cause of enhanced radial mixing is the imperfect "pulsed" flow pattern generated by the commonly used peristaltic pumps. Ideally, the flow should be pulse-free (as obtainable by gravity feed). Increasing the number of rollers to perhaps 12 or 16 appears to help matters, but does not eliminate pulsation.

Conclusions

The random walk model, as adapted for the merging-zones systems, is useful for simulation and quantitative prediction of experimental behavior. A good degree of agreement was found between model and experiment after a somewhat iterative process of matching simulated to experimental conditions. During these experiments, discrepancies were found which were attributed to an unsuspected chemical effect in the experimental system. Removal of this resulted in better agreement of simulation and experiment. Both the model and the chemistry were found to be sensitive to small changes in conditions. This work has shown that the merging-zones systems can be substantially improved by control of the experimental variables and that the totally symmetric strategy in standard use is not necessarily always the best. It has led to an improved understanding of merging-zones systems.

The authors thank Peter D. Wentzell for helpful discussions in completion of this manuscript.

REFERENCES

1 H. Bergamin F°, E. A. G. Zagatto, F. J. Krug and B. F. Reis, Anal. Chim. Acta, 101 (1978) 17.
2 E. A. G. Zagatto, F. J. Krug, H. Bergamin F°, S. S. Jorgensen and B. F. Reis, Anal. Chim. Acta, 104 (1979) 279.
3 B. F. Reis, H. Bergamin F°, E. A. G. Zagatto and F. J. Krug, Anal. Chim. Acta, 107 (1979) 309.
4 B. F. Reis, E. A. G. Zagatto, A. O. Jacintho, F. J. Krug and H. Bergamin F°, Anal. Chim. Acta, 119 (1980) 305.
5 J. Mindegaard, Anal. Chim. Acta, 104 (1979) 185.
6 J. Růžička and E. H. Hansen, Anal. Chim. Acta, 106 (1979) 207.
7 J. Růžička and E. H. Hansen, ChemTech, American Chemical Society, 9 (1979) 756.
8 C. S. Lim, J. N. Miller and J. W. Bridges, Anal. Chim. Acta, 114 (1980) 183.
9 J. Růžička and E. H. Hansen, Anal. Chim. Acta, 114 (1980) 19.
10 D. Betteridge, C. Z. Marczewski and A. P. Wade, Anal. Chim. Acta, 165 (1984) 227.
11 F. H. Pollard and J. V. Martin, Analyst, 81 (1956) 348.
12 A. I. Cohen and L. Gordon, Anal. Chem., 28 (1956) 1445.
13 J. Bosholm, Anal. Chim. Acta, 34 (1966) 71.
14 H. V. Connerty and A. R. Briggs, Am. J. Clin. Pathol., 45 (1966) 290.
15 E. H. Hansen, J. Růžička and A. K. Ghose, Anal. Chim. Acta, 100 (1978) 151.
16 S. Al-Najafi, M.Sc. Thesis, University of Wales, 1984.
17 R. Pribil, Applied Complexometry, Pergamon, Oxford, 1982, p. 32.
18 D. Betteridge, T. J. Sly, A. P. Wade and J. E. W. Tillman, Anal. Chem., 55 (1983) 1292.
19 A. G. Marshall, Biophysical Chemistry, Wiley, New York, 1978, pp. 140—159.
20 C. L. M. Stults, A. P. Wade and S. R. Crouch, Anal. Chim. Acta, 192 (1987) 155.
21 R. C. Weast (Ed.), CRC Handbook of Chemistry and Physics, 59th edn., Section F62, CRC Press Inc., FL, 1979.
22 J. Růžička and E. H. Hansen, Flow Injection Analysis, Wiley, New York, 1981.
23 R. Tijssen, Anal. Chim. Acta, 114 (1980) 71.
24 J. H. M. Van den Berg, R. S. Deelder and H. G. M. Egberink, Anal. Chim. Acta, 114 (1980) 91.

Analytica Chimica Acta, 194 (1987) 61—75
Elsevier Science Publishers B.V., Amsterdam — Printed in The Netherlands

NUMERICAL SOLUTION OF HYDRAULIC MODELS BASED ON THE AXIALLY-DISPERSED PLUG FLOW MODEL BY LAPLACE TRANSFORMS

SPAS D. KOLEV and ERNÖ PUNGOR*

Institute of General and Analytical Chemistry, Technical University of Budapest, Gellért tér 4., H-1502 Budapest XI. (Hungary)

(Received 11th June 1986)

SUMMARY

The problem of solving hydraulic models based on the axially-dispersed plug flow model which are applicable for the mathematical modelling of different flow-through systems both in chemical analysis (e.g., chromatography, flow injection analysis) and chemical industry (e.g., different tubular reactors) is discussed. Methods for numerical inversion of the model solution in the Laplace domain by expanding it into series of orthogonal functions are compared. Best results with respect to precision and consumption of computation time are given by the methods employing Chebyshov polynomials of the first kind and Fourier sine series. These methods were found to be better in these respects than some other frequently used numerical inversion methods.

Many flow-through techniques used in chemical analysis (e.g., chromatography, flow injection analysis) and in the chemical industry incorporate fluid systems which quite often are composed of tubular elements (e.g., empty coiled or straight tubes, packed beds, etc.). The dispersion processes in these systems are frequently described by the axially-dispersed plug flow model [1]. Its mathematical expression in dimensionless form is given by the following partial differential equation:

$$(\partial C/\partial \theta) + (\partial C/\partial X) - (1/P)(\partial^2 C/\partial X^2) = S \quad (1)$$

(Table 1 shows the symbols and their meanings.)

A fluid system of n sections with arbitrary diameters (Fig. 1), given the introduction of matter at $X = X_0$ and absence of chemical reaction, is described by n partial differential equations [2] of the following type:

$$(\partial C_i/\partial \theta) + \gamma_i(\partial C_i/\partial X) - (\gamma_i/P_i)(\partial^2 C_i/\partial X^2) = 0 \quad (i = 1, 2, \ldots, n) \quad (2)$$

The corresponding initial and boundary conditions considered in this work are those proposed by Wehner and Wilhelm [3]:

$$C_i(0, X) = 0 \quad (i = 1, 2, \ldots, n) \quad (3)$$

$$C_i(\theta, X_i^-) = C_{i+1}(\theta, X_i^+) \quad (i = 1, 2, \ldots, n-1) \quad (4)$$

0003-2670/87/$03.50

TABLE 1

Symbols and definitions

$A_{i,j}$	Cubic spline coefficients (Appendix)
a_i	Coefficients (Eqns. 16, 21, 25, 32, 38)
$B_{i,j}$	Cubic spline coefficients (Appendix)
b	Real constant (Eqn. 34)
C	Dimensionless concentration
$\bar{C}$	Laplace transform of C
$\tilde{C}$	Fourier transform of C
$D_{i,j}$	Coefficients (Appendix)
$f(\theta)$	Real Laplace transformable function
$F(s)$	Laplace transform of $f(\theta)$
$g(\theta)$	Real function (Eqn. 28)
h	Time scale constant
i	Imaginary unit
$Im[\ ]$	Imaginary part of a complex number
K_i	Coefficients (Appendix)
l	Distance between the adjacent equally spaced interpolating points (Appendix)
$L_n^{(\lambda)}(\theta)$	Associated Laguerre polynomial
P	Peclet number
$P_n^{(\alpha,\beta)}(x)$	Jacobi polynomial
q	Complex function (Eqn. 40)
r_n	Function defined by Eqn. 12
$Re[\ ]$	Real part of a complex number
S	Source term
s	Laplace complex variable
$T_n(x)$	Chebyshov polynomial of the first kind
$u(\tau - \tau_i)$	Unit step function
$U_n(x)$	Chebyshov polynomial of the second kind
$w_{i,j}$	Lagrangian interpolation coefficients
X	Dimensionless axial distance
x	Jacobi polynomial variable
y_i	ith positive root of Eqn. 45
z	Complex variable equal to $1/s$

Greek letters

α, β	Parameters of Jacobi polynomials
Γ	Gamma function
γ_i	Ratio between the real volume of the test section (usually defined as the section closed between the injection and the measurement points) and the volume which it will have if its diameter is equal to that of the ith section
$\delta(\theta)$	Delta function
$\epsilon(\kappa)$	Function defined by Eqn. 35
θ	Dimensionless time
κ	Function defined by Eqn. 34
λ	Parameter of associated Laguerre polynomials
σ	Real part of s
σ_a	Abscissa of absolute convergency of $\Phi(s)$ (Eqn. 13)
σ_0	Real number larger than σ_a
τ	Imaginary part of s
$\phi(x)$	Function defined by $f(-\ln x)$
$\Phi(s)$	Laplace transform of $\psi(\theta)\, f(\theta)$
$\chi_n(\theta)$	Function defined in Appendix

TABLE 1 (continued)

$\psi(\theta)$	Function defined by $x\omega(x)$
ω	Weight function
Subscripts	
0	Refers to the injection point
m	Refers to the measurement point

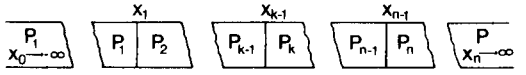

Fig. 1. Scheme of a fluid system with n sections.

$$C_i(\theta, X_i^-) - (1/P_i)(\partial C_i(\theta, X_i^-)/\partial X) = C_{i+1}(\theta, X_i^+) - (1/P_{i+1})(\partial C_{i+1}(\theta, X_i^+)/\partial X) \quad (5)$$

$(i = 1, 2, \ldots, n-1)$

$$C_k(\theta, X_j) = C_0(\theta) \quad (X_{k-1} \leqslant X_j \leqslant X_k, k = 1, 2, \ldots, n) \quad (6)$$

where $X_0 \to -\infty$ and $X_n \to \infty$

$$C_1(\theta, X_0) = \text{finite} \quad (7)$$

$$C_n(\theta, X_n) = \text{finite} \quad (8)$$

A convenient method usually applied for solving the set of partial differential equations represented by Eqn. 2 is that using Laplace transforms [2]. They are defined by the following integral:

$$F(s) = \int_0^\infty f(\theta) \exp(-s\theta)\, d\theta \quad (9)$$

In the general case, performance of the inverse transformation of the solution of the model in the Laplace domain is exceedingly difficult if not impossible. For this reason, analytical solutions of Eqns. 2 are known only in several very simple cases (e.g., for a doubly infinite system, i.e., $P_i = P$ [4]; for a singly infinite system i.e., $P_i = P$ for $i \geqslant k$ and $P_i = \infty$ for $i < k$ [5], or for a closed system, i.e., $P_i = P$ for $i = k$ and $P_i = \infty$ for $i \neq k$ [5]) as presented in Fig. 2.

These solutions however cannot cover the great variety of fluid systems (e.g., chromatographic, flow-injection and industrial systems) which have to be modelled mathematically. This difficulty could be overcome by applying numerical techniques for inversion of Laplace transforms. Several such techniques have been developed over the past twenty years but there is no universal formula which is effective for all types of Laplace transforms. Existing methods for numerical inversion can be divided into three main groups. The

first includes those methods which are based on expansion of the Laplace transform into series of functions. Such methods are those of Zakian [6–9], of Greco et al. [10] and the techniques based on orthogonal functions [11–13]. The second group is composed of methods which solve numerically the Melline integral:

$$f(\theta) = (1/2\pi i) \int_{\sigma-i\infty}^{\sigma+i\infty} F(s) \exp(s\theta)\, ds \tag{10}$$

by replacing the Laplace transform with some interpolation function and then performing the integration [13–17]. The third group of methods exploits the relationship between the Laplace transform and the Fourier transform, thus enabling efficient computational techniques to be applied for the numerical inversion of the Laplace transform [13, 18–21]. Insofar as these methods do not take into consideration some important properties of the Laplace transform (i.e., it is an analytical function only for $Re[s] > \sigma_a$ and that $\lim F(s) = 0$ for $s \to \infty$) they must be used with caution and if possible the results obtained should be checked by some other methods [13].

In this paper, the applicability of some methods based on expansion of the Laplace transform into series of orthogonal functions for solving Eqns. 2 is investigated, in order to choose the most efficient one with respect to precision and consumption of computational time.

TYPES OF ORTHOGONAL FUNCTIONS AND CORRESPONDING NUMERICAL METHODS

The orthogonal functions usually used for numerical inversion of the Laplace transform are of three main types

Shifted Jacobi polynomials

These polynomials [13] are defined by the equation

$$P_n^{(\alpha,\beta)}(x) = (-1)^n \frac{\Gamma(n+\alpha+1)}{\Gamma(\alpha+1)} \sum_{k=0}^{n} (-1)^k \frac{\Gamma(\alpha+1)\Gamma(n+\alpha+\beta+k+1)}{\Gamma(\alpha+k+1)\Gamma(k+1)\Gamma(n-k+1)\Gamma(n+\alpha+\beta+1)} x^k \tag{11}$$

where $0 < x < 1$ and $\alpha, \beta > -1$. They are orthogonal on the interval $[0, 1]$ relative to the weight function $\omega(x)$:

$$\int_0^1 \omega(x) P_n^{(\alpha,\beta)}(x) P_m^{(\alpha,\beta)}(x)\, dx = \begin{cases} 0 & \text{for } m \neq n \\ r_n = \dfrac{\Gamma(n+\alpha+1)\Gamma(n+\beta+1)}{\Gamma(n+1)\Gamma(n+\alpha+\beta+1)(2n+\alpha+\beta+1)} & \text{for } m = n \end{cases} \tag{12}$$

where $\omega(x) = x^\alpha (1-x)^\beta$

If the substitutions $\theta = -\ln x$, $f(-\ln x) = \phi(x)$ and $\psi(-\ln x) = x\omega(x)$ are performed in Eqn. 9 and after that $\phi(x)$ and $F(s)$ are replaced by $\omega(x)\,\phi(x)$ and $\Phi(s)$ the following integral is obtained:

$$\Phi(s) = \int_0^1 x^s \omega(x)\phi(x)\,dx = \int_0^\infty \exp(-s\theta)\,\psi(\theta)\,f(\theta)\,d\theta \tag{13}$$

By giving to s the values $0, 1, 2, \ldots, i$, the so-called weighted moments of $\phi(x)$ are defined. By expanding $\phi(x)$ and x^s in a series of Jacobi polynomials [12]:

$$\phi(x) = \sum_{i=0}^{\infty} (a_i/r_i) P_i^{(\alpha,\beta)}(x) \tag{14}$$

$$x^s = \sum_{i=0}^{\infty} \frac{\Gamma(s+\alpha+1)\Gamma(i+\beta+1)\Gamma(s+1)}{r_i\Gamma(i+s+\alpha+\beta+2)\Gamma(s-i+1)\Gamma(i+1)} P_i^{(\alpha,\beta)}(x) \tag{15}$$

and then using the previously calculated weighted moments of $\phi(x)$, the unknown coefficients a_i (Eqn. 14) can be determined by the following recurrence formula:

$$a_i = \frac{\Gamma(i+\alpha+1)\Gamma(2i+\alpha+\beta+2)}{(2i+\alpha+\beta+1)\,\Gamma(i+\alpha+\beta+1)} \left[\frac{\Phi(i)}{\Gamma(i+1)\Gamma(i+\alpha+1)} - \sum_{k=0}^{i-1} \frac{(2k+\alpha+\beta+1)\Gamma(k+a+\beta+1)}{\Gamma(i-k+1)\Gamma(k+\alpha+1)\Gamma(k+i+\alpha+\beta+2)} a_k\right] \tag{16}$$

In practice, only $F(s)$ is known so that a relationship between $F(s)$ and $\Phi(s)$ is needed. In the general case when the abscissa of absolute convergency of the integral in Eqn. 13 is arbitrary and positive and θ is scaled by h (h is arbitrary and larger than zero), the following relationship should be used [13]:

$$\Phi(s) = hF(\sigma_0 + sh) = \int_0^\infty \exp(-s\theta)\,\psi(\theta)\,f(\theta)\,d\theta$$

$$= \int_0^\infty \exp(-\sigma_0\theta/h)\,f(\theta/h)\exp(-s\theta)\,d\theta \tag{17}$$

where $\sigma_0 > \sigma_a$. The final explicit inversion formula is

$$f(\theta/h) = \psi(\theta)\exp(\sigma_0\theta/h) \sum_{i=0}^{\infty} (a_i/r_i) P_i^{(\alpha,\beta)}(\exp[-\theta]) \tag{18}$$

The following special types of Jacobi polynomials are often used.

Legendre polynomials. These polynomials, $P_n^{(0,0)}(x)$ [13] are characterized by $\alpha = \beta = 0$ and $\psi(\theta) = \exp(-\theta)$.

Chebyshov polynomials of the first kind. Such polynomials, $T_n(x)$ [13] are characterized by $\alpha = \beta = -0.5$ and are obtained from the corresponding

special case of Jacobi polynomials, i.e., $P_n^{(-0.5,-0.5)}(x)$, by multiplication with a constant:

$$T_n(x) = 2^{2n-1}\,[\Gamma(n+1)\Gamma(n)/\Gamma(2n)]\;P_n^{(-0.5,-0.5)}(x) \tag{19}$$

In the calculations it is more convenient to use the trigonometric form of these polynomials, i.e.,

$$T_n(x) = \cos[n \arccos(2x-1)]$$

The final inversion formula is then

$$f(\theta/h) = \frac{2}{\pi \sin\{2 \arccos[\exp(-\theta/2)]\}}\left\{a_0 + \right.$$

$$\left. + 2\sum_{k=1}^{\infty} a_k \cos\{2k \arccos[\exp(-\theta/2)]\}\right. \tag{20}$$

where the unknown coefficients a_i are calculated by the recurrence formula.

$$a_i = 2^{2i-1}\Phi(i) - 0.5\,\frac{\Gamma(2i+1)}{[\Gamma(i+1)]^2}\,a_0 - \sum_{k=1}^{i-1}\frac{\Gamma(2i+1)}{\Gamma(i+k+1)\,\Gamma(i-k+1)}\,a_k \tag{21}$$

Chebyshov polynomials of the second kind. These polynomials, $U_n(x)$ [13] are defined by the equation

$$U_n(x) = 2^{2n}\,\frac{\Gamma(n+1)\Gamma(n+2)}{\Gamma(2n+2)}P_n^{(0.5,0.5)}(x) \tag{22}$$

and the corresponding trigonometric form is

$$U_n(x) = \sin[(n+1)\arccos(2x-1)]/2\,[x(1-x)]^{0.5} \tag{23}$$

The explicit inversion formula is

$$f(\theta/h) = \frac{4}{\pi}\sum_{k=0}^{\infty} a_k \sin\{2(k+1)\arccos[\exp(-\theta/2)]\} \tag{24}$$

where

$$a_i = 2^{2i}\Phi(i) - \sum_{k=0}^{i-1}\frac{k+1}{i+1}\,\frac{\Gamma(2i+3)}{\Gamma(i-k+1)\,\Gamma(i+k+3)}\,a_k \tag{25}$$

Associated Laguerre polynomials

The Laguerre polynomials [13] are defined by

$$L_n^{(\lambda)}(\theta) = \sum_{i=0}^{n}\frac{\Gamma(n+\lambda+1)}{\Gamma(i+\lambda+1)\,\Gamma(i+1)\,\Gamma(n-i+1)}\,(-\theta)^i \tag{26}$$

where $\lambda > -1$. These polynomials are orthogonal on the interval $[0, \infty]$ relative to the weight function $\omega(\theta)$, $\omega(\theta) = \exp(-\theta)\theta^{\lambda}$, and the following equality holds:

$$\int_0^\infty \exp(-\theta)\theta^\lambda \, [L_n^{(\lambda)}(\theta)]^2 \mathrm{d}\theta = \Gamma(k + \lambda + 1)/\Gamma(k + 1) \tag{27}$$

By expanding the functions $g(\theta) = \theta^{-\lambda} f(\theta)$ and $\exp[-(s-1)\theta]$ into series of associated Laguerre polynomials, i.e.,

$$g(\theta) = \sum_{k=0}^{\infty} (a_k/r_k) \, L_k^{(\lambda)}(\theta) \tag{28}$$

$$\exp[-(s-1)\theta] = \sum_{k=0}^{\infty} (1/s^{\lambda+1}) \, (1 - 1/s)^k \, L_k^{(\lambda)}(\theta) \tag{29}$$

and then making the necessary substitutions in the integral Eqn. 9, the following equality is obtained.

$$F(s) = \sum_{k=0}^{\infty} a_k (1/s^{\lambda+1}) \, (1 - 1/s)^k \tag{30}$$

It is expedient to replace $1/s$ by z in Eqn. 30 so that it becomes

$$(1/z^{\lambda+1}) \, F(1/z) = \sum_{k=0}^{\infty} a_k \, (1 - z)^k \tag{31}$$

If $F(s)$ is analytical for $Re[s] > 0.5$ then the unknown coefficients in Eqn. 30 are those obtained when the function $(1/z^{\lambda+1}) \, F(1/z)$ is expanded in Taylor series about $z = 1$:

$$a_k = \frac{(-1)^k}{\Gamma(k+1)} \frac{\mathrm{d}^k}{\mathrm{d}z^k} \left\{ \frac{1}{z^{\lambda+1}} \, F(1/z) \right\}_{z=1} \tag{32}$$

Obviously great computational difficulties will arise in the determination of a_k from this equation if $F(1/z)$ is a more complicated function of $1/z$.

Sine functions

Sine functions of the type $\sin(2i + 1)\kappa$, where $i = 0, 1, 2, \ldots$ and $0 \leqslant \kappa \leqslant \pi/2$ [13] are orthogonal on the interval $[0, \pi/2]$ relative to a weight function equal to one and the following equality is valid:

$$\int_0^{\pi/2} [\sin(2i + 1)]^2 \mathrm{d}\kappa = \pi/4 \text{ where } i = 0, 1, 2, \ldots \tag{33}$$

If the following substitutions

$$\theta = -(1/b) \ln \cos \kappa \text{ where } b > 0 \tag{34}$$

$$f(-(1/b) \ln \cos \kappa) = \epsilon(\kappa) \tag{35}$$

$$s = (2n + 1)b \text{ where } n = 0, 1, 2, \ldots$$

are made in Eqn. 9 and then $\epsilon(\kappa)$ and $(\cos \kappa)^{2n} \sin \kappa$ are expanded into infinite Fourier sine series, i.e.,

$$\epsilon(\kappa) = \sum_{k=0}^{\infty} a_k \sin(2k + 1)\kappa \tag{36}$$

$$(\cos\kappa)^{2n}\sin\kappa = 2^{-2n}\sum_{k=0}^{\infty}\left[\frac{\Gamma(2n+1)}{\Gamma(2n-k+1)\Gamma(k+1)} - \frac{\Gamma(2n+1)}{\Gamma(2n-k+2)\Gamma(k)}\right]$$
$$\sin[2(n-k)+1]\kappa \tag{37}$$

a recurrence formula can be derived for the determination of the unknown coefficients in Eqn. 36:

$$a_i = (4^{i+1}/\pi)bF[(2i+1)b] - \sum_{k=0}^{i-1}\frac{2k+1}{2i+1}\frac{\Gamma(2i+2)}{\Gamma(i+k+2)\Gamma(i-k+1)}a_k \tag{38}$$

The final explicit inversion formula will be

$$f(\theta) = \sum_{k=0}^{\infty} a_k \sin\{(2k+1)\arccos[\exp(-b\theta)]\} \tag{39}$$

In the derivations made above, it is assumed that $\sigma_a \leqslant 0$ and $f(0) = 0$. If the first condition does not hold then $F(\sigma_0 + s)$, where $\sigma_0 > \sigma_a$ should be used instead of $F(s)$, which means that $f(\theta)$ is substituted by $\exp(-\sigma_0\theta)\, f(\theta)$. If the second condition is not fulfilled, then $f(\theta)$ should be replaced by $f_1(\theta) = f(\theta) - f(0)\exp(-\theta)$ which has Laplace transform equal to $F(s) - f(0)/(s+1)$.

COMPARISON OF THE METHODS

The methods described above were tested on three different flow systems composed of one, two and three sections (Fig. 2). The input signal was assumed to be delta-function, i.e., $C_0(\theta) = \delta(\theta)$ (Eqn. 6). The corresponding solutions in the Laplace and time domain in this case are as follows.

For a doubly infinite system (Fig. 2a) [4]

$$\bar{C}_m = \exp[P(0.5-q)]/2q \tag{40}$$

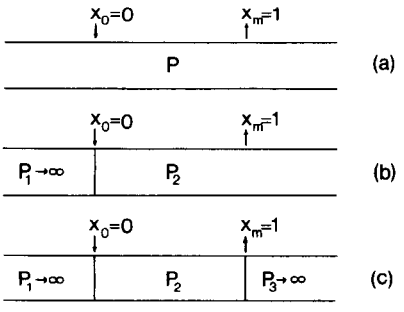

Fig. 2. Schemes of doubly infinite (a), singly infinite (b) and closed (c) systems.

where $q = (s/P + 0.25)^{0.5}$

and $C_m = 1/2\,(P/\pi\theta)^{0.5}\,\exp[-P(1-\theta)^2/4\theta]$

For a singly infinite system (Fig. 2b) [5],

$$\bar{C}_m = \exp[P_2\,(0.5 - q_2)]\,/(0.5 + q_2) \tag{41}$$

$$C_m = \left(\frac{P_2}{\pi\theta}\right)^{0.5} \exp\left[\frac{P_2}{2}\left(1 - \frac{\theta}{2} - \frac{1}{2\theta}\right)\right] - \frac{P_2}{2}\exp(P_2)\operatorname{erfc}\left[\left(\frac{P_2}{4\theta}\right)^{0.5}(1+\theta)\right] \tag{42}$$

For a closed system (Fig. 2c) [5],

$$\bar{C}_m = 2q_2\exp[P_2(0.5-q_2)]\,/[(0.5+q_2)^2 - (0.5-q_2)^2\exp(-2P_2q_2)] \tag{43}$$

$$C_m = \exp\left[\frac{P_2}{2}\left(1-\frac{\theta}{2}\right)\right]\sum_{i=1}^{\infty}\frac{2y_i^2\cos y_i + P_2 y_i \sin y_i}{y_i^2 + P_2^2/4 + P_2}\exp(-y_i^2\theta/P_2) \tag{44}$$

where y_i is the ith positive root of

$$\tan y = P_2\,y/(y^2 - P_2^2/4) \tag{45}$$

Functions 40, 41 and 43 are analytical for $Re[s] = \sigma_0 \geqslant 0$.

In the calculations, the infinite series in Eqns. 18, 28 and 30 were truncated at their tenth term but in Eqn. 44 at the twentieth term. The scale constant (Eqn. 18) and the constant b in Eqn. 34 were taken as unity. Because the Laplace transforms for singly infinite (Eqn. 41) and closed (Eqn. 44) systems are too complicated functions of s, the Taylor series coefficients (Eqn. 32) were determined only in the case of doubly infinite systems (Eqn. 40), according to the formula:

$$a_k = \Gamma(k+1)\exp[P(0.5-q)]\sum_{n=0}^{k}\left\{(-1)^n\frac{1}{[\Gamma(n+1)]^2\Gamma(k-n+1)(2q)^{(n+1)}}\right.$$
$$\left.\sum_{i=0}^{n}\frac{\prod_{j=0}^{i}[n(n+1)-j(j-1)]}{2^i n(n+1)\,\Gamma(i+1)(qP)^i}\right\} \tag{46}$$

where $\lambda = 0$.

The comparison was made with respect to the precision and time consumption of the methods. The second criterion is very important when it is necessary to solve parameter identification problems in which the curve fitting is performed by some nongradient optimization method (e.g., simplex optimization). In such cases, the model used must be solved a considerable number of times and the computation time required for one solution becomes crucial.

The results obtained on a HP-226 personal computer presented in Tables 2—4 show that in the cases of small Peclet numbers, i.e., $P \leqslant 1$, the method based on expansion of the Laplace transform into series of Chebyshov polynomials of the first kind should be preferred whereas for large Peclet

TABLE 2

Concentration vs. time for a doubly infinite system and different Peclet numbers

Time	Analytical solution	Legendre	Chebyshov		Fourier	Laguerre
			First kind	Second kind		
Peclet number = 0.05						
0.20	1.3552E − 01	1.3022E − 01	1.3376E − 01	1.3039E − 01	1.4139E − 01	1.4455E − 01
0.40	9.8620E − 02	9.8492E − 02	9.8541E − 02	9.8874E − 02	1.0491E − 01	1.0321E − 01
0.60	8.1163E − 02	7.9584E − 02	8.0540E − 02	7.9521E − 02	7.5139E − 02	7.8856E − 02
0.80	7.0480E − 02	7.4524E − 02	7.1898E − 02	7.4232E − 02	7.4614E − 02	6.5504E − 02
1.00	6.3078E − 02	6.0943E − 02	6.2563E − 02	6.1161E − 02	6.4882E − 02	5.8808E − 02
1.50	5.1396E − 02	5.4570E − 02	5.2291E − 02	5.4198E − 02	5.1061E − 02	5.3565E − 02
2.00	4.4325E − 02	4.2841E − 02	4.4302E − 02	4.3126E − 02	4.8728E − 02	4.8939E − 02
2.50	3.9448E − 02	3.6189E − 02	3.7585E − 02	3.6553E − 02	3.8633E − 02	4.0571E − 02
3.00	3.5816E − 02	3.8568E − 02	3.6249E − 02	3.7745E − 02	3.2132E − 02	3.1727E − 02
Standard deviation		3.0166E − 03	1.0646E − 03	2.7516E − 03	4.2742E − 03	4.6555E − 03
Duration (s)		3.17	2.45	2.23	2.54	5.23
Peclet number = 1.00						
0.20	2.8343E − 01	2.8331E − 01	2.8183E − 01	2.8483E − 01	2.8292E − 01	2.3212E − 01
0.40	3.5616E − 01	3.5524E − 01	3.5578E − 01	3.5563E − 01	3.5779E − 01	3.3346E − 01
0.60	3.4070E − 01	3.4122E − 01	3.4029E − 01	3.4107E − 01	3.3961E − 01	3.6072E − 01
0.80	3.1147E − 01	3.1168E − 01	3.1280E − 01	3.1072E − 01	3.1417E − 01	3.4476E − 01
1.00	2.8209E − 01	2.8132E − 01	2.8146E − 01	2.8291E − 01	2.7840E − 01	3.0735E − 01
1.50	2.2093E − 01	2.2159E − 01	2.2186E − 01	2.2003E − 01	2.2737E − 01	2.0317E − 01
2.00	1.7603E − 01	1.7507E − 01	1.7587E − 01	1.7720E − 01	1.7168E − 01	1.4693E − 01
2.50	1.4247E − 01	1.4321E − 01	1.4084E − 01	1.4138E − 01	1.2841E − 01	1.3907E − 01
3.00	1.1670E − 01	1.1800E − 01	1.1727E − 01	1.1565E − 01	1.0737E − 01	1.4627E − 01
Standard deviation		7.7407E − 04	9.9472E − 04	9.4721E − 04	6.4143E − 03	2.8566E − 02
Duration (s)		3.17	2.44	2.22	2.54	5.23
Peclet number = 20.0						
0.20	3.1746E − 07	9.2268E − 03	1.8629E − 02	4.0487E − 03	−2.5842E − 03	3.5593E − 02
0.40	2.2159E − 02	7.3818E − 03	7.6742E − 04	1.2088E − 02	2.1496E − 02	3.1886E − 01
0.60	4.2931E − 01	4.4549E − 01	4.5363E − 01	4.4011E − 01	4.3111E − 01	5.6242E − 01
0.80	1.0985E + 00	1.0843E + 00	1.0779E + 00	1.0886E + 00	1.0981E + 00	7.3532E − 01
1.00	1.2616E + 00	1.2601E + 00	1.2553E + 00	1.2624E + 00	1.2592E + 00	8.2556E − 01
1.50	4.4766E − 01	4.3964E − 01	4.4160E − 01	4.4070E − 01	4.4988E − 01	7.2012E − 01
2.00	7.3225E − 02	7.4420E − 02	6.3287E − 02	7.7254E − 02	6.9631E − 02	3.3002E − 01
2.50	8.8637E − 03	2.3846E − 02	4.3683E − 02	1.3428E − 02	6.4070E − 03	−7.2791E − 02
3.00	9.2694E − 04	−6.5341E − 03	7.8464E − 03	−5.5875E − 03	1.9898E − 03	−2.9487E − 01
Standard deviation		1.1130E − 02	1.9013E − 02	7.1533E − 03	2.1345E − 03	2.7149E − 01
Duration (s)		3.17	2.44	2.23	2.54	5.23

numbers, i.e., $P > 1$, the method based on Fourier sine series expansion should be preferred.

These two methods were compared with three others taken as representatives of the above-mentioned three groups of numerical inversion methods: (1) the method with coefficients evaluated as described by Zakian and Gannon [9] and truncation at the tenth term of the corresponding infinite series (see Appendix); (2) the method based on numerical Fourier-transform inversion [19] using cubic-spline interpolation and thirty interpolating points so that the following condition is fulfilled:

TABLE 3

Concentration vs. time for a singly infinite system and different Peclet numbers

Time	Analytical solution	Legendre	Chebyshov		Fourier
			First kind	Second kind	
Peclet number = 0.05					
0.20	2.5339E − 01	2.4289E − 01	2.4980E − 01	2.4375E − 01	2.6505E − 01
0.40	1.7815E − 01	1.7789E − 01	1.7804E − 01	1.7806E − 01	1.9062E − 01
0.60	1.4277E − 01	1.3963E − 01	1.4145E − 01	1.4016E − 01	1.3082E − 01
0.80	1.2124E − 01	1.2928E − 01	1.2414E − 01	1.2829E − 01	1.2942E − 01
1.00	1.0640E − 01	1.0216E − 01	1.0542E − 01	1.0214E − 01	1.1003E − 01
1.50	8.3163E − 02	8.9459E − 02	8.4888E − 02	8.8844E − 02	8.2401E − 02
2.00	6.9272E − 02	6.6349E − 02	6.9416E − 02	6.6192E − 02	7.8073E − 02
2.50	5.9806E − 02	5.3297E − 02	5.5903E − 02	5.5560E − 02	5.8422E − 02
3.00	5.2841E − 02	5.8266E − 02	5.3271E − 02	5.7118E − 02	4.5722E − 02
Standard deviation		5.9890E − 03	2.1708E − 03	5.2241E − 03	8.4664E − 03
Duration (s)		3.16	2.44	2.22	2.54
Peclet number = 1.00					
0.20	4.8833E − 01	4.8815E − 01	4.8534E − 01	4.9200E − 01	4.8872E − 01
0.40	5.5259E − 01	5.5115E − 01	5.5192E − 01	5.5056E − 01	5.5494E − 01
0.60	4.8550E − 01	4.8620E − 01	4.8466E − 01	4.8733E − 01	4.8374E − 01
0.80	4.1265E − 01	4.1303E − 01	4.1515E − 01	4.1049E − 01	4.1578E − 01
1.00	3.5040E − 01	3.4943E − 01	3.4936E − 01	3.5119E − 01	3.4688E − 01
1.50	2.3946E − 01	2.4025E − 01	2.4100E − 01	2.3788E − 01	2.4585E − 01
2.00	1.7046E − 01	1.6958E − 01	1.7060E − 01	1.7156E − 01	1.6636E − 01
2.50	1.2520E − 01	1.2558E − 01	1.2185E − 01	1.2574E − 01	1.1155E − 01
3.00	9.4128E − 02	9.5211E − 02	9.4166E − 02	9.2634E − 02	8.5619E − 02
Standard deviation		8.4332E − 04	1.8568E − 03	1.9005E − 03	6.2119E − 03
Duration (s)		3.17	2.44	2.23	2.54
Peclet number = 20.0					
0.20	5.3051E − 07	1.6677E − 02	2.9818E − 02	8.3709E − 03	−4.9657E − 03
0.40	3.1900E − 02	1.1617E − 02	4.3680E − 03	1.7403E − 02	3.0486E − 02
0.60	5.4371E − 01	5.6525E − 01	5.7497E − 01	5.5841E − 01	5.4697E − 01
0.80	1.2430E + 00	1.2219E + 00	1.2129E + 00	1.2284E + 00	1.2424E + 00
1.00	1.2910E + 00	1.2929E + 00	1.2889E + 00	1.2946E + 00	1.2865E + 00
1.50	3.7019E − 01	3.5767E − 01	3.5809E − 01	3.6012E − 01	3.7429E − 01
2.00	5.0856E − 02	5.4668E − 02	4.3437E − 02	5.7006E − 02	4.4057E − 02
2.50	5.3090E − 03	2.2387E − 02	4.5309E − 02	1.0249E − 02	1.5058E − 03
3.00	4.8820E − 04	−9.9369E − 03	4.5116E − 03	−7.9610E − 03	2.7932E − 03
Standard deviation		1.5544E − 02	2.4394E − 02	1.0323E − 02	3.9531E − 03
Duration (s)		3.17	2.44	2.22	2.54

$$|\bar{C}_m(i\tau)|_{\tau=\tau_{max}} / |\bar{C}_m(i\tau)|_{\tau=0} \leqslant 0.02$$

and (3) the method based on Lagrangian interpolation developed by Semerciyan and Thodos [16] with ten equally spaced interpolating points (see Appendix).

The results obtained (Table 5) show that both in respect to precision and time consumption the methods based on Chebyshov polynomials of the first kind and Fourier sine series expansions should be preferred for solving the types of problems discussed in the present paper.

TABLE 4

Concentration vs. time for a closed system and different Peclet numbers

Time	Analytical solution	Legendre	Chebyshov		Fourier
			First kind	Second kind	
Peclet number = 0.05					
0.20	8.3111E − 01	8.1354E − 01	8.2556E − 01	8.1639E − 01	8.5180E − 01
0.40	6.7932E − 01	6.7871E − 01	6.7900E − 01	6.7733E − 01	7.0302E − 01
0.60	5.5525E − 01	5.4984E − 01	5.5301E − 01	5.5262E − 01	5.3288E − 01
0.80	4.5384E − 01	4.6776E − 01	4.5874E − 01	4.6494E − 01	4.6983E − 01
1.00	3.7096E − 01	3.6374E − 01	3.6946E − 01	3.6221E − 01	3.7629E − 01
1.50	2.2406E − 01	2.3483E − 01	2.2672E − 01	2.3430E − 01	2.2467E − 01
2.00	1.3533E − 01	1.3063E − 01	1.3614E − 01	1.2797E − 01	1.4956E − 01
2.50	8.1741E − 02	6.9995E − 02	7.4759E − 02	7.8677E − 02	7.6293E − 02
3.00	4.9372E − 02	5.8199E − 02	4.8694E − 02	5.7960E − 02	3.6716E − 02
Standard deviation		1.0210E − 02	3.6369E − 03	8.6251E − 03	1.5517E − 02
Duration (s)		3.39	2.66	2.44	2.75
Peclet number = 1.00					
0.20	8.3876E − 01	8.3883E − 01	8.3351E − 01	8.4674E − 01	8.4142E − 01
0.40	8.5157E − 01	8.4912E − 01	8.5019E − 01	8.4729E − 01	8.5496E − 01
0.60	6.9067E − 01	6.9177E − 01	6.8917E − 01	6.9465E − 01	6.8776E − 01
0.80	5.4790E − 01	5.4845E − 01	5.5251E − 01	5.4325E − 01	5.5105E − 01
1.00	4.3355E − 01	4.3231E − 01	4.3165E − 01	4.3502E − 01	4.3186E − 01
1.50	2.4131E − 01	2.4221E − 01	2.4410E − 01	2.3809E − 01	2.4516E − 01
2.00	1.3430E − 01	1.3364E − 01	1.3467E − 01	1.3620E − 01	1.3256E − 01
2.50	7.4747E − 02	7.4482E − 02	6.8493E − 02	7.6716E − 02	6.7153E − 02
3.00	4.1601E − 02	4.2218E − 02	4.1359E − 02	3.8704E − 02	3.7692E − 02
Standard deviation		1.0944E − 03	3.3948E − 03	4.0521E − 03	3.8099E − 03
Duration (s)		3.37	2.64	2.42	2.74
Peclet number = 20.0					
0.20	8.8610E − 07	2.5341E − 02	4.1937E − 02	1.3778E − 02	−6.4795E − 03
0.40	4.5796E − 02	2.0941E − 02	1.3890E − 02	2.7278E − 02	4.3164E − 02
0.60	6.8382E − 01	7.0919E − 01	7.1971E − 01	7.0141E − 01	6.8820E − 01
0.80	1.3887E + 00	1.3611E + 00	1.3494E + 00	1.3696E + 00	1.3872E + 00
1.00	1.2948E + 00	1.3020E + 00	1.2998E + 00	1.3022E + 00	1.2904E + 00
1.50	2.9313E − 01	2.7618E − 01	2.7425E − 01	2.8037E − 01	2.9701E − 01
2.00	3.2860E − 02	3.9972E − 02	3.0411E − 02	4.1039E − 02	2.5826E − 02
2.50	2.8621E − 03	1.9569E − 02	4.3454E − 02	7.1498E − 03	−6.2613E − 04
3.00	2.2308E − 04	−1.2587E − 02	−4.6656E − 04	−9.3334E − 03	2.7766E − 03
Standard deviation		1.9721E − 02	2.9140E − 02	1.3347E − 02	4.3835E − 03
Duration (s)		3.38	2.64	2.43	2.75

Conclusions

The numerical methods for inversion of the Laplace transforms considered in this investigation, based on expansions of the transformed functions into series of orthogonal polynomials, show some considerable advantages connected with computational time consumption and precision in comparison with other numerical methods frequently used for the same purpose.

Among the former techniques, those based on Chebyshov polynomials of the first kind and Fourier sine series were found to give the best results for small and large Peclet numbers, respectively.

TABLE 5

Concentration vs. time for a doubly infinite system with different Peclet numbers

Time	Analytical solution	Chebyshov first kind	Fourier	Zakian	Fourier transform	Lagrange
Peclet number = 0.05						
0.20	1.3552E − 01	1.3376E − 01	1.4139E − 01	1.3551E − 01	2.0311E − 01	2.0050E − 01
0.40	9.8620E − 02	9.8541E − 02	1.0491E − 01	1.1198E − 01	1.7325E − 01	3.5072E − 03
0.60	8.1163E − 02	8.0540E − 02	7.5139E − 02	1.0098E − 01	1.5787E − 01	1.1170E − 02
0.80	7.0480E − 02	7.1898E − 02	7.4614E − 02	9.2510E − 02	1.4754E − 01	2.5973E − 01
1.00	6.3078E − 02	6.2563E − 02	6.4882E − 02	8.5301E − 02	1.3941E − 01	1.3889E − 01
1.50	5.1396E − 02	5.2291E − 02	5.1061E − 02	7.1009E − 02	1.1930E − 01	−2.1495E − 01
2.00	4.4325E − 02	4.4302E − 02	4.8728E − 02	6.0432E − 02	1.0697E − 01	8.2325E − 01
2.50	3.9448E − 02	3.7585E − 02	3.8633E − 02	5.2319E − 02	9.2230E − 02	5.3561E − 01
3.00	3.5816E − 02	3.6249E − 02	3.2132E − 02	4.5905E − 02	6.8982E − 02	−3.0145E + 00
Standard deviation		1.0646E − 03	4.2742E − 03	1.6539E − 02	6.6840E − 02	1.0692E + 00
Duration (s)		2.44	2.54	1.10	38.21	78.06
Peclet number = 1.00						
0.20	2.8343E − 01	2.8183E − 01	2.8292E − 01	2.8285E − 01	2.8843E − 01	2.8343E − 01
0.40	3.5616E − 01	3.5578E − 01	3.5779E − 01	3.5497E − 01	3.5615E − 01	3.5616E − 01
0.60	3.4070E − 01	3.4029E − 01	3.3961E − 01	3.4025E − 01	3.3720E − 01	3.4070E − 01
0.80	3.1147E − 01	3.1280E − 01	3.1417E − 01	3.1162E − 01	3.0509E − 01	3.1147E − 01
1.00	2.8209E − 01	2.8146E − 01	2.7840E − 01	2.8190E − 01	2.7314E − 01	2.8209E − 01
1.50	2.2093E − 01	2.2186E − 01	2.2737E − 01	2.1778E − 01	2.0741E − 01	2.2093E − 01
2.00	1.7603E − 01	1.7587E − 01	1.7168E − 01	1.7059E − 01	1.5413E − 01	1.7603E − 01
2.50	1.4247E − 01	1.4084E − 01	1.2841E − 01	1.3668E − 01	1.0947E − 01	1.4247E − 01
3.00	1.1670E − 01	1.1727E − 01	1.0737E − 01	1.1216E − 01	7.2478E − 02	1.1670E − 01
Standard deviation		9.9472E − 04	6.4143E − 03	3.2591E − 03	2.0723E − 02	1.6565E − 06
Duration (s)		2.44	2.54	1.08	38.18	78.05
Peclet number = 20.0						
0.20	3.1746E − 07	1.8629E − 02	−2.5842E − 03	1.2454E − 02	−9.1487E − 04	4.9863E − 02
0.40	2.2159E − 02	7.6742E − 04	2.1496E − 02	−1.3293E − 03	2.1803E − 02	−1.7404E − 02
0.60	4.2931E − 01	4.5363E − 01	4.3111E − 01	4.2564E − 01	4.2943E − 01	4.9349E − 01
0.80	1.0985E + 00	1.0779E + 00	1.0981E + 00	1.1015E + 00	1.0986E + 00	1.0357E + 00
1.00	1.2616E + 00	1.2553E + 00	1.2592E + 00	1.2619E + 00	1.2608E + 00	1.2191E + 00
1.50	4.4766E − 01	4.4160E − 01	4.4988E − 01	4.4010E − 01	4.4615E − 01	5.0501E − 01
2.00	7.3225E − 02	6.3287E − 02	6.9631E − 02	7.9408E − 02	7.6287E − 02	−1.2900E − 01
2.50	8.8637E − 03	4.3683E − 02	6.4070E − 03	2.9738E − 02	1.8320E − 02	1.0614E − 01
3.00	9.2694E − 04	7.8464E − 03	1.9898E − 03	−9.6482E − 03	1.5076E − 02	6.4907E − 01
Standard deviation		1.9013E − 02	2.1345E − 03	1.2348E − 02	5.8005E − 03	2.3277E − 01
Duration (s)		2.44	2.54	1.09	38.21	78.06

The authors are greatly indebted to Dr. Klára Tóth for valuable discussions and comments.

APPENDIX

Zakian's method [9]

$$C_m = \sum_{i=1}^{n} (K_i/\theta)\, \bar{C}_m\, (2i/\theta)$$

Numerical inversion of the Fourier transform [19]. The Fourier transform is obtained directly from the Laplace transform if s is replaced by $i\tau$, i.e., $\bar{\bar{C}}_m = \bar{C}_m(i\tau)$. The inversion formula for the Fourier transform is

$$C_m = (1/\pi)\int_0^\infty \bar{\bar{C}}_m \exp(i\tau\theta)\,\mathrm{d}\tau = (1/\pi)\left\{\int_0^\infty Re\,[\bar{\bar{C}}_m]\cos\tau\theta\,\mathrm{d}\tau - \int_0^\infty Im\,[\bar{\bar{C}}_m]\sin\tau\theta\,\mathrm{d}\tau\right\} \quad \text{(A1)}$$

If $Re[\bar{\bar{C}}_m]$ and $Im[\bar{\bar{C}}_m]$ are substituted by their cubic spline interpolating functions,

$$Re[\bar{\bar{C}}_m] = \sum_{i=1}^{m} u(\tau-\tau_i)\,[A_{0,i} + A_{1,i}(\tau-\tau_i) + A_{2,i}(\tau-\tau_i)^2 + A_{3,i}(\tau-\tau_i)^3]$$

$$Im[\bar{\bar{C}}_m] = \sum_{i=1}^{m} u(\tau-\tau_i)\,[B_{0,i} + B_{1,i}(\tau-\tau_i) + B_{2,i}(\tau-\tau_i)^2 + B_{3,i}(\tau-\tau_i)^3]$$

and the corresponding integrals in Eqn. A1 are solved, then the final explicit inversion formula will be:

$$C_m = (1/\pi\theta)\sum_{i=1}^{m-1} D_{0,i}\sin il\theta + D_{1,i}\sin(i-1)l\theta + D_{2,i}\cos il\theta + D_{3,i}\cos(i-1)l\theta \quad \text{(A2)}$$

where

$$D_{0,i} = A_{0,i+1} - (1/\theta)\,[B_{1,i} + 2B_{2,i}l + 3B_{3,i}l^2 + (1/\theta)\,(2A_{2,i} + 6A_{3,i}l - (1/\theta)\,6B_{3,i})]$$

$$D_{1,i} = -A_{0,i} - (1/\theta)\,[-B_{1,i} + (1/\theta)(-2A_{2,i} + (1/\theta)\,6B_{3,i})]$$

$$D_{2,i} = B_{0,i+1} + (1/\theta)\,[A_{1,i} + 2A_{2,i}l + 3A_{3,i}l^2 - (1/\theta)\,(2B_{2,i} + 6B_{3,i}l + (1/\theta)\,6A_{3,i})]$$

$$D_{3,i} = -B_{0,i} - (1/\theta)\,[A_{1,i} - (1/\theta)\,(2B_{2,i} + (1/\theta)\,6A_{3,i})]$$

Numerical inversion of the Laplace transform by means of Lagrangian interpolation [16]. The function $\exp(s^{0.5})\,\bar{C}_m$ is presented as Lagrangian interpolation polynomial in $1/(s^{0.5})$ at equally spaced interpolating points:

$$\exp(s^{0.5})\,\bar{C}_m = \sum_{k=0}^{n} \exp(s_k{}^{0.5})\,\bar{C}_m(s_k)\sum_{j=0}^{n} w_{k,j}/s^{j/2} \quad \text{(A3)}$$

Taking into consideration that

$$\chi_n(\theta) = (1/2\pi i)\int_{\sigma-i\infty}^{\sigma+i\infty} [\exp(-s^{0.5})/s^{n/2}]\exp(s\theta)\,\mathrm{d}s \quad \text{(A4)}$$

where $n = 0, 1, 2, \ldots$, the final inversion formula will be

$$C_m = \sum_{j=0}^{n}\sum_{k=0}^{n} [w_{k,j}\exp(s^{0.5})\,\bar{C}_m(s_k)]\,\chi_i(\theta) \quad \text{(A5)}$$

REFERENCES

1 O. Levenspiel and K. B. Bischoff, Adv. Chem. Eng., 4 (1963) 95.
2 S. D. Kolev and E. Pungor, Anal. Chim. Acta, 185 (1986) 315.
3 J. F. Wehner and R. H. Wilhelm, Chem. Eng. Sci., 6 (1956) 89.
4 O. Levenspiel and W. K. Smith, Chem. Eng. Sci., 6 (1957) 227.
5 E. W. Godslave and K. S. Chang, Chem. Eng. Commun., 4 (1980) 699.
6 V. Zakian, Electron. Lett., 5 (1969) 120.
7 V. Zakian, Electron. Lett., 6 (1970) 677.

8 V. Zakian, Electron. Lett., 6 (1970) 474.
9 V. Zakian and D. R. Gannon, Electron. Lett., 7 (1971) 70.
10 G. Greco Jr., G. Iorio and L. G. Gibilaro, Chem. Eng. Sci., 30 (1975) 1069.
11 A. Pethö and J. Kühne, Comput. Chem. Eng., 4 (1980) 63.
12 V. A. Ditkin and A. P. Prudnikov, Operational Calcules, Visshaja Shkola, Moscow, 1975 (in Russian).
13 V. I. Krylov and N. S. Skoblya, Methods of Approximate Fourier Transform and Inversion of the Laplace Transform, Nauka, Moscow, 1974 (in Russian).
14 N. D. P. Dang and L. G. Gibilaro, Chem. Eng. J., 8 (1974) 157.
15 D. H. Kim and K. S. Chang, Chem. Eng. J., 29 (1984) 11.
16 M. Semerciyan and G. Thodos, AIChEJ., 18 (1972) 923.
17 R. Bellman, R. E. Kalaba and A. Lockett, Numerical Inversion of the Laplace Transform, American Elsevier, New York, 1966.
18 W. C. Clements Jr. and K. B. Schnelle Jr., Ind. Eng. Chem. Proc. Design Develop., 2 (1963) 94.
19 J. R. Hays, W. C. Clements Jr. and T. R. Harris, AIChEJ., 13 (1967) 374.
20 W. C. Clements Jr., Chem. Eng. Sci., 24 (1969) 957.
21 L.-K. P. Hsu and H. W. Haynes Jr., AIChEJ., 27 (1981) 81.

Analytica Chimica Acta, 194 (1987) 77—89
Elsevier Science Publishers B.V., Amsterdam — Printed in The Netherlands

A PROGRAM FOR EVALUATING EQUILIBRIUM CONSTANTS FROM SPECTROPHOTOMETRIC DATA BY NON-LINEAR REGRESSION ANALYSIS

L. LAMPUGNANI, L. MEITES[a], P. PAPOFF and T. ROTUNNO*

Istituto di Chimica Analitica Strumentale del C.N.R., Via Risorgimento 35, 56100 Pisa (Italy)

(Received 12th September 1986)

SUMMARY

A new program, CFTSP, is described for computing stability constants and molar absorptivities from data on the absorbances of mixtures of a metal ion with a ligand. It is written in FORTRAN 77, can run on personal computers, and has facilities for interactive data analysis and presentation that ease the operator's task in searching for the equilibrium model that best fits the experimental data. A critical evaluation of the performance of the program is presented, and some general criteria for selecting equilibrium parameters, making use of both synthetic and experimental data, are described.

The characterization and determination of the species involved in chemical equilibria are the aims of many studies in several branches of science, and many authors [1—4] have extensively reviewed the experimental methods and numerical approaches used to obtain stability constants. Spectrophotometry has definite advantages over other techniques for such purposes, including simplicity of operation and direct applicability to a wide range of systems [2, 5—7]. Moreover, the increasing availability of high-performance spectrophotometers with automatic data-collecting capabilities provides an incentive to enhance the use of the spectrophotometric technique. However, these advantages can be severely counteracted by covariation among the equilibrium constants and the molar absorptivities, as well as by the requirement that the absorbance must depend significantly on the total concentration of the reactants, at least in some part of the explored ranges of the wavelength and the total concentration. As is also true for most other techniques, increasing the number of equilibrium species increases the probability that different models may yield acceptable fits to the same set of absorbance data, and thereby makes it more difficult to select the model that most correctly describes the equilibrium under study.

---

[a]Permanent address: Department of Chemistry, George Mason University, 4400 University Drive, Fairfax, VA 22030, U.S.A.

0003-2670/87/$03.50

Since the pioneering work by Dyessen et al. [8], intense activity has been directed toward improving the reliability of the numerical treatment of spectrophotometric data [9], and the increasing availability of powerful computers has lead to the development of many least-squares programs for the evaluation of equilibrium constants [9—26, 28, 29]. Of these, the most popular are LETAGROP(-VRID and -SPEFO) [10, 11], SQUAD [12], and DALSFEK [13]. All are based on the minimization of the sum (U) of the squares of the residuals, but they differ in the iterative procedures they use to approach the minimum of U: Sillén's pit-mapping procedure is used in LETAGROP together with the twist matrix method [10, 11], the Gauss—Newton method [12] in SQUAD, and the Marquardt [13, 25] method in DALSFEK. Each of these programs has distinct merits and claims specific advantages over the others. However, all require computers with large core memories and computer-experienced people. None provides any kind of direct program-operator interaction, and this lack makes it more difficult to choose the best equilibrium model.

This paper describes a new program, CFTSP, that processes spectrophotometric data taken at a fixed wavelength to find the best values of the stability constants, K, and molar absorptivities, ϵ, for the stepwise formation of mononuclear species ML_n and/or binuclear species M_2L_m, with the integers n and/or m running up to 6. CFTSP, written in FORTRAN 77, uses the steepest-descent technique to minimize the sum of the squares of the residuals. Because it requires only 20K of core-memory to process up to 150 spectrophotometric data, it can be executed on a small personal computer. It is made user-friendly by means of several conversational options that facilitate the often difficult search for the best equilibrium model.

All the calculations were performed on an INTEL 330 microcomputer system provided with the iRMX.86 operating system. Briefly annotated listings of CFTSP may be obtained on request from one of the authors (T. R.).

PROGRAM OVERVIEW

The program CFTSP consists of a main section (INOUT) and six subroutines (PPLOT, STAT, CFT4, ERSUM, CALC, and VARPR). Their interaction scheme is shown in Fig. 1.

The routine INOUT manages the conversational input/output of the data. It also organizes the next operations to be undertaken, according to a menu-type dialogue with the operator, after a fit of the guessed model to the data has yielded a convergence. The input data consists of N pairs of values of the total concentrations of metal and ligand, $(c_M^T)_i$ and $(c_L^T)_i$, respectively, which are the independent variables; N corresponding values of the absorbance A_i^{obsd} at a fixed wavelength, which is the dependent variable; and initial estimates of the parameters K_n and ϵ_n for the species involved in the assumed model. Provision is made for the possibility that one or more of the values of these parameters will be known independently and hence not subject to

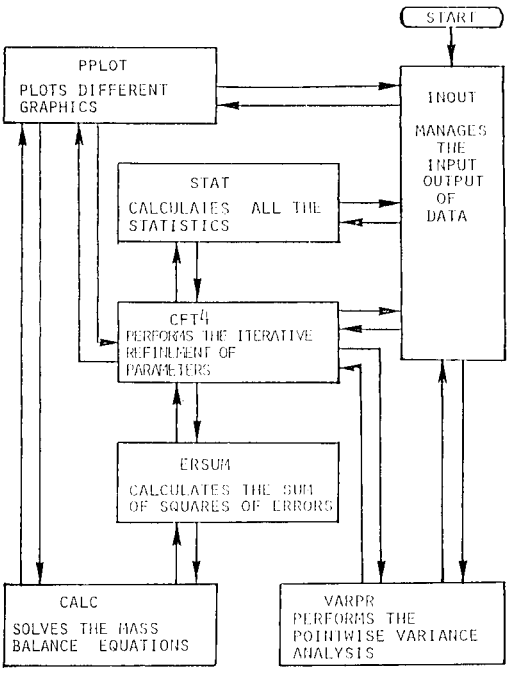

Fig. 1. Block diagram of CFTSP.

refinement by the iterative least-squares procedure. An example of a situation in which this provision is useful will be given in a later section. Finally, INOUT requires some data to make up the internal vectors that describe the stoichiometry of each complex in the guessed model, and some control parameters needed in refining the values of the parameters.

Subroutine CFT4 manages the iterative procedure of finding the values of the parameters that correspond to the minimum on the error surface. It is based on a widely used program [29] that performs non-linear regression analysis by a modified steepest-descent technique together with an extrapolation procedure that speeds convergence.

The CALC routine computes the equilibrium concentrations of all the species, utilizing only the current set of equilibrium constants and the mass-balance equations. This subroutine was written to permit testing different equilibrium models, all involving stepwise formation of the species ML_n and/or M_2L_m, without requiring the user to rewrite the relevant equations for each model tested. By using a special program written in this laboratory [30], it was ascertained that most of the time needed to refine the values of the parameters is spent in solving the mass-balance equations. Several algorithms were therefore tested to optimize the speed of convergence of the subroutine CALC. The successive approximation method was slow and often divergent. The Newton—Raphson method was fast, but gave rise to the

awkward necessity of codifying a different set of analytical derivatives for each model to be tested, and it had a high probability of being divergent [26]. The bisection algorithm [31] was quite slow but was always convergent provided that the search of the roots $(c_L)_i$ and $(c_M)_i$ was begun in the concentration ranges of the metal or ligand delimited by the values zero and $(c_M^T)_i$ or $(c_L^T)_i$. The bisection method was chosen here for solving the mass-balance equations because it is the most robust method, but a quadratic interpolation was added to calculate the next abscissa point that iteratively approaches the real root. This greatly improved the speed of convergence, so that it approached that of the Newton—Raphson method.

The ERSUM routine calculates the absorbance A_i^{calc} of each data point from Beer's law and the equilibrium concentrations of all the species according to CALC, and then sums the squares of the differences $(A_i^{calc} - A_i^{obsd})$. According to an option provided in INOUT, U may be computed as either

$$U_a = \sum_{i=1}^{N} w_i(A_i^{calc} - A_i^{obsd})^2$$

or

$$U_r = \sum_{i=1}^{N} [(A_i^{calc} - A_i^{obsd})/(A_i^{calc} A_i^{obsd})^{1/2}]^2$$

depending on whether it is the absolute or relative errors in the observed absorbances that are believed to be randomly distributed. The value of the weighting factor w_i should be assumed proportional to the inverse of the variance of A_i^{obsd}. The expression for U_r includes a weighting factor that is inversely proportional to the square of the absorbance, modified according to Kohman [27].

The subroutine STAT computes some quantities that aid in estimating the goodness of the fit and in testing the hypothesis represented by the model used. The standard deviation, SD, or the relative standard deviation, RSD, of the residuals represents the random errors in the experimental measurements, if the model is correct, and can be used to evaluate the goodness of the fit of the model to the experimental data. The fit may be considered satisfactory if $SD \leqslant 2s$ [28], where s is the standard error of the absorbance measurements estimated in absence of systematic errors. In addition, STAT calculates the Hamilton R_H-factor, defined as

$$R_H = [\sum_{i=1}^{N} w_i(A_i^{obsd} - A_i^{calc})^2 / \sum_{i=1}^{N} w_i(A_i^{obsd})^2]^{1/2}$$

and the limit value of the R_H-factor

$$R_{lim} = [\sum_{i=1}^{N} w_i u_i^2 / \sum_{i=1}^{N} w_i(A_i^{obsd})^2]^{1/2}$$

where u_i are the residuals calculated from pessimistic estimates of the errors in all the experimental quantities using error propagation rules. If $R_H < R_{lim}$, the fit may be judged acceptable. The values of R_H can also be conveniently used to choose between two different models by applying the R-factor ratio test [3, 23, 32]. Finally, STAT calculates the statistic χ^2 to ascertain whether or not the distribution of the absorbance residuals matches the expected one [33]. All these statistics aid the experimenter in evaluating the reliability of the results but should be taken "cum grano salis", as suggested also by other authors [9, 13, 34].

The subroutine VARPR provides estimates of the standard errors of the refined parameters [35]. The procedure consists of changing a single absorbance value A_i^{obsd} by a suitable quantity ΔA_i^{obsd} without changing any of the other $(N - 1)$ observed absorbances, and calculating a new set of parameters that yields the best fit. It is then possible to calculate the contribution of the ith absorbance to the variance of the nth parameter through the equation

$$s_{i,n}^2 = (\Delta K_n/\Delta A_i^{obsd})^2 s_i^2 \quad \text{or } (\Delta \epsilon_n/\Delta A_i^{obsd})^2 s_i^2$$

where s_i is the standard error of A_i^{obsd}. After N repetitions of the procedure of changing one A_i^{obsd} at a time, the standard error of the nth parameter

$$s_n = [\sum_{i=1}^{N} (s_{i,n}^2)]^{1/2}$$

can be obtained.

Finally, the subroutine PPLOT interactively displays or plots different graphics that portray the effects of the variables on the equilibrium concentrations and other aspects of the behavior of the model employed. If suitably exploited, the potentiality of interactive graphics may be very effective.

Description of the dialogue

Table 1 shows an example of the dialogue between the program and the operator. It refers to the stepwise formation of the mononuclear species ML, ML_2, ML_3, and ML_4. The parameters K_1 and ϵ_1, which pertain to the species ML, are supposed to be known and are not refined. For each parameter to be refined, a relative increment width Δ_n^0 and an indication of the certainty of the sign of the parameter must be provided. Δ_n^0 is the initial value of the quantity Δ_n by which the nth parameter is changed. It varies during the refinement, becoming smaller as the fit converges.

In order to save computational time, it is possible to choose the "sign certain" option. CFTSP then prevents the calculation of chemically meaningless negative values of the equilibrium parameters. To do this, it adjusts the value of each parameter by multiplying or dividing it by $(1 + \Delta_n)$; because Δ_n is always positive, this changes the absolute value of the parameter but not its sign. It is also possible to run the program under the "sign uncertain" option, which allows the signs of the parameters to change during the adjustment. This option is provided because the iterative procedure of CFT4

TABLE 1

Output of the computer-operator dialogue

```
HEAD ?      MODEL ML,ML2,ML3,ML4
INPUT:      RANDOM ERRORS: 1=RELATIVE, 0=ABSOLUTE ?      0
            SIGN OF PARAMETERS: 1=CERTAIN, 0=UNCERTAIN ?      1
            NUMBER OF DATA POINTS ?      81
            NUMBER OF COMPLEXES ?      4
            IS THERE ANY BINUCLEAR COMPLEX ?      NO

BEFORE WRITING THE INITIAL ESTIMATES OF PARAMETERS DEFINE
IF THEY ARE FIXED(F) VARIABLE(V) OR ABSENT(A).
THE INITIAL ESTIMATES MUST THEN BE FOLLOWED BY THEIR RELATIVE
INCREMENT WIDTHS.

ML......K(1),E(1)      F 116.0   0 F 5000    0
ML2.....K(2),E(2)      V 100.0 .5 V 10000 .5
ML3.....K(3),E(3)      V 5.0     .5 V 10000 .5
ML4.....K(4),E(4)      V 100.0 .5 V 10000 .5
M@L.....E(M),E(L)      F 0.0     0 F 0.0     0

PRINT CYCLE: 0=FINAL, N()0)=EVERY NTH CYCLE ?      0
INPUT THE ESTIMATED ABSORBANCE ERROR      0.0001
ALL OK FOR DATA INPUT?      YES



CFTSP MULTIPARAMETRIC CURVE-FITTING
MODEL ML,ML2,ML3,ML4
350 CYCLES

K(1)=1.16000E+02      E(1)=5.00000E+03
K(2)=2.01253E+01      E(2)=7.98489E+03
K(3)=1.03053E+00      E(3)=3.20764E+04
K(4)=2.93553E+01      E(4)=9.35680E+03
E(M)=0.00000E+00      E(L)=0.00000E+00

SUM(DEV)^2=2.178416E-07      STD.DEV.(SD)=5.46272E-05
HAMILTON R-FACTOR=5.88293E-06      R-LIMIT=2.2429E-05
CHI^2=1.172249E+01      (N. OF CLASSES=12)

DO YOU WANT:
1) TO RESTART
2) DATA PRINTOUT
3) TO PLOT THE RESIDUALS
4) TO PLOT THE DISTRIBUTION DIAGRAM
5) PARTIAL ABSORBANCE PRINTOUT
6) PARTIAL ANALYSIS
7) VARPR
8) END

TYPE ?      6

ALPHA'S: REL. ABS.(1) OR REL. CONC.(2) RATIOS ?      1
INPUT THE CONSTRAINS FOR THE ALPHA OF:
ML=      0.5
ML2=     1.0
ML3=     1.0
ML4=     1.0

THE SORTING HAS ISOLATED  23 DATA
DO YOU WANT TO PROCESS(0) OR TO REJECT(1) THEM ?      1

DO YOU WANT OPTION NUMBER ?      8

STOP
```

occasionally tended to force one or more of the values of ϵ_n to assume negative values. This occurrence, which is well known in the literature [11, 20, 21, 24] usually indicates that the guessed model is not correct, but it may also mean that the model is correct and that the path to the minimum has to pass through a region of negative values for some of the ϵ_n values. Under the "sign uncertain" option, the program can overcome this condition and converge to the correct values of the parameters, and has done so in several of our fits.

As a general rule, once the fit has converged, the operator can select different options to verify the reliability of the results as well to test whether another hypothesis might fit the same data. Option 1 starts a new refinement. Option 2 prints out the values of absorbances calculated with the optimized set of constants, the absorbance residuals, and the ratios $(A_i^{\text{obsd}} - A_i^{\text{calc}})/\text{SD}$. Option 3 produces a plot of the absorbance residuals against log $(c_{\text{L}})_i^{\text{calc}}$, in which $(c_{\text{L}})_i^{\text{calc}}$ is the concentration of the free ligand for the ith data point according to the best values of the equilibrium constants. This plot allows one to ascertain whether there is a non-random trend over any limited range of concentrations of the ligand, which would be indicative of a poor fit [36—38]. Option 4 plots the distribution curves for the system, and also the absorbance that is due to each species. Both these diagrams are plotted against log $(c_{\text{L}})_i^{\text{calc}}$. Option 5 gives a pointwise printout of the concentration of each species and of its contribution $(A_{\text{ML}_n})^{\text{calc}}$ to the total absorbance. Option 6 starts the procedure "partial analysis" that allows the sorting of a subset of data points all having some common features. For instance, it can be useful, after a preliminary fit, to isolate from the original data the points for which the ratios $c_{\text{M}}^{\text{T}}/c_{\text{L}}^{\text{T}}$ are so high that the species ML predominates in the equilibrated mixtures. A subsequent fit of the same model to this subset of data will converge to a more precise value of the first formation constant K_1. It might be no less useful to discard the sorted subset and fit the guessed model to the remaining data points, thereby attenuating the effect of the species ML to obtain more precise values of the formation constant of ML_2, ML_3, etc. It is also possible to sort the data with respect to the ratios $(c_{\text{ML}_n}/c_{\text{L}}^{\text{T}})$ and $(A_{\text{ML}_n}^{\text{calc}}/A^{\text{obsd}})$. Points that give rise to a value of the selected ratio that exceeds or equals some specified value can thus be grouped in a subset, which may either be rejected or be subjected to a new refinement. Option 7 starts by asking the operator to identify the set of parameters to be tested for reliability, and uses the procedure VARPR to estimate the standard errors of those parameters. Inspection of the results allows one to obtain more precise values of any desired parameter by adding more experimental measurements of absorbance in regions of the ratio $(c_{\text{M}}^{\text{T}}/c_{\text{L}}^{\text{T}})$ that exert the greatest influence on the value of that parameter.

RESULTS AND DISCUSSION

Testing CFTSP with synthetic data

The program CFTSP was tested extensively with synthetic absorbance data calculated from different models by assuming arbitrary values, which are reported in Table 2, for the formation constants and the molar absorptivities at a fixed wavelength. The models and the species they involve were: |1, 2, 3|, ML + ML_2 + ML_3; |1, 2, 3, 4|, ML + ML_2 + ML_3 + ML_4; |1, 2, 4|, ML + ML_2 + ML_4; |1, 2, 1'|, ML + ML_2 + M_2L; and |1, 2, 3, 4, 5|, ML + ML_2 + ML_3 + ML_4 + ML_5.

For each model, 81 values of absorbance were calculated from initial concentrations of metal c_M^T in the range 0.2 M—6.0×10^{-5} M, and of ligand c_L^T in the range 0.35 M—1.0×10^{-4} M. The values of the initial concentrations were so distributed that, in the c_M^T—c_L^T plane, the points were located at the nodes of a regular net with decimal logarithmic meshes; this guaranteed, as far as possible, a uniform overlap of the zones of presence of the different species. Some of the points thus selected were dropped because they would not produce values of the absorbance between 0.1 and 3.0 with an optical path of 0.1 or 1.0 cm. A corresponding set of "dirty" data was generated for each model by simply rounding the synthetic values of the absorbances to the second decimal digit. The resulting mean error ranged from a minimum of 0.00379 for the model |1, 2, 3| to a maximum of 0.00472 for the model |1, 2, 3, 4|.

Both the clean synthetic data sets and those affected by the rounding errors were processed with CFTSP. The most important aim in this portion of the work was to ascertain how the ability of CFTSP correctly to evaluate the parameters of the model was affected by three main points: the initial estimates of the parameters, the complexity of the guessed model, and the errors affecting the data. For this purpose, at least twenty runs of CFTSP were performed for each of the models considered, varying the initial estimates of the parameters K_n and ϵ_n in a systematic and combinatorial way. The initial estimates of K_1 ranged from 5% to 1000% of the true value, this being the most robust parameter; for each of the remaining K_n, the initial estimates ranged from 5% to 200% of the true value; initial estimates of 10 000 were used for all the ϵ_n. Table 2 lists the mean value of K_n and its standard deviation for all the runs performed for each model. The values of ϵ_n provided no additional information and are consequently not reported. As can easily be seen, the accuracy and the reproducibility of the values obtained for the formation constants decrease slightly both as the number of unknown parameters increases and as the quality of the data degrades. The worst results were obtained when all the initial estimates were farthest from the true values. This was especially true for the estimation of K_3. Considering that very large ranges were used, and that a very low value was assigned to K_3, it can be concluded that generally satisfactory results are obtained. The robustness of the values of K_1 and ϵ_1 is noteworthy: each was correctly

TABLE 2

Values of the formation constants obtained from fits to the same model used in synthesizing the data[a]

Model		K_1	K_2	K_3	K_4	K_5	K_2'
|1, 2, 3|	a	116.26 ± 0.55	19.01 ± 0.78	1.12 ± 0.06			
	b	117.07 ± 1.80	18.86 ± 0.96	1.28 ± 0.32			
|1, 2, 4|	a	116.25 ± 0.76	19.00 ± 1.12		33.03 ± 3.51		
	b	116.89 ± 1.96	21.14 ± 1.44		24.97 ± 5.16		
|1, 2, 2'|	a	117.35 ± 1.88	21.27 ± 0.84				293.91 ± 8.31
	b	119.04 ± 2.27	21.49 ± 1.05				280.67 ± 23.24
|1, 2, 3, 4|	a	115.90 ± 1.23	20.22 ± 0.97	1.23 ± 0.34	28.81 ± 2.40		
	b	114.37 ± 2.75	21.46 ± 1.35	1.47 ± 0.58	23.85 ± 5.71		
|1, 2, 3, 4, 5|	a	117.15 ± 1.43	19.55 ± 0.54	1.38 ± 0.54	26.80 ± 3.80	50.13 ± 30.6	
	b	117.44 ± 1.77	18.07 ± 2.10	1.55 ± 0.90	23.47 ± 4.62	43.01 ± 39.7	

[a]Subsets a refer to data exact to four decimal places; subsets b refer to the same data rounded off to two decimal places and having mean errors ranging from 0.00379 for |1, 2, 3| to 0.00472 for |1, 2, 3, 4|. The true values of the stability constants and molar absorptivities were $K_1 = 116.0$, $K_2 = 20.0$, $K_3 = 1.0$, $K_4 = 30.0$, $K_5 = 60.0$, $K_2' = 300.0$, $\epsilon_1 = 5000$, $\epsilon_2 = 8000$, $\epsilon_3 = 33\,000$, $\epsilon_4 = 9000$, $\epsilon_5 = 9000$, and $\epsilon_2' = 9000$.

estimated within about ±2% in almost all the calculations performed, both for estimating the values of the parameters and for testing the model as described hereafter. Accordingly, a plan was tested for improving the estimates of the parameters. It consisted of fixing the values of K_1 and ϵ_1 at their respective values according to the results of the previous elaborations, while the remaining parameters were refined with a set of further elaborations using the same ranges for the initial estimates as previously described. For instance, using the fixed value $K_1 = 114.37$ gave the following results for the "dirty" data of the model |1, 2, 3, 4|: $K_2 = 20.82 \pm 1.21$, $K_3 = 1.18 \pm 0.34$, $K_4 = 26.33 \pm 3.81$. These values are both more accurate and more precise than those obtained originally.

The ability of CFTSP to force-fit a model to synthetic data originated from a different model was also investigated by fitting all the models in Table 2 to both the clean and "dirty" sets of data obtained from model |1, 2, 3, 4|. The program was unable to fit the model |1, 2, 1'| to these data because overflow errors were generated in attempting to examine too large increments for the parameter describing the equilibrium constant for the binuclear species; that is, the error sum was almost completely insensitive to this parameter. For the model |1, 2, 4|, the program could not converge to a positive value of ϵ_4. The results for the other models are reported in Table 3. The following evidence is relevant to the choice of the correct model. For the clean data of model |1, 2, 3, 4, 5|, it seems that the complex ML_5 is an artifact because the value of K_5 is extremely small and because the value of ϵ_5 undergoes large oscillations when small changes are made in the initial estimates of the parameters. "Dirty" data for the same model gave values of K_5 that did not seem unreasonable, but also gave either values of ϵ_4 that were similarly sensitive to changes in the initial estimates or values of ϵ_5 that were very small. Plots of the residuals for fits of both the clean and "dirty" data to the models |1, 2| and |1, 2, 3| showed clearly that the magnitudes of the deviations increase as the concentration of the free ligand increases, while there was no such trend in the analogous plot for model |1, 2, 3, 4|. The most objective evidence bearing on the choice of the correct model is provided by the standard deviations of the fits and by the Hamilton R-factor analysis. For the exact absorbance data (subsets a), the model |1, 2, 3, 4| is undoubtedly to be preferred because it corresponds to a sharp minimum in the standard deviation from regression. In agreement with this, the models |1, 2| and |1, 2, 3| would be rejected because they give values of R_H that are much larger than those of R_{lim}, while the R_H-factor ratio test [13, 32] leads one to reject the model |1, 2, 3, 4, 5| in favor of the model |1, 2, 3, 4|, at a level of confidence above 99.5%. For the rounded data (subsets b) the trends in the standard deviation from regression and the value of R_H are much less unambiguous, and are effective only in rejecting the models |1, 2| and |1, 2, 3|. The fact that K_1 and K_2 are nearly the same for the models |1, 2, 3, 4| and |1, 2, 3, 4, 5| might be taken to mean that these models are equally likely, and that no real evidence has been gained about the real

TABLE 3

Results of fitting different models to data synthesized for the model |1, 2, 3, 4|[a]

Model		K_1	K_2	K_3	K_4	K_5	10^3 *SD*	10^4 R_H-factor	10^4 R_{lim}
|1, 2|	a	117.84	11.10				12.871	13.840	0.224
	b	118.20	10.19				154.903	169.201	5.601
|1, 2, 3|	a	119.21	8.70	1.75			1.348	1.453	0.224
	b	119.92	11.17	1.87			54.091	58.120	5.601
|1, 2, 3, 4|	a	116.87	20.25	1.13	29.28		0.0325	0.034	0.224
	b	115.11	21.43	1.33	25.70		2.734	2.909	5.601
|1, 2, 3, 4, 5|	a	116.01	20.95	0.89	30.25	$1.7\ 10^{-5}$	0.184	0.194	0.224
	b	115.20	19.80	0.68	25.52	7.8	2.599	2.688	5.601

[a]Subsets a refer to data exact to four decimal places; subsets b refer to the same data rounded off to two decimal places. The initial estimates were: K_1 = 100.0, K_2 = 10.0, K_3 = 5.0, K_4 = 10.0, K_5 = 10.0, and 10 000 for all the ϵ_n. *SD* is the standard deviation from regression.

existence of the species ML_5. Meites [39] previously described some similarly ambiguous cases in the elucidation of the stepwise complex formation from polarographic data. In such cases of indecision, we believe that the simplest possible model should be selected, thus excluding species whose existences are poorly defined throughout the examined range of the total concentrations of the reactants.

It can be concluded that testing different models and varying the initial estimates of the parameters they entail are useful ways of obtaining sound information on the correct model and the values of the parameters. This is also true when the absorbance data are realistically rounded to the second decimal digit, provided that the program performs reliably in converging to acceptable values of the parameters within a large range of variability of the initial estimates.

Testing CFTSP with experimental data

The final test was the application of CFTSP to real chemical systems. Giacomelli et al. [40] studied the equilibrium of the species formed by addition of sodium tetraphenylborate to solutions of some Ni(II) and Co(II) Schiff bases, M(SB), such as Ni(salen), Co(salen) and Ni(salophen) in tetrahdyrofuran (THF) and acetonitrile. The authors proposed the following reactions:

$$Na^+ + M(SB) \underset{}{\overset{K_1}{\rightleftarrows}} [M(SB)Na]^+ + BPh_4^- \overset{K_0'}{\rightleftarrows} [M(SB)Na]^+, BPh_4^-$$

and evaluated the equilibrium constants K_1 and K_0' by processing absorbance data obtained at 20 wavelengths for a series of 17 solutions with different values of the ratio M(SB)/$NaBPh_4$, making use of the non-linear least-squares computer program DALSFEK [13]. The original data were separated into subsets of which each corresponded to a single wavelength, and were used as input to CFTSP. The results reported in Table 4 agree well with those

TABLE 4

Values obtained for the equilibrium constants (M^{-1}) of the reaction between tetraphenylborate and Ni(II) and Co(II) Schiff-base complexes in tetrahydrofuran (THF) and acetonitrile

System	Solvent	Results of CFTSP[a]		Literature values [40]	
		$10^{-3} K_1$	$10^{-3} K'_0$	$10^{-3} K_1$	$10^{-3} K'_0$
Co(salen)/Na^+	THF	5.1 ± 0.6	8.8 ± 0.7	5.5 ± 0.2	8.4 ± 0.3
Ni(salen)/Na^+	THF	6.6 ± 0.9	6.1 ± 0.8	6.2 ± 0.6	6.5 ± 0.5
Ni(salophen)/Na^+	CH_3CN	0.072 ± 0.005		0.074 ± 0.002	
Ni(salen)/Na^+	CH_3CN	0.095 ± 0.004		0.098 ± 0.001	
Ni(salen)/K^+	CH_3CN	0.013 ± 0.005		0.013 ± 0.007	

[a]Mean values and standard deviations from regression for absorbance data at 5 different wavelengths.

obtained from DALSFEK, but CFTSP is much easier to use and requires much less core memory. While all the electrolytes were assumed to be completely dissociated in acetonitrile [41], it was necessary to calculate the concentrations of Na^+ and BPh_4^- in equilibrium with undissociated sodium tetraphenylborate in THF, and the appropriate association constant was taken to be an additional unknown parameter in CFTSP. The value obtained by CFTSP for the association constant of sodium tetraphenylborate in THF was 11 200 ± 600 M^{-1}, in close agreement with the literature value of 10 800 M^{-1} [42]. This agreement is further proof of the ability of CFTSP to converge to reliable values.

REFERENCES

1 H. S. Rossotti, Talanta, 21 (1974) 809.
2 W. A. E. McBryde, Talanta, 21 (1974) 979.
3 F. R. Hartly, C. Burgess and R. M. Alcock, Solution equilibria, Horwood, Chichester, 1980.
4 D. J. Leggett, Am. Lab., 1982, 14(1) (1982) 29.
5 R. W. Ramette, J. Chem. Educ., 44(11) (1967) 647.
6 W. E. Wentworth, W. Hirsh and E. Chen, J. Phys. Chem., 71(2) (1967) 218.
7 K. Conrow, G. D. Thomson and R. E. Bown, J. Am. Chem. Soc., 86 (1964) 1025.
8 D. Dyessen, N. Ingri and L. G. Sillén, Acta Chem. Scand., 15(3) (1961) 15.
9 F. Gaizer, Coord. Chem. Rev., 27 (1979) 195.
10 L. G. Sillén, Acta Chem. Scand., 18 (1964) 1085.
11 L. G. Sillén and B. Warnquist, Ark. Kèmi, 31(29) (1968) 377.
12 D. J. Leggett and W. A. E. McBryde, Anal. Chem., 47(7) (1975) 1005.
13 R. M. Alcock, F. R. Hartley and D. E. Rogers, J. Chem. Soc. Dalton Trans., (1978) 115.
14 I. G. Sayce, Talanta, 15 (1968) 1397.
15 L. Lyhmn, Chem. Scripta, 10 (1976) 49.
16 P. Voznica, J. Havel and L. Sommer, Coll. Czech. Chem. Commun., 54 (1980) 45.
17 M. Meloun and J. Cermak, Talanta, 26 (1979) 569.
18 F. Gaizer and M. Mate, Acta Chim. Acad. Sci. Hung., 103 (1980) 355.

19 J. R. Siefkler, Anal. Chim. Acta, 52 (1970) 545.
20 J. J. Kankare, Anal. Chem., 42(12) (1970) 1322.
21 S. Feldberg, P. Klotz and L. Newman, Inorg. Chem., 11(12) (1972) 2860.
22 G. Heys, H. Kinns and D. Perrin, Analyst, 97 (1972) 52.
23 J. Kragten, P. G. De Jagher and L. G. Decnop-Weever, Anal. Chim. Acta, 180 (1986) 457.
24 D. J. Leggett, Anal. Chem., 49(2) (1977) 276.
25 F. Vierling, M. J. Schwing and J. Meullmstre, Spectra 2000, 79(10) (1982).
26 F. Gaizer and A. Puskas, Talanta, 28 (1981) 925.
27 T. P. Kohman, J. Chem. Educ., 47(9) (1970) 657.
28 D. J. Leggett, S. L. Kelly, L. R. Shine, Y. T. Wu, D. Chang and K. M. Kadish, Talanta, 30(8) (1983) 579.
29 T. Meites and L. Meites, Talanta, 19 (1972) 1131.
30 M. De Blasi, N. Fanelli, G. Giannelli and G. Degli Antoni, Euromicro Newsl., 3 (1977) 27.
31 R. W. Hamming and E. A. Feigenbaum, Introduction to Applied Numerical Analysis, McGraw-Hill, New York, 1971, pp. 36—44.
32 A. Vacca, A. Sabatini and M. A. Gristina, Coord. Chem. Rev., 8 (1972) 45.
33 L. Bologni, A. Sabatini and A. Vacca, Inorg. Chim. Acta, 69 (1983) 71.
34 W. F. Maddams, Appl. Spectrosc., 34(3) (1980) 245.
35 L. Meites, CRC Crit. Rev. Anal. Chem., 8(11) (1979) 1.
36 P. Gans and J. B. Gill, Appl. Spectrosc., 31 (1977) 451.
37 C. Baker, P. S. Johnson and W. F. Maddams, Spectrochim. Acta, Part A, 34 (1978) 683.
38 M. E. R. Robinson, D. I. Bower and W. F. Maddams, Polymer, 19 (1978) 773.
39 L. Meites, Talanta, 22 (1975) 733.
40 A. Giacomelli, T. Rotunno and L. Senatore, Inorg. Chem., 24 (1985) 1303.
41 H. L. Yeagen and B. Kratochvil, Can. J. Chem., (1975) 3448.
42 C. Carvajal, K. J. Tölle, J. Smidt and M. Szwarc, J. Am. Chem. Soc., 87 (1965) 5548.

Analytica Chimica Acta, 194 (1987) 91—98
Elsevier Science Publishers B.V., Amsterdam — Printed in The Netherlands

PREDICTION OF THE SEPARATION IN GAS CHROMATOGRAPHY
Application to the Analysis of Mixtures with Mixed Stationary Phases and Temperature Programming

J. SANZ* and I. MARTÍNEZ-CASTRO

Instituto de Química Orgánica General, Consejo Superior de Investigaciones Científicas, Juan de la Cierva 3, 28006 Madrid (Spain)

G. REGLERO and M. D. CABEZUDO

Instituto de Fermentaciones Industriales, Consejo Superior de Investigaciones Científicas, Juan de la Cierva 3, 28006 Madrid (Spain)

(Received 17th June 1986)

SUMMARY

A mathematical method is developed which predicts the characteristics of a gas chromatographic separation and optimizes some operational parameters. It can be used for isothermal and programmed-temperature conditions and can be applied to both packed and open tubular columns. The optimum composition of a mixed stationary phase for the separation of a complex mixture can be predicted. The method can be implemented in most microcomputers. The method proved satisfactory in obtaining good separations of moderately volatile components of wine flavours.

The gas chromatographic (g.c.) behaviour of a mixture is represented by the retention times and peak widths corresponding to the different sample components. These chromatographic variables depend on operational parameters such as carrier gas flow, temperature and column characteristics (efficiency, selectivity, etc.). The selection of column type and operating conditions is frequently based on previous knowledge and optimization is usually achieved by trial and error. When the mixture to be separated is very complex, the prediction of component separation has to be done by using mathematical methods.

Several methods [1—4] have been proposed for the prediction of chromatographic response in g.c. Some of them use simplified models (a single stationary phase, dead time is neglected); other methods require a mainframe computer.

In this work, a calculation method is developed in order to predict g.c. separation from models based on the band movement through the column. This procedure avoids the above-mentioned problems and can be implemented in a microcomputer. The method can only be applied to columns having the same permeability and phase ratio.

0003-2670/87/$03.50

THEORY

In gas chromatography, elution of the components can be characterized by three variables: t_m (a measure of the carrier gas speed), k (capacity factor, a measure of the solute retention) and w (peak width at half height, related to the resolution between components).

If it is assumed that the carrier gas behaves in the g.c. column as an ideal gas, Darcy's equation [5] can be integrated between column inlet and outlet, giving the following expression:

$$t_m = \eta\, L^2 P_o / B_o j (P_i^2 - P_o^2) \qquad (1)$$

where η is the carrier gas viscosity, L the column length, B_o the column permeability, P_i and P_o the pressure at the inlet and outlet of the column, and j the mobile-phase compressibility factor.

For columns having the same permeability and length, when P_i and atmospheric pressure (P_o) are constant, Eqn. 1 can be rewritten as t_m = (constant) η. Carrier gas viscosity can be related to temperature (T) through an expression proposed by Ettre [6]: $\eta = A(T/273)^B$. Equation 1 can then be written as $t_m = A_t\, T^{B_t}$. Both A_t and B_t can be calculated for a given column geometry, from experimental t_m values at different temperatures, by linear regression of

$$\ln t_m = \ln A_t + B_t \ln T \qquad (2)$$

In considering the capacity factor, the specific retention volume (V_g^0) is related to the vaporization molar heat (ΔH_v) by the expression [7]

$$\ln V_g^0 = (\Delta H_v / R\, T) + \text{(constant)} \qquad (3)$$

which can be rewritten as $V_g^0 = A \exp(B/T)$. For a given column, k and V_g^0 are related by

$$V_g^0 = k\ 273\ V_m / T\, \rho\ V_s$$

where V_m and V_s are the mobile phase volume and the stationary phase volume, respectively; ρ is the liquid phase density.

From these last two equations, it can be deduced that the variation of k at different temperatures can be given by

$$k = A_k\, T \exp(B_k/T) \qquad (4)$$

Although other equations were tested, the best fit from experimental k and T data was obtained from Eqn. 4.

Several equations have been proposed in the literature [2, 3, 8] in order to relate peak width and solute retention (t_r). From them, the expression selected was

$$w = a\, t_r + b \qquad (5)$$

because it is simple and gives a good fit to experimental data ($r = 0.9988$); a and b seem to be independent of column temperature. It is impossible to

predict w accurately even for columns having the same geometry, because the efficiency depends on the coating procedure, which is difficult to reproduce.

Mixed phases

There is still controversy about the calculation of k values for mixed phases [9—11]. Here, it is assumed that for a mixed phase, k can be obtained as a linear combination of the values measured on single-phase standard columns. The expression used is

$$k_{mi} = \sum_{1}^{n} f_n k_{ni} \tag{6}$$

where k_{mi} is the capacity factor in the mixed phase, and f_n and k_{ni} are the weight fraction and capacity factor, respectively, for each pure phase.

It is impossible to predict accurately the value of w for a mixed-phase column. The efficiency of the column should depend on the stationary phase used. Here, it is assumed that, other factors being equal, the peak width for a mixed-phase column can be written as

$$w_{mi} = \sum_{1}^{n} f_n k_{ni} \tag{7}$$

where w_{mi} represents the w value in the mixed phase and w_{ni} in each standard phase. However, peak width will always depend on the column efficiency. Once a given column has been prepared, w values can be calculated more accurately from experimental data by using Eqn. 5.

Programmed temperature

When temperature is continuously varied during a chromatographic run, both gas velocity and capacity factor are continuously changing. However, in a short enough time interval, the same models as used in isothermal columns are valid.

From Darcy's law, the velocity of a band after travelling a length z of the column is

$$v = L\{t_m (1 + k) j [1 + ((P_i/P_o)^2 - 1)(1 - z/L)]^{1/2}\}^{-1} \tag{8}$$

In an interval dt, Eqn. 8 becomes

$$dz/dt = L\{t_m (1 + k) j [1 + ((P_i/P_o)^2 - 1)(1 - z/L)]^{1/2}\}^{-1} \tag{9}$$

If J_p is defined as

$$J_p = j [1 + ((P_i/P_o)^2 - 1)(1 - z/L)]^{1/2}$$

then

$$(J_p/L)\, dz = [t_m (1 + k)]^{-1}\, dt \tag{10}$$

Equation 10 can be integrated between column inlet ($z = 0$, $t = 0$) and outlet ($z = L$, $t = t_r$):

$$\int_0^L (J_p/L)\, dz = \int_0^{t_r} [t_m (1 + k)]^{-1}\, dt \tag{11}$$

The term J_p/L can be written as $(K_1 + zK_2)^{1/2}$

where $K_1 = P^2 j^2/L^2$ and $K_2 = (1-P^2) j^2/L^3$ for $P = P_i/P_o$. The left side of Eqn. 11 can then be integrated to give

$$\int_0^L (J_p/L)\, dz = 1 \tag{12}$$

Equation 11 can then be solved by a numerical procedure, supposing that for small time intervals

$$\int_0^{t_r} [t_m (1 + k)]^{-1}\, dt = 1 = \sum_{t=0}^{t=t_r} \Delta t/[t_{m_t}(1 + k_t)] \tag{13}$$

where k_t and t_{m_t} are the values of capacity factor and dead time at the temperature in a time fraction Δt.

According to Harris and Habgood [12], the peak width of a solute in a programmed-temperature system is similar to the width obtained for the same compound in isothermal conditions at the retention temperature. Although some authors disagree with this view [13], it was found here that this model is accurate enough for the purposes.

METHOD OF CALCULATION

The calculations were done on a microcomputer and all programs were written in BASIC. A chart flow of the program is shown in Fig. 1. The input data for each column include retention times of each solute, dead times at (at least) three column temperatures, and peak widths of solutes of different retention times. The first program (P1) creates input files for the experimental data. P2 uses a linear regression method in order to calculate A_t, B_t, A_k, B_k, a and b values. A_k and B_k can be improved optionally (P3) in order to achieve the best fit in the least-squares sense. P4 calculates t_r and w for a column having the same geometry as that used to obtain A_k and B_k (Fig. 1, path 1) or for columns of different geometry where a, b, A_t and B_t values must be obtained (path 2). The phase ratio must be the same for the original and predicted columns.

These programs can be used in order to optimize the separation in two ways: (1) to obtain the conditions which afford the best resolution for the least resolved pair of solutes, and (2) to optimize the separation of the highest possible number of solutes. A program listing can be obtained from the authors.

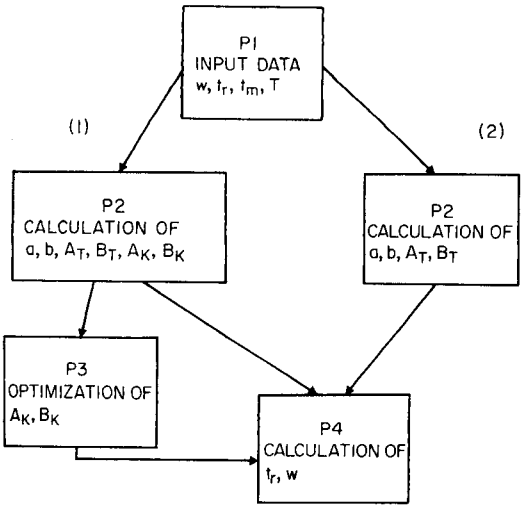

Fig. 1. Flow chart of the programs used in the calculation of t_r and w: (1) same geometry; (2) different geometry.

EXPERIMENTAL

In order to check the proposed models, a column was designed for the separation of eight selected solutes. These were chosen among the most common components of alcoholic beverage flavours, namely, 2-phenylethanol, geraniol, cinnamaldehyde, γ-butyrolactone, ethyl decanoate, ethyl dodecanoate, hexyl hexanoate and 2-phenylethyl acetate.

This mixture was chromatographed on three micropacked columns [14] (deactivated glass pyrex tube, 3 m × 0.80 mm i.d.); the solid support was Volaspher A-2, 120—140 mesh, coated with 4% OV-1, Superox 20M or SP-2310. The carrier gas was nitrogen at a constant pressure drop (2.5 kg cm^{-2}). The permeability and phase ratio were approximately the same for all columns.

In every column the following measurements were made: (a) t_m at four different temperatures, (b) t_r of every solute at three different temperatures, and (c) at least six t_r and w values at different temperatures.

Calculations were done on a Olivetti M-20 microcomputer. The time taken was not large (2—3 h) and did not cause practical troubles.

RESULTS AND DISCUSSION

Tables 1 and 2 show the values of A_t, B_t, A_k, B_k, a and b obtained for each standard column under isothermal conditions. In all cases, the values of the regression coefficients were good.

The maximum resolution of the least-resolved pair of peaks for the flavour mixture was predicted to be achieved for a 3-m column containing a

TABLE 1

Values of A_t, B_t, a, b and their correlation coefficients for the three stationary phases

Column	Set 1[a]			Set 2[b]		
	A_t	B_t	r	a	b	r
OV-1	0.0204781	0.665098	0.9792	0.109645	0.112646	0.9987
SP-2310	0.0008059	1.222430	0.9980	0.213992	0.116269	0.9980
Superox 20M	0.0011727	1.154450	0.9631	0.134132	0.480038	0.9958

[a]Calculated from $t_m = A_t T^{B_t}$. [b]Calculated from $w = a t_r + b$.

TABLE 2

Values of A_k and B_k and correlation coefficients from Eqn. 4 for the compounds and phases selected

Solute	OV-1			Superox 20M			SP-2310		
	A_k	B_k	r	A_k	B_k	r	A_k	B_k	r
2-Phenylethanol	9.65025	5.50923	0.9998	0.79991	7.37838	0.9997	2.93852	6.78833	0.9997
Geraniol	3.47216	6.19515	0.9997	0.56652	7.40474	0.9998	0.55593	7.27359	0.9998
Cinnamaldehyde	9.61060	5.81152	0.9999	1.41565	7.35104	0.9998	2.20169	7.24902	0.9995
γ-Butyrolactone	40.33020	4.47185	0.9997	11.19220	5.82821	0.9998	26.78230	5.78951	0.9997
Ethyl decanoate	1.57658	6.79144	1.0000	1.63818	6.59625	0.9998	0.45162	7.04306	0.9996
Ethyl dodecanoate	0.82940	7.47256	0.9999	1.89327	6.3428	0.9999	0.19140	7.72116	0.9997
Hexyl hexanoate	1.79600	6.71536	0.9999	2.06928	6.43602	0.9996	0.55448	6.90506	0.9952
2-Phenylethyl acetate	6.96725	5.88983	0.9999	0.85928	7.20882	0.9993	1.19992	7.07115	0.9989

TABLE 3

Experimental and calculated t_r and w values of the selected compounds on the mixed-phase column. Column: deactivated glass pyrex tube, 3 m × 0.80 mm i.d. Solid support: Volaspher A-2, 120—140 mesh, coated with 4% of a mixed phase composed of 55% OV-1 and 45% Superox 20M; t_m = 1.05 min. Temperature program: 60°C, 3°C min^{-1}, 180°C.

Solute	t_r (min)		w (min)	
	Exper.	Calc.	Exper.	Calc.
2-Phenylethanol	32.76	32.48	0.28	0.28
Geraniol	32.09	31.71	0.26	0.28
Cinnamaldehyde	37.10	37.24	0.34	0.30
γ-Butyrolactone	21.57	21.19	0.28	0.28
Ethyl decanoate	30.04	30.08	0.28	0.28
Ethyl dodecanoate	38.74	38.74	0.32	0.29
Hexyl hexanoate	29.29	29.22	0.24	0.29
2-Phenylethyl acetate	30.92	30.98	0.20	0.28

mixed phase composed of 55% OV-1 and 45% Superox 20M. The optimum predicted temperature program was 60°C, 3°C min^{-1}, 180°C. Table 3 shows the calculated and experimental values of t_r and w. Optional iteration did not improve the results.

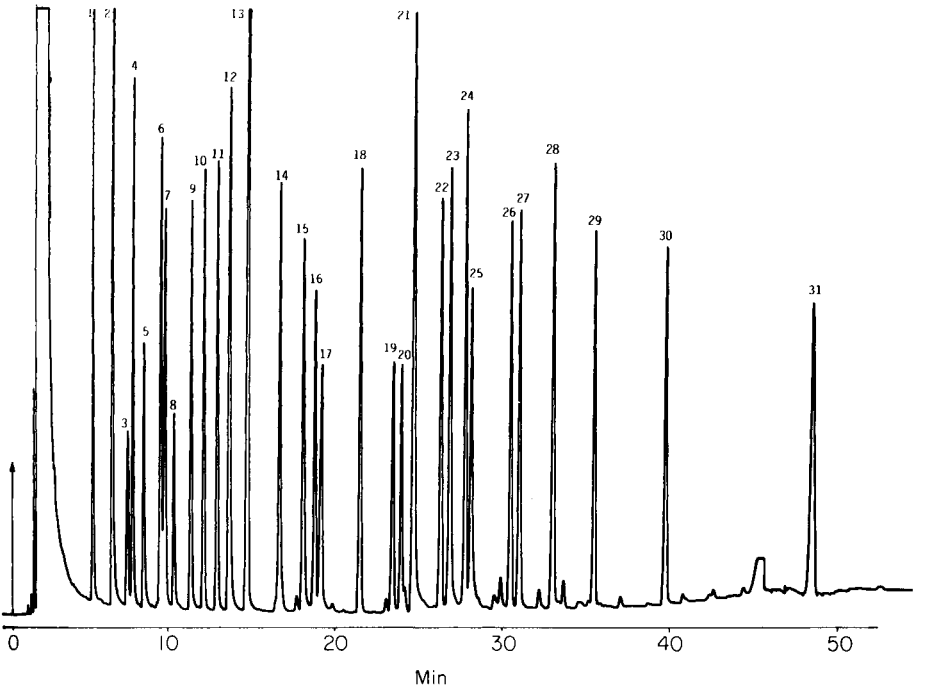

Fig. 2. Chromatographic separation of a mixture containing some medium-volatility components of wine flavour. Micropacked column (10 m × 0.85 mm) with a stationary phase of 5% OV-1/Superox 20M/SP-2310 (80:10:10) on Volaspher A-2 (120—140 mesh). Initial temperature 60°C, programming rate 3°C min^{-1}, final temperature 200°C, hydrogen carrier gas. Peaks: (1) isoamyl alcohol; (2) acetoin; (3) *trans*-2-hexenal; (4) ethyl pyruvate; (5) ethyl lactate; (6) 1-hexanol; (7) *cis*-3-hexen-1-ol; (8) *trans*-2-hexen-1-ol; (9) furfural; (10) ethyl hexanoate; (11) hexyl acetate; (12) 1-heptanol; (13) benzaldehyde; (14) ethyl heptanoate; (15) methyl octanoate (internal standard); (16) linalol; (17) γ-butyrolactone; (18) ethyl octanoate; (19) ethyl succinate; (20) α-terpineol; (21) benzyl alcohol; (22) ethyl nonanoate; (23) 2-phenylethanol; (24) 2-phenylethyl acetate; (25) geraniol; (26) hexyl hexanoate; (27) ethyl decanoate; (28) cinnamaldehyde; (29) ethyl undecanoate; (30) ethyl dodecanoate; (31) ethyl tetradecanoate.

A mixed-phase column was also designed in order to separate the components of wine flavour having medium volatility. The highest number of resolved peaks was obtained by using the column and conditions shown in Fig. 2.

These results provide strong support for the validity of the method.

This work was made possible by financial assistance from the Comision Asesora de Investigacion Científica y Técnica, Project 237/84. One of us (G.R.) is also grateful to the Consejo Superior de Investigaciones Científicas for a grant. The authors thank Dra. M. Herraiz, C.S.I.C., and Dr. J. Almy, California State University, Stanislaus, for their critical review.

REFERENCES

1 M. J. Molera, J. A. García-Domínguez and J. Fernández Biarge, J. Chromatogr. Sci., 11 (1973) 538.
2 V. Bartu, J. Chromatogr., 260 (1983) 255.
3 V. Bartu and S. Wicar, Anal. Chim. Acta, 150 (1983) 245.
4 L. Podmaniczky, L. Szepesy, K. Lakszner and G. Schomburg, Chromatographia, 20 (1985) 623.
5 R. J. Laub and R. L. Pecsok, Physicochemical Applications of Gas Chromatography, Wiley, New York, 1976, p. 17.
6 L. S. Ettre, Chromatographia, 18 (1984) 243.
7 R. J. Laub and R. L. Pecsok, Physicochemical Applications of Gas Chromatography, Wiley, New York, 1976, p. 111.
8 T. W. Smuts, T. S. Buys, T. G. du Toit and J. N. du Toit, J. High Resolut. Chromatogr. Chromatogr. Commun., 4 (1981) 358.
9 R. J. Laub and J. H. Purnell, J. Chromatogr., 112 (1975) 71.
10 J. K. F. Huber, E. Kenndler and H. Markens, J. Chromatogr., 167 (1978) 291.
11 P. Sandra and M. Van Roelenbosch, Chromatographia, 14 (1981) 345.
12 W. E. Harris and H. W. Habgood, Programmed Temperature in Gas Chromatography, Wiley, New York, 1966, p. 115.
13 J. S. Fritz and D. M. Scott, in J. Gasparic (Ed.), Chromatographic Data, Elsevier, Amsterdam, 1983, p. 193.
14 G. Reglero, M. Herraiz, M. D. Cabezudo, E. Fernández-Sánchez and J. A. García-Domínguez, J. Chromatogr., 348 (1985) 327.

Analytica Chimica Acta, 194 (1987) 99—107
Elsevier Science Publishers B.V., Amsterdam — Printed in The Netherlands

INTEGRATED SYSTEM FOR POTENTIOMETRIC STRIPPING DETERMINATIONS

LAURIE E. LOCASCIO[a] and JIŘÍ JANATA*
Center for Sensor Technology, University of Utah, Salt Lake City, UT 84112 (U.S.A.)
(Received 28th April 1986)

SUMMARY

An automatic system for potentiometric stripping was designed and tested for the determination of lead(II) and cadmium(II) in the 10^{-3}—10^{-6} M range. It consists of solid-state integrated circuitry containing a chemically-sensitive field-effect transistor (CHEMFET) and a transistor control switch. Flow of solutions, application of potentials during the electrode preparation, plating and stripping periods and data acquisition are controlled by a cheap microprocessor. It is shown that 200-μl samples in the concentration range mentioned above can be dealt with in less than 2.5 min with relative standard deviations below 10%. The detection limit of the system is at present restricted by the slow sampling rate of the microprocessor used. The upper value of the usable concentration range is limited by the maximum practical concentration of the oxidant.

Potentiometric stripping methods have several advantages over other available procedures for the determination of trace metals [1—4]. The most obvious advantage is that several different metals can be quantified simultaneously in a small volume of a single sample. This paper describes a system in which the plating/stripping cycle is performed on a specially designed integrated circuit chip [5, 6] and the sample manipulation is done by a flow-injection manifold based on solenoid valves [7]. The operation of the system is controlled with an inexpensive VIC-20 Commodore microprocessor.

EXPERIMENTAL

Description of the system

Integrated circuit. A chemically-sensitive field-effect transistor (CHEMFET) with a resistively coupled gate [5, 6] was used in this work. The chip contains two n-channel field-effect transistors (FET), one CHEMFET and one metal-oxide semiconductor field-effect transistor (MOSFET); the latter will be referred to as the control FET. The schematic diagram of the integrated circuit chip is shown in Fig. 1 inside the area bordered by the dashed line. The CHEMFET gate is covered with a thin layer of platinum for the

[a]Present address: National Bureau of Standards, Analytical Chemistry Division, Washington, DC 20234, U.S.A.

0003-2670/87/$03.50

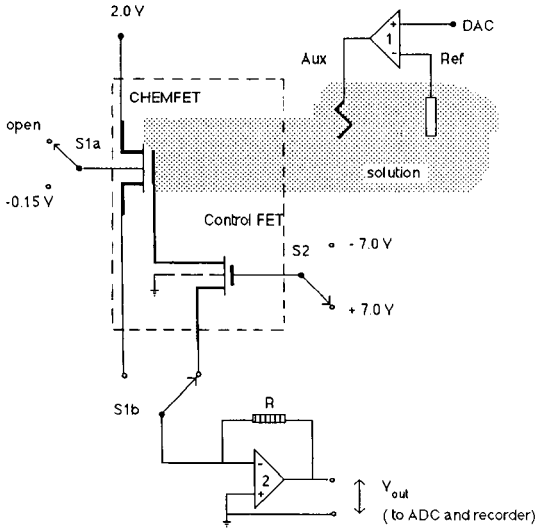

Fig. 1. Circuit diagram of the integrated potentiometric stripping system. The auxiliary electrode (Aux) is connected to the output of operational amplifier 1 and supplies the necessary current to maintain a constant potential on the reference electrode (Ref). A D/A converter which is connected to the positive input of the same amplifier sets the potential of the reference electrode. S1a and S1b are switched by a DPDT relay and S2 is switched independently by an SPDT relay. When S1a, S1b, and S2 are in the positions shown in the diagram, the CHEMFET is in the plating mode. When S1a, S1b, and S2 are in their alternative positions, the CHEMFET is in the stripping mode. The output voltage of operational amplifier 2 is recorded during the stripping cycle. The value of feedback resistor R is 25.9 kohms. The part of the circuit inside the dashed line area is on one integrated silicon chip.

purpose of making ohmic contact to the solution. There are direct outside connections to the gate and source electrodes of the control FET, and the drain of the control FET is connected to the platinum gate of the CHEMFET. Therefore, when the control FET is biased fully on (+7.0 V), the voltage applied to the control drain becomes the voltage applied to the CHEMFET gate which acts as a platinum electrode onto which the mercury film can be deposited. The CHEMFET gate becomes isolated and is electrically floating when the control gate is biased fully off (—7.0 V). In that case the drain current in the CHEMFET is controlled by the total applied voltage on the gate which contains the contribution from the mercury/solution interface. Thus, by using this integrated circuit, one has the means to switch from plating to stripping without the need for additional external instrumentation.

The current flowing through the CHEMFET is converted to a voltage (amplifier 2). This voltage is then related to the voltage on the CHEMFET platinum gate by the gain factor of the device and by the gain factor of the current-to-voltage converter. The current follower output is digitized with a standard A/D converter.

It is important that during the stripping cycle all potentials at the CHEMFET gate are held constant except that of the mercury/solution interface. That potential is the only variable during the stripping cycle so that the current change in the CHEMFET is a true representation of the reaction being monitored.

In a typical Hg/Pt junction, formation of intermetallic species may account for an interfering potential change and would appear as drift in the signal. When mercury is plated onto the platinum electrode, the two metals amalgamate and form compounds of $PtHg_2$, and $PtHg_4$ [8]. Sufficient time must be allowed for amalgamation prior to the measurement step, otherwise this reaction will generate a time-varying potential and distort the signal. A waiting period of 1 h is sufficient to make the film stable enough to minimize the drift.

Flow-injection manifold. Pressurized helium was used for propulsion of the solution through the flow-injection manifold. Micro-miniature solenoid pinch valves (Angar Scientific Company, Model 401) were used [7] and were activated by the microprocessor. Because the VIC-20 5-V power supply with a 100-mA maximum rating was not sufficient to activate the valves, an auxiliary power supply was used in conjunction with a relay-driver chip to provide the necessary power.

A diagram of the final flow manifold is presented in Fig. 2. In the configuration shown, valves V4 and V5 are open and sample is aspirated into the sample loop. When V3 and V6 are open, the sample is injected as carrier is propelled through the system. When V1 and V6 are open, background electrolyte flows through the system. Valves V7 and V2 can be opened independently to allow detergent and precoating solution to pass through the flow cell. At the flow rate of 1 ml min^{-1}, it takes approximately 2 min for injected solution to pass from the sample loop (SL) to the flow cell (FC). Therefore, in order to reduce the overall measurement time, the detergent and the precoating solution pass only through the flow cell and bypass the rest of the manifold. The manifold was made from 0.5 mm i.d. teflon tubing; the distance from the sample loop to the flow cell was 10 cm.

Microprocessor control. The circuit used for the control of the plating and stripping cycles is based on a Commodore VIC-20 personal computer. This computer is user-friendly, expandable and inexpensive compared to other available microprocessors; however, it is relatively slow.

The control circuit (Fig. 1) applies a positive voltage to the reference electrode while grounding the platinum gate of the CHEMFET during the plating of a metal onto the gate. In that case, all grounds are connected together so that the CHEMFET gate is negative with respect to the Ag/AgCl reference electrode during the plating cycle. The chip is fabricated in such a way that there is direct access to the gate region through the control FET when it is biased fully on [5]. Therefore, a positive potential of 7.0 V is applied to the gate of the control FET through which the platinum CHEMFET gate can be

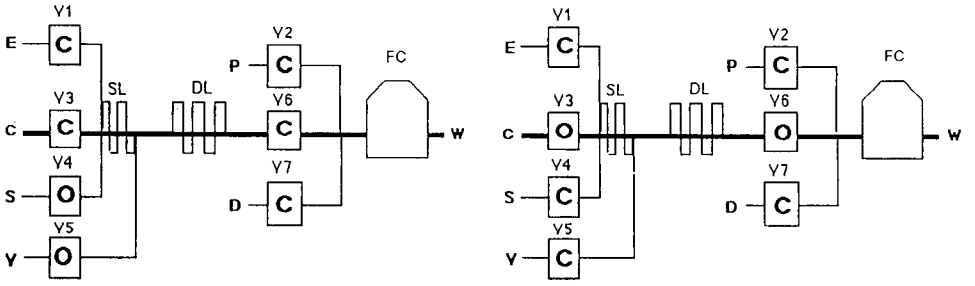

Fig. 2. Diagram of the flow-injection system. The symbol C indicates when the solenoid valves V1—V7 are closed and O indicates when they are open. The symbols in the figure are defined as follows: (E) background electrolyte, 0.1 M HNO_3; (C) carrier solution, $Hg(NO_3)_2$/0.2 M sodium acetate/0.1 M HNO_3; (S) sample solution, metal ion/0.2 M sodium acetate/0.1 M HNO_3; (V) vacuum (15 cm Hg); (P) precoating solution, 1 mM $Hg(NO_3)_2$/0.1 M $HClO_4$; (D) detergent, 0.3% Brij-35 in 0.1 M HNO_3; (SL) sample loop; (DL) dispersion loop; (FC) flow cell; (W) waste. The system is shown with valves in the "filling" position. For "injection" (right side), only V3 and V6 are open.

grounded during the plating cycle. The potential applied to the reference electrode is set by the output voltage of the digital-to-analog converter between 0.0 and ±5.0 V. The range up to +5 V applied to the auxiliary electrode (amplifier 1) is needed in precoating the mercury film and in plating metals onto the working electrode, while the —5 V range is used to clean the CHEMFET gate surface.

In the process of switching from the plating cycle to the stripping cycle, three changes must take place in the circuit configuration: (1) the control FET must be biased fully off so that the CHEMFET platinum gate region becomes electrically floating and its potential with respect to the solution is dictated only by the chemical reaction which is taking place at the mercury film/solution interface; (2) the bias on the substrate of the FET must be changed from ground to a small negative potential in order to ensure that there is no leakage of current through the substrate p/n junctions; and (3) the CHEMFET source must be connected to the input of the current follower (amplifier 2) which registers the variation in the drain-source current during the stripping part of the cycle. This output is also recorded by an analog-to-digital converter and is stored into system random access memory. Data are gathered at a sampling rate of 100 Hz, and are transferred to a sequential file on the Commodore 1541 disk drive.

The source and substrate of the CHEMFET are connected to a double-pole double-throw relay which is switched after the plating time indicated by the user. At this time, the voltage on the gate of the control FET is switched from +7.0 V to —7.0 V. This serves to isolate the CHEMFET gate electrically as mentioned above. Simultaneously, the substrate goes from ground to —0.15 V, and the CHEMFET source, which was floating, is now connected to the input of a current-to-voltage converter. The timing diagram for the whole procedure is shown in Fig. 3.

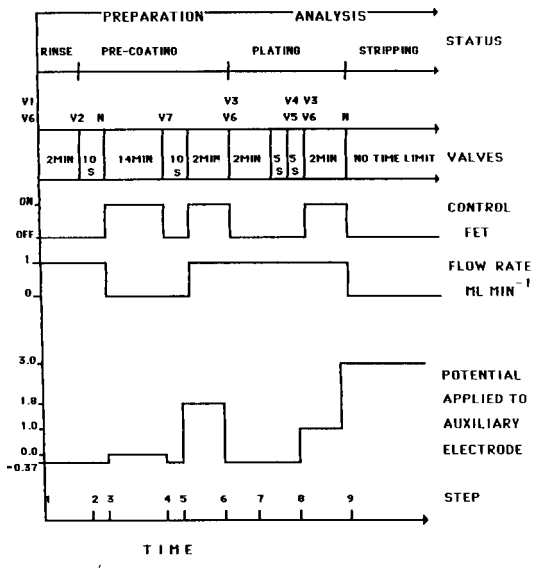

Fig. 3. The timing diagram. When the control FET is ON, the potential at the working electrode has the same magnitude (but opposite polarity) as that shown for the auxiliary electrode.

Solutions and electrodes

Solutions were prepared from triply distilled water and reagent-grade chemicals. Stock sample solutions were 10^{-2} M lead(II) nitrate and cadmium-(II) nitrate in 0.1 M nitric acid. After dilution, sodium acetate was added to the final sample solutions to a final concentration of 0.2 M to serve as the background electrolyte. These solutions will be referred to in the following sections as the plating solution and sample solution, respectively. The stripping (oxidizing) solution was 0.02 M mercury(II) nitrate in 0.1 M nitric acid. A 1.0 mM solution of mercury(I) nitrate dissolved in 0.1 M perchloric acid was used as the precoating solution to create the mercury film. A 0.3% solution of Brij-35 (Sigma Diagnostics, 30% w/v) in 0.1 M nitric acid was used to eliminate bubble formation in the flow cell.

A home-made silver/silver chloride double-junction electrode with saturated KCl and a 4 M KNO_3 salt bridge was used as the reference electrode. A platinum wire was used as the auxiliary electrode and the platinum gate of the CHEMFET was the working electrode with an area of 0.15 mm^2. It was cleaned before use by placing it in an oxygen radio-frequency plasma for 1 h in order to remove organic deposits. The preparation and encapsulation of the CHEMFET integrated circuit has been described previously [5, 6].

Procedure

The stripping solution, which contained the oxidizing species, mercury-(II), was deaerated for 15 min under vacuum of 15-cm Hg created with a

Nalgene hand-held pump in order to prevent the trapping of air bubbles in the manifold. It was not necessary to deaerate the sample solutions, precoating solutions, and background electrolyte prior to the start of the experiment. The solutions were placed in containers pressurized with helium from which they were propelled through the flow manifold. The sample loop was filled by aspiration with a vacuum of 15-cm Hg created with the hand-held vacuum pump.

Before the beginning of the plating cycle, the surface of the platinum gate was cleaned in a series of precisely controlled steps which included application of various solutions and potentials (Fig. 3, Steps 1—5). Details are available [9]; it suffices to say here that the reproducibility of the results was predicated by the use of this computer-controlled sequence.

Once the surface was clean, the precoating cycle was started. The purpose of this cycle was to obtain a smooth mercury film on the working microelectrode. A 1.0 mM solution of mercury(II) nitrate in 0.1 M perchloric acid was flushed through the flow cell for 10 s (Step 2). During this time, the CHEMFET gate was isolated from the outer circuitry by the control FET. The valves were then closed and the CHEMFET was connected and placed at 0 V vs. reference electrode for 14 min (Step 3). At this point, the surface of the gate appeared grey under the microscope because the mercury had plated out as tiny beads and not as a smooth film. The platinum gate was again disconnected and a 0.3% detergent solution in 0.1 M nitric acid (in order to eliminate adhering bubbles of hydrogen) was flushed through the flow cell for 10 s (Step 4). The valves remained open and the gate was connected and held at —1.8 V vs. reference electrode for 2 min. During this time, hydrogen was vigorously evolved from the exposed platinum. The hydrogen overpotential of bright platinum is ca. —0.4 V and is reduced to ca. —0.2 V on platinum that has been plated with mercury and then cleaned [10]. At the end of this sequence, a smooth mercury film, which was lustrous under the microscope, was obtained.

If this was the first experiment of the series, the microprocessor would automatically cause the entire system to be rinsed with the stripping solution for 2 min (Step 6). If it was not the first experiment, the flow manifold would be rinsed for 5 s with stripping solution while the CHEMFET gate was disconnected. The vacuum and sample valves were opened for 5 s to aspirate solution into the 200-μl sample loop (Step 7). Once the sample valves had been closed, the gate was electrically connected and was placed at —1.0 V against reference electrode (Step 8). The valves for the stripping solution were opened simultaneously and this pushed the sample through the dispersion loop where it was dispersed, and on to the detector. After a 2-min plating time, all valves were closed and the gate of the CHEMFET was electrically isolated (Step 9). The potential on the CHEMFET gate at this time was equal to the solution potential plus the potential of the mercury/solution interface. Because the mercury/metal layer at the CHEMFET gate is electrically isolated from the external circuit at this point, +3.0 V with respect to the transistor substrate can be applied to the reference electrode in order to increase the

gain of the CHEMFET during the detection (stripping) phase. It should be noted that all current during the plating/cleaning period passes through the platinum auxiliary electrode.

RESULTS

There are several factors which affect the determination of metals in flowing solutions when potentiometric stripping is used. These factors include sample size, dispersion, the ratio of Hg^{2+} to M^{n+} and flow rate during the stripping and plating steps. Experiments were done to establish the effects of some of these parameters on the precision of data in processing samples containing 100 μM lead(II). In all experiments, the sample size was 200 μl, the plating voltage was —1.0 V, the ratio of Hg(II) to M(II) was 25, and the flow rate during stripping was equal to the flow rate during plating. In the first set of experiments, the flow rate was 0.2 ml min^{-1} and the plating time was 5 min. The second set of experiments was done on a new mercury film with a flow rate of 1.0 ml min^{-1} and a plating time of 2 min. It was found that the use of a faster flow rate during the plating period improved the precision from 7.3% (relative standard deviation, r.s.d.) to 2.7% for the 1.0 ml min^{-1} flow rate. The flow conditions during the stripping period were also found to be important. In the first case, the flow rate during the stripping step was equal to the flow rate during the plating period. In the second case, the flow in the system was stopped by closing the valves at the time when stripping was initiated. The stripping times when the flow was stopped were approximately twice as long as when the flow was continued (Fig. 4) yielding better precision and accuracy.

The effect of the ratio of concentration of Hg(II) to Pb(II) was investigated. In all experiments, the flow rate was 0.2 ml min^{-1}, the plating time was 5 min, the plating voltage was 1.0 V, and the sample size was 200 μl. The first two experiments were designed to establish the effect of an increase in metal concentration on the precision. For the same ratio of Hg(II)/M(II) = 2.5, it was found that the r.s.d. was 12.6% for 10 μM lead and 2.5% for 100 μM lead. Additional results are summarized in Table 1. It can be seen that as the Hg(II)/M^{n+} ratio is increased from 2.5 to 100 the r.s.d. decreases from 12.6% to 1.9%. This improvement in precision is due to the elimination of the effect of variation in the mass transport of the oxidant, mercury(II), to the surface of the mercury film. However, the resulting increased rate of stripping, and consequently shorter times, impose the lower limit on precision, particularly for the relatively low sampling rate achievable with the Commodore microprocessor. Thus, for r.s.d. <10% and one concentration of the stripping solution, up to two decades of concentration of the assayed metal can be covered. A faster microprocessor would broaden the dynamic range at the low concentrations.

The procedure was tested over the range of 1 mM to 10.0 μM for both lead(II) and cadmium(II) in aqueous solution. In experiments where lower levels of metal were present, the concentration of mercury(II) ions in the

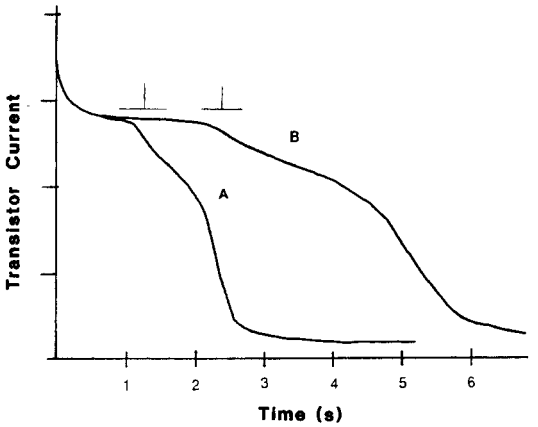

Fig. 4. Comparison of the stripping curves: (A) at constant flow; (B) with stopped flow. Experiments were done consecutively on the same mercury film. Conditions for both curves: plating potential (V_{pl}), −1.03 V; plating time (t_{pl}), 2 min; flow rate, 1 ml min^{-1}; sample solution, 1×10^{-4} M Pb(II)/0.2 M sodium acetate/0.1 M HNO_3; stripping solution, 2.5×10^{-4} M Hg(II)/0.2 M sodium acetate/0.1 M HNO_3. The second change of the transistor output is due to the discharge of the double-layer capacitor. The filtered digital time-derivatives of curves A and B are shown above the experimental curves.

TABLE 1

Effect of the ratio of oxidant to metal (M^{n+})[a]

Experiment	Hg^{2+}/M^{n+}	$[M^{n+}]$ (mM)	t_{str} (s)	R.s.d. (%)
1	2.5	6.04	0.76	12.6
2	25	7.43	0.54	7.2
3	100	0.27	0.0054	1.9

[a]Conditions: flow rate, 0.2 ml min^{-1}; sample size, 200 μl; N = 5; plating time, 5 min; plating potential, −1.0 V vs. Ag/AgCl.

stripping solution was also decreased in order to obtain longer stripping times but not below a Hg/M ratio of 100. In each case, experiments were done without renewing the mercury film. Experiments were done in order to establish if the plot of time vs. concentration was linear for both metals. The concentration of Hg(II) in all cases was 2.5×10^{-4} M, the flow rate was 1 ml min^{-1} and the sample volume was 200 μl. The flow was stopped at the time when the stripping was initiated. For both metal ions, the plot of concentration vs. time was linear with a correlation coefficient of 0.999 for Pb(II) and 0.997 for Cd(II).

DISCUSSION

The potentiometric stripping method is an ideal system on which the principle of design of integrated analytical microsystems can be demonstrated because many different steps have to be executed simultaneously or in a precisely timed sequence. These steps fall into three categories (Fig. 3): (1) control of flow in the flow-injection manifold, (2) control of potentials applied to the reference electrode, and (3) rapid switching ON and OFF of the potentiometric detector (CHEMFET). The result is a system which can deal automatically with 200 μl samples of 10^{-5}—10^{-3} M Pb(II) or Cd(II) in less than 2.5 min with better than 10% r.s.d.

The operation of the present system has not been optimized with respect to any specific application. In principle, it should be possible to use this approach for trace heavy metal determinations in samples containing particulates, such as whole blood or suspensions, because the dilutional error encountered during direct flow-injection approach [11, 12] would be circumvented by the integration during the plating period.

Assistance from Mr. Royce Johnson with the design of the microprocessor is greatly appreciated. This work was supported by the NIGMS Grant 22952.

REFERENCES

1 D. Jagner, H. Josefson, S. Westerlund and K. Åren, Anal. Chem., 53 (1981) 1406.
2 B. Hoyer and L. Kryger, Anal. Chim. Acta, 167 (1985) 11.
3 J. K. Christiansen, L. Kryger and N. Pind, Anal. Chim. Acta, 136 (1982) 39.
4 J. F. Coetzee, A. Hussam and T. R. Petrick, Anal. Chem., 55 (1983) 120.
5 R. Smith, R. J. Huber and J. Janata, Sensors and Actuators, 5 (1984) 127.
6 R. Smith, Thesis, University of Utah, Salt Lake City, UT, 1982.
7 J. J. Harrow and J. Janata, Anal. Chem., 55 (1983) 2461.
8 M. Z. Hassan, D. F. Untereker and S. Bruckenstein, J. Electroanal. Chem. Interfac. Electrochem., 42 (1973) 161.
9 L. E. Locascio, Thesis, University of Utah, Salt Lake City, UT, 1986.
10 A. M. Hartley, A. G. Herbert and J. A. Cox, Electroanal. Chem. Interfacial Chem., 17 (1968) 81.
11 C. Labar and L. Lamberts, Anal. Chim. Acta, 132 (1981) 23.
12 J. J. Harrow and J. Janata, Anal. Chim. Acta, 174 (1985) 123.

Analytica Chimica Acta, 194 (1987) 109—117
Elsevier Science Publishers B.V., Amsterdam — Printed in The Netherlands

AXIAL DISPERSION IN COILED TUBULAR REACTORS
The Effect of Curvature at Low Dean Numbers

DENYS F. LECLERC, CARR J. SMITH and E. CLIFFORD TOREN, Jr.*

Department of Pathology, University of South Alabama Medical Center, 2451 Fillingim Street, Mobile, AL 36617 (U.S.A.)

(Received 15th September 1986)

SUMMARY

Deforming tubing (e.g., coiling) reduces axial dispersion in flow-injection systems and post-column reactors. An improvement is presented for a previous theoretical treatment of axial dispersion in coiled tubes. New experimental data are also presented for different coil radii. Changes were necessary because smaller-than-predicted dispersion improvements were observed. This contradicts earlier treatments that predict a linear dependence on the aspect ratio of the coil. Evidence is presented that this is explained by assuming a boundary layer thickness much smaller than the radius of the tube and proportional to the ratio of radial velocities. This is a special case of earlier theory and it predicts an almost curvature-independent change in dispersion. The inclusion of the critical Reynolds number, Re_c, to form a reduced parameter, (Re/Re_c), accounts for all observations, including some previously-defined empirical constants. The dispersion is found to increase as $(Re/Re_c)^{2/3}Sc$ at low fluid velocities and to decrease as $(Re_c^{1/6}/(Re/Re_c)^{4/3}Sc^{0.08})$ at higher velocities. Experiments are reported for several coil radii and with a range of proteins and protein mixtures.

Secondary flow improves dispersion in post-column reactors and in flow-injection systems. Secondary flow occurs when fluid passes through a curved tube. The parabolic flow pattern that is typical of Poiseuille flow becomes distorted by centrifugal forces; consequently, radial or secondary flow creates a recirculating pattern in which fluid flows back inwardly along the inner wall of the tube. This recirculating flow is confined to a so-called boundary layer, the thickness of which is but a small fraction of the inner radius of the tube. This generates two symmetrical flow cells between which there is little exchange of liquid. Therefore, there is less axial dispersion because dispersion occurs over smaller distances. Secondary flow also stabilizes laminar flow. Turbulence develops at higher Reynolds numbers than in corresponding straight tubes.

In some previous work on dispersion in coiled tubes [1], plate heights at higher fluid velocities were found to be much lower for coils than for similar straight tubes. Others [2, 3] have observed a maximum in the dispersion curve that was not predicted by previous theoretical treatments [4, 5]. Experiments by Tijssen [3] and in this laboratory [1] established that the

0003-2670/87/$03.50

dispersion curve is a function of the 2/3 power of the Reynolds number at lower fluid velocities and is inversely proportional to the 4/3 power of the Reynolds number at higher velocities. Tijssen [3, 6] showed that this sudden decrease in dispersion occurs because the boundary layer thickness changes with velocity. This has also been shown in theoretical studies by Mori and Nakayama [7]. With several assumptions, the logarithm of the dispersion can be shown to decrease linearly with the logarithm of the dimensionless parameter $De^2Sc^{1.14}$, at fluid velocities above the dispersion maximum, where De is the Dean number, and Sc is the Schmidt number. (All variables and parameters are defined in Table 1.) This was empirically confirmed in earlier work [1]. However, closer examination of the Mori—Nakayama equations for the boundary layer reveals that they are applicable only when the Dean number exceeds 50, while the experimental fluid velocity encountered in previous studies corresponds to Dean numbers that are smaller than 50 [1, 3]. Therefore, a modification of present theory is needed.

An expression for the boundary layer can be derived, assuming a constant thickness along the circumference of the inner wall of the tube, provided that both the fluid velocity and the radius of curvature are quite high. In this paper, a modification of an earlier development given by Tijssen [6] is discussed, and a result quite different from that obtained by Mori and Nakayama [7] is obtained. The boundary layer thickness is a function of the ratio of secondary to axial velocities rather than of the inverse square root of the Dean number. This appears to be a special case of the theory given earlier [1].

THEORY

According to Tijssen [3], the plate height, H, for coiled tubes is described by

$$H = (2\kappa r^2 \bar{u})/D_r \tag{1}$$

where κ is a parameter dependent on the velocity profile of the radius, r, of the tube, $\bar{u}$ is the mean linear fluid velocity and D_r is an effective mass-transfer number having the units of diffusivity. D_r is related to the molecular diffusion coefficient, D_m, and merely reflects the additional contribution of radial flow to diffusion processes. Thus $D_r = D_m + D_s$, where D_s is the additional contribution of secondary flow. At low fluid velocities, both κ and D_r have constant values. Therefore, in binary mixtures, the D_r of each solute will reflect the value of its molecular diffusion coefficient. Consequently, a radial mass-transfer number can be formulated for mixtures:

$$D_r^{mix} = zD_r^A + (1 - z)D_r^B \tag{2}$$

where z is the mass fraction of A in the mixture, assuming that D_s^A, D_s^B and D_r^{mix} can be expressed in terms of either D_r^A or D_r^B if both D_m^A and D_m^B are known.

TABLE 1

Notations and definitions

D_r	Effective radial mass transfer number ($cm^2\ s^{-1}$)	$\bar{u}$	Mean fluid velocity ($cm\ s^{-1}$)
D_s	Secondary flow component of D_r ($cm^2\ s^{-1}$)	u_s	Secondary flow velocity ($cm\ s^{-1}$)
D_m	Molecular diffusion coefficient ($cm^2\ s^{-1}$)	v	Boundary-layer velocity ($cm\ s^{-1}$)
De	Dean number (dimensionless) (= $Re\ \lambda^{1/2}$)	δ	Boundary-layer thickness (cm)
H	Plate height (coiled tubes) (cm)	η	Viscosity (poise)
L	Tube length (cm)	κ	Velocity profile parameter (dimensionless)
Pe	Peclet number (dimensionless) (= $4r/H$)	λ	Aspect ratio (dimensionless) (= r/R)
r	Tube radius (cm)	μ_1	First moment of elution profile (s)
R	Coil radius (cm)	μ_2	Second moment of elution profile (s^2)
Re	Reynolds number (dimensionless) [$2ru(\rho/\eta)$]	ρ	Density ($g\ cm^{-3}$)
Re_c	Critical Reynolds number [= $2100(1 + 12\lambda^{1/2})$]	ν	Kinematic viscosity (= η/ρ stoke)
Sc	Schmidt number (dimensionless) (= $\eta/\rho D_m$)		

Earlier [1] it was established that for coiled tubes the plate height varies with $Re^{2/3}$ at lower fluid velocities. By rewriting Eqn. 1 in dimensionless terms, the reciprocal of the Peclet number can be expressed as

$$Pe^{-1} = (H/4r) = (D/\kappa \bar{u} r)(\kappa Re^{2/3} Sc)/4(D_r/D_m) \quad (3)$$

At velocities below the dispersion maximum, both κ and (D_r/D_m) are constant, with $\kappa = 1/16$ and D_r/D_m approximately equal to 4 and D is the natural diffusivity defined earlier [1]. The latter value reflects the fact that the tube is split into two recirculating cells [3]. This situation is radically altered if the liquid is made to flow at higher velocities: both parameters become dependent on fluid velocity and, in the case of D_r/D_m, on the thickness, δ, of the boundary layer. In turn, the boundary-layer thickness also depends on fluid velocity. Mori and Nakayama [7] have shown that for $De > 36$, the form of this dependence is $(\delta/r) \propto De^{-1/2}$, whereas, at lower velocities and lower curvature, results by Adler [8] and Tijssen [6] give, after rearrangement, $(\delta/r) \approx 1.5\,(u_s/v) \sin\phi$ for $\delta \ll r$, where u_s is the secondary flow velocity. This assumes that the maximum velocity, v, in the boundary layer is a sinusoidal function of the cylindrical angle ϕ. The boundary-layer thickness, δ, thus becomes independent of $\sin\phi$. Furthermore, when $\phi \approx 90°$, the boundary layer velocity is directly related to $\bar{u}$ and consequently $(\delta/r) \propto 1.5\,(u_s/\bar{u})$ for $\delta \ll r$. This suggests that as the fluid velocity and the curvature of the tube increase, a stronger secondary flow first contributes to the build-up of a boundary layer which eventually attains maximum thickness, before diminishing as predicted by Mori and Nakayama [7].

Tijssen [3] has proposed the following expression for (D_r/D_m) at higher velocities:

$$(D_r/D_m) = [(32/3)(u_s r/\nu) Sc]/(\delta/r)^2 \quad (4)$$

Substituting the above dependence for δ/r on $(u_s/\bar{u})$, rearranging and applying the definitions of the Reynolds and Schmidt numbers, one obtains

$$(D_r/D_m) = [(32/27) Re^2 Sc]/(u_s r/\nu) \quad (5)$$

According to Mori and Nakayama [7], $(u_s r/\nu) = 0.966\, De^{1/2}$. After introduction of a constant Re_c, the expression for (D_r/D_m) then becomes

$$(D_r/D_m) \approx (32/27)\,(Re/Re_c)^{3/2} Sc\, \lambda^{-1/4} \tag{6}$$

where Re_c is the critical Reynolds number for the onset of turbulence, λ is the aspect ratio equal to (r/R), and R is the radius of the coil. The critical Reynolds number is 2100 $(1 + 12\lambda^{1/2})$ in coiled tubes.

Kalb and Seader [9] reported that, for very high Schmidt numbers, their previously reported correlation was valid for low Dean numbers and consequently, the velocity-profile parameter, κ, becomes

$$\kappa = (6/5)\,(De^{1/2} Sc^{0.08-0.12})^{-1} \tag{7}$$

Finally, substitution of Eqns. 6 and 7 for κ and (D_r/D_m) in the expression for Pe^{-1} (Eqn. 3) gives a high-velocity result that is curvature-independent:

$$Pe^{-1} \approx (Re_c^{3/2})/(Re^{4/3} Sc^{0.08}) \tag{8}$$

This also suggests that for lower velocities, $Pe^{-1} \approx (Re/Re_c)^{2/3} Sc$, which would therefore explain the experimental factor of 256 as $(240 < (Re_c)^{2/3} < 280)$, for the values of R used in this study.

Therefore, for $De < 50$, the effect of a looser coil on Pe^{-1} should show a slight increase at lower velocities and a somewhat greater decrease at higher velocities, because the critical Reynolds number is smaller for a greater coil radius.

The inverse of the reduced dispersion [1] can be expressed as a product of dimensionless numbers, $Pe\ (Re/Re_c)^{2/3} Sc$. Dispersion in coiled tubes can thus be summarized for higher fluid velocities:

$$Pe(Re/Re_c)^{2/3} Sc \propto Re^2 Sc^{1.08} \qquad (De < 50) \tag{9}$$

Therefore, dispersion maxima should occur at values of $Re^2 Sc^{1.08}$ which are approximately equal to $1.055\, Re_c^{13/6}$. Only data from the low-Dean-number region have been collected so far in this laboratory. Nevertheless, results will also be fitted to the parameter $De^2 Sc^{1.14}$ to establish which one best fits the experimental results.

EXPERIMENTAL

Apparatus

The apparatus has been described in the paper by Fulton et al. [10]. The carrier delivery unit, injection system, and the dual-detector system used was described earlier [1].

Three types of reactors were fabricated. The first was identical to the coil system described earlier [1]: it included a 1790-cm pre-delay coil and a 2955-cm main reactor. Coils were fabricated by winding the tubing around 4.76-cm o.d. poly(vinyl chloride) (PVC) pipes. The second type of reactor consisted of identical tubing coiled around 11.43 cm o.d. pipes. In this case, the pre-delay coil was 1150 cm long and the main reactor 2160-cm long. The

coiled tubes were 508-μm (i.d.) 316 stainless steel (Alltech Associates, Deerfield, IL). The third type of reactor was fabricated by twisting 768-μm 316 stainless steel tubing around pegs mounted on wooden spheres of 12.7-cm diameter. The twisting was done repetitively as shown in Fig. 1. These reactors were 800 and 2550 cm long, respectively.

Reagents

Protein solutions (1.2—1.6 g l^{-1}) were prepared in a 0.08 M sodium sulfate/0.01 M sodium acetate buffer, pH 7.0. [12]. This buffer was also used as the carrier, after filtering through a 0.5-μm filter. Horse heart cytochrome C, bovine pancreas chymotrypsinogen, bovine serum albumin, rabbit muscle aldolase, bovine liver catalase, horse spleen ferritin and porcine thyroglobulin were used as sample solutes. All compounds except for thyroglobulin were provided in a calibrated molecular weight kit (no. 2666 Mol-Ranger; Pierce Chemical Co., Rockford, IL). Thyroglobulin was obtained in powder form (T1126; Sigma Chemical Co.). Binary mixtures of cytochrome C and 25, 50, 75 and 90 mass-% thyroglobulin were prepared.

Samples were injected into the system at flow rates ranging from 0.0833 to 12 ml min^{-1}. Only one experiment was done per flow rate because values of plate height can be obtained in three different ways, one by using moments and two from differences in the dual-detection system [1]. A convolution

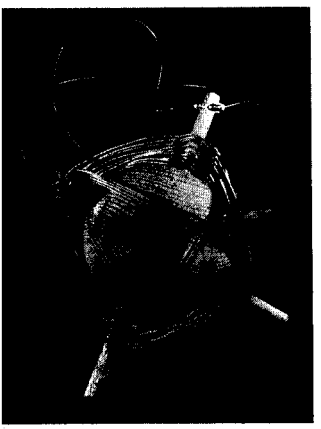

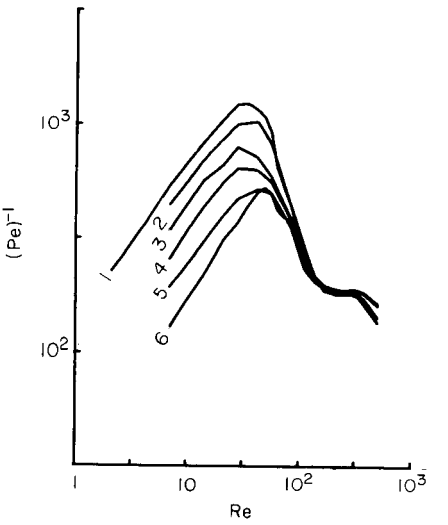

Fig. 1. Twisted coil reactor. Six pegs are distributed octahedrally around a wooden ball (12.7-cm diameter).

Fig. 2. Inverse Peclet number $(Pe)^{-1}$, as a function of Reynolds number, Re, for binary mixtures. Mass ratios of thyroglobulin to cytochrome C: (1) 100/0; (2) 90/10; (3) 75/25; (4) 50/50; (5) 25/75; (6) 0/100.

can also be performed to calculate the vessel dispersion number [1], H/2L: the upstream detector profile is transformed into a simulated downstream profile. Details of the procedure have been reported [1, 10]. The detection wavelength was 214 nm.

Data acquisition, software, and calculations

Hardware and software for data acquisition were described previously [1, 10]. Data acquisition was begun within 0.2 s of injection.

The plate height, H, can be calculated from the ratio of the first and second moments, μ_1 and μ_2, of the sample profile, $H = (\mu_2/\mu_1^2)L$, in which μ_1 and μ_2 are calculated as described before [1]. Schmidt numbers were calculated for each solute, using values of diffusion coefficients given by Walters et al. [11] and Sober [12]. These data are presented in Table 2, along with the corresponding molecular weight of the corresponding solutes.

RESULTS AND DISCUSSION

Binary mixtures

Results are shown in Fig. 2. Theoretical values of D_r (mixture) in terms of D_r (thyroglobulin) were calculated using Eqn. 2, and are shown in Table 3 along with experimental values obtained from Fig. 2. The agreement is quite good, considering the errors involved in the determination of plate heights and of molecular diffusion coefficients. It can be seen that each diffusing species therefore contributes independently to the observed overall diffusivity.

Coiled reactors

As evidenced by Fig. 3, there is very little change in dispersion behavior when a change in coil radius is made. In all likelihood, this is the result of the experimental conditions encountered here. In opposition to what was predicted by previous treatments [1, 3], the dispersion does not change very

TABLE 2

Molecular weights, diffusion coefficients and Schmidt numbers of solutes

Compound	Molecular weight	D_m (10^{-7} cm^2 s^{-1})	Schmidt number
Cytochrome C	13 500	11.6[a]	8500
α-Chymotrypsinogen	25 000	9.5[b]	10 600
Albumin	67 000	6.1[b]	15 700
Aldolase	158 000	4.6[b]	21 700
Catalase	240 000	4.1[b]	24 500
Ferritin	540 000	3.25[b]	30 900
Thyroglobulin	650 000	3.45[a]	28 600
		2.65[b]	37 300

[a]Data from [11]. [b]Data from [12].

TABLE 3

Dispersion of protein mixtures of cytochrome C and thyroglobulin

Mixture (% Thyroglobulin)	D_r (mixture)/D_r (thyroglobulin)	
	Theoretical	Experimental
90	1.23	1.22
75	1.59	1.59
50	2.18	2.08
25	2.76	2.80
0	3.36	3.40

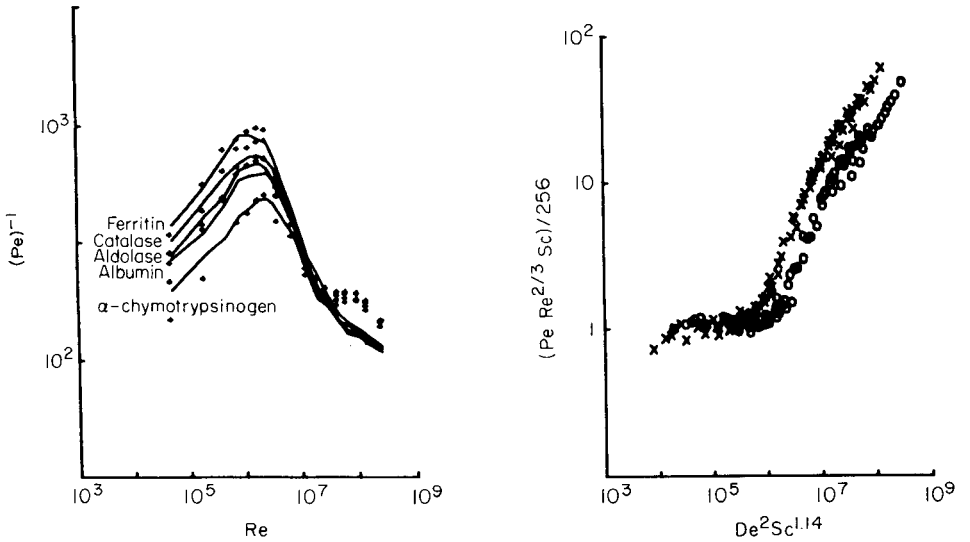

Fig. 3. Inverse Peclet number $(Pe)^{-1}$, as a function of the Reynolds number, Re, for two coil radii, R. Data points relate to R = 2.49 cm; solid lines relate to R = 5.82 cm.

Fig. 4. Inverse reduced dispersion, $Pe\ Re^{2/3}\ Sc/256$, as a function of $De^2Sc^{1.14}$ for two coil radii, R: (○) R = 2.49 cm; (×) R = 5.82 cm.

much with coil radius for fluid velocities above the dispersion maximum. However, the observed behavior can be readily accounted for by the theoretical development given above. It appears that the curvature of tubing used here is not sufficient to induce the type of velocity-profile modifications predicted for pipes of strong curvature and much greater diameter.

Therefore, the data given in Fig. 4. show that the Dean number is not the relevant parameter for the conditions applied here. If this were the case, there would be a single curve, instead of the two shown. The type of clustering seen in Fig. 5 indicates that both the normalized dispersion, $Pe\ (Re/Re_c)^{2/3}Sc$,

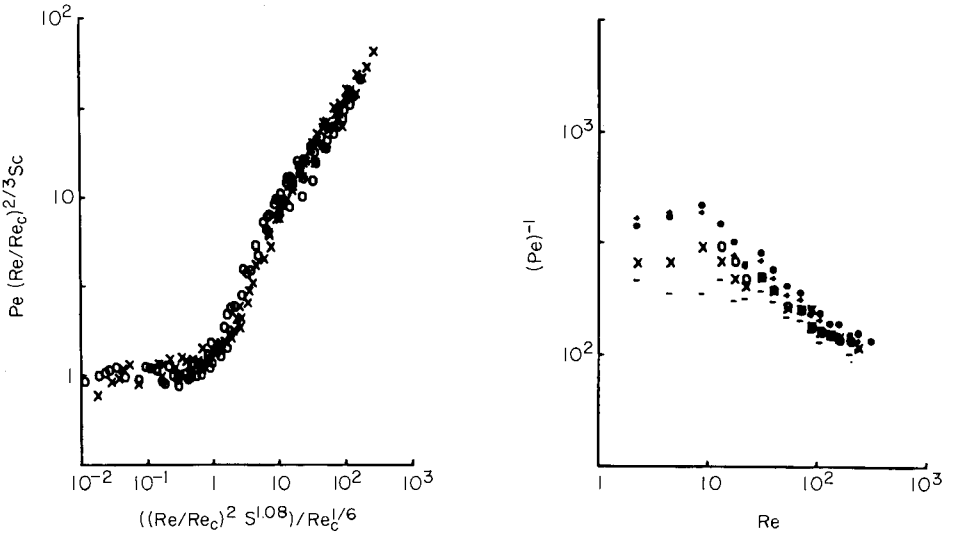

Fig. 5. Normalized dispersion, $Pe\,(Re/Re_c)^{2/3}Sc$, as a function of $[(Re/Re_c)^2Sc^{1.08}]/(1.055\ Re_c^{1/6})$ for two coil radii, R:(○) R = 2.49 cm; (×) R = 5.82 cm.

Fig. 6. Inverse Peclet number, Pe^{-1}, as a function of the Reynolds number, Re, for the twisted reactor shown in Fig. 1: (-) α-chymotrypsinogen; (×) albumin; (○) aldolase; (+) catalase; (•) ferritin.

and the parameter $[(Re/Re_c)^2Sc^{1.08}]/(1.055\ Re_c^{1/6})$, are appropriate to fit these experimental data. The agreement with theory is certainly better than that of Fig. 4. While the fit is by no means exact, the experimental results can be explained by a theory that does not require a dependence on the Dean number. The critical Reynolds number Re_c does, however, play a central role. There seems to be a strong relationship between the onset of turbulence at high fluid velocities and the observation of a dispersion maximum at much lower velocities. Also, the dependence of the Schmidt number at velocities below the dispersion maximum is very real and is confirmed by these experiments.

Twisted reactors

The importance of geometry (as shown in Fig. 1) in governing dispersion in tubular reactors is demonstrated by the curves shown in Fig. 6. Although the mathematical description of this geometry is difficult, it is easily constructed and provides for reproducible geometries. Dispersion is very low, despite indications of a maximum at very low fluid velocities. Although the dispersion seems to be a function of the Schmidt number at lower fluid velocities, it is not yet clear exactly what the influence of the Schmidt number is at very low fluid velocities. There is no influence of the Schmidt number

TABLE 4

Comparison of vessel dispersion numbers obtained by two different methods of calculation for the twisted reactor configuration

Flow rate (ml h^{-1})	Vessel dispersion number		Flow rate (ml h^{-1})	Vessel dispersion number	
	Moments	Convolution		Moments	Convolution
5	0.0250	0.0440	160	0.0130	0.0190
10	0.0290	0.0440	240	0.0110	0.0140
20	0.0330	0.0490	450	0.0080	0.0100
40	0.0220	0.0290	720	0.0075	0.0090
70	0.0250	0.0250			

at higher velocities: the same staircase-like pattern is obtained for all solutes. The unusual shape of the dispersion curve for high fluid velocities may be a reflection of the geometry of the reactor. Even with the relatively straight geometry between pegs, the dispersion is much less than for similar coils.

The vessel dispersion number, $H/2L$, was calculated for a few representative flow rates as described earlier [1]. The results presented in Table 4 show that, as predicted, the accuracy of the calculation is not affected by the reactor geometry.

Much remains to be done in order to gain full understanding of dispersion behavior in tubular reactors of various geometries. In the case of helically coiled reactors, the region of high Dean number must be investigated to establish whether the theory needs adjustments.

We are indebted to Dr. Peter A. Bloxham for the development of much of the software used for the calculations, and to Joe Ann Thomas for technical assistance. This work was supported by grant number CHE-8101121 from the National Science Foundation and was presented in part at the Pittsburgh Conference and Exposition, Atlantic City, NJ (March, 1986).

REFERENCES

1 D. F. Leclerc, P. A. Bloxham and E. C. Toren, Jr., Anal. Chim. Acta, 184 (1986) 173.
2 R. N. Trivedi and K. Vasudeva, Chem. Eng. Sci., 30 (1975) 317.
3 R. Tijssen, Sep. Sci. Technol., 13 (1978) 681.
4 L. C. Truesdell, Jr. and R. J. Adler, AIChE J., 16 (1970) 1010.
5 L. R. Austin, Jr. and R. J. Adler, AIChE J., 19 (1973) 85.
6 R. Tijssen, Chromatographia, 3 (1970) 525.
7 Y. Mori and W. Nakayama, Int. J. Heat Mass Transfer, 8 (1965) 57; 10 (1967) 681.
8 M. Z. Adler, Angew. Math. Mech., 14 (1934) 257.
9 C. E. Kalb and J. D. Seader, AIChE J., 20 (1974) 340.
10 J. A. Fulton, T. D. Schlabach, J. E. Kerl, E. C. Toren, Jr. and A. R. Miller, J. Chromatogr., 175 (1979) 269.
11 R. R. Walters, J. F. Graham, R. M. Moore and D. J. Anderson, Anal. Biochem., 140 (1984) 190.
12 H. A. Sober (Ed.), Handbook of Biochemistry, 2nd edn., CRC Press, Cleveland, OH, 1970, pp. C-3 to C-30.

Analytica Chimica Acta, 194 (1987) 119—127
Elsevier Science Publishers B.V., Amsterdam — Printed in The Netherlands

FLOW-INJECTION DETERMINATION OF NITRITE AND NITRATE WITH BIAMPEROMETRIC DETECTION AT TWO PLATINUM WIRE ELECTRODES

A. HULANICKI, W. MATUSZEWSKI and M. TROJANOWICZ*
Department of Chemistry, University of Warsaw, Warsaw (Poland)
(Received 21st May 1986)

SUMMARY

The flow-injection determination of nitrite is based on oxidation of iodide by nitrite. The triiodide formed is detected amperometrically in a flow-through cell with two teflonized graphite or platinum wire electrodes polarized with a voltage of 100 mV. More sensitive and faster response was observed with the platinum wire electrodes. The same detector is used for determination of nitrate after reduction to nitrite in a reductor column containing copperized cadmium. Detection limits under optimized conditions are 6 $\mu g\ l^{-1}$ for both nitrite- and nitrate-nitrogen. Effects of oxygen and interfering metal ions are discussed.

The problem of nitrite and nitrate determinations is important for environmental protection, food and agricultural analysis. Because the flow-injection technique is especially advantageous in the case of large numbers of routine determinations, many papers have been devoted to this subject. Most common are spectrophotometric determinations of nitrite based on formation of azo dyes [1—7] or amperometric determinations with a glassy carbon working electrode [8—10]. The same procedures were used for flow-injection determination of nitrate after their preliminary reduction to nitrite [1–3, 5, 11—13]. Direct nitrate determination was also based on ultraviolet absorption [14] or potentiometric measurements with nitrate ion-selective electrode [15, 16]. The best detection limits, in the sub-$\mu g\ l^{-1}$ range for nitrite-nitrogen [1, 6, 7] and ca. 1.5 $\mu g\ l^{-1}$ for nitrate-nitrogen [1, 11], have been reached with spectrophotometric detectors. For both analytes, amperometric detectors are unsuitable below the mid-$\mu g\ l^{-1}$ range [9, 10, 12, 13] and potentiometry offers even worse determination limits [15, 16].

The aim of this study was to investigate the possibility of flow-injection determination with two platinum electrodes polarized with a small potential difference. It is based on measurement of iodine concentration formed in the reaction between iodide and nitrite. This principle was used in the coulometric determination of nitrite by Karlsson and Torstensson [17]. Initially, a flow cell with two semitubular electrodes of teflonized graphite was used [18]. In this paper, it is shown that two platinum wire electrodes enable

0003-2670/87/$03.50

even smaller amounts of nitrite to be determined. Recently, a similar method of detection was used for the determination of sulphur(II) compounds on the basis of an induced iodine/azide reaction [19], and for the determination of molybdenum based on its catalysis of the iodide/hydrogen peroxide reaction [20].

EXPERIMENTAL

Apparatus

The measuring system used in present work consisted of a multichannel peristaltic pump MP-13GJ-4 (Ismatec, Zürich, Switzerland), a home-made rotary injection valve and flow cells connected to an a.c./d.c. polarograph (PLP 225C; Cobrabid, Warszawa, Poland). The polarograph output was connected to a potentiograph (E-436; Metrohm, Herisau, Switzerland) used as a strip-chart recorder or to a line recorder (TZ 2100; Laboratorni Pristroje, Praha, Czechoslovakia).

The design of the flow-through cells with teflonized graphite or platinum wire electrodes is shown in Fig. 1. Platinum electrodes were made of platinum wire of diameter 0.3 mm. An exposed length of wire electrode to flowing solution was usually 8 mm or in some indicated in text cases 4 mm. Working area of teflonized graphite semitubular electrodes was estimated as 20 mm^2. The constant polarizing voltage (usually 100 mV) is applied from the potentiostat circuit of a polarograph. The bore of the tube around the platinum electrodes was 1.2 mm; the bore through the graphite electrode was 1.2 mm.

The manifold of the system used (Fig. 2) was composed of propylene tubings (0.9 mm internal diameter) with home-made perspex connectors. Pump tubes were from Elkay (Boston, MA). The reduction column was a glass tube (2 mm internal diameter) filled with cadmium granules (<0.3 mm particle size). Daily, prior to measurements, the cadmium was copperized by passing 3 ml of 0.1 M copper(II) sulphate solution at a flow rate of 5 ml min^{-1}.

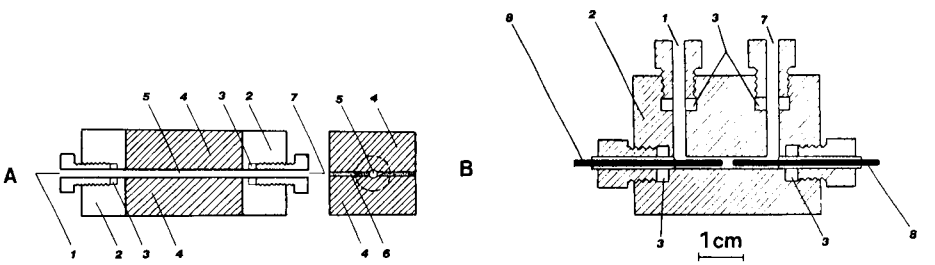

Fig. 1. Schematic diagram of flow-through cells for amperometric detection with two polarized teflonized graphite (A) or platinum wire electrodes (B): (1) inlet; (2) perspex body; (3) silicone rubber spacer; (4) teflonized graphite; (5) measuring channel; (6) epoxy layer separating the teflonized graphite semitubular electrodes; (7) outlet; (8) Pt wire electrodes.

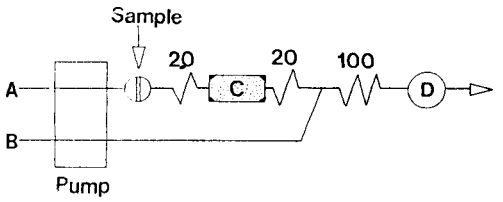

Fig. 2. Manifold of the flow-injection system used for determination of nitrate with a copperized cadmium column (C). For the nitrite determination, the column was omitted.

Solutions and soil extracts

Stock standard nitrate solutions (0.01 M) were prepared by dissolution of 0.8499 g of sodium nitrate in 1 l of triple-distilled water. Stock standard nitrite solutions (0.01 M) were prepared by dissolution of 0.6899 g of sodium nitrite in 1 l of triple-distilled water. Less concentrated standard solutions were obtained by successive dilutions. Carrier solutions containing potassium iodide and sulphuric acid were prepared daily. All reagents used were of analytical-grade purity.

Aqueous soil extracts were prepared by vigorous shaking of 50 g of freshly sampled greenhouse soil for 45 min with 150 ml of distilled water, followed by double-vacuum filtering.

RESULTS AND DISCUSSION

Iodine detection with the polarized electrodes

The determination of nitrite and nitrate is based on the linear dependence of the current on the concentration of iodine in the presence of large excess of iodide. With 100-mV applied voltage, the resulting current for micromolar concentrations was compared for semitubular electrodes from teflonized graphite [18] and for platinum wire electrodes. The latter offered nearly double the sensitivity (Fig. 3). The linearity of the response was confirmed in the iodine concentration range from 10 μM to 1 mM. Comparison of the analytical signals for very low concentrations with the baseline noise indicated that iodine could be detected in the submicromolar range.

Optimization of nitrite determination

The indirect amperometric determination of nitrite with two polarized electrodes is based on its reaction with iodide in the acidic medium

$$2HNO_2 + 3I^- + 2H^+ \rightarrow 2NO + I_3^- + 2H_2O$$

where the triiodide formed gives a perfectly reversible couple. This thermodynamically feasible reaction can suffer interference from the oxidation of nitrogen oxide with dissolved oxygen, $2NO + O_2 \rightarrow 2NO_2$. The nitrogen dioxide formed can either disproportionate into nitrous and nitric acids or react further with excess of iodide giving again nitrogen oxide as a product [21, 22]:

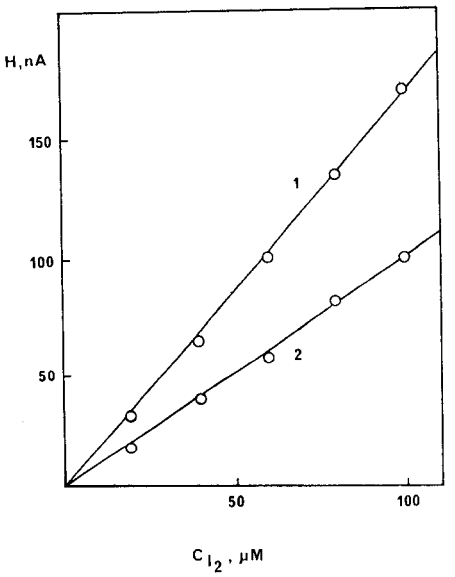

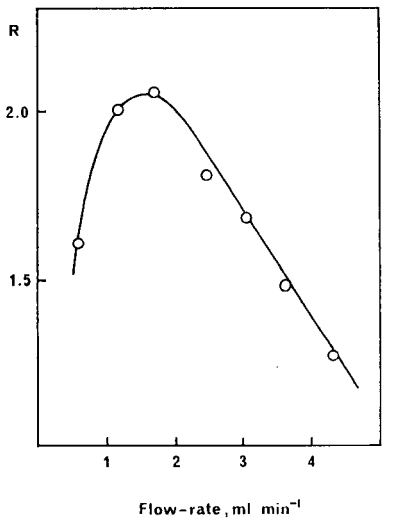

Fig. 3. Calibration plots obtained for injections of 250 μl of iodine solutions in 0.2 M potassium iodide: (1) flow cell with 8-mm long platinum wire electrodes; (2) flow cell with teflonized graphite electrodes. Flow rate in each line 2.4 ml min^{-1}.

Fig. 4. Effect of flow rate on the ratio (R) of the peak heights for injection of 160 μl of air-saturated and argon-deaerated 1.0 mM nitrite solutions in the flow cell with teflonized graphite electrodes.

$$2NO_2 + 6I^- + 4H^+ \rightarrow 2I_3^- + 2NO + H_2O$$

The sequence of reactions indicates complicated mechanisms which indeed cause many problems in classical procedures [21]. However, in the strictly controlled conditions of flow-injection analysis, application for the determination of nitrite is quite feasible.

In order to estimate the effect of oxygen on the nitrite flow-injection peaks, two series of experiments were conducted, in which the effect of flow rate was examined for solutions saturated with atmospheric oxygen or deaerated with argon. The ratio of the peak heights obtained at various flow rates is shown on Fig. 4. Most favourably, the peak heights for the air-saturated samples compared to deaerated samples were almost doubled for flow rates between 1 and 2 ml min^{-1}.

The choice of the optimal flow rate must also take into account the change in peak height with flow rate as well as peak broadening and the rate of return to the base line, which influences the sampling rate. As expected, increasing the flow rate decreased the peak height (Table 1), but the peak broadening and the above-mentioned effect of oxygen favoured a flow rate of 2.4 ml min^{-1} in each channel as the most advantageous for the determination of small amounts of nitrite in presented measuring system.

TABLE 1

Optimization of 0.4 mM nitrite determination

Parameter	Value of optimized parameter	Peak height (μA)	Other conditions
Flow rate[a] (Q, *ml min*$^{-1}$)	0.6	3.89	0.2 M KI in 0.1 M H_2SO_4 in line B (Fig. 2); V_s = 360 μl
	1.2	3.42	
	2.4	2.83	
	3.6	2.50	
	4.9	2.19	
Acidity	3 M CH_3COOH	2.67	0.4 M KI in given acid solution in line B (Fig. 2); Q = 2.4 ml min^{-1}; V_s = 360 μl
	0.1 M H_2SO_4	3.48	
	0.4 M H_2SO_4	3.56	
	0.8 M H_2SO_4	3.69	
Iodide (M) in line B	0.05	2.33	KI in 0.1 M H_2SO_4 in line B; Q = 2.4 ml min^{-1}; V_s = 360 μl
	0.2	3.28	
	0.4	3.14	
Sample volume (V_s, μl)	36	0.49	0.2 M KI in 3 M acetic acid in line B; Q = 2.4 ml min^{-1}
	360	4.44	
	1050	4.59	
Electrode length[c] *(mm)*	4	0.10	0.2 M KI in 0.1 M H_2SO_4 in line B; Q = 2.4 ml min^{-1}; V_s = 360 μl
	8	0.14	

[a]Flow rate in each line (A and B). [b]Equilibrium signal. [c]For 0.04 mM nitrite injected.

Optimization of the conditions for determination also requires consideration of such parameters as medium acidity, iodide concentration and sample volume (Table 1). The highest peaks were observed with 0.1 M H_2SO_4/0.2 M potassium iodide in line B of Fig. 2. With a constant geometry of the manifold, it was found that the peak height increased up to sample volumes of 360-μl, which was only 3% lower than the equilibrium signal.

As could be expected, the surface area of the amperometric electrodes directly influenced the current magnitude. When short (4.0 mm long) wire electrodes were used instead of 8.0-mm electrodes, the analytical signal decreased by ca. 25%. Further measurements were done with the longer electrodes in spite of slightly larger tailing.

In the range 2—30 μM of nitrite, the peaks recorded under optimal conditions (Fig. 5) gave a linear calibration plot which passed through the origin of the coordinate system. With maximal amplification on the TZ 2100 recorder, the limit of detection was 4×10^{-7} M (6 μg l^{-1} nitrite-nitrogen). The calibration graph was also linear from 30 μM to 1 mM nitrite, but this line did not pass through the origin. The reasons for this behaviour are not known but when the procedure for the micromolar concentration range is used, it does not have any specially harmful effect.

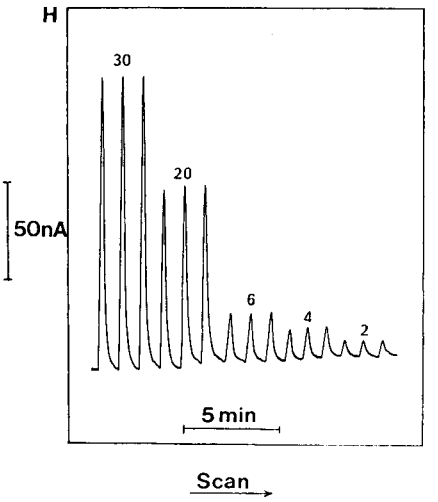

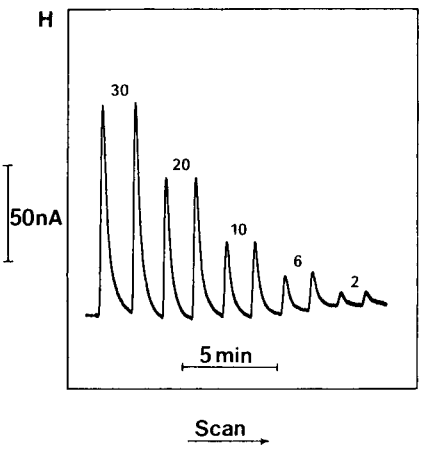

Fig. 5. Flow-injection peaks obtained for nitrite under the optimized conditions with a flow cell having two 8-mm long Pt wire electrodes. Flow rate in each line 2.4 ml min^{-1}; injected sample volume 360 μl. Concentration of injected nitrite solutions is indicated in μM on the peaks.

Fig. 6. Flow-injection peaks obtained for nitrate under optimized conditions with an 80-mm reduction column. Other conditions as for Fig. 5.

Optimization of nitrate determination

Application of the above procedure for the determination of nitrate requires preliminary nitrate reduction in flow conditions. This reduction is usually done with copperized cadmium [1, 3, 5, 11], but zinc [2] and cadmium [13] have also been used. Starting with the early paper of Anderson [1], who used a microcolumn with copperized cadmium and carrier solutions containing sodium and ammonium chlorides [1], various concentrations of salts have been used, sometimes also with addition of EDTA [3, 5, 11].

The first step in optimization of the nitrate determination was to check whether the column influenced the peak height in any way other than the effect of increased dispersion. The amperometric detector was therefore replaced by a potentiometric detector with a potassium ion-selective electrode and 5 mM KCl was injected into a 0.05 M NaCl carrier. For manifolds without a column and with columns of 30-mm and 80-mm length, the calculated dispersion coefficients were 3.1, 4.7 and 6.4, respectively. The decrease in the nitrite peak heights calculated on this basis was in good agreement (within 3%) with the peak heights observed experimentally. This indicates that the nitrite peaks were not influenced by passing the solutions through the reductor column.

The cadmium column was activated by passing 0.2 M copper(II) sulphate through it. The efficiency of reduction depended on the amount of copper. When an 80-mm column was used, 85 μmol of copper(II) produced only ca.

50% reduction of 1 mM nitrate. Complete reduction was achieved when 200 μmol of copper(II) was passed through the column. Such a column could be used for several hours without visible decrease of efficiency. The composition of the electrolyte flowing through the column significantly affected the peak height (Table 2). When only distilled water was used, the peak was ten times smaller than with the optimal concentration of ammonium chloride. Ammonium sulphate was almost as effective as the chloride but potassium chloride reduced the response. The length of the reductor column was of prime importance. The 30-mm column used in the optimal flow conditions produced only 40% reduction of 50 μM nitrate compared to the 80-mm column.

The addition of EDTA for elimination of some cationic interferences decreased the efficiency somewhat. With the 80-mm reductor column, for 6—50 μM solutions of nitrate, the efficiency was around 103% with no EDTA present; this may be explained by partial elution of copper ions from the column, which then oxidize some iodide ions. When 0.6– 3.9 g l^{-1} EDTA was added to the carrier stream ions. (B in Fig. 2), the efficiency of reduction was 95—96%.

The peak heights recorded for 2—30 μM nitrate (Fig. 6) provided a linear calibration graph, which could be extended up to 800 μM nitrate. As in the case of nitrite, the detection limit was 4×10^{-7} M (6 μg l^{-1} nitrate-nitrogen).

Copper(II) and iron(III) interferences

Both copper(II) and iron(III) oxidize iodide to iodine and the presence of those cations in samples can cause positive errors (Table 3). A small addition of EDTA to the iodide solution in sulphuric acid effectively masked such interferences, and had no influence on the nitrite signal.

Another effect was observed in determination of nitrate; 5 mg l^{-1} copper(II) did not affect the determination of 0.1 mM nitrate, but iron(III) reduced the peak height significantly (Table 3). Addition of EDTA to the iodide solution in stream B (Fig. 2) eliminated this interference.

TABLE 2

Peak heights for reduction of 50 μM nitrate in the 80-cm column with different electrolytes as carrier solutions

Carrier solution	Conc. (g l^{-1})	Peak height (nA)	Carrier solution	Conc. (g l^{-1})	Peak height (nA)
Water	—	17	NH_4Cl	0.05	38
KCl	10	110		0.1	112
$(NH_4)_2SO_4$	10	165		0.5	165
				1	172
				5	179
				10	181
				20	165

TABLE 3

Effect of copper(II) and iron(III) on amperometric determination of nitrite and nitrate

Analyte	Interfering species	Peak height change (%)	
		No masking	0.3% EDTA
20 μM nitrite	15 μM Cu(II)	31	0
	77 μM Cu(II)	230	1.6
	17 μM Fe(III)	13	0
	85 μM Fe(III)	78	0
100 μM nitrate	17 μM Fe(III)	−5.7	0
	85 μM Fe(III)	−56	−4.7

TABLE 4

Determination of nitrate-nitrogen in soil extracts

Sample	Nitrate-nitrogen found (mg l^{-1})	
	Flow-injection amperometry	Potentiometry
1	9.6	9.6
2	7.5	7.3
3	7.4	7.3
4	7.7	7.9

Determination of nitrate in soil extracts

To check the practical utility of the developed procedure, nitrate was determined in greenhouse soil extracts. The flow-injection determinations with the amperometric detector were compared with potentiometric determinations using a nitrate-selective electrode (Table 4). The potentiometric determinations were done by the standard addition method with slope correction for dilution [23]. The differences at the 7—9 mg l^{-1} level did not exceed 0.2 mg l^{-1}.

REFERENCES

1 L. Anderson, Anal. Chim. Acta, 110 (1979) 123.
2 J. Růžička and E. H. Hansen, Anal. Chim. Acta, 114 (1980) 19.
3 M. F. Giné, H. Bergamin F°, E. A. G. Zagatto and B. F. Reis, Anal. Chim. Acta, 114 (1980) 191.
4 E. A. G. Zagatto, A. O. Jacintho, J. Mortatti and H. Bergamin F°, Anal. Chim. Acta, 120 (1980) 399.
5 J. F. Van Staden, Anal. Chim. Acta, 138 (1982) 403.
6 S. Nakashima, M. Yagi, M. Zenki, A. Takahashi and K. Toei, Anal. Chim. Acta, 155 (1983) 263.

7 A. Rios, M. Dolores Luque de Castro and M. Valcárcel, Analyst, 109 (1984) 1487.
8 A. G. Fogg, N. K. Bsebsu and M. A. Abdalla, Analyst, 107 (1982) 1040.
9 A. G. Fogg and N. K. Bsebsu, Analyst, 109 (1984) 19.
10 J. E. Newberry and M. Pilar Lopez de Haddad, Analyst, 110 (1985) 81.
11 S. Nakashima, M. Yagi, M. Zenki, A. Takahari and K. Toei, Fresenius' Z. Anal. Chem., 319 (1984) 506.
12 R. C. Schothorst, M. Van Son and G. den Boef, Anal. Chim. Acta, 162 (1984) 1.
13 A. G. Fogg, A. Y. Chamsi and M. A. Abdalla, Analyst, 108 (1983) 464.
14 J. Slanina, F. Bakker, A. G. Bruijn-Hes and J. J. Möls, Fresenius' Z. Anal. Chem., 289 (1978) 38.
15 E. H. Hansen, A. K. Ghose and J. Růžička, Analyst, 102 (1977) 705.
16 S. Alegret, J. Alonso, J. Batroli, J. M. Paulis, J. L. F. C. Lima and A. A. S. C. Machado, Anal. Chim. Acta, 164 (1984) 147.
17 R. Karlsson and L. G. Torstensson, Talanta, 21 (1974) 945.
18 A. Hulanicki, W. Matuszewski and M. Trojanowicz, Paper presented at Euroanalysis V Conference, Kraków, Poland, 1984.
19 J. Kurzawa, Anal. Chim. Acta, 173 (1985) 343.
20 M. Trojanowicz, A. Hulanicki, W. Matuszewski, M. Palys, A. Fuksiewicz, T. Hulanicka-Michalak, S. Raszewski, J. Szyller and W. Augustyniak, Anal. Chim. Acta, 188 (1986) 165.
21 See, e.g., I. M. Kolthoff and R. Belcher, Volumetric Analysis, Vol. 3, Interscience, New York, 1957, p. 310.
22 M. H. Boyer and J. B. Ramsey, J. Am. Chem. Soc., 75 (1953) 3802.
23 W. Matuszewski, A. Żytnikowski and M. Trojanowicz, Chem. Anal. (Warsaw), 25 (1980) 897.

Analytica Chimica Acta, 194 (1987) 129—138
Elsevier Science Publishers B.V., Amsterdam — Printed in The Netherlands

AMPEROMETRIC DETECTION OF CATIONIC NEUROTRANSMITTERS AT NAFION-COATED GLASSY CARBON ELECTRODES IN FLOW STREAMS

JOSEPH WANG*, PENG TUZHI and TERESA GOLDEN
Department of Chemistry, New Mexico State University, Las Cruces, NM 88003 (U.S.A.)
(Received 21st November 1986)

SUMMARY

Substantial improvements in amperometric monitoring of flowing streams are obtained by using Nafion-coated working electrodes. The charged coating tends to exclude anionic and neutral interferences, thus adding a new dimension of selectivity to electrochemical detection for flow-injection and liquid-chromatographic systems. A highly selective response is observed for cationic neurotransmitters in the presence of otherwise interfering substances (e.g., ascorbic acid, uric acid, bilirubin or chlorpromazine). The permselectivity and transport characteristics are evaluated with respect to solution pH, solvent, flow rate, film thickness, and other variables. The reduced flow-rate dependence results in low noise levels and detection limits of 0.04 and 0.10 ng of norepinephrine and epinephrine, respectively. A bilayer electrode coating, with a cellulose acetate film over the Nafion layer, offers a bifunctional (selectivity, protection) capability. Applicability to urine samples is demonstrated.

Amperometric detection for flowing streams has proven to be a viable technique in many analytical problems demanding high sensitivity and selectivity. Most work has focused on the development of new electrode materials or detector configurations, new detection schemes, or new applications. Despite the high level of activity in the area of chemically modified electrodes, there have been only few reports on their utility for detection in flow systems. Most work in this area has involved tailoring an electrocatalytic response (i.e., lowering the detector operating potential) for detection of compounds with kinetically-hindered redox reactions [1—4]. Another aspect of chemically modified electrodes, the permselectivity of various polymeric films, can also be advantageous for amperometric monitoring of flowing streams. A thin-layer glassy-carbon detector coated with a base-hydrolyzed cellulosic film was recently described [5]. The film prevents electroinactive macromolecules, which normally foul electrode surfaces by adsorption, from reaching the carbon surface but remains permeable to small molecules of analytical interest. Substantial improvements in the selectivity toward small analytes have also been demonstrated in flow-injection and liquid-chromatographic systems. Other permselective polymeric films, that may also offer improved detection in flowing streams, have not been studied for this purpose.

0003-2670/87/$03.50

This paper describes the properties, advantages, and utility of a glassy-carbon thin-layer detector coated with the perfluorosulfonated polymer Nafion. Because of their ion-exchange properties, stability, and versatility, Nafion films have been extensively examined in recent years [6—9]. The preferential incorporation of organic counter-ions into the polymer has offered sensitivity and selectivity advantages for trace [7] and in-vivo [9] measurements, respectively, of such species. Surprisingly, work aimed at utilizing the unique characteristics of Nafion polymers to improve amperometric detection in flowing solutions has not been reported. The present work demonstrates that such detection can be substantially enhanced with electrodes coated with charged Nafion films, which tend to exclude anionic interferences. Hence, new discriminative properties based on analyte charge are obtained (analogous to the size exclusion of cellulosic coatings), offering significant selectivity improvements when various species are monitored. Such behavior and advantages of Nafion-coated amperometric detectors are elucidated in this paper.

EXPERIMENTAL

Apparatus and reagents

The flow-injection system and the Bioanalytical Systems Model LC-303 liquid chromatograph were described previously [5]. A glassy-carbon thin-layer electrochemical detector (Model TL-5, Bioanalytical Systems) was used. The Ag/AgCl reference electrode and stainless-steel auxiliary electrode were located in a downstream compartment. An EG & G PAR Model 174 polarographic analyzer was used in the flow-injection experiments.

Stock solutions of dopamine, epinephrine, norepinephrine, serotonin, uric acid, chlorpromazine, bilirubin, desipramine, lidocaine (Sigma) and ascorbic acid (Baker) were prepared fresh each day. A 5% solution of Nafion (1100 EW) was obtained (Solution Technology, Mendenhall, PA). Cellulose acetate (39.8% acetyl content) was from Aldrich. A 0.05 M phosphate buffer (K_2HPO_4/KH_2PO_4, adjusted to pH 4 with phosphoric acid) was used as electrolyte and carrier in the flow-injection experiments. The chromatographic mobile phase was a 0.075 M chloroacetic acid solution adjusted to pH 4 with perchloric acid; the mobile phase contained 25 mg l^{-1} sodium octyl sulfate and 200 mg l^{-1} disodium ethylenediaminetetracetate. The urine samples were obtained from a healthy volunteer, filtered by passing through a glass filter (10—15-μm porosity), and diluted with the mobile phase solution.

Surface modification

Prior to the coating, the amperometric response of the bare surface was evaluated. For this purpose, the electrode was polished with 0.05-μm α-alumina particles, rinsed with double-distilled water, and allowed to air-dry. The same surface was modified by coating the disk and its surroundings with 6 μl of the 5% Nafion solution. The film was allowed to dry in air for 5 min.

The bilayer coating was prepared in two steps. First, the electrode and its surroundings were coated with 6 μl of the 5% Nafion solution; the Nafion film was allowed to air-dry. The outer cellulosic layer was formed by placing 10 μl of a 5% (v/v) cellulose acetate solution (in a 1:1 mixture of acetone and cyclohexanone) from a syringe on top of the Nafion layer; the solvents were then allowed to evaporate in air. Following this, the coated electrode was placed in stirred 0.07 M potassium hydroxide, where hydrolysis proceeded for the desired time.

After the modification, the cell was assembled and equilibrated with the flowing supporting electrolyte (or mobile phase) solution, while the working potential was applied. Amperometric measurements were made after the background current had decayed to a steady-state value.

RESULTS AND DISCUSSION

Transport characteristics

The utility of Nafion-coated electrodes for amperometric detection requires detailed knowledge of their permeability under the hydrodynamic conditions characterizing flowing systems. Because charge is expected to play a major role in the selectivity, the effect of solution pH on the permeability was explored. Figure 1 shows the dependence of the film permeability on the sample pH for different analytes possessing different charges. The ratio between the flow-injection peak current at the film-coated electrode over that at the bare electrode, is used as a measure of the permeability. Over the pH range tested, 1.5—7.4, the film is negatively charged, thus tending to exclude anionic or neutral species. For example, a negligible response is observed for ascorbic acid and uric acid. In contrast, passage of cationic species is maintained; the primary neurotransmitters, serotonin and dopamine, that are protonated over this pH range, yield well-defined peaks. For these species, high sensitivity is maintained; their peak sizes represent significant fractions of their responses at the bare electrode. Facile response was observed also for the neurotransmitters, epinephrine and norepinephrine, while the electrode was practically insensitive to bilirubin and the drugs, chlorpromazine, lidocaine or despiramine (not shown). Hence, selective detection of primary neurotransmitters is expected without interference from other oxidizable substances (endogeneous or exogeneous) present in body fluids. The pH profiles shown in Fig. 1 represent the net effect of the pH on the charges of the film and analytes examined. As will be shown below, the peak for the coated electrode approaches, and even exceeds, that of the bare electrode in liquid-chromatographic detection of primary neurotransmitters. Such increase in permeability, compared to that of Fig. 1, is attributed to longer residence times of solutes in the detector compartment, associated with the chromatographic band-broadening. Similar effects were observed for cellulosic coating following injections of different sample volumes [5].

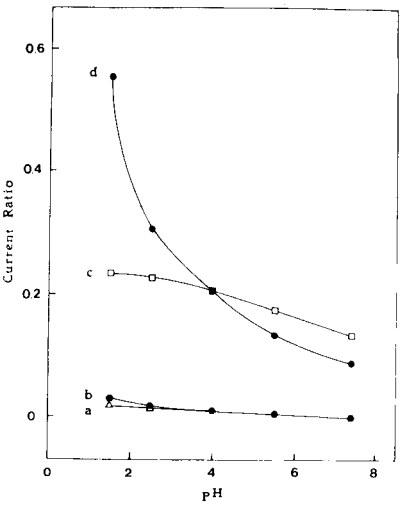

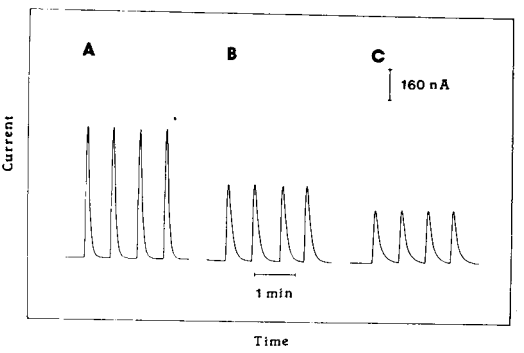

Fig. 1. Dependence of the film permeability (current ratio as defined in the text) on the solution pH for 2×10^{-5} M ascorbic acid (a), uric acid (b), serotonin (c) and dopamine (d). Flow-injection measurements with 20-μl sample loop, 1.0 ml min^{-1} flow rate and +0.90 V applied potential. Electrolyte and carrier, 0.05 M phosphate buffer adjusted to different pH values with phosphoric acid.

Fig. 2. Flow-injection current/time profiles for 4×10^{-5} M dopamine at glassy carbon electrodes: (A) bare; (B) coated with 3 μl of Nafion solution; (c) coated with 6 μl of Nafion solution. Supporting electrolyte and carrier, 0.05 M phosphate buffer solution (pH 4); other conditions as in Fig. 1.

In addition to solution pH, the film permeability depends on the supporting electrolyte and/or solvent used. The extent of ascorbic acid rejection was used to evaluate this effect (Table 1). None of the solvents tested yields complete blockage of ascorbic acid under the flow conditions of the thin-layer cell. Effective (>90%) rejection of ascorbic acid was observed in 0.05 M phosphate buffer (pH 4), 0.05 M chloroacetic acid (pH 4), 0.05 M perchloric acid, and 10% methanol/90% phosphate buffer (pH 4) solutions. In contrast, a relatively large permeability (ca. 0.2) was observed using 0.05 M hydrochloric acid, 10% propanol/90% phosphate buffer (pH 4) and 10% acetonitrile/90% phosphate buffer (pH 4) solutions. Such differences in permeability are probably attributable to differences in solvent swelling, particularly the water content. Diffusion of accompanying co-ions in cation-exchange polymers with high water content has been reported [10, 11], including the transport of oxalate through Nafion membranes [12]. Most subsequent flow-injection and liquid-chromatographic work reported here used 0.05 M phosphate buffer (pH 4) and 0.075 M chloroacetic acid (pH 4) solutions, respectively, that yielded 97% rejection of ascorbic acid. The use of solvents with relatively large permeability of ascorbate (or other accompanying co-ions) may be beneficial in applications such as dual-electrode

TABLE 1

Effect of solution conditions on permeability of bare and film-coated electrodes for ascorbic acid[a]

Solution	Current at peak maximum (nA)		Ratio (coated/bare)
	Bare electrode	Coated electrode	
0.05 M phosphate buffer (pH 4)	404	12	0.03
0.05 M HCl	366	83	0.22
0.05 M $HClO_4$	396	35	0.08
10% acetonitrile/90% 0.05 M phosphate buffer (pH 4)	348	69	0.19
0.05 M chloroacetic acid (adjusted to pH 4)	437	13	0.03
10% methanol/90% 0.05 M phosphate buffer (pH 4)	384	26	0.06
10% propanol/90% 0.05 M phosphate buffer (pH 4)	313	67	0.21

[a]Flow-injection conditions, same as in Fig. 1.

detection, where differences in peak ratios may assist in assessing the peak identity. No loss of film integrity was observed in the presence of organic solvents. For example, a series of 60 repetitive injections of the 10% acetonitrile/90% phosphate buffer solution containing 2×10^{-5} M ascorbic acid yielded a mean peak current of 70.1 nA (with range 68.6—71.2 nA) and a relative standard deviation of 1.1% under the conditions given in Table 1.

The rejection of anionic interferences depends also on the thickness of the Nafion film. Coatings prepared using 2, 4, and 6 μl of the Nafion solution yielded $i_{p,c}/i_{p,b}$ values of 0.08, 0.05, and 0.02, respectively, for flow-injection measurements of 2×10^{-5} M ascorbic acid (conditions as in Fig. 1 using a pH 4 phosphate buffer). Hence, permeability of accompanying ions increases as the film thickness decreases. As expected, the use of thinner films results also in increased permeability of counter ions; thus high selectivity is maintained as indicated from the ratio of anion-to-cation peak currents. Most subsequent work was performed using the 6-μl coatings.

Because transport through the film is a major contributor to the total diffusional transport, the response of the Nafion-coated electrode exhibits negligible dependence on flow rate. The effect of flow rate was evaluated, over the 0.2—1.2 ml min^{-1} range from chromatograms for injections of 50 ng of norepinephrine (applied potential, +0.6 V). A slight increase in peak current was observed over the 0.2—0.6 ml min^{-1} range, after which the

response exhibited independence from flow rate. A log-log treatment of the resulting data yielded two straight lines with slopes of 0.144 (over the 0.2—0.6 ml min^{-1} range) and —0.04 (over the 0.6—1.2 ml min^{-1} range). Hence, at high flow rates, film control of the current is observed. As will be shown below, such flow-rate independence results in lower noise level (and detection limits) compare to analogous measurements at the bare electrode. (The latter should yield a log-log plot with a slope of 0.333.) Measurements in systems with poorly controlled flow rate may also benefit from the behavior of the Nafion-coated detector.

Coated electrodes exhibit slower response characteristics than bare ones, because the transport through the film is the major contributor to the total diffusional resistance. Nagy et al. [9] reported that the apparent diffusion coefficient for dopamine in Nafion films is lower by three orders of magnitude than the corresponding value in aqueous solutions. Figure 2 shows characteristic flow-injection current/time profiles for 4×10^{-5} M dopamine at bare and Nafion-coated electrodes. All electrodes exhibited rapid increase of the current, with 2-s response time to reach 90% of maximum signal. The slow "wash-out" characteristics of the coated electrodes resulted in wider peaks. The peak widths (at 0.6 C_{max}) were 6.2 and 6.8 s for the 3-μl and 6-μl coated electrodes, compared to 4.6 s for the bare electrode. The difference in peak heights for the different Nafion coatings is due to the more facile transport through the thinner film. The slower response characteristics of the coated electrode are not a matter of major concern, as high injection rate and resolution are maintained in flow-injection and liquid-chromatography systems, respectively.

The potential of the permselective transport characteristics of Nafion-coated glassy carbon detectors for selective amperometric detection in flow-injection systems is illustrated in Fig. 3. With the bare electrode (A, C), it is not feasible to detect epinephrine or dopamine selectively in the presence of uric acid or ascorbic acid, respectively, because of the additive (oxidation) response. In contrast, the Nafion-coated electrode (B, D) effectively excludes the uric acid or ascorbic acid from reaching the surface; as a result, the epinephrine or dopamine response is not affected by the presence of these compounds, even at excess levels (compare peaks (a) and (c) in parts B and D). The Nafion-coated electrode exhibited similar improvements in selectivity for other mixtures of electroactive species. For example, measurements of 2×10^{-5} M serotonin were not affected by the presence of 1×10^{-4} M chlorpromazine. Similarly, selective measurement of 5×10^{-5} M dopamine was obtained in the presence of 5×10^{-5} M bilirubin. For both mixtures, analogous experiments at the bare electrode yielded additive response (not shown; conditions as in Fig. 2C except that a pH 9 phosphate buffer was used to illustrate the bilirubin exclusion). Hence, the in-situ "separation", based on the analyte charge, at the detector surface enhances the selectivity of flow-injection measurements. This may eliminate the need for a sample pretreatment or separator column, commonly required when such mixtures of oxidizable compounds are assayed.

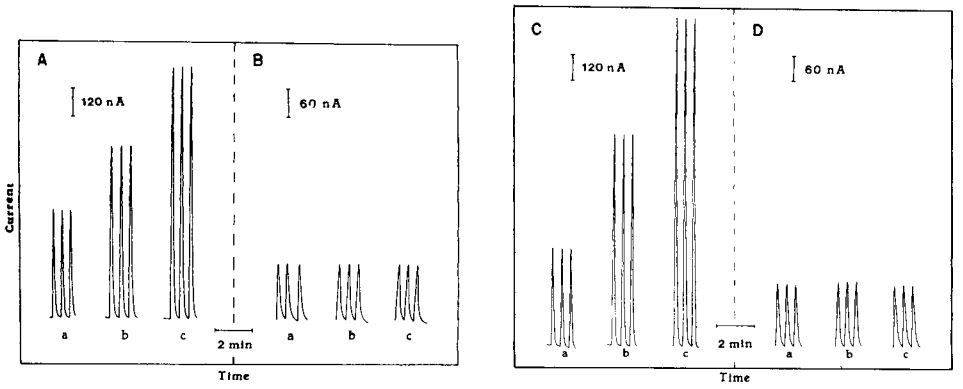

Fig. 3. Flow-injection determination of dopamine in the presence of ascorbic acid (A, B) or epinephrine in the presence of uric acid (C, D) at the bare (A, C) and Nafion-coated (B, D) electrodes: (a) 2×10^{-5} M dopamine (A) or epinephrine (C); (b) same as (a) but after addition of 2×10^{-5} M ascorbic acid or uric acid; (c) same as (b) but after addition of 2×10^{-5} M ascorbic acid or uric acid. Conditions as in Fig. 1, with a 0.05 M phosphate buffer (pH 4) solution.

Figure 4 shows chromatograms for a sample mixture containing ascorbic acid, uric acid, norepinephrine, and epinephrine obtained at the bare (A) and coated (B) electrodes. The effective rejection of anionic species is indicated from the nearly complete elimination of the ascorbic acid and uric acid peaks (1 and 2, respectively). In contrast, the large permeability of cationic neurotransmitters through the Nafion coating results in large peaks (3 and 4). The charge-exclusion characteristics of the Nafion-coated electrode can thus provide simplification of chromatograms recorded amperometrically. Such properties can be used to improve the selectivity and provide better assessment of peak purity. For example, Fig. 5 compares chromatograms for diluted (50-fold) urine sample, spiked with norepinephrine and epinephrine (15 ng injected) obtained at the bare and coated electrodes. At the bare electrode (A), the neurotransmitter peaks (designated as 3 and 4) are accompanied by eight peaks of variable sizes, representing various endogeneous oxidizable compounds. One of these compounds (t_R = 9.5 min) co-elutes with norepinephrine, resulting in a partially overlapping response. Most of these peaks are eliminated at the Nafion-coated electrode (B); as a result, a pure norepinephrine peak is obtained. Because of their high levels in urine, ascorbic acid and uric acid yield defined peaks (designated as 1 and 2) even at the coated electrode, despite their effective (ca. 95%) rejection by the Nafion film. Besides the simplification of chromatograms achieved at the coated electrode without lowering the operating potential, peak identity information may be improved substantially by comparing the response of the bare and coated electrodes (recorded separately or simultaneously in dual-electrode operation). Improvements in the response are expected also for the detection of primary neurotransmitters in samples containing their anionic and neutral metabolites.

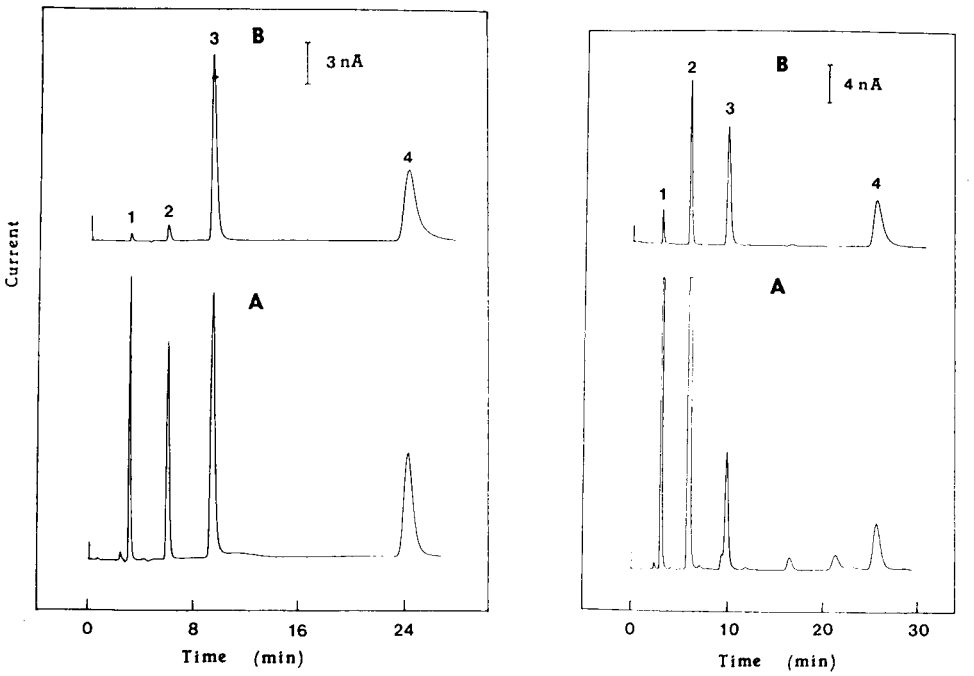

Fig. 4. Chromatograms for injections of 10 ng of ascorbic acid (1), 10 ng of uric acid (2), 20 ng of norepinephrine (3) and 20 ng of epinephrine (4) obtained (A) at the bare electrode, and (B) at the coated electrode. Applied potential, +0.60 V; mobile phase, 0.075 M chloroacetic acid solution adjusted to pH 4; flow rate, 1.0 ml min^{-1}.

Fig. 5. Chromatograms for diluted (50-fold) urine sample, spiked with norepinephrine and epinephrine (15 ng injected, peaks 3 and 4) obtained (A) at the bare electrode and (B) at the coated electrode. Conditions as in Fig. 4.

Chromatograms for injections of a mixture containing 5 ng each of norepinephrine and epinephrine were used to estimate the detection limit. The peaks were similar to those shown in Fig. 4, when the instrumental expansion was increased 6-fold. However, the Nafion-coated electrode exhibited a lower noise level than the bare electrode as a result of its reduced flow-rate dependence. The signal-to-noise characteristics indicated detection limits of 0.04 ng of norepinephrine and 0.10 ng of epinephrine (S/N = 3); the bare electrode yielded values of 0.125 and 0.30 ng, respectively.

Calibration plots, constructed from repetitive injections of dopamine solutions of increasing concentration (2—16) $\times$ 10^{-5} M, indicate improved linearity at the coated electrode under the conditions for Fig. 1, with a pH 4 phosphate buffer. Response was linear over the entire concentration range tested (slope, 81.1 $\times$ 10^{5} nA M^{-1}; intercept, 8.8 nA; correlation coefficient, 0.999). Some curvature was observed in the response at the bare electrode for concentrations higher than 12 $\times$ 10^{-5} M; the resulting plot had a slope of

187 × 10^5 nA M^{-1}, intercept of 64 nA and correlation coefficient of 0.998. A series of twenty successive injections of a 3 × 10^{-5} M epinephrine solution was used to evaluate the precision of the response (conditions as in Fig. 1, with a pH 4 phosphate buffer). A mean peak current of 210.7 nA, with a range of 205.6—216.0 nA, and a relative standard deviation of 1.5% were obtained. The bare electrode yielded a mean peak current of 659.4 nA, with a range of 656.0—672.0 nA, and a relative standard deviation of 0.7%. Hence, a high degree of reproducibility (without memory effects) is observed at the coated and bare electrodes.

Another important function of polymeric coatings is to minimize electrode fouling caused by adsorption of surface-active compounds. The size-exclusion characteristics of cellulose-coated electrodes have been particularly useful for this purpose [5]. In contrast, Nafion-coated electrodes do not offer such protection (Fig. 6, plots a). For epinephrine (A) and dopamine (B) solutions (containing 200 mg dl^{-1} gelatin and albumin, respectively), a rapid loss in electrode activity is observed, up to 80% decrease in the response for the 30 repetitive injections shown. This extent of electrode poisoning was larger than that observed at the bare electrode, indicating possible interaction between the film and the surfactants. It is possible, however, to design a bilayer polymer assembly, with a cellulose acetate film over the Nafion layer, to prevent electrode passivation while maintaining the permselectivity of the Nafion membrane. Such a bilayer electrode exhibits a uniform level of

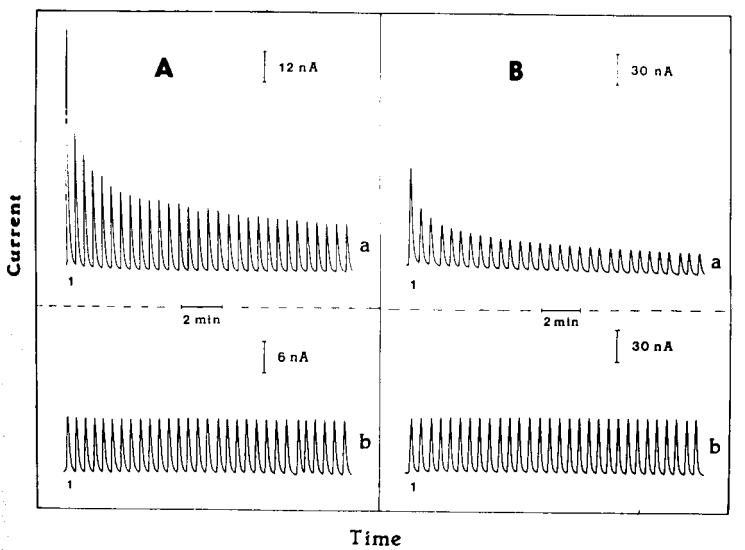

Fig. 6. Detection peaks at Nafion-coated (a) and bilayer-coated (b) electrodes. Repetitive injections of 2 × 10^{-5} M epinephrine (A) or dopamine (B) solutions, containing 200 mg dl^{-1} gelatin and albumin, respectively. Conditions as in Fig. 1, with a 0.05 M phosphate buffer (pH 4). Hydrolysis time (b), 40 min.

activity in the presence of gelatin and albumin (Fig. 6, plots b). Hence, the outer cellulosic layer blocks the large surfactant molecules from reaching the inner Nafion layer. The utility of a similar bilayer-modified electrode for improving the selectivity of cyclic voltammetric measurements was demonstrated recently [13]. The data in Fig. 6 indicate that amperometric monitoring of flowing streams can also benefit from the concept of bifunctional electrode coating, utilizing two different permselective overlaid films.

In conclusion, this study has demonstrated that the use of permselective (charged) electrode coating can enhance the power of amperometric detection in flowing solutions. The additional separation step, performed in-situ at the electrode surface, permits effective exclusion of anionic interferences. As a result, substantial improvements in the selectivity are observed for detecting primary neurotransmitters in flow-injection and liquid-chromatography systems. Additional advantages were achieved by using bifunctional electrode coating consisting of two different permselective overlaid films. Such features reduce further the attention necessary for sample cleanup. The recently introduced solution-cast Nafion films, which offer high stability in numerous organic solvents [14], should be useful for additional chromatographic separations. Analogous improvements may be achieved by using positively-charged coatings that would exclude cationic interferences [15]. It is clear that the versatility of tailoring electrode surfaces can benefit flow measurements in many practical situations. Work along these lines is in progress in this laboratory.

This work was supported by the National Institutes of Health (Grant No. GM 30913-03) and the American Heart Association. T. G. acknowledges the support of Battelle Pacific Northwest Labs. for the award of a summer fellowship during the course of this work.

REFERENCES

1 M. K. Halbert and R. P. Baldwin, Anal. Chem., 57 (1985) 591.
2 L. M. Santos and R. P. Baldwin, Anal. Chem., 58 (1986) 848.
3 J. Wang and B. Freiha, Anal. Chem., 56 (1984) 2266.
4 Y. Ikariyama and W. R. Heineman, Anal. Chem., 58 (1986) 1803.
5 J. Wang and L. D. Hutchins, Anal. Chem., 57 (1985) 1536.
6 H. S. White, J. Ledy and A. J. Bard, J. Am. Chem. Soc., 104 (1982) 4811.
7 M. N. Szentirmay and C. R. Martin, Anal. Chem., 56 (1984) 1898.
8 N. Oyama, T. Ohsaka, K. Sato and H. Yamamoto, Anal. Chem., 55 (1983) 1429.
9 G. Nagy, G. A. Gerhardt, A. F. Oke, M. E. Rice, R. N. Adams, R. B. Moore, M. N. Szentirmay and C. R. Martin, J. Electroanal. Chem., 188 (1985) 85.
10 P. Meares, in J. Crank and G. S. Park (Eds.), Diffusion in Polymers, Academic, London, 1986.
11 N. Oyama and F. C. Anson, Anal. Chem., 52 (1980) 1192.
12 I. Rubinstein and A. J. Bard, J. Am. Chem. Soc., 103 (1981) 5007.
13 J. Wang and P. Tuzhi, Anal. Chem., 58 (1986) 3257.
14 R. B. Moore and C. B. Martin, Anal. Chem., 58 (1986) 2569.
15 J. Wang, T. Golden and P. Tuzhi, Anal. Chem., 59 (1987) 740.

Analytica Chimica Acta, 194 (1987) 139—149
Elsevier Science Publishers B.V., Amsterdam — Printed in The Netherlands

PENETRATION OF MERCURY-ADSORBED PHOSPHOLIPID MONOLAYERS BY POLYNUCLEAR AROMATIC HYDROCARBONS

A. NELSON

Institute for Marine Environmental Research, Prospect Place, The Hoe, Plymouth PL1 3DH (Great Britain)

(Received 16th September 1986)

SUMMARY

The penetration of phospholipid monolayers (dioleoyl lecithin) adsorbed on mercury by polynuclear aromatic hydrocarbons (PAH) is described. The PAH studied were anthracene, phenanthrene, pyrene, benzo[a]anthracene, fluoranthene and perylene. The penetration is monitored by measuring the differential capacitance of the monolayer; the uptake of PAH causes a potential shift (up to −0.25 V) in the cathodic capacitance peaks. This occurs without displacement of the lipid from the mercury. The differential capacitance is measured by out-of-phase (90°) a.c. voltammetry and rapid cyclic voltammetry. The PAH permeate the mercury-adsorbed lipid layers from dilute aqueous solution; the order of affinity is benzo[a]anthracene > fluoranthrene = pyrene > anthracene = phenanthrene. The rates of penetration vary for the different compounds and depend on their water solubility.

In recent years there has been increased interest in the response of marine organisms to polynuclear aromatic hydrocarbons (PAH). This interest is due to the toxic effect of these contaminants on the biota in relation to their carcinogenicity and to the bio-accumulation of the compounds at various trophic levels [1]. There have been three main approaches to these problems: analytical, bioassay, and predictive. In the analytical approach, attempts are always made to determine the total concentration of pollutant in various environmental compartments. This approach has been undertaken in order to find out more about the biogeochemical cycling of the toxic compounds [2]. More recent work has attempted to define the speciation and consequent bio-availability of these contaminants in the environment by using physicochemical principles [3].

Bio-assay methods use a variety of indicator organisms to test the bio-accumulation and toxicity of contaminating substances [1, 4]. Indeed, the link between the analytically measured chemical species and its toxicity and bio-accumulation is of critical importance in environmental studies [1]. This concept is used in predictive models which examine the physical properties and chemical structure of the contaminant and relate this information to its toxic action [5]. As an example, the method involves simple examination of the phase-partitioning behaviour of the toxicant, e.g., its octanol/water partition coefficient, which can often be related to its bio-accumulation [1].

0003-2670/87/$03.50

In this paper, the penetration of mercury-adsorbed lipid monolayers by PAH in aqueous electrolyte is described. The influence of the PAH on the electrical transitions of these lipids was also investigated. The lipid-coated electrode consists of a phospholipid monolayer deposited on a mercury electrode; the formation and properties of these phospholipid membranes have been described in detail elsewhere [6]. This work was undertaken to examine the possibility of applying these lipid-coated electrodes to the assay of PAH in natural waters.

EXPERIMENTAL

The apparatus, materials and methods for preparing the monolayers and monitoring the electrical properties of the film have been described [6]. Briefly, a phospholipid monolayer is deposited on a hanging mercury drop electrode in a standard base electrolyte (0.55 mol dm^{-3} KCl). Subsequently, either a test extract of PAH is added to the electrolyte, or the electrode is transferred to a fresh test solution containing PAH. Standard solutions were prepared from authentic PAH which were dissolved in acetone (5×10^{-3} mol dm^{-3}). Diluted working solutions in acetone were prepared as necessary. A small quantity of the working solutions (1—5 μl) was added to the electrolyte. The acetone, itself, was shown to have no influence on the conformation of the monolayer. Six PAH compounds were examined in this study: anthracene, phenanthrene, pyrene, benzo[a]anthracene, fluoranthene and perylene.

A PAH extract from asphalt was also used to test the response of the membrane to a range of PAH. The PAH extract had a total concentration of 1.5×10^{-3} mol dm^{-3} PAH expressed as pyrene equivalent. The relative proportions of PAH in the mixture, determined by gas chromatography, are shown in Table 1. Small quantities of the extract were added to the test electrolyte in these experiments. All electrochemical measurements in the membrane were of differential capacitance (C_d). The potential and height of the cathodic capacitance peaks [6] were measured; these are sensitive to PAH penetration. The measurements were obtained by using a.c. voltammetry, recording the out-of-phase (90°) current and also using rapid cyclic voltammetry. All potentials are quoted versus Ag/AgCl (3.5 mol dm^{-3} KCl).

TABLE 1

Polynuclear aromatic compounds in the asphalt extract used, with their contents as a percentage of the total PAH measured

Compound	% present	Compound	% present	Compound	% present
Phenanthrene	17	Benzofluorene	4.7	Benzo[e]pyrene	3.9
Anthracene	5.6	Benzo[a]anthracene	6.2	Benzo[a]pyrene	4.7
Methylphenanthrenes	4.1	Chrysene/triphenylene	7.2	Indo[1,2,3-cd]pyrene	2.1
Fluoranthene	20	Benzofluoranthene	9.8	Benzo[ghi]perylene	2.6
Pyrene	12				

The penetration experiments were done in the following way. To monitor the penetration by the various test compounds, the compound was added to the required concentration. The solution was then stirred and the cathodic capacitance peaks were continually monitored by rapid cyclic voltammetry at 84 V s^{-1} between −0.6 V and −1.1 V. In this way, the rate of penetration could be followed by the shift in potential and changed height of these peaks. After 15 min, an a.c. voltammogram was recorded. The equilibration experiments of the lipid film with PAH were done similarly. To observe expulsion of the PAH from the PAH-penetrated membrane, the coated electrode was transferred to a fresh solution of electrolyte. The solution was stirred and the membrane scanned at 230 V s^{-1} from −0.06 V to −1.5 V. Taking the potential more cathodic than −1.25 V removes PAH from the film and with the rapid cyclic voltammetric method, the layer can be continually monitored.

RESULTS AND DISCUSSION

Influence of the PAH on the lipid film

Solutions containing 2×10^{-7} mol dm^{-3} PAH were used. The PAH penetrate the lipid film to varying extents from dilute solution. Their effect on the capacitance/potential plot is displayed in Fig. 1, which shows that PAH penetration shifts the cathodic capacitance peaks. The effect is similar for all phospholipid layers of phosphatidyl choline (PC; lecithin) and phosphatidyl ethanolamine (PE). Here results are reported for dioleoyl lecithin (di-O-PC) films. These are the most suitable for this kind of work because they exhibit the best reproducibility and stability of conformation. Penetration by PAH also reduces the value of the capacitance minimum, although not initially. For pyrene, benzo[a]anthracene and fluoranthene, this decrease is ~20%. Penetration of PAH into the hydrocarbon region of the lipid can be inferred from this decrease, which corresponds to an increase in thickness of the lipid layer (see below). The preservation of the fluidity of the lipid monolayer is shown by the continued stability of the film on the electrode and the preservation of the fundamental character of the capacitance/potential profile. The significance of all the capacitance regions is the same as in the pure lipid [6]. The low capacity region inhibits faradaic ionic reactions and the membrane becomes permeable at the onset of the first cathodic capacitance peak. It is important to note that, although the penetration shifts the cathodic capacitance peaks, it has no effect on the final −1.25 V peak.

The PAH penetration also affects the potential of zero charge (*PZC*); the capacitance minimum shifts negatively by ca. 0.1 V on penetration of the di-O-PC monolayer with pyrene, benzo[a]anthracene and fluoranthene. A combined interaction of the PAH with lipid and mercury is indicated because the PAH was found not to penetrate the lipid at an air/electrolyte interface. This was readily shown by adsorbing lipid on to mercury at the air/water interface above a subphase electrolyte containing PAH. The most convenient

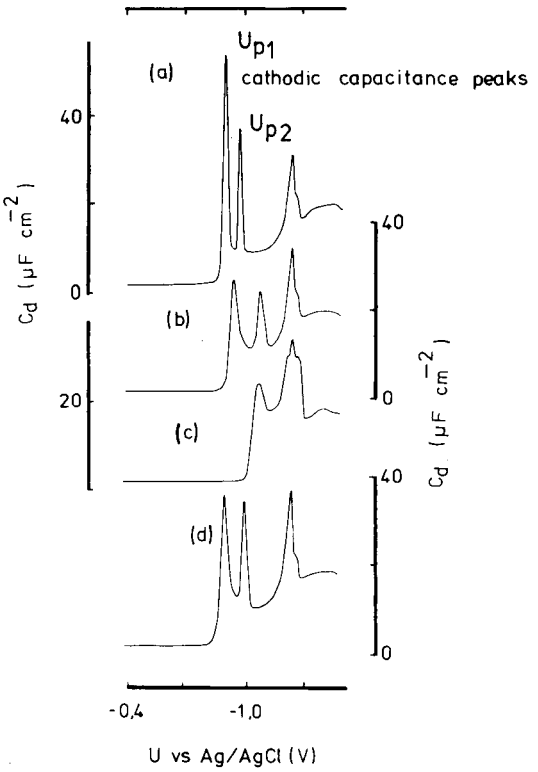

Fig. 1. Differential capacitance (C_d) vs. potential (U) for different monolayers: (a) di-O-PC monolayer; (b) monolayer penetrated by phenanthrene; (c) monolayer penetrated by pyrene; (d) after expulsion of PAH from the film in base electrolyte. Differential capacitance measured by phase-sensitive a.c. voltammetry, phase angle 90°, amplitude 10 mV, scan rate 5 mV s^{-1}, 75 Hz. For (b) and (c), 2×10^{-7} mol dm^{-3} PAH in base electrolyte, 0.55 mol dm^{-3} KCl.

monitor of the extent of penetration is the shift in potential and the changed height of the capacitance peaks. Initial experiments showed that from a 2×10^{-7} mol dm^{-3} concentration of PAH in the electrolyte, pyrene, fluoranthene and benzo[a]anthracene caused a large shift in these peaks, whereas phenanthrene and anthracene initiated smaller changes. This divides the PAH into two groups with respect to their effect on the lipid monolayer. A further effect of the PAH penetration is to shift the increase in anodic capacitance [6] negatively.

The surface excess of PAH in the lipid was measured. Thus the quantity of ^{14}C-phenanthrene which had penetrated a lipid film (supported on a mercury pool) from a 2×10^{-7} mol dm^{-3} solution was measured after 2 h and was found to be 0.75×10^{-10} mol cm^{-2}.

The PAH-penetrated film was stable at all potentials up to −1.1 V, but if the potential was taken cathodic of the −1.25 V peak, the PAH was expelled

from the film. This is in accord with previous conclusions on the properties of the film [6]. The cathodic capacitance peaks represent re-orientation and an increase in permeability of the film; the final peak represents a major structural change which leads to expulsion of the PAH. The rate of this expulsion varies for different PAH (see below), the time for complete loss of PAH varying from 1 to >60 min. It is significant that the capacitance/potential profile of the lipid film after expulsion of PAH is usually very similar to that of the pure lipid except for some residual PAH (Fig. 1d). This confirms that, in most cases, the PAH has no disrupting influence on the film and it truly penetrates the film rather than displacing it from the surface.

Equilibrium penetration of PAH into the lipid film

The penetration of PAH into the film from different solution concentrations was monitored. Equilibrium penetration can be defined as that which occurs after stirring for 15 min, scanning continuously between −0.6 V and −1.1 V during that time. However, in the case of perylene, penetration continued after 15 min (see below). Scanning the potential across the two capacitance peaks reduced the rate of penetration of PAH but allowed the film to be continuously monitored during penetration. Additionally, when the membrane was held in open circuit during penetration, there was some drift in membrane structure. Because the measuring technique involves traversing the potentials of the two capacitance peaks, it is reasonable to maintain the potential scanning across these capacitance peaks during the penetration period. After each penetration experiment, the capacitance was recorded by a.c. voltammetry and, in this instance, the extent of shift of the cathodic capacitance peaks and the value of the capacitance minimum were observed. The results are displayed in Fig. 2. Various points can be noted. First, the shift in the capacitance peak is non-linear with respect to the concentration of PAH in solution; the non-linearity is more marked for penetration by phenanthrene than by pyrene. Secondly, the initial penetration by PAH does not cause a decrease in the capacitance minimum. From previous work [6], it is assumed that a reciprocal relationship exists between the capacitance and the thickness of the hydrocarbon region of the film. However, the dielectric constant of the penetrating PAH is higher than that of an alkane hydrocarbon which is about 2. For example, the dielectric constant of phenanthrene is given as 2.8 [7]. At low surface excess of PAH, this will have little effect on the capacitance, but at higher penetrations the capacitance will increase if there is no thickening of the membrane. Because there is a decrease in capacity minimum with penetration by PAH at higher concentrations of PAH, the data indicate that the initial stages of penetration occur with little increase in thickness of the film but that the film thickens at higher penetrations.

Potential shift of the cathodic capacitance peaks

The PAH penetrates the membrane in the potential domain of the capacity minimum. In the potential region negative to the cathodic capacitance peaks,

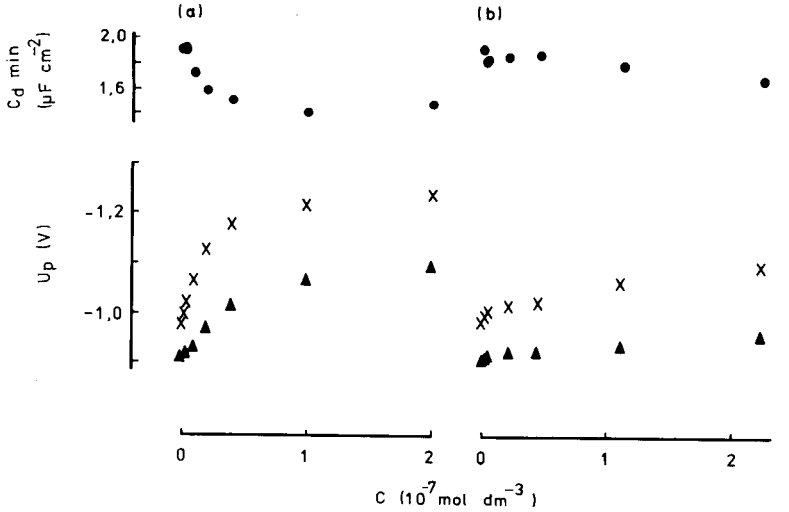

Fig. 2. Equilibrium penetration of PAH into di-O-PC monolayer in 0.55 mol dm^{-3} KCl. Potential of cathodic capacitance peaks, U_{p1} (▲) and U_{p2} (×), and the capacity minimum, $C_{d\,min}$ (•), of di-O-PC vs. concentration (C) of (a) pyrene and (b) phenanthrene in solution. Penetration time 15 min; differential capacitance measured by a.c. voltammetry as in Fig. 1.

there is over 90% suppression of pyrene penetration of the monolayer. Indeed, capacitance curves following the second capacitance peak, U_{p2}, always coincided for monolayers with varying degrees of penetration. As a result, it is proposed that this potential region represents an equivalent energetic state of the membrane. Conceptually, the penetration of the membrane by PAH stabilises the monolayer within the capacity minimum region relative to the monolayer outside of this potential domain. This causes a negative shift in the cathodic capacitance peaks. This stabilisation or Gibbs energy decrease is the driving force for membrane penetration by PAH.

At higher PAH concentrations, the decrease in capacity minimum indicates that the membrane is thickening, which suggests that the mechanism of penetration is changing. This change can be seen from the capacitance data. When the potential shift of the capacitance peaks is plotted against the log concentration (log C) of PAH in solution (Fig. 3), the shift of the peak concurrent with thickening of the membrane has a different relationship with log C than that caused by penetration without thickening.

Contributions to the Gibbs energy of interaction between PAH and the lipid membrane on the mercury will be: (a) the lipid solubility of the hydrocarbon relative to its solubility in water, which in many cases is equivalent to the octanol/water partition coefficient; and (b) the π-electron interaction between PAH and the lipid-coated mercury. The evidence for the latter effect is the shift in *PZC* on penetration and the increased cathodic capacitance peak shift induced by the same concentrations of those PAH containing more

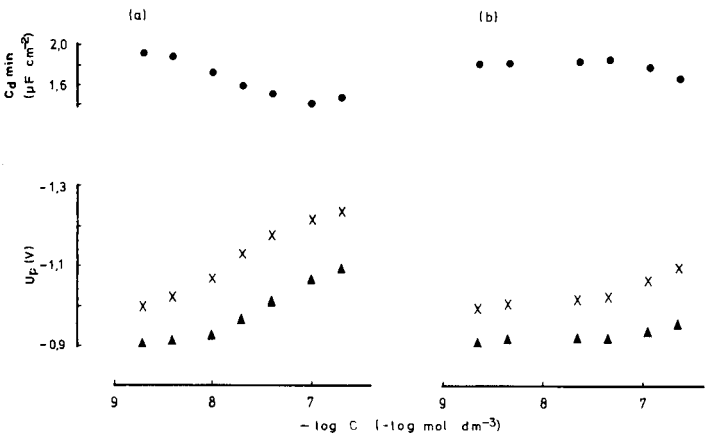

Fig. 3. Potential of cathodic capacitance peaks, U_{p1}(▲) and U_{p2}(×), and the capacity minimum, $C_{d\ min}$(●) of di-O-PC vs. the log concentration (log C) of (a) pyrene and (b) phenanthrene. Base electrolyte 0.55 mol dm^{-3} KCl; penetration time 15 min; differential capacitance measured by a.c. voltammetry as in Fig. 1.

aromatic rings. Thus from observation of the relative shifts of the cathodic capacitance peaks (Table 2), the affinity of PAH for the lipid membrane can be placed in the following order: benzo[a]anthracene > pyrene = fluoranthene > anthracene = phenanthrene. The π-electron interaction has been noted previously for the adsorption of PAH on a bare mercury surface [8].

Rate of penetration of PAH into the lipid film

The rate of penetration of PAH into the lipid film varies for each compound and can be used to aid the identification of individual PAH. The penetration rate was monitored empirically by observing the percentage decrease in capacitance of the first cathodic capacitance peak (initially at −920 mV) during the rapid cyclic voltammetric scans and also the cathodic shift in its potential (Fig. 4a). These two parameters are plotted against each other in Fig. 4(b) for films penetrated by various PAH. A linear relationship is observed for up to 60% reduction in the peak height. Scatter in the data is likely to result from inaccuracy in measuring the potential on the oscilloscope during the experiment. For this reason, the fractional depression of this peak is used here as an indicator of the extent of penetration up to 60% suppression of the peak. Results for the rates of penetration are displayed in Fig. 4(c). In these experiments, the PAH added to the solution was in excess of that necessary to give maximum shift of the capacitance peak after continued equilibration with the film (2×10^{-7} mol dm^{-3}). The rates of penetration vary within the two groups of compounds and depend to some extent on the solubility of the PAH in water (Table 2). Notably the rate of anthracene and phenanthrene penetration into the membrane differs significantly. The rate

TABLE 2

Properties of PAH and their penetratability into di-O-PC monolayers on mercury electrodes[a]

PAH	M.W.	Water soly. ($\mu g\ dm^{-3}$)	Suppression of U_{p1}[b] (%)	Time for expulsion[c] (min)	Log K_{ow}[d]	Max. shift in U_{p1}[e] (V)	Max. decrease in $C_{d\,min}$[f] (%)
Anthracene	178	44.6	21	1	4.54	−0.056	6.8
Phenanthrene	178	1070	42	0.5	4.56	−0.060	8.6
Pyrene	202	132	46	8	5.17	−0.191	21
Fluoranthene	202	206	61	8	4.90	−0.191	19
Benzo[a]anthracene	228	9.4	18	>60	5.61	−0.250	18
Perylene	252	0.4	4	—	6.53	−0.006	0

[a]All data on the physical properties are from [2] except perylene which is from [9]. [b]U_{p1}, first cathodic capacitance peak; suppression relates to 2-min penetration. [c]Time for expulsion of PAH from membrane. [d]Octanol/water partition coefficient. [e]Maximum shift in U_{p1} after 15-min penetration. [f]$C_{d\,min}$, capacitance minimum.

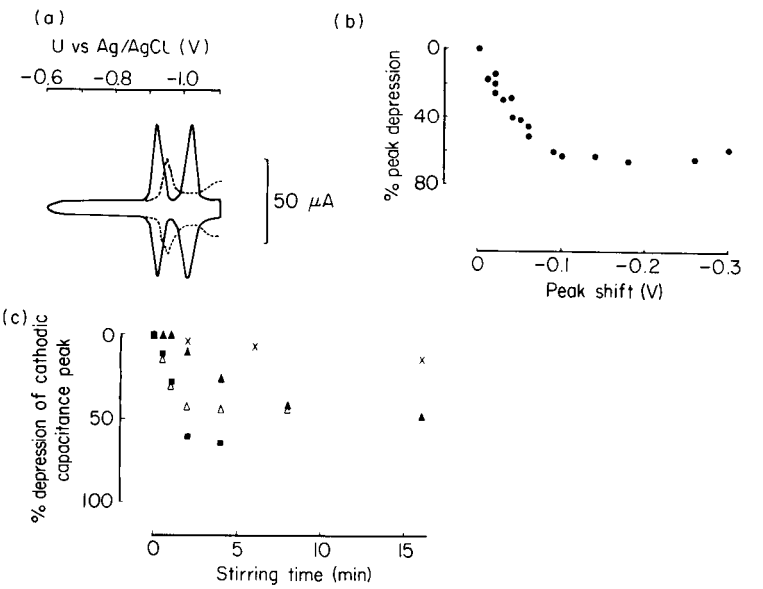

Fig. 4. Cathodic capacitance peaks of di-O-PC penetrated by PAH monitored by rapid cyclic voltammetry at 84 V s^{-1} from −0.6 to −1.1 V. Base electrolyte 0.55 mol dm^{-3} KCl; PAH concentration 2 × 10^{-7} mol dm^{-3}. (a) Oscilloscope trace of capacitance peaks of di-O-PC before (——) and after (— — —) penetration by phenanthrene. (b) Plot of % decrease of the first capacitance peak (U_{p1}) vs. its potential; recorded for all PAH penetrations into di-O-PC. (c) Plot of % decrease of the first capacitance peak vs. PAH penetration time for different PAH: (▲) anthracene; (△) phenanthrene; (■) fluoranthene; (X) perylene.

of penetration of PAH into the lipid film from various matrices can be measured. Figure 5(a) shows the rate of penetration of the lipid film by an asphalt PAH extract (6×10^{-9} mol dm^{-3} pyrene equivalent) added to the pure base electrolyte and also to a natural sea-water sample (salinity 34‰).

The removal of the PAH from the lipid film is also of interest. Table 2 shows the relative times for maximum removal of the PAH from the lipid film. As with the penetration rate, there is some relationship with water solubility.

Preliminary applications

A PAH extract from asphalt was added to the base electrolyte in order to assess its composition qualitatively. The electrolyte was made up to 6×10^{-8} mol dm^{-3} (pyrene equivalent) with the PAH extract. This approaches the flattened region of the capacitance peak shift/PAH concentration curve (cf. Fig. 2). The traces showed that penetration after 15 min gave a maximum shift to the cathodic capacitance peaks (−0.191 V for U_{p1}), possibly indicating high proportions of pyrene, fluoranthene and benzo[a]anthracene in the extract. The rate of penetration also fell between that observed for these three compounds (Fig. 5a). During expulsion, there remained considerable PAH in the lipid after 60 min. These qualitative tests indicated that there was a significant proportion of pyrene, fluoranthene and benzo[a]anthracene in the extract. The composition of the extract shows this to be the case (see Experimental). These three PAHs represent 38% of the measured PAH in the sample, whereas phenanthrene and anthracene constitute 23%. Presumably

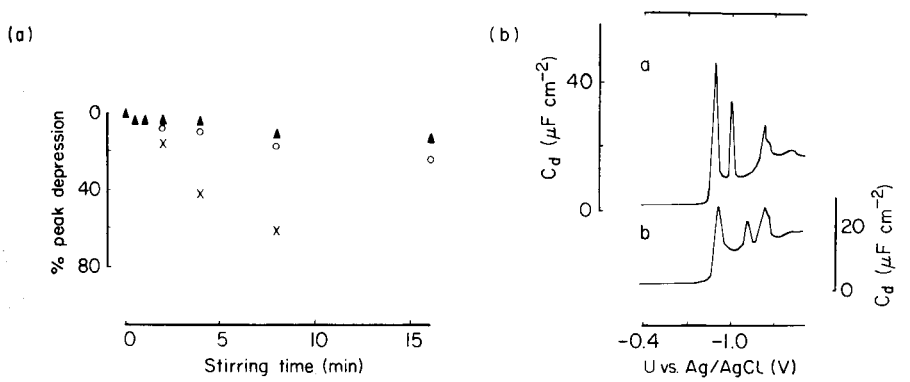

Fig. 5. (a) Plot of percentage decrease of the capacitance peak vs. PAH penetration time: (o) asphalt PAH extract, 6×10^{-9} mol dm^{-3} pyrene equivalent in 0.55 mol dm^{-3} KCl; (▲) asphalt PAH extract, 6×10^{-9} mol dm^{-3} pyrene equivalent in sea water (salinity 34‰); (×) asphalt PAH extract, 6×10^{-8} mol dm^{-3} pyrene equivalent in 0.55 mol dm^{-3} KCl; capacitance peaks were monitored by rapid cyclic voltammetry as in Fig. 4. (b) Differential capacitance (C_d) versus potential (U) for: (a) di-O-PC film in the sea water; (b) di-O-PC film penetrated by pyrene from 2×10^{-8} mol dm^{-3} pyrene in the sea water; differential capacitance measured by a.c. voltammetry as in Fig. 1.

the other 4- and 5-membered ring PAHs in the extract contribute significantly to the observed membrane response.

The penetration of the lipid membrane with the isomers anthracene and phenanthrene has been compared to their effect on the stability of the lysosomal membrane of the digestive gland cells of the edible mussel, *Mytilus edulis* exposed to these PAH [4]. The acute effect of the isomers on the membrane is quite different for each one. This is presumably partly related to the rate of equilibration of the lipid membrane with the PAH. However, at the end of the experiment, the concentration of PAH in the lipids was the same.

With respect to interferences, the shift in cathodic capacitance peaks appears to be specifically related to PAH penetration. This is probably because the mechanism of penetration depends on the presence of conjugated aromatic rings and on the high values of lipid/water partition coefficients and limited water solubilities; these characteristics are unique to the PAH system. Other moieties in solution such as humic acids, proteins, alkanes, polychlorinated hydrocarbons, major ions and heavy metals such as Cd^{2+} and Pb^{2+}, have other very characteristic effects on the lipid membrane and will not normally obscure the capacitance peak shift (see, e.g., Fig. 5b). However, high concentrations of organic matter (>20 mg l^{-1}) will tend to displace the lipid from the mercury. Detailed studies on the selectivity of the lipid coated electrode are to be reported in a subsequent paper.

Conclusions

Polynuclear aromatic hydrocarbons (PAH) penetrate mercury-adsorbed phospholipid monolayers from dilute aqueous solution. The penetration causes a shift and decrease in height of the cathodic capacitance peaks and these can be measured readily. The extent of penetration varies for different compounds.

The rates of penetration are variable and depend to some extent on the water solubility of the PAH. Thus water solubility enhances the rate of transfer of the PAH from the hydrophilic to the hydrophobic region of the lipid monolayer. The penetration is, in most cases, reversible and the PAH can be expelled from the film at potentials more cathodic than the re-orientation peak at −1.25 V. The PAH does not displace the lipid film from the mercury.

The findings in this paper have stimulated studies on the applications of the lipid-coated electrode to the assay of PAH in natural waters. Results will be reported in a future paper.

The author thanks Dr. Jim Readman for the PAH extract and gas chromatographic measurements and Drs. Readman, Donkin and Mantoura for very helpful comments on this work. The support of the Natural Environment Research Council, of which the Institute for Marine Environmental Research is a component part, is gratefully acknowledged.

REFERENCES

1 A. Nelson and P. Donkin, Mar. Pollut. Bull., 16 (1985) 164.
2 J. W. Readman, R. F. C. Mantoura, M. M. Rhead and L. Brown, Est. Coast. Shelf. Sci., 14 (1982) 369.
3 J. W. Readman, R. F. C. Mantoura and M. M. Rhead, Fresenius Z. Anal. Chem., 319 (1984) 126.
4 M. N. Moore and S. V. Farrar, Mar. Env. Res., 17 (1985) 222.
5 J. Harris, A. J. Bale, B. L. Bayne, R. F. C. Mantoura, A. W. Morris, L. A. Nelson, P. J. Radford, R. J. Uncles, S. A. Weston and J. Widdows, Ecol. Mod., 22 (1984) 253.
6 A. Nelson and A. Benton, J. Electroanal. Chem., 202 (1986) 253.
7 R. C. Weast (Ed.), Handbook of Chemistry and Physics, CRC Press, Cleveland, OH, 1974, p. E58.
8 A. M. Gerovich, Dokl. Akad. Nauk. SSSR, 96 (1954) 543.
9 D. Mackay, A. Bobra, W. Y. Shiu and S. H. Yalkousky, Chemosphere, 9 (1980) 701.

Analytica Chimica Acta, 194 (1987) 151—162
Elsevier Science Publishers B.V., Amsterdam — Printed in The Netherlands

FACTORS AFFECTING THE PRECISION OF A NEW METHOD FOR DETERMINING THE REDUCED AND OXIDIZED FORMS OF A REDOX COUPLE BY A SINGLE POTENTIOMETRIC TITRATION

LOUIS MEITES*[a] and NICOLANGELO FANELLI

Istituto di Chimica Analitica Strumentale (C.N.R.), Dipartimento di Chimica e Chimica Industriale dell'Università, Via del Risorgimento 35, 56100 Pisa (Italy)

(Received 21st October 1986)

SUMMARY

In a potentiometric titration of a solution that contains both the reduced form Red_2 and the oxidized form Ox_2 of a redox couple, at concentrations of $c^0_{Red_2}$ M and $c^0_{Ox_2}$ M, respectively, using as reagent a solution that contains the oxidized and reduced forms Ox_1 and Red_1 at concentrations of c_{Ox_1} M and c_{Red_1} M, respectively, the reaction that occurs is

$$n_1Red_2 + n_2Ox_1 = n_1Ox_2 + n_2Red_1;\ K_t = \exp[n_1n_2(E_1^{0\prime} - E_2^{0\prime})/0.02569]$$

if all of the reactants and products are monomeric and if the titration is done at 25°C. By applying weighted non-linear regression analysis to the data obtained in such a titration, if c_{Ox_1} is known, it is possible to evaluate four parameters: $c^0_{Red_2}$, $c^0_{Ox_2}$, and the formal potentials $E_2^{0\prime}$ and $E_1^{0\prime}$ for the couple titrated and the reagent couple, respectively. For the common situation in which n_1 and n_2 are equal, this paper describes the ways in which the precisions of all four parameters depend, over a wide range of conditions, on their values and on the precisions of measurement of the volume of reagent and the potential of the indicator electrode.

About a dozen years ago, several groups of authors [1—4] showed, more or less simultaneously, that applying non-linear regression analysis to data obtained in potentiometric titrations yields values of the physicochemical parameters characterizing those titrations that are both more accurate and more precise than those that can be obtained in any other way. Isbell et al. [1] showed this to be true for potentiometric precipitation titrations. In titrations of acetate ion, a very weak base, with hydrochloric acid in aqueous solutions, Barry and Meites [3] achieved precisions one to two orders of magnitude better than could be secured by conventional techniques of end-point location, and showed that titrations could still be done successfully even with solutions so dilute that there is no point of maximum slope on the titration curve. Ingman et al. [2] were able to analyze mixtures of acetic and propionic acids by titrating them with a strong base even though the

[a]Permanent address: Department of Chemistry, George Mason University, 4400 University Drive, Fairfax, VA 22030, U.S.A.

0003-2670/87/$03.50

values of pK_a for these acids differ by only 0.12, so that the titration curve does not have a point of inflection near the equivalence point of the titration of the stronger acid.

The use of non-linear regression analysis not only improves the accuracy and precision of the results, but also increases the efficiency of experimentation by making it possible to evaluate several parameters simultaneously from the data obtained in a single titration. Some such possibilities are classical, such as the evaluation of pK_a from the titration curve obtained on titrating a weak acid with a base, although the use of regression analysis always leads to a substantial improvement of precision. Others, such as the simultaneous determination of a weak base in the solution being titrated and standardization of the strong acid used as the titrant [4], would scarcely be possible if any other technique were used for interpreting the data.

There have been several investigations [5–7] of the ways in which the precisions of measurement of the volume of reagent and the pH effect the precisions of the parameters computed from data obtained in acid–base titrations of different types, including titrations of weak [5] and strong [6] acids with strong bases and titrations of mixtures of two weak acids with a strong base [7]. This paper describes the results of a similar study of a novel method in which data obtained in a potentiometric redox titration are used to evaluate the concentrations of both the reduced form and the oxidized form of the redox couple present in the solution being titrated. Although its conceptual foundation is very simple, the method is novel because it would be difficult or impossible to implement in any other way.

THEORY AND PROCEDURE

Consider the titration of V^0 cm^3 of a solution containing the reduced form Red_2 of the redox couple

$$Ox_2 + n_2e = Red_2; E^{0\prime} = E_2^{0\prime}$$

at a concentration of $c^0_{Red_2}$ M with a c_{Ox_1} M solution of the oxidizing agent Ox_1, which is the oxidized form of the couple

$$Ox_1 + n_1e = Red_1; E^{0\prime} = E_1^{0\prime}$$

The solution being titrated must contain Ox_2 at some finite concentration, for if it did not it would be an infinitely powerful reducing agent and would reduce dissolved oxygen, hydrogen ion, water, or some other oxidizing agent. Similarly, the titrant must contain some Red_1 because it would be an infinitely powerful oxidizing agent if it did not, and would oxidize chloride ion, water, or some other reducing agent. The initial concentration of Ox_2 in the solution being titrated, and the concentration of Red_1 in the titrant, are denoted by $c^0_{Ox_2}$ and c_{Red_1}, respectively.

To minimize the effects of round-off errors, the following procedure was adopted for calculating the composition of the titration mixture at any point

on the titration curve for any combination of the parameters being evaluated. Let V be the volume, in cm^3, of reagent that has been added. Then, if no reaction occurred, the concentrations of the species would be given by

$$[Red_2]_a = V^0 c^0_{Red_2}/(V + V^0); [Ox_2]_a = V^0 c^0_{Ox_2}/(V + V^0)$$
$$[Red_1]_a = V c_{Red_1}/(V + V^0); [Ox_1]_a = V c_{Ox_1}/(V + V^0) \quad (1)$$

The subscript "a" denotes this initial approximation. Of course the reaction

$$n_1 Red_2 + n_2 Ox_1 = n_1 Ox_2 + n_2 Red_1$$

does occur. For convenience, both n_1 and n_2 are henceforth assumed to be equal to 1, so that the results pertain to titrations like those of mixtures of iron(II) and (III) with cerium(IV), or of titanium(III) and (IV) with copper(II) in solutions containing high concentrations of chloride. If the equivalence point has not yet been reached, a second approximation is made by assuming that the reaction is complete (that is, that all of the added Ox_1 has been consumed by reacting with the excess of Red_2 that is still present). On this basis, the concentrations are given by

$$[Red_2]_b = [Red_2]_a - [Ox_1]_a = (V^0 c^0_{Red_2} - V c_{Ox_1})/(V + V^0)$$
$$[Ox_2]_b = [Ox_2]_a + [Ox_1]_a = (V^0 c^0_{Ox_2} + V c_{Ox_1})/(V + V^0)$$
$$[Red_1]_b = [Red_1]_a + [Ox_1]_a = (V c_{Red_1} + V c_{Ox_1})/(V + V^0)$$
$$[Ox_1]_b = 0 \quad (2)$$

where the subscript "b" denotes this second approximation. Now the reaction is assumed to reach equilibrium. To do so, D mmol cm^{-3} of Ox_1 and D mmol cm^{-3} of Red_2 must be produced, and D mmol cm^{-3} of Ox_2 and Red_1 must be consumed. The resulting concentrations at equilibrium will be

$$[Red_2] = [Red_2]_b + D; [Ox_2] = [Ox_2]_b - D$$
$$[Red_1] = [Red_1]_b - D; [Ox_1] = [Ox_1]_b + D = D \quad (3)$$

The equilibrium constant K_t is given by

$$K_t = [Ox_2]\,[Red_1]/[Red_2]\,[Ox_1] = \exp[(E^{0\prime}_1 - E^{0\prime}_2)/0.02569] \quad (4)$$

if the reaction occurs at 25°C. Combining Eqns. 3 and 4 yields a quadratic equation that can readily be solved for D. The result was used to compute $[Red_2]$ and $[Ox_2]$ from Eqns. 2 and 3, and the potential E of an indicator electrode immersed in the mixture could then be computed from the Nernst equation for the Ox_2/Red_2 couple. Value of E at points beyond the equivalence point were computed by a completely analogous procedure.

For each desired combination of the assumed values of the parameters, including the standard errors of measurement σ_V and σ_E of the volume of reagent and the potential, respectively, the theoretical coordinates of 30 points along the titration curve were computed from the above equations. The first point always corresponded to $f = 0$, where f is the familiar titration parameter and is defined by

$$f = Vc_{\mathrm{Ox}_1}/V^0c^0_{\mathrm{Red}_2} \tag{5}$$

in the present application. The value of f at each subsequent point was obtained by adding an increment Δf to the last preceding value. The algorithm used to generate the values of Δf was

(1) if $2 < N < 5$, $\Delta f = 0.01$; (2) if $N > 5$, $\Delta f = |1 - f|/4$

where N is the ordinal number of the point being generated and f denotes the value at the $(N-1)$th point. As the equivalence point is approached, the second of these equations yields progressively smaller values of Δf, but any value below 0.01 was discarded and replaced by 0.01. The resulting values of f, rounded off to the nearest 0.001 unit, were 0, 0.02, 0.04, 0.06, 0.08, 0.24, 0.482, 0.612, 0.709, 0.782, 0.836, 0.877, 0.908, 0.931, 0.948, 0.961, 0.971, 0.981, 0.991, 1.001, 1.011, 1.021, 1.031, 1.041, 1.051, 1.064, 1.080, 1.100, 1.126, and 1.157. A human chemist performing the same titration might well attempt to secure points distributed in about this way. Although this data-acquisition schedule is generally similar to those used in other recent publications [5—7], it is not exactly identical with any of them. The results given below will depend to some extent on the way in which the data are distributed along the titration curve, and the discussion therefore emphasizes their trends rather than their exact values.

The data thus synthesized were incorporated into a computer program, VARPWR, which has been described previously [8] and which uses weighted non-linear regression analysis to estimate the variances of the parameters (which are $c^0_{\mathrm{Red}_2}$, $c^0_{\mathrm{Ox}_2}$, $E^{0\prime}_1$, and $E^{0\prime}_2$) for any assumed combination of the standard errors of measurement σ_V and σ_E of the volume of reagent V and the potential E, respectively. It does so in the following way. It applies an increment $\Delta V = M\sigma_V$ to the volume for each point in turn. The quantity M is a constant that is chosen by the operator at the time of execution. Small values of M exaggerate the importance of round-off errors, while large ones compromise the accuracy of the finite-difference approximation described below. Every use of the program must therefore include an examination of the effect of varying M so that an appropriate value can be selected [8]. In this work, it was found that the results of several representative calculations were not sensibly affected by changing M from 2 to 8, and the value $M = 4$ was used in obtaining all the results that are reported.

For each of the perturbed sets of data thus produced, the program computes the best values of the parameters V_i by weighted non-linear regression and finds the differences ΔV_i between these and the corresponding values used in generating the data. Values of $\Delta V_i/\Delta V$ are stored as estimators of the partial derivatives $\partial V_i/\partial V$ at the point under consideration, the original value of E at that point is restored, and the next point is treated in the same way. After the values of $\Delta V_i/\Delta V$ have been obtained and the original value of V for the last point has been restored, an increment $\Delta E = M\sigma_E$ is applied to the potential for each point in turn, and estimates of the partial derivatives $\partial V_i/\partial E$ are obtained and stored in the same way. Finally, the values of the derivatives are combined to yield estimates of the variances of the parameters.

In weighted regression, one must minimize the quantity Q defined by the equation

$$Q = (E_{meas} - E_{calc})^2/[\sigma_V^2(dE/dV)^2 + \sigma_E^2]^2 \quad (6)$$

To obtain the necessary expression for dE/dV in the weighting factor within square brackets, the following procedure was adopted for $f < 1$. Differentiating the Nernst equation for the Ox_2/Red_2 couple gives

$$dE/dV = 0.02569\ \{(1/[Red_2])(d[Red_2]/dV) - (1/[Ox_2])(d[Ox_2]/dV)\} \quad (7)$$

Values of $d[Red_2]/dV$ and $d[Ox_2]/dV$ can be obtained by differentiating Eqns. 3 and the expression for D, and can be combined with the previously computed values of $[Red_2]$ and $[Ox_2]$ to yield a value of dE/dV at each point in turn.

Partly to permit examining the effects of round-off errors, partly to guide the choice of a value of M as was described above, and partly to ensure that the arbitrary conditions for termination were sufficiently stringent, several replicate computations were made with different starting points, different values of M, and different conditions for termination. It was concluded that the results given below are generally reliable within 2% or better. This degree of certainty more than suffices for any real purpose.

The computations described above were made in FORTRAN on Radio Shack TRS-80 Model II microcomputers. Those based on Eqn. 8 were made in BASIC on a TAB 132/15-G microcomputer.

RESULTS AND DISCUSSION

Table 1 shows how the standard errors of $E_1^{0\prime}$ and $E_2^{0\prime}$, and the relative standard errors of $c^0_{Red_2}$ and $c^0_{Ox_2}$, depend on the standard errors of measurement of the volume and potential under typical conditions. In synthesizing the data that correspond to these conditions, the values of $E_1^{0\prime}$ and $E_2^{0\prime}$ were taken to be 1.44 and 0.68 V, respectively. These are the literature values for the couples involved in a titration of iron(II) with cerium(IV) in 1 M sulfuric acid as supporting electrolyte.

As long as both σ_V (which is always expressed in cm^3) and σ_E (which is always expressed in V), are small, the standard error of $E_1^{0\prime}$, which pertains to the reagent couple, is roughly a third to a half as large as σ_E, whereas the standard error of $E_2^{0\prime}$, which pertains to the couple being titrated, is roughly equal to, or a little larger than, σ_E. The value of $E_1^{0\prime}$ is chiefly determined by the data at points that follow the equivalence point. Because that point is very precisely defined, and because the value of c_{Ox_1} is taken to be known, the concentrations of both Red_1 and Ox_1 can be calculated with good precision. It may be remarked that, although allowance was made, as shown in the heading of the Table, for the presence of a little Red_1 in the reagent solution, the amount of Red_1 thus contributed to any titration mixture is negligible compared with the much larger amount arising from the titration

TABLE 1

Standard errors of the parameters for $E_1^{0\prime} = 1.44$ V, $E_2^{0\prime} = 0.68$ V, $V^0 = 25$ cm^3, $c^0_{\mathrm{Red}_2} = c^0_{\mathrm{Ox}_2} = c^0_{\mathrm{Ox}_1} = 0.1$ M, and $c^0_{\mathrm{Red}_1} = 10^{-6}$ M

σ_V (cm^3)	σ_E (mV)	$\sigma_{E_1^{0\prime}}$ (mV)	$\sigma_{E_2^{0\prime}}$ (mV)	$\sigma_{c^0_{\mathrm{Red}_2}}/c^0_{\mathrm{Red}_2}$ (%)	$\sigma_{c^0_{\mathrm{Ox}_2}}/c^0_{\mathrm{Ox}_2}$ (%)
0.005	0.5	0.204	0.521	0.0189	2.92
	1	0.362	0.963	0.0210	5.60
	2	0.680	1.92	0.0332	11.6
	5	1.63	4.98	0.0382	34.3
	10	3.27	11.7	0.0788	110
0.01	0.5	0.226	0.565	0.0273	3.06
	1	0.418	1.08	0.0398	6.03
	2	0.745	2.00	0.0487	11.8
	5	1.74	5.15	0.0958	34.5
	10	3.32	11.1	0.123	111
0.02	0.5	0.275	0.631	0.0447	3.30
	1	0.462	1.17	0.0569	6.35
	2	0.852	2.07	0.0789	12.3
	5	1.98	5.60	0.121	36.2
0.05	0.5	0.438	0.828	0.106	4.02
	1	0.642	1.43	0.122	7.30
	2	1.04	2.50	0.146	13.6
	5	2.18	5.74	0.197	36.6

reaction. The results are therefore almost independent of c_{Red_1} unless its value is improbably large. This is why c_{Red_1} is not included among the parameters that might be evaluated in a practical application of the method. In contrast, the value of $E_1^{0\prime}$ is chiefly determined by the data at points that precede the equivalence point. There is little uncertainty in the concentration of Red_2 at any such point, but the concentration of Ox_2 at equilibrium depends largely on the value of $c^0_{\mathrm{Ox}_2}$, whose uncertainty limits the precision of $E_1^{0\prime}$.

Although the relative standard error of $c^0_{\mathrm{Red}_2}$ does increase as σ_E increases, it is in general roughly equal to σ_V/V^*, where V^* is the volume of reagent required to reach the equivalence point. As V^* was always equal to 25 cm^3 in these calculations, the value $\sigma_V = 0.01$ cm^3 corresponds, for example, to $\sigma_V/V^* = 0.04\%$, which is close to the geometric mean of the values of $\sigma c^0_{\mathrm{Red}_2}/c^0_{\mathrm{Red}_2}$ given in Table 1 for values of σ_E ranging from 0.5 to 10 mV. The relative standard error of $c^0_{\mathrm{Ox}_2}$ is much larger because it interacts with the uncertainty in $E_2^{0\prime}$. If $\sigma_V = 0.01$ cm^3 and $\sigma_E = 0.001$ V (Table 1, line 7), the standard error of $E_2^{0\prime}$ is 1.08 mV. On combining the value of E at the first point, where $V = 0$, with the Nernst equation for the $\mathrm{Ox}_2/\mathrm{Red}_2$ couple and a value of $(1.00^2 + 1.08^2)^{1/2} = 1.47$ mV for the standard error of the difference between the measured potential at this point and the value of $E_2^{0\prime}$,

it can be seen that the uncertainties in E and $E_2^{0\prime}$ alone correspond to a relative uncertainty of $10^{1.47/59.15} = 5.9\%$ in $c^0_{Ox_2}$. This differs very little from the calculated value of 6.03% for the relative standard error.

Changing the assumed values of $E_1^{0\prime}$ and $E_2^{0\prime}$ to 1.34 and 0.78 V, respectively, decreases the value of K_t by three orders of magnitude (to 2.9×10^6) but has virtually no effect on the results given in Table 1. Further changes to 1.24 and 0.88 V, respectively, which correspond to $K_t = 1.2 \times 10^6$, yield the results shown in Table 2. The precisions of all the parameters deteriorate as $E_1^{0\prime} - E_2^{0\prime}$ decreases, but so slowly that the values in these Tables would not seriously misrepresent the precisions of the results obtained from any titration that would normally be regarded as feasible.

In the discussion of Table 1, it was explained why the concentration of Red_1 in the reagent solution has very little influence on the calculations, and why it is therefore impossible to take c_{Red_1} as an adjustable parameter. Under conditions identical with those of Table 1, except that c_{Red_1} was taken to be 1×10^{-4} M instead of 1×10^{-6} M, the calculated precisions of all the parameters agreed almost exactly with those given in Table 1. The results obtained with $c_{Red_1} = 0.01$ M are shown in Table 3. Increasing the value of c_{Red_1} improves the precisions of all the parameters, but the effect, like that of changing the value of $E_1^{0\prime} - E_2^{0\prime}$, is too small to have much importance.

TABLE 2

Standard errors of the parameters for $E_1^{0\prime} = 1.24$ V, $E_2^{0\prime} = 0.88$ V, $V^0 = 25$ cm^3, $c^0_{Red_2} = c^0_{Ox_2} = c^0_{Ox_1} = 0.1$ M, and $c^0_{Red_1} = 10^{-6}$ M

σ_V (cm^3)	σ_E (mV)	$\sigma_{E_1^{0\prime}}$ (mV)	$\sigma_{E_2^{0\prime}}$ (mV)	$\sigma_{c^0_{Red_2}}/c^0_{Red_2}$ (%)	$\sigma_{c^0_{Ox_2}}/c^0_{Ox_2}$ (%)
0.005	0.5	0.204	0.535	0.0197	3.00
	1	0.381	1.01	0.0300	5.88
	2	0.713	2.09	0.0506	12.4
	5	1.84	5.29	0.107	36.9
	10	3.47	13.3	0.163	129
0.01	0.5	0.222	0.553	0.0261	3.03
	1	0.410	1.06	0.0392	6.01
	2	0.779	2.12	0.0626	12.4
	5	1.89	5.49	0.116	36.7
	10	3.46	11.9	0.155	113
0.02	0.5	0.311	0.661	0.0551	3.37
	1	0.478	1.18	0.0611	6.40
	2	0.852	2.19	0.0839	12.6
	5	1.90	5.44	0.124	36.4
	10	3.57	13.3	0.176	130
0.05	0.5	0.485	0.895	0.124	4.27
	1	0.747	1.57	0.155	7.70
	2	1.18	2.73	0.190	14.2
	5	2.02	5.61	0.207	37.1
	10	4.03	12.8	0.305	119

TABLE 3

Standard errors of the parameters for $E_1^{0\prime}$ = 1.44 V, $E_2^{0\prime}$ = 0.68 V, V^0 = 25 cm³, $c^0_{\mathrm{Red}_2}$ = $c^0_{\mathrm{Ox}_2}$ = $c^0_{\mathrm{Ox}_1}$ = 0.1 M, and $c^0_{\mathrm{Red}_1}$ = 10^{-2} M

σ_V (cm³)	σ_E (mV)	$\sigma_{E_1^{0\prime}}$ (mV)	$\sigma_{E_2^{0\prime}}$ (mV)	$\sigma_{c^0_{\mathrm{Red}_2}}/c^0_{\mathrm{Red}_2}$ (%)	$\sigma_{c^0_{\mathrm{Ox}_2}}/c^0_{\mathrm{Ox}_2}$ (%)
0.005	0.5	0.202	0.530	0.0188	2.97
	1	0.361	0.973	0.0209	5.68
	2	0.835	2.22	0.0281	12.6
	5	1.75	5.15	0.0380	34.8
	10	3.27	11.7	0.0788	110
0.01	0.5	0.225	0.556	0.0272	3.02
	1	0.417	1.05	0.0397	5.95
	2	0.744	2.02	0.0488	12.0
	5	1.73	5.12	0.0958	34.3
	10	3.33	12.1	0.123	116
0.02	0.5	0.274	0.625	0.0446	3.27
	1	0.462	1.16	0.0570	6.33
	2	0.852	2.18	0.0798	12.5
	5	1.93	5.53	0.119	35.6
	10	3.36	12.2	0.140	116
0.05	0.5	0.435	0.836	0.106	4.06
	1	0.640	1.42	0.122	7.24
	2	1.04	2.50	0.146	13.5
	5	2.17	5.73	0.196	37.4
	10	3.86	12.6	0.224	117

TABLE 4

Standard errors of the parameters for $E_1^{0\prime}$ = 1.44 V, $E_2^{0\prime}$ = 0.68 V, V^0 = 25 cm³, $c^0_{\mathrm{Red}_2}$ = $c^0_{\mathrm{Ox}_1}$ = 0.1 M, $c^0_{\mathrm{Red}_1}$ = 10^{-6} M, and different values of $c^0_{\mathrm{Ox}_2}$

σ_V (cm³)	σ_E (mV)	$\sigma_{E_1^{0\prime}}$ (mV)	$\sigma_{E_2^{0\prime}}$ (mV)	$\sigma_{c^0_{\mathrm{Red}_2}}/c^0_{\mathrm{Red}_2}$ (%)	$\sigma_{c^0_{\mathrm{Ox}_2}}/c^0_{\mathrm{Ox}_2}$ (%)
A. $c^0_{\mathrm{Ox}_2}$ = 0.01 M					
0.005	0.5	0.203	0.202	0.0187	2.03
	1	0.361	0.365	0.0210	3.97
	2	0.833	0.845	0.0287	8.45
	5	1.75	1.69	0.0455	20.9
	10	3.27	2.84	0.0779	45.7
0.01	0.5	0.227	0.218	0.0269	2.11
	1	0.418	0.414	0.0392	4.14
	2	0.743	0.753	0.0478	8.14
	5	1.73	1.80	0.0953	21.3
	10	3.32	3.48	0.122	47.7

TABLE 4 (continued)

v (cm³)	σ_E (mV)	$\sigma_{E_1^{0\prime}}$ (mV)	$\sigma_{E_2^{0\prime}}$ (mV)	$\sigma_{c^0_{Red_2}}/c^0_{Red_2}$ (%)	$\sigma_{c^0_{Ox_2}}/c^0_{Ox_2}$ (%)
0.02	0.5	0.276	0.249	0.0440	2.30
	1	0.463	0.449	0.0558	4.30
	2	0.852	0.837	0.0787	8.44
	5	1.97	2.05	0.120	22.0
	10	3.37	3.50	0.139	47.8
0.05	0.5	0.439	0.342	0.103	3.04
	1	0.641	0.561	0.120	4.93
	2	1.04	0.977	0.144	9.02
	5	2.17	2.13	0.196	22.4
	10	3.84	3.88	0.222	48.6
B. $c^0_{Ox_2}$ = 0.001 M					
0.005	0.5	0.204	0.169	0.0185	6.07
	1	0.361	0.304	0.0209	11.3
	2	0.832	0.700	0.0277	23.4
	5	1.75	1.48	0.0455	60.4
	10	3.26	2.79	0.0769	135
0.01	0.5	0.227	0.189	0.0267	7.34
	1	0.417	0.345	0.0390	12.3
	2	0.741	0.620	0.0468	23.2
	5	1.74	1.48	0.0952	60.4
	10	3.32	2.83	0.122	135
0.02	0.5	0.278	0.231	0.0442	10.3
	1	0.462	0.386	0.0553	14.8
	2	0.848	0.699	0.0783	25.0
	5	1.96	1.70	0.118	62.3
	10	3.37	2.85	0.138	136
0.05	0.5	0.451	0.347	0.107	18.4
C. $c^0_{Ox_2}$ = 0.0001 M					
0.005	0.5	0.203	0.166	0.0185	47.5
	1	0.362	0.296	0.0210	84.9
	2	0.832	0.678	0.0289	172
0.01	0.5	0.227	0.187	0.0267	60.2
	1	0.417	0.339	0.0388	96.4
0.02	0.5	0.279	0.230	0.0443	87.6
	1	0.464	0.387	0.0556	123
0.05	0.5	0.454	0.354	0.108	183

The effect of changing the value of $c^0_{Ox_2}$, and with it the value of the ratio $c^0_{Red_2}/c^0_{Ox_2}$, is much more substantial and is illustrated by Table 4. Decreasing $c^0_{Ox_2}$ hardly affects the precisions with which $E_1^{0\prime}$ and $c^0_{Red_2}$ can be evaluated, but it improves the precision of $E_2^{0\prime}$ and worsens that of $c^0_{Ox_2}$. Were it

not for the weighting factor in Eqn. 4, an improvement in the precision of $E_2^{0\prime}$ would be accompanied by an improvement in the relative precision of $c^0_{Ox_2}$. As $c^0_{Ox_2}$ decreases, however, the slope of the initial portion of the titration curve increases, and the weights assigned to the data in that region decrease. Those points are the ones that contain most of the information about the value of $c^0_{Ox_2}$, for as the titration progresses the amount of Ox_2 in the original solution becomes less and less important in comparison with the amount that has been formed in by oxidizing Red_2 with the reagent. By decreasing the weights assigned to the points that would be most useful in evaluating $c^0_{Ox_2}$, decreasing the value of this quantity worsens the precision that can be obtained in evaluating it, and this effect swamps the improvement that would otherwise result from improving the precision of $E_2^{0\prime}$.

Although the values that were attributed to σ_V and σ_E in these calculations cover the ranges that are likely to be of practical interest, they are unlikely to be exactly duplicated in any real titration, and the same thing is true of the other variables investigated. To facilitate interpolation, the values obtained for the standard or relative standard errors of each parameter on changing the value of each variable in turn were fitted to the equation

$$\sigma_{V_i} = [(k_1 \sigma_V)^2 + (k_2 \sigma_E)^2]^{1/2} \tag{8}$$

assuming the relative (rather than the absolute) errors in σ_{V_i} (or, if V_i denotes a concentration, in σ_{V_i}/V_i) to be randomly distributed. The qualities of these fits can be gauged from the fact that the relative standard deviations from regression ranged from 6.2 to 10.4% for $\sigma_{E_1^{0\prime}}$, from 7.2 to 9.4% for $\sigma_{E_2^{0\prime}}$, from 16.4 to 27.2% for $\sigma_{c^0_{Red_2}}/c^0_{Red_2}$, and from 4.6% to 27.4% for $\sigma_{c^0_{Ox_2}}/c^0_{Ox_2}$. All of these numbers exceed the precisions attributed above to the calculated standard or relative standard errors of the quantities to which they pertain, and some of them do so by very wide margins. In designing an experiment or in interpreting its results, however, it is very important to know whether a desired level of precision can be expected or has been attained, but it makes no real difference whether the theoretically attainable precision is, say, 0.5% or 0.6%. Equation 8 is clearly only a rather crude approximation to the truth, but several different empirical modifications of it produced so little improvement that they did not seem to be worth their greater complexity. Accordingly the results of the fits to that equation are summarized in Table 5.

The use of this table can be illustrated by supposing that one wishes to estimate the standard error of $E_2^{0\prime}$ that might be obtained if $E_1^{0\prime} - E_2^{0\prime} = 0.46$ V, $c^0_{Red_2}/c^0_{Ox_2} = 300$, $c^0_{Ox_1}/c^0_{Red_1} = 10^5$, and σ_V and σ_E are 0.01 cm^3 and 0.001 V, respectively. Logarithmic interpolation between the values given for $c^0_{Red_2}/c^0_{Ox_2} = 100$ and 1000, with $E_1^{0\prime} - E_2^{0\prime} = 0.76$ V and $c^0_{Ox_1}/c^0_{Red_1} = 10^5$, gives $k_1 = 6.9$ and $k_2 = 320$. Greater accuracy is hardly warranted. The first of these numbers is 0.48 times, and the second is 0.30 times, the value obtained with $E_1^{0\prime} - E_2^{0\prime} = 0.76$ V, $c^0_{Ox_1}/c^0_{Red_1} = 10^5$, and $c^0_{Red_2}/c^0_{Ox_2} = 1$. Similar interpolation between the values given for $E_1^{0\prime} -$

TABLE 5

Values of the coefficients k_1 and k_2 in Eqn. 8
(The first three columns give the values of the parameters assumed in the calculations. The last four columns give, in the form "k_1, k_2", the values of the coefficients in Eqn. 8 that correspond to values of the standard errors $\sigma_{E_1^{0\prime}}$ and $\sigma_{E_2^{0\prime}}$ expressed in mV and to values of the relative standard errors $\sigma_{c^0_{\mathrm{Red}_2}}/c^0_{\mathrm{Red}_2}$ and $\sigma_{c^0_{\mathrm{Ox}_2}}/c^0_{\mathrm{Ox}_2}$ expressed as percentages.)

$(E_1^{0\prime} - E_2^{0\prime})$ (V)	$c^0_{\mathrm{Red}_2}/c^0_{\mathrm{Ox}_2}$	$c^0_{\mathrm{Ox}_1}/c^0_{\mathrm{Red}_1}$	Values of k_1, k_2 for			
			$\sigma_{E_1^{0\prime}}$	$\sigma_{E_2^{0\prime}}$	$\sigma_{c^0_{\mathrm{Red}_2}}/c^0_{\mathrm{Red}_2}$	$\sigma_{c^0_{\mathrm{Ox}_2}}/c^0_{\mathrm{Ox}_2}$
0.76	1	10^5	9.63, 375	14.5, 1070	3.03, 11.6	39.2, 6800
		1000	9.57, 379	13.7, 1100	2.88, 14.8	20.9, 7400
		10	9.44, 378	13.7, 1100	3.05, 11.8	23.1, 7300
	10	10^5	9.53, 379	6.90, 383	2.98, 12.0	42.7, 4300
	100		9.17, 373	7.0, 316	3.01, 11.6	367, 12 200
	1000		8.55, 404	6.7, 333	2.18, 29.0	3760, 87 400
0.56	1		9.5, 380	13.4, 1109	2.89, 14.9	18.5, 7300
0.36			11.4, 381	15.7, 1134	3.09, 20.4	28.1, 7600
		1000	11.3, 385	15.8, 1131	3.08, 20.7	23.3, 7500
		10	11.1, 387	15.9, 1122	3.01, 21.4	42.6, 7100

$E_2^{0\prime} = 0.36$ and 0.56 V, with $C^0_{\mathrm{Red}_2}/c^0_{\mathrm{Ox}_2} = 1$ and $c^0_{\mathrm{Ox}_1}/c^0_{\mathrm{Red}_1} = 10^5$, given $k_1 = 13.9$ and $k_2 = 1115$, of which the first is 0.96 times, and the second is 1.04 times, the value for $E_1^{0\prime} - E_2^{0\prime} = 0.76$ V, $c^0_{\mathrm{Ox}_1}/c^0_{\mathrm{Red}_1} = 10^5$, and $c^0_{\mathrm{Red}_2}/c^0_{\mathrm{Ox}_2} = 1$. Combining these pairs of coefficients suggests that the value of k_1 under the desired conditions is 0.48×0.96 times as large as it is under the reference conditions ($E_1^{0\prime} - E_2^{0\prime} = 0.76$ V, $c^0_{\mathrm{Ox}_1}/c^0_{\mathrm{Red}_1} = 10^5$, and $c^0_{\mathrm{Red}_2}/c^0_{\mathrm{Ox}_2} = 1$), and is therefore equal to $0.48 \times 0.96 \times 14.5 = 6.7$. Similarly, the value of k_2 under the desired conditions can be estimated as $0.30 \times 1.04 \times 1070 = 334$. Combining these estimates with Eqn. 8 and the assumed values of σ_V and σ_E gives

$$E_2^{0\prime} = [(6.7 \times 0.01)^2 + (334 \times 0.001)^2]^{1/2} = 0.34 \text{ mV}$$

Direct calculation with $E_1^{0\prime} = 1.23$ V, $E_2^{0\prime} = 0.77$ V, $c^0_{\mathrm{Red}_2}/c^0_{\mathrm{Ox}_2} = 300$, and $c^0_{\mathrm{Ox}_1}/c^0_{\mathrm{Red}_1} = 10^5$ gave $\sigma_{E_2^{0\prime}} = 0.365$ mV. The relative error of 7.4% in the estimate resulting from these interpolations is consistent with the relative standard deviations from regression in the fits that led to the values of k_1 and k_2 on which the estimate is based. It seems certain that estimates made in this fashion will be accurate enough for any real purpose as long as they do not go beyond the ranges considered in this work.

This work was aided by the generous support of the Consiglio Nazionale delle Richerche and M.P.I., to which one of us (L.M.) is indebted for a visiting fellowship during the summer of 1986.

REFERENCES

1 A. F. Isbell, Jr., R. L. Pecsok, R. H. Davies and J. H. Purnell, Anal. Chem., 45 (1973) 2363.
2 F. Ingman, A. Johansson, S. Johansson and R. Karlson, Anal. Chim. Acta, 64 (1973) 113.
3 D. M. Barry and L. Meites, Anal. Chim. Acta, 68 (1974) 435.
4 D. M. Barry, L. Meites and B. H. Campbell, Anal. Chim. Acta, 69 (1974) 143.
5 G. Kateman, H. C. Smit and L. Meites, Anal. Chim. Acta, 152 (1983) 61.
6 H. C. Smit, G. Kateman and L. Meites, Anal. Chim. Acta, 153 (1983) 121.
7 M. Betti, P. Papoff and L. Meites, Anal. Chim. Acta, 182 (1986) 133.
8 L. Meites, The General Non-Linear Regression Program CFT4A, The George Mason Institute, Fairfax, VA, 1985, pp. 218—222.

Analytica Chimica Acta, 194 (1987) 163—170
Elsevier Science Publishers B.V., Amsterdam — Printed in The Netherlands

APPLICATION OF ION-SELECTIVE ELECTRODES IN ENVIRONMENTAL ANALYSIS
Determination of Acid and Fluoride Concentrations in Rain-water with a Flow-Injection System

J. FUCSKÓ, K. TÓTH and E. PUNGOR*

Institute for General and Analytical Chemistry, Technical University of Budapest, Gellért tér 4, H-1111 (Hungary)

J. KUNOVITS

Radelkis Electrochemical Company, Budapest, Laborc 1/3 (Hungary)

H. PUXBAUM

Institute for Analytical Chemistry, Technical University, Vienna (Austria)

(Received 8th July 1986)

SUMMARY

A flow-injection method is described for the measurement of acid and fluoride concentrations. The conditions were optimized to ensure small sample and reagent consumption, low detection limit and the highest rate of analysis allowed by the potentiometric sensor. With a microcapillary pH-sensitive glass electrode, 20-μl sample volumes and 1.0—1.5 ml min^{-1} carrier flow rates, strong acids were determined at concentrations as low as 10^{-5} M (0.2 nmol of acid in 20 μl). The relative standard deviation was about 1% at 10^{-4} M strong acid concentration at an injection rate of 500—550 h^{-1}. With a flow-through fluoride-selective electrode, 250-μl sample volumes and a 1 ml min^{-1} carrier flow rates, fluoride concentrations as low as 10^{-7} M were measured (ca. 0.5 ng of fluoride in 250 μl). The injection rate was 40 h^{-1} at concentrations below 10^{-6} M, but 60 h^{-1} above 10^{-5} M. The methods were used successfully for determining the acid and fluoride concentrations in rain-waters.

Potentiometric analysis of natural waters (e.g., rain water) involves difficulties if ion-concentrations near the detection limit of the sensor are to be quantified, or if the ionic strength of the sample is too low or the concentration of interferents is relatively high.

It is especially difficult to define and measure quantities related to hydrogen ion concentration (e.g., pH, acidity) in samples with low buffer capacity and low ionic concentrations [1—3]. Theoretically sound pH values corresponding to accepted definitions can only be measured with specially designed apparatus [1, 4, 5] which enables the errors most frequently occurring in batch pH measurement to be minimized. Such errors include "stirring error", problems of contamination, circuit disruption and liquid-junction potentials and the change in activity coefficients with ionic strength. Acidity determinations [4] by an indirect method (in general, by coulometric titra-

0003-2670/87/$03.50

tion and potentiometric end-point detection) usually involves the same type of errors as pH measurement.

The application of the above methods in routine laboratories, however, requires much time and care and representative standard samples which are stable and easy to prepare. Although attempts have been made to design and use appropriate standards, representative for precipitation water samples, the problem is far from being solved. Thus, further efforts in acidity and pH determinations to use reference standards which have a less complex composition than that of the sample, and so are easier to prepare in a reproducible way, and to apply a simple faster method of measurement, appear to be worthwhile.

It has been shown for acid precipitation (pH < 4.5) by a great number of measurements that the acidity is in most cases caused by strong mineral acids (H_2SO_4, HNO_3) [6, 7]. Therefore, other components present in low concentration have only a slight effect on the buffer capacity and ionic strength of the sample, and do not significantly influence the acidity itself. Accordingly, with such samples, dilute aqueous solutions of strong mineral acids can be used as standards; the pH of both the standard and sample are measured with a pH glass electrode and the acid concentration of the sample is expressed.

The rate of analysis can be increased by applying a non-equilibrium "dynamic potentiometric method", e.g., the flow-injection technique. When the flow injection technique is used, the potentiometric signal measured depends primarily on the pH of the solution, but is affected also by the hydrodynamic parameters of the flow system and by the dynamic characteristics of the detector. Hence the signal measured is not directly correlated with the pH of the solution. Using dilute aqueous solutions of strong mineral acids as standards, Slanina et al. [8] developed a flow-injection method for determining the acid concentration in rain-water samples. With a computer-controlled flow-injection system, at a flow rate of about 4 ml min^{-1} and a sample volume of 0.5 ml, a rate of 60—120 samples per hour was achieved for hydrogen ion concentrations exceeding 10^{-5} M.

The lanthanum fluoride single-crystal fluoride ion-selective electrode has excellent selectivity properties and a fairly good detection limit. The determination of fluoride by ion chromatography poses problems in the presence of formate and acetate because of peak overlapping. An obvious solution to the problem appears to be to develop a separate flow-injection method with a fluoride ion-selective electrode. Using such a system, Slanina et al. [8] reported a detection limit for the fluoride determination of the order of 10^{-6} M at a flow rate of 4 ml min^{-1} and sample volume of 0.5 ml. Van den Winkel et al. [9] achieved a sample injection rate of 120 h^{-1} for the fluoride determination in the concentration range 10^{-5}—5×10^{-4} M with a flow rate of 5.5 ml min^{-1}.

The aim of the present work was to develop a flow-injection system for acid and fluoride determination with a lower reagent and sample consumption

and a higher rate of sample throughput than those of the methods described earlier, and with a detection limit similar to that reported for fluoride by ion chromatography.

EXPERIMENTAL

Apparatus

The scheme of the flow-injection system used is shown in Fig. 1. The flow rate of the carrier solution was controlled by nitrogen overpressure in the reservoir. The value of the overpressure was adjusted by a pneumatic pressure controller (MMG 0880, Hungary). A loop-type injector (Labor MIM OE-320, Hungary) was used for sample introduction (20-μl loop for hydrogen ion and 250-μl loop for fluoride determination). The dispersion tube was a 1-m length of Pierce teflon tube with internal diameters of 0.3 and 0.6 mm for acid and fluoride determination, respectively.

A pH-sensitive microcapillary glass electrode (Radelkis OP-0753P, Hungary) and a flow-through fluoride-selective electrode (Radelkis OP-F-7443) were used as indicator electrodes, and a double-junction Ag/AgCl electrode (Radelkis OP-820P) was used as reference electrode. E.m.f. measurements were made with a digital pH meter (Radelkis type OP-208 or OP-211/1), and the signal was recorded by an x-t recorder.

Reagents

Standard solutions were prepared from analytical-grade hydrochloric acid and sodium fluoride with double-distilled water and stored in polyethylene containers.

For the acid concentration determinations, 0.5 or 1 M potassium nitrate containing a low concentration ($<10^{-4}$ M) of buffer (acetate or phosphate buffer or a linear buffer composition as described by Slanina et al. [8]) was used as carrier solution.

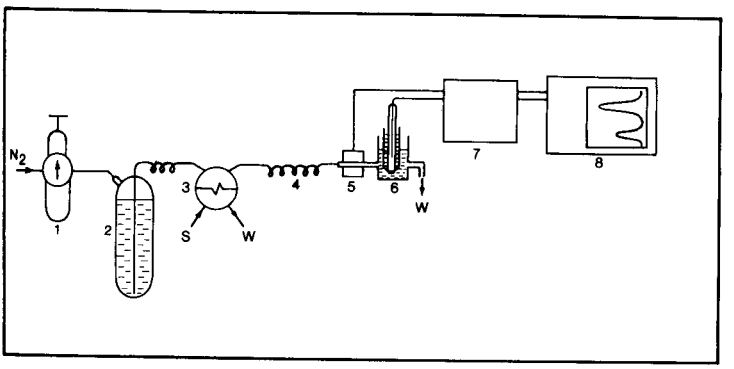

Fig. 1. Schematic diagram of the flow-injection measuring system: (1) pressure controller; (2) carrier tank; (3) loop-type injector; (4) tube; (5) indicator electrode; (6) reference half cell; (7) pH/mV meter; (8) recorder.

For the fluoride determinations, samples and standards were diluted in a 1:1 ratio with TISAB solution. The TISAB solution used contained 3.07 g l^{-1} EDTA, 9 g l^{-1} sodium chloride and an acetate buffer with a total acetate concentration of 1.5 M, adjusted to pH 5.0—5.3. The carrier solution was prepared by diluting the above TISAB solution with an equal volume of water and adding sodium fluoride solution to yield the required low concentration of fluoride.

RESULTS AND DISCUSSION

As the first step, electrodes with suitable geometric, dynamic and hydrodynamic characteristics were selected to meet the demands of the flow-through method to be developed. The microcapillary-type pH glass electrode (type OP-0753P, Radelkis) with a 58.2 mV/pH slope of the calibration curve and excellent dynamic properties, and a flow-through fluoride electrode (type OP-F-7443, Radelkis) were found to be best for the purpose.

Determination of acid concentration

The pH-sensitive microcapillary glass electrode has a tube-shaped membrane (0.5 mm internal diameter and 10—12 mm long) as the sensing surface, providing a total volume of about 3 μl. Hence, its hydrodynamic peak-broadening effect is very small.

It is well known that the stability of the signal (or of the baseline in flowing systems), as well as the response time of glass electrodes, depends primarily on the buffer capacity of the solutions used [10]. Thus, the electrode response becomes slower and the interference caused by impurities (absorption of CO_2, etc.) becomes much more pronounced in solutions as the buffer capacity decreases. Accordingly, in flow systems, the baseline fluctuation is significant if carrier solutions of low buffer capacity are used; it is essential to maintain an appropriate buffer capacity of the carrier solution. However, because of dispersion, the sample reacts with the buffer. The sensitivity of the measurement is therefore dependent on the buffer capacity of the carrier solution, especially for samples of low concentration. In such cases, to ensure the required sensitivity and low detection limit, a low buffer capacity of the carrier solution is desirable. A buffer concentration between 10^{-5} and 10^{-4} M was found to ensure sufficient stability and rapid re-establishment of the baseline and the measurement of 10^{-5} M acid with appropriate precision. For example, $2.5—5 \times 10^{-5}$ M acid concentrations could be determined at an injection rate of 500 h^{-1} with a relative standard deviation of about 5%, using an acetate buffer of about 5×10^{-5} M total concentration, a 1.0—1.5 ml min^{-1} carrier flow rate and a 20-μl sample volume.

The pH and the nature of the buffer is also of importance in determining the shape of the calibration curve. The peak obtained for an injected sample is larger when a carrier of higher pH is used, but interference from CO_2 is also greater, and the pH of the carrier solution changes to a greater extent during storage, because of CO_2 absorption. A carrier with a pH between 5

and 6 was found to be best suited for measuring the acid content in rain-water. The acetate buffer (with EDTA) used in fluoride determination (pH 5.0—5.3) proved to be suitable, so it was added in an appropriate ratio to the potassium nitrate carrier solution. Figure 2 shows the recordings for 10^{-5}—5×10^{-4} M standards in the flow-injection system, while Fig. 3 is a typical calibration curve.

The calibration curve (peak height, ΔE vs. log c) is not linear at low acid concentrations, but with appropriate choice of the carrier, a linear portion on the calibration curve can be obtained for acid concentrations above 2×10^{-4} M. At acid concentrations below 2×10^{-4} M, fitting of a non-linear curve is necessary, and the relationship between the peak height, ΔE and log c depends on the nature, concentration and pH of the buffer and also on the hydrodynamic parameters (length and internal diameter of the tubing and flow rate). As it would be very difficult to construct a theoretically correct physical and mathematical model to describe the calibration curve, it is advisable to have many calibration points within the non-linear section to ensure reliable curve fitting.

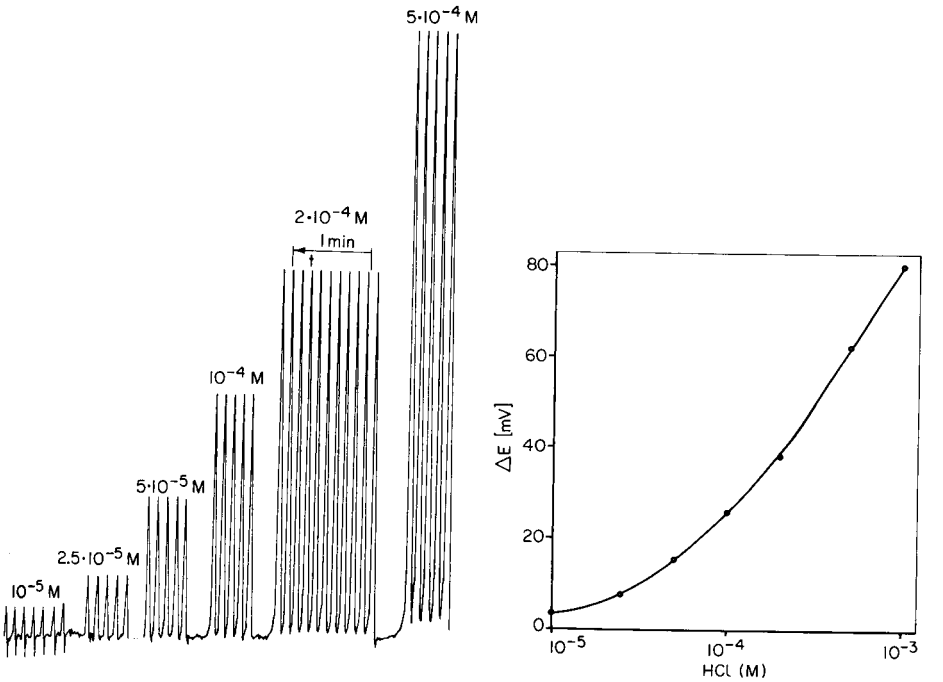

Fig. 2. Flow-injection recordings of 10^{-5}—5×10^{-4} M strong acid standards. Conditions: tube length, 1 m (0.33 mm i.d.); flow rate, 1.3 ml min^{-1}; carrier solution, 1 M KNO_3/ca. 5×10^{-5} M HAc/NaAc (pH ≈ 5).

Fig. 3. Flow-injection calibration for strong acid standards in the 10^{-5}—10^{-3} M range. Conditions as for Fig. 2.

The standard deviation of the peak-height measurements was <0.2 mV; the signal range (potential change) corresponding to a concentration change from 10^{-5} to 10^{-4} M was about 20 mV. The precision of the acid determination was about 1% at 10^{-4} M concentration. The acid concentration of 16 rain-water samples examined was found to be $<8 \times 10^{-5}$ M.

Determination of fluoride concentration

The lower limit of linear response of the fluoride electrodes used was 10^{-5} M. In choosing the parameters of the flow-injection method, the unfavourable dynamic characteristics (slow response) of the electrode at low concentrations were considered. As there may be significant differences between the properties of individual electrodes, four fluoride ion-selective electrodes of different ages were compared by preparing calibration graphs in the injection mode under identical conditions. The calibration curves shown in Fig. 4 indicate the fact observed earlier by other workers (e.g., Stahr et al. [11] and Mertens et al. [12]) that electrodes in use for a longer period of time have slower responses than new ones. Accordingly, a smaller fraction of the equilibrium potential change is reached during the residence time of the sample solution in the detector cell by an old than by a new electrode. In the flow-injection calibration, this is manifested by an apparent reduction in sensitivity with the age of the electrode. In the present experiments, the newest of the electrodes tested (electrode 1) produced a potential difference signal in the concentration range below 5×10^{-6} M more than twice that produced by the oldest electrode (4) which had been in use for about 3 years. Hence, for the determination of low fluoride concentrations in flow injection analysis it is advisable to use new or renewed electrodes [11] to ensure the required sensitivity. It is also advisable to increase the residence time of the sample in the detector cell because of the relatively slow response at low concentrations. As the volume of the detector cell is about 20 μl, a relatively large (250 μl) sample volume was chosen with a carrier flow rate of about 1 ml min^{-1} in the determination of concentrations below 10^{-6} M.

To stabilize the baseline, and to increase the rate of electrode response, fluoride was added to the carrier solution, as suggested before [8, 9]. The choice of the concentration of fluoride in the carrier is a compromise: it should ensure a relatively fast response without reducing the sensitivity significantly. The effects of hydrodynamic parameters and of the fluoride concentration in the carrier stream on the calibration curve are shown in Figs. 5 and 6, respectively. As shown by Fig. 6, the sensitivity (ΔE signal corresponding to a given concentration change) is higher at a lower fluoride concentration in the carrier, whereas the rate of measurement is lower because of the slower electrode response. As a compromise, the concentration in the carrier was chosen at 1×10^{-6} M fluoride. When the samples injected have a concentration lower than that of the carrier, negative peaks appear. As these negative peaks are reproducible within 0.05 mV, concentra-

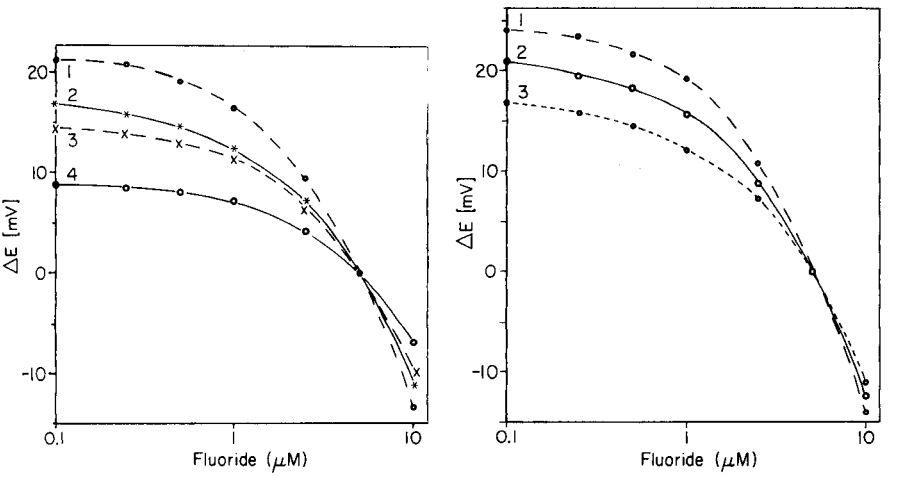

Fig. 4. Calibration curves for flow-through fluoride electrodes of different ages. General conditions: flow rate (v), 1.6 ml min^{-1}; carrier solution, TISAB containing 5×10^{-6} M fluoride. Age of electrodes: (1) new; (2, 3) ca. 1 year; (4) 3 years.

Fig. 5. Calibration of a fluoride electrode under different hydrodynamic conditions: (1) tube length 2 m (0.33 mm i.d.); (2, 3) tube length 1 m (0.6 mm i.d.). Flow rates (ml min^{-1}): (1) 0.62; (2) 0.86; (3) 1.6.

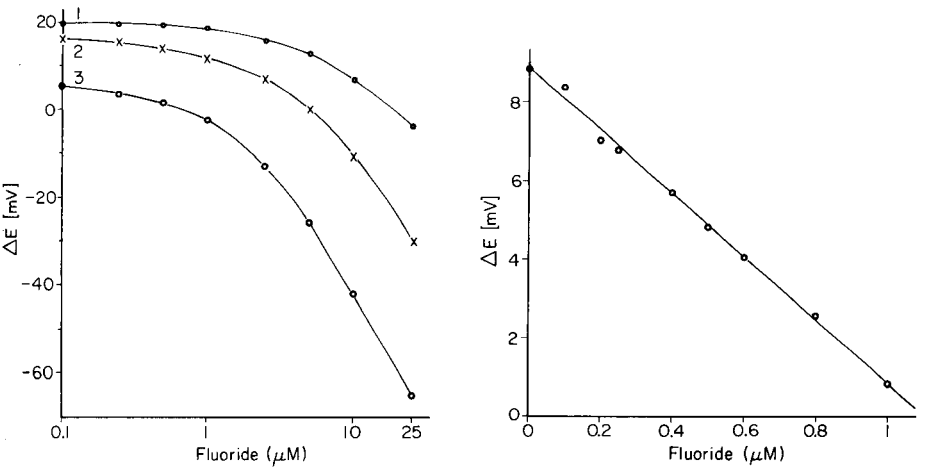

Fig. 6. Calibration curves in carrier solutions of different fluoride concentrations: (1) 1.8×10^{-5} M; (2) 5×10^{-6} M; (3) 1×10^{-6} M.

Fig. 7. Calibration curve in carrier solution containing 1×10^{-6} M fluoride.

tions below 10^{-6} M can be determined by appropriate calibration. A calibration curve taken in the range $0—10^{-6}$ M with a linear concentration scale is shown in Fig. 7; the ΔE vs. c calibration appears to be linear under the experimental conditions used. However, because of the dynamic, non-equi-

librium nature of the measurement, this linearity cannot be explained by an equilibrium model similar to that derived by Trojanowicz and Matuszewski [13] for measurements with precipitate-based electrodes in the range near the detection limit.

The standard deviation of the measurement was about 0.05 mV, corresponding to a concentration of about 10^{-8} M, based on the calibration curve measured. However, the error from other sources, (e.g., from the preparation of highly diluted standards) may exceed this. In addition, the deviation of the experimental points from the fitted straight line is often greater than this standard deviation. Accordingly, it is more justifiable to give a detection limit of 10^{-7} M, and a relative standard deviation of 5% at 10^{-6} M fluoride concentrations. The injection rate is 40—60 h^{-1}.

The technique described was used to determine fluoride in 18 rain-water samples. The concentration was found to be in the range $1—5 \times 10^{-7}$ M. The fluoride concentration in tap water was of the order of 10^{-6} M, measured in 1 M citrate containing TISAB.

The authors thank the Hungarian Academy of Sciences for financial support (Project MTA-KKA 499/85).

REFERENCES

1 A. K. Covington, P. D. Whalley and W. Davison, Pure Appl. Chem., 57 (1985) 877.
2 R. G. Bates, Crit. Rev. Anal. Chem., 10 (1981) 247.
3 R. G. Bates, Determination of pH: Theory and Practice, 2nd edn., Wiley, New York, 1973.
4 W. F. Koch, G. Marienko and J. W. Stolz, National Bureau of Standards, Washington, DC 20234, NBSIR 82-2581, 1982.
5 W. F. Koch and G. Marienko, Sampling and Analysis of Rain, American Society for Testing and Materials, Special Technical Publication 823, Philadelphia, 1983, p. 10.
6 H. Puxbaum, G. Holdwachs, G. Glatzel and H. Löffler, Osterr. Chem. Ztg., 84 (1984) 33.
7 H. Malissa, H. Puxbaum and B. Wopenka, Fresenius' Z. Anal. Chem., 301 (1980) 279.
8 J. Slanina, W. A. Lingerak and F. Bakker, Anal. Chim. Acta, 117 (1980) 91.
9 P. Van den Winkel, G. de Backer, M. Vandeputte, F. Mertens, L. Dryan and D. L. Massart, Anal. Chim. Acta, 145 (1983) 207.
10 A. Wikby and B. Karlberg, J. Electroanal. Chem., 43 (1973) 325.
11 H. M. Stahr, P. F. Ross and W. Hyde, Microchem. J., 25 (1980) 232.
12 J. Mertens, P. Van den Winkel and D. L. Massart, Anal. Chem., 48 (1976) 272.
13 M. Trojanowicz and W. Matuszewski, Anal. Chim. Acta, 138 (1982) 71.

Analytica Chimica Acta, 194 (1987) 171—176
Elsevier Science Publishers B.V., Amsterdam — Printed in The Netherlands

RESPONSE OF POLY(VINYL CHLORIDE) ELECTRODES BASED ON THE NEUTRAL CARRIER 1,4,7,10-TETRAOXACYCLODODECANE

MICHAEL D. HAMPTON*, CRAIG A. PETERS and LISA A. WELLINGTON
Department of Chemistry, University of Central Florida, Orlando, FL 32816 (U.S.A.)
(Received 10th June 1986)

SUMMARY

Ion-selective electrodes based on the neutral carrier, 12-crown-4, in a poly(vinyl chloride) matrix were found to respond ideally, or almost ideally, to potassium, sodium, barium, strontium, magnesium, cobalt(II), nickel(II) and aluminum ions. The electrode showed good selectivity for Al^{3+} over Co^{2+} and Mg^{2+}, and for Co^{2+} over Mg^{2+}. Little selectivity was found for the other ions tested.

Ion-selective electrodes based on neutral carriers have been investigated extensively [1]. One particular group of compounds, naturally occurring antibiotics, has found application as neutral carriers [2, 3]. Ion-selective electrodes based on valinomycin in particular have been shown to exhibit ideal response to and excellent selectivity for potassium ions [1—4]. In 1967, a class of compounds, crown ethers, with structures quite similar to naturally occurring antibiotics was reported [5]. Because of their complexing abilities, crown ethers and their analogs have been intensively investigated, one facet of these studies being their use as neutral carriers in ion-selective electrodes [1, 6—12]. Gadzekpo and Christian [11] reported the use of 1,4,7,10-tetraoxacyclododecane (12-crown-4) as the neutral carrier for lithium in a lithium-selective electrode. These authors found the response of the electrode to be Nernstian at low lithium ion concentrations ($<10^{-4}$ M) and much less than Nernstian at higher concentrations ($>10^{-3}$ M).

Most of the reports of ion-selective electrodes based on crown ethers have included the responses of these electrodes only to alkali and alkaline earth metal cations. This paper describes the response of a poly(vinyl chloride) electrode with 12-crown-4 as the neutral carrier to a number of other cations.

EXPERIMENTAL

Reagents and apparatus

The 12-crown-4 (Aldrich Chemical Company) was used as received. The metal ions were used as the chloride salts except for lead(II), iron(III), strontium, and zinc which were used as the nitrate salts. Solutions were prepared with doubly deionized water. Sodium and potassium ion solutions

0003-2670/87/$03.50

were standardized by ion-exchange chromatography. Solutions of the other ions were standardized by either direct or back-titration with ethylenediaminetetraacetic acid (EDTA). The EDTA (Aldrich Gold Label disodium EDTA) was converted to the tetra-acid form prior to use. Poly(vinyl chloride) was 99%+ (Gold Label, Aldrich). The tetrahydrofuran was Mallinckrodt ChromAR grade. The tetrakis(4-chlorophenyl)borate was of analytical grade (p.a. grade, Fluka).

Potentials were measured with a Corning 155 pH/ion meter. A saturated calomel electrode (SCE) with either a cracked bead or fiber junction was used as the external reference electrode. A silver chloride electrode was used as the internal reference electrode for all ions except for lead(II), iron(III), strontium and zinc for which the internal reference electrode was a saturated calomel electrode with a cracked bead junction.

Electrode preparation

Membranes were prepared by dissolving 100 mg of poly(vinyl chloride) (PVC), 250 mg of dibutyl phthalate, and 50 mg of 12-crown-4 in the minimal amount of tetrahydrofuran. Membranes containing the potassium tetrakis(4-chlorophenyl)borate (KTClPB) had 71 mg of the compound added before dissolution in tetrahydrofuran. The mixture was poured into a small, flat-bottom dish (5.4-cm diameter), covered with filter paper, and allowed to stand overnight. The resulting membrane (ca. 0.1 mm thick) was then sectioned with a cork borer and mounted across the opening of a polycarbonate tube (5 mm i.d.) using a glue of PVC in tetrahydrofuran.

Procedures

The electrodes were filled with a solution (the internal solution) which contained the primary ion at a concentration of 0.1 M and was saturated with silver chloride. The internal solutions in the electrodes used for lead(II), zinc, strontium and iron(III) ions did not contain AgCl. The filled electrode was conditioned by soaking in an approximately 0.05 M solution of the primary ion for 24 h and then it was placed in doubly deionized water for 1 h.

The electrode response was examined by immersing the membrane electrode in a measured amount of doubly deionized water, typically 50 or 100 ml, along with a saturated calomel reference electrode. A standardized solution, typically about 0.05 M, of the primary ion was then added incrementally to the stirred solution from a buret. The potential was recorded when the reading became stable (±0.1 mV/5 sec) after each addition. The data were plotted as observed potential (E) vs. the logarithm of the activity of the primary ion.

Activity coefficients were calculated from

$$-\log f_i = 0.5085\, Z_i^2(\mu)^{1/2}/(1 + 0.3281\, a_i(\mu)^{1/2})$$

where f_i is the activity coefficient of ion i, Z_i is the charge on ion i, μ is the ionic strength, and a_i is the effective hydrated diameter (Å) of ion i.

The slopes of the linear regions of the response curves were calculated by linear least-squares using a Hewlett-Packard 9845B computer. The selectivity coefficients were evaluated by the separate-solutions method using approximately 0.05 M solutions. All measurements for response curves and selectivity coefficients were done in triplicate with one membrane.

RESULTS AND DISCUSSION

The responses of the 12-crown-4 electrode to varying activities of eleven metal ions were examined. The activity range studied was 10^{-4} M to 10^{-2} M. This narrow range was chosen to limit the effects of changes in ionic strength. The upper activity limit was chosen to restrict the study to ionic strengths for which the activity coefficients are well behaved ($\mu < 0.1$ M). In the activity range studied, the responses of the electrodes to changing activity of the electroactive species showed only small deviations from linearity in the potential vs. logarithmic activity plots. Figure 1 shows the response of the electrode to changing activity of nickel(II) ions. This plot, which is typical for the 12-crown-4 based electrodes, displays a linear region with deviations from linearity at the activity extremes (activity greater than 7.8×10^{-4} M and less than 1.2×10^{-2} M for this ion). This is also the approximate activity range over which other investigators have obtained similar responses from crown ether-based membrane electrodes [9, 13].

Crown ethers containing only oxygen donor atoms are known to be poor ligands for transition metal ions but are noted for their ability to form very stable complexes with alkali and alkaline-earth metal ions. As a result, electrodes based on crown ethers are generally evaluated only with respect to these metal ions [1]. In this study, the response of the electrode based on 12-crown-4 to a number of representative ions was investigated. Table 1 lists

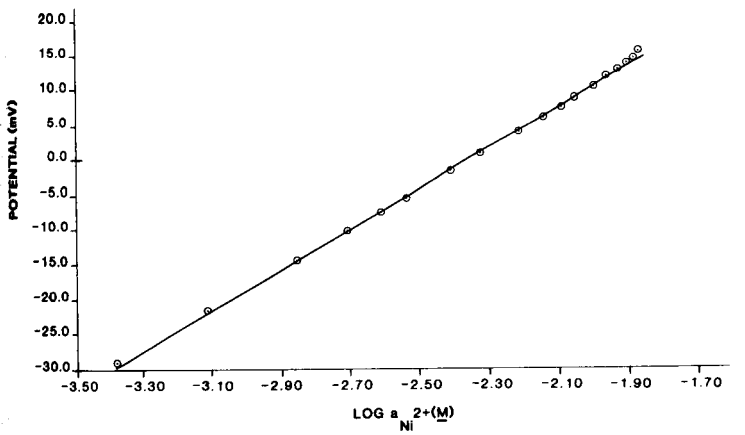

Fig. 1. Response curve of electrode for nickel(II) ions.

TABLE 1

Slopes and activity limits of linear regions of electrode response curves[a]

Ion	Li^+	Ba^{2+}	Sr^{2+}	Fe^{3+}	Mg^{2+}	Co^{2+}
Slope (mV/decade)	45.1	29.6	29.4	71.7	28.9	28.9
Activity limits (10^{-3} M)	6.10—25.5	0.54—9.51	0.52—17.7	0.25—3.25	0.37—13.5	0.74—13.2
Ion	Ni^{2+}	Cu^{2+}	K^+	Na^+	Al^{3+}	
Slope (mV/decade)	28.9	77.0	55.9	53.8	22.2	
Activity limits (10^{-3} M)	0.63—11.7	3.51—13.3	0.44—26.7	4.11—27.5	0.26—2.84	

[a]The electrode tested contained KTClPB as specified under Experimental.

the activity ranges and slopes of the linear regions of the response curves to eleven metal ions. The selectivity coefficients of the electrode for aluminum, cobalt(II), nickel(II), magnesium and potassium ions as primary ions are listed in Table 2. As can be seen, the electrode responds to a wide variety of cations. The responses to Ba^{2+} and Sr^{2+} are within 1% of ideal and the response to Mg^{2+} is within 2% of Nernstian. More interestingly, the responses to Co^{2+} and Ni^{2+} ions are also within 2% of ideal. The slopes of the linear regions of the curves for Na^+ and K^+ were slightly less than Nernstian (Table 1). The slope of the linear region of the curve for aluminum ion was slightly higher than ideal. The responses to Fe^{3+} and Cu^{2+} ions were significantly hyper-Nernstian.

In the study by Gadzekpo and Christian, the neutral carrier (12-crown-4) was immobilized in a PVC membrane by using triisononyl trimellitate as the plasticizer [11]. Their electrode was reported to have two linear response ranges, one with a slope of 28.8 mV/decade at high lithium ion concentrations and another with a slope of 61.1 mV/decade at lower lithium ion concentrations. The decreased slope at high lithium ion concentrations was attributed to the formation of complexes containing two lithium ions per crown ether molecule within the membrane. The slope of the linear region of the response curve for lithium produced by the electrode used here was considerably higher than that obtained by Gadzekpo and Christian, 45.1 mV/decade vs. 28.8 mV/decade even at relatively high lithium ion concentrations. When the lipophilic anion was not added to the electrode, the response curve for lithium ion had a slope of 21.3 mV/decade, similar to Gadzekpo and Christian's electrode. It is most likely that, here also, a 2:1 complex of Li^+ to crown ether is being formed in the membrane without the KTClPB present. When the lipophilic anion (TClPB) was present in the membrane, its counter ion, K^+, probably complexed enough of the crown ether to reduce the amount of 2:1 complex that Li^+ could form within the electrode membrane.

With dibutyl phthalate as plasticizer, it was necessary to include tetrakis(4-chlorophenyl)borate in the membrane to obtain a stable, reproducible

TABLE 2

Selectivity coefficients[a], $K_{i,j}^{pot}$

Interfering ion, j	Selectivity coefficient				
	$i = Mg^{2+}$	$i = K^{+}$	$i = Ni^{2+}$	$i = Al^{3+}$	$i = Co^{2+}$
Co^{2+}	1.19	10.9	0.06	3.2×10^{-4}	1.00
Mg^{2+}	1.00	0.24	2.07	7.9×10^{-5}	4.65×10^{-4}
K^{+}	1800	1.00	67500	9850	452
Cu^{2+}	8.63	0.13	0.32	0.04	0.18
Li^{+}	2.25	3.57	0.54	0.73	7350
Zn^{2+}	2.75	0.28	0.72	2.81	0.16
Sr^{2+}	7.33	0.17	0.07	1.00	0.09
Na^{+}	38.2	3.88	0.20	1020	1180
Al^{3+}	0.97	0.89	0.27	1.00	0.61
Ba^{2+}	63.7	0.27	0.07	0.13	1.69
Pb^{2+}	17.6	0.82	14.7	76.3	0.10
Fe^{3+}	0.50	0.43	0.07	4.18	4.59
Ni^{2+}	1.02	1.08	1.00	0.10	2.92

[a]See footnote to Table 1.

potential. In the absence of KTClPB in the membrane, up to 1 h was required to obtain a stable potential, whereas stable potentials were obtained in seconds with KTClPB in the membrane. Further, without the lipophilic anion present, the electrode gave response curves with negative slopes to nickel(II), cobalt(II) and magnesium ions (—33.2, —31.1, and —29.2 mV/decade, respectively). With KTClPB in the membrane, the electrode gave near-Nernstian response to these three ions (Table 1).

As stated above, the electrodes incorporating tetrakis(4-chlorophenyl)-borate responded to iron(III) and copper(II) ions with significantly greater than ideal slopes. Electrodes without the lipophilic anion produced slopes of 32.4 mV/decade for Fe(III) and 25.5 mV/decade for Cu(II) ions. The slope of the iron(III) response curve of the electrode without KTClPB may be due to the formation of a doubly charged complex ion of Fe(III) in the test solution. The response to Cu(II) was close to Nernstian without KTClPB in the membrane. The greater slopes of the response curves of the electrode with KTClPB for iron(III) and copper(II) are due to the presence of the TClPB in the membrane; the exact cause was not investigated.

Table 2 shows that the 12-crown-4 electrode is selective for aluminium over magnesium and cobalt(II) ions; selectivity coefficients were 7.9×10^{-5} and 3.2×10^{-4}, respectively. The electrode is also selective for cobalt(II) over magnesium ions, with a selectivity coefficient of 4.65×10^{-4}. While this electrode does exhibit selectivity in some specific situations, it is not reasonable to consider it to be generally selective for any particular ion. The 12-crown-4 electrode investigated by Gadzekpo and Christian [11] exhibited selectivity

for Li^+. The 12-crown-4 electrode studied here was not selective for Li^+ with or without the tetrakis(4-chlorophenyl)borate in the membrane. This is probably due to the use of a different plasticizer and a larger ion concentration than used by Gadzekpo and Christian.

In conclusion, these electrodes show fast response but generally poor selectivity. They may be useful as general cation indicating electrodes, or in applications such as chromatographic detectors.

The author acknowledges support by the Naval Research Laboratory/ Underwater Sound Reference Detachment and the University of Central Florida Division of Sponsored Research.

REFERENCES

1 See, e.g., W. E. Morf and W. Simon, in H. Freiser (Ed.), Ion-selective Electrodes in Analytical Chemistry, Vol. 1, Plenum, New York, 1978.
2 L. A. R. Pioda, V. Stanhova and W. Simon, Anal. Lett., 2 (1969) 665.
3 M. Mascini and F. Pallozzi, Anal. Chim. Acta, 73 (1974) 375.
4 U. Fiedler and J. Růžička, Anal. Chim. Acta, 67 (1973) 179.
5 C. J. Pedersen, J. Am. Chem. Soc., 89 (1967) 7017.
6 O. Ryba and J. Petranek, J. Electroanal. Chem. Interfacial Electrochem., 44 (1982) 25.
7 M. Yamauchi, A. Jyo and N. Ishibashi, Anal. Chim. Acta, 136 (1982) 399.
8 A. V. Bogatsky, N. G. Lukyanenko, V. M. Golubev, N. Yu. Nazarova, L. P. Karpenko, Yu. A. Popkov and V. A. Shapkin, Anal. Chim. Acta, 157 (1984) 151.
9 J. Petranek and O. Ryba, Anal. Chim. Acta, 72 (1974) 375.
10 K. M. Aalmo and J. Krane, Acta Chem. Scand., Ser. A, 36 (1982) 227.
11 V. P. Y. Gadzekpo and G. D. Christian, Anal. Lett., 16 (1983) 1371.
12 O. Ryba and J. Petranek, J. Electroanal. Chem. Interfac. Electrochem., 67 (1976) 321.
13 S. Kitazawa, K. Kimura, H. Yano and T. Shono, Analyst, 110 (1985) 295.

Analytica Chimica Acta, 194 (1987) 177—187
Elsevier Science Publishers B.V., Amsterdam — Printed in The Netherlands

THE DETERMINATION OF ARSENIC AND SELENIUM IN COAL BY CONTINUOUS FLOW HYDRIDE-GENERATION ATOMIC ABSORPTION SPECTROMETRY AND ATOMIC FLUORESCENCE SPECTROMETRY

LES EBDON* and JOHN R. WILKINSON[a]

Department of Environmental Sciences, Plymouth Polytechnic, Drake Circus, Plymouth, Devon PL4 8AA (Great Britain)

(Received 2nd July 1986)

SUMMARY

Concentrated perchloric acid is used to digest coal for subsequent determination of arsenic and selenium by hydride-generation atomic absorption and fluorescence spectrometry. Arsenic and selenium are removed from potentially interfering metal ions by co-precipitation with lanthanum hydroxide. The detection limits, 58 and 36 ng g^{-1} by atomic absorption and 25 and 10 ng g^{-1} by atomic fluorescence, for arsenic and selenium in coal, respectively, are adequate for the normal levels of these metals.

Coal combustion has been identified as a potential source of pollution from volatile trace metals. Some studies [1] on the fate of such elements during combustion have shown that up to 85%, 60% and 55% of the mercury, arsenic and selenium, respectively, originally present in the coal could not be accounted for in the waste streams examined. Other workers [2] have suggested that almost all the arsenic and selenium present in the coal appear in the fly ashes and exhaust gases.

Several instrumental methods have been used to determine arsenic and selenium in coal and related materials including neutron activation (with [3—6] or without [7—9] prior combustion or ashing), x-ray fluorescence spectrometry [6, 10] and spark-source mass spectrometry [11, 12]. Other workers have used a variety of dissolution techniques with subsequent determination by spectrophotometry [13], atomic absorption spectrometry (a.a.s.) [14] anodic stripping voltammetry [15] and gas chromatography [16, 17] (with a microwave-induced plasma detector), and by electrothermal a.a.s. [18, 19]. Ashing techniques have been used to prepare coal samples for determination of arsenic and selenium. Following treatment with magnesium nitrate/nickel nitrate to prevent volatilization losses, powdered coal was ashed at 450—500°C followed by determination of arsenic by electrothermal a.a.s. [20]. This approach was extended by Ebdon and Pearce [21]

[a]Present address: EDT Research, 14 Trading Estate Road, London NW10 7LU, Great Britain.

0003-2670/87/$03.50

to the direct determination of arsenic in whole coal by ashing a slurried sample in the graphite tube for electrothermal a.a.s.

Coal samples have been ashed at similar temperatures with mixtures of magnesium oxide and sodium carbonate [18] prior to determination by hydride-generation a.a.s. Nadkarni [22] has also applied hydride-generation a.a.s. to coals, reporting the determination of arsenic, selenium, antimony, bismuth, lead, tin and tellurium, after decomposition in a Parr bomb. Several factors, e.g., oxidation state, pH and certain cations, have been shown [23] to affect the accuracy in hydride-generation a.a.s. Methods which minimize or eliminate these interferences involve the use of masking agents [24] and separation techniques [25, 26].

In this paper, a method is described in which concentrated perchloric acid is used to digest coal prior to determination of arsenic and selenium by hydride-generation a.a.s. and atomic fluorescence spectrometry (a.f.s.). Interfering cations are removed by a simple coprecipitation step which isolates the arsenic and selenium on lanthanum hydroxide.

EXPERIMENTAL

Apparatus

The continuous flow system and the miniature atom cell used to quantify arsenic and selenium by a.a.s. and a.f.s. have been described previously [27]. The instrumentation and operational conditions were also similar to those previously reported. An atomic absorption spectrometer (IL-151, Instrumentation Laboratory) was used for all measurements. For the atomic absorption measurements, hollow-cathode lamps (S. J. Juniper & Co., Harlow) operated at 4 mA were used as sources. For the atomic fluorescence measurements, electrodeless discharge lamps excited in a Broida 3/4-wave microwave cavity (210L) powered by a Microtron 200 Mark III microwave generator (Electromedical Supplies, Wantage, Oxon.) were used as sources; the net power supplied to the arsenic lamp was 37 W and to the selenium lamp was 64 W. For both a.a.s. and a.f.s., the arsenic wavelength of 193.7 nm and the selenium wavelength of 196.0 nm were used, with a spectral bandpass of 2.0 nm. The continuous flow hydride generator was as described previously [27] and the hydrides formed were swept to an air/hydrogen flame which burnt on a glass Y burner. An argon carrier gas (flow rate 120 ml min^{-1}) and an auxiliary hydrogen flow (180 ml min^{-1}) were used to augment the flame.

Lanthanum(III) hydroxide was precipitated by mixing the appropriate solutions in a centrifuge tube (PTFE, 100 ml) which, after cooling, was inserted into a heavy-duty centrifuge (MSE Super Minor Centrifuge, MSE Scientific Instruments, Crawley).

Silica residues, obtained on dissolution of coal with concentrated perchloric acid, were tested for arsenic by standard x-ray fluorescence and x-ray diffraction techniques. Low-temperature ashing was done in a Nanotech

Plasma Prep P100 (Nanotech Thin Films, Prestwich, Manchester). Forward power was 115 ± 5 W and reflected power ca. 5 W.

Reagents

Unless otherwise stated the reagents used were of analytical grade (BDH). The water used was distilled then deionized. Sodium tetrahydroborate(III) solution was prepared by dissolving 1 g of the solid (Fisons Scientific Apparatus, Loughborough; general-purpose-reagent) in 0.1 M sodium hydroxide (100 ml). Solutions prepared this way remained usable for 2—3 days.

Arsenic and selenium standard solutions were prepared by serial dilution of stock solutions of 1000 μg ml^{-1} (Hopkin and Williams, Chadwell Heath). Working standards, typically in the range 1—100 ng ml^{-1}, were prepared with the following diluents. Arsenic solution diluent was prepared by dissolving sodium iodide (10 g) in 5 M hydrochloric acid (1.0 l). Selenium solution diluent was prepared by dissolving sodium bromide (10 g) in 5 M hydrochloric acid (1.0 l).

Solutions of lanthanum(III) chloride, sodium iodide and sodium bromide were each prepared by dissolving 10 g of the solid in water (100 ml). Ammonia solution was prepared by diluting concentrated (0.88) ammonia liquor with an equal volume of water. The copper solution (500 μg ml^{-1} in 2 M nitric acid) was prepared by dissolving copper foil (0.50 g) in 4 M nitric acid (500 ml) and diluting to 1 l with water.

Standard reference material coals (SRM 1632a and 1635) were obtained from the National Bureau of Standards, Washington, DC.

Procedures

Dissolution of coal in concentrated perchloric acid. Powdered coal, (0.7 g) was added to a three-necked round-bottomed digestion flask and a double surface condenser was fitted to the B24 neck of the flask. Concentrated perchloric acid (35 ml, 72% w/v) was added through the second neck of the flask, which was then stoppered and the flask was swirled repeatedly to ensure mixing and thorough wetting of the coal. The third neck was used to insert a thermometer. The mixture was heated gently with a Bunsen burner until effervescence began (5—10 min). At this point, the reaction became vigorous and self-sustaining. Heating was discontinued until effervescence subsided (5—10 min), whereupon the mixture was heated strongly until the carbonaceous matter was completely dissolved. The mixture was then refluxed for ca. 10 min and allowed to cool. This procedure yielded a sample solution in $\leqslant$45 min. When more concentrated sample solutions were required, the mixture was cooled after the initial effervescence had ceased and a second portion of coal (0.3—0.7 g) was added through the second neck of the flask. The procedure was continued as described above and the total reaction time was typically 1 h. After cooling, first in air and then in an ice/water mixture, the solution and silica residues were transferred with condenser and flask washings (10—12 ml, 5 M hydrochloric acid) to a 50-ml volumetric flask.

As a safety precaution, iced water (ca. 200 ml) was placed in a separating funnel, fitted in the vertical arm of a two-way adaptor located in the top of the condenser. In initial experiments, when any smouldering and/or ignition of the coal was observed, the iced water was immediately discharged into the reaction flask to cool and quench the mixture. Once the technique had been established, however, no such problems were encountered.

Separation of arsenic and selenium by co-precipitation with lanthanum hydroxide. An aliquot of the perchloric acid digest (10—20 ml) was transferred to a 100-ml PTFE centrifuge tube and lanthanum chloride solution was added (2 ml, 10% w/v). Sodium iodide solution (1 ml, 10% w/v) or sodium bromide solution (1 ml, 10% w/v) was added for arsenic or selenium determination, respectively. After mixing, ammonia solution (25—50 ml, 50% v/v) was poured quickly into the mixture. For arsenic determinations, the solution was cooled by immersion in cold water. For selenium determinations, the solution was allowed to cool in air (10—15 min), the heat of neutralization being used to accelerate reduction of selenium(VI) to selenium(IV). The lanthanum hydroxide precipitate was separated by centrifuging at ca. 3000 rpm for 2—3 min. A second aliquot (1 ml) of lanthanum chloride solution was added and the mixture centrifuged as before. The supernatant liquor was carefully discarded and the precipitate dissolved in the minimum volume of hydrochloric acid (5 M, containing 1% w/v sodium bromide or sodium iodide for selenium or arsenic determinations, respectively). The resulting solution was transferred to a volumetric flask (10—25 ml) and made up to volume with the appropriate hydrochloric acid diluent. Arsenic or selenium was quantified in this solution by hydride-generation a.a.s. or a.f.s.

Low-temperature ashing of coal samples. A sample of powdered coal (typically 0.5 g) was spread thinly on a cover glass which was placed in the sample chamber of the ashing unit. After evacuation of the chamber, a small flow of oxygen (20 ± 2 ml min^{-1}) was introduced, the forward power was set to ca. 100 W and the plasma was initiated. The forward power was increased to a nominal setting of 115 W and the plasma tuned to produce minimum reflected power (typically 5 W). The sample was allowed to ash in the oxygen plasma for periods ranging between 24 and 90 h. On completion of the ashing cycle, the oxygen supply was switched off and the pressure in the sample chamber allowed to rise slowly to atmospheric pressure. The ash was mixed with 15 ml of a 500 μg ml^{-1} copper solution in 2 M nitric acid and heated at 80°C for 30 min. The suspension was allowed to cool to ca. 30°C and filtered directly into a 25-ml volumetric flask. The precipitate was washed and the solution made up to volume with the same copper solution. Arsenic was quantified by electrothermal a.a.s. under the conditions listed in Table 1.

RESULTS

Dissolution of coal in concentrated perchloric acid

During initial attempts to digest coal, the volume of acid per unit weight of coal was varied in order to establish which proportions yielded rapid and

TABLE 1

Instrumentation and optimum operating conditions used in the determination of arsenic by electrothermal a.a.s.

Component	Model[a]	Operating conditions
Spectrometer	PE-272	PMT voltage 620 V, wavelength 193.7 nm, spectral bandpass 0.7 nm
Autosampler	AS-1	Sample volume 20 μl, 4 replicates per sample
Recorder	056	1 cm min^{-1}; 10 mV f.s.d.
Sources, hollow-cathode lamp		7.5 mA
deuterium arc		4 mA
Furnace	HGA-76B	see below

Furnace operating conditions

Parameter	Cycle		
	Dry	Char	Atomize
Temperature (°C)	150	1250	2700
Time (s)	20	15	8
Argon flow (ml min^{-1})	50	50	stopped

[a]All from Perkin-Elmer.

safe dissolution of the coal while preventing undue dilution of the sample solution. It was found to be essential to wet the coal thoroughly with the acid but, wherever possible, with a minimum of agitation. If the acid and coal were not intimately mixed, small inclusions or 'pockets' of dry coal tended to react rather vigorously during preliminary heating of the mixture. In some cases when the ratio of acid to coal was small (typically $\leqslant$20 ml: 1 g), these inclusions tended to persist to the stage of vigorous heating of the mixture, and ignition of the coal occurred. Similarly, when the coal and acid mixture was shaken too vigorously prior to heating, a thin layer of coal dust was seen to collect on the inside of the flask above the level of the acid. During heating of the mixture this coal dust was seen to smoulder, suggesting imminent ignition. When this happened, the iced water stored in the separating funnel in the top of the condenser was immediately discharged into the flask to quench the mixture and prevent potential explosion. The minimum acid-to-coal ratio necessary to minimize these problems was 40:1; in practice 50:1 was preferred.

The sample solution concentrations of coal were of the order of 1.4% w/v. This concentration represented arsenic concentrations of 130 and 5 ng ml^{-1} and selenium concentrations of 36 and 12 ng ml^{-1} for the standard reference coals 1632a and 1635, respectively. While these levels could be measured by the proposed detection systems, the relative standard deviation (RSD) obtainable for arsenic and selenium in SRM 1635 was unlikely to be better than 10%. Consequently, sample solution concentrations were

increased by adding more coal during digestion. This proved to be relatively simple and increased the time taken for sample dissolution by only 15–20 min.

Determination of arsenic and selenium in the perchloric acid digests

Initial attempts to quantify arsenic and selenium directly in the perchloric acid digests of the standard coals by the hydride-generation methods described resulted in low recoveries of both elements, typically 80 ± 5%. Possible reasons suspected were the adsorption of arsenic and selenium on silica precipitated during digestion, depletion of the available reductant concentration because of reaction between perchloric acid and sodium tetrahydroborate(III), interferences during hydride generation by certain transition metals, notably copper and nickel, and volatilisation losses during digestion with refluxing perchloric acid.

After digestion of the two coal samples, the residue from both solutions was filtered on to a Nuclepore 0.8-μm filter and examined by x-ray fluorescence and x-ray diffraction methods. The x-ray diffraction confirmed that the material was largely quartz, with small amounts of kaolinite and alumina. Both samples produced x-ray fluorescence spectra in which arsenic peaks were observed (detection limit 5 $\mu g\ g^{-1}$). Selenium was not observed in either spectrum but this was probably because the maximum levels of selenium expected in the residue were below the detection limit of the method (5 $\mu g\ g^{-1}$). The silica was returned to each of the solutions and the samples refluxed for 10–15 min. After a second filtration, the silica was again examined by x-ray fluorescence spectrometry, which showed that the arsenic had been desorbed. However, examination of these solutions by hydride-generation a.a.s. showed that the recoveries of arsenic were still low (typically

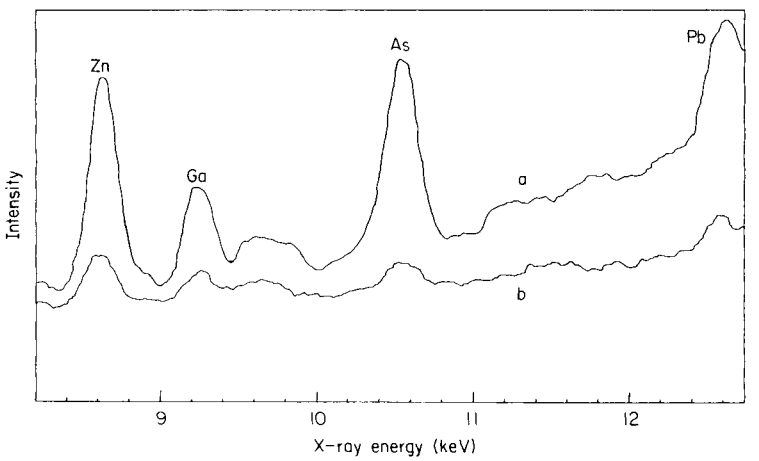

Fig. 1. X-ray fluorescence spectrum of silica residues from perchloric acid digestion of NBS SRM 1632a: (a) before refluxing; (b) after refluxing.

80%) so this source of error was discounted. The x-ray fluorescence spectra obtained from one coal residue are shown in Fig. 1.

Metal ion interference was then considered to be the most plausible source of error. To investigate this possibility, various 'synthetic' coal solutions were prepared containing the concomitant trace metals present in SRM 1632a (chromium, copper, iron, lead, manganese, nickel, vanadium and zinc) as well as arsenic and selenium. Two solutions containing these metals in the ratios reported for the 1632a coal sample were prepared in 5 M hydrochloric acid and in a 1 + 1 mixture of 5 M hydrochloric acid and concentrated perchloric acid. Two other solutions were prepared with the same acids and having the same arsenic and selenium concentrations but increased metal concentrations (10 μg ml^{-1} each).

When measured by hydride-generation a.a.s., all the solutions containing trace metals gave apparently low recoveries of arsenic and selenium (typically 80–90%) relative to solutions made up in 5 M hydrochloric acid and containing no added transition metals. The solutions which were 10 μg ml^{-1} in each metal gave slightly lower recoveries than the solutions directly representative of SRM 1632a. The results are given in Table 2. Although rigorous attempts to identify the effects of specific metals were not made, copper and nickel in particular were investigated. Solutions of both arsenic and selenium containing copper or nickel (at SRM 1632a concentration ratios) were examined directly by hydride-generation a.a.s. In each case, recoveries were low, typically 90% and 80% for nickel and copper solutions, respectively.

TABLE 2

Comparison of responses from various solutions with and without the trace metals present in SRM 1632a, measured by hydride-generation a.a.s.

Solution[a]	Recovery (%)[b]			
	As 20	Se 20	As 100	Se 100
A	100	100	100	100
B	103	97	102	99
C	86	90	90	89
D	86	90	91	84
E	79	83	84	80
F	82	80	83	80

[a]A, 5 M HCl containing As and Se.
B, 5 M HCl/72% $HClO_4$ (1 + 1) containing As and Se.
C, 5 M HCl containing (in ng ml^{-1}) As (20), Cr (70), Cu (35), Fe (2000), Pb (25), Mn (60), Ni (40), Se (5), V (90), Zn (60).
D, 5 M HCl/72% $HClO_4$ (1 + 1) with the metals as in C.
E, 5 M HCl containing As (20 ng ml^{-1}), Se (5 ng ml^{-1}); Cr, Cu, Fe, Pb, Mn, Ni, V and Zn (10 000 ng ml^{-1} each).
F, 5 M HCl/72% $HClO_4$ (1 + 1) with the metals as in E. [b]For nominal concentrations of 20 and 100 ng ml^{-1} Se or As, as shown. All solutions contained sodium iodide or sodium bromide (1% w/v), respectively.

When the lanthanum hydroxide single precipitation procedure was applied in ammoniacal solution, in order to separate the analytes from the metal ions, arsenic was recovered quantitatively, but only 93 ± 2% of the selenium was recovered. Quantitative recoveries of both elements were obtained when the double precipitation procedure was used. Clearly, the coprecipitation procedure removed any excess of perchloric acid and possible loss of reductant was not investigated further.

The perchloric acid/lanthanum hydroxide co-precipitation method was used to prepare sample solutions of SRMs 1632a and 1635. Arsenic and selenium were quantified by hydride-generation a.a.s. and a.f.s. The results are given in Table 3. In attempts to increase the recovery of arsenic from SRM 1635, the concentrations of the lanthanum chloride and ammonia solutions were increased. However, the results for arsenic for SRM 1635 were not improved, but the results were within the NBS quoted range.

A range of non-standard coals was examined for arsenic and the results obtained were compared with results obtained independently [21] by the British Standard BS-1016 method and by neutron activation. The results are shown in Table 4.

Low-temperature coal ashing

Experiments were done in which the weight of coal taken and the ashing time were varied in order to find the optimum conditions for rapid preparation of the ash. The ash leachates (with nitric acid) were examined for arsenic by carbon-furnace a.a.s. (see Table 1) with the results shown in Table 5. These results suggest that the sample needs to be ashed for more than 24 h if subsequent quantitative leaching of the arsenic from the ash is to be achieved. In one experiment, the ash was not filtered from the leachate and an ash slurry was examined instead. The recovery of arsenic was within 6% of the value

TABLE 3

Determination of arsenic and selenium in reference coals by hydride-generation a.a.s. and a.f.s.

Coal sample	SRM 1632a		SRM 1635	
Element ($\mu g\ g^{-1}$)	As	Se	As	Se
Certificate value	9.32 ± 1	2.6 ± 0.7	0.42 ± 0.15	0.9 ± 0.3
Hydride-generation a.a.s.				
Mean	9.34	2.58	0.32	0.90
Standard deviation	0.23	0.08	0.02	0.03
RSD (%)	2.4	2.9	7	5
No. of results	9	7	5	5
Hydride-generation a.f.s.				
Mean	9.27	2.64	0.30	0.90
Standard deviation	0.25	0.05	0.02	0.03
RSD (%)	2.7	1.9	7	5
No. of results	5	5	5	5

TABLE 4

Comparison of the arsenic concentrations found in this work with independent determinations [21] on six coal samples

Sample	Arsenic concentration ($\mu g\ g^{-1}$)				
	This work	Independent results			
	Hydride-generation a.a.s.	Neutron activation	BS-1016	Electrothermal a.a.s.	
				A[a]	B[b]
1	18.5	28.0	16.7	17.7	—
2	16.7	20.0	14.1	22.7	12.0
3	17.3	32.0	13.2	22.7	16.0
4	8.4	11.3	7.0	14.3	12.5
5	4.6	—	2.9	6.7	4.8
6	15.2	—	10.8	13.5	8.9

[a]Calibrated with aqueous solutions matched for nickel and magnesium content. [b]Calibrated with aliquots of slurried coal (sample 1) assuming an arsenic content of 16.7 $\mu g\ g^{-1}$.

TABLE 5

Recovery of arsenic from low-temperature coal ash from NBS SRM 1632a (Bituminous Coal)[a] by electrothermal a.a.s.

Sample weight (g)	Arsenic found ($\mu g\ g^{-1}$) for different ashing times	
	24 h	72 h
0.050	7.4 ± 1	10.0 ± 0.4
0.200	6.5 ± 1	9.18 ± 0.4[b]
0.500	6.0 ± 1	9.14 ± 0.4

[a]Certificate value, 9.32 ± 1 $\mu g\ ml^{-1}$. [b]Arsenic found for a slurry, 8.8 ± 1.3 $\mu g\ g^{-1}$.

obtained for the filtered leachate, though precision was worse, presumably because of light scattering in the furnace by ash particulates.

DISCUSSION

The perchloric acid digestion procedure is seen to be a simple, rapid and efficient method for the dissolution of coal. The elevated temperatures required to reflux concentrated perchloric acid (200—210°C) do not lead to losses by volatilisation of arsenic or selenium. The strenuous reflux conditions used also minimize undesirable emission of perchloric acid fumes. Thus the tendency towards dehydration of the acid, which may subsequently introduce potential explosive hazards, is avoided. When applied as recom-

mended, this method was completely safe and reliable, and showed no tendencies towards ignition and/or over-vigorous reaction. It has been used routinely to dissolve numerous coal samples, of widely varying compositions, in a rapid and reproducible manner.

Talmi and Norvell [17] experienced problems of adsorption of selenium on precipitated silica when dissolving environmental samples in a mixture of nitric, perchloric and sulphuric acids. Such problems were avoided in this work by refluxing the coal digest to desorb arsenic and selenium from the residual silica.

Direct examination of the perchloric acid digests by the proposed hydride-generation methods failed to yield quantitative recoveries of arsenic and selenium. The results of a series of experiments indicated that these low recoveries were due to inhibition by certain transition metals (probably nickel and copper) during generation of the hydrides. A possible explanation is that species such as copper arsenide, copper selenide, nickel arsenide and nickel selenide were precipitated during mixing of the sodium tetrahydroborate and sample solutions, when the pH of the solution rises sharply. Thus, appreciable amounts of both arsenic and selenium are made unavailable for reduction and low recoveries result. The large excess of lanthanum ions added during the precipitation step ensures that arsenic and selenium are preferentially precipitated with the lanthanum, while the copper and nickel remain in solution as their ammine complexes.

The results obtained for the various coals are encouraging in terms of accuracy and precision. Values obtained for both elements in both standard coals by hydride-generation a.a.s. and a.f.s. are within the NBS quoted ranges, although the value obtained for arsenic in SRM 1635 is towards the lower end of the range. The certified value is based on figures obtained by determinations by a.a.s. and activation analysis. Authors [4, 28—30] who determined arsenic in SRM 1635 by instrumental activation methods have reported average values substantially higher than the NBS value, and often with poorer precision. This is probably because such low concentrations are close to the detection limits of the methods used, but there may be some interferences. Consequently, a certificate value based on the results obtained by use of these techniques may be biased towards the high end of the range.

The use of the miniature flame as the atom cell for a.a.s. or a.f.s., together with the reproducible digestion conditions and continuous hydride generation provides a suitably accurate and precise method for the determination of arsenic and selenium in coal. Interferences that occur during generation of the hydrides are prevented by a simple rapid co-precipitation procedure. The detection limits of 58 and 36 ng g^{-1} by a.a.s. and 25 and 10 ng g^{-1} by a.f.s. for arsenic and selenium, respectively, are adequate for typical arsenic and selenium concentrations in coals. When extra sensitivity is required, these detection limits can be improved by a factor of 2—3 by increasing the amount of coal dissolved per digestion, although correspondingly longer digestion times are required.

Finally, the potential of the low-temperature oxygen plasma ashing technique as a suitable method for preparing coal samples for subsequent determination of arsenic and selenium was investigated. Ashing was found to be time-consuming, and would considerably lengthen the analytical procedure.

The authors thank the British Gas Corporation, London Research Station and the Science and Engineering Research Council for the award of a SERC CASE Studentship to one of us (J. R. W.).

REFERENCES

1 N. E. Bolton, J. A. Carter, J. F. Emery, C. Feldman, W. Fulkerson, L. D. Hulett and W. S. Lyon, in S. P. Babu (Ed.), Trace Elements in Fuel, Advances in Chemistry series, American Chemical Society, Washington, DC, Vol. 141, 1975, p. 175.
2 G. T. Moore and V. J. Elia, Paper presented at the 71st Annual Meeting Air Pollution Control Association, Houston, Texas 78-34.2 (June 1978).
3 J. N. Weaver, Anal. Chem., 45 (1973) 1950.
4 J. J. Rowe and E. Steinnes, J. Radioanal. Chem., 37 (1977) 849.
5 R. R. Greenberg, Anal. Chem., 51 (1979) 2004.
6 R. R. Ruch, H. J. Gluskoter and N. F. Shimp, Occurrence and Distribution of Potentially Volatile Trace Elements in Coal: an Interim Report, Illinois State Geological Survey, Environmental Geology Notes, 61 (April 1973).
7 M. Gallorini, R. R. Greenberg and T. E. Gills, Anal. Chem., 50 (1978) 1479.
8 D. Knab and E. S. Gladney, Anal. Chem., 52 (1980) 825.
9 E. Orvini, T. E. Gills and P. D. LaFleur, Anal. Chem., 46 (1974) 1294.
10 R. D. Giaque, R. B. Garrett and L. Y. Goda, Anal. Chem., 51 (1979) 511.
11 D. W. Koppenaal, R. G. Lett, F. R. Brown and S. E. Manahan, Anal. Chem., 52 (1980) 44.
12 T. Kessler, A. G. Sharkey Jnr. and R. A. Friedel, Analysis of Trace Elements in Coal by Spark Source Mass Spectrometry, U.S. Bur. Mines Rep. Invest., (1973) 7714.
13 G. I. Spielholtz and H. Diehl, Talanta, 13 (1966) 991.
14 G. I. Spielholtz, G. C. Toralballa and R. J. Steinberg, Mikrochim. Acta, 1 (1971) 918.
15 R. W. Andrews and D. C. Johnson, Anal. Chem., 48 (1976) 1056.
16 Y. Talmi and A. W. Andren, Anal. Chem., 46 (1974) 2122.
17 Y. Talmi and V. E. Norvell, Anal. Chem., 47 (1975) 1510.
18 S. K. Gangwal, P. M. Grohse, D. E. Wagoner, D. J. Minick, C. M. Sparacino and R. A. Zweidinger, Environmental Protection Agency Report (1979) Washington, DC, 600/7-79/201.
19 P. Aruscavage, J. Res. U.S. Geol. Surv., 5 (1977) 405.
20 B. W. Haynes, At. Absorpt. Newsl., 17 (1978) 49.
21 L. Ebdon and W. C. Pearce, Analyst (London), 107 (1982) 942.
22 R. A. Nadkarni, Anal. Chim. Acta, 135 (1982) 363.
23 B. Welz and M. Melcher, Analyst (London), 109 (1984) 569, 573, 577.
24 G. F. Kirkbright and M. Taddia, Anal. Chim. Acta, 100 (1978) 145.
25 S. Nakashima, Analyst (London), 103 (1978) 1031.
26 M. Thompson, B. Pahlavanapour, S. J. Walton and G. F. Kirkbright, Analyst (London), 103 (1978) 705.
27 L. Ebdon, J. R. Wilkinson and K. W. Jackson, Anal. Chim. Acta, 136 (1982) 191.
28 J. J. Rowe and E. Steinnes, Talanta, 24 (1977) 433.
29 M. S. Germani, I. Gokmen, A. C. Sigleo, G. S. Kowalczyk, I. Olmez, A. M. Small, D. L. Anderson, M. P. Failey, M. C. Gulovali, C. E. Choquette, E. A. Lepel, G. E. Gordon and W. H. Zoller, Anal. Chem., 52 (1980) 240.
30 J. M. Ondov, W. H. Zoller, I. Olmez, N. K. Aras, G. E. Gordon, L. A. Rancitelli, K. H. Abel, R. H. Filby, K. R. Shah and R. Ragaini, Anal. Chem., 47 (1975) 1102.

Analytica Chimica Acta, 194 (1987) 189—197
Elsevier Science Publishers B.V., Amsterdam — Printed in The Netherlands

PRECISION AND ACCURACY OF QUANTITATIVE EMISSION SPECTROMETRY WITH PARTICULAR REFERENCE TO GOLD ALLOYS

R. DE MARCO and D. J. KEW

Royal Melbourne Institute of Technology, GPO Box 2476V, Melbourne, Victoria 3001 (Australia)

C. CHADJILAZAROU and D. W. OWEN

Engelhard Industries P/L (Aust.), Settlement Road, Thomastown, Victoria 3074 (Australia)

J. V. SULLIVAN*

CSIRO, Division of Chemical Physics, PO Box 160, Clayton, Victoria 3168 (Australia)

(Received 14th October 1986)

SUMMARY

An emission spectrometric method is described for the determination of major constituents in metal samples. The metal sample is made the hollow-cathode of a demountable emission source. Use of the hollow-cathode discharge permits intensity measurements of the analytical lines (resonance lines) to be made with high signal-to-noise ratio. For ultimate precision and accuracy, such as is required in the determination of gold in gold alloys, internal standardization is also necessary. The precision is approximately 0.03% (w/w) (standard deviation) and the accuracy is 0.03% (w/w).

De Marco et al. [1, 2] have described a technique for emission spectrometry which permits precise and accurate determinations of major constituents in metal samples. The source was a hollow-cathode lamp [3, 4]. The high efficiency of excitation of the hollow-cathode discharge ensured that very good signal-to-noise ratio was obtained, even for low currents, when resonance lines were used as the analytical lines. Operation of the source at low current meant that there was little or no self-absorption present to affect the linearity of calibration graphs.

Analysis of gold alloys requires that the constituents, particularly the gold, be determined with very high accuracy. The accepted method for the determination of gold is fire assay which permits an absolute accuracy of 0.02—0.04% (w/w). To be acceptable, any other method for the determination of gold, e.g., emission spectrometry, must allow determinations to be made with comparable accuracy. To achieve this, it is essential to compensate for fluctuations in the discharge conditions and in the sputtering process.

Earlier attempts at the accurate analysis of gold alloys [5, 6] involved the use of an internal standardization procedure to correct for variations occurring from sample to sample. No compensation was made for variation from

0003-2670/87/$03.50

standard to standard. These efforts were not completely successful, and the precision and accuracy of 0.1% (r.s.d.) obtained for some determinations could not be achieved routinely, nor for all constituents.

The theory and application of the internal standardization procedure are discussed fully below and the results which can be achieved, in respect of precision and accuracy, are illustrated by the analysis of thirty-eight samples of gold alloy, especially prepared for this study.

The determinations of gold, silver and copper by fire assay, gravimetric techniques and atomic absorption spectrometry were done at Engelhard Industries P/L (Aust.) and were independent of emission analyses which were done at RMIT (R. DeM, D. J. K. and J. V. S.).

EXPERIMENTAL

Samples

The samples were prepared from gold and silver refined by Engelhard, and from electrolytic-grade copper. The specifications of the metals were: Au, 99.998%; Ag, 99.99%; Cu, 99.95% (minimum). The appropriate amounts of these metals were melted together by using a high-frequency discharge and were then cast into rod form in a carbon mould. Each sample was then machined to size [3] and the hollow cathode (3 mm deep and 3 mm in diameter) was drilled. Of the thirty-eight samples prepared, ten contained 88% (nominal) gold and another ten contained 96% (nominal) gold. The remaining eighteen samples consisted of duplicates at nine different values of concentration in the range 80—98% gold. Material remaining after preparation of the cathode samples was used in the chemical analyses.

Preliminary experiments indicated the presence of a matrix effect which necessitated the use of at least two standards. It was assumed that the effect was due to the presence of a Cu—Au compound, most likely CuAu.

All samples were heated in hydrogen to 280°C for several hours in an effort to produce some ordering of the CuAu phase. The two standards (84% and 96% gold, respectively), the two samples (3 and 7 of Table 1) and the two samples containing 88.97% Au were subsequently heated in hydrogen to 450°C for several hours to form disordered alloys.

Instrumentation

The experimental techniques for the emission measurements have been described elsewhere [1, 2]. The analytical lines were Au I 242.795 nm, Ag I 338.289 nm and Cu I 327.396 nm, respectively. No spectral interference was encountered.

The source was operated at 3 mA and the spectral band-pass used on the Varian-Techtron 0.5-m grating spectrometer was 0.04 nm. A current of 3 mA was chosen because experiments showed that calibration curves of intensity vs. concentration were linear up to at least 6 mA.

Internal standardization

The foundation for accurate emission spectrometry was laid by Gerlach [7] who, in 1925, introduced the concept of referring the intensity of the analytical line to that of a "homologous" line of some element present in fixed concentration in samples and standards alike. Great care had to be taken in the selection of the reference line so that fluctuations in the excitation and detection (photographic) processes, would affect it in a manner identical to that experienced by the analytical line.

In such a case, the intensity ratio of the two lines would not be affected significantly by changes in experimental parameters and would depend only on the concentration of the unknown element. Good improvement in precision and accuracy was achieved when intensity ratios rather than absolute intensities were measured.

The fundamental relationship used in quantitative emission spectrometry is $I = kC$, where I is the intensity of the analytical line, C the concentration of the constituent, and k a constant called the slope factor. This factor is measured using standards of known composition. Many factors affect the intensities of the lines emitted by the discharge source. These include changes in discharge parameters such as the dimension of the hollow cathode and the values of the operating pressure, current and voltage. In addition, there may be changes in the sputtering efficiency caused by the presence of gas inclusions in the metal, the condition and cleanliness of the surface and possible metallurgical effects. Compensation for all of these must be made when standards and samples are measured if the highest precision and accuracy are to be attained.

Because resonance lines respond to changes in discharge conditions in a similar fashion, particularly when a hollow cathode is used, the ratio I_a/I_b is independent of any fluctuation of discharge conditions. The subscripts a and b refer to particular elements in standards and samples. Further, because

$$I_a/I_b = k_a C_a/k_b C_b$$

the ratio k_a/k_b is also independent of these fluctuations. The k values for any system can thus be measured as ratios and for the ternary alloys discussed below,

$$K_{Au} = 1.00$$

$$K_{Cu} = k_{Cu}/k_{Au} = I_{Cu} C_{Au}/I_{Au} C_{Cu} \quad (1a)$$

$$K_{Ag} = k_{Ag}/k_{Au} = I_{Ag} C_{Au}/I_{Au} C_{Ag} \quad (1b)$$

where the K values are the relative slope factors.

When the concentrations in samples are to be measured, one could similarly use intensity ratios and derive concentration ratios. The determination of concentration of any constituent from such a ratio would require, in addition, knowledge of the concentration of an internal standard.

One way of avoiding the use of such a standard is to normalize the data by writing

$$C_a = C_a / \sum_{i=1}^{n} C = [(I_a/K_a)/ \sum_{i=1}^{n} I_i/K_i)] \ 100\% \qquad (2)$$

where, in order to determine C_a, all I and K must be measured. This technique enables compensation to be made for fluctuations in the measured intensities of the analytical lines in the samples. Another advantage of the use of Eqn. 2 is that greater precision and accuracy can be obtained by cancellation of error, as discussed in the Appendix.

If the concentration, C_a, of a constituent is known, then $\Sigma(I_i/K_i)$ may be evaluated from

$$\Sigma(I_i/K_i) = [(I_a/K_a)/C_a]100\%$$

and can be used for finding the concentration of all other constituents, the intensities of the analytical lines having been measured.

Bengtson [8] has proposed an empirical intensity expression to take account of fluctuations in sputtering efficiency and discharge parameters. He used the expression to derive corrected values for the elemental concentrations in copper-based alloys, with a single steel reference sample, and was able to improve the accuracy of measurement by orders of magnitude.

The method described in this paper is shown to correct for the fluctuations of the parameters considered by Bengtson.

RESULTS AND DISCUSSION

The accuracy of the emission technique for gold was evaluated by comparing the results obtained with those obtained by the accepted method, i.e., fire assay. Application of the emission method required measurement not only of the intensities of the analytical lines but also of the relative slope factors. These were calculated by using standards of known composition in conjunction with Eqns. 1(a) and 1(b). Systematic bias was excluded by using different chemical techniques for the analysis of standards and samples, respectively.

It was found that two standards were required, one for the range 80—90% gold and another for the range 90—100% gold. The standard used for samples in the former range was prepared from weighed amounts of gold, silver and copper and contained 84% gold, 8% silver and 8% copper, the concentrations being confirmed by chemical analysis. The relative slope factors were K_{Au} = 1.00, K_{Ag} = 10.21 and K_{Cu} = 11.26. The standard used for the latter range contained 96.02% gold, 2.00% silver and 1.98% copper. The concentrations of silver and copper were determined by flame atomic absorption spectrometry (a.a.s.) and the gold by difference. The error for the gold determination could be expected to be less than 0.04%. The relative slope factors were K_{Au} = 1.00, K_{Ag} = 12.48 and K_{Cu} = 13.64.

TABLE 1

Concentrations of gold, silver and copper, in prepared alloys[a]

Sample	Metal concentration (%, w/w)					
	Gold		Silver		Copper	
	A	B	A	C	A	D
1	79.91	79.88	10.04	10.02	10.05	9.72
2	81.92	81.95	8.95	8.98	9.13	9.06
3	85.95	85.93	7.02	7.05	7.03	6.93
4	87.97	87.95	6.02	6.01	6.01	5.93
5	89.98	89.93	5.01	5.03	5.00	4.95
6	91.96	91.92	4.05	3.96	3.97	4.02
7	93.96	93.94	3.03	2.99	3.00	3.01
8	95.95	95.91	2.06	2.02	2.01	2.02
9	97.87	97.86	1.13	1.07	1.00	1.04

[a]A, Emission spectrometry; B, fire assay; C, gravimetry; D, flame a.a.s. Results are the average of duplicate runs on ordered samples. Two standards were used.

Table 1 shows results obtained for gold, silver and copper by emission spectrometry and the internal standardization procedure. For comparison, the results obtained by chemical methods of analysis are included. It can be seen that for gold, where the comparison is between emission spectrometry (A) and fire assay (B), the concentrations generally agree to within 0.04% absolute. For silver, where the comparison is between emission spectrometry (A) and gravimetry (C), the agreement between results is better than 2% relative; for copper the agreement between results is better than 3% relative.

The need for the two standards is probably associated with an inter-element effect caused by the presence of an ordered phase, CuAu. Table 2 shows the K values obtained for the standards. The results obtained with the 96% standard show little difference between the slope factors for the ordered and disordered alloys. This can be expected because there is little copper present to form any significant amount of CuAu. However, with the 84% standard there is a marked difference in the K values of the respective elements. This trend was confirmed with the samples (3 and 7).

TABLE 2

Relative slope factors, K, for gold, silver and copper in standards containing 84 and 96% (w/w) gold, respectively, for ordered and disordered phases

Element	Relative slope factor, K			
	84% (gold)		96% (gold)	
	Ordered	Disordered	Ordered	Disordered
Gold	1.000	1.000	1.000	1.000
Silver	10.21	12.33	12.48	12.52
Copper	11.26	13.41	13.64	13.68

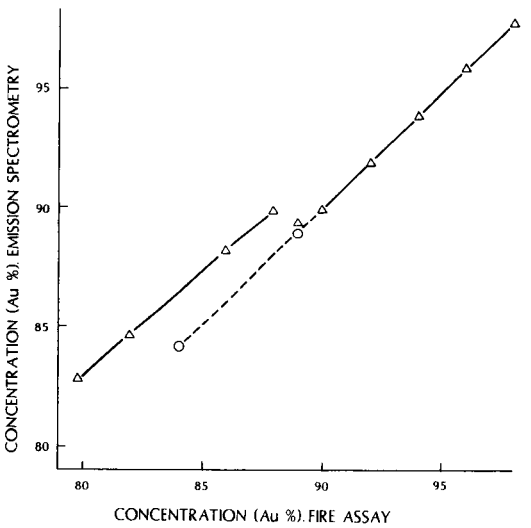

Fig. 1. Concentration of gold found by emission spectrometry, based on the 96% gold standard, vs. concentration found by fire assay: (△) samples heated to 280°C for 8 h to promote ordering; (○) samples heated to 450°C for several hours to promote ordering.

Figure 1 shows a plot of the concentrations of gold found by emission spectrometry versus those found by fire assay. The standard used was the 96% gold alloy, and the slope of this plot should be unity over the entire range of concentrations. The curve has two segments; the lower one has a slope of 0.877 whilst the upper one has a slope of 1.00. Thus, it is clear that the use of the 96% standard will lead to systematic error if used for the lower range. An interesting effect is observed with the samples containing 88.97% gold, 5.44% silver and 5.59% copper. The sample which had been ordered lies on neither curve, whereas the sample which had been disordered gives a value lying on the upper segment. These results suggest that no significant ordering occurs in the range 90—98% gold. However, once the concentration of copper exceeds 5%, ordering becomes significant and separate standards are required if the best accuracy is to be attained. The necessity for different standards depending on the concentration range can be avoided if all samples are disordered, as shown by previous results [2] and by the fact that the 84% and 89% disordered gold alloys give results which lie on the upper segment.

Table 3 shows the relative standard deviation (r.s.d.) obtained in the spectrometric determinations of gold, silver and copper. Two sets of gold alloy were used, each set containing ten samples. $(R.s.d.)_I$ refers to the precision of intensity measurement arising solely from instrumental factors; it was obtained for each element by repeated measurement of the intensities of the respective analytical lines for one sample which was not removed from the source between determinations. $(R.s.d.)_u$ refers to the precision of measure-

TABLE 3

Relative standard deviation (r.s.d.) of spectrometric determinations of the concentrations of gold, silver and copper[a]

Element	Concentration (w/w)	$(r.s.d.)_I$ (%)	$(r.s.d.)_u$ (%)	$(r.s.d.)_s$ (%)
Gold	88	0.18	7	0.04
	96	0.18	8	0.02
Silver	6	0.15	7	0.50
	2	0.40	15	1.00
Copper	6	0.16	7	0.60
	2	0.40	15	0.50

[a]The relative standard deviation $(r.s.d.)_I$ is the instrumental precision. $(R.s.d.)_u$ refers to the uncorrected concentrations. $(R.s.d.)_s$ refers to the concentrations after internal standardization.

ment of concentration without application of the internal standardization procedure; the apparent lack of precision is in part due to the fact that no attempt was made to maintain a strict tolerance on the dimensions of the hollow cathode. $(R.s.d.)_s$ denotes the precision obtained when correction is applied.

It can be seen that, even though the precision with which intensity measurement can be made is 0.2—0.4%, the precision with which the concentration of the major constituent can be obtained is an order of magnitude better because of cancellation of error (see Appendix). This cancellation is not as effective for minor constituents, as is shown in Table 3.

Conclusion

The demountable hollow-cathode lamp is a useful source for emission spectrometry because it emits sharp, intense and stable resonance lines. Use of such lines for analysis ensures good signal-to-noise ratio and, if major constituents are determined, discharge currents of the order of 5 mA can be used. This means that self-absorption effects are minimal, leading to linear calibration graphs. Because the discharge currents used are relatively low, the power supply provided with an atomic absorption spectrometer will normally be adequate.

There is evidence that a metallurgical effect caused by ordering of the alloy can affect the precision and accuracy. Experimental results suggest that disordered alloys, containing 80—100% (w/w) gold, can be analysed by using a single standard. The method of internal standardization developed increases the precision and accuracy of measurements of concentrations significantly, by compensating for fluctuations in the parameters considered by Bengtson's [8] treatment.

The method described is particularly suitable for the determination of gold in gold alloys where accuracy comparable with that of fire assay is required.

The authors thank the management of Engelhard Industries (Aust.) P/L for the loan of materials used to make the gold alloys.

APPENDIX. PROPAGATION OF ERROR FOR THE INTERNAL STANDARDIZATION PROCEDURE

Equation 2, which is used for evaluating the concentration of an unknown constituent, a, is expanded to include errors:

$$C_a + \Delta C_a = [(I_a/K_a) + \Delta_a]/\{[(I_a/K_a) + \Delta_a] + [(\Sigma I_r/K_r) \pm \Delta_r]\}\,100\%$$
$$\approx C_a\,[1 + \Delta_a/(I_a/K_a) - \Delta_a/\Sigma(I_i/K_i) \mp \Delta_r/\Sigma(I_i/K_i)]$$
$$\approx C_a\,[1 \mp \Delta_r/\Sigma(I_i/K_i)] \qquad \text{(A1)}$$

Here Δ_r is the error associated with measurement of the minor constituents and $\Delta_a/(I_a/K_a) \approx \Delta_a/\Sigma(I_i/K_i)$ for a major constituent.

A more accurate expression for Eqn. A1 can be derived from the propagation of error expression:

$$s^2_{C_a} = \sum_{i=1}^{n} [(\partial C_a/\partial I_i)^2\ s^2_{I_i} + (\partial C_a/\partial K_i)^2\ s^2_{K_i}]$$

where s_{C_a} is the standard deviation of the concentration of constituent, a; s_{I_i} is the standard deviation of the intensity of constituent i; and s_{K_i} is the standard deviation of the relative slope factor of constituent, i.

For the gold alloys discussed above,

$$s^2_{C_1} = [C_1 - C_1^2/100]^2\ (\text{r.s.d}_{I_1})^2 + [C_1\ C_2/100]^2\ (\text{r.s.d}^2_{I_2} + \text{r.s.d}^2_{K_2} + \text{r.s.d}^2_{I_3} + \text{r.s.d}^2_{K_3}) \qquad \text{(A2)}$$

because $C_2 = C_3$; components 1, 2 and 3 refer to gold, silver and copper, respectively.

Table A1 shows the standard deviations, s_{calc} and s_{exptl}, for gold. The values of s_{calc} were calculated from Eqn. A2, in which the various $(\text{r.s.d.})_I$ values were obtained from Table 3. The values of s_{exptl} were obtained from Table 3 by converting $(\text{r.s.d.})_s$ to absolute values. The good agreement between the experimentally found and the calculated standard deviations indicates that the internal standardization procedure successfully corrects for fluctuations in the discharge.

TABLE A1

Standard deviation (s) of spectrometric determinations of gold in two sets of gold alloy[a]

Gold concentration % (w/w)	s_{calc}	s_{exptl}
88	0.03_2	0.03_5
96	0.02_0	0.01_9

[a] s_{calc} refers to the calculated standard deviation obtained with Eqn. A2 in which the $(\text{r.s.d.})_I$ values come from Table 3; s_{exptl} is the experimentally found standard deviation and is the absolute value of $(\text{r.s.d.})_s$ in Table 3.

REFERENCES

1 R. De Marco, D. Kew and J. V. Sullivan, Spectrochim. Acta, Part B, 41 (1986) 591.
2 R. De Marco, D. Kew, D. Owen and J. V. Sullivan, Proc. 10th Int. Precious Met. Inst. Conf., Lake Tahoe, NV, June 1986.

3 J. V. Sullivan, Anal. Chim. Acta, 105 (1979) 213.
4 G. S. Lomdahl and J. V. Sullivan, Spectrochim. Acta, Part B, 39 (1984) 1395.
5 H. Jäger, Anal. Chim. Acta, 58 (1972) 57.
6 P. Pille, P. R. Lowe, A. M. Gillespie and L. R. P. Butler, Anal. Chim. Acta, 104 (1979) 11.
7 W. Gerlach, Foundations and Methods of Chemical Analysis by the Emission Spectrum, Hilger, London, 1929, Chap. V.
8 A. Bengtson, Spectrochim. Acta, Part B, 40 (1985) 631.

Analytica Chimica Acta, 194 (1987) 199—209
Elsevier Science Publishers B.V., Amsterdam — Printed in The Netherlands

POSITIVE SECONDARY-ION MASS SPECTRA AND THIN-LAYER CHROMATOGRAPHY/MASS SPECTROMETRY OF PHENOTHIAZINE DRUGS

MICHELE S. STANLEY and KENNETH L. BUSCH*
Department of Chemistry, Indiana University, Bloomington, IN 47405 (U.S.A.)
(Received 21st November 1986)

SUMMARY

The positive secondary-ion mass spectra of phenothiazine drugs contain abundant protonated molecules and structurally informative fragment ions that are characteristic of the *N*-substituent. Because the secondary-ion current is carried by a few characteristic ions, selected-ion monitoring is used with chromatographic separation for the determination of these drugs in mixtures. Drugs are extracted in situ from thin-layer chromatograms, and the secondary-ion mass spectra are obtained without destruction of the chromatogram. The spectra are dependent upon the solvent used and not the nature of the underlying chromatographic matrix. Spatially-resolved selected-ion monitoring of the protonated molecule provides the *x*-*y* spatial profiles of the sample in the chromatogram. Extended irradiation leads to a beam-induced tailing that alters the profile.

Phenothiazine-derived drugs are a pharmacologically diverse group of substances possessing antiemetic, antipsychotic, sedative, antipruritic, antidyskinetic, analgesic, and antihistaminic properties [1]. Separation of the drugs from their metabolites, or from other components present in a biological matrix, often involves thin-layer chromatography or (with sample derivatization) gas chromatography, with the latter often coupled to a mass spectrometer for the identification of eluting peaks.

Several investigators have reported the electron-ionization mass spectra of phenothiazine-based drugs [2—6]. The electron-ionization mass spectra of many of the phenothiazine-based drugs are dominated by low-mass ions, with the molecular ions often below 10% in relative abundance. Exact mass measurements and metastable-ion studies have established both primary and secondary fragmentation pathways. Labelling studies have been used to establish the processes by which the molecular ions fragment, including several pathways that involve hydrogen scrambling.

Chemical-ionization mass spectrometry has also been applied to determinations of the phenothiazines in preliminary studies [7, 8]. In contrast to the mass spectra obtained with electron ionization, the protonated molecule is often the base peak in these mass spectra. Stable molecular ions, $M^{+\cdot}$, were also formed under conditions of chemical ionization for many of the phenothiazine

0003-2670/87/$03.50

derivatives studied. Most of the fragmentation observed in the chemical-ionization spectra was correlated with dissociation of the group attached to the ring-bridging nitrogen. Derivatives with a polar group X at the 2-position of the ring also underwent characteristic loss of HX.

Other ionization techniques developed in the past few years are used for the determination of nonvolatile or marginally volatile compounds. Secondary-ion mass spectrometry has been shown to provide excellent sensitivity for compounds such as the phenothiazine derivatives that readily form ammonium salts [9]. In addition, a chromatography/secondary-ion mass spectrometry instrument permits direct monitoring of samples separated by thin-layer chromatography [10]. Phenothiazine drug mixtures separated in thin-layer chromatograms serve to demonstrate the analytical potential of this system. The positive secondary-ion mass spectra of ten phenothiazine derivatives are reported and discussed in this paper. Sputtering of the sample from a thin-layer chromatogram follows an in situ extraction, and spatially resolved mass spectral data for the protonated molecules of the phenothiazine drugs are generated.

EXPERIMENTAL

Positive secondary-ion mass spectra were obtained on a custom-built secondary-ion mass spectrometer [10] based on an Extrel quadrupole mass analyzer. Neat samples were introduced on a copper platform attached to the direct-insertion probe. A total of 10—20 μl of glycerol solution containing 5 μg of the phenothiazine was spread over a 1-cm^2 area. The primary beam consisted of 8-keV cesium ions emitted from a thermionic source. The primary-ion current density at the sample surface was approximately 10^{-6} A cm^{-2} with a beam diameter of approximately 2 mm. Spectra were recorded directly on an x-y recorder at a scan speed of 0.5 daltons per second; neither spectral averaging nor background subtraction was used. Spectra of the dissolved sample could be obtained as long as the glycerol persisted, about 30 min in most cases.

The phenothiazine drugs were purchased from Sigma (St. Louis, MO) and used without further purification. With the exception of perphenazine, which is sold as the free amine, all were processed as the salt forms. Chlorpromazine, ethopropazine, promethazine, and triflupromazine were obtained as hydrochloride salts, and trifluoperazine as the dihydrochloride. Acetopromazine and propiomazine were used as the maleate salts, trimeprazine as the hemi(+)tartrate, and prochlorperazine as the edisylate salt.

Thin-layer chromatography plates used were aluminum-backed, 0.2-mm thick silica gel, commercially prepared (Merck) with a fluorescent indicator. They were pretreated by prior development with the solvent system. All reagent-grade solvents were obtained from Mallinkrodt. The developing solvent was methanol/ammonia (100:1.5, v/v) [11]. The plates were then developed in a 9 × 9 × 4-cm glass tank to a height of 5 cm and air-dried. A

short-wave ultraviolet light was used for preliminary spot location. The phenothiazine drugs were spotted in approximately 25-μg quantities in separate channels by using flame-drawn melting-point tubes with either dichloromethane or methyl acetate solvent. For data from discrete samples (see Fig. 2), the spots located by ultraviolet spectroscopy were excised and attached to the direct-insertion probe. Glycerol (7 μl) was added to the thin-layer chromatography plate with a pipet. As the glycerol is absorbed into the silica gel, some spreading of small sample spots may occur, but because the sample spots are several millimeters in diameter after development, this is of no practical consequence in these experiments.

For acquisition of spatially resolved data (see Figs. 3 and 4), a threitol phase-transition matrix [12] was used to minimize lateral spreading, and because of its lower vapor pressure, to extend the period over which spectra could be recorded. The threitol was applied as a liquid to the developed chromatogram to ensure extraction of the sample from the matrix, and then allowed to solidify. Energy from the primary ion beam liquefies the surface of the threitol, providing the reservoir of sample necessary for a stable and persistent secondary-ion emission. Spatially-resolved selected-ion-monitoring data were acquired by setting the quadrupole to pass the protonated molecule of interest, and adjusting the x and y manipulators to move the chromatographic spot into the point of instrument focus. Ion abundances so obtained were manipulated by the plotting routines of ASYST scientific software, which produced the axonometric and contour plots.

RESULTS AND DISCUSSION

Secondary-ion mass spectra

Positive, secondary-ion mass spectra were obtained for ten phenothiazine-based drugs: acepromazine, chlorpromazine, ethopropazine, perphenazine, prochloroperazine, promethazine, propiomazine, trifluoperazine, trifluopromazine, and trimeprazine. The structures of these drugs vary in the substituent on the nitrogen and the group (if any) substituted onto the aromatic ring at the 2-position. Because these compounds exist in the glycerol or threitol solution as preformed ions, a relatively abundant signal for the intact cation can be expected to appear in the positive secondary-ion mass spectra. This expectation was confirmed, and the intact cation is the base peak in seven of the ten spectra presented here, and an abundant ion in the remaining spectra. This result contrasts with the electron-ionization mass spectra, in which the molecular ions can be of very low relative abundance, but is similar to the data obtained with chemical ionization. A complete comparison of the chemical ionization and secondary-ion mass spectra is given elsewhere [13].

An ion at m/z 133 is uniquitous in the secondary-ion mass spectra shown here, corresponding to cesium originating in the primary-ion beam. The relative abundance of the cesium ion is a function of the amount of glycerol

remaining on the probe tip, and rises with irradiation time. The abundances of the protonated molecules of the phenothiazine drugs are initially high; the abundance of all ions in the spectrum of the drug decrease with respect to the cesium ion with time (15—20 min). Replenishment of the glycerol on the probe tip increases the abundances to their original levels. Mass spectral data for the phenothiazine derivatives obtained immediately after insertion of the sample into the mass spectrometer are summarized in Table 1. Selected spectra are given in Fig. 1 to demonstrate the quality of the spectra. In the discussion, the derivatives are grouped in terms of similar *N*-substituents.

The protonated molecule of acepromazine at *m/z* 327 is the base peak in the positive, secondary-ion mass spectrum (Fig. 1A). In contrast, the electron-ionization mass spectrum contains the molecular ion with a relative abundance of less than 10%. The ion at *m/z* 254 (relative abundance of 30%) is formed by cleavage in the nitrogen side-chain, viz., loss of dimethylethylamine from the protonated molecule. Loss of small neutral molecules is characteristically observed in the positive secondary-ion mass spectra of onium salts,

TABLE 1

Positive secondary-ion mass spectral data for phenothiazine derivatives. Only the major ions are reported.
(The protonated molecules are marked by asterisks. Me = methyl and Et = ethyl)

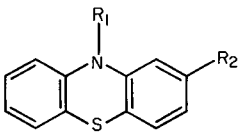

Compound	M.w.	R_1	R_2	Major ions *m/z* (relative intensity)
Chlorpromazine	318	$(CH_2)_3N(Me)_2$	Cl	319*(100), 246(30), 233(15), 232(20), 214(35), 198(16)
Acepromazine	326	$(CH_2)_3N(Me)_2$	$OCOCH_3$	327*(100), 254(30), 240(21), 222(30), 198(20)
Trifluprom azine	352	$(CH_2)_3N(Me)_2$	CF_3	353*(100), 280(30), 266(18), 248(50), 198(12)
Prochloroperazine	373	Me—N—C_4H_8—N—Me_3	Cl	374*(25), 246(55), 233(25), 232(48), 214(100), 198(62), 180(35), 141(40)
Trifluoperazine	407	Me—N—C_4H_8—N—Me_3	CF_3	408*(100), 280(38), 266(25), 248(67), 141(18)
Promethazine	284	$CH_2CHMeNMe_2$	H	285*(95), 240(16), 212(7), 198(100), 180(12)
Propiomazine	340	$CH_2CHMeNMe_2$	COEt	341*(25), 296(14), 268(5), 254(100), 198(30), 197(55)
Ethopropazine	312	$CH_2CH_2NEt_2$	H	313*(100), 240(12), 198(90), 180(10)
Trimeprazine	298	$CH_2CHMeNEt_2$	H	299*(100), 212(60), 198(40), 180(82)
Perphenazine	403	$HOCH_2CH_2$—N—C_4H_8—N—Me_3	Cl	404*(100), 246(75), 232(45), 214(75), 198(25), 171(30), 143(53)

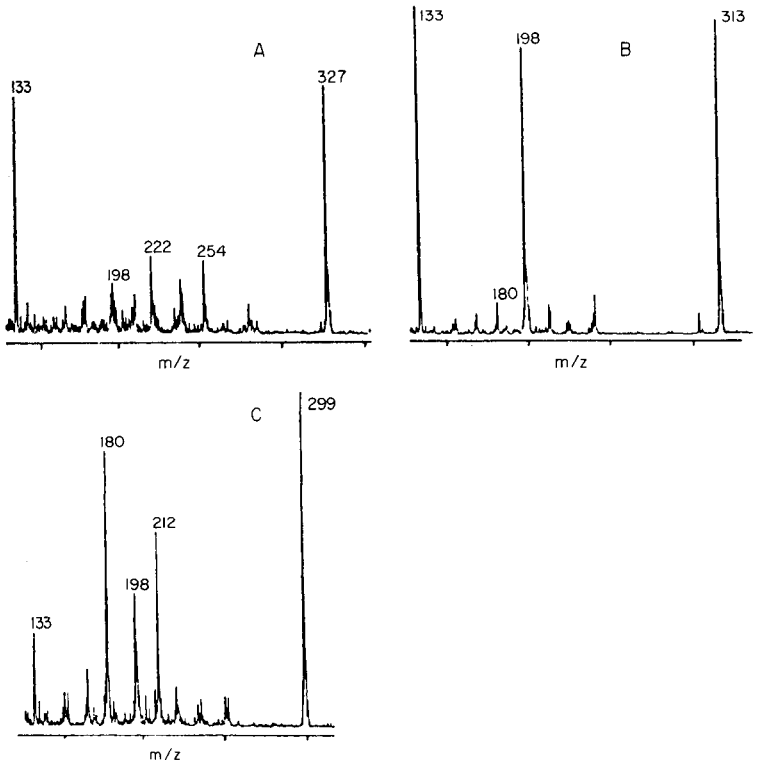

Fig. 1. Positive secondary-ion mass spectra: (A) acepromazine; (B) ethopropazine; (C) trimeprazine.

including ammonium, phosphonium, and sulfonium salts [14—16]. Additional loss of the sulfur atom from the phenothiazine skeleton forms the ion at *m/z* 222. The ion at *m/z* 198 is characteristic of the phenothiazine skeleton, and is found in all of the mass spectra reported here. The remaining ion in the secondary-ion mass spectrum is that at *m/z* 240, thought to result from the loss of neutral dimethylpropylamine to form the substituted phenothiazin-10-yl structure.

Similar fragmentations are noted in the mass spectrum obtained for chlorpromazine. The protonated molecule at *m/z* 319 is the base peak in the spectrum, and the characteristic skeletal ion at *m/z* 198 is also observed. Loss of 73 daltons (dimethylethylamine) occurs (as with acepromazine) to produce the fragment ion at *m/z* 246, which retains the chlorine isotopic signature. The fragment ion at *m/z* 232 (also observed in the methane chemical-ionization mass spectrum of chlorpromazine) is the substituted phenothiazin-10-yl ion, and that at *m/z* 214 is formed by loss of a sulfur atom from the ion at *m/z* 246. An ion at *m/z* 233 is the more stable even-electron analog of the ion at *m/z* 232. Chlorpromazine darkens on exposure to light [17], and

decomposition after prolonged exposure to the primary-ion beam is evidenced by darkening of the sample. Such decomposition can occur because the primary-ion gun is a light as well as an ion source. Interpretation of the secondary-ion mass spectrum of trifluprομazine is straightforward, as the same fragmentation processes (loss of 73, 87, and 105 daltons) are observed in this spectrum, along with the characteristic ions of the phenothiazine skeleton.

The second class of phenothiazine drugs investigated comprised those that contain a more complicated *N*-substituent, which again seems to direct the majority of the fragmentation processes. The positive secondary-ion mass spectrum of prochloroperazine is a case in point. The protonated molecule (*m/z* 374) fragments by loss of 128 and 142 daltons to produce the chlorine-containing fragment ions at *m/z* 246 and 232, respectively. Both of these losses originate in the *N*-substituent chain, with 128 daltons corresponding to CH_3—N—C_4H_8—N—C_2H_5 and 142 daltons to CH_3—N—C_4H_8—N—C_3H_7. The base peak at *m/z* 214 is formed by loss of a sulfur atom from the ion at *m/z* 246. This ion appears in the electron-ionization mass spectrum of prochloroperazine; an analogous process is described for chlorpromazine, as discussed above. The ion at *m/z* 180 corresponds to $C_{13}H_{10}N^+$ (from the phenothiazine skeleton) and that at *m/z* 141 to the *N*-substituent itself. Substitution of $-CF_3$ for —Cl yields trifluoperazine rather than prochloroperazine, and the main fragmentation processes (losses of 128 and 142 daltons) are analogous.

Promethazine and propiomazine vary in R_2, but share a common *N*-substituent that results in a similar pattern of fragmentation. Initial loss of 45 daltons from the protonated molecule corresponds to loss of dimethylamine, and produces the abundant fragment ions at *m/z* 240 for promethazine and *m/z* 296 for propiomazine. Loss of dimethylethylamine (73 daltons) produces *m/z* 212 for promethazine and *m/z* 268 for propiomazine. Loss of dimethylpropylamine (87 daltons) generates *m/z* 198 for promethazine and *m/z* 254 for propiomazine. The ions at *m/z* 198 and *m/z* 180 are characteristic of the phenothiazine skeleton.

The final three phenothiazine drugs studied vary in the nature of the *N*-substituents, but the general procedure of spectral interpretation remains the same. In ethopropazine (Fig. 1B), the protonated molecule at *m/z* 313 fragments by loss of dimethylethylamine (73 daltons) to create the fragment ion at *m/z* 240. The protonated molecule of trimeprazine (Fig. 1C) at *m/z* 299 loses diethylmethylamine (87 daltons) to form the fragment ion at *m/z* 212. Perphenazine provides the most diverse secondary-ion mass spectrum of these last few examples, but the interpretation is again straightforward. The protonated molecule at *m/z* 404 loses 158 daltons to provide the fragment ion at *m/z* 246; this loss involves the bulk of the *N*-substituent, leaving $RN{=}CH_2^+$, with the accompanying loss of the additional methylene (the entire *N*-substituent) to form *m/z* 232, which retains the chlorine atom. The ion at *m/z* 214 also contains chlorine, and corresponds again to the loss of sulfur from the fragment ion at *m/z* 246. The remaining ions in the mass

spectrum are found at *m/z* 171 and *m/z* 143 (neither of which contains chlorine) that correspond to the fragments of the *N*-substituent.

As concluded by Melikian et al. [8], the high relative abundances of the protonated molecules of the phenothiazine drugs make them ideal candidates for selected-ion monitoring in gas chromatography/mass spectrometry. They are also suitable for the spatially resolved selected-ion monitoring experiments described in the next section. Further, the ubiquitous appearance in the positive ion spectra of ions characteristic of the phenothiazine skeleton (*m/z* 197 and *m/z* 198, for example) allow a class-specific selected-ion monitoring experiment to be completed in a similar fashion.

Direct detection for chromatography

The particle-induced desorption techniques, such as secondary-ion mass spectrometry, have been used to monitor directly organic samples separated within a chromatographic matrix. The advantages of both *x* and *y* dimensions of information, the ability to rescan the area of interest, and the variability of the spatial resolution are apparent in previous work [10]. The initial application of secondary-ion mass spectrometry, and of any particle-induced desorption technique to chromatographic determinations was described by Unger et al. [18] in 1981. Since then, published work has included applications for substrates used in paper chromatography, thin-layer chromatography, and electrophoresis.

Secondary-ion mass spectrometry sputters material from the top nanometer or so of a surface. If the flux of primary ions is kept below about 10^{-9} A cm^{-2} (static secondary-ion mass spectrometry), damage to the organic material is minimized, although the flux of secondary ions attainable is limited because the bulk of the sample is not accessible. The restriction in flux is not necessary if a reservoir can be established in which the organic sample can be extracted from within the chromatogram, and cycled to the surface of the chromatogram from which sputtering and ionization occurs. Because the samples have been separated in a chromatogram, the spatial resolution of the separation should not be compromised. When spot sizes are small enough that solvent diffusion through the chromatographic matrix limits the spatial resolution, transport of the sample molecules (in the *z* axis) to the surface, without significant diffusion in *x* and *y* (the plane of chromatographic development), can be accomplished with the use of a phase-transition matrix [12]. Diffusion in *x* and *y* was not a limiting factor in these experiments, and so glycerol was used as the liquid matrix. Because the sample surface is that of the liquid, the mass spectrum of a dissolved sample should not be a function of the underlying chromatographic support. The secondary-ion mass spectra of all ten phenothiazine drugs were obtained using glycerol as an extraction solvent from a silica-gel thin-layer chromatogram. The spectra were very similar to those obtained for discrete-sample solutions. Changes in the relative abundances of the ions were a function of changes in the sample concentration, but were not major. Figure 2 contains the thin-layer

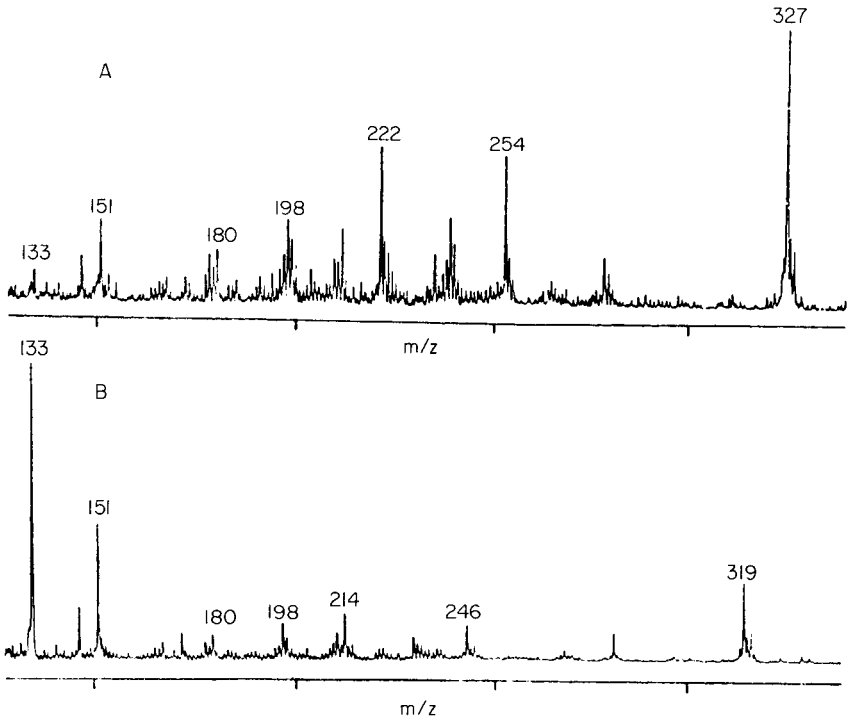

Fig. 2. Thin-layer chromatography/glycerol:secondary-ion mass spectra: (A) acepromazine; (B) chloropropazine.

chromatography/glycerol:secondary-ion mass spectra of acepromazine and chlorpromazine.

Spatially-resolved selected-ion-monitoring mass spectral data are obtained by moving the chromatogram with the x and y manipulators, and monitoring the changes in the absolute abundance data for the selected ion as the sample spot is brought into and out of the point of instrument focus. The mass spectral data provides the spatial information about the shape of the spot on the surface of the chromatogram. Further, with spots of unknown sample composition, the spectrum can be interpreted to provide the identity of the compound at those x-y coordinates. The x-y-mapped absolute abundance of the protonated molecule of trimeprazine separated in a thin-layer chromatogram is given in Fig. 3. The total amount of sample in this 3 × 4-mm oval spot was 5 μg, and, in this case, liquid threitol was used as the extraction solvent. The spectrum persists for well over 2 h, ample time even for the manual recording of the x-y spectral intensities. The spacing of the grid lines on the axonometric plot is 0.50 mm. Excellent S/N is apparent, and the spot boundaries are clearly defined. Each spot of a phenothiazine drug separated in a thin-layer chromatogram provides similar data for the protonated molecule.

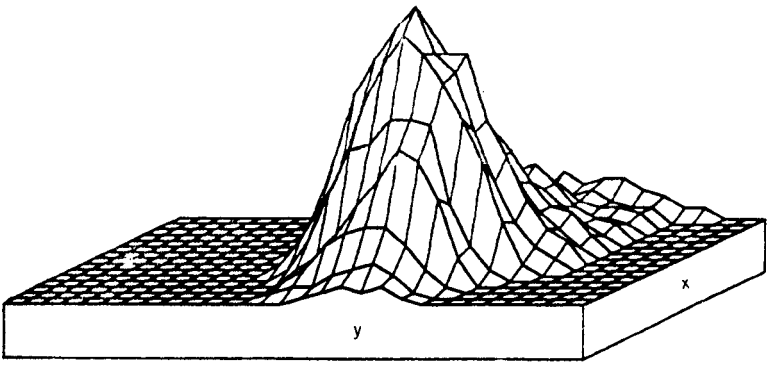

Fig. 3. Spatially-resolved selected-ion monitoring (*m/z* 299) for trimeprazine originally separated in a thin-layer chromatogram.

Examination of the data in Fig. 3 shows that the initially symmetrical chromatographic spot (as determined by visual inspection) provides abundance data that indicates an unsymmetrical spot. This is shown more clearly in the contour plot in Fig. 4. The direction from which the primary cesium ion beam impinges upon the sample (angle of incidence for the primary ion beam is 45 degrees) is indicated on the figure. Over time, the primary beam itself can promote the diffusion of the sample solution across the surface, and the beam-induced tailing may distort the measured shape of the spot profile when an extended time is spent in data acquisition. The phenomenon is similar to the beam-induced mixing that has been suggested to occur in the secondary-ion mass spectrometry of solid organic compounds [14], and is distinct from chromatographic tailing.

Figure 5 is a plot of spatially-resolved mass spectral data: the isoabundance contours of the protonated molecules of two overlapped phenothiazine spots are evident. Contour A is data from the protonated molecule of promethazine at *m/z* 285. Contour B is data from the protonated molecule of trimeprazine at *m/z* 299. For ions that are common to both secondary-ion mass spectra (ions at *m/z* 198 and *m/z* 180, for example), double-lobed contour plots are generated.

CONCLUSIONS

Poole et al. [19] have summarized the current state-of-the-art in high-performance thin-layer chromatography, emphasizing the recent advantages in reproducible sample application and development that presage a return to thin-layer chromatography as a quantitative separation method. Nevertheless, detection systems, specifically for the identification of compounds separated by thin-layer chromatography, are not as sophisticated as the current methods for sample application and chromatographic development. Mass spectrometry has catalyzed the development of gas chromatography/mass spectrometry

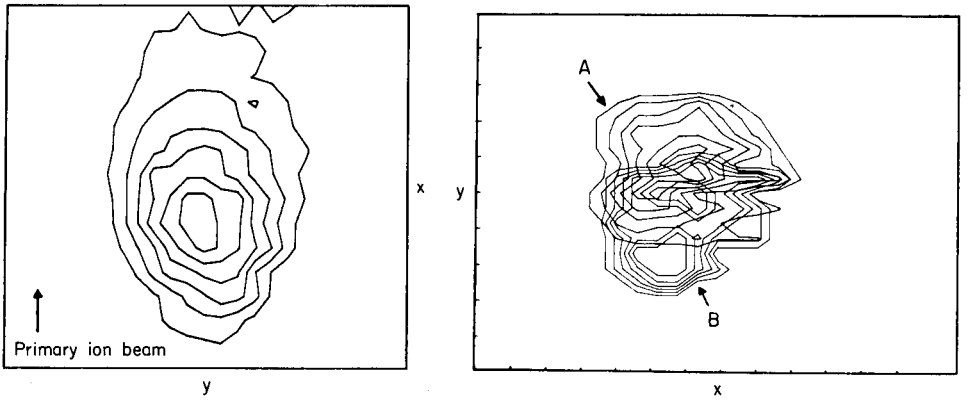

Fig. 4. Contour plot of spatially-resolved selected-ion monitoring data showing the effects of extended irradiation on the spot shape.

Fig. 5. Contour plots of the abundance of the protonated molecules: (A) promethazine (*m/z* 285); (B) trimeprazine (*m/z* 299). The sample spots are incompletely resolved by thin-layer chromatography.

and liquid chromatography/mass spectrometry as powerful analytical tools for complex mixtures. It is likely to have a similar impact with thin-layer and paper chromatography. The present work shows that the thin-layer chromatography/mass spectrometry experiment is presently feasible, and that organic compounds can be determined in situ by using particle-induced desorption ionization techniques. The phenothiazine-based drugs were used as a demonstration of the potential of this technique, as they are a widely used group of psychoactive compounds, the determination of which often involves thin-layer chromatography. The secondary-ion mass spectra of these compounds contain abundant protonated molecules that can be used for spatially-resolved selected-ion monitoring experiments. Thin-layer chromatographic separation of these drugs followed by direct in situ mass spectrometric monitoring has been demonstrated in this paper. As in gas chromatography/mass spectrometry and liquid chromatography/mass spectrometry, the volume of data generated by this chromatography/mass spectrometry method is tremendous. A data system that controls chromatographic movement in the *x-y* plane, and manipulates mass spectral data in terms of mass and relative abundance, is currently being developed for the chromatography/secondary-ion mass spectrometer. The sophisticated image interpretation software that has been developed over the last few years will be used in this detection system. The present results emphasize the creation of a stable reservoir of sample, and delineate some of the time restraints inherent to sputtering of the surface by an energetic particle beam. In the direct determination of phosphonium salts separated by thin-layer chromatography, a detection limit of 20 ng (*S/N* of 2) has been achieved. The present limit of detection for the phenothiazine drugs ranges from 50 to

250 ng, depending, for example, upon the relative abundance of the protonated molecule. Further work is directed towards achieving greater sensitivity so that direct mass spectrometric detection can be used in conjunction with the widely used thin-layer chromatographic separation of these compounds.

The construction of the secondary-ion mass spectrometer was supported by the Whitaker Foundation, and the applications were supported by the National Institutes of Health (grant number GM 36454-01).

REFERENCES

1 M. Gordon (Ed.), Psychopharmacological Agents, Vol. II, Academic, New York, 1964.
2 A. M. Duffield, J. C. Craig and L. R. Kray, Tetrahedron, 24 (1968) 4267.
3 J. N. T. Gilbert and B. J. Millard, Org. Mass Spectrom., 2 (1969) 17.
4 J. Heiss and K. P. Zeller, Org. Mass Spectrom., 2 (1969) 819.
5 D. Simov and I. G. Taulov, Org. Mass Spectrom., 5 (1971) 1133.
6 L. C. Vishwakarma and A. R. Martin, J. Heterocycl. Chem., 19 (1982) 849.
7 B. Finkle, R. L. Foltz and D. Taylor, J. Chromatogr. Sci., 12 (1974) 304.
8 A. P. Melikian, N. W. Flynn, F. Petty and J. D. Wander, J. Pharm. Sci., 66 (1977) 228.
9 R. J. Day, S. E. Unger and R. G. Cooks, J. Am. Chem. Soc., 101 (1979) 501.
10 J. W. Fiola, G. C. DiDonato and K. L. Busch, Rev. Sci. Instrum., 57 (1986) 2294.
11 C. Korczak-Fabierkiewicz and G. Cimbura, J. Chromatogr., 53 (1970) 413.
12 G. C. DiDonato and K. L. Busch, Anal. Chem., 58 (1986) 3231.
13 R. A. Flurer and K. L. Busch, Org. Mass Spectrom., submitted for publication.
14 A. Ba-Isa, K. L. Busch, R. G. Cooks, A. Vincze and I. Granoth, Tetrahedron, 39 (1983) 591.
15 K. J. Kroha and K. L. Busch, Org. Mass Spectrom., 21 (1986) 507.
16 K. L. Duffin and K. L. Busch, Int. J. Mass Spectrom. Ion Proc., 74 (1986) 141.
17 E. G. C. Clarke, Isolation and Identification of Drugs, Pharmaceutical Press, London, 1969, p. 257.
18 S. E. Unger, A. Vincze, R. G. Cooks, R. Chrisman and L. D. Rothman, Anal. Chem., 53 (1981) 976.
19 C. F. Poole, S. Khatib and T. A. Dean, Chrom. Forum, 1 (1986) 27.

Analytica Chimica Acta, 194 (1987) 211—219
Elsevier Science Publishers B.V., Amsterdam — Printed in The Netherlands

SPECTRAL SIMPLIFICATION IN PROTON MAGNETIC RESONANCE SPECTROMETRY FOR 3-(4-AMINOPHENYL)-3-ETHYL-2,6-PIPERIDINEDIONE (AMINOGLUTETHIMIDE) WITH ACHIRAL AND CHIRAL LANTHANIDE SHIFT REAGENTS

ALEXANDER HATZIS, ROBERT ROTHCHILD* and PAUL SIMONS

The City University of New York, Toxicology Research and Training Center, John Jay College of Criminal Justice, Department of Science, 445 West 59th Street, New York, NY 10019-1199 (U.S.A.)

(Received 4th November 1986)

SUMMARY

The 60-MHz ^{1}H-NMR spectra of racemic aminoglutethimide (*A*; 3-(4-aminophenyl)-3-ethyl-2,6-piperidinedione) are studied with the achiral shift reagent, tris(6,6,7,7,8,8,8-heptafluoro-2,2-dimethyl-3,5-octanedionato)europium(III) (*B*) and the chiral reagents, tris[3-(trifluoromethylhydroxymethylene)-*D*-camphorato]europium(III) (*C*) and tris[3-heptafluoropropylhydroxymethylene-*D*-camphorato]europium(III) (*D*). Appreciable values of the enantiomeric shift difference, $\Delta\Delta\delta$, were observed for both sets of aryl protons and the methyl protons in $CDCl_3$ solutions at 28°C with added *C* or *D*. Optical purity determinations were done with good reliability by using the methyl resonance and a *D*:*A* molar ratio near 0.5. Results are discussed in terms of possible coordination of the europium at the amine or amide carbonyl groups. Some significant differences in results with *B*, *C* and *D* were noted.

Aminoglutethimide, *A*, was originally introduced for treatment of epilepsy because of its anticonvulsant properties. When it was found to inhibit adrenal function [1], the drug was withdrawn in 1966. These antisteroid effects led to studies of its efficacy in the treatment of certain cancers [2—4]. Its use for metastatic breast cancer has been associated with its aromatase inhibition.

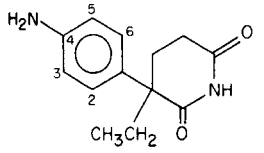

A

The optical resolution of aminoglutethimide as the tartrate has been achieved and absolute configurations have been assigned to the enantiomers as *R*-(+) and *S*-(—) [5]. The availability of the optical antipodes and the considerable medical possibilities of aminoglutethimide have led to much work being reported recently on the relative effects of the different enantiomers.

0003-2670/87/$03.50

Some examples include findings that the dextrorotatory isomer was 2 or 3 times more potent as an inhibitor of corticosterone secretion in rats than the racemate [5]; that the *D*-isomer was about 2.5 times more potent than the *L*-isomer in inhibition of side-chain cleavage of cholesterol [6]; that the luteolytic potency of the *D*-isomer was nearly 5 times greater than that of the *L*-isomer in rabbits and 25 times greater in rats [7]; and the *D*-isomer was 38 times more potent than the *L*-isomer in the inhibition of aromatization of testosterone by human placental microsomes [8]. The dextrorotatory enantiomer of *A* has been used for reducing adrenal hyperfunction; major biological activities of this and other related glutarimides have been found to reside in the *D*-isomers [9]. These and other results have been summarized by Salhanick [10].

Methods for the direct determination of optical purity of drugs and for ^{1}H-NMR spectral simplification using lanthanide shift reagents have been studied in this laboratory. The methods have been reviewed [11–15] and have been applied to a number of drugs. Results for glutethimide have been reported [16]. A comparative study of some five- and six-membered ring compounds, including imides, hydantoins, etc., that are closely related to *A* has been described [17]. Comparative studies with *A* were therefore of considerable theoretical and practical interest; the studies for the analog, glutethimide, encouraged the idea of applying the shift reagent technique to *A*. The results presented here for aminoglutethimide suggest that efficient NMR spectral simplification and optical purity assay can readily be achieved with analytical utility.

EXPERIMENTAL

A sample of racemic aminoglutethimide (Cytadren, lot no. M-892) was kindly provided by CIBA Pharmaceutical Co., Summit, NJ 07901. Samples of the pure enantiomers, (+)-*A* (CGS 2396, sample no. 775-875) and (−)-*A* (CGS 2501, sample no. 16-185c) were obtained from the same source. Chloroform-*d*, (99.8 atom % D; Aldrich Chemical Co. or Norell), was dried and stored over 3A molecular sieves. Shift reagents (Aldrich Chemical Co.) were stored in a desiccator over P_2O_5. Materials were used as supplied except as noted.

The solubility of aminoglutethimide in $CDCl_3$ was found to be rather low. In general, an accurately weighed portion of drug (about 25 mg) was added to about 700 mg of $CDCl_3$ containing about 0.2% tetramethylsilane (TMS) as internal standard in the usual sample tube and dissolved by shaking; increments of shift reagent were added and dissolved by shaking, and the spectra were run immediately.

For quantitative runs on non-racemic mixtures of drug, samples were prepared by directly weighing portions of each enantiomer into the sample tube using an accurate balance. Alternatively, the non-racemic samples were prepared by mixing weighed portions of the racemic material with either of the

pure enantiomers. Reported chemical shifts in measurements involving chiral shift reagents are average values for enantiomeric protons where enantiomeric shift differences are observed.

All spectra were run on a Varian EM-360A 60-MHz ^{1}H-NMR spectrometer at a probe temperature of 28°C. Chemical shifts are reported in parts per million (δ) relative to TMS as internal standard and are accurate to ±0.05 ppm. In spectra where TMS was obscured by shift reagent peaks, chloroform (present as an impurity in the solvent) was used as internal standard.

RESULTS AND DISCUSSION

The achiral lanthanide shift reagent tris(6,6,7,7,8,8,8-heptafluoro-2,2-dimethyl-3,5-octanedionato)europium(III), abbreviated as Eu(FOD)$_3$, *B*, and the chiral reagents, tris[3-(trifluoromethylhydroxymethylene)-*D*-camphorato]europium(III), abbreviated as Eu(TFC)$_3$, *C*, [also known as Eu(FACAM)$_3$] and tris[3-(heptafluoropropylhydroxymethylene)-*D*-camphorato]europium(III), abbreviated as Eu(HFC)$_3$, *D*, [also known as Eu(HFBC)$_3$] were used in these studies. These reagents have proven particularly useful for enhanced dispersion of spectral features to permit assignments and, with *C* or *D*, to achieve direct determination of optical purity. Here, parallel studies were done, first with the achiral *B* to facilitate spectral elucidation and then with chiral *C* or *D* to demonstrate the potential use of the technique for optical purity assays. As in the case of glutethimide [16], both with and without added *B* or *C*, the 60-MHz ^{1}H-NMR spectra of *A* are complex and have not been completely interpreted. In the unshifted spectrum of *A* as a 0.141 molal solution in $CDCl_3$, the imide resonance appears as a broad singlet at 8.2 δ, the amino group as a broad singlet at 3.7 δ and the methyl group as a clean triplet ($^3J \approx 7.3$ Hz) at 0.85 δ. Whereas the aromatic protons of glutethimide appeared virtually as a singlet in the absence of shift reagent, the strong mesomeric electron releasing effect of the amino group in *A* results in an $(AB)_2$ pattern for the aryl H of aminoglutethimide. The approximate doublets ($J \approx 8.5$ Hz) centered near 6.7 and 7.05 δ are assigned to $H_{3,5}$ and $H_{2,6}$, respectively, of the aromatic ring. Calculated values using substituent chemical shifts [18] were 6.39 and 6.81 δ for these hydrogens; the values given for the NH_2 and CH_3 substituents were used. The remaining six nonequivalent hydrogens of *A* appear as overlapped complex multiplets from 1.75 to 2.65 δ. These spectral data are in good agreement with an earlier report, which did not specify sample concentration or temperature [19].

As increments of *B* are added, gross spectral changes occur. The NH_2 resonance moves most rapidly downfield. At a molar ratio of about 0.7, the aryl hydrogens have almost collapsed to a singlet at 9.2 δ, which is again resolved to an $(AB)_2$ pattern at still higher levels of *B*. A molar ratio of *B*:*A* up to 1.48 was studied, at which point line broadening was modest. Although assignments of these aryl hydrogens cannot be considered unequivocal (in the absence of, e.g., deuterium-labeled analogs), a "crossover" of chemical

shifts of the aryl protons seems reasonable, resulting in $H_{2,6}$ being further downfield at low levels of shift reagent and $H_{3,5}$ being further downfield at high shift reagent levels. It should also be noted that the δ plot for NH_2 becomes significantly steeper at *B*:*A* ratios above about 0.5. The plot for NH seems to indicate a slight decrease in slope at these higher levels of *B*. Higher shift reagent levels may increasingly favor complexation at the NH_2 group relative to the imide system. This would be expected to enhance deshielding of the NH_2 at high *B*:*A* ratios and would sharply increase deshielding of $H_{3,5}$ (*ortho* to the NH_2) relative to $H_{2,6}$, based on proximity considerations. The present assignments to $H_{3,5}$ are consistent with increased slope of the δ plot occurring at roughly comparable *B*:*A* ratios as for the similar slope change of the NH_2. Results with *B* are summarized in Fig. 1A, assuming "crossover" of the aryl protons.

This ambiguous "crossover" effect of the aryl protons of *A* was not seen in spectra shifted by *C* up to a *C*:*A* molar ratio of 0.679, the highest level examined. Appreciable peak broadening here precluded study of higher molar ratios. The slope of the plot for the NH_2 signal is clearly seen to increase throughout the range of *C*:*A* ratios studied, and a gentle decrease in slope for NH is observed at the higher *C*:*A* ratios. Furthermore, the slope of the $H_{3,5}$ plot increases relative to that for $H_{2,6}$ at the higher shift reagent levels. These observations are consistent with those for *A* using *B*, but suggest that the crossover point of the signals of the aryl protons would occur at higher molar ratios for *C* than for *B*. Figure 1B summarizes these results with *C*.

Enantiomeric shift differences, $\Delta\Delta\delta$, are readily observed for several of the resonances of *A* in spectra shifted by *C*, confirmed by comparisons with spectra shifted by the achiral *B*. Here, the enantiomeric shift difference is defined as the magnitude of the chemical shift difference for enantiomeric nuclei when a chiral shift reagent is present. Figure 2 shows enantiomeric

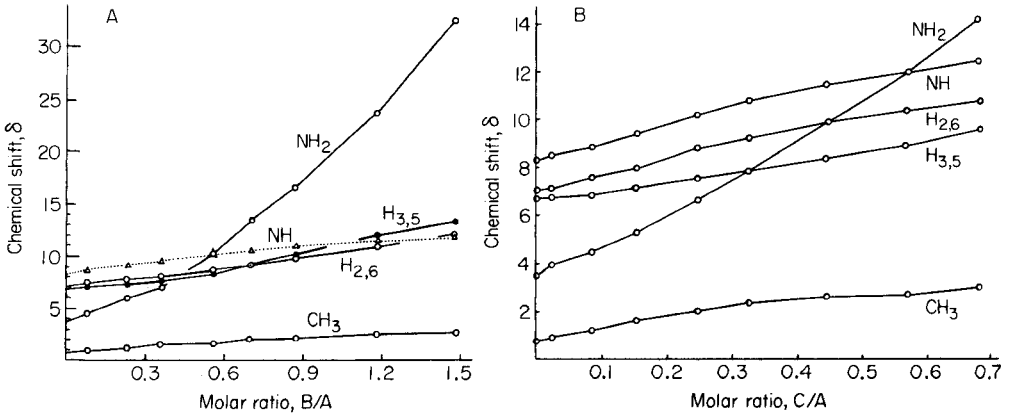

Fig. 1. Variation of chemical shift, δ, with molar ratio: (A) $Eu(FOD)_3$/aminoglutethimide; (B) $Eu(TFC)_3$/aminoglutethimide.

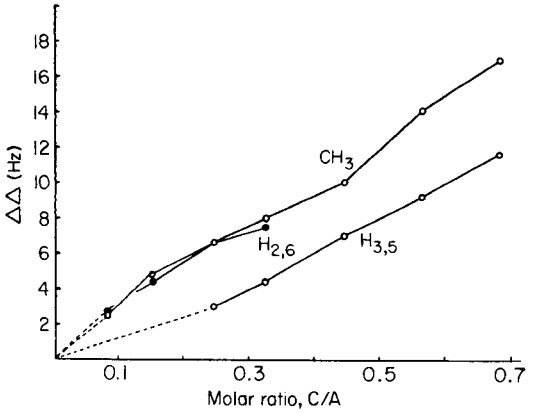

Fig. 2. Variation of enantiomeric shift difference, $\Delta\Delta\delta$ (in Hz), with molar ratio of $Eu(TFC)_3$/aminoglutethimide.

shift differences achieved with *C*, for a sample of racemic *A*(0.161 molal in $CDCl_3$). Even at the low *C*:*A* ratio of 0.0858, $\Delta\Delta\delta$ is clearly seen for the CH_3 (2.6 Hz) and the downfield aryl protons, $H_{2,6}$ (2.7 Hz). The downfield aryl protons assigned to $H_{2,6}$ consistently display greater $\Delta\Delta\delta$ than the upfield aryl protons, $H_{3,5}$. This is in keeping with the greater proximity of $H_{2,6}$ to the chiral center of *A*. The values of $\Delta\Delta\delta$ became considerable at higher molar ratios, i.e., about 17 Hz for CH_3 and 11.6 Hz for $H_{3,5}$ at a *C*:*A* ratio of 0.679; the $\Delta\Delta\delta$ for $H_{2,6}$ is probably similar to that of the CH_3. However, peak broadening and coincidental overlaps make accurate measurements of these enantiomeric shift differences unfeasible; such a high *C*:*A* is unsuitable for quantitation of optical purity of *A*.

With a low *C*:*A* molar ratio of 0.0858, the CH_3 signal could be quantitatively useful for optical purity determinations simply by peak-height measurements of the center two peaks of the clearly doubled triplet; good sensitivity should result because of the intensity of these sharp peaks. For higher *C*:*A* ratios near 0.56, the $H_{3,5}$ signal is well separated from NH_2, $H_{2,6}$ and $CHCl_3$ peaks, and is quantitatively useful. The $H_{3,5}$ signal appears as a fairly clean, symmetrical triplet, allowing simple peak-height measurements of the outer branches. As little as 10% of a minor enantiomer should be detectable under these conditions.

To extend and improve these results, the chiral reagent *D* was used. A portion of racemic *A*, 0.245 molal, was treated with increments of *D*, resulting in the induced shifts summarized in Fig. 3. As with *B* and *C*, largest $\Delta\Delta\delta$ values are observed for the amino signal. However, results with *D* differ from those described above in that the slope of the amino signal shows essentially no deviations from linearity up to a *D*:*A* ratio of 0.791, the highest level examined. As was seen for runs with *B* and *C*, the slope of the imino signal does decrease at higher shift reagent levels. A "crossover" in chemical

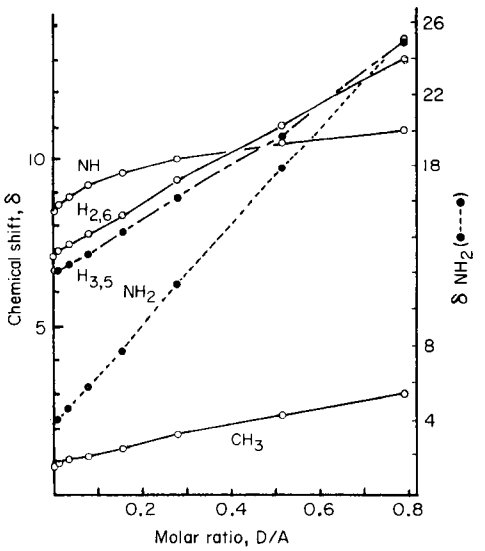

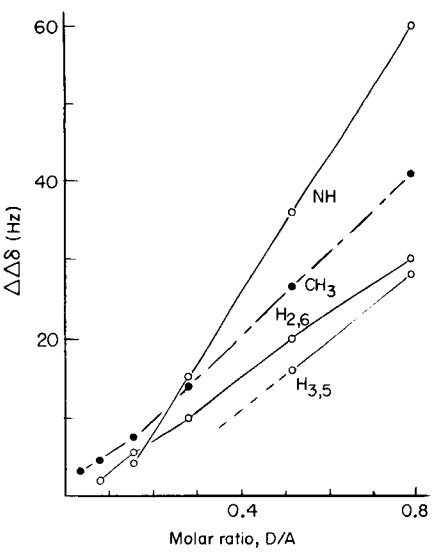

Fig. 3. Variation of chemical shift, δ, with molar ratio of Eu(HFC)$_3$/aminoglutethimide.

Fig. 4. Variation of enantiomeric shift difference, $\Delta\Delta\delta$ (in Hz), with molar ratio of Eu(HFC)$_3$/ aminoglutethimide.

shifts of the aryl proton signals is assigned for *D*, as with *B*. Importantly, for determinations of enantiomeric excess, results with *D* are substantially better than with C. The $\Delta\Delta\delta$ values with *D* are presented in Fig. 4. At the very low *D*:*A* ratio of 0.073, $\Delta\Delta\delta$ is clearly seen for the CH_3 signal (4.4 Hz) and the downfield aryl proton, $H_{2,6}$ (1.8 Hz). At higher levels of *D*, the enantiomeric CH_3 triplets are completely separated from each other, although some overlap with peaks of *D* may interfere, e.g., near a *D*:*A* ratio of 0.280. At this molar ratio, $\Delta\Delta\delta$ for the NH signal of 16.0 Hz is seen, with the valley height only 40.6%, very suitable for quantitative work. Using a *D*:*A* ratio of 0.791, $\Delta\Delta\delta$ was seen for $H_{3,5}$ (30.0 Hz) with a valley height of 23.2%, for $H_{2,6}$ (28.0 Hz) with a valley height of 18.4%, with NH (60.0 Hz) almost baseline-separated, and the CH_3 (40.0 Hz) overlapped with *D* resonances. The upfield branch of the NH signal overlaps one of the CH_2 resonances making optical purity determination based on this imide signal unfavorable. Valley heights given above refer to the height of the valley between the absorptions of the enantiotopic nuclei relative to the maximum height of the resonance for the particular enantiotopic nuclei. At this high *D*:*A* ratio, the downfield aryl signals (assigned to $H_{3,5}$) displayed both larger $\Delta\Delta\delta$ and more peak broadening than the signals assigned to $H_{2,6}$.

Quantitative utility was conclusively demonstrated by use of *D* with several non-racemic standard solutions of *A*. These studies also allowed determination of the sense of nonequivalence for selected signals. The triplet

methyl signals were used for quantitation of optical purity of *A*. Two samples of relatively high optical purity were examined using a high molar ratio of *D*:*A* to separate the methyl signals fully. A third sample of relatively low optical purity was examined with both low and high levels of the shift reagent. With low reagent levels, the two triplets are severely overlapped but excellent peak sharpness still allows facile measurements of the peak heights of the central peak of each triplet. With high reagent levels, the triplets did not overlap one another, and the peak height of the central peak of each triplet was determined by two methods. In Method (a), the peak height was measured to a projected horizontal baseline. In Method (b), a tangent skim method was used to determine the baseline to be used for peak-height measurement. The latter method was applied because of slight overlap of the upfield triplet with shift reagent absorptions. Sample spectra for some of these nonracemic samples of *A* with added *D* are shown in Fig. 5. Quantitative data are summarized in Table 1. In all of the cases examined, quite good agreement was

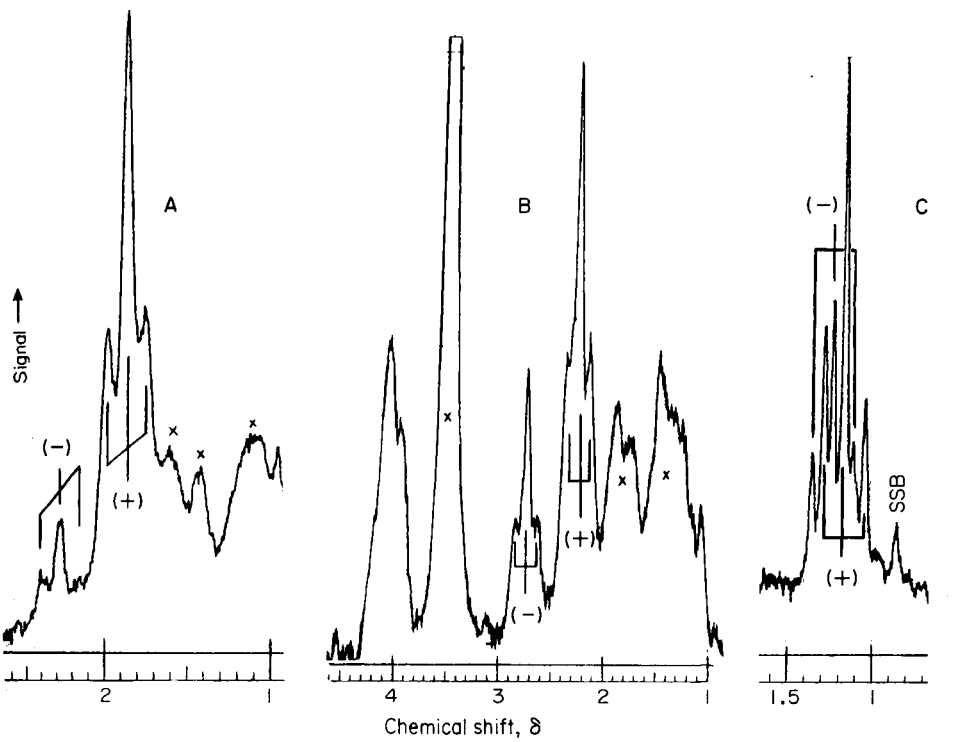

Fig. 5. Upfield regions of spectra for nonracemic samples of *A* with added *D*. The branches of each triplet from the methyl signals of the two enantiomers of *A* are indicated; the signal of (−)-*A* is downfield in each case. Peaks marked "X" are from the shift reagent. Sweep width of actual full recorded spectrum was 10 ppm in each case. The peak marked SSB is a spinning side-band of TMS, the internal chemical shift standard. Actual ratios of (+)-*A* to (−)-*A* (and the molar ratios of *D* to total *A*) were: (A) 85.4:14.6 (0.462); (B) 66.6:33.4 (0.561); (C) 66.6:33.4 (0.0918). See text for details.

TABLE 1

Results of optical purity determinations for non-racemic samples of *A* using *D*, based on the methyl signal

Total *A* (molality)	Actual enantiomer ratio, by weight (+)-*A*/(−)-*A*	Molar ratio of *D* to total *A*	Enantiomer ratio found
0.215	85.4:14.6	0.462 (Fig. 5A)	84.2:15.8[a] 86.2:13.8[b]
0.220	92.9:7.1	0.493	92.8:7.2[a] 94.0:6.0[b]
0.225	66.6:33.4	0.561 (Fig. 5B)	67.9:32.1[a] 67.1:32.9[b]
0.225	66.6:33.4	0.0918 (Fig. 5C)	64.9:35.1[a]

[a]Measured as peak height of central peak of triplet to projected horizontal baseline. [b]Measured as peak height of central peak of triplet to project "skimming" baseline (tangent skim method).

found between actual and found values, with either baseline method. In all cases, the minor triplet appeared downfield, implying that (+)-*A* has a positive sense of magnetic non-equivalence for the methyl resonance. When reagent *D* was used, as little as 5% of the minor enantiomer should be readily detectable using the CH_3 signal and *D*:*A* ratios near 0.5.

In conclusion, ^{1}H-NMR spectral simplification of *A* by using *B*, *C* and *D* has been demonstrated. Several nuclei of *A* display appreciable $\Delta\Delta\delta$ values with the chiral reagents *C* or *D*. Enantiomeric excess determinations for *A* can most readily be done by using *D* with the methyl signal being suitable for quantitative purposes.

Purchase of the NMR spectrometer and supplies was made possible by Grant SER80-15293 from the National Science Foundation. This research was supported (in part) by grants number 6-63225 and 6-65225 from the PSC-CUNY Research Award Program of the City University of New York. Additional support was provided by the U.S. Education Department Minority Institutions Science Improvement Program and the Sandoz Research Institute. We thank Professor Bonnie Nelson for her assistance in computerized literature searching.

REFERENCES

1 A. M. Camacho, R. Cash, A. J. Brough and R. S. Wilroy, J. Pediatr., 6 (1966) 852.
2 D. N. Orth and G. W. Liddle, N. Engl. J. Med., 285 (1971) 243.
3 A. Lipton and R. J. Santen, Cancer (Philadelphia), 33 (1974) 503.
4 E. J. Sanford, J. R. Drago, T. J. Rohner Jr., R. Santen and A. Lipton, J. Urol., 115 (1976) 170.

5 N. Finch, R. Dziemian, J. Cohen and B. G. Steinetz, Experientia, 31 (1975) 1002.
6 V. I. Uzğiris, C. A. Whipple and H. A. Salhanick, Endocrinology, 101 (1977) 89.
7 C. A. Whipple, T. Colton, J. M. Strauss, J. Hourihan and H. A. Salhanick, Endocrinology, 103 (1978) 1605.
8 P. E. Graves and H. A. Salhanick, Endocrinology, 105 (1979) 52.
9 R. Dziemian and N. Finch, U.S. Pat. 3944671 (March 16, 1976); Chem. Abstr., 84 (26) (1976) 184912n.
10 H. A. Salhanick, Cancer Res. (Suppl.), 42 (1982) 3315s and references therein.
11 C. Kutal, in R. E. Sievers (Ed.), Nuclear Magnetic Resonance Shift Reagents, Academic, New York, 1973, p. 87.
12 A. F. Cockerill, G. L. O. Davies, R. C. Harden and D. M. Rackham; Chem. Rev., 73 (1973) 553.
13 R. R. Fraser, in J. D. Morrison (Ed.), Asymmetric Synthesis, Vol. 1, Academic, New York, 1983, p. 173.
14 P. L. Rinaldi, Prog. Nucl. Magn. Reson. Spectrosc., 15 (1982) 291.
15 G. R. Sullivan, in E. L. Eliel and N. L. Allinger, (Eds.), Topics in Stereochemistry, Vol. 10, Interscience, New York, 1978, p. 287.
16 S. Thomson Eberhart and R. Rothchild, Appl. Spectrosc., 37 (1983) 292.
17 J. Avolio, S. Thomson Eberhart, R. Rothchild and P. Simons, Appl. Spectrosc., 40 (1986) 531.
18 R. J. Abraham and P. Loftus, Proton and Carbon-13 NMR Spectroscopy, Heyden, Philadelphia, 1978, p. 28.
19 N. Defay and C. Dorlet, J. Pharm. Belg., 27 (1972) 335.

Analytica Chimica Acta, 194 (1987) 221—233
Elsevier Science Publishers B.V., Amsterdam — Printed in The Netherlands

EXTRACTION RATE IN LIQUID-LIQUID SEGMENTED FLOW INJECTION ANALYSIS

L. NORD*, K. BÄCKSTRÖM, L.-G. DANIELSSON and F. INGMAN
Royal Institute of Technology, S-100 44 Stockholm (Sweden)
B. KARLBERG
Bifok AB, Box 124, S-191 22 Sollentuna (Sweden)
(Received 8th September 1986)

SUMMARY

The extraction mechanism in liquid-liquid segmented flow-injection systems is investigated. A film is formed on the tubing wall by the phase with the highest affinity to the tubing material. This film surrounds the segments of the other phase. To a great extent the extraction takes place at the interface of this film. The extraction rate is influenced by the segment length, the inner diameter of the tubing and the flow velocity. Short segments, small inner diameter and high linear flow velocity lead to a high extraction rate. These findings indicate that miniaturization of the flow system will lead to faster extraction and to decreased sample-zone broadening.

Extraction in liquid-liquid segmented systems for flow analysis has, since its introduction in 1978 [1], proved to be a powerful tool in automated analysis. The sample introduction is made either by injection into a carrier (flow injection analysis, f.i.a.) or by continuous pumping of the sample. In a recent review of the development of f.i.a., various extraction applications were covered [2].

In any automated flow extraction system, regardless of the method of sample introduction used, two aspects should be critically regarded, namely the sample dispersion and the extraction rate. While the sample dispersion mechanism in liquid-liquid segmented flow systems has been studied [3], very little is known about the influence of different extraction rates on the analytical behaviour of such systems. If the extraction mechanism of the segmented flow can be elucidated, it would be possible to use the inherent advantage of liquid-liquid segmented f.i.a., namely the very reproducible control of residence time, mixing and interfacial area, as the basis for a new tool for measurements of extraction kinetics. Thus the aims of the work presented in this paper are to elucidate the extraction mechanism, to determine the influence of the system design on the extraction rate, and to develop guidelines to optimize the system design with respect to dispersion and extraction rate.

0003-2670/87/$03.50

THEORY

Fundamental considerations

In a previous work, Nord and Karlberg [3] studied film formation and intrasegmental mixing in a liquid-liquid segmented flow system and their influence on the sample dispersion. The situation in the segmented flow can be described as follows. First, a film is formed by the phase that has the highest affinity to the tubing material, e.g., the organic phase in a PTFE (teflon) tubing and the aqueous phase in a glass capillary. Secondly, laminar flow prevails; the linear flow velocity is zero at the tubing surface while it is twice the mean flow velocity in the centre of the tubing. Because the film is very thin, it becomes part of a relatively stationary layer at the tubing wall. Thirdly, the segments move along the tube at the mean flow velocity; the difference between the local flow velocities (that in the centre of the tubing and that at the tubing wall) forces the liquid in the segments into a circulating flow. Finally, small eddies are formed within the segments so that the intrasegmental mixing is improved.

Figure 1A shows a simplified model for the extraction process in the segmented stream (for symbols, see Table 1). A species X is extracted from the aqueous phase to the organic phase in a segmented flow where the film on the tubing wall is formed by the organic phase. It is reasonable to assume that the concentration of X is homogeneous in the aqueous segments when they are formed in the segmentor at the start of the extraction. As the extraction begins, diffusion zones develop on both sides of the phase boundary. In the aqueous segment, the concentration of X in the diffusion zone is lower than in the bulk while in the organic segments the concentration in the diffusion zone is higher than in the bulk. In Fig. 1A, the bulk zones are marked off by broken lines. The internal circulation in the segments extends the diffusion zones along the flow lines into the segments. The thickness of

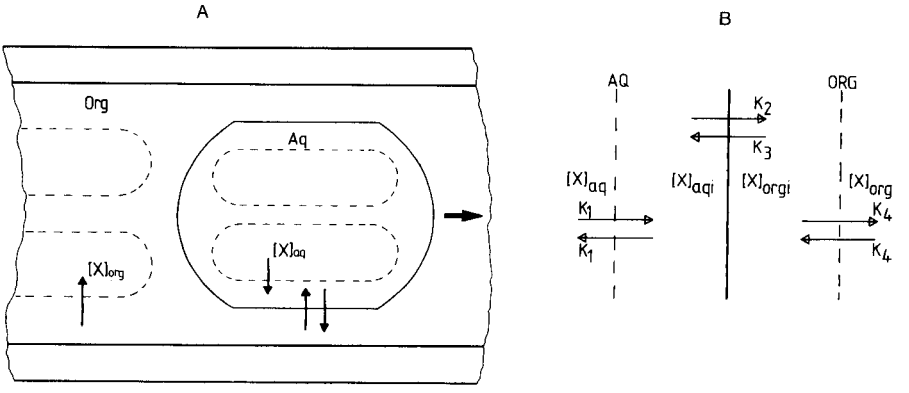

Fig. 1. (A) The extraction mechanism model in the segmented stream. (B) The extraction process for an uncharged species X.

TABLE 1

List of symbols

K_1, K_4	Mass transport rate constants (cm s^{-1})
K_2, K_3	Interfacial transfer rate constants (cm s^{-1})
D	Diffusion coefficient (cm^2 s^{-1})
ΔZ	Diffusion layer thickness
Q_1, Q_2, Q_3	Flux across the interface (mol cm^{-2} s^{-1})
K_d	Distribution constant
$[X]_{aqi}, [X]_{orgi}$	Interface concentrations
$[X]_{aq}, [X]_{org}$	Bulk concentrations
V_{aq}, V_{org}	Volume of the aqueous and organic phases
S/V	Interfacial area/volume ratio
l_s	Segment length
α_t	Extraction rate constant, time (s^{-1})
α_l	Extraction rate constant, length (m^{-1})
K_{tot}	Extraction rate constant (unit interfacial area/volume ratio (S/V)) (cm s^{-1})
d_t	Tubing inner diameter
d_f	Film thickness
C	Initial concentration in the aqueous phase
t_c	Residence time in the extraction coil, from phase segmentation to phase separation
H	Recorded deflection
H_{min}, H_{max}	H at zero coil length and H at equilibrium
$\bar{u}$	Mean linear flow velocity

the diffusion zone depends on the amount of convective mixing in the segments. It is obvious that the mass transport from the bulk to the interface in the aqueous segment and from the interface to the bulk of the organic segment forms a substantial part of the resistance to extraction. In previous dispersion studies [3], it was concluded that tubing diameter, segment length and flow velocity are important parameters to be considered in this context.

Figure 1B shows the extraction process for the case when the analyte transfer across the interface is assumed to follow first-order kinetics. The diffusive transport to and from the interface can be described by the constants K_1 and K_4, consisting of $D/\Delta Z$ where D is the diffusion coefficient and ΔZ is the thickness of the diffusion layer. Consequently, the greater the convection, the smaller the ΔZ value and the greater the K_1 and K_4 values.

The flux across the interface, can be described by

$$Q_1 = K_1 ([X]_{aq} - [X]_{aqi})$$

$$Q_2 = K_2 [X]_{aqi} - K_3 [X]_{orgi}$$

$$Q_3 = K_4 ([X]_{orgi} - [X]_{org})$$

If steady-state conditions prevail at the interface it follows that

$$Q_1 = Q_2 = Q_3 = (V/S)\, d\,[X]_{org}/dt$$

Working through the equations will eliminate $[X]_{aq}$, $[X]_{aqi}$ and $[X]_{orgi}$ (for the case when $V_{aq} = V_{org}$). The subsequent integration gives

$$1 - (1 + 1/K_d)\,[X]_{org}/C = \exp[-t_c\,(S/V)\,K_1\,K_4\,(K_2 + K_3)/(K_1\,K_3 + K_1\,K_4 + K_2\,K_4)] \quad (1)$$

K_d is the distribution constant equal to K_2/K_3.

When the mass transport to the interface is fast compared to the transport over the interface, a similar expression is obtained

$$1 - (1 + 1/K_d)\,[X]_{org}/C = \exp[-t_c\,(S/V)\,(K_2 + K_3)] \quad (2)$$

From Eqns. 1 and 2, it can be concluded that the ratio between the interface area and phase volume (S/V) is important to the extraction rate. Furthermore, from Eqn. 1, one can see that K_1 and K_4 must be 100 times greater than K_2 and K_3 in order to make the measured extraction rate constant equal to 98% of $K_2 + K_3$. This simplified model does not take all the possible kinetic aspects of an extraction into account. The chemistry of an extraction may well include slow reactions such as formation or degradation of complexes. In such cases, the importance of the mass transport processes may decrease in favour of a kinetic process actually taking place in one phase only. Nevertheless, knowledge of the interfacial transfer and dispersion mechanisms will aid the choosing of optimal conditions in such cases.

A necessary first step is to establish the actual pathway of the extraction in the segmented flow and the magnitude of the mass transport. This is most easily done in a system where no chemical reaction takes place, e.g., extraction of caffeine from aqueous solution into chloroform.

Flow system considerations

The peaks obtained in an extraction in f.i.a. are influenced by processes other than extraction. Examples are sample dispersion and adsorption on the tubing walls. In the present work, the mechanism of extraction and the influence of the manifold parameters on its rate were studied. It was therefore necessary to eliminate the influence of these other processes. The simplest way to achieve this is to pump the sample continuously to reach a steady state.

As only the extraction process of the segmented flow in the coil was to be studied, the extraction that could take place in the segmentor and the separator had to be minimized. Obviously, the residence time of the sample in the segmentor, the separator and the shortest connection between them must be kept as small as possible. The volume of the segmentor can probably not be made smaller than twice the segment volume. The latest development of the membrane phase separator allows the use of extremely small working volumes, compared with the flow rate and the segment volume. The separator used in this study had a 2.8-μl cavity for the segmented flow. This should be compared to a typical segment volume of 3 μl (l_s = 8 mm, d_t = 0.7 mm) and a total flow rate of 30 μl s^{-1}. The shortest possible connection tubing between

segmentor and separator is 5 cm; for 0.35-mm i.d. tubing, this means a volume of 5 μl. Thus, the minimum total volume of the extraction manifold is about 15 μl, giving a residence time of 0.5 s.

EXPERIMENTAL

Apparatus

Figure 2 shows the manifold used for the studies of extraction rate. The equipment comprised a peristaltic pump (Gilson Minipuls) and a spectrophotometer (Perkin-Elmer LC-55) with an 8-μl flow cell. Segmentors were made from T-connectors made of poly(vinyl difluoride) (PVDF) and Kel-F with 0.5 and 0.7 mm internal diameter. The internal diameter of the outflow channel was in some cases enlarged up to 1.5 mm to make production of large segments possible. Also the original Karlberg type of segmentor [1] was used to produce the largest segments. Extraction coils were made of PTFE with 0.35, 0.5 and 0.7 mm i.d. and with lengths between 5 and 180 cm. A membrane phase separator with a rigid support was used; the two cylindrical cavities had a volume of 2.8 μl each [4]. PTFE restriction coils, 0.35 mm i.d., were placed after the flow cell and the phase separator, in order to force the organic phase through the membrane and to increase the total pressure enough to avoid solvent evaporation.

Chemicals

Chloroform and a 1:1 (v/v) mixture of n-pentanol and n-heptane were used as organic phases. The aqueous phases were 0.01 M sodium hydroxide and 0.01 M nitric acid, respectively. Sample solutions were 1.2×10^{-5} M caffeine (0.01 M NaOH) and 40 mg l^{-1} bromocresol green (BCG) (0.01 M HNO_3).

RESULTS AND DISCUSSION

Rate-measuring technique

The measurements were made in the following way. First, aqueous phase without extractant was pumped into the system to establish a baseline. Then

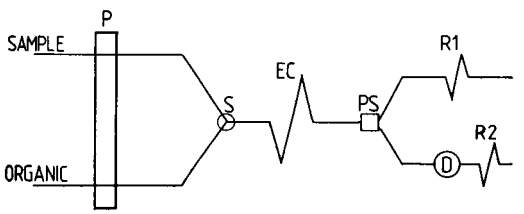

Fig. 2. Manifold configuration for the experiments: P, peristaltic pump; S, segmentor; EC, extraction coil; PS, phase separator; R1, R2, restrictors; D, spectrophotometric detector.

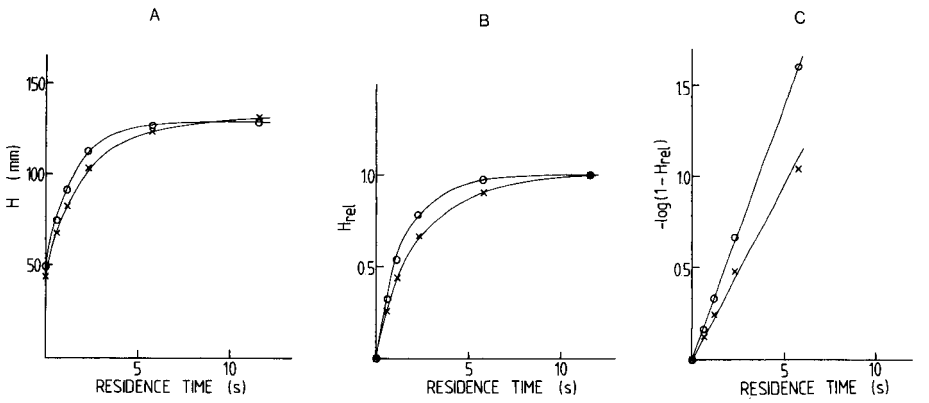

Fig. 3. Extraction of caffeine into chloroform: (○) l_s = 4 mm; (×) l_s = 9 mm. (d_t = 0.7 mm; extraction-coil lengths 0—100 cm.) (A) Measured deflection (H) vs. residence time; (B) relative deflection H_{rel}; (C) logarithmic representation, $-\log(1 - H_{rel})$.

aqueous phase containing the extractant was pumped using extraction coils of varying lengths. In each case the resulting absorbances were recorded. Typical results are shown in Fig. 3A. Two segment lengths were compared. The shorter segment length gives a faster extraction but the difference is difficult to quantify. In Fig. 3B the results are normalized by the equation

$$H_{rel} = (H - H_{min})/(H_{max} - H_{min})$$

so that the difference in the extraction degree in the reference manifold (zero coil-length) is compensated for. For Fig. 3C, the data obtained were treated as if they had originated from a process following first-order kinetics by plotting $-\log(1 - H_{rel})$ versus the residence time. If one identifies with Eqns. 1 and 2, the slope of the straight line, α_t, can be related to an overall rate constant K_{tot} by

$$K_{tot} = \alpha_t \, (V/S) \ln 10$$

When the mass transport to and from the interface is fast, Eqn. 2 is valid and $K_{tot} = (K_2 + K_3)$. At slow mass transport, Eqn. 1 is valid and $K_{tot} = K_1K_4$ $(K_2 + K_3)/(K_1K_3 + K_1K_4 + K_2K_4)$. If $-\log(1 - H_{rel})$ is plotted versus the extraction-coil length instead of the residence time (t_c), the dimension of the slope, α_l, will be the reciprocal coil length (m^{-1}). As coil length is an important design parameter in f.i.a., it is sometimes an advantage to describe the extraction rate by α_l. In this way, the extraction rate in a flow-injection extraction system can be quantified. Furthermore, the extraction rate can be described by a constant, K_{tot}, which is independent of the interfacial area/phase volume ratio, S/V.

The segment length

Figure 4A shows the results from an extraction of bromocresol green (BCG) into a pentanol/heptane mixture done with different segment lengths.

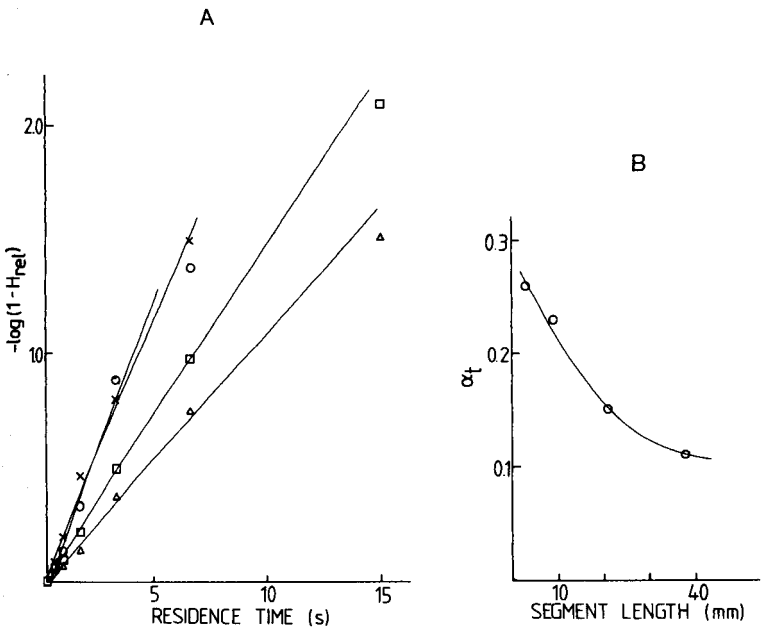

Fig. 4. Influence of segment length on extraction rate for the extraction of BCG into pentanol/heptane. (A) $-\log(1 - H_{rel})$ vs. residence time (s) for different segment lengths, l_s: (○) 3; (×) 9; (□) 21; (△) 38 mm (d_t = 0.7 mm). (B) extraction rate (α_t, s^{-1}) vs. segment length.

It is obvious that the extraction in the segmented stream is fast, taking between 7 and 15 s to reach 98% extraction. This corresponds to a value of $-\log(1 - H_{rel}) = 1.7$. Figure 4B shows the α_t values plotted versus the segment length. When the segment length is decreased, the extraction rate is increased. For long segments, the rate curve seems to level out reaching a α_t value around 0.1.

These results give some clues to the extraction mechanism. The ratio of the interfacial area/phase volume, equals

$$S/V = (d_t + l_s)/[(d_t^2/6) + (d_t\, l_s/4)]$$

which means that when the segment length is decreased from 3.8 to 0.3 cm, S/V increases from 57.5 to 61.0 (cm^{-1}), a change of less than 10%. This small increase in the interfacial area/volume ratio can only explain a minor fraction of the increase in extraction rate.

It is possible to distinguish two different phase boundary zones in the aqueous segment where the extraction takes place. These zones are: (A) the wall zone concentric with the tubing wall and surrounded by the organic phase film; and (B) the menisci zone, i.e., the zone at the segment ends. The segment surface at the tubing wall accounts for more than 90% of the total segment surface area when the segments are longer than 7 mm. In this film

region, the flow velocity relative to the tubing wall is very small and mass transport is likely to occur through diffusion only. This is certainly also valid for the mass transport within the organic film interspaced between the aqueous phase boundary and the tubing wall. The segmented flow was photographed during the continuous extraction of BCG from an aqueous to an organic phase of pentanol/heptane (Fig. 5). At the segment ends, no visible colour could be seen inside the meniscus of the aqueous segment. In the organic segment, a coloured zone appeared surrounding the meniscus.

The mass transfer to the interface is slow compared to the transfer across it, both at the film zone and at the menisci zone. This means that the overall extraction at the segment ends should not be faster than elsewhere in the segment. The contribution to the total extraction from the menisci should therefore be in proportion to their fraction of the total interfacial area. However, as discussed before [3], mass transfer between the bulk and the stationary layer of the organic, film-forming phase on the tubing wall may be enhanced by eddies appearing at the tubing wall just behind the aqueous segments. Thus, the shorter the segment length, the larger the number of mixing points. By decreasing the segment length, one can increase the mass transport rate.

In a manifold where the extraction is allowed to reach equilibrium, fluctuations in the segment length are unlikely to change the analytical precision. Conversely, in a manifold where the extraction coil is short so that the

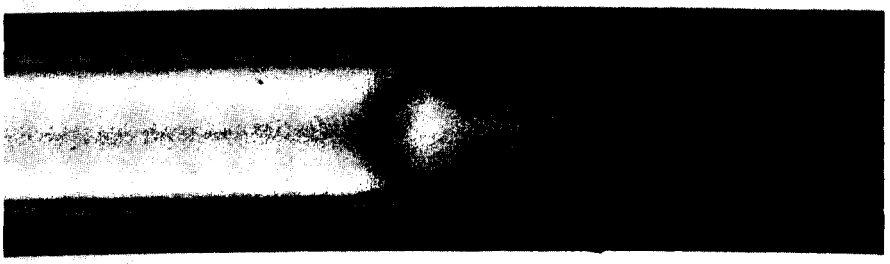

Fig. 5. Photograph of continuous extraction of BCG into pentanol/heptane. PTFE extraction coil, 0.7 mm i.d.

extraction is incomplete, the precision of the method can be influenced by fluctuations in the segment length.

Inner diameter of extraction tubing

The inner diameter of the extraction coil is an important design parameter. When the diameter is varied in an otherwise fixed manifold, both the flow velocity and the segment length are altered. To investigate the influence of the inner diameter on the extraction rate, two extreme system design cases were set up and studied. First, the flow velocity and the segment length were kept constant while the tubing diameter was varied. Secondly, the flow rate and the segment volume were kept constant. The results from these experiments are summarized in Table 2. In practice, it is difficult to keep the segment length constant while changing the tubing diameter, but by using different segmentors it was possible to come quite close.

Table 2A shows that the absolute rates α_t and α_l increase dramatically when the tubing diameter is decreased. In contrast to α_t, the rate constant, K_{tot}, is based on the unit surface area/phase volume ratio (S/V). By comparing α_t and K_{tot}, it is possible to elucidate to what degree the increased extraction rate is a consequence of an increased value of S/V. K_{tot} is almost constant when the diameter is changed. This means that the increase in extraction rate is mainly an effect of an increased S/V value. This is surprising as one would think intuitively that a decrease in diameter would shorten the diffusion distances and so improve the intrasegmental mixing and the extraction rate. However, the diffusion layers may be very thin. Thus, the diameter after a change from 0.7 to 0.35 mm would still be magnitudes greater than the diffusion distances.

Table 2B shows the results obtained by decreasing the diameter while keeping the volumetric flow rate and the segment volume constant. The flow velocity and segment length will change when the diameter is varied. In this case α_l decreases only 20% when the diameter is changed from 0.7 to

TABLE 2

Influence of the inner diameter of the tubing on the extraction rate of caffeine into chloroform

d_t (mm)	l_s (mm)	$\bar{u}$ (cm s^{-1})	α_l (m^{-1})	α_t (s^{-1})	K_{tot} (cm s^{-1})
A. Flow velocity and segment length constant					
0.7	8	9.2	2.4	0.22	9.0×10^{-3}
0.5	5	9.2	4.0	0.37	10.6×10^{-3}
0.35	5—10	8.7	6.3	0.54	10.9×10^{-3}
B. Flow rate and segment volume constant					
0.7	4	9.4	2.6	0.24	9.7×10^{-3}
0.5	8	18.3	2.9	0.53	15×10^{-3}
0.35	15—20	37.4	2.1	0.77	15.5×10^{-3}

0.35 mm. In practice, this means that the extraction is complete at about the same coil length although the residence time is 4 times shorter in the coil with the narrower bore. Consequently, α_t increases rapidly when the diameter decreases. Also K_{tot} increases to some extent. If one compares the results in Table 2A and B, it is possible to conclude that the increased flow velocity does have some effect on the extraction rate.

When applied to manifold design, these results give a strong argument for miniaturization. When a slow extraction is encountered in a practical situation, one might be tempted to use a wide-bore extraction coil in order to increase the residence time. But, as can be seen from Table 2B, this will not improve the situation as the extraction rate will decrease.

The flow velocity

Figure 6 shows the results obtained by changing the flow rate while keeping the inner diameter of the tubing constant (0.7 mm). In this case, the flow rate will be proportional to the flow velocity. The segment length and the area/volume ratio (S/V) are constant. If one considers a case when the mass transport to the interface is fast compared to the transfer across the interface, α_l will be inversely proportional to the flow rate and α_t will be constant.

Figure 6 shows that the extraction rate is controlled by both the mass transport to the interface and the transfer across the interface. When the flow rate increases, α_t increases to a constant value. This suggests that the mass transport to and from the interface increases with the flow rate. At high flow rates, it becomes fast enough to make the interfacial transfer the main resistance to extraction. The increased mass transport is likely to result from an increase in the convective constituent of the intrasegmental mixing. The increased film thickness may also be a factor. If the film is thin enough to become saturated by the extractant, this will of course impede the extraction. It can be calculated, however, that the volume of organic phase in the film around one segment would extract 85% of the molecules if it was equilibrated with one aqueous segment, assuming common conditions (d_t = 0.7 mm, d_f = 0.01 mm, K_d = 100). In other words, it is less likely that the film thickness per se would have a great influence on the mass transport rate.

It is clear from Fig. 6 that optimization of the extraction rate with respect to the total flow rate depends on whether the coil length or the residence time should be minimized. This choice depends, of course, on the specific situation.

Measurements of extraction kinetics

The fact that the α_t curve in Fig. 6B levels out at high flow rates has another interesting aspect, namely, the possibility of using the flow-injection extraction as a tool for measurements of extraction rate constants. In Fig. 7, results from Fig. 6 and Table 2 are plotted as K_{tot} versus linear flow velocity. The K_{tot} curve gives further indication that the mass transport to and from the interface at high flow velocities in narrow-bore tubings is fast compared to the transfer across the interface. The kinetics of the specific extraction

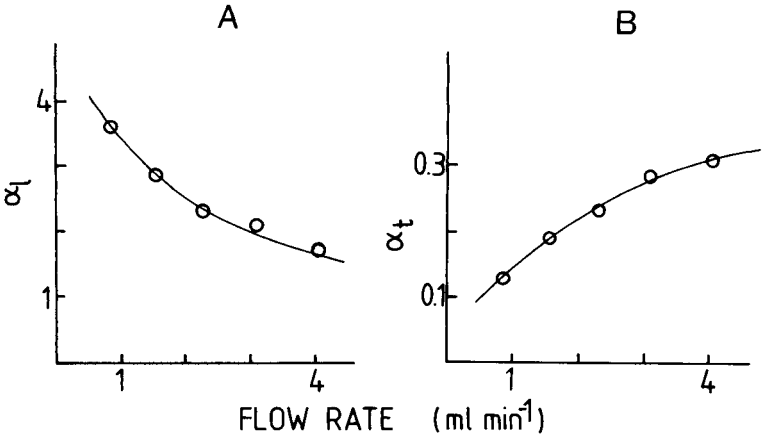

Fig. 6. Influence of the flow rate on the extraction rate for the extraction of caffeine into chloroform: (A) α_l (m^{-1}); (B) α_t (s^{-1}), l_s = 8 mm, d_t = 0.7 mm.

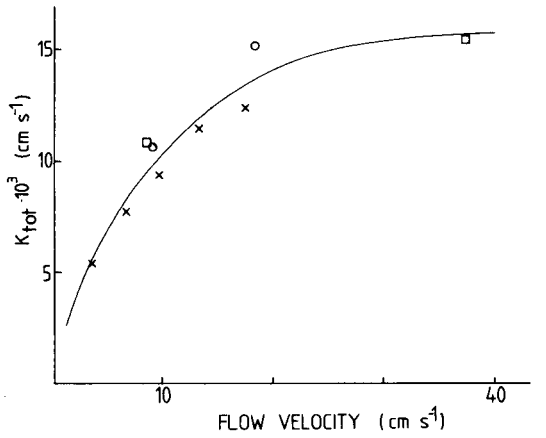

Fig. 7. Extraction rate (K_{tot}, cm s^{-1}) for caffeine into chloroform as a function of flow velocity for different inner diameters of the tubing: (×) d_t = 0.7, (○) d_t = 0.5, (□) d_t = 0.35 mm.

determines how vigorous the mixing must be to make the transfer across the interface the dominating resistance to extraction. Under such conditions, it is possible to apply an equation similar to Eqn. 2 in order to evaluate the constants experimentally. This potentially important use of flow-injection extractions needs further investigation and it must be evaluated and compared to standard methods such as the falling drop technique [5, 6].

Extraction rate and sample dispersion

The extraction rate will influence the degree of dispersion, because it determines the residence time (t_c) necessary for complete extraction. The dispersion in the segmented flow occurs in the phase that forms the film on the tubing wall [3]. Thus, the concentration and the residence time of the analyte in that phase will influence the dispersion. The concentration versus time curve shows this effect (Fig. 3B). The critical quantity for the dispersion is $\int_0^{t_c} H_{rel}\,dt$, which for the organic phase is the area under the curve and for the aqueous phase the area between the curve and $H_{rel} = 1$. For a first-order extraction from the aqueous to the organic phase the area under the curve is

$$\int_0^{t_c} H_{rel}\,dt = t_c + [\exp(-\alpha_t\, t_c)] - 1)/\alpha_t$$

For an extraction which is complete to a degree of 99% at $t_c = 1$, the integration is 0.78 for the organic phase and 0.22 for the aqueous phase. At 90% of complete extraction, the integration is 0.30 for the organic phase and 0.20 for the aqueous phase. Thus, the conditions favour dispersion in the organic (film-forming) phase rather than in the aqueous phase. By choosing the tubing material so that the aqueous phase forms the film, lower dispersion is obtained provided that the thicknesses of the aqueous and organic films are about the same. Furthermore, the integration for the organic phase increases 2.5 times when going from 90 to 99% of complete extraction. When the extracting phase forms the film, the dispersion can be decreased by using a coil half the length of that necessary to reach 99% extraction. The 10% loss in yield may well be compensated for by decreased dispersion for cases where thick films are formed.

For an analytical flow-injection extraction system, the aim of optimization must be to obtain complete extraction and minimum dispersion within the shortest possible time. It is therefore interesting to compare earlier findings about the influence of the design parameters on the dispersion [3] with their influence on the extraction rate, (Table 3). A decrease in the segment length and the tubing diameter both affect the extraction rate and the dispersion in the desired way. The flow velocity situation is somewhat more complicated. When the flow velocity decreases, the extraction rate based on time (α_t) decreases, but based on coil length (α_l) it increases. Thus, if minimum

TABLE 3

Summary of the influence of the design parameters on extraction rate and dispersion

Parameter decreased	Extraction rate		Sample zone broadening
	α_t	α_l	
Segment length	Increases	Increases	Decreases
Tubing diameter	Increases	Increases	Decreases
Flow velocity	Decreases	Increases	Decreases

volumetric dispersion is desired, the coil length should be as short as possible and the flow velocity should be kept low. However, this means that the extraction will not be as fast (in time) as possible.

CONCLUSIONS

The results show that the main path for extraction in liquid-liquid segmented flow is via the film surrounding the segments of the non-film-forming phase. Two important factors influencing the extraction rate are the interfacial area to volume ratio and the mass transport in the segments to and from the interface. For the relatively narrow-bore tubings used in f.i.a., the interfacial area consists almost only of the film interface.

A few condensed guidelines to improved extraction rate can be established. First, the extraction rate is greatly increased if the interfacial area/segment volume ratio is increased. This can be accomplished by decreasing the inner diameter of the extraction tubing. Secondly, shorter segments lead to better mixing and consequently to an increased extraction rate. Thirdly, increased flow velocity increases the extraction rate based on residence time. This results in minimum residence time for a given degree of extraction. Fourthly, decreased flow velocity increases the extraction rate based on extraction coil length. This results in minimum extraction coil length for a given degree of extraction.

It is clear that the manifold parameters of flow velocity, inner diameter, segment length and coil length can be varied in a reproducible manner and thus the mixing within the phases and the interfacial area can also be varied reproducibly. Furthermore, this work indicates that it might be possible to reach a degree of intrasegmental mixing large enough to reach conditions at which the extraction rate is controlled by the extraction kinetics only. This would mean that flow-injection extraction could be used as a new tool for the study of extraction kinetics.

The authors are indebted to Dr. Bernie Bubnis for valuable discussions. The work was financially supported by the Swedish Natural Science Research Council.

REFERENCES

1 B. Karlberg and S. Thelander, Anal. Chim. Acta, 98 (1978) 1.
2 J. Růžička and E. H. Hansen, Anal. Chim. Acta, 179 (1986) 1.
3 L. Nord and B. Karlberg, Anal. Chim. Acta, 164 (1984) 233.
4 K. Bäckström, L.-G. Danielsson and L. Nord, Anal. Chim. Acta, 169 (1985) 43.
5 S.-O. Jansson, T. Nordgren and G. Schill, Acta Pharm. Suec., 14 (1977) 435.
6 T. Nordgren, Dissertation, Uppsala, 1979.

Analytica Chimica Acta, 194 (1987) 235—245
Elsevier Science Publishers B.V., Amsterdam — Printed in The Netherlands

DETERMINATION OF ORGANOLEAD COMPOUNDS BY LIQUID CHROMATOGRAPHY WITH ON-LINE EXTRACTION AND ULTRAVIOLET DETECTION

D. S. BUSHEE and I. S. KRULL*

Department of Chemistry and The Barnett Institute, 341 Mugar Building, Northeastern University, 360 Huntington Avenue, Boston, MA 02115 (U.S.A.)

S. B. SMITH, Jr. and R. G. SCHLEICHER

Analytical Instruments Division, Allied Analytical Systems, Inc., 590 Lincoln Street, Waltham, MA 02254 (U.S.A.)

(Received 31st March 1986)

SUMMARY

Detection limits by ultraviolet detection in liquid chromatography (LC) for organolead species are improved by the use of a post-column, on-line, continuous liquid-liquid extraction system. Extraction of the organolead species is followed by membrane separation of the extracts from the aqueous mobile phase. Optimization of the membrane used in the phase separator, ratios of aqueous-to-organic flow rates, extractor dimensions and shape, aqueous salt content, the detection wavelength, and other operational parameters are described. Improvements of detection limits over conventional LC methods with ultraviolet detection range from a factor of 2 for triethyllead chloride, up to a factor of over 10 for trimethyllead chloride. Calibration plots are linear over several orders of magnitude. Extraction efficiencies as a function of the organic extractant flow rate are discussed. The optimized approach is applied to spiked, distilled-water samples.

Methods for trace-metal speciation have received increased attention and emphasis within the past decade. In part, this is due to the realization that total amounts present can be less important than the particular species [1—4]. Both inductively-coupled plasma emission spectrometry (ICP) and direct-current plasma emission spectrometry seem to offer significant advantages over other detection modes for liquid chromatography (LC). However, there is the problem of adequate detection limits for real samples. One successful approach to lowering detection limits has involved the use of post-column hydride formation [5, 6]. However, such techniques are only practical for a limited number of elements, such as arsenic, tin, and selenium.

Post-column extraction has become popular for improved detection of organics [4, 7]. The combined sensitivity and selectivity have expanded the range of applications for some detectors such as the mass spectrometer and Fourier-transform infrared spectrometer [8, 9]. With post-column extraction, a compatible organic solvent is chosen to introduce the analyte into the

0003-2670/87/$03.50

detector without sacrificing the chromatographic separation. Such an approach might prove useful in interfacing liquid chromatography and atomic spectrometry [10]. Flow injection followed by liquid-liquid extraction has also been used as a sample introduction method for atomic absorption spectrometry (AAS) to eliminate spectral and matrix interferences [11].

This paper describes reversed-phase chromatographic separations for various organoleads, an on-line post-column liquid-liquid extraction system, a modified membrane phase separator, and results for system optimization. Also presented are detection limits for the ultraviolet detector and the extraction/ultraviolet detector, calibration plots and linearities for three organoleads, system variances, extraction efficiencies, and optimized flow rates and extractants. Finally, the extraction/ultraviolet approach was applied to spiked, distilled-water samples prepared in a blind study.

EXPERIMENTAL

Instrumentation

The instrumentation is outlined in Fig. 1. A Constametric III pump (LDC/Milton Roy, Riviera Beach, FL), a Constametric I pump, a low-pressure pump (Eldex Laboratories, Menlo Park, CA), and an injection valve (Model 7125, Rheodyne) with a 200-μl fixed loop were used. The u.v.-visible detector was a variable-wavelength Hitachi Model 100-40 spectrophotometer with a Model 155-00 flow cell module (Altex Scientific, Berkeley, CA) or a linear diode-array detector (Model 1040A, Hewlett-Packard). Peak height and peak area data from the u.v. detector were collected with a Hewlett-Packard Model 3380A reporting integrator; u.v. absorption was monitored at either 230 or 270 nm, depending on the solvent.

A Waters 150-mm × 3.9-mm C_{18} Resolve column (5 μm) was used for the separations. The mobile phase consisted of 0.1 M ammonium acetate adjusted to pH 4.6 with anhydrous acetic acid and 20% (v/v) methanol, all at a flow rate of 1.0 ml min^{-1} [12].

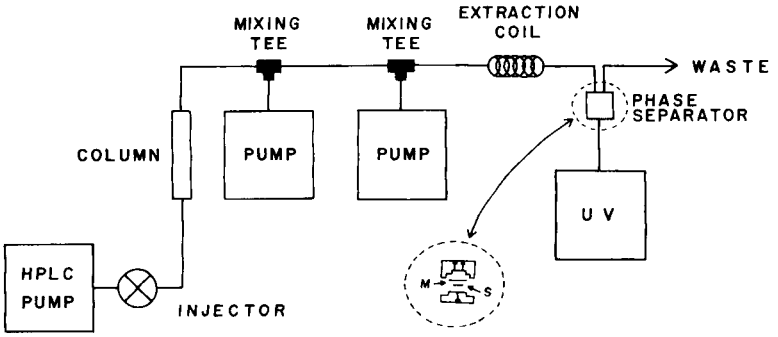

Fig. 1. Schematic diagram of the complete instrumentation. M = membrane separator, *S* = glass disk support.

Chemicals, reagents, standards and solvents

Chloroform was distilled-in-glass Omnisolv grade (EM Science, Cherry Hill, NJ). The mobile-phase water was from a Corning Mega-Pure still. All mobile phase, reagent, and chloroform solutions were filtered through Millipore 0.45-μm filters. Reagent-grade sodium iodide and ammonium acetate were obtained from Alfa Products or Aldrich Chemical Co.

Lead standards were obtained from either Alfa Products, Thiokol Corp., Ventron Division or Strem Chemicals (Newburyport, MA) and were used as received. The purity of the standards was determined by LC/ICP and LC/ultraviolet methods. Triethyllead chloride was found to be 70% pure by LC/ultraviolet. It contained 30% lead chloride, determined with an external standard. The triethyllead chloride was shown by LC/ICP, to contain a second lead species, with retention time the same as lead chloride. For lead chloride, trimethyllead chloride and diphenyllead chloride only a single peak was present. Because no commercial standard was available with 100% triethyllead chloride, it was necessary to identify and quantify the lead contaminant, as above. The purity factor was included in the detection limit and linear range determinations, as well as in the method validation studies.

Membrane phase separator and interface

The membrane phase separator was based on a design of Fossey and Cantwell [13] which had been modified slightly by changing the positions of the inlet and outlet ports. In the Fossey-Cantwell design, the membrane was supported by a teflon sheet with channels. Optimized conditions with their separator consisted of a 1:1 ratio of organic/aqueous flow rates, at which point 50% of the organic solvent passed through the detector before any of the aqueous phase passed through the membrane and entered the detector.

The inset in Fig. 1 illustrates the membrane phase separator. It was machined from a 1.5-in. diameter rod of Kel-F (Plastic Profiles, E. Hanover, NJ). Polypropylene tube end-fittings (1/16-in.; Rainin Instruments, Woburn, MA) were used to couple the separator and connecting tubings. The membrane was supported by a borosilicate microfiber glass disk (Type AP40, Millipore). Polytetrafluoroethylene (PTFE) membranes were obtained from Millipore Corp. in a range of pore sizes. The membrane and glass disk were cut to diameters of 3/4-in. and 1/2-in., respectively.

The mixing tees were glass-lined, stainless steel pieces (1/16-in. o.d., 0.5-mm i.d.), with 25-mm long side arms (Scientific Glass Engineering, Austin, TX). Polytetrafluoroethylene tubing (1/16-in. o.d. $\times$ 0.032-in. i.d. $\times$ 0.016-in. wall thickness; Cole Parmer, Chicago, IL) was used for all the post-column extraction coils and woven coils. A back-pressure regulator (Scientific Systems, State College, PA) was placed at the aqueous waste outlet of the separator and adjusted to achieve 100% separation of the two phases.

Determination of extraction efficiencies

The extraction efficiency for each organolead into chloroform was evaluated by collecting peaks from the LC system with the extraction detector and quantifying the lead in the collected fractions by flame atomic absorption spectrometry (AAS). An Instrumentation Laboratory Model 951 spectrometer was fitted with a small-volume sample cup (part no. 12311900; Allied Analytical Systems). An air/acetylene flame was monitored at 283.7 nm with a bandwidth of 1.0 nm. Samples (50 μl) were injected for both unknowns and standards. The same organolead standard was used as that injected into the LC system. Samples were prepared for AAS by taking 1-ml aliquots of the collected peak fractions and concentrating these, with stirring, under a stream of nitrogen in Reacti-Vials (VWR Scientific, Boston, MA) containing 0.5 ml of diluted (1 + 4) nitric acid as a keeper solvent. Standard lead solutions were prepared in this same acid. Recoveries of each organolead species were determined by spiking each standard into an equivalent volume of chloroform, and then processing each of these solutions in triplicate as for the extracted species in the LC system. Recoveries (%) were used to calculate the true percent extractions, where necessary.

RESULTS AND DISCUSSION

Unless noted otherwise, uncertainties are reported as one standard deviation (±1 s.d.).

Membrane evaluation and optimization

A series of membranes was evaluated for the phase separator in a flow-injection system. The polytetrafluoroethylene membranes ranged in pore size from 0.02 to 10 μm. Several of these were available in laminated and unlaminated forms. In all cases, the unlaminated membranes performed better than the corresponding laminated one of the same pore size. Laminated membranes were also more difficult to seat properly in the phase separator. It was necessary to over-tighten the separator halves with the laminated membranes to prevent leaking and this placed unusual stress on the Kel-F.

Testing of the flow-rate ranges with each membrane was done with distilled water and chloroform. The usefulness of each membrane was tested in two ways (see Table 1). In the first experiment, the chloroform flow rate was kept constant at 0.5 ml min^{-1}, while the aqueous flow rate was increased in steps of 0.10 ml min^{-1}, starting at 0.5 ml min^{-1}. The flow rate of the water phase was increased until breakthrough of the water was observed. Breakthrough was indicated by an increase in the absorbance at 254 nm, and by visually monitoring the effluent from the phase separator. Flow rates one increment before breakthrough are listed in Table 1 (second column) as the highest water flow rate tolerated by each membrane. Such data were used to calculate the highest ratio of water to chloroform flow rates which the mem-

TABLE 1

Evaluation of membranes for phase separator

Membrane type (pore size, μm)	Maximum tolerable parameters		
	Water flow (ml min^{-1})	Water/organic ratio	Flow rate at 1:1 ratio (ml min^{-1})
PTFE, unlaminated (0.02)	NB[a]	NB[a]	NB[a]
Fluoropore, unlaminated (0.2)	4.3	8.6:1	4.0
Fluoropore, laminated (0.2)	3.3	6.6:1	4.0
Fluoropore, laminated (0.5)	2.5	5.2:1	4.0
Fluoropore, unlaminated (0.5)	2.1	4.2:1	4.0
Fluoropore, laminated (1.0)	2.3	4.8:1	4.0
Fluoropore, laminated (3.0)	1.6	3.2:1	1.8
Mitex, unlaminated (5.0)	0.8	1.7:1	1.1
Mitex, unlaminated (10.0)	0.8	1.7:1	1.0

[a]No breakthrough.

brane would withstand before breakthrough (Table 1, third column). The second test done on each membrane was to determine breakthrough occurrence as a function of increasing flow rates, with the ratio of aqueous to organic phases kept constant (1:1). Both flow rates were initially set at 0.5 ml min^{-1} and increased in 0.10 ml min^{-1} increments until the breakthrough of water. The results are listed in Table 1 (fourth column). All of these values were obtained with a 100% separation of the organic from aqueous phases. With the 0.02-μm membrane, no breakthrough was observed at any flow rate, but it was limited by the aqueous/organic separation. At best, only 40% of the organic phase was transferred across the membrane, probably because of the small pore size. The filter was also easily clogged with particulate matter in the mobile phase in the flow-injection mode.

The overall results indicate that the smaller the pore size, the greater the range of useful flow rates. The 0.2-μm unlaminated membrane was chosen for all further work. By using a 0.5 ml min^{-1} flow of chloroform, a maximum water flow rate of 4.3 ml min^{-1} was possible. This is almost a 9:1 ratio of aqueous to organic phases, spanning a wide range of possible chromatographic flow rates. The highest aqueous/mobile phase flow rate for a 1:1 ratio of phases was 4.0 ml min^{-1} (Table 1). This upper limit was not due to membrane failure, but to pressure limitations on the analytical column at high flow rates.

Extractor configuration and length

Liquid-liquid extractors in LC have involved various configurations of flexible teflon tubing, but the simplest has been a coiled or helical arrangement. The use of a knitted open tubular weave has been found to reduce band broadening for some applications [14]. This weave is a series of alter-

nating right and left loops, which effectively reduces axial dispersion in homogeneous systems. The effect of using this weave with a solvent-segmented system was studied.

The band broadening in the extraction/ultraviolet system was determined in the flow-injection mode, using acetophenone as a model compound, because of its good ultraviolet-absorbing properties as compared with organolead species. The variance, V, was calculated from the equation suggested by Foley and Dorsey [15].

$$V = \overline{M}_2 = W_{0.1}^2/[1.764(B/A)^2 - 11.15(B/A) + 28]$$

where $\overline{M}_2$ is the variance or second statistical moment, $W_{0.1}$ is the peak width at 10% of the peak height, and B/A is equal to the asymmetry factor. This formula is valid for asymmetry factors ranging from 1.00 to 2.76.

The average peak variances for the coil and weave configurations were 3186 ± 223 and 3297 ± 504, respectively. All tubing was of the same internal diameter, and both coil and weave were 3 ft. long. The Student's t-test, with a 95% confidence interval, showed no statistical difference between the variances observed with the coil or weave. Thus, solvent segmentation in a coiled tube is as effective in reducing band broadening as the knitted open tube.

Extraction efficiency, measured as peak area, is compared for the three tubing configurations in Table 2 for five different injection volumes. The areas indicated were normalized relative to the response obtained with the coil for a 25-μl injection volume. When little or no time was allowed for the extraction (i.e., with the 3-in. length of straight tubing), the relative area was always less than with the coil or weave present. This was expected, because some time was necessary for the equilibrium to be established between the two phases. There was no obvious difference between the coil and weave, suggesting no real difference in extraction efficiencies. There was no reduction in band broadening with the weave, nor was there any real increase in extraction efficiency. Because it was simpler to use a coil, and because back-pressure was lower, the coil was used in the remainder of these studies.

The optimum extraction time was determined by varying the length of the extraction coil (fixed internal diameter) while monitoring the peak area for 2.4 mg l^{-1} trimethyllead (TML) in the LC mode. Figure 2 shows the change in u.v. response with increasing length of extraction coil. A 3-ft length of tubing was used in all further work.

Optimization of extraction conditions

The membranes used above cannot tolerate high concentrations of organic solvents. The addition of an auxiliary stream of water after the chromatographic step partially overcomes this limitation. This changes the organic/aqueous ratio so that the membrane tolerates 50% methanol in the mobile phase. This does not affect the chromatographic separation, nor does it

TABLE 2

Extraction efficiencies with and without various extractors[a]

Injection volume (μl)	Relative area[b]		
	No extractor	Coil	Weave
25	0.7 (1.2)	1.0 (1.9)	1.0 (12.2)
50	1.4 (5.6)	1.9 (1.8)	1.8 (3.3)
100	2.6 (3.1)	3.6 (0.8)	3.1 (6.4)
150	3.8 (5.5)	5.3 (1.5)	5.1 (0.6)
200	4.9 (4.6)	6.7 (4.0)	6.4 (4.2)

[a]Relative areas should theoretically be even multiples of 25-μl injections, but amounts extracted at high injection volumes decreased. [b]Average and RSD (%) for three injections.

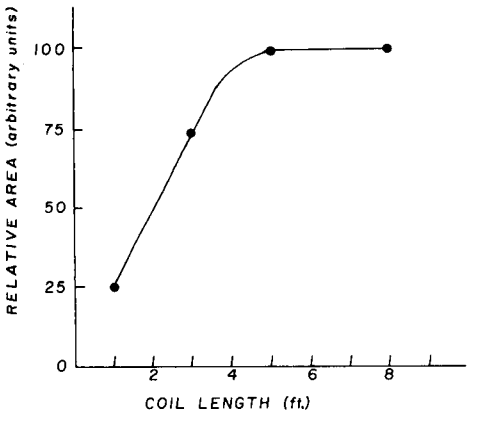

Fig. 2. Effect of changing extraction coil length on peak-area response of 2.4 mg l^{-1} lead as TML in the LC system.

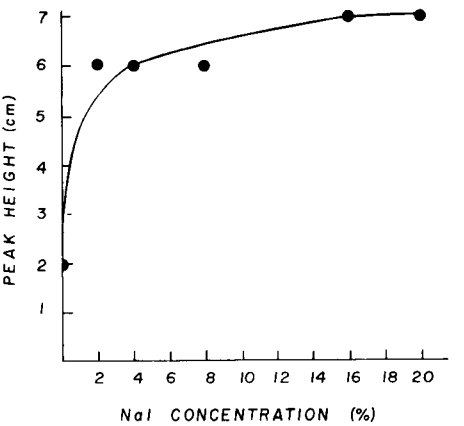

Fig. 3. Effect of increasing sodium iodide concentration on peak-height response of 88 mg l^{-1} lead as TML in the LC system.

increase band broadening, because the post-column effluent is solvent-segmented. The sample is initially diluted and extracted into a larger volume of organic phase. The addition of the post-column aqueous stream makes a wider range of mobile phases compatible with the membrane separator.

Extraction of trimethyllead chloride (TML) was not possible without the post-column addition of an inorganic salt. Several salts were tested, including sodium chloride, sodium iodide, sodium carbonate, ammonium acetate, and sodium acetate; only NaCl and NaI were effective. Sodium iodide was chosen because it is less corrosive. The concentration was varied from 0 to 20% while the peak-height response for an 88 mg l^{-1} lead solution

of TML was monitored (Fig. 3). The diameter of each dot represents the standard deviation of three replicate determinations. The flow rate of the iodide solution was held constant at 1.0 ml min^{-1} throughout. A concentration of 4% (w/v) sodium iodide was used for further work. Changes in the flow rate of this solution from 1.0 to 3.0 ml min^{-1} did not change the peak-height response. A 1.0 ml min^{-1} flow rate was used in all further work. Sodium iodide acts as a salting-out agent, suppressing the dissociation of the trialkyllead salts [16]. Tri- and di-alkyllead salts with the anion of a strong acid have a high degree of ionic character and the trialkyllead halides exist as solvated cations in aqueous media.

De Jonghe et al. [16] showed that chloroform was the best solvent for extraction of organolead species. The flow rate of chloroform was varied from 0.3 ml min^{-1} to 1.0 ml min^{-1} as the peak areas for a TML solution were monitored (Fig. 4). As the chloroform flow rate increased, the concentration of the analyte in each peak decreased. The 0.65 ml min^{-1} flow rate was used for further studies because the peaks were more reproducible.

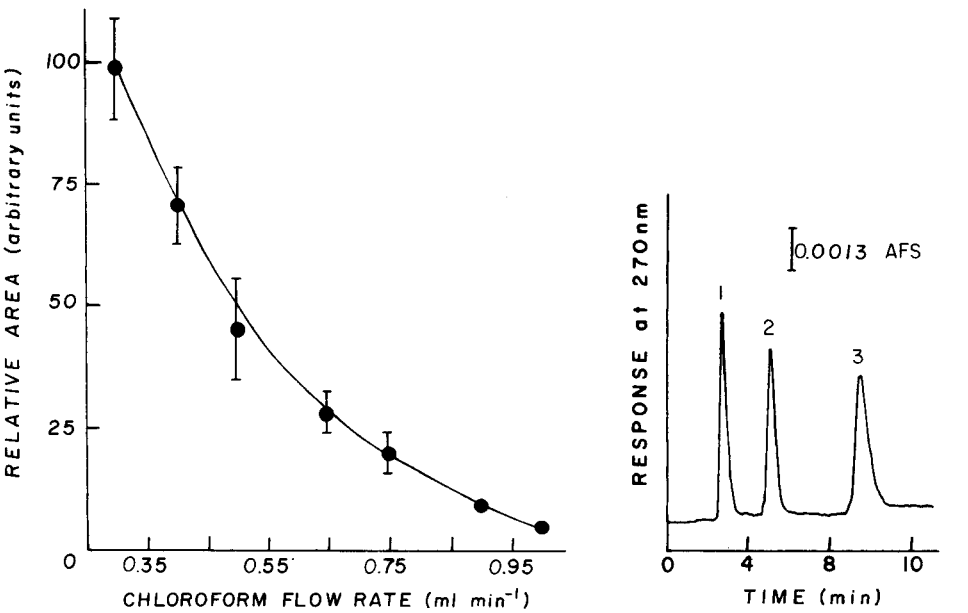

Fig. 4. Effect of changing the chloroform flow rate on peak area of 2.4 mg l^{-1} lead as TML in the LC system.

Fig. 5. Chromatogram of organolead compounds (each at ca. 3 mg l^{-1} Pb): (1) TML; (2) TEL; (3) $(C_6H_5)_2PbCl_2$. LC conditions: mobile phase of 0.1 M ammonium acetate, 20% methanol (pH 4.6) at 1.0 ml min^{-1} on a 15 cm × 3.9 mm Waters Resolve column, 200-μl injections. Detection conditions: 4% sodium iodide added post-column at 1.0 ml min^{-1}; chloroform added at 0.65 ml min^{-1}; detection at 270 nm.

Wavelength selection

The u.v.-visible absorption spectra for the lead compounds were obtained by monitoring the effluents with a linear diode-array detector; wavelengths ultimately chosen were 230 nm for LC with u.v. detection only and 270 nm for the extraction/ultraviolet method. The auxiliary stream, at 1.0 ml min^{-1}, consisted of either distilled water or 4% sodium iodide. The optimum wavelengths of absorbance were about the same for each compound regardless of the added reagent. The only differences between the responses for any given compound were intensity, which increased from water to sodium iodide, which confirmed the enhanced extraction of the lead compounds.

Extraction efficiencies of organolead species in the LC system

Figure 5 is a chromatogram for a typical separation of trimethyllead chloride (TML), triethyllead chloride (TEL), and diphenyllead dichloride. Lead(II) ions, if present, would elute just after the solvent front, retention time ca. 1.5 min. Under these solvent conditions, inorganic lead was not extracted. The total procedure required less than 10 min.

The extraction efficiency into chloroform was determined by flame AAS. Samples were collected from the u.v. detector, at a set time and flow rate, resulting in a known volume. At least four samples were separately collected for each compound, using two different flow rates (0.65 ml min^{-1} and 0.40 ml min^{-1}). Total lead in an aliquot was quantified by flame AAS, using a small sample cup, by comparison against a standard of the same species. Table 3 summarizes the extraction efficiencies. Also indicated are

TABLE 3

Extraction efficiencies of organolead species[a]

Compound	Extraction efficiency (%)[b]		Recovery (%)
	0.40 ml min^{-1}	0.65 ml min^{-1}	
Trimethyllead	84 ± 1	55 ± 1	108 ± 3
Triethyllead	83 ± 2	93 ± 2	99 ± 6
Diphenyllead dichloride	72 ± 2	62 ± 2	108 ± 4

[a]Flame atomic absorption quantitation of peaks collected from the u.v. detector at two different chloroform flow rates. LC conditions as in text. [b]At least five data points.

TABLE 4

Linearity study for organolead compounds by LC with extraction/ultraviolet detection

Compound	Linear range (mg l^{-1})	Slope	*y* intercept
Trimethyllead chloride	0.080—76	2.07 ± 0.14	6.71 ± 4.92
Triethyllead chloride	0.140—169	1.58 ± 0.06	5.13 ± 5.35
Diphenyllead dichloride	0.280—39	1.61 ± 0.05	−1.98 ± 0.95

percent recoveries obtained by extracting known, spiked levels into separate chloroform solutions; the spikes were similar in concentration to those in the extraction samples. All of the results were highly reproducible. Extraction efficiencies were 55—93%, and percent recoveries of standards were high. For two of the three organoleads, extraction efficiencies were higher at lower flow rates, as expected.

Detection limits and linear dynamic ranges for organolead compounds

Detection limits (mg l^{-1}) without and with extraction, respectively, were 1.1 and 0.08 for TML, 0.3 and 0.14 for TEL, 0.7 and 0.3 for O_2PbCl_2, and 0.2 for $PbCl_2$ (no $PbCl_2$ detected with extraction); a 3:1 signal/noise ratio was the criterion. The detection limit for trimethyllead chloride was improved about ten-fold with extraction. Other organoleads did not exhibit such enhancements, probably because they already have u.v. activity without extraction. With the proposed LC system, each species exhibited a linear dynamic response over 2—3 orders of magnitude by peak height and area. Linear regression analysis showed correlation coefficients from 0.996 to 0.999 (Table 4).

Method validation

Results were obtained for a series of five spiked distilled-water samples containing the lead compounds in ranges (mg l^{-1} Pb) of 0.09—46 for TML, 0.16—162 for TEL, and 0.38—38 for diphenyllead dichloride. Most of the results agreed well with the spiked levels, with a few expected exceptions; differences between spiked and determined values were in the range of 18—0.008 mg l^{-1}. Standard deviations for triplicate runs ranged from 0.002 to 1.0 mg l^{-1}. Least-squares fits determined vs. spiked values yielded slopes for TML, TEL, and diphenyllead dichloride of 1.06 ± 0.01, 0.92 ± 0.08, and 0.99 ± 0.01, respectively, intercepts of −0.3 ± 0.3, 3 ± 6, and −0.2 ± 0.2 mg l^{-1}, respectively, and correlation coefficients from 0.977 to 1.000.

We acknowledge with appreciation the assistance of B. Karcher, Northeastern University, in the preparation of various spiked water samples. W. LaCourse, Northeastern University, made valuable suggestions for the improved phase separator used. We appreciate the interest and encouragement of K. Panaro, M. Lookabaugh, and S. Kryzsko of the Boston District Office, Food and Drug Administration. Special thanks to Waters Chromatography Division of Millipore Corporation for technical discussions and donation of the membranes used. This work was supported by a research and development contract from Allied Analytical Systems. We further thank the Hewlett-Packard Company for the gift of the photodiode-array detector. This is contribution number 284 from The Barnett Institute at Northeastern University.

REFERENCES

1 J. C. MacDonald (Ed.), Inorganic Chromatographic Analysis, Wiley, New York, 1985.
2 W. M. Blakemore, in M. C. Bowman (Ed.), Handbook of Carcinogens and Other Hazardous Substances. Chemical and Trace Analysis, M. Dekker, New York, 1982, Chap. 9.
3 I. S. Krull, in M. Bernhard, F. E. Brinckman and P. J. Sadler (Eds.), The Importance of Chemical Speciation in Environmental Processes, Springer, Berlin and Heidelberg, 1986, p. 579.
4 I. S. Krull, in J. F. Lawrence (Ed.), Environmental Analysis by Liquid Chromatography, The Humana Press, Clifton, NJ, 1984, Chap. 5.
5 I. S. Krull and K. W. Panaro, Appl. Spectrosc., 39 (1985) 960.
6 D. S. Bushee, I. S. Krull, P. R. Demko and S. B. Smith Jr., J. Liq. Chromatogr., 7 (1984) 8671.
7 J. F. Lawrence, U. A. Th. Brinkman and R. W. Frei, in I. S. Krull (Ed.), Reaction Detection in Liquid Chromatography, M. Dekker, New York, 1986, Chap. 6.
8 C.-P. Tsai, A. Sahil, J. M. McGuire, B. L. Karger and P. Vouros, Anal. Chem., 58 (1986) 2.
9 C. C. Johnson, J. W. Hellgeth and L. T. Taylor, Anal. Chem., 57 (1985) 610.
10 K. L. Jewett and F. E. Brinckman, in T. M. Vickrey (Ed.), Liquid Chromatography Detectors, M. Dekker, New York, 1983, Chap. 6.
11 J. A. Sweileh and F. F. Cantwell, Anal. Chem., 57 (1985) 420.
12 M. Blaszkewicz and B. Neidhart, Int. J. Environ. Anal. Chem., 14 (1983) 11.
13 L. Fossey and F. F. Cantwell, Anal. Chem., 54 (1982) 1693.
14 I. S. Krull (Ed.), Reaction Detection in Liquid Chromatography, M. Dekker, New York, 1986, Chaps. 1 and 7.
15 J. Foley and J. G. Dorsey, Anal. Chem., 55 (1983) 730.
16 W. R. A. De Jonghe, W. E. Van Mol and R. C. Adams, Anal. Chem., 55 (1983) 1050.

Analytica Chimica Acta, 194 (1987) 247—260
Elsevier Science Publishers B.V., Amsterdam — Printed in The Netherlands

A LOW-PRESSURE BEENAKKER-TYPE MICROWAVE-INDUCED HELIUM PLASMA SOURCE AS A SIMULTANEOUS MULTI-ELEMENT GAS CHROMATOGRAPHIC DETECTOR

J. C. EVANS*, K. B. OLSEN and D. S. SKLAREW

Environmental Sciences Department, Pacific Northwest Laboratory, Richland, WA 99352 (U.S.A.)

(Received 16th October 1986)

SUMMARY

A low-pressure version of a Beenakker-type microwave-induced helium plasma optical emission spectroscopy detector for gas chromatographic effluents is described. The plasma is sustained in a 1.3-mm i.d. quartz tube and is viewed axially through a quartz window. Operating characteristics of the source were studied for power levels of 15—115 W, for carrier-gas flows of 20—1000 ml min^{-1}, and for pressures of 2—700 torr. A gas chromatographic system involving a fused-silica capillary column is used as the sample introduction system for compounds containing carbon, hydrogen, nitrogen, sulfur, and chlorine. Elemental response factors and the precision of elemental response ratios were studied. The use of this detector in evaluating empirical formulae is also discussed. Empirical formulae for a number of hydrocarbons and sulfur-containing aliphatic and heterocyclic compounds are presented, together with a discussion of the factors that affect accuracy and precision. It is concluded that this type of detector combines some of the best features of the atmospheric-pressure Beenakker and the Evenson-type sources.

The feasibility of interfacing gas chromatography with atomic emission spectrometry was first demonstrated by McCormack and co-workers more than 20 years ago [1]. Since that time, several different atomic excitation sources have been investigated as element-specific detectors for gas chromatography effluents. These excitation sources include inductively-coupled argon plasmas (ICP) [2, 3], direct-current plasmas [4], surface-wave-generated plasmas [5], and most recently, afterglow sources [6]. Both argon and helium have been used as plasma support gases; however, in the case of microwave-induced plasmas (MIP), helium has proven particularly useful for the detection of elements such as nitrogen, sulfur, and the halogens that are difficult to excite. The majority of work done in recent years with helium-plasma detection has involved the use of either the low-pressure Evenson-type 1/4-wave cavity [7] or the atmospheric-pressure TM_{010} cavity [8—10]. Both sources have advantages and disadvantages. The low-pressure Evenson source provides optimal excitation energy, but the transverse viewing geometry used decreases sensitivity. Tube erosion and carbon build-up in the active region can also cause degradation of long-term stability. The TM_{010} cavity originally described

0003-2670/87/$03.50

by Beenakker [8, 9] provides a more efficient method for coupling microwave energy into the plasma and provides an axial geometry with inherently better light transmission. These systems have been operated at atmospheric pressure in analytical applications. The high pressure causes decreased sensitivity for nitrogen and other elements that are difficult to excite. The atmospheric-pressure source is also prone to tube erosion with prolonged use, ignition difficulties, and slow stabilization after ignition. A recently-developed tangential-flow version of the atmospheric pressure Beenakker-type cavity minimizes some of these problems at the expense of high gas flow rates [11]. A solution to this dilemma is to combine the most attractive features of both systems. A low-pressure Beenakker-cavity excited source fulfills those requirements.

A study of plasma properties for both argon and helium plasmas at pressures ranging from 10 to 760 torr was recently reported by Goode et al. [12] who used a TM_{010} cavity for plasma excitation. While this work concentrated on the measurement of excitation temperatures and electron densities, it also suggested that use of that type of source as a quantitative tool was feasible.

A low-pressure version of a Beenakker source was constructed by simply terminating a standard low-power Beenakker plasma tube with a tee fitted with a quartz window and a vacuum port. In that geometry, the quartz window was sufficiently far removed from the plasma region that fogging and tube erosion were not problems and the optical geometry was otherwise identical to that of an atmospheric-pressure source. This paper details the operating characteristics of a low-pressure Beenakker plasma source and discusses its application to determination of empirical formulae.

EXPERIMENTAL

Instrumentation

The configuration of the low-pressure Beenakker MIP source is depicted in Fig. 1. Carrier gas flow and scavenge gas mixture were controlled by a Matheson SP-760 Dyna-Blender dual-channel mass flow controller (Matheson, East Rutherford, NJ). The cavity was supplied by Scientific Equipment Services (Bancroft, Milton Keynes, United Kingdom).

Two spectrometers were used. Initially, the Beenakker source was mounted on a Spectraspan IIIB spectrometer (Beckman Instruments, Irvine, CA). The Spectraspan is an ultrahigh-resolution, 0.75-m echelle spectrometer equipped with an exit aperture cassette and matching photomultiplier tubes (Hamamatsu R268, R292, and R374 end-window phototubes) aligned for 20 emission lines specifically chosen for use with a helium MIP source. Wavelengths used in this study were as follows: carbon, 247.9 nm; hydrogen, 656.1 nm; sulfur, 545.4 nm; nitrogen, 746.9 nm; chlorine, 479.5 nm; helium, 388.9 nm; and silicon, 251.6 nm.

Most of the results presented here were obtained with the echelle spectrometer. For the empirical formulae work, the source was remounted on an

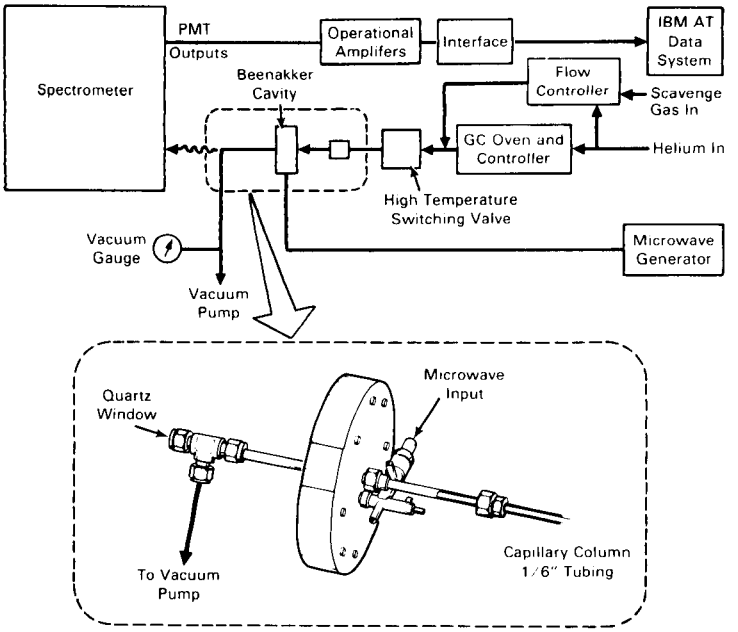

Fig. 1. Experimental configuration of low-pressure Beenakker MIP source.

MPD-850 spectrometer (Applied Chromatography Systems, Luton, United Kingdom), an instrument with lower resolution providing better optical stability. The MPD-850 spectrometer is a 0.75-m direct-reading, multichannel optical emission spectrometer with secondary slits and phototubes (IP28 and R446) for 12 elemental lines distributed about the Rowland circle. The wavelengths of the lines of interest in this study were the same for both the echelle and MPD-850 spectrometers. Both systems were equipped with identical microwave generators (Applied Chromatography Systems). The microwave generators were operated at 2450 MHz over a range of 15 to 115 W.

A common data-acquisition system was used either simultaneously or alternately for both systems. The system consists of five operational amplifiers with outputs connected to three Nelson Analytical Model 763S Dual-Channel Intelligent Interfaces (Nelson Analytical, Cupertino, CA). Chromatograms were stored in the interface for the duration of each run. Each interface is capable of storing up to 100 000 data points with a linear dynamic range of six decades. Data were acquired at a rate of 10 points per second per channel. At the end of each run (20 min at 20°C min^{-1} or 30 min at 10°C min^{-1}), data were automatically transferred to an IBM-AT computer and stored on a 20-megabyte hard disk. Data display and integration were done with the Nelson 3000 Series software package. Helium and silicon line intensities were monitored on the echelle system directly at the phototube output using Keithley picoammeters (Keithley Instruments, Cleveland, OH).

With the exception of the solvent venting system, both systems had identical chromatographic systems consisting of HP-5880A (Hewlett-Packard) gas chromatographs (GC) equipped with splitless injectors. The GC on the echelle system was equipped with an air-actuated, four-port, zero dead-volume solvent venting valve (Valco Instruments Co., Houston, TX) operated under control of the GC program. The venting valve was omitted from the MPD-850 GC system in order to simplify system set-up. The connection between the capillary column and the venting valve is particularly delicate and a source of serious maintenance problems.

Both systems included identical transfer lines consisting of 25-cm lengths of stainless steel tubing (1.6-mm o.d., 0.5-mm i.d.). The capillary columns were threaded through the tubing into the plasma tube to within a few millimeters of the active region. The capillary column should be positioned as closely as possible to the plasma to minimize loss of resolution caused by dead volume in the plasma tube. Particular care was taken to ensure that the plasma did not actually contact the capillary column, because it could fuse the end of the column. Gas was introduced into the transfer line through a Swagelok tee inside the GC oven. The transfer lines were resistively heated by direct connection of low-voltage, high-current power supplies. All seals, including those to the inlet and outlet of the quartz plasma tube and the GC capillary column, were made with Swagelok fittings with graphite ferrules.

Materials

Chromatographic separations were achieved with 30-m (0.25-mm i.d., 1-μm thick film) bonded phase DB-5 (1% vinyl, 5% phenylmethyl polysiloxane) fused silica capillary columns (J & W Scientific, Rancho Cordova, CA). Ultrahigh-purity helium (Liquid Air Corporation, San Francisco, CA) used as carrier gas was further purified by passage over a liquid nitrogen-cooled molecular sieve and supplied to both the MIP and the GC from a single source. Scavenging gas was either research-grade oxygen (Industrial Gas Division, Air Products and Chemicals, Tamaqua, PA) or hydrogen produced electrolytically by a hydrogen generator (General Electric Company, Aircraft Equipment Division, Willmington, MA). Quartz plasma tubes (150-mm long, 7.4-mm o.d., 1.4-mm i.d.) were supplied by Applied Chromatography Systems.

Sources of chemicals were: anthracene, n-decane, 1,3,5-trithiane, and 1-octanethiol (Chem Services, West Chester, PA); 2-methylthiophene, benzothiophene, dibenzothiophene, and thianthrene (Aldrich Chemical Co.); atrazine (Supelco., Bellefonte, PA); and n-hexylbenzene, n-tetradecane, n-docosane, n-hexacosane (Alltech Associates, Deerfield, IL). Chromatography-grade distilled-in-glass dichloromethane (Burdick and Jackson, Muskegon, MI) was used as the solvent in all cases.

Procedures

All heated parts of the assembled system were heated overnight or longer at 325°C. The helium and oxygen lines were purged repeatedly at high flow

rates to remove air. Plasmas were ignited with a Tesla coil. The plasma source on the solvent-vented system was operated continuously after start-up. The source on the unvented system (MPD-850) was ignited 2.5 min after injection. Stabilization occurred very rapidly at low pressure. The first set of experiments was done with the 388.8-nm helium line monitored for effects of varying different plasma parameters sequentially while holding the others constant. Parameters varied included forward power, helium flow rate, plasma pressure, and scavenger flow for both oxygen and hydrogen. Plasma pressure was measured at the outlet of the plasma tube with a precision pressure gauge (0—1500 torr absolute; Heise, Newtown, CT). The pressure was controlled by throttling the vacuum pump with a ball valve while maintaining a constant helium carrier flow rate of 50 ml min^{-1}. The intensity for the 251.6-nm silicon line was monitored as a function of scavenger flow rate for both oxygen and hydrogen; carrier-gas flow rate was held constant at 50 ml min^{-1} at 20 torr and at a power level of 75 W.

Background signals were measured as a function of power level for carbon, chlorine, hydrogen, and nitrogen. These measurements were done by connecting a digital voltmeter to the outputs of the respective operational amplifiers. Elemental response factors were measured by repeated injections of an atrazine standard ($C_8H_{14}N_5Cl$) as a function of power level, helium flow rate, and scavenger flow rate. Appropriate increments of power, or carrier or scavenger flow rates were made while other conditions were held constant at 75 W power, 50 ml min^{-1} carrier flow rate, or 0.2% oxygen scavenger depending on the individual experiment. Chromatographic conditions were as follows: splitless injection; injector temperature, 250°C; hold at 40°C for 1 min; temperature program at 20°C min^{-1} to 300°C and hold at 300°C for 6 min. The atrazine solution was 400 μg ml^{-1} in dichloromethane. All injections were as close as possible to 1 μl. For plotting purposes, the data were renormalized to 1-μl volumes using the amounts injected. The same data were used to calculate elemental response ratios by dividing by the appropriate data for carbon. The data were also used to calculate effective signal-to-background ratios by dividing one set of renormalized results by the other for each element. The units of signal-to-background are thus arbitrary and dependent on gain but serve to demonstrate relative effects.

Based on results obtained above, the following were the standard operating conditions used for the remaining experiments: 70 W forward power, 20 torr pressure, 50 ml min^{-1} carrier flow, and 0.2% oxygen scavenger flow.

Various sulfur-containing compounds were carefully selected from the inventory available at this laboratory, and their retention times were measured. Some hydrocarbons, both aromatic and aliphatic, were also selected to serve as reference peaks. The compounds studied included 2-methylthiophene, n-decane, octanethiol, benzothiophene, n-hexylbenzene, 1,3,5-trithiane, n-tetradecane, dibenzothiophene, anthracene, n-eicosane, thianthrene, n-docosane, and n-hexacosane. Considerations involved in the choice of compounds included purity, stability, chromatographic separation from other

compounds, and diversity of compound types. An effort was made to provide a sufficiently large number of compounds in a single chromatogram so that comparisons could be made on an internal-standard basis for both similar and dissimilar types of compound.

A mixture of the selected compounds was prepared by weighing into a 10-ml volumetric flask and diluting to volume with dichloromethane. The concentrations in the stock solution were 0.8—1.5 mg ml^{-1} per compound. All subsequent measurements were made on freshly prepared dilutions of the stock solution. A representative chromatogram of a 5-fold dilution of the stock solution is given in Fig. 2; chromatographic conditions were as described above. The broad baseline feature in the hydrogen chromatogram could be minimized but not eliminated by repeated baking of the system. Because the hump was not present in the carbon channel, it was apparently caused by

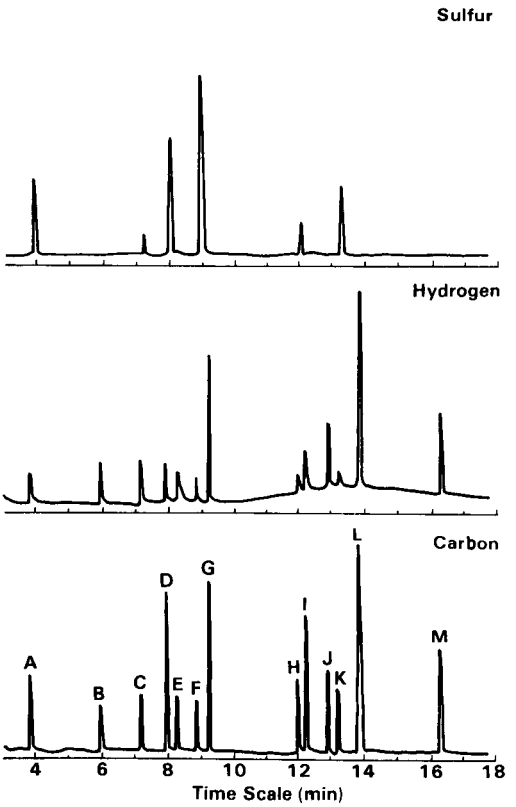

Fig. 2. Multi-element chromatogram for carbon, hydrogen, and sulfur channels; 1-μl injection of sulfur/hydrocarbon mixture; temperature program rate of 20°C min^{-1} to 300°C. Concentrations were 160—320 μg ml^{-1} in dichloromethane: (A) 2-methylthiophene; (B) n-decane; (C) octanethiol; (D) benzothiophene; (E) n-hexylbenzene; (F) 1,3,5-trithiane; (G) n-tetradecane; (H) dibenzothiophene; (I) anthracene; (J) n-eicosane; (K) thianthrene; (L) n-docosane; (M) n-hexacosane.

water. This behavior was essentially absent on the MPD-850 system after prolonged conditioning at 325°C.

To determine the linear range of the system, a series of two-fold dilutions of the stock solutions was used, starting with the stock solution and continuing to a 128-fold dilution. All injections were renormalized to 1 μl. Chromatographic and plasma conditions were held constant as described above. Peak areas determined by the computer system were used as response factors. These data were also used to test the constancy of ratios of response factors for hydrogen vs. carbon and hydrogen vs. sulfur as a function of concentration.

A 5-fold dilution of the stock solution was used to calculate empirical formulae. To improve chromatographic resolution and resulting integration accuracy, the temperature program was decreased to 10°C min^{-1}. To minimize optical drift, the inlet slit was increased from its normal setting of 50 μm to 200 μm. Four injections were made under identical conditions with elemental responses obtained as peak areas. Peak height was also tested but was found to give somewhat poorer precision. The source was then moved to the MPD-850 system. The system was baked and retention times were measured for the 10°C min^{-1} program rate. Four injections of the 5-fold dilution were made and treated in the same manner as described above. Element-to-carbon ratios, R, were computed for each peak in the eight chromatograms according to the expression:

$$R = (E_u/C_u)\,(C_r/E_r)\,(n_E/n_C)$$

where E and C are the responses for the element of interest, i.e., sulfur or hydrogen, u and r represent unknown and reference, and n is the number of atoms in the reference.

Tetradecane was used as the internal reference for the hydrocarbons and 2-methylthiophene was used as the reference for the sulfur compounds. All other compounds were treated as unknowns. For the sulfur compounds, the carbon number could be calculated by adjusting the sulfur number to be a whole integer and taking the reciprocal of the above expression. The hydrogen number was then calculated by multiplying the hydrogen-to-carbon ratio by the calculated carbon number. In most cases, the molecular formulae could be inferred from the empirical formulae by reference to the peak retention time, thus allowing differentiation between, for example, a C_6 and a C_{12} compound. This procedure does break down when the sulfur-to-carbon ratio is close to unity as is the case with trithiane. For the hydrocarbons and trithiane, it was assumed that the carbon number is known for the calculation of the hydrogen number.

RESULTS AND DISCUSSION

Initial experience with the low-pressure Beenakker source was encouraging. Plasma ignition with a Tesla coil is simple and reliable. After ignition, the plasma stabilizes very rapidly requiring no retuning after its initial set-up.

Reflected power levels are quite low and stable. Tube erosion was not detectable after several weeks of operation, although there was some noticeable discoloration. Tolerance to a wide range of operating parameters was remarkable. The plasma remained ignited over the entire operating range of the microwave generator (15—115 W). Temporary substitution of a different microwave generator (Model 420B, Micro-Now Co., Chicago, IL) demonstrated that this range could be extended up to at least 400 W without difficulty. A similarly wide range of gas flow rates and pressures was tolerated (25—1000 ml min^{-1} and 2—700 torr, respectively). The wide operating range suggested that it should be possible to find a set of optimal conditions providing adequate plasma stability to determine empirical formulae. Imprecision of about 0.5% for elemental ratios would be required if the technique were used for primary identification of compounds based on empirical formulae. Hagen et al. [13] demonstrated that such a level of precision is possible for Cl/C ratios using an Evenson source, while Uden et al. [14] obtained similar results for H/C ratios determined with an atmospheric-pressure Beenakker source. Direct-inlet experiments with the low-pressure Beenakker source showed that a long-term imprecision of 0.6% was attainable for hydrogen-to-carbon ratios. Determination of accurate empirical formulae over a wide variety of conditions will require that the ratio be invariant with compound type and analyte amount; previous studies shed little light on that subject. This work suggests that some correction factors may be needed.

Plasma optimization

Measurements for plasma optimization were made by monitoring the 388.8-nm He I line. The relative intensity of this line should reflect the excitation temperature of the plasma. Strong excitation of helium should thus be indicative of strong analyte excitation. Figure 3 shows the effect of differing power levels and helium gas flows on the He I line intensity. The line intensity vs. power relationship is approximately linear with power up to about 40 W where it begins to become flat; between 60 and 110 W, the line intensity increases only about 25% for a power increase of almost 100%. Helium line intensity was only weakly dependent on flow rate, decreasing by only about 50% in response to a factor of 10 increase in flow rate. By contrast, the intensity was markedly affected by pressure (see Fig. 3). All subsequent work was done at a plasma pressure of 20 torr.

Helium line intensity was also studied as a function of percentage of scavenger gas added to the carrier flow for both hydrogen and oxygen. For both gases, intensity decreased rapidly with the addition of scavenger gas, implying that the amount of gas added should be held to the minimum needed to prevent carbonization of the plasma tube. The Si I line was also monitored to test the effect of the addition of scavenger gas on the intensity of the silicon line; the line intensity was barely detectable above background at low pressure with an oxygen scavenger but increased significantly with added hydrogen. This is of interest because it provides a measure of the rate

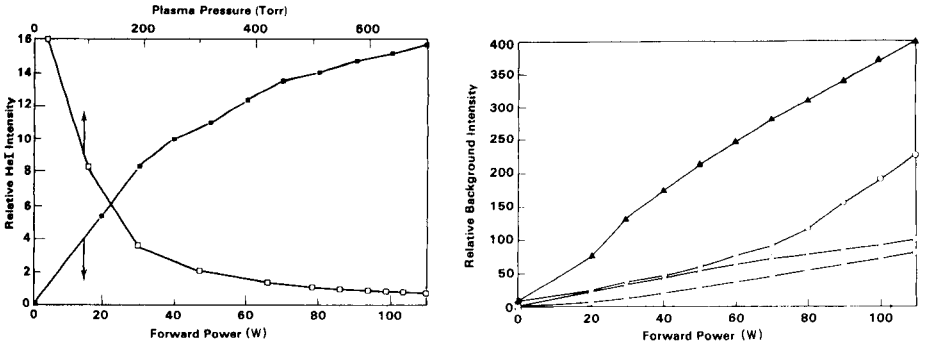

Fig. 3. Intensity of helium I line (388.8 nm) vs. forward power to the plasma (■) and plasma pressure (□).

Fig. 4. Relative background signal as a function of plasma power for: (□) carbon; (○) hydrogen; (△) chlorine; (▲) nitrogen.

of tube erosion. The low-pressure Beenakker source showed no appreciable physical evidence of tube erosion even after more than a month of daily operation with a 0.2% oxygen scavenger. This observation is in contrast to our earlier experience with various configurations of atmospheric-pressure Beenakker-type sources.

Figure 4 shows a plot of background vs. power level for the lines of carbon, hydrogen, nitrogen and chlorine. Sulfur is not plotted but behaved in a manner similar to chlorine for which background signals derive primarily from continuum emission. Carbon, hydrogen, and nitrogen have small internal background contributions that are difficult to eliminate. Elemental responses as functions of power level are plotted in Fig. 5, from the areas for atrazine calculated by the computer system. The behavior is complex at low power with an approximately linear increase above 40 W, except for hydrogen, which shows an apparent dip above 80 W. This behavior is better illustrated in Fig. 6, where the same data in the form of elemental ratios show an apparent dip in the hydrogen-to-carbon ratio above 80 W, which appears to be significant within the level of precision of the data. From these data, it is concluded that the most favorable operating power is between 60 and 75 W. Slight variations in plasma power regulation should have little influence on the precision of elemental ratios in that range.

Varying the helium flow rate at a constant power of 75 W resulted in a sharp decrease in sensitivity between 25 and 50 ml min^{-1} caused by dilution effects. The effect on elemental ratios is shown in Fig. 7. A flow rate of 50 ml min^{-1} was chosen as a trade-off between sensitivity and stability; however, at higher flows (i.e., above 100 ml min^{-1}), elemental response ratios appear to be essentially independent of flow rate. For the determination of empirical formulae, it may be desirable to sacrifice some sensitivity to improve precision.

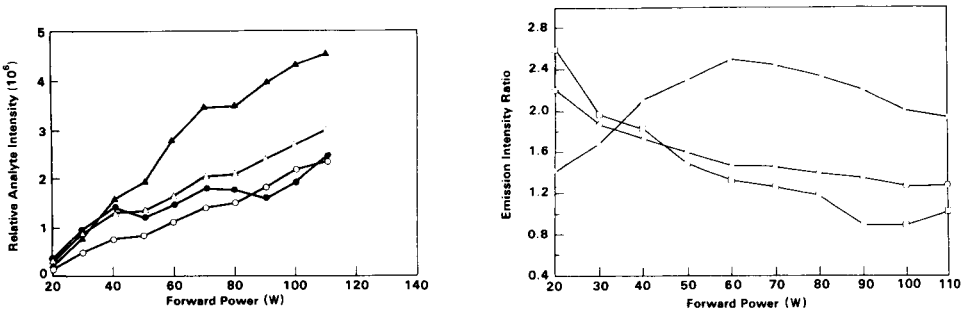

Fig. 5. Relative analyte response factors as a function of plasma power for: (○) carbon; (●) hydrogen; (△) nitrogen; (▲) chlorine. (1-μl injection of 400 μg ml^{-1} atrazine standard.) Nitrogen data are multiplied by 10 to plot on the same scale.

Fig. 6. Elemental response ratios for hydrogen (□), nitrogen (○), and chlorine (△) normalized to carbon and plotted vs. plasma power for 1-μl injections of 400 μg ml^{-1} atrazine standard. Nitrogen data are multiplied by 10 to plot on the same scale.

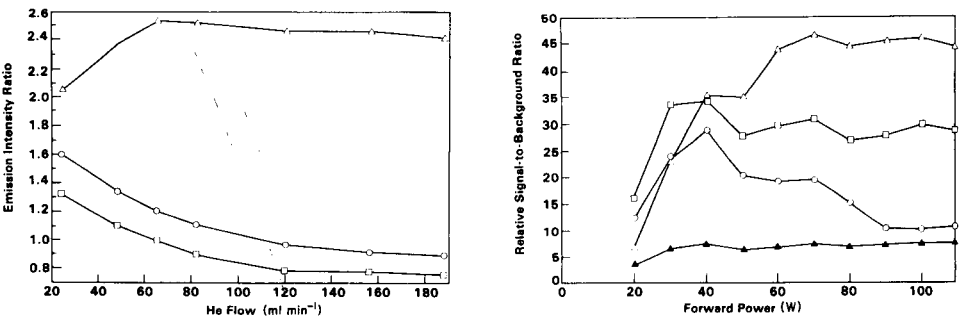

Fig. 7. Elemental response ratios for hydrogen (□), nitrogen (○), and chlorine (△) normalized to carbon and plotted vs. helium flow rate for 1-μl injections of 400 μg ml^{-1} atrazine standard. Nitrogen data are multiplied by 10 to plot on the same scale.

Fig. 8. Signal-to-background ratios for nitrogen (▲), hydrogen (○), carbon (□), and chlorine (△) vs. forward power for 1-μl injections of 400 μg ml^{-1} atrazine standard. Units are arbitrary and provide only a relative scale.

The elemental response data were combined with the background data discussed above to calculate a relative signal-to-background ratio for various conditions. The signal-to-background ratio is plotted vs. forward power in Fig. 8. Interestingly, the ratio appears most favorable for carbon and hydrogen at relatively low power (40 W). The ratio peaks at around 70 W for chlorine and remains constant thereafter. For nitrogen the ratio is relatively flat and lower than for the other elements. A power setting of 70 W was used for

all subsequent experiments. Signal-to-background ratio was also studied as a function of helium flow rate. Largest ratios were observed at very low flow rates. This observation is consistent with the expectation that dilution effects associated with increased helium flow rate should reduce sensitivity. The effect is least pronounced for nitrogen, which has the greatest internal background caused by air contamination. In that case, background and signal are diluted almost equally. A flow of 50 ml min^{-1} was confirmed as a compromise between sensitivity and stability although, as previously discussed, a two-fold higher flow may have advantages when empirical formulae are to be determined.

Elemental responses and response ratios were also studied as a function of scavenger flow. Sulfur and nitrogen sensitivities showed little effect; carbon and hydrogen showed a small decrease up to 2% oxygen; the chlorine response showed considerable sensitivity to scavenger flow rate. The hydrogen-to-carbon ratio appeared to be rather erratic when the scavenger flow rate was increased. All subsequent work was done at 0.2% oxygen, which appeared to be adequate to prevent carbonization of the tube. A hydrogen scavenger can be used at the same levels for alternative applications involving elements that form nonvolatile oxides, such as Hg, As, and P [15].

Dynamic range

Several experiments were done with serial two-fold dilutions (1- to 128-fold) of the 1 mg ml^{-1} stock solution of the sulfur/hydrocarbon mixture described above. The 128-fold dilution was still well above the detection limit for all three elements. A typical calibration curve, including the least-squares line, is given in Fig. 9. The carbon and hydrogen plots were similar; compounds used for these plots included three sulfur heterocyclic compounds and an aliphatic hydrocarbon. Five sulfur-heterocyclic compounds were used for the plot shown in Fig. 9. When plotted on linear coordinates, some curvature was evident for all three elements at high concentrations; this may be the result of resonance absorption, which would be a disadvantage of the axial geometry, but it may simply be due to chromatographic overload.

The same data were used to test the constancy of elemental ratios at various concentrations. The data for the hydrogen-to-carbon ratio are shown in Fig. 10 for a single compound (n-decane). Other compounds, including the heterocycles, exhibited similar behavior. The plot shows some dependence on analyte level, even at relatively low concentrations. It is clear that some correction based on the measured carbon level is needed. In contrast, the plot for the sulfur-to-carbon ratio (Fig. 10) is quite flat, except at the highest level.

Empirical formulae

Two sets of experiments were conducted to estimate the reproducibility of empirical formulae calculated from the element response ratios (see Table 1). The results for the MPD-850 system are slightly more accurate than those

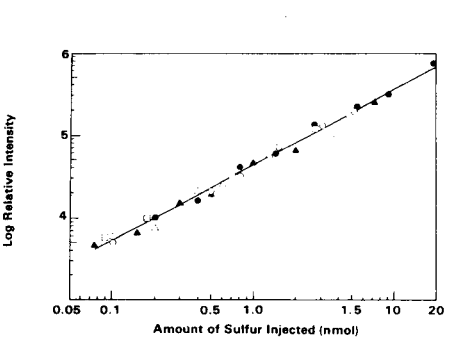

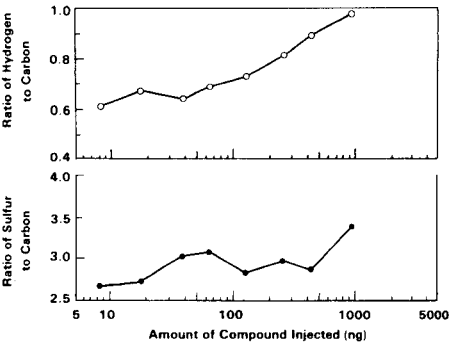

Fig. 9. Calibration plot for sulfur response as a function of the amount of the element injected for five selected compounds: (▲) dibenzothiophene; (○) 2-methylthiophene; (●) trithiane; (△) thianthrene; (□) benzothiophene. (——) Regression line.

Fig. 10. Hydrogen-to-carbon and sulfur-to-carbon ratios plotted vs. total amount of compound injected. Data are for 1-μl injections of serial two-fold dilutions of n-decane and 2-methylthiophene in dichloromethane.

TABLE 1

Empirical formulae found with the echelle and MPD-850 systems

Compound	Empirical formula		
	True	Echelle	MPD-850
n-Decane	$C_{10}H_{22}$	$C_{10}H_{21.5}$	$C_{10}H_{22.1}$
n-Hexylbenzene	$C_{12}H_{18}$	$C_{12}H_{15.8}$	$C_{10}H_{17.5}$
Anthracene	$C_{14}H_{10}$	$C_{14}H_{8.8}$	$C_{14}H_{11.1}$
n-Eicosane	$C_{20}H_{42}$	$C_{20}H_{44.7}$	$C_{20}H_{42.6}$
n-Docosane	$C_{22}H_{46}$	$C_{22}H_{46.2}$	$C_{22}H_{46.2}$
n-Hexacosane	$C_{26}H_{54}$	$C_{26}H_{52.9}$	$C_{26}H_{54.2}$
1,3,5-Trithiane	$C_3H_6S_3$	$C_{2.8}H_{5.0}S_3$	$C_{2.9}H_{5.0}S_3$
Thianthrene	$C_{12}H_8S_2$	$C_{12.1}H_{7.3}S_2$	$C_{12.1}H_{7.4}S_2$
Dibenzothiophene	$C_{12}H_8S$	$C_{11.4}H_{7.8}S$	$C_{12.1}H_{7.8}S$
Octanethiol	$C_8H_{18}S$	$C_{8.0}H_{16.3}S$	$C_{8.4}H_{18.5}S$
Benzothiophene	C_8H_6S	$C_{7.9}H_{6.0}S$	$C_{8.1}H_{6.0}S$

found by using the echelle spectrometer. The poorer precision obtained with the echelle system appears to result from wavelength drift caused by the use of an aluminum base and poor thermal isolation in the echelle spectrometer. For the hydrocarbon data, agreement was excellent for the MPD-850 system but only fair for the echelle system. Precision (see Figs. 11 and 12) was somewhat worse than expected for both sets of data. The hydrogen-to-carbon ratios for the sulfur compounds are somewhat less precise than those for the pure hydrocarbons (Fig. 12). Subtle compound-specific effects may be present that affect the accuracy of the elemental ratios.

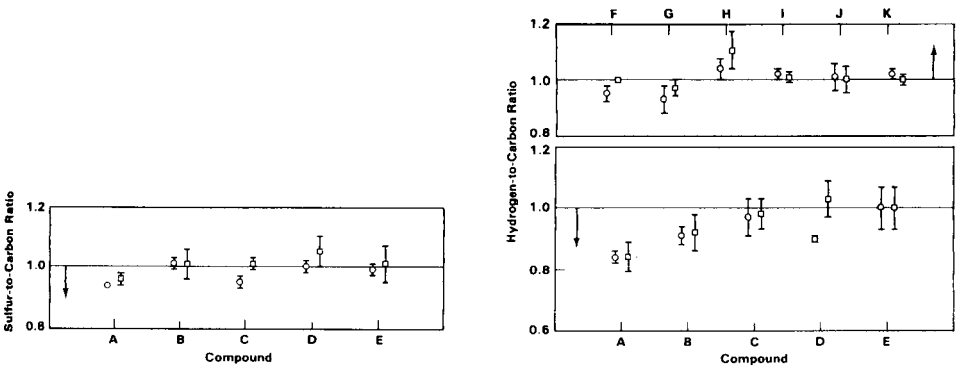

Fig. 11. Measured sulfur-to-carbon ratios normalized to the known value for each sulfur compound: (A) trithiane; (B) thianthrene; (C) dibenzothiophene; (D) octanethiol; (E) benzothiophene. Averages and standard deviations (n = 4) for the echelle (○) and MPD-850 (□) configurations. 2-Methylthiophene served as internal standard.

Fig. 12. Measured hydrogen-to-carbon ratios normalized to the known value for each compound: (A) trithiane; (B) thianthrene; (C) dibenzothiophene; (D) octanethiol; (E) benzothiophene; (F) n-decane; (G) n-hexylbenzene; (H) anthracene; (I) n-eicosane; (J) n-docosane; (K) n-hexacosane. Averages and standard deviations (n = 4) for the echelle (○) and MPD-850 (□) configurations. N-Tetradecane served as internal standard.

It should be possible to obtain 1% or better precision by internal standardization. This has already been demonstrated in a series of recent publications [14, 16, 17]. That level of precision was adequate to distinguish between alkanes and alkenes. Precision and accuracy were less favorable for chloride-to-carbon ratios measured by Uden et al. [14]. By contrast, Hagen et al. [13] were able to obtain a precision for chloride-to-carbon ratios in the range 0.1—2%, using an MPD-850 system equipped with a 1/4-wave low-pressure Evenson source but relatively poor precision for hydrogen-to-carbon ratios. The results of those studies, as well as the present work, suggest that MIP detection is useful for determination of empirical formulae but that additional work is needed to identify and correct sources of error.

The authors thank Dr. Stuart Scheppele for his support and interest in this study. Thanks are also given to Art Graf for instrumentation support and Mindy Strong for technical editing assistance. This study was supported by the U.S. Department of Energy through contract DE-AC06-76RLO 1830.

REFERENCES

1 A. J. McCormack, S. C. Tong and W. D. Cooke, Anal. Chem., 37 (1965) 1470.
2 D. L. Windsor and M. B. Denton, J. Chromatogr. Sci., 17 (1979) 492.
3 D. Sommer and K. Ohls, Fresenius' Z. Anal. Chem., 295 (1979) 337.
4 R. J. Lloyd, R. M. Barnes, P. C. Uden and W. G. Elliott, Anal. Chem., 50 (1978) 2025.
5 J. Hubert, M. Moisan and A. Ricard, Spectrochim. Acta, Part B, 33 (1979) 1.

6 G. W. Rice, A. P. D'Silva and V. A. Fassel, Spectrochim. Acta, Part B, 40 (1985) 1573.
7 R. M. Dagnall, S. J. Pratt, T. S. West and D. R. Means, Talanta, 17 (1970) 1009.
8 C. I. M. Beenakker, Spectrochim. Acta, Part B, 31 (1976) 483.
9 C. I. M. Beenakker, Spectrochim. Acta, Part B, 32 (1977) 173.
10 J. P. J. van Dalen, P. A. de Lezenne Coulander and L. de Galan, Spectrochim. Acta, Part B, 33 (1978) 545.
11 S. R. Goode, B. Chambers and N. P. Buddin, Spectrochim. Acta, Part B, 40 (1985) 329.
12 S. R. Goode, N. P. Buddin, B. Chambers, K. W. Baughman and J. P. Deavor, Spectrochim. Acta, Part B, 40 (1985) 317.
13 D. F. Hagen, J. S. Marhevka and L. C. Haddad, Spectrochim. Acta, Part B, 40 (1985) 335.
14 P. C. Uden, K. J. Slatkavitz, R. M. Barnes and R. L. Deming, Anal. Chim. Acta, 180 (1986) 401.
15 K. B. Olsen, D. S. Sklarew and J. C. Evans, Spectrochim. Acta, Part B, 40 (1985) 357.
16 K. J. Slatkavitz, L. D. Hoey, P. C. Uden and R. M. Barnes, Anal. Chem., 57 (1985) 1846.
17 P. C. Uden, H. J. Perpall and Y. J. Yoo, Proceedings of the 1986 Winter Conference on Plasma Spectrochemistry, January 1986, p. 88.

Analytica Chimica Acta, 194 (1987) 261—268
Elsevier Science Publishers B.V., Amsterdam — Printed in The Netherlands

SUBSTOICHIOMETRIC ISOTOPE-DILUTION ANALYSIS FOR STRONTIUM BY LIQUID-LIQUID EXTRACTION WITH A MACROCYCLIC CROWN ETHER OR CRYPTAND

NOBUO SUZUKI*, TOMOKO FUKAYA and HISANORI IMURA
Department of Chemistry, Faculty of Science, Tohoku University, Sendai 980 (Japan)
(Received 4th September 1986)

SUMMARY

Strontium(II) is substoichiometrically extracted into 1,2-dichloroethane with 1.0×10^{-4} M cryptand-2.2.2 or 18-crown-6 in the presence of 1.0×10^{-2} M picrate at pH 8—10 or 7—9, respectively. A constant substoichiometric amount of strontium(II) is extracted (relative standard deviation, 0.5%). The method combined with isotope dilution is applied to determine strontium(II) in a seaweed sample (*Laminaria religiosa* Miyabe); the values obtained were 546 ± 9 $\mu g\ g^{-1}$ with cryptand-2.2.2 and 546 ± 7 $\mu g\ g^{-1}$ with 18-crown-6.

Substoichiometric isotope-dilution analysis can provide very high accuracy and precision. The method does not require quantitative recovery of the element of interest from a sample matrix, and the determination can be made by measuring only the radioactivity of the substoichiometric extract without comparison with a standard. In recent reviews [1—3], only one reference to a substoichiometric determination of strontium, by 8-quinolinol extraction, is cited [4]. Macrocyclic crown ethers and cryptands are effective organic reagents for alkali and alkaline earth ions. Strontium ion would be expected to form stable complexes with 18-crown-6 and cryptand-2.2.2 if its ionic diameter (2.32 Å) [5] is compared with the cavity diameters of these reagents, 2.9 ± 0.3 Å for 18-crown-6 [6] and 2.8 Å for cryptand-2.2.2 [7]. The extraction of Sr^{2+} with 18-crown-6 and picrate as counter anion into benzene has been investigated [8] but not with cryptand-2.2.2.

In the present paper, the extraction of Sr^{2+} with 18-crown-6 and cryptand-2.2.2 into 1,2-dichloroethane is examined for several counter anions. Then the substoichiometric extraction of Sr^{2+} with a substoichiometric amount of 18-crown-6 or cryptand-2.2.2 in the presence of an excess of picrate is investigated in detail. The method is applied to the determination of strontium in a seaweed sample.

EXPERIMENTAL

Reagents and apparatus

A radioisotope, ^{85}Sr, was produced from rubidium chloride (Merck, Suprapur) by the (p,n) reaction with 18-MeV protons in the Tohoku Uni-

0003-2670/87/$03.50

versity Cyclotron and Radioisotope Center. After proton bombardment, the target was dissolved in 9 M hydrochloric acid, fed into a cation-exchange column (Dowex 50W-X8; 1.2-cm inner diameter, 20 cm high), and eluted with 9 M hydrochloric acid. After elution of the rubidium fraction containing the radioactive byproduct of ^{86}Rb, carrier-free ^{85}Sr was eluted with a 4 M hydrochloric acid and the effluent was evaporated to dryness. The residue was heated with concentrated nitric acid to decompose organic impurities completely and then evaporated to dryness. The ^{85}Sr was redissolved in 0.01 M hydrochloric acid. Its radiochemical purity was checked with a Ge(Li) detector connected with a multichannel analyzer.

A standard solution of strontium (2.016 g l^{-1}) was prepared from strontium nitrate (Merck, Suprapur). The radioactive Sr^{2+} working solution was prepared by adding a few drops of the carrier-free ^{85}Sr solution to an aliquot of the standard solution before dilution to a suitable exact volume.

18-Crown-6 and cryptand-2.2.2, both from Merck, were used as received. 1,2-Dichloroethane was washed with redistilled water. A tetramethylammonium hydroxide solution (Merck) was standardized with potassium hydrogenphthalate and used to adjust the pH of the aqueous phases. Other reagents were of analytical-reagent grade and were used as obtained.

The seaweed examined was brown algae (*Laminaria religiosa* Miyabe), collected in Onagawa, Miyagi, and immediately frozen at −20°C. It was dried by lyophilization for 48 h and powdered. The sample was dried for 2 h at 85°C before use.

The γ-activity of ^{85}Sr was measured with an NaI(Tl) well-type scintillation counter. The equilibrium pH value of aqueous phases was measured with a glass electrode.

General extraction procedure for strontium(II)

A 5-ml portion of an aqueous solution (pH 1—13) containing 5×10^{-5}—3×10^{-4} M radioactive Sr^{2+} and 1×10^{-3}—1×10^{-2} M picric acid was placed in a 30-ml extraction vial with a fitted cap. A 5-ml portion of a 1×10^{-4}—1×10^{-3} M solution of cryptand or crown in 1,2-dichloroethane was added and shaken for 30 min. After centrifugation, the γ-activity of each phase was measured.

Recommended procedure for the substoichiometric isotope-dilution method

About 1 g of a dry sample of seaweed was weighed into a decomposition vessel and a known amount of radioactive Sr^{2+} was added. Then concentrated nitric acid and 30% hydrogen peroxide (each about 10 ml) were added, heated until a clear solution was obtained, and evaporated to dryness. The residue was dissolved in 2 ml of 4 M hydrochloric acid, and 2 ml of 5×10^{-2} M tartaric acid, 3 ml of 0.8 M ammonium acetate, and 25 ml of water were added. After addition of 5 ml of 0.3 M ammonium oxalate, aqueous 2.5 M ammonia was added dropwise to adjust the pH to 4—5 while the solution was heated. The oxalate precipitate of strontium and calcium was separated

by centrifugation and washed with water. It was dissolved in 4 M hydrochloric acid and reprecipitated as the oxalate; if necessary, this procedure was repeated. Then the precipitate was dissolved with concentrated nitric acid and evaporated to dryness to produce the nitrates of strontium and calcium. To the residue was added 0.2 ml of 1:1 (v/v) ethanol/diethyl ether. Calcium nitrate dissolved in the organic solution and was removed. The residue of strontium nitrate was dissolved in 3 ml of water and used for the substoichiometric extraction. To this sample solution, picric acid was added to give a 0.01 M concentration, and the pH value was adjusted to 8—10 for the cryptand and to 7—9 for 18-crown-6 with tetramethylammonium hydroxide. This aqueous solution was shaken for 30 min with an equal volume of a 1,2-dichloroethane solution containing a substoichiometric amount (1×10^{-4} M) of the cryptand or 18-crown-6. The γ-activity of an aliquot of the organic phase was measured.

RESULTS AND DISCUSSION

Extraction of strontium(II) with macrocyclic compounds

Extraction of Sr^{2+} (5.0×10^{-5} M) with 1.0×10^{-3} M cryptand-2.2.2 in 1,2-dichloroethane was investigated in the presence of some counter ions (1.0×10^{-2} M). The log D values with picrate, β-naphthalenesulfonate, and trichloroacetate were 2.20 ± 0.02 at pH 7.36, −1.88 ± 0.01 at pH 7.35 and −2.76 ± 0.06 at pH 7.39, respectively. Picrate was thus effective in this ion-pair extraction system. When the pH was adjusted with sodium hydroxide or ammonia instead of tetramethylammonium hydroxide, the extraction of Sr^{2+} with 1.0×10^{-3} M cryptand and 1.0×10^{-2} M picrate decreased remarkably, the log D value became 0.33 at pH 8.16 adjusted with sodium hydroxide, and −0.76 at pH 9.38 adjusted with ammonia. This decrease is ascribed to association of these alkaline cations with the cryptand [6]. Tetramethylammonium hydroxide is suitable for pH adjustment because the molecule is much larger than the cavity of the cryptand and so there is no specific interaction with cryptand.

The general extraction curves of Sr^{2+} with 1.0×10^{-3} M cryptand or 18-crown-6, which are in excess over Sr^{2+}, in the presence of 1.0×10^{-2} M picrate are shown in Fig. 1. The decrease in the distribution ratios of Sr^{2+} with the cryptand in the lower pH region is attributed mainly to protonation of the cryptand in the aqueous phase. The protonated cryptand is a diprotic acid and has pK_a values of 7.28 and 9.60 [7]. In contrast, appreciable protonation of the crown compound is not plausible in such a pH region, considering the lower basicity of crown. The decrease in the distribution ratio of Sr^{2+} with 18-crown-6 observed in the lowest pH region in this experiment may be attributed to depression of the dissociation of picric acid (pK_a = 0.38 [9]). In the higher pH region, the distribution ratios are independent of pH.

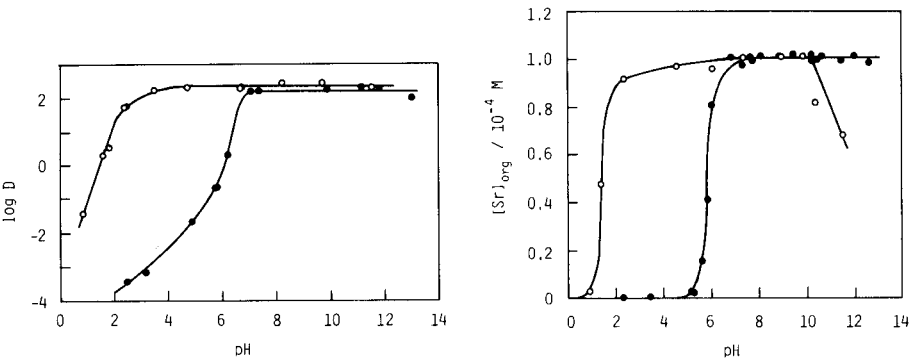

Fig. 1. Extraction of Sr^{2+} (5.0×10^{-5} M) with 1.0×10^{-3} M macrocyclic compound and 1.0×10^{-2} M picrate: (○) 18-crown-6; (●) cryptand-2.2.2.

Fig. 2. Effect of pH on the substoichiometric extraction of Sr^{2+} with the macrocyclic compound in the presence of an excess of picrate: (○) 18-crown-6; (●) cryptand-2.2.2. Conditions: 2.9×10^{-4} M Sr^{2+}, 1.0×10^{-4} M macrocycle, 1.0×10^{-2} M picrate.

Substoichiometric extraction of strontium(II) with macrocyclic extractants

As was previously demonstrated in the substoichiometric extraction of uranium(VI) with a β-diketone and a neutral ligand [10], when a set of two different kinds of reagent is used in the substoichiometric extraction, two types of procedure are possible. In the present ion-pair extraction, one procedure is extraction with a substoichiometric amount of the macrocyclic compound in the presence of an excess of picrate; the other is with a substoichiometric amount of picrate in the presence of an excess of the macrocyclic extractant, but here the former procedure was preferred (Fig. 2). It is clearly seen that a constant amount of Sr^{2+} can be extracted with the same substoichiometric amount of cryptand-2.2.2 or 18-crown-6 at pH 8—10 and 7—9, respectively. The extracted amount of strontium at the plateau region in Fig. 2 is in good agreement with the amount expected from a quantitative 1:1 reaction of strontium with the substoichiometric amount of cryptand or crown compound. The substoichiometric extraction equilibrium was achieved by shaking for 30 min; no change in the strontium concentration in the organic phase was observed from 10 to 240 min for the cryptand and from 5 to 240 min for 18-crown-6. A decrease in the extracted amount of strontium was observed at pH > 10 in the crown system. At such high pH, the total recovery of strontium radioactivity from both phases decreased; this can be ascribed to formation of insoluble strontium carbonate with carbon dioxide in air.

Figure 3 shows the effect of the picrate concentration on the substoichiometric extraction of strontium at a fixed substoichiometric amount of the macrocyclic compound. A constant amount of strontium is extracted over a wide range of picrate concentration: 4×10^{-3}—2.4×10^{-2} M for cryptand-2.2.2 and 8×10^{-3}—2.4×10^{-2} M for 18-crown-6. The extracted amount

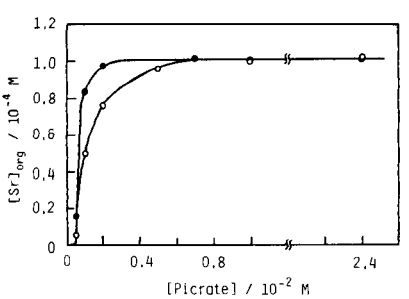

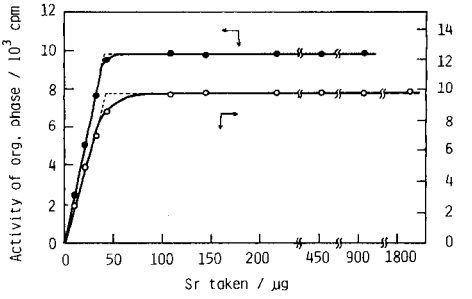

Fig. 3. Effect of picrate concentration on the substoichiometric extraction of Sr^{2+} with the macrocyclic compound: (○) 18-crown-6; (●) cryptand-2.2.2. Conditions: 2.9×10^{-4} M Sr^{2+}, 1.0×10^{-4} M macrocycle, pH 7.3—8.5.

Fig. 4. Precision of the substoichiometric extraction from aqueous solutions (5 ml) containing varying amounts of Sr^{2+}. Conditions: 1.0×10^{-4} M macrocycle, 1.0×10^{-2} M picrate. Symbols as in Fig. 3.

of strontium is in good agreement with the amount expected from the substoichiometric amount of the macrocyclic compound, and this shows that the extraction of strontium with an excess of picrate alone is negligible.

Reproducibility of the substoichiometric extraction

Substoichiometric extractions with 1.0×10^{-4} M cryptand-2.2.2 or 18-crown-6 in the presence of 1.0×10^{-2} M picrate were applied to a series of solutions containing various amounts of radioactive Sr^{2+}. Figure 4 shows that the radioactivity of the organic phase increases with increase in the amount of strontium up to the point corresponding to a 1:1 mole ratio of Sr^{2+} to macrocyclic compound. Beyond this point, i.e., under substoichiometric conditions, a constant amount of strontium is extracted. The precision of the substoichiometric extraction is very high; the relative standard deviation (RSD) for the radioactivities of the organic extracts was 0.42% (n = 5) in the cryptand system and 0.45% (n = 5) in the crown system. Strontium at the ca. 10 μg ml^{-1} level was determined accurately by using these macrocyclic compounds.

Effect of diverse ions

The effect of diverse ions, which may be present in large quantities in biological materials, on the substoichiometric extraction was investigated by adding varying amounts of non-active ions to 5 ml of aqueous solution containing 0.13 mg of strontium. The radioactivities of ^{85}Sr obtained in the presence and absence of the diverse ion were compared. The results are summarized in Table 1. It is obvious that the selectivity in the substoichiometric extraction of strontium with 18-crown-6 is higher than that with cryptand-2.2.2. No significant interference from large amounts of sodium, magnesium or anions was observed in the crown system but, of these ions, sodium caused serious interference in the cryptand system. Large amounts of other

TABLE 1

Effect of diverse ions on the substoichiometric extraction of strontium[a]

Diverse ion	Amount added (mg)	Interference[b] (%)		Diverse ion	Amount added (mg)	Interference[b] (%)	
		Cryptand	Crown			Cryptand	Crown
Na^+	0.013	−5.7	0.1	Ba^{2+}	0.0013	−1.9	−2.2
	0.63	−80.8	1.5		0.005	−7.1	−5.4
K^+	0.013	−51.1	−1.7		0.013	−16.9	−9.6
	0.63	−98.9	−40.5	Cl^-	3.1	−1.1	−1.6
Rb^+	0.13	−70.1	−2.3		16	−4.7	−2.9
Mg^{2+}	0.13	−0.6	−2.0	NO_3^-	3.1	0.8	−0.5
	0.63	1.6	−1.3		16	−2.3	−2.3
	2.50	−1.0	−1.4	SO_4^{2-}	0.13	−0.8	−1.1
Ca^{2+}	0.13	−0.6	−2.1	$C_2O_4^{2-}$	0.13	1.2	−0.6
	0.63	−8.4	−4.0				
	2.50	−53.7	−10.8				

[a]Sr taken, 0.13 mg per 5 ml, [cryptand], 1.1×10^{-4} M; [crown], 1.0×10^{-4} M; [picrate], 1.0×10^{-2} M. [b]Calculated as $100\ (a - a_s)/a_s$, where a is the activity of ^{85}Sr in the presence of the diverse ion and a_s is that in its absence.

alkali and alkaline earth ions, especially barium even in small amounts, interfered seriously. Hence, preseparation of strontium was needed, as mentioned in the experimental section. Alkali and other metal ions, except for Ca^{2+} and Ba^{2+}, can be readily separated by the oxalate precipitation method. In this work, the separation efficiency of Sr^{2+} from Ca^{2+} and Ba^{2+} was examined by using the radiotracers, ^{47}Ca and ^{135m}Ba, which were produced by the photonuclear reaction of the corresponding carbonate salts with 50-MeV bremsstrahlung in the Tohoku University electron linear accelerator. When Sr^{2+} (1 mg) was precipitated as oxalate together with Ca^{2+} (10 mg) in the presence of Ba^{2+}, about 10% of Ba^{2+} was coprecipitated. Then, after the conversion of oxalate to nitrate, about 98% of Ca^{2+} was dissolved with the ethanol/ether solution and removed from the residue of strontium nitrate. The recovery of Sr^{2+} after this preseparation was 55—83%. Because quantitative recovery is not required for final substoichiometric determination, the practical procedure can be greatly simplified.

Determination of strontium by the substoichiometric isotope-dilution method

The accuracy and precision of the method was evaluated by determining strontium in a synthetic mixture containing some interfering ions. The results are shown in Table 2, where the substoichiometric extraction of strontium was done successively from the same aqueous solution obtained after the preseparation. The results obtained from the successive extractions are consistent and there is no interference from the diverse ions. A consistent average value of 1426 μg was obtained with the two macrocyclic extraction systems; this agrees well with the added amount (1411 μg), the relative

TABLE 2

Substoichiometric determination of strontium(II) (1411 μg) in a synthetic mixture containing other alkaline earth metals

Other ions added	Active Sr spike, M_s (μg)	Reagent	No. of extraction[a]	Activity from solution a (cpm)	Sr found[b] (μg)
Mg (18.3 mg)	1209	Cryptand[c]	1	5932	1425
Ca (18.3 mg)			2	5895	1442
Ba (0.037 mg)			3	5964	1411
		Crown[d]	1	6222	1421
			2	6232	1417
			3	6180	1439

[a]Successive substoichiometric extractions are designated as 1, 2, and 3. [b]The amount of Sr found, M_x, is calculated from $M_x = M_s[a_s/a - 1]$. [c]Activity from spike, 12922 cpm (a_s); mean Sr found, 1426 ± 15 μg; RSD, 1.1%; deviation from Sr taken, +1.0%. [d]Activity from spike, 13534 cpm (a_s); mean Sr found, 1426 ± 12 μg; RSD, 0.8%; deviation from Sr taken, +1.0%.

difference being only 1.0%. The present method is thus accurate and precise, and is suitable for real samples.

The proposed method was applied to a seaweed sample, *Laminaria religiosa* Miyabe. The results are shown in Table 3. Two portions of the sample were used after addition of different amounts of radioactive strontium. The results obtained from the successive substoichiometric extractions are consistent. The value obtained with cryptand-2.2.2 (546 ± 9 μg g^{-1}) is in good

TABLE 3

Substoichiometric determination of strontium in a seaweed sample

Sample taken (g)	Active Sr spike (μg)	Reagent	Activity from test solution (cpm)	Sr found (μg g^{-1})
1.0164	907	Cryptand[a]	7962	556
			8063[b]	538
		Crown[c]	8393	547
			8344[b]	555
1.0043	599	Cryptand[d]	5778	552
			5849	538
		Crown[e]	6418	541
			6420	541

[a]Acitivity from spike, 12922 cpm. [b]Successive substoichiometric extraction. [c]Activity from spike, 13534 cpm. [d]Activity from spike, 11122 cpm. [e]Activity from spike, 12238 cpm.

agreement with that obtained with 18-crown-6 (546 ± 7 $\mu g\ g^{-1}$). These results are notably consistent despite the different selectivities for strontium of the two reagents. This consistency indicates that the results are accurate and do not involve error from interfering ions in the sample. The substoichiometric extraction with the cryptand or crown compound in the presence of an excess of picrate can be applied to the determination of strontium in various types of sample.

REFERENCES

1 K. Kudo and N. Suzuki, J. Radioanal. Chem., 59 (1980) 605.
2 K. Kudo and N. Suzuki, Trends Anal. Chem., 3 (1984) 20.
3 G. N. Bilimovich, J. Radioanal. Nucl. Chem., 88 (1985) 171.
4 I. E. Zimakov and V. V. Usatenko, Tr. Vses. Nauch. Issled. Inst. Vet. Sanit., 48 (1974) 144. CA, 86 (1977) 39726s.
5 R. D. Shannon and C. T. Prewitt, Acta Crystallogr., Sect. B, 25 (1969) 925.
6 I. M. Kolthoff, Anal. Chem., 51 (1979) 1R.
7 J. M. Lehn and J. P. Sauvage, J. Am. Chem. Soc., 97 (1975) 6700.
8 Y. Takeda and H. Kato, Bull. Chem. Soc. Jpn., 52 (1979) 1027.
9 R. C. Weast, (Ed.), CRC Handbook of Chemistry and Physics, CRC Press, Cleveland, OH, 1979.
10 N. Suzuki, K. Yoshida and H. Imura, Anal. Chim. Acta, 129 (1981) 221.

Analytica Chimica Acta, 194 (1987) 269—274
Elsevier Science Publishers B.V., Amsterdam — Printed in The Netherlands

Short Communication

FLOW-INJECTION SINGLE-POINT TITRATION OF ACIDS WITH BIAMPEROMETRIC DETECTION AT POLARIZED PLATINUM ELECTRODES

WOJCIECH MATUSZEWSKI, ADAM HULANICKI and MAREK TROJANOWICZ*
Department of Chemistry, University of Warsaw, Pasteura 1, 02 093 Warsaw (Poland)
(Received 18th September 1986)

Summary. Flow-injection single-point titration of acids is based on biamperometric measurement of iodine formed quantitatively in the reaction of iodide with iodate. Results are presented for determination of sulphuric, hydrofluoric, monochloroacetic, formic and acetic acids. The slopes of the calibration plots, which are linear for about 1—10 mM acid, depend on the strength of the acid, decreasing from sulphuric acid to acetic acid. With microcomputer on-line data processing, relative standard deviations were about 0.2%.

One of the attractive possibilities of flow-injection analysis is flow-injection titration with various detection methods. Several papers have been already published on flow-injection acid/base titrations. Růžička and co-workers established appropriate dispersion in flow-injection systems by use of a mixing chamber [1] or a tube reactor [2] for acid/base gradient titrations with spectrophotometric detection. Single-point acid/base titrations, in which the sample is injected into a buffer carrier solution were reported by Åstrom [3] who used potentiometric detection with a glass electrode for titrations of 0.01—0.1 M acids and bases. A similar procedure was used in flow-injection measurements of the pH of soil extracts with a potentiometric detector based on a pH-sensitive PVC membrane tubular electrode [4]. The concept of single-point titration was also utilized by Schick [5] for titrations of alkaline solutions with colorimetric detection and sulphuric acid with potentiometric detection. A gradient titration with a potentiometric detector based on glass and antimony electrodes was reported by Simpson and Holler [6].

In this work, an indirect amperometric detector with two polarized platinum electrodes was applied for detection in single-point flow-injection titrations. This detection system based on the reversible redox couple I_2/I^- has already been utilized in flow-injection determinations of nitrite and nitrate [7] and catalytic determination of molybdenum(VI) [8]. The reaction utilized is

$$IO_3^- + 8I^- + 6H^+ \rightleftharpoons 3I_3^- + 3H_2O \qquad (1)$$

0003-2670/87/$03.50

which proceeds rapidly and is quantitative. It is a classical reaction for the iodimetric titration of acid contents [9] and was recently applied in a flow-injection procedure with an ultraviolet spectrophotometric detector [10].

Experimental

Reagents. A carrier solution containing iodide and iodate of the required concentrations was prepared daily by dissolving appropriate amounts of potassium iodide and sodium iodate. Standard solutions of sulphuric and acetic acid were prepared by dilution of standard volumetric concentrates (POCh, Gliwice, Poland). Solutions of monochloroacetic, formic and hydrofluoric acids were prepared from analytical-grade reagents and standardized by titration with standard sodium hydroxide solution. All solutions were prepared in triple-distilled water.

Apparatus. The measuring system used consisted of a multichannel pump (MP-13GJ-4; Ismatec, Zurich, Switzerland), a home-made rotary injection valve, and a flow cell connected to an a.c./d.c. polarograph (PLP 225C; Cobrabid, Warszawa) which was in turn connected to a potentiograph (E-436; Metrohm, Herisau, Switzerland) used as a strip-chart recorder.

The flow-through cell used was the same as described earlier [7, 8]; the platinum wire electrodes were 0.3 mm in diameter and 8 mm long [7]. A constant polarizing voltage of 100 mV was applied from the polarograph.

The manifold used was made from polypropylene tubing (internal diameter 0.9 mm) with home-made perspex connectors. Samples of acids (15 μl) were injected into a stream of distilled water, which merged with a stream of potassium iodide/sodium iodate solution before the detector inlet. Both solutions were pumped at the same flow rate (2.4 ml min^{-1}). The tube length between the injection and merging points was 5 cm, and the distance between the merging point and the detector was 10 cm.

Microcomputer data processing. Measurements with on-line processing of experimental data were done by using an IMP-86 microcomputer (Impol II, Warszawa), which is compatible with the IBM PC/XT, equipped with 512-Kbyte RAM, 2 floppy-disk drives, 10-Mbyte hard disk, and an Epson GX-80 printer. Voltage output from the polarograph was connected to one of the 16 channels of the 12-bit A/D converter. The main steps of the software are shown in Fig. 1. The program was written in BASIC and used in measurements in a compiler version; details are available from the authors on request.

Results and discussion

As shown earlier [7, 8], biamperometric detection with two platinum electrodes polarized at a small constant voltage provides a linear relationship between the measured current and iodine (triiodide) if enough iodide is present in the solution. Detection limits are in the submicromolar range. That relationship can be also used to monitor the progress of the oxidation of iodide by iodate (reaction 1).

Some results obtained in flow-injection measurements with sulphuric acid indicated that the linearity of the relationship between the measured current

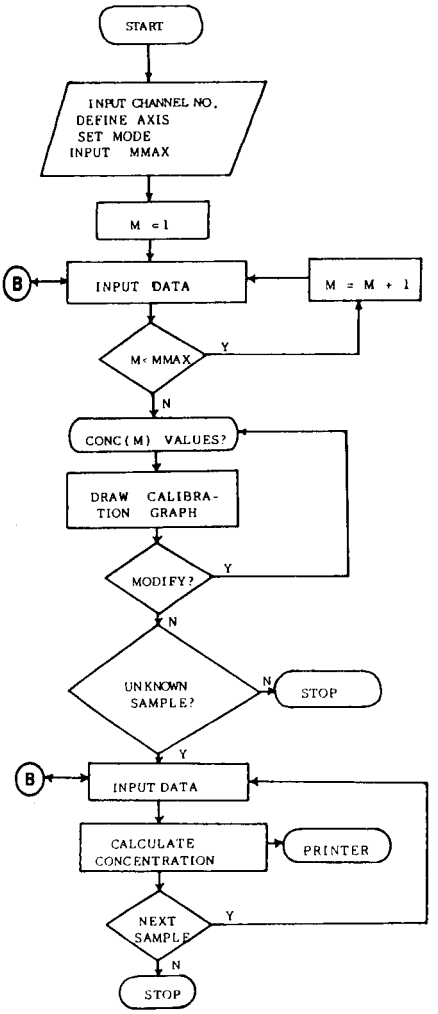

Fig. 1. Overall flow chart of the software used in microcomputer data processing: M, peak number; MMAX, number of injections in calibration run; CONC(M), concentration of standard solutions. Points B are connected to subprograms concerning data input and smoothing and analog-to-digital conversion.

and the acid concentration depends on the iodide and iodate concentrations in the carrier solution (Fig. 2). With too little iodide, the linear ranges are very short; with too little iodate, the linear range is short and there is a positive intercept (Fig. 2A). These measurements indicated that the optimum concentrations of iodide and iodate in the flow-injection manifold used were 2 M iodide and 50 mM iodate.

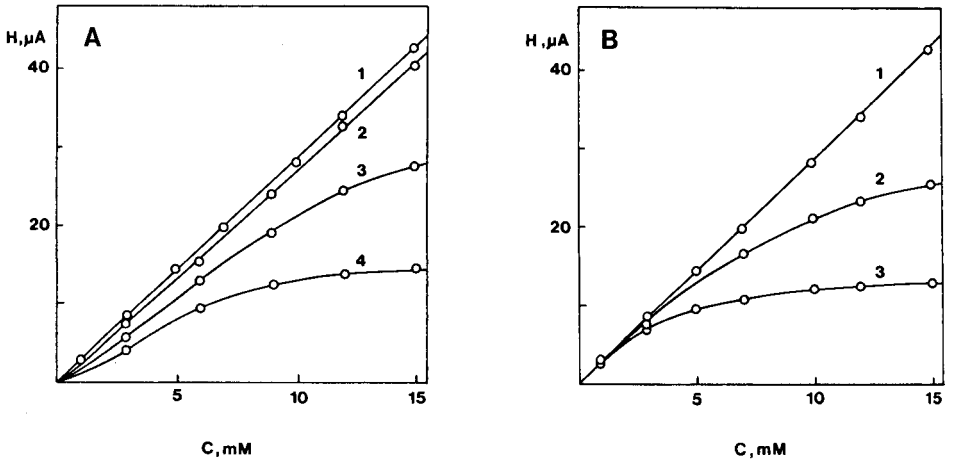

Fig. 2. Calibration plots obtained for single-point flow-injection titration of sulphuric acid. (A) Constant 2 M iodide concentration with variable iodate concentration: (1) 50, (2) 5.0, (3) 1.0, (4) 0.5 mM. (B) Constant 50 mM iodate concentration and variable iodide concentration: (1) 2.0, (2) 0.5, (3) 0.2 M.

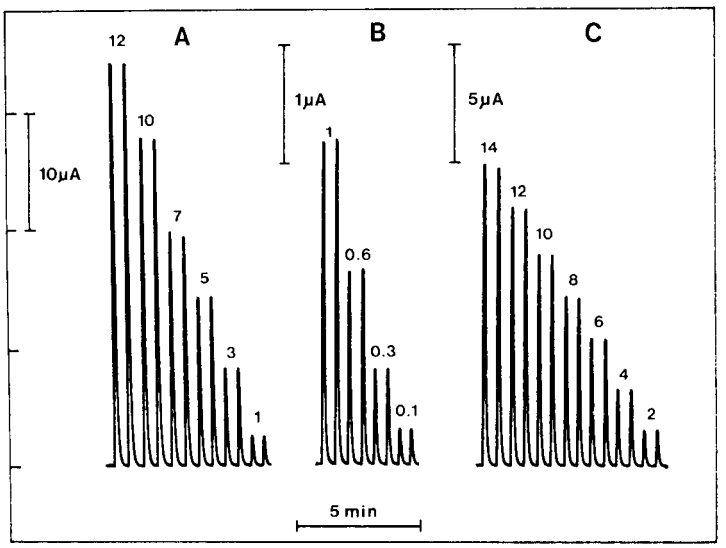

Fig. 3. Peaks recorded in the flow-injection titration of sulphuric acid (A, B) and acetic acid (C) with 2 M iodide and 50 mM iodate in the carrier solution. Concentrations of the injected solutions are given in mM on the peaks.

Effect of strength of the acid. The flow-injection peaks recorded for two ranges of sulphuric acid concentration (Fig. 3A and B) and for acetic acid (Fig. 3C) were reproducible and sharp with fast return to baseline; similar outputs were obtained for 2–12 mM hydrofluoric acid. As the strength of

the acid decreased, the slopes of the calibration plots from the flow-injection measurements decreased (Table 1) though the linearity of the plots was maintained. The deviations of the experimental plots from the origin were very small. The slope dependence on acid strength corresponds to the usual difficulties encountered in utilizing reaction 1 for titrimetric determinations of weak acids [9]. In such titrations, the removal of hydrogen ions during the reaction sets up a buffer system that stops further progress of the reaction. In titrimetric procedures, good results can be obtained by adding an excess of standard thiosulphate and back-titrating with iodine after a suitable interval [9]. In spite of some decrease in the calibration slope for weaker acids, the flow-injection method of acid determination seems to be an attractive alternative to the classical procedures.

Precision of determination. The advantages of on-line data processing with microcomputers interfaced with measuring equipment are widely documented

TABLE 1

Parameters of the linear calibration plots[a] obtained for different acids under optimized conditions for the concentration range 2—20 mM (1—10 mM for sulphuric acid)

Acid	Correlation coefficient	S (μA mM^{-1})	A (μA)
Sulphuric	0.9995	2.76	−0.16
Monochloro-acetic	0.9995	1.37	−0.29
Formic	0.9998	1.33	−0.03
Acetic	0.9997	1.05	−0.25

[a]The equation is $i = A + SC$, where i is the measured current, C the concentration of acid in the injected sample, S the slope of the linear calibration plot and A the intercept on the current axis at $C = 0$.

TABLE 2

Effect of A/D sampling frequency in microcomputer data acquisition on the precision of single-point titrations of 9 mM sulphuric acid

Sampling frequency (sample/s)	Sampling time (ms)	Number of samples	Mean value of peak height[a]	RSD (%)
16.4	61	10	2.768	0.17
13.5	74	10	2.765	0.19
7.9	126	10	2.749	0.54
5.0	200	10	2.736	0.80
2.0	500	5	2.037	18
—[b]	—[b]	8	2.528	0.54

[a]At polarograph output (V). [b]Measurements without on-line data processing.

and accepted. Instead of the dedicated microprocessor control and processing system used earlier [8], the present measurements were obtained with on-line processing using a commercially available microcomputer. Because of the rapid changes in the measured signals, the precision of the results depends significantly on the rate of analog-to-digital conversion. Table 2 shows a comparison of data obtained in on-line processing at different current-sampling times with results obtained using a strip-chart recorder. As can be seen, the precision of the observed results changes dramatically with current-sampling rate. With current-sampling times below 100 ms, the precision of the acid titration was improved significantly.

REFERENCES

1 J. Růžička and E. H. Hansen, Anal. Chim. Acta, 114 (1980) 19.
2 A. U. Ramsing, J. Růžička and E. H. Hansen, Anal. Chim. Acta, 129 (1981) 1.
3 O. Astrom, Anal. Chim. Acta, 88 (1977) 17; 97 (1978) 259; 105 (1979) 67.
4 Cui Hongbo, E. H. Hansen and J. Růžička, Anal. Chim. Acta, 169 (1985) 209.
5 K. G. Schick, Adv. Instrum., 39 (1984) 279.
6 S. F. Simpson and F. J. Holler, Anal. Chem., 54 (1982) 43.
7 A. Hulanicki, W. Matuszewski and M. Trojanowicz, Anal. Chim. Acta, 194 (1987) 119.
8 M. Trojanowicz, A. Hulanicki, W. Matuszewski, M. Pałys, A. Fuksiewicz, T. Hulanicka-Michalak, S. Raszewski, J. Szyller and W. Augustyniak, Anal. Chim. Acta, 188 (1986) 165.
9 I. M. Kolthoff, E. B. Sandell, E. J. Meehan and S. Bruckenstein, Quantitative Chemical Analysis, MacMillan, New York, 1969.
10 O. F. Kamson, Anal. Chim. Acta, 179 (1986) 475.

Analytica Chimica Acta, 194 (1987) 275—279
Elsevier Science Publishers B.V., Amsterdam — Printed in The Netherlands

Short Communication

SULPHUR(IV) IN RAIN WATER AND ANTARCTIC ICE BY ION CHROMATOGRAPHY

DIANA M. DAVIES

CSIRO Division of Atmospheric Research, Private Bag 1, Mordialloc, Victoria 3195 (Australia)

JOHN P. IVEY*

Australian Government Analytical Laboratories, P.O. Box 84, Kingston, Tasmania 7150 (Australia)

(Received 19th November 1985)

Summary. Sulphur(IV) is quantified as the α-hydroxysulphonic acid, hydroxymethanesulphonate, which is stabilized in samples and standards by a stoichiometric excess of formaldehyde. The addition of 0.2% (v/v) formaldehyde to the very dilute eluent protects against oxidation of the adduct, which is eluted as a single symmetrical peak, completely resolved from all other anions including methanesulphonate. The detection limit is 0.1 $\mu g\ l^{-1}$ S(IV). The method is applied in the analysis of Tasmanian rain water and Antarctic ice.

Precipitation is an important mechanism for removal of sulphur from the atmosphere both as sulphur(IV) and sulphur(VI). Sulphur dioxide in the Antarctic and pristine maritime sites originates mainly from reduced sulphur compounds produced by marine biogenic activity rather than from anthropogenic sources. Sulphur emission from Mt. Erebus and other vulcanism, principally as sulphur dioxide (4.2×10^7 kg y^{-1}), has been estimated to represent only a small portion of the total sulphur input to the Antarctic air mass. Although Delmas [1] has considered the deposition of sulphur dioxide on snow as a contributor to the Antarctic sulphur budget (in addition to measured sulphate), no attempt has been made, to our knowledge, to establish the existence of sulphur(IV) in Antarctic ice. To date, sulphate and methanesulphonate are the only sulphur species shown to be present in Antarctic ice [2].

Past methods for the determination of sulphite have been well reviewed by Dasgupta et al. [3] who considered ion chromatography to be the promising approach. The major problem in quantifying sulphite by ion chromatography has been that of oxidation of the samples and standards prior to and during elution with alkaline eluents. Stevens et al. [4] found that oxidation of sulphite in water samples was a problem, as did Hansen et al. [5] who concluded that the method was unreliable. Oxidation continued to be a problem even after the complete removal of oxygen from their eluent.

0003-2670/87/$03.50

Holcombe et al. [6] stabilized standard solutions by the addition of 10% formaldehyde as an oxidation inhibitor. The stabilization technique was successfully adapted by Dasgupta et al. [3, 7] who found that the resultant adduct, hydroxymethanesulphonate, was extremely stable in slightly acidic solution. They recommended the use of formaldehyde for absorption of atmospheric sulphur dioxide after investigating the possible utility of a range of carbonyl compounds. Lindgren et al. [8] also found formaldehyde to be the most effective stabilizing agent after examining the possible use of alcohols, and aldo- and keto-hexoses. Again difficulties were encountered because of oxidation during chromatography. Dasgupta [9] overcame the problem of oxidation during chromatography by the use of an eluent containing formaldehyde, but appears to have abandoned the method because of low retention times and possible separator column degradation believed to be caused by formaldehyde. McCormick and Dixon [10] also reported the successful use of formaldehyde for stabilization of high levels of sulphite (mg l^{-1}) in photographic fixers and the addition of formaldehyde to their eluent.

In this study, stabilization of sulphite as the hydroxymethanesulphonate adduct is used in the determination of low levels of sulphur(IV) (μg l^{-1}) in rain water and in Antarctic ice and snow. The method has advantages over spectrophotometric methods which measure only sulphite.

Experimental

Instrumentation. The ion-chromatographic system consisted of a Waters Associates M45 pump, a Rheodyne 7000 injector with a 5.5-ml stainless-steel loop, a Dionex IonPac AS3 fast-run anion separator and a Dionex hollow-fiber anion suppressor (64667). The eluent flow rate was 2.0 ml min^{-1}. The detector was a modified Waters 430 conductivity detector with the cell heating block set to 27°C.

Sufficient sensitivity for rain-water samples was provided by 1 μS full-scale deflection but 0.2 μS f.s.d. was required for Antarctic ice and snow. The chromatograms were recorded with a Servogor 120 chart recorder. The sample loop was filled from a 10-ml polyethylene syringe fitted with a Millex-HA 0.45-μm filter (Millipore).

Materials. Distilled/deionized water and analytical-reagent grade chemicals were used throughout. Formaldehyde solution (36—38% w/w, Ajax Chemicals) was diluted to 2% (v/v) and passed through a 25-mm diameter column containing well washed Amberlite IR-45 (OH) ion-exchange resin having a packed volume of ca. 70 ml.

The eluent (pH 7.8) consisted of 0.0009 M sodium hydrogencarbonate containing 0.2% (v/v) of freshly ion-exchanged formaldehyde, filtered through a 0.45-μm filter. Standards were prepared from anhydrous sodium sulphite (May and Baker) which was dissolved and then serially diluted in 0.2% (v/v) formaldehyde.

Procedures. Rain water (70 ml) from a rural site (Kingston, Tasmania) was collected in a clean vessel containing 5.0 ml of the 2% formaldehyde.

The sample was stored in a Whirlpak (Nasco) taking care to exclude air from the sample.

Antarctic ice-core samples consisted of a small portion of ice (40 g) retained after melting 200 g sections of ice core in scrubbed air. Details of the ice-core samples and preparation for analysis are described in detail elsewhere [11]. The 40-g samples were stored in Whirlpaks at −17°C prior to analysis. A portion (5.0 ml) of 2% formaldehyde was added to the weighed ice portion and the Whirlpak was sealed, excluding as much air as possible, before the ice was melted at room temperature. Snow samples were weighed in a Whirlpak and treated in the same manner as the ice.

The ice and surface-snow samples were injected within an hour of completely thawing and the rain water samples were injected as soon as sufficient volume had been collected. This was to ensure that losses of the low levels of anions to the containers were minimal.

Results and discussion

The initial clean-up of the formalydehyde solution with ion-exchange resin was essential. This reduced the background conductivity of the prepared eluent to a minimum, by removing large amounts of contaminating chloride and formate from the formaldehyde. Furthermore, if untreated formaldehyde were added to samples and standards, the eluting formate and chloride peaks would interfere with the analyte peak. To establish that as much as possible of the chloride and formate had been removed (<5 $\mu g\ l^{-1}$), the formaldehyde was analyzed in the same system prior to eluent preparation.

Formaldehyde solution oxidizes slowly in air to formic acid and at alkaline pH undergoes a Cannizzaro reaction to a small extent, also forming formate [12]. It was thus found that the prepared eluent should be discarded after 24 h because of the formation of formate and that the formaldehyde solution should be prepared as required. No separator column degradation was caused by formaldehyde in the eluent although Dasgupta [9] suggested that demethylation and Schiff-base formation may occur at the quaternary ammonium exchange sites. As a precautionary measure, the system was flushed with 0.001 M hydrogencarbonate on completion of a run.

Repeated injections of freshly prepared standards showed that, with the conditions described, formation of the adduct was complete in <15 min and that the adduct was stable for at least 24 h. Standards were prepared in the range of 0.1—10 $\mu g\ l^{-1}$ as sulphur and resulted in a four-point linear calibration (correlation coefficient = 0.999). The hydroxymethanesulphonate peak was symmetrical and well resolved from the methanesulphonate which was present in these samples (Fig. 1). Later-eluting peaks, such as sulphate, were retained on the separator column and thus not observed. The detection limit was found to be 0.1 $\mu g\ l^{-1}$ S(IV). The identity of the hydroxymethanesulphonate peak in rain water (Fig. 2) was confirmed by standard addition. No contamination was found from the use of Whirlpaks which proved to be convenient containers.

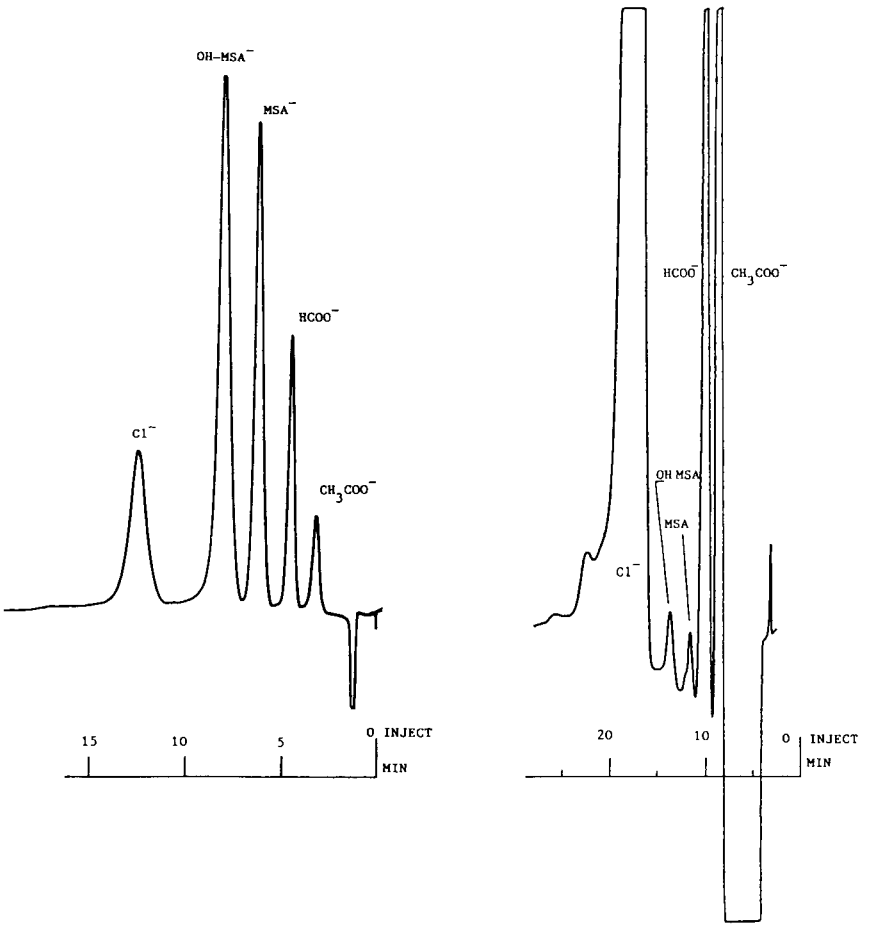

Fig. 1. The separation of hydroxymethanesulphonate (OH-MSA) from methanesulphonate (MSA), showing residual formate and chloride contaminants not removed from the formaldehyde by ion-exchange. The eluent was 0.001 M $NaHCO_3$/0.2% (v/v) formaldehyde with a flow rate of 2.0 ml min^{-1}.

Fig. 2. Hydroxymethanesulphonate (OH-MSA, 4.3 $\mu g\ l^{-1}$ S) and methanesulphonate (MSA), acetate, formate and chloride, in rain water from a rural site. Conditions are as for Fig. 1.

Dasgupta and DeCesare [7] found the adduct to be most stable at a pH of 4—5 and buffered their absorber accordingly. To avoid the addition of further possible interfering ions, samples were not buffered here. After the addition of formaldehyde, the natural acidity of the samples and residual acidity in the formaldehyde resulted in a pH range of 5.6—5.9 at which the adduct was found to be stable.

The possibility of using electrochemical detection as a more selective alternative to conductivity detection was considered, but the adduct was not electrochemically active at +0.8 V in the eluent used. Carbonate was not added to the samples to reduce the water dip, as suggested by Irgum [13]. Earlier, it was found that addition of eluent to samples, when large sample volumes are used, resulted in extreme peak broadening. As the water dip did not interfere, the concentration effect of the anions on the head of the analytical column (which occurs during the passage of the water) was utilized.

A trial determination of sulphur(IV) in rain water by this method showed low levels in water from the Tasmanian site (4—15 $\mu g\ l^{-1}$ S). Sulphur(IV) could be present both as sulphite and as hydroxymethanesulphonate if any formaldehyde was present. Formate, derived in part from atmospheric formaldehyde, was also present in those samples which had a pH at which the adduct would be stable. The results obtained are within the range of those of Tsunogi (rural Japan) [14] and also of Guiang et al. [15] who reported low levels of sulphite in rural U.S.A. rain water. Unfortunately, their results were found to be artificially low as the samples were not preserved against oxidation [16] and also sulphite would certainly have oxidized to sulphate in their chromatography system. Thus, the method presented here should be useful for monitoring sulphur(IV) in rain water.

The amount of sulphur(IV) as either sulphite or hydroxymethanesulphonate in Antarctic ice and surface-snow samples was less than 0.1 $\mu g\ l^{-1}$ S. When compared with a mean methanesulphonate concentration of 2.69 $\mu g\ l^{-1}$ S and a mean sulphate concentration of 15.06 $\mu g\ l^{-1}$ S, it can be seen that sulphur(IV) does not contribute significantly to the Antarctic sulphur budget at our site [2]. The contributing sulphur species identified to date are present as sulphur(VI).

REFERENCES

1 R. J. Delmas, Nature, 299 (1982) 677.
2 J. P. Ivey, D. M. Davies, V. Morgan and G. P. Ayers, Tellus, 5 (1986) 88.
3 P. K. Dasgupta, K. B. DeCesare and M. Brummer, Atmos. Environ., 16 (1981) 917.
4 T. S. Stevens, V. T. Turkelson and W. R. Albe, Anal. Chem., 49 (1977) 1176.
5 L. D. Hansen, B. E. Richter, D. K. Rollins, J. D. Lamb and D. J. Eatough, Anal. Chem., 51 (1979) 633.
6 L. J. Holcombe, B. F. Jones, I. I. Illsworth and F. B. Meserole, in J. D. Mulik and E. Sawicki (Eds.), Ion Chromatographic Analysis of Environmental Pollutants, Ann Abor, MI, 1979, p. 401.
7 P. K. Dasgupta and K. B. DeCesare, Atmos. Environ., 16 (1982) 2927.
8 M. Lindgren, A. Cedergren and J. Lindberg, Anal. Chim. Acta, 141 (1982) 279.
9 P. K. Dasgupta, Atmos. Environ., 16 (1982) 1265.
10 M. J. McCormick and L. M. Dixon, J. Chromatogr., 322 (1985) 478.
11 J. P. Ivey and D. M. Davies, Anal. Chim. Acta, 194 (1987) 281.
12 K. Irgum, Anal. Chem., 57 (1985) 1335.
13 K. Irgum, Anal. Chem., 57 (1985) 1496.
14 S. Tsunogi, Geochem. J., 5 (1971) 175.
15 S. F. Guiang, S. V. Krupa and G. C. Pratt, Atmos. Environ., 18 (1984) 1677.
16 M. Radojevic, Atmos. Environ., 19 (1985) 685.

Analytica Chimica Acta, 194 (1987) 281—286
Elsevier Science Publishers B.V., Amsterdam — Printed in The Netherlands

Short Communication

ION CHROMATOGRAPHIC DETERMINATION OF SELECTED IONS IN ANTARCTIC ICE

J. P. IVEY*[a]

Australian Government Analytical Laboratories, P.O. Box 84, Kingston, Tasmania 7150 (Australia)

D. M. DAVIES

CSIRO Division of Atmospheric Research, Private Bag 1, Mordialloc, Victoria 3195 (Australia)

(Received 3rd January 1986)

Summary. Ion chromatography is used to measure the concentrations of chloride, nitrate, sulphate, ammonium and sodium ions at the $\mu g\ l^{-1}$ level in Antarctic ice and to investigate the occurrence of methanesulphonate, fluoride, formate, acetate and nitrite. Of the latter group of ions, only methanesulphonate was found in measurable concentrations.

The composition of Antarctic ice, in particular its soluble impurities, has been used to give insight into such questions as paleoatmospheric composition [1], and the natural cycling of nitrogen and sulphur compounds [1, 2]. Recently, the presence of biogenic methanesulphonic and other organic acids in the maritime environment [3—5] has raised questions as to their presence or otherwise in Antarctic ice. If they are present, they can be expected to contribute to ice acidity and in the case of methanesulphonic acid to the sulphur budget [6]. Methanesulphonate measurements may also aid in the definition of the relative sulphate contributions from marine biogenic productivity and volcanic activity [1].

The sample preparation protocol is of fundamental importance in the eventual reliability of the analytical results. The problems associated with gaseous species in the preparation of ice for analysis have been noted in earlier work [7]. In this communication, the manner in which the preparation problem was overcome is discussed as well as the optimization of the instrumentation for the determination of each ion, or group of ions.

Experimental

Sample preparation. Ice cores were collected as part of the Australian National Research Expedition (ANARE) glaciology research program at Law Dome (66 30′S, 111 00′E). The core was cut into 15 equal (depth) sections

[a]Present address: Department of Analytical Chemistry, University of New South Wales, P.O. Box 1, Kensington, N.S.W. 2033, Australia.

0003-2670/87/$03.50

for each annual accumulation layer as shown by the oxygen isotope record. Each section was then trimmed to leave ca. 200 g of the inner part of the core. The method of washing and melting the 200-g sections was developed in three stages, only results obtained from the final two methods were utilized elsewhere [8]. All manipulations were done in a clean air laminar flow cabinet. All plastic ware was washed copiously with distilled/deionized water and then filled with distilled/deionized water, sealed, and allowed to stand for at least 24 h prior to use. The three stages were as follows.

(1) Initially about 25% of the 200-g block was removed by washing in distilled/deionized water (resistivity > 18 M ohm cm^{-2}) after which a further 25% was removed by placing the washed ice in a polyethylene funnel and allowing the ice to melt as described by Legrand et al. [7]. Chloroform (multiply extracted with distilled/deionized water) was added to a polyethylene receiver vessel. The purpose of this was to preserve any organic acids which have been shown to be labile in the absence of a biocide [5]. Frozen distilled/deionized water taken through the procedure, however, showed disconcerting levels of acetate, formate and traces of nitrite by ion chromatography. The clean air cabinet was obviously allowing acidic (and presumably basic) gases through its filter, with the potential further to contaminate the melting sample with nitric acid and sulphurous/sulphuric acids and ammonia.

(2) Air from a compressed air source was cleaned by passage through an in-line gas absorption tube containing Ascarite (8—20 mesh). The scrubbed air was then piped to an inverted funnel over the polyethylene funnel used to contain the melting ice (Fig. 1). A gas absorption tube packed with oxalic acid was included in the same line for removing ammonia. A 0.45-μm filter was last in line. The effectiveness of this can be seen in Fig. 2, for which two different samples were allowed to melt in the laminar flow cabinet (A) and the scrubbed-air (B) melt systems.

(3) When the above system was used, any formate and acetate present were below the detection limit of the present method and thus no chloroform was required. The ice was washed with distilled/deionized water until 50% remained which was then simply melted in a sealed polyethylene bag (Whirlpak). The Whirlpaks were checked for possible contaminants by running blank determinations with distilled/deionized water.

Equipment. The ion-chromatographic system for the determination of anions consisted of a Waters Associates M45 pump, a Rheodyne fixed-volume injector (model 7000), a Dionex 030985 fast-run anion separator column, a Dionex 035350 hollow-fibre or Dionex 030829 suppressor column and a Waters model 430 conductivity detector. The same instrumentation was used for the determination of sodium and ammonium except that a Wescan 269004 cation separator column and a Dionex cation suppressor column were used. As indicated by Legrand et al. [7] a large (5.5-ml) sample loop was found to be preferable to a concentrator column for the introduction of samples with low concentrations of analyte species. Samples

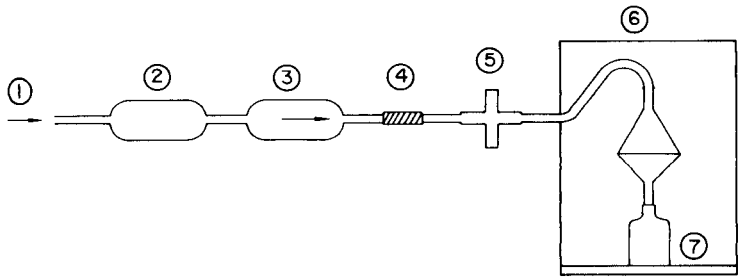

Fig. 1. Air-purification system used in the melting of ice cores: (1) compressed air source; (2) acid gas trap of ascarite (8—20 mesh); (3) alkali gas trap of oxalic acid; (4) self-indicating soda lime; (5) particle filter; (6) laminar flow clean cabinet; (7) polyethylene receiving bottle.

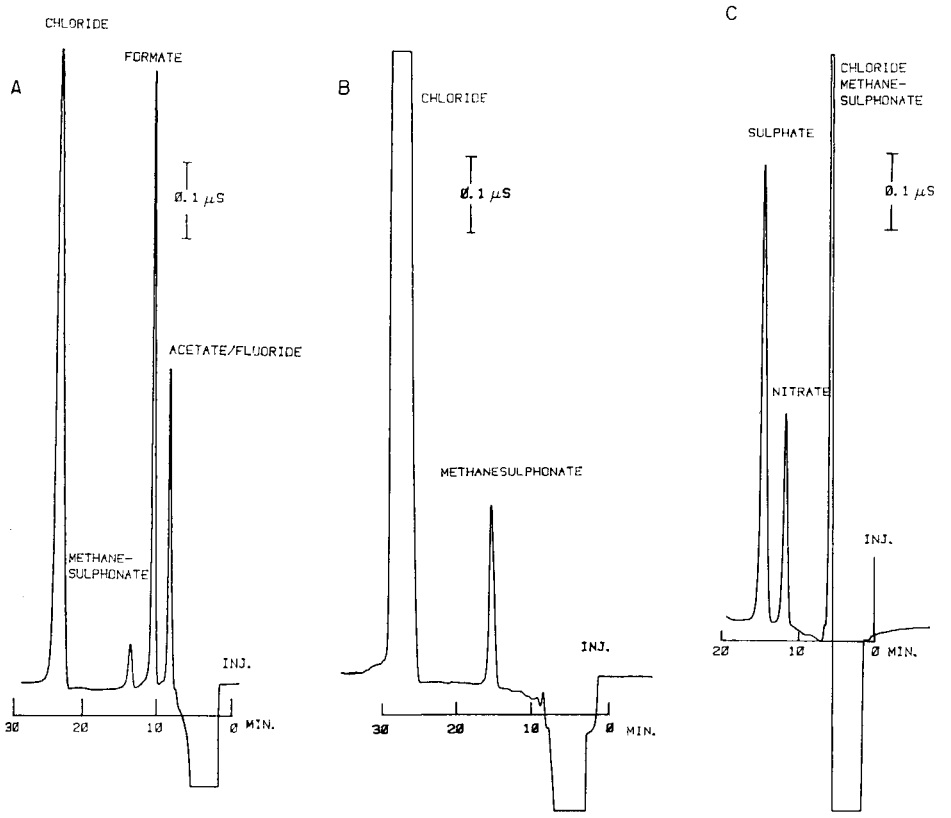

Fig. 2. Chromatograms of sample ice. (A) Ice melted in a clean air cabinet without contaminating gas removal showing the separation of acetate/fluoride, formate, methanesulphonate and chloride at respective concentrations of about 105, 5.8 and 50 ng ml^{-1}. (B) Ice melted after contaminating gas removal; methanesulphonate and chloride at respective concentrations of 16.7 and 310 ng ml^{-1}. (C) Sample ice with nitrate and sulphate concentrations of 17 and 31 ng ml^{-1}, respectively. Conditions: injection volume of 5.5 ml, flow rate 2.0 ml min^{-1}, chart speed 0.25 cm min^{-1}, eluents as in Table 1.

were loaded into the loop with a cleaned 10-ml polyethylene syringe. Eluent concentrations and conditions are shown in Table 1.

Comparative measurements of sodium and determinations of magnesium were done on a Varian atomic absorption spectrometer model 1475 with an air/acetylene flame.

Results and discussion

Legrand et al. [7] used an eluent for nitrate and sulphate which did not allow chloride to be quantified. They chose to use an alternative column specifically for chloride determinations. Here, the same column was used for all determinations but with a more dilute eluent for chloride. In the method of Legrand et al. [7], chloride elutes at a retention time of less than 2 min after passage of the water dip. Acetate, formate, methanesulphonate and fluoride all elute prior to chloride. Fluoride has been reported previously as being present in Antarctic ice but accurate quantitation was not possible because of interference from the water dip [1]. To examine the possible existence of these poorly retained anions, a very dilute eluent (0.0007 M sodium hydrogen carbonate) was used. Figure 2B is a typical sample chromatogram and Fig. 2A shows the degree of separation achieved. Fluoride was resolved from acetate though not adequately; but because no peak was observed at the acetate/fluoride retention time in any sample, this was not a problem. Chloride was also quantified with this system by using very high attenuation.

Methanesulphonate ion was found in all samples examined. The concentration was between 9 and 0.2 $\mu g\ l^{-1}$ as sulphur (S); the latter is the detection limit at twice the baseline noise. Standards with concentrations of 1.0, 2.5, 5.0, 7.5 and 10.0 $\mu g\ l^{-1}$ (S) typically gave a linear peak height vs.

TABLE 1

Summary of conditions for quantifying selected ions in Antarctic ice[a]

Ion	Eluent	Detection limit (ng)	Range of standards (ng ml^{-1})
Sodium	0.004 M HNO_3	1	0—500
Ammonium		2	0—50
Fluoride/acetate		5/20	—
Formate		20	0—100
Methane sulphonate	0.0007 M $NaHCO_3$	1	0—30
Chloride		2	0—800
Nitrite		4	0—5
Nitrate	0.002 M Na_2CO_3	2	0—25
Sulphate		3	0—150

[a]Injection volume 5.5 ml; flow rate 2.0 ml min^{-1}; columns etc. as discussed in text; sensitivity 5 μS f.s.d. for cations, 1 μS and 5 μS for chloride, with both 0.0007 M hydrogen carbonate and 0.002 M carbonate eluents.

mass calibration with a correlation coefficient of 0.9998, a standard error of 0.14 and an intercept of 0.02 $\mu g\ l^{-1}$ (S).

Nitrate and sulphate were both quantified by using 0.002 M sodium carbonate as eluent (Fig. 2C). Nitrite elutes between chloride and nitrate but was not observed in samples melted in scrubbed air or samples melted in polyethylene bags. Detection limits are given in Table 1.

Sodium and ammonia were quantified by ion chromatography. Potassium was not measured in the present study. Comparison of the sodium results from ion chromatography and those obtained by a.a.s. on 30 samples is shown in Fig. 3. In general, the agreement between the two methods is reasonable (r = 0.988) and certainly comparable to a similar comparison between ion chromatographic and neutron activation measurements of sodium content [7]. Accurate sodium and magnesium results are particularly important as they are used to define the relative contributions made to the sulphate budget from sea salt and gas to particle conversion [9]. The a.a.s. measurements of sodium and magnesium were done without the addition of an ionization suppressant to either standards or samples in order to avoid contamination of the samples.

Ammonium concentrations were in the range 0—1 $\mu g\ l^{-1}$; most samples were at, or about, the detection limit of 0.5 $\mu g\ l^{-1}$ for the equipment used. The relative absence of ammonia from our samples indicates that the methodology for sample preparation is sound. Presence of ammonia has been found to be indicative of sample contamination [7].

Conclusion

Whilst it is always preferable to be able to quantify all the species of interest from a single chromatogram, this is not practicable in the determination of anions in Antarctic ice. Valuable information may be lost if the concen-

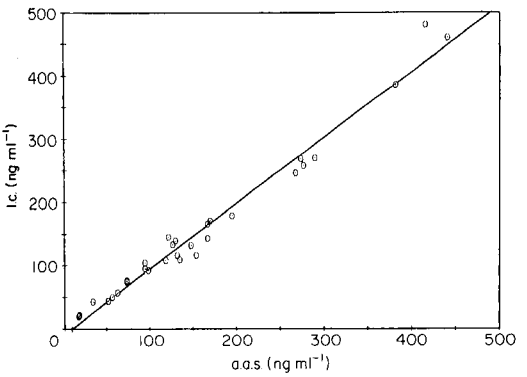

Fig. 3. Comparison of sodium concentration obtained by a.a.s. (x axis) and ion chromatography (y axis) of 30 ice-core samples (ng ml^{-1}). Corr. coeff. 0.988, slope 1.034 and x intercept 8.8.

trations of early eluting species are not measured. The methodology presented above allows such measurement and forms the basis of work regarding the presence of methanesulphonate in Antarctic ice [8].

Experience leads to the conclusion that it is necessary not only to filter the air to remove particulate matter prior to contact with melting ice but also to exclude potentially contaminating gases.

REFERENCES

1 J. M. Palais and M. Legrand, J. Geophys. Res., 90 (1985) 1143.
2 M. R. Legrand and R. J. Delmas, Atmos. Environ., 18 (1984) 1867.
3 E. S. Saltzman, D. L. Savoie, R. G. Zika and J. M. Prospero, J. Geophys. Res., 88 (1983) 10897.
4 G. P. Ayers, J. P. Ivey and H. S. Goodman, J. Atmos. Chem., 4 (1986) 173.
5 W. C. Keene, J. N. Galloway and J. D. Holden, J. Geophys. Res., 88 (1983) 5122.
6 R. J. Delmas, Nature, 299 (1983) 677.
7 M. Legrand, D. DeAngelis and R. J. Delmas, Anal. Chim. Acta, 156 (1984) 181.
8 J. P. Ivey, D. M. Davies, V. Morgan and G. P. Ayers, Tellus, 5 (1986) 88.
9 W. C. Keene, A. A. P. Pszenny, J. N. Galloway and M. E. Hawley, J. Geophys. Res., 9 (1986) 6647.

Analytica Chimica Acta, 194 (1987) 287—292
Elsevier Science Publishers B.V., Amsterdam — Printed in The Netherlands

Short Communication

USE OF CYCLODEXTRIN-BONDED PHASES FOR LIQUID CHROMATOGRAPHIC SEPARATION OF STYRENE POLYMERS

C. ALLEN CHANG*[a], HONG JI, QIHUI WU and MICHAEL P. EASTMAN

Department of Chemistry, University of Texas at El Paso, El Paso, TX 79968-0513 (U.S.A.)

SHIH-TSE LAI

American Tech. and Ventures, 2132 Michelson Dr., Irvine, CA 92715 (U.S.A.)

(Received 11th August 1986)

Summary. The use of β- and γ-cyclodextrin bonded columns is successful for the separation of styrene polymers. Two retention mechanisms are involved: below 50% dichloromethane in heptane, normal adsorption behavior is observed; above 50%, a size-exclusion mode prevails. Good chromatograms under isocratic and gradient-elution conditions are shown, together with their applications in determination of molecular weights of polymers.

It has been demonstrated recently that the use of cyclodextrin bonded-phase columns provides good separations of mixtures containing a large number of geometrical isomers, e.g., substituted anilines, benzoic acids, and phenols in both normal-phase and reversed-phase liquid chromatography (LC) [1—4]. Thus, apart from their novel applications in reversed-phase chiral resolution [5—7], cyclodextrin columns can be used conventionally with great versatility.

The separation mechanism involved in the cyclodextrin columns in normal-phase chromatography is believed to be similar to that of polar-bonded phases with amine and alkylhydroxy functional groups. In particular, hydrogen bonding between analytes and the stationary phase is significant and its presence is thought to be important even in reversed-phase chromatography when water is introduced in the mobile phase [4, 8]. However, the hydrogen bonding is eventually diminished when the water content of the mobile phase is high and the separation mechanisms become those of reversed-phase chromatography which are mainly caused by inclusion phenomena.

In view of the multi-mode behavior of cyclodextrin bonded-phases, it was of interest to test their use for the separation of polymers. For the

[a]Current address: Separations Technology Division, Aluminum Company of America, ALCOA Technology Center, ALCOA Center, PA 15069, U.S.A.

0003-2670/87/$03.50

separation of polystyrenes, some other chemically bonded phases have been shown to behave as a reversed-phase substrate, a normal-phase adsorbent, and a size-exclusion medium, depending on the precise mobile-phase compositions [9].

In this communication, β- and γ-cyclodextrin bonded phases are used for the LC separation of polystyrenes. Emphasis is placed on the versatility of such columns in polymer separation and on comparison of columns of β- and γ-cyclodextrins, which have different cavity sizes because of the number of glucose units in their cyclic structures, i.e., 7 for β-cyclodextrin 8 for γ-cyclodextrin.

Experimental

A Beckman 332 liquid chromatograph with two Altex 110A pumps and a microprocessor control unit together with a Micromeritics (Norcross, GA) 786 variable-wavelength (200—600 nm) detector was used. A Micromeritics Model 7500 liquid chromatography system was also used; this system was equipped with a Model 750 solvent delivery system, a Model 752 ternary solvent mixer, and a Model 731 column compartment with a universal injector and a variable-temperature controller (ambient to 150°C).

Pressure-Lok series C-160 (Precision Sampling, New Orleans, LA) 25-μl syringes were used for sample injection. Chromatograms were recorded with a Linear Model 555 single-channel recorder.

Bonded columns (25 cm × 4.6 mm i.d. for β-cyclodextrin and 25 cm × 4.6 mm i.d. for γ-cyclodextrin; Aztec, Whippany, NJ) were used for all experiments.

Styrene polymer standards (PS-500, PS-800, PS-1000, PS-3000, PS-3.7 × 10^4, PS-2.33 × 10^5, PS-6 × 10^5, PS-1.03 × 10^6) were obtained from Perkin-Elmer and other sources. High-performance liquid chromatographic (HPLC) grade solvents were used.

Before the separation experiments, the columns were pre-equilibrated with the mobile phase. After pre-equilibration, a flow rate of 1 ml min^{-1} was set for the chromatographic process.

For each separation, the polymer was dissolved in the eluent and 3-μl samples containing 1—2 mg ml^{-1} of each solute were injected into the system. Back-pressures of <1000 and 3000 psi were usually observed during normal-phase and reversed-phase experiments, respectively. All data points were collected by averaging results for three or more separations. Published methods were used for evaluation of t_0 values for the β- and γ-cyclodextrin columns [10].

Results and discussion

Figure 1A illustrates a typical separation of the components of polystyrene PS-800 on a β-cyclodextrin bonded phase with heptane as the mobile phase. Partial resolution is observed for the stereoisomers of the individual oligomers which may correspond to the syndiotactic, isotactic, and atactic microstructures. Similar chromatograms were obtained for the PS-500 and

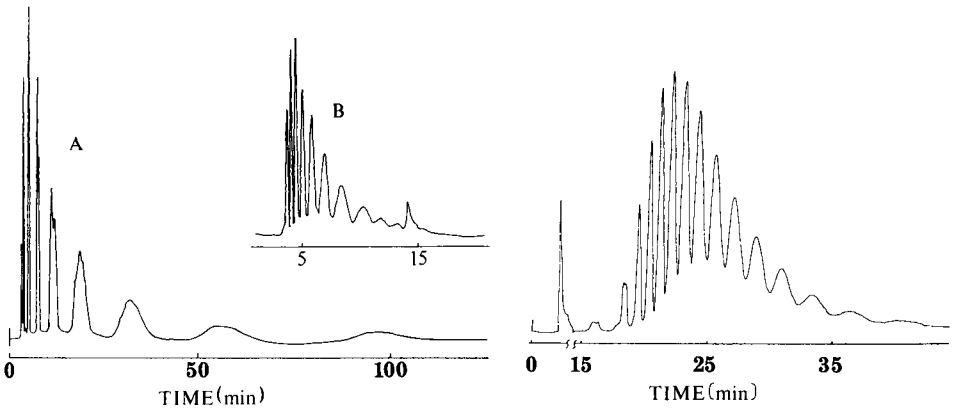

Fig. 1. Chromatograms for a polystyrene standard (PS-800) on (A) β-cyclodextrin; (B) γ-cyclodextrin. Mobile phase, pure heptane; flow rate, 1 ml min^{-1}; detection at 254 nm.

Fig. 2. Chromatogram for a polystyrene standard (PS-1000) on γ-cyclodextrin. Linear gradient (45 min) from 3/97 dichloromethane/heptane to 20/80 dichloromethane/heptane; flow rate, 1 ml min^{-1}, detection at 254 nm.

PS-1000 samples. However, the resolution of stereoisomers was lost when a γ-cyclodextrin column was used (Fig. 1B). Because of their limited solubility, higher-molecular-weight samples could not be tested when pure heptane was used as the mobile phase. Addition of polar solvents such as dichloromethane to the heptane diminished the resolution of the stereoisomers. However, with gradient elution conditions, the styrene oligomers were separated to a satisfactory degree (Fig. 2).

The normal-phase peaks in β-cyclodextrin columns usually eluted more slowly than the corresponding peaks in γ-cyclodextrin columns under identical experimental conditions. This indicates that the β-cyclodextrin column provides longer retention presumably because of the higher surface coverage with β-cyclodextrin. However, the inclusion process may not be significant under those elution conditions.

Figure 3 compares the plots of capacity factors (k') vs. the composition of mobile phase for the separation of PS-800 sample on both β- and γ-cyclodextrin columns at a flow rate of 1 ml min^{-1}. When the dichloromethane concentration was <50% (v/v) in heptane, each separated peak was eluted faster as the proportion of strong solvent was increased, i.e., the normal-phase chromatographic process. When the dichloromethane concentration in heptane was >50%, all the individual peaks corresponding to different degrees of polymerization merged into one and the peak was eluted before the solvent peak. The higher-molecular-weight samples were also dissolved in the more polar solvents and each was eluted as a single peak with a retention time less than t_0. The retention times obtained were inversely related to the molecular weights of the samples, i.e., typical size-exclusion chromatographic (SEC) behavior (Fig. 4). Thus, there exists a

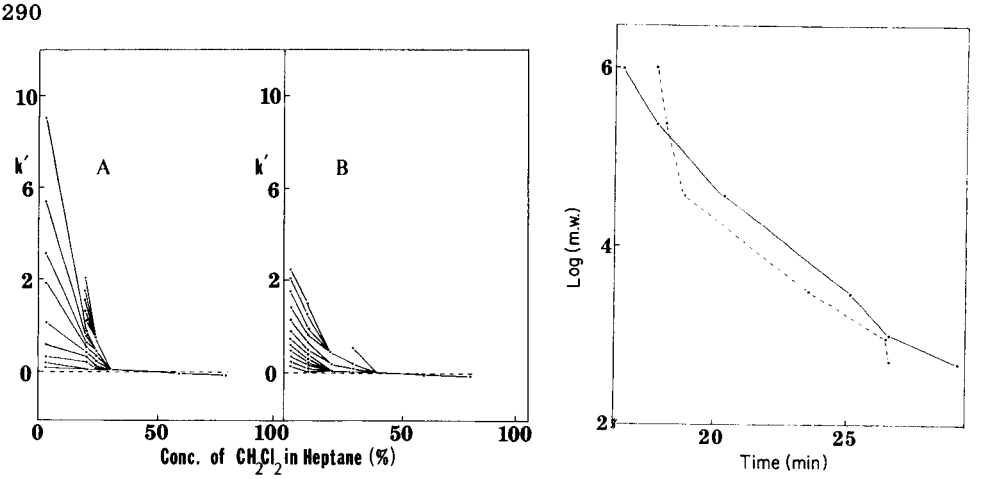

Fig. 3. Dependence of k' on mobile-phase composition (from 100% heptane to 100% dichloromethane) for styrene oligomer peaks of different degrees of polymerization: (A) styrene oligomer PS-800 on β-cyclodextrin; (B) styrene oligomer PS-800 on γ-cyclodextrin. Flow rate, 1 ml min^{-1}.

Fig. 4. Calibration curves for determination of molecular weight of polystyrene in 80/20 dichloromethane/heptane: (——) on γ-cyclodextrin bonded phase; (- - - -) on β-cyclodextrin bonded phase. Flow rate, 0.1 ml min^{-1}.

mobile-phase composition, ψ_m, between the two modes of LC separation [9]. Below ψ_m, the polystyrene is eluted in the order of that expected when the column packings act as normal-phase adsorbents. Above ψ_m, the mobile phase is strong enough to eliminate individual solute/stationary phase interactions, and the column functions as a SEC medium.

The value of ψ_m seems to vary only slightly with different bonded-phase columns. For example, it is 45% dichloromethane in iso-octane when a Partisil PAC column is used to separate polystyrene samples [9]. This is expected because at high dichloromethane concentrations, the specific bonded-phase/substrate interactions are eliminated and only the pore size of silica is significant in SEC separation.

Figure 5 shows that the retention of styrene oligomers is related linearly to the composition of mobile phase, ψ, and the degree of polymerization, n. When the solvent strength is weak, the retention behavior of styrene oligomers on the β- and γ-cyclodextrin columns can be explained in terms of the competition between the adsorptivity of the chemically bonded phase and the solubility of oligomers in the mobile phase. The relationship can be expressed as

$$\log k' = (A - B\psi) + (C - D\psi)n \qquad (1)$$

where A, B, C and D are constants [9]. When the composition of mobile phase is fixed, Eqn. 1 becomes a Martin-type equation: $\log k' = U + Vn$. For any individual oligomer peak, n is a constant and Eqn. 1 becomes a Snyder-type equation: $\log k' = \log k_s - S\psi$, where $\log k_s$ is the extrapolated

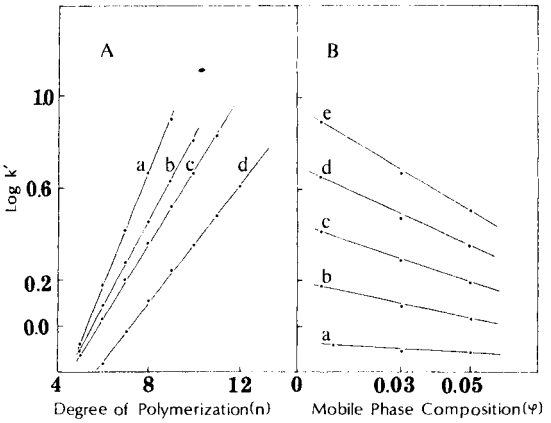

Fig. 5. Plots of log k' for styrene oligomer (PS-800) on a β-cyclodextrin bonded phase: (A) vs. degree of polymerization, n; (B) vs. mobile-phase composition. Plots a—e refer to the different peaks obtained.

value of log k' in the pure weak solvent. It is noted that Eqn. 1 is a general expression for the isocratic retention of oligomeric series. Both the Martin and Snyder equations are special cases of Eqn. 1.

The size-exclusion method can be used to determine molecular weights with ultraviolet detection in accordance with the number of chromophores per molecule. The same idea has led to the development of a peak-area correction method for molecular-weight (m.w.) determinations of styrene oligomers by chemically bonded-phase LC [11]. Calculation of the m.w. of PS-800 was based on data from a β-cyclodextrin column. Some formulae involved are as follows:

number-averaged m.w., $M_n = \Sigma M_i A_i / \Sigma A_i$

weight-averaged m.w., $M_w = \Sigma M_i^2 A_i / \Sigma M_i A_i$

Z-average m.w., $M_Z = \Sigma M_i^3 A_i / \Sigma M_i^2 A_i$

where M_i and A_i are the increments of m.w. and peak area, respectively. For a sample containing multiple chromophores, the corrected area for the individual oligmomer peak is $A_i' = A_i/n$, where n is the degree of polymerization. The uncorrected areas, A_i were 4, 30, 13.7, 18.3, 129.5, 147, 148, 178.5, 200, 173, 143, 110 for i = 1, 2, 3, ... 12, respectively. The m.w. values, based on the corrected area, from the four preceding equations were M_n = 791.2, M_w = 900.2, and M_Z = 974.6 where M_i = 58 + 104n. These values are consistent with the manufacturer's specifications.

Figure 6 shows the chromatograms of a mixture of several polystyrene samples obtained under the size-exclusion mode on the β- and γ-cyclodextrin columns. The partial resolution of these peaks indicates that these columns can also be used for determination of the molecular weights of polymers.

In conclusion, it is clear that β- and γ-cyclodextrin columns can be used

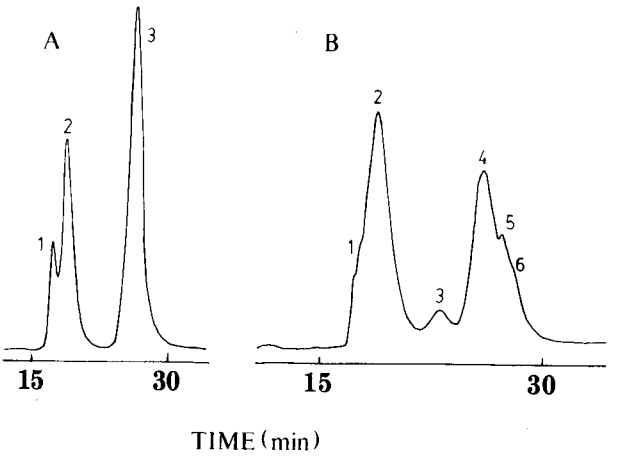

Fig. 6. Chromatograms for a mixture of several polystyrene samples: (A) β-cyclodextrin; (B) γ-cyclodextrin. Peak identification: (A) (1) PS-1.0 $\times 10^6$, (2) PS-3.7 $\times 10^4$, (3) PS-800 and PS-1000; (B) (1) PS-1.0 $\times 10^6$, (2) PS-2.33 $\times 10^5$, (3) PS-3.7 $\times 10^4$, (4) PS-3000, (5) PS-1000, (6) PS-500. Eluent, 80/20 dichloromethane/heptane at 0.1 ml min^{-1}.

to separate polymers such as polystyrene under normal-phase conditions in addition to their unusual selectivities in reversed-phase and chiral separations. The elution order and other chromatographic characteristics are very similar to those found when a phenyl-bonded column is used for the separation of polystyrene samples [12], despite the vast differences in surface modification of the two bonded phases. This is presumably due to the fact that polystyrene samples do not possess specific functional groups which are capable of hydrogen-bonding or higher-order interactions. Thus, even though the two bonded phases are not alike, the separations are quite similar.

REFERENCES

1 C. A. Chang, H. Abdel-Aziz, N. Melchor, Q. Wu, K. H. Pannell and D. W. Armstrong, J. Chromatogr., 347 (1985) 51.
2 C. A. Chang, Q. Wu and D. W. Armstrong, J. Chromatogr., 354 (1986) 454.
3 C. A. Chang, Q. Wu and L. Tan, J. Chromatogr., 361 (1986) 199.
4 C. A. Chang and Q. Wu, Anal. Chim. Acta, (1987) in press.
5 D. W. Armstrong, J. Liq. Chromatogr., 7 (S-2) (1984) 353.
6 D. W. Armstrong, W. DeMond, A. Alak, W. L. Hinze, T. E. Riehl and K. H. Bui, Anal. Chem., 57 (1985) 234.
7 D. W. Armstrong, T. J. Ward, R. D. Armstrong and T. E. Beesley, Science, 232 (1986) 1132.
8 C. A. Chang, Q. Wu and M. P. Eastman, J. Chromatogr., 371 (1986) 269.
9 S.-T. Lai, L. Sangermano, C.-K. Chou and D. C. Locke, J. Chromatogr., 324 (1985) 436.
10 W. L. Hinze, T. E. Riehl, D. W. Armstrong, W. DeMond, A. Alak and T. Ward, Anal. Chem., 57 (1985) 237.
11 S.-T. Lai and L. Sangermano, J. Chromatogr., 322 (1985) 338.
12 S.-T. Lai, L. Sangermano and D. C. Locke, J. Chromatogr., 312 (1984) 313.

Analytica Chimica Acta, 194 (1987) 293—298
Elsevier Science Publishers B.V., Amsterdam — Printed in The Netherlands

Short Communication

LIQUID-LIQUID EXTRACTION OF SILVER ION WITH BENZOTHIACROWN ETHER DERIVATIVES

MASATOSHI OUE*

Department of Chemical Engineering, Nara National College of Technology, Yata, Yamato-Koriyama, Nara 639-11 (Japan)

KEIICHI KIMURA and TOSHIYUKI SHONO

Department of Applied Chemistry, Faculty of Engineering, Osaka University, Yamada-oka, Suita, Osaka 565 (Japan)

(Received 26th June 1986)

Summary. The extraction behavior of mono-, poly-, and bis-(benzothiacrown ether)s is studied for alkali, alkaline-earth, heavy, and transition metal ions in the presence of picrate. These ethers show high selectivity for silver ion. Silver extractions from binary and quaternary mixtures of silver with heavy or transition metal ions were successful, except for mixtures with mercury(II) ion. Silver was extracted from a copper ore with ca. 80% recovery.

Crown compounds are capable of complexing various cations. The kind of heteroatoms in the crown ring, i.e., oxygen, nitrogen, sulfur, or phosphorus, affects not only the cation affinity but also the cavity size. It is well known that crown ethers containing only oxygen as the heteroatoms are most likely to complex alkali and alkaline-earth metals [1]. Thiacrown ethers, in which some or all of the ring oxygen atoms are replaced by sulfur, show affinity to heavy or transition metal ions [2, 3]. Poly- and bis-(crown ether) derivatives which have monocyclic ethers in the side arm tend to form 2:1 (crown ether unit/cation) sandwich-type complexes with particular cations. Percent extraction of some cations is often increased compared with the corresponding monocyclic analogs [4, 5]. This is also the case for poly- and bis-(thiacrown ether) derivatives [6].

The liquid-liquid extraction of heavy and transition metals by poly- and bis-(thiacrown ether) derivatives [6] is efficient and highly selective for silver ions. This communication is concerned with applications of this extraction to Ag^+ recovery from several artificial samples and from actual copper ore. The thiacrown ethers examined are shown below (cf. Table 1).

Experimental

Chemicals. Benzothiacrown ether derivatives used as extraction reagents have been described [6]. 1,4,8,11-Tetrathiacyclotetradecane (TTC) was synthesized by a method similar to that of Rosen and Busch [7]. Metal nitrates were used for extractions (Wako Pure Chemicals).

0003-2670/87/$03.50

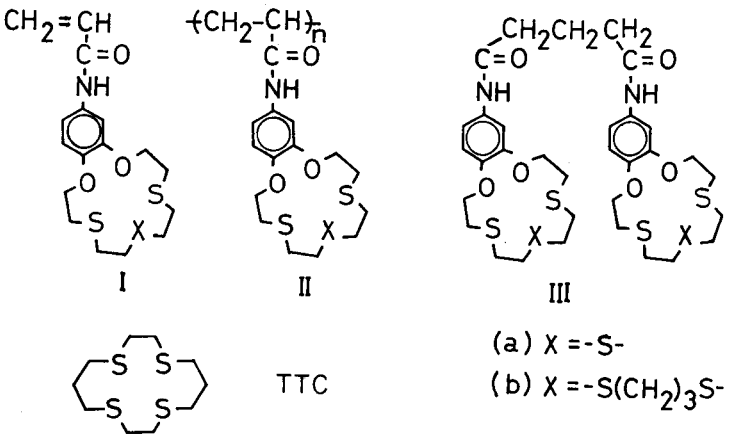

Liquid-liquid extraction. The procedure was as reported previously [6]. Equal volumes (10 ml) of an aqueous solution 1×10^{-5} M in metal nitrate and 1×10^{-4} M picric acid and a 5×10^{-5} M (for monomeric unit) solution of the benzothiacrown ether derivative in chloroform were placed in a stoppered flask and shaken for 40 min at 25.0 ± 0.1°C. After complete phase separation, the metal ion concentration in the aqueous phase was determined by flame emission or atomic absorption spectrometry (A-185 Jarrell Ash). When the percent extraction was small, the metal ion was quantified in the organic phase; the organic phase was evaporated, the residue dissolved in 10 ml of 6 M nitric acid, and the metal determined as before.

Selective separation of Ag^+ from mixtures containing Hg^{2+}, Zn^{2+}, Cu^{2+}, Pb^{2+}, Fe^{3+}, and Bi^{3+}. Extraction was done from aqueous 1×10^{-5} M silver(I) solution containing appropriate concentrations of the interfering ions and 1×10^{-4} M picric acid, into chloroform which contained 5×10^{-5} M (monomeric unit) in the benzothiacrown ether derivative. The ratio of interfering ions to Ag^+ in the aqueous phase was 10 for the binary systems and 1 for quaternary systems.

Silver recovery from a copper ore. The copper ore used was from South America and was a gift from Mitsubishi Metal Co. The sample contained about 80 g silver per tonne after drying. Dried ore (5.03 g) was ground finely in a mortar and then stirred with 10 ml of concentrated nitric acid at room temperature until no further dissolution occurred. The residual insoluble material was filtered off. The filtrate was diluted 1000-fold with deionized water. Silver ion was extracted from a 10-ml aliquot as described above but without picric acid present. In some cases, after the silver determination, a further 5 ml of the diluted aqueous solution was again extracted with 5 ml of the chloroform solution of the reagent.

Results and discussion

Liquid-liquid extraction. In the previous work [8], silver picrate was extracted efficiently by poly- and bis-(thiacrown ether)s **II** and **III**, while silver

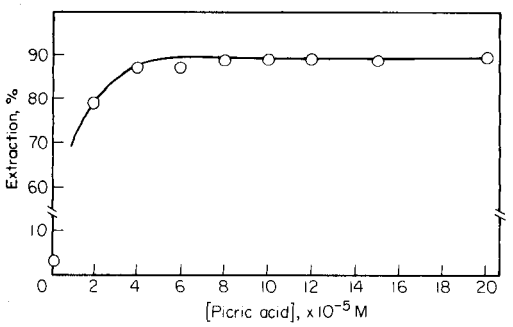

Fig. 1. Relationship between silver extraction and picric acid concentration in extraction with poly(thiacrown ether)s IIa. Silver ion concentration 1 × 10^{-5} M; crown ether unit concentration 5 × 10^{-5} M.

nitrate was extracted only slightly. Thus the cation extraction by the thiacrown ether derivatives depended on the counter anion and picrate was better than nitrate as the anion. However, for practical applications, one cannot consider only pure metal picrates. Therefore, picric acid was added to aqueous silver nitrate solutions to increase the percent extraction. Figure 1 shows the relationship between picric acid concentration in the aqueous phase and Ag^+ percent extraction by compound IIa. Without picric acid, the percent extraction for Ag^+ was very low. Increasing picric acid concentrations enhanced the Ag^+ extraction and the percent extraction became constant (at about 90%) at a picric acid/metal ratio of about 8; a ratio of 10 was adopted routinely.

With that ratio of picric acid, various metal ions were extracted by using the thiacrown ethers with the results shown in Table 1. For comparison, TTC was also tested. Silver(I), Hg^{2+}, and Pd^{2+} were extracted by TTC, the percent extraction being 52.7, 33.3, and 27.3%, respectively. The other heavy or transition metals, and alkali and alkaline-earth metal ions, were scarcely extracted. These results are supported by the affinity of thiacrown ethers, but TTC does not possess high ion selectivity for soft metal ions. In contrast, benzothiacrown ether derivatives I—III(a, b) showed excellent selectivities for Ag^+ and Hg^{2+}. Though the extraction abilities of the monocyclic thiacrown ethers are lower than those of the poly and bis derivatives, the mono derivatives are more selective for silver than the poly or bis compounds. The high affinity of the poly- and bis-(thiacrown ether)s for Ag^+ and Hg^{2+} can be explained by the fact that the thiacrown ethers easily form 2:1 (crown ether unit to cation) sandwich-type complexes which are more favorable than the 1:1 complexes for extraction.

Silver ion separation from binary and quaternary metal systems. Silver in actual samples often co-exists with Cu^{2+}, Zn^{2+}, or Pb^{2+}. Recovery of silver from silver-containing products (silver plate, batteries, jewellery, etc.) is now often used to conserve source materials. Separation of silver from such materials is difficult because of the variety of materials.

TABLE 1

Extraction of various metal ions by thiacrown ethers[a]

Metals	Extraction[b] (%)						
	Ia	IIa	IIIa	Ib	IIb	IIIb	TTC
Na^+	0.4	0.6	0.3	0.6	1.0	0.4	0.0
K^+	0.2	0.4	0.1	0.3	0.3	0.2	0.5
Ca^{2+}	0.0	0.6	0.0	0.0	0.8	0.0	0.8
Fe^{3+}	0.1	0.4	0.3	0.1	0.3	0.3	2.8
Co^{2+}	0.1	0.1	0.3	0.0	0.2	0.3	8.3
Cu^{2+}	0.0	0.8	0.6	0.2	1.5	0.7	7.1
Ag^+	70.3	90.6	86.7	71.6	90.6	88.4	52.7
Zn^{2+}	0.4	1.4	1.3	0.4	2.1	1.5	10.0
Cd^{2+}	0.0	0.2	0.2	0.1	0.4	0.5	2.6
Hg^{2+}	0.0	90.4[c]	25.1	0.0	90.4[c]	25.3	33.3
Pb^{2+}	0.9	1.5	1.5	1.3	1.5	1.5	5.0
Pd^{2+}	0.0	0.0	0.0	0.0	0.0	0.0	27.3

[a][ThiaCr unit]/[metal] = 5×10^{-5} M/1×10^{-5} M. In IUPAC nomenclature, **Ia** is 2,3-(4′-acryloylaminobenzo)-1,4-dioxa-7,10,13-trithiacyclopentadeca-2-ene; **IIa** is poly[2,3-(4′-acryloylaminobenzo)-1,4-dioxa-7,10,13-trithiacyclopentadeca-2-ene]s; **IIIa** is 1,3-bis[(3′,-4′-benzo-1″,4″-dioxa-7″,10″,13″-trithiacyclopentadeca-2″-ene)aminocarbonyl]propane; **Ib** is 2,3-(4′-acryloylaminobenzo)-1,4-dioxa-7,10,14,17-tetrathiadioxacyclononadeca-2-ene; **IIb** is poly[2,3-(4′-acryloylaminobenzo)-1,4-dioxa-7,10,14,17-tetrathiacyclononadeca-2-ene]s; **IIIb** is 1,3-bis[(3′,4′-benzo-1″,4″-dioxa-7″,10″,14″,17″-tetrathiacyclononadeca-2″-ene)-aminocarbonyl]propane.

[b]Evaluated from the metal ion concentration in the aqueous phase.

[c]Some precipitate was formed at the interface between organic and aqueous phases. The values of percent extraction are, therefore, apparent ones.

It is clear that the benzothiacrown ethers tested are efficient extractants for Ag^+ alone. To establish their behavior in the case of binary and quaternary cation systems containing silver and other heavy or transition metals, tests were made with various other metal ions present. For the binary systems

TABLE 2

Selective extraction of silver ion from binary cation systems[a]

Thiacrown ether	Extraction (%)							
	Ag^+	Cu^{2+}	Ag^+	Zn^{2+}	Ag^+	Pb^{2+}	Ag^+	Hg^{2+}
Ia	39.7	0.1	33.0	7.0	37.8	1.1	1.3	0.5
IIa	94.9	1.2	96.9	8.4	99.2	1.9	1.3	45.2
IIIa	96.2	0.6	96.3	4.7	97.2	1.9	0.0	0.6
Ib	91.0	0.8	87.5	6.7	91.9	1.2	0.0	0.6
IIb	97.4	1.6	98.2	6.1	99.2	1.9	0.0	47.6
IIIb	97.4	1.1	97.3	4.7	97.6	1.9	0.0	35.5

[a][MNO_3] = 1×10^{-4} M, [$AgNO_3$] = 1×10^{-5} M, [crown ether unit concentration] = 5×10^{-5} M.

with Ag^+ and Cu^{2+}, Zn^{2+}, or Pb^{2+} (Table 2), the extraction efficiency for Ag^+ did not vary much for the poly- and bis-(thiacrown ether)s, but the monocyclic compounds were less effective than for silver alone. However, mercury(II) ions had a disastrous effect on all the Ag^+ extractions; compounds **IIa, IIb** and **IIIb** extracted only Hg^{2+} from the binary mixture. This might be partly due to the formation of the 2:1 (thiacrown unit/Hg^{2+}) complex, which is apt to precipitate irreversibly in these systems. The silver separations from Cu^{2+}, Zn^{2+}, and Pb^{2+} in the binary systems were reasonably effective at 10:1 M^{2+}/Ag^+ ratios.

In the quaternary system with Ag^+, Cu^{2+}, Fe^{3+} and Bi^{3+} (Table 3), there were no remarkable differences in the silver extraction ability compared with extractions of silver alone and selectivity was good.

Silver separation from copper ore. Separation of silver from copper ores was examined. Picric acid was not added because extraction of Ag^+ as the picrate proved to be impractical. Sevdic et al. [9] reported that a high concentration of acid in the aqueous phases enhances cation extraction with thiacrown ether derivatives. Therefore, the copper ore was dissolved in concentrated nitric acid and then this solution was diluted with water. Table 4 shows the results. Extraction was done twice successively from the aqueous phase. Although the ratio of Cu^{2+} over Ag^+ was about 5×10^3 in the original sample, Ag^+ was extracted to the extent of 6—20% in the first extraction. Only a little copper was extracted with any of the reagents. The percent extraction of Ag^+ was 52.6—73.8% with the poly and bis derivatives in the second extraction. A maximum of about 80% total extraction of Ag^+ was attained (Table 4). Thus some thiacrown ethers are quite promising for selective silver extraction from copper ores.

TABLE 3

Selective extraction of silver ion from quaternary cation systems[a]

Thiacrown ether	Extraction (%)			
	Ag^+	Cu^{2+}	Fe^{3+}	Bi^{3+}
Ia	40.7	0.3	0.9	0.1
IIa	80.6	0.3	0.8	0.2
IIIa	73.8	2.0	1.4	0.3
Ib	70.8	1.4	0.0	0.1
IIb	83.7	0.4	1.0	0.2
IIIb	73.8	1.6	1.0	0.2

[a] $[MNO_3] = 1 \times 10^{-5}$ M, [crown ether unit] $= 5 \times 10^{-5}$ M.

TABLE 4

Silver extraction from copper ore sample[a]

Thiacrown ether	First extraction (%)		Second extraction (%)	
	Ag^+	Cu^{2+}	Ag^+	Cu^{2+}
Ia	6.0	2.8	—	—
IIa	19.9	3.7	73.8	0.9
IIIa	14.3	2.9	66.7	0.7
Ib	13.6	2.8	—	—
IIb	14.7	3.7	68.8	1.4
IIIb	17.1	3.3	52.6	1.1

[a]The concentration ratio of Cu^{2+}/Ag^+ in the copper ore was about 5×10^3. Picric acid was not added.

REFERENCES

1 C. J. Pedersen, J. Am. Chem. Soc., 89 (1967) 2495.
2 V. B. Pett, L. L. Diaddario, Jr., E. R. Dockal, P. W. Corfield, C. Ceccarelli, M. D. Glick, L. A. Ochrymowycz and D. B. Rorabacher, Inorg. Chem., 22 (1983) 3661.
3 R. M. Izatt, R. E. Terry, L. D. Hansen, A. G. Avondet, J. S. Bradshaw, N. K. Dalley, T. E. Jensen and J. J. Christensen, Inorg. Chim. Acta, 30 (1978) 1.
4 K. Kimura, T. Maeda and T. Shono, Talanta, 26 (1979) 945.
5 S. Kopolow, T. E. Hogen Esch and J. Smid, Macromolecules, 6 (1973) 133.
6 M. Oue, A. Ishigaki, Y. Matsui, K. Kimura and T. Shono, J. Polym. Sci., Polym. Chem. Ed., 23 (1985) 2033.
7 W. Rosen and D. H. Busch, J. Am. Chem. Soc., 91 (1969) 4694.
8 M. Oue, A. Ishigaki, Y. Matsui, T. Maeda, K. Kimura and T. Shono, Chem. Lett., (1982) 275.
9 D. Sevdić, Lj. Jovanovac and H. Meider-Goričan, Mikrochim. Acta, (1975) 235.

Analytica Chimica Acta, 194 (1987) 299—302
Elsevier Science Publishers B.V., Amsterdam — Printed in The Netherlands

Short Communication

A MODIFIED METHOD FOR THE DETERMINATION OF LEAD IN ZIRCONS BY DIFFERENTIAL-PULSE ANODIC STRIPPING VOLTAMMETRY

M. M. PALRECHA, R. PARTHASARATHY and M. SANKAR DAS*

Analytical Chemistry Division, Bhabha Atomic Research Centre, Trombay, Bombay 400 085 (India)

(Received 28th July 1986)

Summary. Zircons (20—100 mg) are decomposed within 1 h by fusion with potassium hydrogenfluoride followed by fuming with sulphuric acid. With differential-pulse anodic stripping voltammetry, after deposition for 1 min, the limit of detection for lead is 2 ng ml^{-1} and the limit of quantitation is 6.6 ng ml^{-1}. Results (7—247 mg kg^{-1} lead) are reported for nine zircons.

Application of differential-pulse anodic stripping voltammetry (d.p.a.s.v.) for the determination of heavy metals at $\mu g\ l^{-1}$ levels is well established. Application of this technique for the determination of lead in zircon, an ubiquitous refractory mineral, widely used for radiometric dating, is reported in this communication.

Krogh [1] recommended dissolution of zircon with hydrofluoric acid in a Parr bomb for the isotopic examination of lead needed for dating purposes. Unfortunately samples (ca. 20 mg) had to be heated in the bomb at 220°C for one week. In the proposed method, zircon samples (up to 100 mg) were decomposed within 1 h by fusion with potassium hydrogenfluoride followed by fuming with sulphuric acid. In an earlier paper [2], zircon was fused with sodium carbonate and borax, and a.s.v. was applied to determine lead. It was found that the solutions obtained after that decomposition were turbid so that reproducibility was poor if the voltammograms were not recorded immediately. Calderoni [3] applied d.p.a.s.v. for the determination of lead in igneous rock after decomposing the sample with hydrofluoric acid and perchloric acid; hydroxylammonium chloride served as supporting electrolyte.

Among the various methods of attacking zircon, fusion with potassium hydrogenfluoride followed by fuming with sulphuric acid was found to provide a clear stable solution for d.p.a.s.v. This procedure was applied for the determination of lead in zircons from various geological environments with a view to estimating their ages [4].

0003-2670/87/$03.50

Experimental

Chemical. For the lead standard solution (100 μg ml^{-1}), dissolve 100 mg of pure lead (Merck) in 5 ml of 1 + 1 nitric acid (BDH, Aristar) and dilute to 1 l with distilled water. Prepare working solutions (10 μg ml^{-1}) by suitable dilution. Supplies of potassium hydrogenfluoride from E. Merck (purified crystals), J. T. Baker (analyzed reagent) and Hopkins & William (general-purpose reagent) were available in this laboratory. They were certified for "heavy metal contents as lead", but not specifically for lead. These samples were analyzed and found to contain 0.3—20 mg kg^{-1} lead. A particular supply from Hopkins & William which contained 0.3 mg kg^{-1} lead was selected.

Apparatus. A Princeton Applied Research polarographic analyzer Model 174 A with the SMDE 303-A was used.

Procedure. Mix the zircon sample (usually 50 mg) with 0.5 g of potassium hydrogen-fluoride in a platinum crucible and heat gently until it has melted. Place the crucible over a burner and heat gradually until a clear melt is formed. Cool and add 0.5 ml of Suprapur (Merck) concentrated sulphuric acid. Then heat the crucible on a sand bath to fumes of SO_3. Take the cooled melt up in deionized water with a drop of concentrated nitric acid added to keep lead in solution and dilute to 25 ml.

Transfer 10 ml of the sample solution to the SMDE cell and deaerate it with pure nitrogen (IOLAR grade, Indian Oxygen Ltd.). The d.p.a.s. voltammograms were recorded at a scan rate of 5 mV s^{-1} with 50-mV modulation amplitude, after preconcentration at —0.6 V (vs. Ag/AgCl) for 1 min.

Results and discussion

The method of fusion reported earlier [2] yielded turbid solutions because of silicic acid precipitation which tended to dislodge the mercury drop. The clear stable solutions obtained with the present procedure gave reproducible peak currents even after a week.

The mean process blank for lead (with 0.5 g of KHF_2 and 0.5 ml of sulphuric acid) was 8.3 ng ml^{-1} with a standard deviation of 1.1 ng ml^{-1} (n = 8) corresponding to a limit of detection (LOD) and limit of quantitatin (LOQ) [5] of 2 ng ml^{-1} and 6.6 ng ml^{-1}, respectively ($\overline{S}_{B1} = tS_{B1}/n^{1/2}$, where t = 5.4 for 7 d.f. at the 99.9% confidence level). The lowest concentration of 7 mg kg^{-1} lead in sample 2, is measured at 14 ng ml^{-1} which is well above the LOQ. Calibration is done by the standard addition method (Fig. 1). As d.p.a.s.v. is more sensitive than the a.s.v. technique used earlier, lead can be determined in as little as 20—30 mg of zircon; 500 mg of zircon was needed for the earlier procedure.

Table 1 gives the results obtained by the proposed method for zircons from various geological environments. The results are the means of three independent determinations. Replicate analyses of the in-house standard zircon MK Z-V yielded a value of 34 ± 3 mg kg^{-1} (n = 6) of lead, indicating good precision and accuracy; the previously reported value was 33 ± 3 mg kg^{-1} [2].

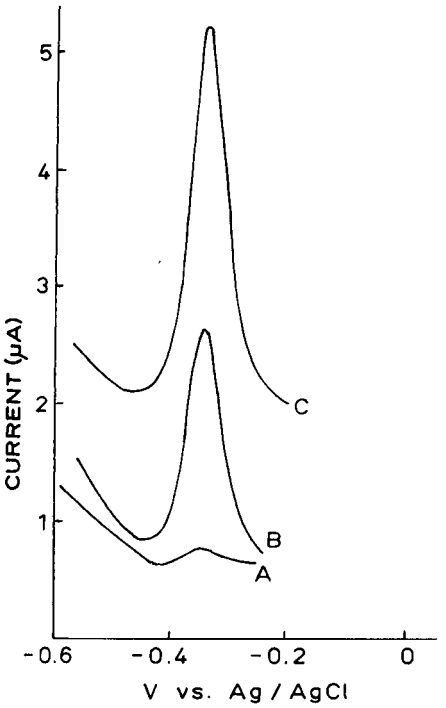

Fig. 1. Voltammograms obtained in a typical run: (A) blank (0.5 g KHF_2 + 0.5 ml H_2SO_4 in 25 ml); (B) sample (KUN Z.R., 47.5 mg in 25 ml); (C) sample with standard addition (1 μg Pb added to 10 ml of solution B). Conditions: scan rate 5 mV s^{-1}, modulation amplitude 50 mV, deposition potential −0.6 V, deposition time 1 min, rest time 0.5 min.

TABLE 1

Lead content of zircons

Sample identity	Sample description	Lead content[a] (mg kg^{-1})
MK. Z.V.	Beach sand; Manavalakurchi, Tamil Nadu (TN)	34 ± 3 (n = 6)
Kas. S.B.	Pegmatite; Kasipatnam, Andhra Pradesh (AP)	7
J_z	Pegmatite; Odara (Kerala)	77
H_z	Gneissic charnockite; Komalam (Kerala)	45
Tvm. Z.M.	Acidic charnockite; Pachalur (Kerala)	247
Kun. Z.R.	Nepheline syenite; Kunavaram (AP)	43
Put. Z.R.	Syenite associated with charnockite; Kanyakumari (TN)	32
NS-137.Z	Pink granite; Shivpuri nr. Malkajgiri Hyderabad (AP)	126
O_z	Beach sand, detrital; Chatrapur (Orissa)	37

[a]Mean of 3 analyses with an uncertainty of ±10% of the value.

REFERENCES

1 T. E. Krogh, Geochim. Cosmochim. Acta, 37 (1973) 485.
2 K. A. Khasgiwale, R. Parthasarathy and M. Sankar Das, Anal. Chim. Acta, 59 (1972) 485.
3 G. Calderoni, Talanta, 28 (1981) 65.
4 R. Parthasarathy, M. M. Palrecha and M. Sankar Das, J. Geol. Soc. India, 27 (1986) 110.
5 G. L. Long and J. D. Winefordner, Anal. Chem., 55 (1983) 712A.

Analytica Chimica Acta, 194 (1987) 303—309
Elsevier Science Publishers B.V., Amsterdam — Printed in The Netherlands

Short Communication

FOURIER-TRANSFORM INFRARED PHOTOACOUSTIC SPECTROSCOPY EVALUATED FOR NEAR-SURFACE CHARACTERIZATION OF POLYMERIC MATERIALS

CHARLES Q. YANG and WILLIAM G. FATELEY*
Department of Chemistry, Kansas State University, Manhattan, KS 66506 (U.S.A.)
(Received 21st May 1986)

Summary. Fourier-transform infrared photoacoustic spectroscopy was applied to the near-surface study of various polymeric materials including aluminum/polyethylene composite films, poly(vinyl chloride) composites, and various chemically-modified textile materials. Examples are given for surface identification of polymers, distribution of chemical additives in textile materials, and characterization of polymer surface degradation. This approach has various advantages over conventional infrared sampling techniques for the study of polymeric materials.

Photoacoustic spectroscopy (PAS) was first introduced for the study of polymer structures in the ultraviolet and visible spectral regions [1]. However, the relative paucity of structural information in these regions for most polymeric materials limits the usefulness of PAS. Fourier-transform infrared (FTIR) photoacoustic spectroscopy became a reality when photoacoustic detection was combined with an interferometer and a large data system in the late 1970s [2]. The high throughput and multiplexing advantages of FTIR spectrometers have made FTIR/PAS a practical technique with suitable signal-to-noise ratio [3, 4].

The FTIR/PAS approach demonstrates a number of advantages over the conventional transmission or reflection techniques. Opaque or highly scattering samples can be examined satisfactorily and samples are not altered or disturbed during the experiment, because little or no sample separation is needed for photoacoustic detection. Rough, brittle or other intractable solid samples can be examined by FTIR/PAS without sampling difficulties. In many industrial applications, polymeric samples are unsuitable for transmission or attenuated total reflectance measurements. In many cases, FTIR/PAS is the only alternative for infrared spectroscopic examination.

Fourier-transform infrared photoacoustic spectroscopy can be used as a surface probe to investigate the surface layers of solid materials, because only the heat generated within one thermal diffusion length from the sample surface can propagate into the gas and cause photoacoustic signals. Thermal diffusion length is inversely proportional to the square root of modulation

0003-2670/87/$03.50

frequency, which is the product of optical velocity and infrared frequency (in wavenumber) [5]. For optically opaque and thermally thick samples, i.e., when both optical penetration length and thermal diffusion length are smaller than sample thickness, the thermal diffusion length can be varied by changing the optical velocity if that length is smaller than the optical penetration length. Therefore, the effective sampling depth of PAS can be reduced by increasing the optical velocity of the interferometer and nondestructive depth-profiling is possible [5].

This communication describes applications of PAS to the study of a variety of polymeric materials including textile fibers, yarns, fabrics, poly(vinyl chloride) (PVC) composites, and aluminum/polyethylene composite films.

Experimental

An IBM IR-98 spectrometer was used to make all the FTIR/PAS measurements. Resolution for all the PAS measurements was 8 cm^{-1}; no smoothing function was used. Helium passing through a liquid nitrogen trap was used to purge the sample chamber. Carbon black was used as a reference material.

Cotton yarns sized with various polymeric sizing agents were provided by Southern Regional Research Center, U.S. Department of Agriculture. Finished cotton fabrics were provided by United Merchants and Manufacturers. The finishing agents used were dimethyloldihydroxyethylene urea (DMDHEU; Valrez 248) and methylated DMDHEU (Valrez ULF). The aluminum/polyethylene composite films were provided by Jiangsu Communication Cable Comapany, P.R. of China.

Results and discussion

Surface identification. The Cr(III) fumarato coordination compound, Volan-82, is an excellent bonding agent in promoting durable adhesion of low-density polyethylene to aluminum [6, 7]. If polyethylene laminated on aluminum foil with Volan-82 is peeled off, then retention of polymer on the substrate surface indicates cohesive failure [8]. Such a surface was examined here by using scanning electron microscopy (SEM), Auger electron spectroscopy (AES), x-ray photoelectron spectroscopy (XPS) and FTIR/PAS. No differences between the peeled aluminum surface and a blank aluminum-foil surface could be found by using SEM. However, the infrared spectrum exhibited peaks at 2925 cm^{-1} and 2850 cm^{-1} (Fig. 1), corresponding to the CH asymmetric and symmetric stretching vibrational frequency. This observation indicates that polyethylene was retained on the surface. Although the presence of carbon on the surface was confirmed with AES and XPS, it was not possible to identify polyethylene by either AES or XPS. The thickness of the polyethylene was estimated to be less than 1000 Å by using Auger sputter depth profiling. This example demonstrates that FTIR/PAS can be used to identify an ultra-thin polymer film on a metal surface.

Fourier-transform infrared photoacoustic spectroscopy was also used to identify sizing agents in the surface layer of cotton yarns. When untreated

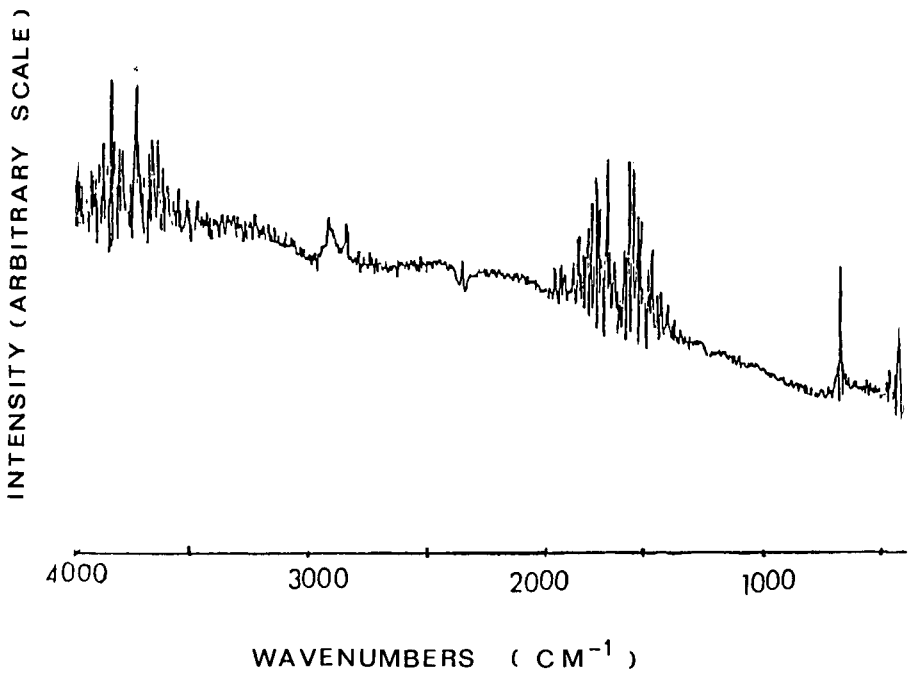

Fig. 1. Photoacoustic infrared spectrum of the aluminum surface when polyethylene was peeled from the aluminum/polyethylene composite film.

cotton yarn and yarn sized with a polyacrylate were examined by FTIR/PAS (Fig. 2, spectra A and B), it was found that the infrared spectrum of the sized yarn was similar to the spectrum of the untreated cotton yarn except for a band at 1735 cm^{-1} from the carbonyl of the polyacrylate. However, when the spectrum of the untreated yarn was subtracted from the spectrum of the sized yarn, most of the spectral features of the polyacrylate sizing agent (Fig. 2, spectrum D) appeared in the difference spectrum (Fig. 2, spectrum C), so that the sizing agent could be identified.

The sensitivity of surface identification using FTIR/PAS can also be enhanced by changing the optical velocity of the interferometer. A chemically-modified poly(ethylene terephthalate) (PET) fiber and the finishing agent were found to have similar infrared spectra except that the finish had an intense band at 2880 cm^{-1} corresponding to the asymmetric stretching of CH_2 of the poly(ethylene oxide) in the finish molecule. The amount of the finishing agent applied to the PET fiber was so small that the infrared spectrum of the modified PET fiber was almost identical to the spectrum of an untreated PET fiber. However, when the chemically-modified fiber was measured with different optical velocity, a shoulder at 2880 cm^{-1} pertaining to the finishing agent became more intense with an increase in the optical velocity (Fig. 3). This could be interpreted as evidence of the presence of more

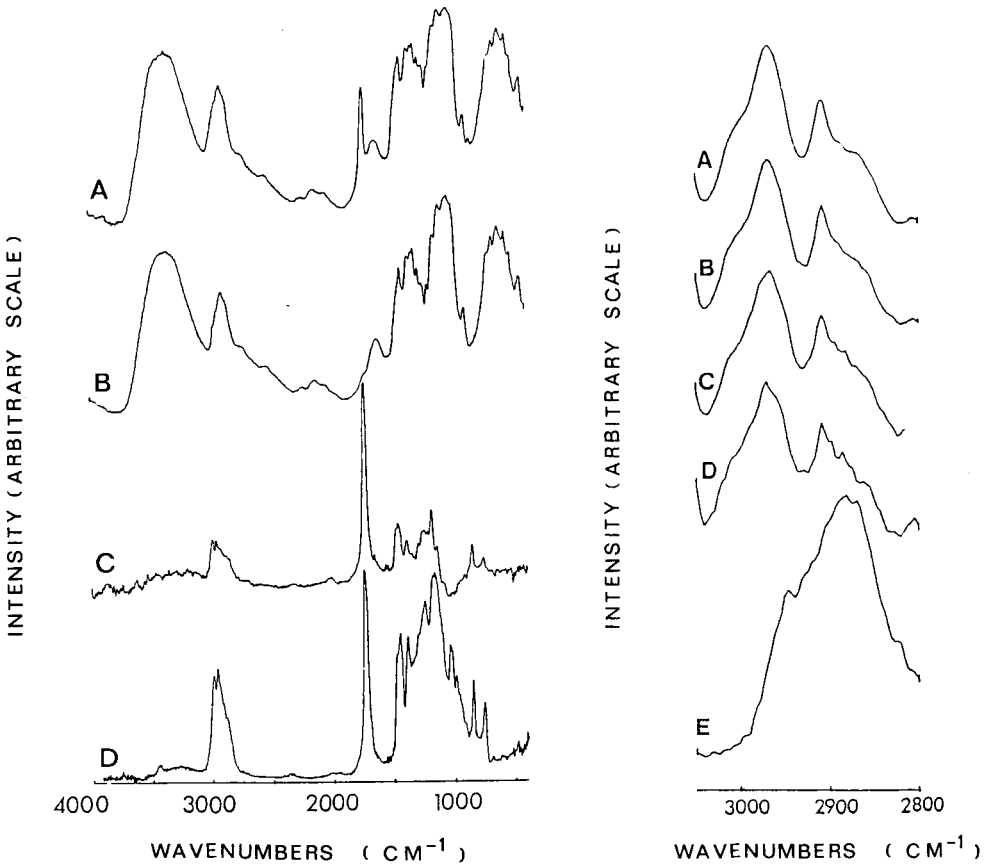

Fig. 2. Photoacoustic infrared spectra: (A) cotton yarn sized with the polyacrylate; (B) untreated cotton yarn; (C) difference, A — B; (D) the polyacrylate sizing agent.

Fig. 3. Photoacoustic infrared spectra of the chemically-modified PET fiber collected at different optical velocities: (A) 0; (B) 3; (C) 6; (D) 9 cm s^{-1}. (E) Photoacoustic infrared spectrum of the finishing agent.

finishing agent in a thinner surface layer of the fiber, because increasing the optical velocity reduces the sampling depth of PAS as was discussed above.

Determination of penetration of chemical additives in textile materials. Two finishing agents, Valrez 248 and Valrez ULF, were applied to cotton fabrics with conventional padding and foam-finishing techniques [9]. The cotton fabrics treated with Valrez ULF using conventional padding and foam-finishing techniques were examined with FTIR/PAS for both intact and ground portions of the two fabric samples in order to compare results for surface layers and bulk materials. The carbonyl peak intensities at 1720 cm^{-1} for the cotton fabrics and the corresponding powdered samples are summarized

in Table 1. The peak ratios of 0.92 and 1.10 for the foam finishing treatment suggest a more homogeneous finish distribution for this technique than for the padding treatment. This explains the observation that wrinkle recovery angle was generally higher for the foam-finished cotton fabrics than for the conventionally finished fabrics [9], because a more homogeneous distribution of the finishing agents throughout the cotton fabrics would allow more fibers to be cross-linked, thereby improving the wrinkle recovery properties.

The distribution of various sizing agents in the cotton yarns was also studied by using FTIR/PAS, again for ground (40-mesh screen) and unground samples. The intensity of a band at 1735 cm^{-1}, from the carbonyls of the polyacrylate sizing agent, was lower for ground yarns than for intact yarns, indicating that the polyacrylate is more concentrated in the surface layer than in the bulk.

The distribution of the sizing agents in the cotton yarns can also be investigated by FTIR/PAS depth profiling. The polyacrylate-sized cotton yarn was examined with FTIR/PAS using different velocities. Ratios of the peak intensity at 1730 cm^{-1} to the peak intensity at 1430 cm^{-1}, chosen as a reference because it represents the CH bending of cellulose molecules in the cotton yarn, were evaluated as a function of optical velocity. The intensity ratio was used as a semiquantitative measure of the amount of the polyacrylate sizing agent compared to the amount of cellulose within the PAS sampling depth. When the optical velocity was increased from 0.235 cm s^{-1} to 1.119 cm s^{-1}, the thermal diffusion length was decreased from 6.1 μm to 2.8 μm. A corresponding increase in the peak intensity ratio (Fig. 4) was probably due to a higher concentration of the sizing agent in the surface layer than in the underlying layers.

Characterization of surface oxidization and degradation. A cotton fabric weathered outdoors for 100 h and an unweathered fabric were examined by using FTIR/PAS. The infrared spectra of the weathered and the unweathered fabrics were almost identical. However, when the spectrum of the unweathered fabric was subtracted from the spectrum of the weathered cotton fabrics, poorly resolved carbonyl bands assumed to be due to various oxidation products of cellulose were observed in the difference spectrum.

TABLE 1

Carbonyl peak intensities (1720 cm^{-1}) of the treated cotton fabrics

Finishing agent	Finishing technique	Carbonyl peak intensity (Arbitrary unit)		Carbonyl peak intensity ratio (powder/fabric)
		Fabric	Powder	
Valrez 248	Conventional	1.14	0.65	0.57
Valrez 248	Foam-finishing	1.06	0.98	0.92
Valrez ULF	Conventional	1.11	0.64	0.58
Valrez ULF	Foan-finishing	0.80	0.88	1.10

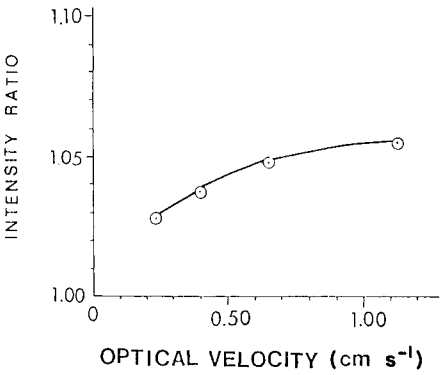

Fig. 4. Peak intensity ratio, I (1730 cm^{-1})/I (1430 cm^{-1}).

Bands at 1722 and 1704 cm^{-1} are possibly due to carbonyls of aldehyde, ketone and carboxylic acid formed as the oxidization products of the $-CH_2OH$ and —CHOH— groups of cellulose.

A poly(vinyl chloride) (PVC) composite was weathered in the desert for 6 months and then examined by PAS at two velocities; the spectra were compared to that of an unweathered PVC composite. A broad band at 3300 cm^{-1} observed in the weathered samples could be assigned to hydrogen-bonded OH stretching, indicating the presence of hydroxyl groups in the weathered PVC composite. A band at 1034 cm^{-1} probably corresponding to the alcoholic CO stretching vibration, suggested the formation of —CHOH— through the hydrolysis of poly(vinyl chloride) during the weathering process. The intensity of the peak at 1034 cm^{-1} increased as the optical velocity was increased from 0.235 cm s^{-1} to 0.665 cm s^{-1}. Because the thermal diffusion length of PVC at 1034 cm^{-1} for optical velocities of 0.235 and 0.665 cm s^{-1} were 12.8 and 7.6 μm, respectively, a more intense peak at 1034 cm^{-1} observed at a faster optical velocity indicated that more chloride groups underwent hydrolysis in the outer 7.6 μm of the surface layer than in the underlying layers. The carbonyl in the unweathered PVC composite was due to dibutyl phthalate, which was used as a plasticizer. The broadening of the carbonyl peak observed in the spectrum of the weathered PVC composite was due to the oxidation of the PVC. Shoulders at 1720 and 1701 cm^{-1} could probably be assigned to the carbonyls of ketone and carboxylic acid formed during the oxidation process. It was also noticed that the carbonyl peak in the spectrum of the cross-section of the weathered PVC was similar to that of the unweathered PVC composite, indicating that the bulk of the composite was not oxidized during the weathering process.

When the spectra of the weathered PVC composite were measured with three different optical velocities, it was found that the intensities of the shoulders at 1720 and 1701 cm^{-1} increased as the optical velocity was increased. The thermal diffusion length of poly(vinyl chloride) at 1720 cm^{-1}

decreased from 9.9 to 5.9 μm for optical velocities of 0.235 to 0.665 cm s^{-1}, respectively. An observed increase in peak intensity as a result of increased optical velocity indicated that the oxidation products had higher concentrations in the surface layers. This is consistent with the observation that oxidation of the composite was a near-surface phenomenon as mentioned above.

Special acknowledgement is made to Dr. R. R. Bresee, Department of Clothing, Textile and Interior Design, Kansas State University, and Dr. T. A. Perenich, Department of Clothing, Textile, Furnishing and Interiors, the University of Georgia, for their valuable advice. This work was done with the support of the U.S. Department of Energy, Grant No. DE-FG02-85ER13347.

REFERENCES

1 L. H. Lee, Polym. Sci. Technol., Part A, 12 (1980) 87.
2 M. G. Rockley, Chem. Phys. Lett., 68 (1979) 455.
3 T. A. Graham, W. M. Grim III and W. G. Fateley, in J. R. Ferraro and L. J. Basile (Eds.), Fourier-Transform Infrared Spectroscopy, Vol. 4, Academic, New York, 1985, p. 345.
4 J. F. McClelland, Anal. Chem., 55 (1983) 89A.
5 A. Rosenwaig, Photoacoustics and Photoacoustic Spectroscopy, Wiley, New York, 1980, pp. 34, 271.
6 J. A. Robertson and J. W. Trebilcock, Tappi, 58 (1975) 106.
7 C. Q. Yang and Q. L. Zhou, in L. H. Lee (Ed.), Adhesive Chemistry, Plenum, New York, 1984, p. 801.
8 R. C. Hartlein, Ind. Eng. Chem. Process. Des. Dev., 10 (1971) 92.
9 T. A. Perenich, Text. Chem. Color., 16 (1984) 241.

Analytica Chimica Acta, 194 (1987) 311—315
Elsevier Science Publishers B.V., Amsterdam — Printed in The Netherlands

Short Communication

NUCLEAR MAGNETIC RELAXATION DISPERSION MEASUREMENT OF WATER MOBILITY AT A SILICA SURFACE

CARL F. POLNASZEK[a], DOUGLAS A. HANGGI[b] and PETER W. CARR

Department of Chemistry, University of Minnesota, Minneapolis, MN 55455 (U.S.A.)

ROBERT G. BRYANT*

Department of Biophysics, University of Rochester Medical Center, Rochester, NY 14642 (U.S.A.)

(Received 3rd November 1986)

Summary. Nuclear magnetic relaxation rates are measured as a function of magnetic field strength corresponding to proton Larmor frequencies ranging from 0.01 to 42 MHz for silica gel samples with a nitroxide free radical covalently attached at the surface. The field dependence of the relaxation rate is interpreted using a translational model for the relaxation equation to yield a translational diffusion coefficient for the water, in the immediate vicinity of the radical attached to the surface, of 2.1×10^{-6} cm^2 s^{-1} at 278 K for Si-4000 silica.

The dynamic behavior of solvents close to surfaces is fundamental to the understanding of a number of processes. Characterization of diffusive behavior at a surface region has considerable fundamental importance for both gas and liquid chromatography where a small ratio of mobilities in the surface region to those in the interstitial mobile phase may result in excessive band broadening [1—3]. Horvath and Lin [1] and Chen and Weber [2] have proposed that the dynamics of the solute dissociation from the surface may be an important broadening mechanism when very small particles (<10 μm) are used in high-performance liquid chromatography. The dynamics of the dissociation process may be limited either by chemical kinetics or by translational diffusion through the surface layer of bound ligand. Limited diffusion in the surface region could be an important factor in the dissociation process, especially in polymeric films of bonded phases [1]. The pores of silica gel are never perfectly uniform. Internal tortuosity and restricted pores may decrease the apparent diffusion coefficient inside the particle. However, the method used in this study reports the translational mobility of the solvent measured over a distance approximately 10 Å from the labelled position at the surface. Thus, effects of diffusion barriers are minimized.

[a]Present address: FMC Corporation, 4800 East River Road, Minneapolis, MN 55421 (U.S.A.).
[b]Present address: 3M Company, St. Paul, MN (U.S.A.).

0003-2670/87/$03.50

The technique exploits the translational contribution to the electron-nuclear dipole-dipole interaction that drives nuclear magnetic relaxation in solutions or suspensions containing paramagnetic centers. In the case for which the electron spin relaxation time is very long, the correlation time that dominates the nuclear spin lattice relaxation rate of the solvent protons is the translational correlation time for the solvent in the vicinity of the paramagnetic center [4—7]. Because the strength of the dipole-dipole interaction falls very rapidly with distance, the range over which the relaxation mechanism dominates is ca. 10 Å; however, the whole sample is affected by the interaction because of rapid mixing between the surface region and the bulk solution [5]. Nitroxide free radicals, which have the requisite long relaxation time for the unpaired electron, have been used to measure translational mobility at a protein surface [4, 5] and at a lipid surface. In the present case, localization of the radical at the silica surface was accomplished by covalent attachment. The mobility of water is thus measured within ca. 10 Å of the paramagnetic label, which is at the surface.

Experimental

Nuclear magnetic relaxation measurements were made over a wide frequency range using a relaxation spectrometer constructed in this laboratory in collaboration with Dr. Seymour Koenig and Dr. Rodney Brown III, of the IBM Watson Laboratory, Yorktown Heights, New York. This instrument measures proton spin-lattice relaxation rates over a range of magnetic field strengths corresponding to proton Larmor frequencies from 0.01 to 42 MHz with constant signal-to-noise ratio by rapidly switching the d.c. magnetic field from a high soaking field, in which spins are polarized, to a relaxation field of interest followed by pulsing the field back to a convenient field at which the magnetization is sampled. Measurement of the magnetization as a function of the time at the relaxation field permits accurate measurement of the relaxation rate. In the measurements reported here, the free induction decay following a single 90° pulse was captured by a sample-and-hold circuit, digitized by an IBM-7406 Device Coupler, and analyzed directly in an IBM-5120 computer that controlled the spectrometer. Field switching times are approximately 15 ms, and 30 points were used in the decay fit for each relaxation time reported at each field strength measured.

The spin lattice relaxation rate was interpreted by using the equation

$$(1/T_{1p}) = 2.786 \times 10^{-11}\ c/Db\,[3j(\omega_I) + 7j(\omega_s)] \tag{1}$$

where c is the molar concentration of nitroxide, D the relative translational diffusion coefficient, which is the sum of the diffusion constants of the nitroxide and of water, b the effective distance of closest approach of the two spins, and $j(\omega)$ is the spectral density given by

$$j(\omega) = [1 + (5/8)z + (1/8)z^2]/[1 + (1/2)z^2 + (1/6)z^3 + (4/81)z^4 + (1/81)z^5 + (1/648)z^6] \tag{2}$$

where $z = (2\omega b^2/D)$, ω_I is 2π times the proton Larmor frequency, and ω_s, the electron Larmor frequency, is 658 ω_I. As the diffusion coefficient for water is much greater than that for the immobilized nitroxide, the relaxation rate depends primarily on the translational motion of the water near the nitroxide radical. The field dependence of the relaxation rate was fitted using this equation which has been tested previously [5], and shown to provide accurate measures of the translational diffusion coefficient in water when a low-molecular-weight nitroxide is used as the paramagnetic center.

LiChrosphere Si-4000 silica (10-μm diameter, 400-nm mean pore diameter; Merck) was silylated with triethoxy-γ-aminopropylsilane (Petrarch Systems, Levittown, PA) after the method of Waterton and Hall [8] which yields approximately monolayer coverages of bonded silane. In the procedure, 1.0 g of silica was outgassed under vacuum while suspended in 10 ml of deionized water, after which 200 μl of the silane reagent, freshly diluted in 2.0 ml of water, was added with vigorous stirring for 1 min during which time the silane absorbed onto the silica. The solution was then promptly vacuum-filtered without washing in order to remove excess of reagent. The silica gel was then dried for 24 h at 50°C followed by 24 h in a vacuum oven at 110°C and 0.026 Pa in order to cure the bonded phase. Silica gels prepared in this manner have been widely used as high-performance liquid chromatographic phases in both normal-phase and ion-exchange modes, as well as supports for the immobilization of biological macromolecules for immobilized enzyme reactors and affinity chromatographic applications. The silanol blocking properties of aminosilanes on silica surfaces is well documented [9], with the majority of bonded ligands folding so as to allow the amino group to hydrogen-bond with the silanol surface. As a result of these interactions, amino-bonded silica displays significantly less silanophilic interactions relative to other bonded phases, while retaining significant reactivity towards amine-sensitive reagents.

Nitroxide spin labels were immobilized on the amino-silicas by reacting succinimidyl 2,2,5,5-tetramethyl-3-pyrroline-1-oxyl-3-carboxylate (amino-acyl-SL) with the amino-bonded silica [10]. The reaction vessel was outgassed and the reaction allowed to proceed for 3 days. Excess of unreacted spin label was removed by washing the silica with deionized water, methanol, and ether. The sample was dried for 24 h in a vacuum oven at 358 K. Deionized water was added to the silica sample, the sample centrifuged at the lowest speed using a bench-top clinical centrifuge, an aliquot drawn off for electron spin resonance studies (ESR), and a vortex plug inserted to force excess of water from the silica portion of the sample. The water above the plug was removed by pipet. The nuclear magnetic relaxation dispersion measurements and the ESR studies were conducted as previously reported [4, 5].

Results and discussion

The water proton spin-lattice relaxation rates measured as a function of field strength are shown in Fig. 1 for both unmodified and derivatized

silica surfaces. The nitroxide concentration was nominally 2.2×10^{-3} M. The minor field dependence associated with the lower field strengths in the control sample, which is interesting in its own right and will be treated elsewhere, was subtracted from the derivatized data set and the resulting curve was fitted to the relaxation Eqn. 1. The parameters obtained at 278 K that yield the solid curve in Fig. 1 are: $D = 2.1 \times 10^{-6}$ cm^2 s^{-1} and $B = 1.8$ Å, assuming a field-independent electron relaxation rate of 3.5×10^9 s^{-1}.

This result for the translational mobility of water close to the silica gel surface is smaller than that for pure water at the same temperature, 1.8×10^{-5} cm^2 s^{-1}. The value of the diffusion constant obtained here represents an average over the volume within approximately 10 Å of the radical label; thus, it is not a number characterizing just the first one or two monolayers because the label is attached to the silica by a tether of finite length. Nevertheless, the mobility of the solvent in this region close to the silica surface is attenuated by almost a factor of ten. Similar observations have been reported using this technique on a protein [4, 5]. The major uncertainties in this measurement derive from the length and flexibility of the tether attaching the radical label to the surface, adding uncertainty to the precise region sampled by the measurement, the assumption that any complexes formed between the nitroxide radical and the solvent are short-lived, and the approximations of the theory discussed in detail previously [5].

These results are in reasonable agreement with a neutron diffraction study of deuterium oxide in silica samples with pores similar to those used in this study. This neutron diffraction study showed that modification of the solvent properties by the interface is limited to approximately 10 Å or less

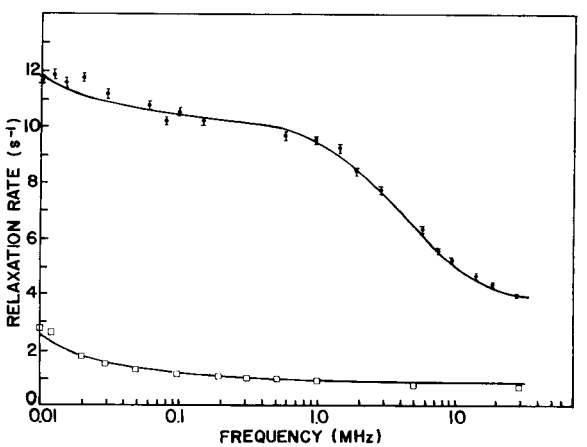

Fig. 1. The water proton nuclear magnetic spin lattice relaxation rate measured as a function of magnetic field strength for slurries of Si-4000 derivatized with an aminopropyltriethoxysilane that was labeled with an aminoacyl nitroxide. The temperature was 278 K and the label concentration was 2.2×10^{-3} M. (□) The control curve obtained on the same material without the spin label attached. The solid curve through the upper points is a theoretical fit to the data as described in the text.

[11]. Also, the structural arrangement of the water was reported to be similar to that in the bulk. These data and conclusions are consistent with earlier nuclear magnetic relaxation studies that address water mobility at silica surfaces [12—15] though the method exploited in these experiments is fundamentally different. In summary, these results support the view that the water mobility at the silica-gel hydrophilic surface is clearly attenuated, but the water is hardly immobilized, a fact that will be important in modelling solvent participation in the dynamics of chemical separations.

This work was supported in part by the National Institutes of Health and the National Science Foundation.

REFERENCES

1 C. Horvath and H. -J. Lin, J. Chromatogr., 149 (1978) 43.
2 J. C. Chen and S. G. Weber, Anal. Chem., 55 (1983) 127.
3 J. C. Giddings, Dynamics of Chromatography, M. Dekker, New York, 1965.
4 C. F. Polnaszek and R. G. Bryant, J. Am. Chem. Soc., 106 (1984) 428.
5 C. F. Polnaszek and R. G. Bryant, J. Chem. Phys., 81 (1984) 4038.
6 R. G. Bryant, C. F. Polnaszek, S. D. Kennedy, J. Hetzler and D. Hickerson, Med. Phys., 11 (1984) 712.
7 C. F. Polnaszek and R. G. Bryant, Magn. Reson. Med., 2 (1985) 296.
8 L. D. Waterton and J. C. Hall, J. Am. Chem. Soc., 101 (1979) 3697.
9 C. -H. Chiang, H. Ishida and J. Koenig, J. Colloid Interface Sci., 74 (1980) 396.
10 B. J. Gaffney, in L. G. Berliner (Ed.), Spin Labeling Theory and Applications, Academic, New York, 1976, pp. 183—238.
11 D. C. Steytler, D. C. Dore and C. J. Wright, Mol. Phys., 48 (1983) 1031.
12 J. A. Glasel, Nature, 227 (1970) 704; J. Am. Chem. Soc., 96 (1974) 970.
13 R. T. Pearson and W. Derbyshire, J. Colloid Interface Sci., 46 (1974) 232.
14 G. Belfort, J. Scherfig and D. O. Seevers, J. Colloid Interface Sci., 47 (1974) 106.
15 E. Almagor and G. Belfort, J. Colloid Interface Sci., 66 (1978) 146.

Analytica Chimica Acta, 194 (1987) 317—322
Elsevier Science Publishers B.V., Amsterdam — Printed in The Netherlands

Short Communication

ELECTROCHEMICAL DIGITAL SIMULATION: RE-EVALUATION OF THE CRANK-NICOLSON SCHEME

DIETER BRITZ* and KARSTEN THOMSEN
Kemisk Institut, Aarhus Universitet, 8000 Aarhus (Denmark)

(Received 1st February 1987)

Summary. It has been found that in those cases where the boundary concentration is determined by a known current, the standard Crank-Nicolson method can produce very poor results. Chronopotentiometry is used as an example.

Although the Crank-Nicolson technique [1, 2] is perhaps not used in most digital simulation, there is general agreement that it is superior in accuracy, stability and computational efficiency (the last despite the extra computing required by the method) compared with the standard explicit technique [2, 3]. This agreement is possibly based on such test-case experiments as the diffusion-limited potential step (see below), where the Crank-Nicolson method indeed performs very well. In a current investigation of the implicit boundary-value technique of Heinze, Störzbach and Mortensen (HSM) [4], we were surprised to find very poor results by the Crank-Nicolson method, when the HSM method was not applied; this occurred whenever the concentration c_0 at the electrode is determined by the current (strictly, by the concentration gradient, which is proportional to it). In this communication, a clear example of this is given for the case of chronopotentiometry and remedies are suggested.

Definitions

In the following, the equation to be solved is

$$\partial c/\partial t = D\,\partial^2 c/\partial x^2 \qquad (1)$$

where c is the concentration, t the time, D the diffusion coefficient of the substance under study, and x the distance from the electrode. If c_b is the bulk concentration and τ the (arbitrary) duration of the experiment to be simulated, the standard normalizations [2], i.e., $C = c/c_b$, $T = t/\tau$ and $X = x/(D\tau)^{1/2}$, then lead to the dimensionless equation

$$\partial C/\partial T = \partial^2 C/\partial X^2 \qquad (2)$$

Time ($0 \leqslant T \leqslant 1$) is divided into discrete intervals δT and space into intervals of length H; the sample-point distribution 0, H, $2H$, $3H$, . . . $(m + 1)H$ is used, with c_{m+1} always held at bulk concentration. The concentration

0003-2670/87/$03.50

gradient at the electrode is given the symbol G_0. The quantity λ is defined as $\lambda = \delta T/H^2$.

Evaluation method

For evaluation of a given technique, one has two choices. The error is best expressed as

$$err = q_{sim}/q_{known} - 1 \tag{3}$$

and presented as $\log|err|$, where q_{sim} is the simulated quantity of interest, and q_{known} its known exact value. This error can be plotted either against $\log H$ (the usual numerical analysis practice) or, for practical purposes, against $\log(cpu/s)$, where *cpu* denotes actual computing time required in s. The latter is used here.

The relative efficiency of a given method with respect to another is the inverse ratio of the *cpu* time required by that method to that required by the reference method, here, always the explicit point-method [2]. In evaluating any Crank-Nicolson scheme, there is the problem that one has free choice of both δT and H, because of the stability of the method; λ may take any value (within reason). One way to handle this is to draw contour plots of $\log|err|$ in the $(H, \delta T)$ plane and superimpose contours of the required *cpu* on these. For any desired accuracy, the corresponding contour can then be followed to the minimum *cpu* value, resulting in the optimum $(H, \delta T)$ pair. This is tedious and can be expensive (in terms of computing time) but it turns out that λ values around $1 \leqslant \lambda \leqslant 3$ are usually optimum.

A Digital Equipment VAX 11/780 computer was used for the numerical experiments, programmed in FORTRAN, with all floating-point variables in double precision. *Cpu* was measured to a precision of 0.01 s by a VAX VMS system routine.

Results

Diffusion-limited potential-step experiment (the Cottrell equation). With the boundary condition $C_0 = 0$ (all T), the solution for $G_0(T)$ is $G_0(T) = 1/(\pi T)^{1/2}$ or $1/\pi^{1/2}$ at $T = 1$. The gradient G_0 must be calculated from the simulated C values; the equation used [5] is

$$G_0 \approx (1/A_n H) \sum_{i=0}^{n-1} B_{n,i} C_i \tag{4}$$

for some different n, with A and B coefficients as given elsewhere [5]. Figure 1(a) shows error against *cpu* using the explicit point-method, with a constant $\lambda = 0.45$ and $0.0001 \leqslant \delta T \leqslant 0.01$. Note that, fortuitously, $n = 3$ gives the smallest errors but $n = 5$ is to be considered the most reliable result [5]; $n > 4$ all give the same result.

Figure 2 shows the $\pm 10^{-4}$ accuracy contour in the $(H, \delta T)$ plane, for the Crank-Nicolson method, with $n = 5$, and superimposed *cpu* contours. There are two local *cpu* minima: points A and B. Clearly, the latter (if it can be

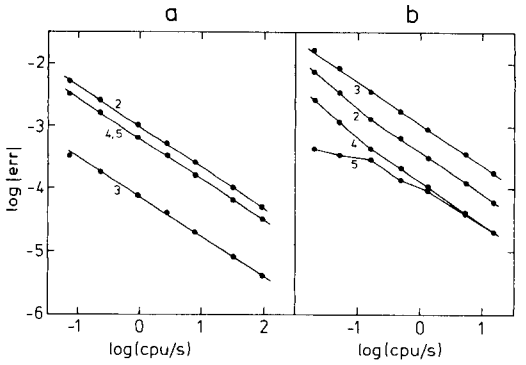

Fig. 1. Log|*err*| in $G_0(T = 1)$ against log(*cpu*/s) for the simulation of the diffusion-controlled potential-step experiment: (a) explicit point method, $\lambda = 0.45$ ($0.0001 \leqslant \delta T \leqslant 0.01$); (b) standard Crank-Nicolson scheme, $\lambda = 1$ ($0.001 \leqslant \delta T \leqslant 0.1$). In both cases, the controlled variable was δT, n as marked on the curves.

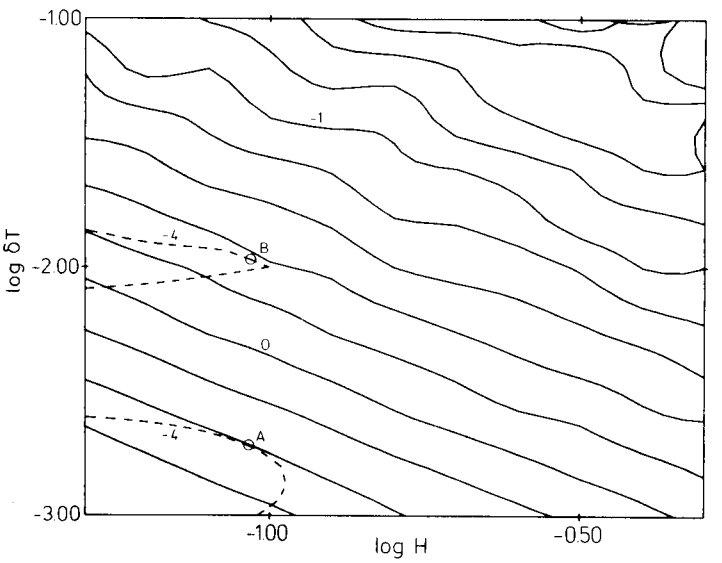

Fig. 2. Contours of (a single value of) log|*err*|: (— — —) from the simulation of the diffusion-controlled potential-step experiment by the Crank-Nicolson scheme, in the (H, δT) plane; (——) contours of log(*cpu*/s) for simulation by the Crank-Nicolson method in the same plane. The log(*cpu*/s) contours are equispaced and a few are marked.

trusted) gives the greater efficiency, at $\delta T = 0.01$ and $H = 0.1$ ($\lambda = 1$). In Fig. 1(b), this λ value is used for various δT and the error plotted against *cpu*, for some n. For some desired accuracy (e.g., $\pm 10^{-4}$ error), the relative efficiency then is close to 40; that is, 1/40 the computing time is required to yield that accuracy with the Crank-Nicolson method, relative to the explicit method. If point A were chosen, to be on the safe side ($\lambda = 0.25$),

the relative efficiency is still about 7. Here, then, the Crank-Nicolson technique performs well.

Chronopotentiometry. The known transition time τ (from the Sand equation) is the normalizing time; this leads to a constant G_0 equal to $\pi^{1/2}/2$ and the simulated quantity of interest here is the dimensionless transition time, which should be unity. In the explicit method, the procedure at each T, to proceed to the next time $T + \delta T$, is to first adjust C_0 so as to satisfy Eqn. 4, by rearranging to

$$C_0 = (-1/B_{n,0}) \left[\sum_{i=1}^{n-1} B_{n,i} C_i - A_n G_0 H \right] \tag{5}$$

For example, if $n = 2$, this becomes simply $C_0 = C_1 - G_0 H$. Then, diffusion is simulated. This is repeated until C_0, as calculated in Eqn. 5 falls below zero and the actual simulated transition time is calculated by linear interpolation. Figure 3(a) shows the errors in that time for $\lambda = 0.45$ and the same range of δT as used in Fig. 1(a), again plotted against *cpu*, for some marked n. Again, $n = 3$ is atypical but results are the same for all $n > 4$.

When the Crank-Nicolson method is used, a strategy problem arises, in fact, this lies at the heart of performance of that method. The Crank-Nicolson expression for C_1', i.e., the new C_1 value at $T + \delta T$, is

$$C_1' = C_1 + (\lambda/2) [C_0 - 2C_1 + C_2 + C_0' - 2C_1' + C_2'] \tag{6}$$

It may be noted that there is a "present" (T) value of C_0 and a "future" value ($T + \delta T$), C_0', which (for the moment) cannot be predicted. The most

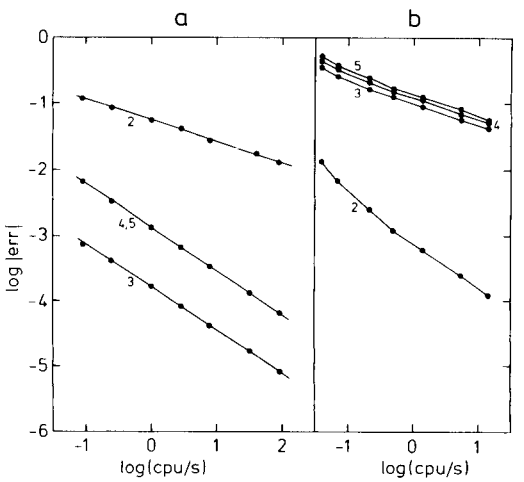

Fig. 3. Log|*err*| in the computed transition time in the simulation of chronopotentiometry: (a) explicit point method, $\lambda = 0.45$ ($0.0001 \leqslant \delta T \leqslant 0.01$); (b) standard Crank-Nicolson scheme, $\lambda = 1$ ($0.001 \leqslant \delta T \leqslant 0.1$). The controlled variable was δT and n is marked.

rational method here is to do as in the explicit method and use Eqn. 5 to compute C_0, and let C'_0 be equal to it. Equation 6 then becomes

$$C'_1 = C_1 + (\lambda/2)\,[2C_0 - 2C_1 + C_2 - 2C'_1 + C'_2] \qquad (7)$$

with C_0 the newly calculated value. The alternative is to keep the previous C_0 and use a new C'_0 but this choice turns out to be worse, not surprisingly. Figure 3(b) shows the result of the first (better) alternative, using a (reasonable) $\lambda = 1$. The surprise is that, as n increases (and thus, C_0 is an increasingly better fit to the concentration profile), results become worse. At $n = 5$, the Crank-Nicolson method is far inferior to even the explicit method; it was not practical to estimate a relative efficiency at accuracies better than $\pm 10^{-1}$, where the efficiency is about 0.1. Even with $n = 2$, comparing with the explicit method ($n = 5$), the efficiency is not much above unity.

Discussion

There is no obvious explanation for the unexpected behaviour of the Crank-Nicolson method with respect to n, in chronopotentiometry. However, higher n definitely does produce more reliable results. In this case, higher n point out a weakness of the Crank-Nicolson method. In essence, smaller n appear to produce discretization errors that tend to cancel errors produced by the Crank-Nicolson method.

Why the method fails here is not clear. One, rather vague, explanation is that the equality $C_0 = C'_0$ violates the philosophy behind the Crank-Nicolson scheme. The same phenomenon was observed in Crank-Nicolson simulation of quasireversible chronoamperometry and adsorption kinetics; in all these cases, C_0 had to be computed via G_0. In all cases the HSM technique [4] of including C'_0 in the implicit equation system completely eliminated the problem and led to Crank-Nicolson efficiencies (relative to the explicit method) one to two orders of magnitude greater. This will not, unfortunately, appeal to casual workers in this area because that method requires rather careful preparation. A more practical solution to the problem of increasing efficiency, the whole-system Runge-Kutta integration method, will be described in a later paper. In the above test case of chronopotentiometry, as well as others, it outperformed the standard explicit method and has the advantage of being very easy to program.

Conclusion

The standard Crank-Nicolson scheme can no longer be considered a method of choice in electrochemical digital simulation, especially in those systems where a known concentration gradient at the electrode determines the boundary concentration, unless one is prepared to include C'_0 in the system of equations as an implicit quantity [4].

We thank Ole Østerby, of the Computer Science Department, Aarhus University, for helpful comments.

REFERENCES

1 J. Crank and P. Nicolson, Proc. Cambridge Philos. Soc., 43 (1947) 50.
2 D. Britz, Digital Simulation in Electrochemistry, Springer, Berlin, 1981.
3 S. W. Feldberg, in A. J. Bard (Ed.), Electroanal. Chem., Vol. 3, 1969, p. 199.
4 J. Heinze, M. Störzbach and J. Mortensen, J. Electroanal. Chem., 165 (1984) 61.
5 D. Britz, Anal. Chim. Acta, 193 (1987) 277.

Analytica Chimica Acta, 194 (1987) 323—327
Elsevier Science Publishers B.V., Amsterdam — Printed in The Netherlands

Short Communication

ANALYTICAL REACTIONS OF ISOMERIC METHOXYCYCLOHEPTATRIENES

HARVEY W. YUROW* and SAMUEL SASS

U.S. Army Chemical Research, Development and Engineering Center, Aberdeen Proving Ground, MD 21010-5423 (U.S.A.)

(Received 21st October 1986)

Summary. Methods for distinguishing among the isomeric 1-, 3- and 7-methoxycycloheptatrienes are reported. Treatment with anisaldehyde in strong perchloric acid produced a blue solution for the first two compounds only (with detection limits of the order of 2 μg), while irradiation at 256 nm prior to treatment gave magenta solutions for the first and third compounds only. Absorbance was linear with respect to concentration, at least in the range 0.5—8 μg ml^{-1}. Both the 1- and 3-isomers were oxidized by cerium(IV) to tropylium salts while the 7-isomer was resistant to attack. Similarly, the 7-isomer did not react with sodium tetrachloropalladate(II) on filter paper while the other two compounds gave black spots.

The compound, 1-methoxy-1,3,5-cycloheptatriene (1-MCT), which is of interest as a safe sensory irritant [1], is formed by heating the 7-isomer, with the 3-isomer being formed as an intermediate [2, 3]. Because mixtures of the three compounds often occur, methods of differentiation are required. These methods, which involve photochemical transformations [4—6] and oxidation to tropylium ion [7], form the basis of this communication.

Experimental

Reagents. The methoxycycloheptatrienes were supplied by Organic Chemistry Branch, Chemical Division, U.S. Army Chemical Research, Development and Engineering Center. A sample of the 7-isomer was also prepared from tropylium fluoroborate (Willow Brook Labs) and methanol. Although not confirmed, the samples of this isomer were assumed to be free of the other isomers. Two samples of the 3-isomer were tested. The one for the photochemical study contained 76.5% of the compound, 5.5% of the 1-isomer, 17% of nondistillable impurities and 1% of the 7-isomer. The sample used for the remainder of the studies contained 70.8% of the 3-isomer, 22.3% of the 1-isomer and 6.9% of nondistillable impurities. The 1-isomer sample was 90.0% with 4.6% of the 3-isomer and 5.4% of nondistillable impurities. These values were obtained by gas-liquid chromatography. Cycloheptatriene (97%) and tropolone were obtained from Aldrich Chemical Company. Anisaldehyde (Matheson, Coleman and Bell) was prepared fresh

0003-2670/87/$03.50

daily as a 25% (v/v) solution in reagent-grade methanol. Other chemicals used were perchloric acid (G. F. Smith; double-distilled grade, 70—72%) and cerium(IV) ammonium nitrate (G. F. Smith; primary standard grade); sodium tetrachloropalladate(II) was prepared from palladium(II) chloride and the required amount of sodium chloride in aqueous solution. Acetonitrile was Eastman spectroscopic grade.

Equipment. Photometric measurements were made with a Bausch and Lomb Spectronic 20 photometer. Ultraviolet radiation for photochemistry was produced by General Electric 15-W, 45-cm ultraviolet lamps. Photochemistry was done in quartz test tubes (Southern New England Ultraviolet Co.). Titrations were done with a 2-ml Gilmont microburet.

Spectrophotometric determination of 1- and 3-methoxycycloheptabrienes. A 25-μl aliquot of the compound in methanol was pipetted into the test tube and the micropipet rinsed with 25 μl of methanol that was also added. The mixture was treated with 100 μl of anisaldehyde in methanol followed by 1.0 ml of water. Rapid addition of 3.0 ml of concentrated perchloric acid and mixing was followed by measurement between 10 and 15 min at 650 nm on the Spectronic 20 vs. a reagent blank.

Differentiation among the three isomers. The 1- and 3-isomers gave a strong cyan color with anisaldehyde as previously described, while 7-MCT gave a pale yellow color. The three isomers in methanol (1 mg ml^{-1}) were irradiated for 1 h in 15-ml stoppered quartz test tubes with 256-nm radiation supplied by two u.v. lamps at a distance of 5 cm. Subsequent treatment of 25-μl aliquots by the anisaldehyde procedure followed by 20-min heating at 50°C gave strong magenta colors (maximum at 560 nm) with 7-MCT and 1-MCT, and a gray color with 3-MCT. With prolonged heating, 3-MCT developed a pink color. While the above conditions did not give maximum absorbance for the 1-isomer, they did give good qualitative differentiation of it from the 3-isomer.

Titrimetric determination of 1- and 3-methoxycycloheptatriene. Cycloheptatriene derivatives not substituted on the 7-position were rapidly oxidized to tropylium salts with strong oxidants. The reagent used in this procedure was cerium(IV) ammonium nitrate standardized against arsenic(III) oxide with osmium(VIII) oxide catalyst and iron(II)-phenanthroline indicator. The samples were then titrated as follows. A 1-ml sample containing approximately 1 mg of the compound in 1 ml of acetonitrile was pipetted into a 5-ml Erlenmeyer flask followed by 3 ml of 1:1 (v/v) acetonitrile/1 M nitric acid. One drop of 0.005 M iron(II)-phenanthroline indicator was added and the sample was titrated to a pale blue color at ambient temperature with 0.1 M cerium(IV) in 1 M nitric acid, using a Gilmont micrometer buret. Additions near the end-point were at 30-s intervals. A reagent blank was subtracted.

Spot tests for 1- and 3-methoxycycloheptatriene. In the first spot test, a drop of compound (1 mg ml^{-1}) in methanol was added to filter paper (Whatman 50) soaked in 1% sodium tetrachloropalladate(II) and then dried. A gray spot was formed with a detection limit of 5 μg cm^{-2}.

The anisaldehyde reagent also was used as a spot test for 1- and 3-MCT. The test was used on Gelman glass-fiber, type A, and the sample in methanol was applied with a micropipet. The reagent, consisting of 100 μl of 25% anisaldehyde, 1 ml of water and 3 ml of concentrated sulfuric acid, was then applied. A positive test consisted of a cyan spot after 10 min while the blank remained pale pink. The detection limit was 1 $\mu g\ cm^{-2}$.

Results and discussion

The 1- and 3-isomers gave intense colors on condensation with anisaldehyde in strong acid solution in a test tube. With concentrated sulfuric acid, a transitional cyan color rapidly changing to magenta (λ_{max} = 560 nm) was produced. With concentrated perchloric acid, a cyan color (λ_{max} = 650 nm) formed within 10 min. Because anisaldehyde condenses with a number of compounds to give purple or magenta hues, it was reasoned that the blue given with perchloric acid, although somewhat less intense than the color for sulfuric acid, would be more characteristic for the cycloheptatriene derivatives, so this was made the method of choice. The cyan hue had a peak at 650 nm, where the reagent blank gave negligible absorption. Under the above conditions, cycloheptatriene itself gave negligible color at 0.5 mg while 25 μg of the 7-isomer gave a pale yellow hue. Tropolone (25 μg) gave a negative test.

Calibration plots for the 1- and 3-isomers followed Beer's Law in the concentration range studied, i.e., 0.5—8 $\mu g\ ml^{-1}$. A least-squares fit for the 1-isomer gave: Absorbance = $(0.115 \pm 0.002)C + (-0.008 \pm 0.010)$, at a 0.05 level of significance, with a correlation coefficient of 1.0000. A similar fit for the 3-isomer gave: Absorbance = $(0.111 \pm 0.005)C + (-0.009 \pm 0.018)$, with a coefficient of 0.9998.

Spectrophotometric measurements for 1-MCT following irradiation and treatment with anisaldehyde indicated linearity in the concentration range 4—32 μg in 0.1 ml of methanol. Samples of 3-MCT and 1-MCT (1 $mg\ ml^{-1}$) in methanol treated by u.v. irradiation for 1 h gave absorbance values of 0.102 and 0.530, respectively, for 25-μg aliquots. Because the sample of 1-MCT was 90.0% pure, a 100% sample would give an estimated absorbance of 0.588. Applying this value to the 3-MCT sample which contained 5.5% of 1-MCT and 1% of 7-MCT (which gave a comparable result to 1-MCT), a value of 0.588×0.065 plus a reagent blank of 0.013 must be subtracted from the absorbance value of 0.102 for 7-MCT to give a net absorbance value of 0.051. This value was sufficiently small in comparison to that for 1-MCT that quantitative differentiation was feasible.

Titration of the three isomers with cerium(IV) indicated that 7-MCT consumed a negligible amount of oxidant as would be expected from a cycloheptatriene compound substituted in the 7-position. The 1- and 3- isomers gave respectively 2.04 and 2.12 equivalents each of titrant corresponding to oxidation to tropylium cation.

Cycloheptatriene is an unusual compound in that thermal, chemical and photochemical pathways are readily available for its decomposition. Thermal

decomposition gives toluene while hydrolysis of cyano derivatives produces phenylacetic acid, indicating a tendency to contraction to a phenyl ring. Oxidation or electrophilic attack results in the formation of cycloheptatrienyl (tropylium) cation, a relatively stable carbonium ion with aromatic character. Photochemical decomposition causes bicyclization to bicyclo[3.2.0]hepta-3,6-diene with a quantum yield of 0.03 [3—6].

Of interest in this study were the isomeric 1-, 3- and 7-methoxy derivatives of cycloheptatriene. As expected, the 1- and 3-isomers, having an active methylene group, condensed with anisaldehyde in acidic solution to give colored derivatives. The 7-isomer, lacking an active methylene group, did not give a color, while samples of the 1- and 3-isomer exposed to air for extended periods gave a weaker color than did fresh samples, possibly indicating alteration of the 7-position, e.g., via oxidation to a tropone derivative. In addition, the 7-methoxy isomer was reported to be readily cleaved in acid solution to give tropone while the 1- and 3-isomers were much more resistant to decomposition [3]. Tropone did not give the anisaldehyde test.

Cycloheptatriene derivatives undergo both thermal and photochemical isomerization. The thermal scheme is [3]:

7-isomer → 3-isomer ⇌ 1-isomer ⇌ 2-isomer

Irradiation of the 7-, and the 1-isomer with 256-nm radiation was reported to give 1-methoxybicyclo[3.2.0]hepta-3,6-diene in high yield (>90%), which on heating gave the 3-isomer [4]. The 3-isomer produced the bicyclic compound in only a 3% yield, plus unidentified products. This difference in reactivity can be used for purposes of differentiation.

Oxidation of cycloheptatriene and derivatives not blocked in the 7-position gave relatively stable tropylium ions, e.g., $C_7H_7^+$ via a two-electron change [7]. Thus it was not unexpected that only the 7-isomer did not react with cerium(IV) at ambient temperatures. When the titration was done at elevated temperature, e.g., 50°C, the tropylium ion was reported to be further oxidized to benzene, carbon monoxide and benzaldehyde, but because the iron(II)-phenanthroline indicator gave a fading end-point, a potentiometric technique was required [8].

The reaction of 1- or 3-MCT with an aqueous solution of sodium tetrachloropalladate(II) may serve as a moderately sensitive spot test for the compounds. When the compounds were mixed with reagent, a dark brown precipitate formed that rapidly turned black. This precipitate was found to be more than metallic palladium alone. When heated to 130°C, it decomposed vigorously to give a colorless oil (40% yield) that solidified on cooling, and a gray residue (60% yield), both of unknown composition.

REFERENCES

1 G. A. Grant, Canadian Patent 1172957 (1984); Chem. Abstr., 102 (1985) 27605 n.
2 W. R. Hydro, U.S. Patent 4249025 (1981); Chem. Abstr., 94 (1981) 191978 y.

3 T. Nozoe and K. Takahashi, Bull. Chem. Soc. Jpn., 38 (1965) 665.
4 G. W. Borden, O. L. Chapman, R. Swindell and T. Tezuka, J. Am. Chem. Soc., 89 (1967) 2979.
5 T. Tezuka, O. Kikuchi, K. N. Houk, M. N. Paddon-Row, C. M. Santiago, N. G. Rondan, J. C. Williams and R. W. Gandour, J. Am. Chem. Soc., 103 (1981) 1367.
6 R. Srinivasan, J. Am. Chem. Soc., 84 (1962) 4141.
7 M. J. S. Dewar, C. R. Ganellin and R. Pettit, J. Chem. Soc., (1958) 55.
8 L. B. Young, Diss. Abstr. B, 29 (1968) 128B.

Analytica Chimica Acta, 194 (1987) 329—338
Elsevier Science Publishers B.V., Amsterdam — Printed in The Netherlands

Book Reviews

G. Vernin and M. Chanon (Eds.), *Computer Aids to Chemistry*. Ellis Horwood, Chichester, 1986 (ISBN 0-85312-774-3). ix + 394 pp. Price £49.50.

Chemistry, like each other branch of science, utilizes intensively scientific progress and technological achievements in computer science. With this progress the spectrum of computer applications changes. Development of fast processing units and large capacity memory devices enables complicated theoretical calculations to be made and large data sets to be stored and processed. Continuous progress in miniaturization has resulted in the common use of microcomputers for on-line control of laboratory experiments and industrial chemical processes.

The authors of this volume have had to make an arbitrary choice, as to what can best illustrate the most advanced applications of computers in chemistry. The selection made is very fortunate. Several different examples indicate well the great advantage of computer applications in dealing with large amounts of data acquired during experiments as well as data bases created for various purposes. Substantial attention is also paid to a review of the most frequently used numerical methods.

Chapter I, devoted to computer-aided organic synthesis, compares various concepts in existing software and their evolution. The most frequently used numerical methods are presented in Chapter IV, dealing with kinetic applications; in Chapter V, discussing multivariate analysis of chemical data sets with factorial methods; and in Chapter VI, describing X-ray structure analysis. Besides Chapter I, the design and utilization of large data bases is discussed in Chapter VII, introducing the reader to interpretation of data from a coupled gas-chromatography/mass spectrometry system. The utilization of commercial literature information systems is another application of large data bases. Problems of on-line access to chemical information are discussed in Chapter VII, with much information on existing systems. A valuable supplement to this volume are two chapters relating microcomputers to teaching chemistry; Chapter II on teaching chemistry with microcomputers, discussing fundamentals and presenting some available software; and Chapter III, recommending computer graphics as a new tool in chemical education.

A drawback of the reviewed volume is that is practically ignores the problems of on-line computer applications in measurement systems, which is currently a very broad field of chemical applications of computers. Even in the discussion of data acquisition in crystallographic measurements or mass spectrometry, hardware problems are neglected. They are also omitted from the list of recent literature on the use of computers in chemistry that is included in Chapter VIII. Very little attention is paid also to optimization problems.

Every chapter is written by different authors, mainly French, and obviously they differ as regards style and depth of presentation of a given subject. I consider Chapters I and V to be the best written. Without doubt the book is valuable and addressed to a variety of readers, providing a general picture of advanced computer chemistry with a good selection of basic references. At least three Chapters are devoted to analytical problems.

Marek Trojanowicz

Alf Bjørseth and Thomas Ramdahl, *Handbook of Polycyclic Aromatic Hydrocarbons, Vol. 2.* Emission Sources and Recent Progress in Analytical Chemistry. M. Dekker, New York, 1985 (ISBN 0-8247-7442-6). xi + 416 pp. Price $114 ($95 in the USA and Canada).

The first volume dealt at length with the analytical chemistry of polycyclic aromatic hydrocarbons (PAHs). The present text considers the emission of PAHs from coal and biomass combustion and from automobiles and atmospheric reactions of PAHs, as well as further analytical aspects (developments in gas and liquid chromatographic procedures, determination of occupational exposure, reference materials, and a chapter specifically on 6-nitrobenzo[a] pyrene determination in cells). In addition there is a long chapter (87 pp) on nitrogen-containing PAHs in coal-derived materials. The chapters contain a lot of useful tabulated data, and there is a considerable amount of information on chromatographic separations. The book certainly demonstrates the great effort that is being made to obtain reliable analytical data on this very important class of pollutants, and will be a valuable companion for all workers in this field.

J. B. Pedley, R. D. Naylor and S. P. Kirby, *Thermochemical Data of Organic Compounds, 2nd edn.* Chapman and Hall, London, 1986 (ISBN 0-412-27100-1). xi + 791 pp. Price £55.00.

This book provides in printed form the thermochemical computer data base on standard enthalpies of formation which has been developed at the University of Sussex. Publication began with the distribution of CATCH tables in loose leaf form, followed by a bound volume in 1977, and this is now the second edition.

Included in the text are summarising lists of original data, with references, concerning enthalpies of combustion by bomb calorimetry, and enthalpies of reaction and of vaporization. These data have been correlated to give recommended enthalpies of formation of about 3000 organic compounds of the elements C, H, O, N, S and the halogens, based upon the literature up to 1983. The text also describes predictive schemes which may be used to obtain values for other compounds in terms of their structure.

This is an authoritative work of reference for enthalpy of formation at 298.15 K in the ideal gas state at 1 atmosphere pressure. As the authors suggest, these data may be used to give an indication of the feasibility of processes given that the enthalpy change is often the dominant factor. The book does not contain any values of heat capacity or of entropy. It is well produced and the cross referencing is excellent.

P. G. Francis

A. J. Freeman and C. Keller, *Handbook on the Physics and Chemistry of the Actinides, Vol. 4.* North-Holland Physics Publishing, Amsterdam, 1986 (ISBN 0-444-86983-s). 567 pp. Price Dfl. 325.

Volumes 1 and 2 reviewed aspects of the physics of the actinides, Volume 3 dealt with the chemistry, as does the present volume, which covers subjects as varied as uranium hexafluoride, the crystal structure of actinide chalcogenides and pnictides, biochemistry of actinides, thorium halide spectroscopy, tertiary actinide—transition metal—carbon/nitrogen systems, thermochemical properties of the elements and noble metal intermetallics, chemical behaviour in natural aquatic systems, minor actinides in nuclear power stations, organoactinide compounds and fabrication of U/P mixed oxide fuel elements. There is not much of direct interest to analytical chemists, but the toxicological and environmental information will be welcomed by those working in these areas. Numerous further volumes are planned, as would be expected from the rapidly increasing knowledge of this interesting group of elements.

Malcolm S. Cresser and L. C. Ebdon, *Annual Reports on Analytical Atomic Spectroscopy, Vol. 14* (reviewing 1984). Royal Society of Chemistry, London, 1985 (ISBN 0-85186-677-8). xiii + 445 pp. Price £65.00.

It has been a pleasure over the years to have reviewed several of these volumes, as they matured from an exciting new concept to an eagerly awaited companion. The latest volume continues the trend. A total of 2635 publications and conference presentations has been scoured, to generate a well organized, wide ranging but detailed coverage of analytical atomic spectroscopy. As usual it covers basic developments, commercial instrumentation, methodology and applications to various types of samples (chemicals, metals, refractories, minerals, air, water, soils, plants, fertilizers, food and beverages, and body tissues and fluids). The camera-ready copy presentation is very clear, and the tabular arrangement of much of the material makes it relatively easy to locate information. It even manages the odd quip (e.g., p.16!) After this volume, the Annual Reports will be published in sections in the Journal of Analytical Atomic Spectroscopy as Atomic Spectroscopy Updates. This

should ensure that the material continues to be up-to-date and widely available.

A. Townshend

A. Hulanicki (Ed.), *Euroanalysis V. Reviews of Analytical Chemistry*. Akademiai Kiado, Budapest, 1986 (ISBN 963-05-4186-6). xiii + 185 pp. Price £13.25.

This book is a compilation of the lectures presented at the opening, plenary and keynote sessions of the fifth European Conference on Analytical Chemistry (Euroanalysis V) held in Cracow, Poland, during the week of August 26—31, 1984. The contents are therefore intended to provide an overview of the present state of European analytical chemistry.

The two opening lectures provide general surveys of "The History of Analytical Chemistry in Poland" and "Analytical Chemistry in Science and Society". The four plenary lectures cover a wide range of topics, from flow potentiometric stripping analysis to environmental specimen banking and from chemical analysis of extraterrestrial material to computer systems for the laboratory. There are also seven keynote lectures, with a distinct emphasis on environmental analysis and process control, which are undoubtedly two areas of increasing importance for the application of analytical chemistry.

This book satisfies the requirement of providing a permanent record of the proceedings and major themes of Euroanalysis V, and is also reasonably priced. However the range of topics covered and the general nature of most contributions make it difficult to identify the readership at whom this publication is aimed, other than those who attended the conference.

B. Welz (Ed.), *Fortschritte in der Atomspektrometrischen Spurenanalytik, Band 2*. VCH, Weinheim, 1986 (ISBN 3-527-26539-2), xi + 663 pp. Price DM 168.

This book contains contributions treating the topic of atomic spectrometric trace analysis in connection with the 3rd Colloquium held in March 1985 at Konstanz. Worthy of particular note are the overview articles concerning atomic absorption spectrometry and ICP spectrometry. In these, the most recent status of the appropriate techniques is presented and indications as to possible further developments (such as multielement-AAS, laser vaporization and ICP/MS) are made; the respective authors are highly competent experts on the subject matter (J. M. Ottaway, K. Dittrich and J. M. Mermet).

In all, the book contains 59 contributions covering almost every aspect of AAS as well as ICP/OES in the framework of the symposium. Emphasis is placed on work involving applications and problems encountered in practical operating conditions. The major group of contributors is engaged with urgent environmental analytical problems (14 papers). Contributions to the

determination of trace elements in biological substances branch into the field of clinical chemistry. Ten authors contribute directly to methods in clinical chemistry, medical research and occupational health. In these papers, it becomes particularly evident how spectrometric analysis techniques have gained significance in respect to the "human sphere of life". Although the individual articles are, to some degree, highly specialized, the references made therein to analytical problems will assist in the solution of questions in similar analytical tasks in other fields.

The fact that contemporary themes are emphatically treated is demonstrated by lectures on the AAS of solids, a technique which has gained increasing importance during the past two years. Likewise, data processing has become considerably more modern and convenient in AAS; this is also an aspect of the original contributions. In addition, instrumental developments and the theoretical backgrounds of methods are often discussed.

H. Berndt

M. E. Rose (Ed.), *Mass Spectrometry, Vol. 8.* Royal Society of Chemistry, 1985 (ISBN 0-85186-328), xii + 360 pp. Price £70.00.

The eighth volume of this Specialist Periodical Report series reviews the mass spectrometry literature published between July 1982 and June 1984 in eleven chapters. It is a measure of the importance of this publication within the field that it continues to attract considerable international and commercial support, four of the chapters being contributed from outside the United Kingdom and two from industry.

Specialist chapters are concerned with photoelectron-photoion coincidence spectroscopy, Fourier transform ion cyclotron resonance, and quantitative fast atom bombardment of materials in solution. The regular features detailing trends in instrumentation and application of computers to mass spectrometry are contributed from an industrial source and the senior reporter provides a review of current practice in gas chromatography—mass spectometry and high performance liquid chromatography—mass spectrometry. Another regular inclusion, mass spectral analysis in drug metabolism, pharmacokinetics and toxicity studies is present, but the normally recurrent chapter concerned with natural products is missing from this volume. An interesting new departure is the presence of a section on the mass spectral investigation of inorganic and organo-metallic compounds. This is an area which has received little coverage previously in this series and will be welcomed by a large number of research workers in the inorganic field. The breadth of coverage and extremely comprehensive listing of references makes this book highly recommendable to all mass spectroscopists who wish to remain abreast of current trends in their field. Analytical chemists in general will also find this volume useful in

providing an insight into the maze of techniques and methods that make up present-day mass spectrometry.

A. D. Roberts

J. H. Futrell (Ed.), *Gaseous Ion Chemistry and Mass Spectrometry*. Wiley, New York, 1986 (ISBN 0-471-82803-3). xii + 335 pp. Price £57.50.

This book has grown from the lecture notes of a workshop, held in 1983 at the University of Utah, on gas-phase ion chemistry and physics (the third most important application of mass spectrometry, according to the editor). Eight of the original lecturers, all recognized specialists from three different countries, have contributed chapters to the book. The 13 chapters are divided into sections on (i) underlying theory (unimolecular dissociation and collision theory), (ii) fundamentals of electron impact (EI) and photo-ionization, and descriptions of mass analysers, (iii) swarm and beam techniques for studying collision processes, and (iv) applications (photodissociation spectroscopy, state-to-state dynamics studies, ion/molecule reaction kinetics, cluster ions, and biomedical research). Readers of this journal should be aware that the book is not analytical in nature but covers some physical chemistry and instrumentation that underpins one of our most valuable analytical methods. Neither should the all-embracing title be taken to imply comprehensive coverage: selected topics only are presented.

It is easy to be critical of books of this nature. Several important areas are hardly covered, if at all, and such omissions could be construed as weaknesses. However, the volume does not aim to be exhaustive and it does provide clear didactic treatments of classical collision theory, mechanisms of EI ionization and fragmentation, the development of ion cyclotron resonance, swarm experiments like the flowing afterglow and drift-tube methods, and the active area of cluster ions. There is also a good introduction to biomedical applications through the use of illustrative examples, although this short chapter sits uncomfortably in a text largely concerning physical chemistry. The book is a useful topping-up text for students with a good background in physical sciences wishing to apply themselves, and mass spectrometry, to selected fields of ion chemistry.

M. E. Rose

R. L. S. Patterson, *Biomedical Identification of Meat Species*. Elsevier/ Applied Science Publishers, London, 1984 (ISBN 0-85334-408-6). viii + 213 pp. Price £25.

This publication contains the proceedings of a Scientific Workshop held in Brussels on November 27—28 1984. The meeting was organised under the

auspices of the Commision of the European Communities' Research Programme.

This book is divided into four sections. Section 1 is concerned with the differentiation of fresh meat from different species of domestic and farm animals, including deer and ostrich, using various electrophoretic procedures in particular those based on SDS-PAG electrophoresis and isoelectric focusing. The principal problems to be encountered using these techniques are also outlined. The second section covers some of the classical immunological techniques that are available for the identification of various minced meats, particularly those of muscle from such animals as antelope, kangaroo, sheep, pig, horse and cow. Alternative methods based on various enzymes including PGM, PGD and AK were shown to exhibit both quantitative and staining differences between species.

The antithesis, that is the identification of cooked meats, is described in the next section. Here identification is explored on the basis of the isoelectric focusing patterns of the heat stable components from adrenal and muscle tissues, or through the immunological reactions of various stable muscle antigens. A method of differentiation based on the distribution pattern of the major fatty acids over the triglycerides found in a number of farm animals is also described.

The final area discussed at this workshop outlined the practical problems and procedures in relation to a species testing programme and which tests to apply, and recent improvements in existing techniques.

J. Sutton

K. K. Stewart and J. R. Whitaker (Eds.), *Modern Methods of Food Analysis.* AVI, Westport, CT, 1984 (ISBN 0-87055-462-X). xx + 421 pp. Price £58.25.

The Institute of Food Technologists and the International Union of Food Science and Technology jointly sponsored a symposium on Modern Methods of Food Analysis held in New Orleans in June 1983. This book is a collection of the presentations given at the meeting and is dedicated to the memory of George F. Stewart for his contributions to the field of food science.

It is apparent from the contents of the book that the aim of the meeting was to acquaint food scientists with a variety of analytical techniques and sample treatment procedures. There are sixteen chapters, of which nine describe particular analytical techniques (atomic spectrometry, reflectance spectroscopy, bioassays, microbiological assays, sensory analysis, gas chromatography, flow injection analysis, liquid chromatography and automation), three are applications orientated (nutrients, flavours and pesticides) and four discuss aspects of the analytical process (systems approach, sample preparation, reference materials and quality assurance).

From the standpoint of an analytical chemist the chapters discussing the analytical process are of most interest and clearly show some of the particular

problems associated with the analysis of food samples, e.g. sample preparation and method validation. The chapters describing analytical techniques generally contain very basic information which is available in standard textbooks.

The range and the level of material presented in this book, together with the price tag, suggest that it will have only a limited appeal to analytical scientists.

Richard R. Muccino (Ed.), *Synthesis and Applications of Isotopically Labelled Compounds 1985.* Elsevier, Amsterdam, 1986 (ISBN 0-444-42612-4). xxxiv + 557 pp. Price $129.75/Dfl 350.

This is a compilation of the plenary and invited lectures and selected other material presented at the Second International Symposium on this topic, Missouri, U.S.A., September 1985. It reflects, in camera ready copy on glossy paper, the whole spectrum of the subject ranging from applications in medicine, metabolism and binding studies, aspects of n.m.r. of ^{2}H, ^{3}H and ^{15}N, instrumentation for isotopic studies to synthesis of labelled compounds and reaction mechanism studies. In addition to these 107 papers there are lists of posters and delegates, and a brief subject index. The standard of presentation is generally high, with figures, sometimes of great delicacy, clearly reproduced. The book should be of much interest to all who use isotopic species in their research.

Topics in Current Chemistry, Vol. 134. Springer, Berlin 1986 (ISBN 3-540-16403-0). vii + 162 pp. Price DM 124.

This volume, curiously entitled "Analytical Problems", contains three articles: surface enhanced Raman scattering of bimolecules (Koglin and Séquaris), sampling and sample preparation of environmental material (Melcher, Peters and Emmel) and chemical reactions in alkali metals (Borgstedt). The first is an intriguing account of a powerful new spectroscopic technique, the last an interesting review of a very specialist field with no particular analytical implication. Analytical chemists will find most to interest them in the second article — certainly an area of analytical problems. Air, water and solid sampling is dealt with. Devices for collecting air samples, and for isolating air particulates are described (and detector tubes, although strictly not relevant). Various water pretreatment procedures are described, as are extraction of solids, sample clean-up and water and solids sampling. The article therefore provides a compact but comprehensive treatment of one of the more neglected areas of environmental analysis. The volume also contains the author index to Vols. 101—134.

A. Maehly and Raymond L. Williams (Eds.), *Forensic Science Progress, Vol. 1*. Springer, Berlin, 1986 (ISBN 3-540-12936-7). ix + 172 pp. Price DM 138.

This new review series meets a great need in a field that is growing rapidly and which attracts the interest and talents of a wide variety of scientists. This variety will be accommodated by this series, and is reflected in the diverse contents of this first volume: forensic soil characterization (J. I. Thornton), determination of blood groups in tissue samples (H. Mukoyama and S. Seta), accidental or suicidal death by use of firearms (P. J. Thatcher) and the scientific detection of art forgeries (J. Riderer). The first group articles are comprehensive reviews, liberally sprinkled with case histories. The last is disappointingly brief, and almost completely lacking in anecdotal material. If subsequent volumes are generally as well produced as this one, the series should be very successful.

J. M. van Rossum and R. A. A. Maes, *Pharmacokinetics: Classic and Modern*. VCH, Weinheim, 1985 (ISBN 3-527-27343-3). 64 pp. Price DM 25.

This booklet provides a succinct account of the basic concepts of pharmacokinetics, the quantitative treatment of the manner and rate of distribution, metabolism and elimination of xenobiotics in living organisms, usually mammals. The classical (compartment models) and systems dynamics approaches are described. The booklet sets the scene for the series of reports by the German Senate Commission for Clinical-Toxicological Analysis on the monitoring of individual drugs, several of which have already been reviewed in this journal.

TrAC — Trends in Analytical Chemistry, Reference Edition, Vol. 4: 1985. Elsevier, Amsterdam, 1986 (ISBN 0-444-42635-3). viii + 280 pp. Price Dfl 295.00.

Trends in Analytical Chemistry is a monthly journal published by Elsevier which gives accounts of recent developments in analytical chemistry and related areas, including computer applications. It also includes news items, conference reports, book reviews and comments. Each year, the review articles are published together in one book. Volume 4 is the collected articles for 1985. They provide, in great variety, accounts of the "trends" in the subject: techniques, instrumentation, applications, basic phenomena, computer programs etc., each in 3—6 pages. They give a concise, readily available account of modern analytical chemistry, which should be available to all students and practitioners in the subject.

WHO International Agency for Research on Cancer, *Evaluation of the Carcinogenic Risk of Chemicals to Humans, Vol. 39. Some Chemicals used in Plastics and Elastomers.* 1986 (ISBN 92-832-1239-8). 411 pp. Price S.Fr. 60.

This particular volume, which resulted from a meeting of an IARC Working Group in Lyon, June 1985, continues as in the previous volumes by providing information on studies identifying a carcinogenic risk to humans, in this instance for a number of vinyl and vinylidene compounds, the nylon monomers aminoundecanoic acid and caprolactam, other monomers including toluene diisocyanate and melamine, and dichloroacetylene. The information provided is extensive and detailed, and includes data on industrial production and use, impurities and analysis as well as the carcinogenic effects. The volume incorporates a cumulative index.

Analytica Chimica Acta, 194 (1987) 339
Elsevier Science Publishers B.V., Amsterdam — Printed in The Netherlands

Erratum

M. H. Pochon, The Choice and Installation of On-Stream Analyzers with Emphasis on Infrared Instruments.

Anal. Chim. Acta, 190 (1986) 235—243.

The first two sentences of this paper after the summary (p. 235) shold read:

The term "on-stream" will be used here in preference to "on-line" which is now in common use in a somewhat different sense by computer specialists. On-stream analysis can, of course, be made either in-line or in a bypass.

ANALYTICA CHIMICA ACTA, VOL. 194 (1987)

AUTHOR INDEX

CLUE

A Microcomputer Program for Hierarchical Clustering

Authors: A. Thielemans, M.P. Derde and D.L. Massart

- performs the clustering task of arranging objects into groups based on their mutual similarities and hierarchical relationships
- determines the coherence between several groups of objects characterised by many variables
- can cluster up to 50 objects each determined by 50 variables
- available for Apple II series, IBM-PC, + IBM-PC/AT and compatibles
- clear, fully descriptive manual
- full source code listing
- easy to use
- US $ 405.00

AVAILABLE FROM:

Elsevier Scientific Software (JIC)
52 Vanderbilt Avenue
New York, NY 10017 USA
Phone: (212) 916 1250
Telex: 420643

or
Elsevier Scientific Software
P.O. Box 330
1000 AH Amsterdam
THE NETHERLANDS
Phone: (020) 5862 828
Telex: 18582

Write or call us for further information on our other programs

No shipping charge if paid in advance

ELSEVIER SCIENTIFIC SOFTWARE

Apple is a registered trademark of Apple Computer Inc.
IBM-PC is a registered trademark of IBM

INSTRUMENTUNE-UP

A Computer Program for Improving the Performance of Common Laboratory Instruments

Authors: S.N. Deming and S.L. Morgan

- adjust as many as ten continuous variables simultaneously
- based on the sequential simplex method of optimization
- available for the Apple II series and IBM-PC
- clear, fully descriptive manual with tutorial
- full source code listings
- easy to use
- US $ 205.00

No shipping charge
if paid in advance

AVAILABLE FROM

Elsevier Scientific Software (JIC)
52 Vanderbilt Avenue
New York, NY 10017 USA
Phone: (212) 916 1250 Telex: 420643
or
Elsevier Scientific Software
P.O. Box 330
1000 AH Amsterdam
THE NETHERLANDS
Phone: (020) 5862 828 Telex: 18582

"The program was extremely easy to use. . ." (G.M. Hieftje in TrAC)

". . . the package can be recommended for its full documentation and ease of use. . ." (The Analyst)

". . . this "no frills" software package could be easily successfully used by anyone with a desire for instrumentation optimization." (J.A. Holcombe in the Journal of American Chemical Society)

"The package constitutes a very competent microcomputer implementation of simplex optimization algorithm. . . "(E.L. Short in Chemistry and Industry)

GC
UV
AAS
IR
HPLC

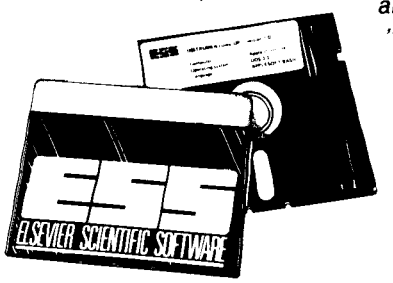

Write to us for further information on our other programs

Apple is a registered trademark of Apple Computer, Inc.
IBM-PC is a registered trademark of IBM.

ESS
ELSEVIER SCIENTIFIC SOFTWARE

INFORMATION FOR AUTHORS

"Information for Authors" was published in Vol. 190, No. 2, pp. 375–378. A free reprint is available from the
ır from:

Editorial Services Ltd., Mayfield House, 256 Banbury Road, Oxford OX2 7DH (Great Britain)

›f contribution. The journal welcomes original research papers, short communications and reviews.
are written by invitation of the editors, who welcome suggestions for subjects. Short communications are
omplete descriptions of limited investigations, and should generally not exceed six printed pages. Preliminary
ications of important urgent work can be printed within four months of submission, if the authors are
to forgo proofs.

:ripts. The preferred language of the journal is English, but French and German manuscripts are also
le. For authors whose first language is not English, French or German, linguistic improvement is provided as
e normal editorial processing. Authors should submit three copies of the manuscript in double-spaced typing
ide of the paper only, with a margin of 4 cm, on pages of uniform size. If any variety of machine copying is
g. xerox), authors should ensure that all copies are easily legible and that the paper used can be written on
ı ink and pencil. Authors are advised to retain at least one copy of the manuscript. Manuscripts should be
by a sheet of paper carrying (a) the title of the paper, (b) the name and full postal address of the person to
oofs are to be sent, (c) the number of pages, tables and figures.

on on the *submission of papers* is given on the inside front cover.

ry. Research papers and reviews begin with a Summary (50–250 words) which should comprise a brief
ccount of the contents of the paper, with emphasis on new information. Short communications and
ry communications require summaries, which should not exceed 50 words. Uncommon abbreviations,
ıd reference numbers must not be used. The Summary should be suitable for use by abstracting services
ewriting. Papers in French or German require a Résumé or Zusammenfassung preceded by a Title and
in English; authors are encouraged to provide translations where necessary.

:tion. The first paragraphs of the paper should contain an account of the reasons for the work, any essential
background (as briefly as possible and with key references only) and preliminary experimental work.

Figures should be prepared in black waterproof drawing ink on drawing or tracing paper of the same size as
/hich the manuscript is typed. One original (or sharp glossy print) and two photostat (or other) copies are
Attention should be given to line thickness, lettering (which should be kept to a minimum) and spacing on
raphs, to ensure suitability for reduction during printing. Axes of a graph should be clearly labelled, along the
l outside the graph itself.

s should be numbered with Arabic numerals, and require descriptive legends. Explanatory information should
l not in the figure, but in the legend, which should be typed on a separate sheet of paper. Simple straight-line
e not acceptable, because they can readily be described in the text by means of an equation or a sentence.
f linearity should be supported by regression data that include slope, intercept, standard deviations of the
l intercept, standard error, and the number of data points; correlation coefficients are optional.

phs should be glossy prints and be as rich in contrast as possible; colour photographs cannot be accepted. In
ine diagrams are more informative and less liable to dating than photographs of equipment, which are
not usually acceptable.

r outputs for reproduction as figures must be good quality on blank paper, and should preferably be
l as glossy prints.

:lature, abbreviations and symbols. In general, the recommendations of the International Union of Pure
ied Chemistry (IUPAC) should be followed, and attention should be given to the recommendations of the
l Chemistry Division in the journal *Pure and Applied Chemistry* (see also *IUPAC Compendium of Analytical
ature*, 1978).

ces. The references should be collected at the end of the paper, numbered in the order of their appearance in
not arranged alphabetically), and typed on a separate sheet.

: of references, the following forms should be adopted.

ıd and M. Salberg, Anal. Chim. Acta, 76 (1975) 131.

Daniel, A. D. Shendrikar, K. D. Reizneir and P. W. West, Anal. Chem., 48 (1976) 2240.

›f the journal must be abbreviated as in the Bibliographic Guide for Editors and Authors.

Perrin, Masking and Demasking of Chemical Reactions, Interscience–Wiley, New York, 1970, p. 188.

mann, in G. Svehla (Ed.), Wilson and Wilson's Comprehensive Analytical Chemistry, Vol. 9, Elsevier,
dam, 1979, p. 89.

›apers are unnecessary. Citations of reports which are not widely available (e.g., reports from government
:entres) should be avoided if possible. Authors' initials should not be used in the text, unless real confusion
caused by their omission. If the reference cited contains three or more names, only the first author's name
by et al. (e.g., McDaniel et al.) should be used in the text; but the reference list must contain the initials and
all authors.